TIME AND PROBABILITY OF FAILURE
OF
TIMBER FRAMED WALLS IN FIRE

by

Paul Clancy

BE Hons (Qld), MEngSc (Melb)

A thesis submitted in fulfillment of the requirements for the degree of
Doctor of Philosophy at Victoria University of Technology

Centre of Environmental Safety and Risk Engineering
Faculty of Engineering and Science
Victoria University of Technology
Victoria
Australia

December 1999

Declaration of Originality of Work

This thesis contains no material which has previously been submitted for an award or degree at any University. To my knowledge, the work reported in this thesis is original and contains no material published by other investigations, except where appropriate reference has been given to the source of the material.

Paul Clancy

ABSTRACT

The general aim of the research for this thesis was to develop models to predict the performance of fire resistant light-timber framed walls, in relation to requirements of new performance-based building fire regulations being introduced around the world. The performance bases that were adopted in the modelling, were time and probability of failure. The models that were developed for a wide range of wall types, and have been specifically validated for ordinary cavity walls and double framed walls. Validation involved numerical checks for convergence and energy conservation, and the undertaking of eight full scale wall furnace experiments with well controlled conditions. Values of thermal properties of materials in the walls were obtained with simple independent experiments. These experiments helped to clarify appropriate values from the wide ranges which have been previously published. Model predictions were evaluated against results published in the literature. The models comprise specific models for fire severity, heat transfer, structural response and probability of failure. This research has developed the heat transfer model named ADIDRAS, a probability model, and undertaken all linkages of models to produce the time and probability of failure models. A model developed by a colleague, Young, was adopted for the structural response model. The time and probability of failure models can incorporate most fire severity models. In this research, two fire severity models were incorporated; one was the standard fire, and the other was the real fire severity model of Kawagoe and Lie. ADIDRAS, in several respects, is an advance on previous heat transfer models for structures containing cavities. It analyses thermal diffusion with alternating direction implicit finite difference analysis which enhances numerical stability without the loss of computation speed of explicit procedures. It uses the discrete radiation method which enables analysis of radiant heat transfer through smoke and cavities of any shape. Previous models have analysed only cavities without re-entrant corners. It was deduced that when the interfaces between studs and gypsum board on the fire side reach temperatures greater than 400°C, the interfaces open to form gaps due to shrinkage in these materials. These gaps prevent much of the heat transferring directly from gypsum board to the studs, and divert the heat to the cavity by radiation. This diversion explains some anomalies between experimental results and predictions of previously published heat transfer models. It is shown that temperatures in studs are insensitive to the transmissivity of radiant heat in smoke. The structural model and the time of failure model have been applied, to obtain for the first time, relationships between the time of failure and a number of variables including vertical load, elastic modulus of timber, strength of timber, height of wall, size and spacing of studs, initial crookedness of studs and thickness of gypsum board. The time of failure model has established failure, induced by the vaporisation of moisture, is critical for walls that are either higher than walls commonly built (higher than 3.6 metres), or are more heavily loaded than is currently permitted in timber structural engineering codes. It was found that the time of failure is most sensitive to fire temperature, vertical load, elastic modulus of timber in compression, and density and specific heat of timber. It is sensitive also to the thickness and thermal properties of gypsum board, and the sectional dimensions of studs; however, these variables are unlikely to vary much for walls built to specifications in common building construction. It is considered that the

probability of failure model is the first theoretically-based reliability model for light-timber framed structures exposed to fire. Several applications of the model have been demonstrated. It was shown that the variabilities of thermal properties of gypsum board and wood are low compared with the large variabilities of mechanical properties inherent in timber. In the applications demonstrated, typical variations of all variables led to a coefficient of variation (CoV) in the time of failure of 0.12 for typical walls subjected to standard (AS1530.4) fire. Exposure to a real fire did not significantly affect this CoV. Unlike the standard fire, the real fire did not necessarily lead to collapse. There is much scope for reducing fire resistances of walls without significantly increasing the risk to life.

Acknowledgements

The author wishes to acknowledge the following:

- The support, encouragement and patience of his family.

- The supervision of Professor Vaughan Beck and the assistance of staff at the Centre for Environmental Safety and Risk Engineering, at Victoria University of Technology, including Professors Ian Thomas and Michael Hasofer. Assistance has also been provided by Associate Professor Graham Thorpe of the School of the Built Environment.

- Dr Bob Leicester for his guidance and making available the laboratory at CSIRO Division of Building, Construction and Engineering, Highett, Victoria, Australia. The project greatly benefited from the expertise, enthusiasm, and timely service of CSIRO laboratory staff.

- Mr Bob Appleton, Director of Fire Research at Forest and Wood Products, Research and Development Corporation, Australia for his encouragement, guidance and financial assistance he arranged through Australian timber industries. Through his encouragement and assistance, the project was able to attract further funds via the API scholarship mentioned below, and make valuable contacts and obtain critical appraisal from researchers overseas.

- Mr Scott Young who undertook extensive model development, testing and publication which resulted in a comprehensive, fast and numerically stable structural response model.

- Staff at BHP-Research Melbourne Laboratories for making their services and facilities available for the project. As mentioned for CSIRO above, their expertise, enthusiasm and timely service was of great benefit to the project.

- The Australian Government for its financial assistance by means of an Australian Postgraduate Industry (API) scholarship which was awarded to Mr Scott Young.

- Victoria University of Technology for its support schemes for research from which this project benefited by means of funding and time release from other duties. The assistance and encouragement provided by the former Department of Civil and Building Engineering and the present School of the Built Environment are also acknowledged.

Contents

Page

Nomenclature

A = area of surface (m^2)

A_i = area of surface i (m^2)

a_1 = a factor which varies depending on the kind of wood, carbon, and direction of heat flow ($W.m^{-1}.K^{-1}$). Refer to equation (2.44)

a_2 = temperature coefficient = 1.2 ($W.m^{-1}.K^{-2}$). Refer to equation (2.44)

b = rate constant (s^{-1})

C = coefficient for determining Nusselt number in equation (2.47)

C = confidence level

CoV = coefficient of variation

c = specific heat ($J.kg^{-1}.K^{-1}$)

c_0 = specific heat of oven dry wood with temperature ($J.kg^{-1}.K^{-1}$)

c_u = specific heat of moist wood with temperature ($J.kg^{-1}.K^{-1}$)

d_p = diameter of pores; that is, cell cavities (m)

E = elastic modulus ($N.m^{-2}$)

E = emissive power ($W.m^{-2}$)

E_A = activation energy ($J.mol^{-1}$)

E_b = emissive power of black body ($W.m^{-2}$)

$E(x)$ = expected value of x. Also known as the mean value. Same as, $\bar{x}$.

e = emissive radiant heat as a function of angle of emission ($W.m^{-2}$)

e = eccentricity (m)

$F(d_p, \varepsilon)$ = function of geometry and emissivity of cell cavities ($F \leq 1$)

F_{cv} = a convective factor, usually 1.6 ($W.m^{-2}.K^{-1.33}$) for free turbulent convection required for equation (2.50)

F_{ij} = view factor = proportion of radiant heat that is emitted from surface i and is incident on surface j

$F_R(x)$ = cumulative probability, that is probability of the structural resistance (strength) being less than the value, x.

f = function such as temperature, over a domain

$f_S(x)$ = probability density, that is frequency, of forces (or moments) are equal to, x

G = radiant heat absorbed as a function of angle of incidence

G = reliability failure function

$g(x)$ = joint probability function for normal vector x

g = gravitational acceleration = 9.81 ($m.s^{-2}$)

H = height (m)

H = hyperplane in standard normalised, n dimensional space. The plane of failure is the one for which H equals zero.

H_i = radiant heat incident on surface, i from all other surfaces and from any radiant heat emitted from smoke. ($W.m^{-2}$) Refer to equation (3.6).

h = convective heat transfer coefficient ($W.m^{-2}.K^{-1}$)

$h(y)$ = joint probability function for standard normal vector y

I = second moment of area (m^4)

$I(x)$ = indicator function which is equal to one if x has the logical value of, "true" and zero if it has the logical value of, "false"

$I_{\lambda e}(\lambda,\theta,\phi)$ = radiation intensity ($W.m^{-2}.sr^{-1}.\mu m^{-1}$)

$I_e(\theta,\phi)$ = radiation intensity ($W.m^{-2}.sr^{-1}$)

k = thermal conductivity ($W.m^{-1}.K^{-1}$)

k = effective length factor which, when multiplied with the actual length, gives the length of pin-ended column which buckles at the same load as the actual column

k_{amb} = conductivity at ambient conditions. ($W.m^{-1}.K^{-1}$)

k_g = thermal conductivity of gas in cell cavities ($W.m^{-1}.K^{-1}$)

k_r = value of thermal conductivity that gives the same rate of heat transfer as radiation through cavities, cracks or pores in material ($W.m^{-1}.K^{-1}$)

k_s = thermal conductivity of solid material ($W.m^{-1}.K^{-1}$)

k_w = thermal conductivity of bound water ($W.m^{-1}.K^{-1}$)

k_x = thermal conductivity in "x"direction ($W.m^{-1}.K^{-1}$)

L = characteristic length which is typically for an external wall surface is its height and for a cavity, its width (m)

L_e = effective length; that is the length of stud with pinned supports each end and buckles at the same load as the actual studs (m)

M = bending moment (N.m)

N = number of simulations.

$\overline{Nu}_H$ = Nusselt number for external wall surface, based on height, H of wall.

$\overline{Nu}_L$ = Nusselt number $= \dfrac{h.L}{k}$

P_{cr} = Concentric vertical load concentric on the studs (N)

Pr = Prandtl number

p = probability

p_f = probability of failure

q = energy (J)

$\dot{q}''_{bound}$ = heat influx to achieve a given temperature at the boundary node at a given time ($W.m^{-2}$)

$\dot{q}''_{c_{bound}}$ = convective heat flux exchange between the boundary node and surface node ($W.m^{-2}$)

$\dot{q}''_{r_{bound}}$ = one dimensional radiant exchange between the boundary node and surface node ($W.m^{-2}$)

$\dot{q}_r$ = radiant heat passing through some particular surface (W)

$\dot{q}''$ = heat passing through a surface of unit area ($W.m^{-2}$)

$\dot{q}'''$ = source heat rate, assumed positive for exothermic heating ($W.m^{-3}$)

$\dot{q}''_c$ = convective heat transfer per unit area ($W.m^{-2}$)

$\dot{q}''_k$ = conductive heat transfer per unit area = $k_x \frac{\partial T}{\partial x}$

$\dot{q}''_r$ = total rate radiation is emitted per unit of surface area ($W.m^{-2}$)

$\dot{q}''_{stor}$ = $\rho c \frac{\partial T}{\partial t} dx$

R = universal gas constant = 8.314 ($J.mol^{-1}K^{-1}$)

R = radiant heat resulting from reflection of incident radiant heat ***e***, which is defined above

R = structural resistance

Ra_H = Rayleigh number based on dimension H

Ra_L = Rayleigh number based on dimension L.

r = distance travelled by ray of radiation (m)

r_i = radiant heat emitted from surface i ($W.m^{-2}$). Refer to equation (3.16).

S = specific gravity

S = applied structural actions

$s_{ab}.\Delta x$ = distance between nodes "a" and "b" (m)

$s_{bc}.\Delta x$ = distance between nodes "b" and "c" (m)

T = temperature (°C or K)

T_f = average temperature of boundary layer (K)

T_s = temperature at surface (°C or K)

T_∞ = temperature in gas beyond boundary layer at surface (°C or K)

t = time (s)

t_f = time of failure

t_{fa} = actual time of failure

t_{fm} = time of failure predicted with model

u = moisture content

Var (x) = the variance of variable, x

W_i = radiant heat emitted from each surface, i ($W.m^{-2}$). Refer to equation (3.6)

x = distance in the orthogonal "x" direction (m)

x = force or moment

$\boldsymbol{x}$ = vector of actions including forces and moments

$\bar{x}$ = mean value of x

x_S = particular value of structural action such as moment, shear or axial force

$x_{\cdot tof.i.20}$ = variable input for the time of failure model; value applicable for temperature equal to 20°C

$x_{\cdot pof.i.20}$ = value generated for probability of failure model; value applicable for temperature equal to 20°C

y = distance in the orthogonal "y" direction (m)

$\boldsymbol{y}$ = standard normalised vector of actions including forces and moments

$Z = \frac{\text{weight of specimen at temperature, T}}{\text{Initial weight of specimen at ambient conditions}}$ (Refer to equation 2.45)

α = thermal diffusivity = $\frac{k}{\rho c}$ ($m^2.s^{-1}$)

α = thermal diffusivity of air ($m^2.s^{-1}$). Refer to equation (2.48)

α = surface absorptivity

α_j = generated random parameter applied to variable, $x_{\cdot tof.j.20}$ to obtain $x_{\cdot pof.j.20}$

α'_j = independently generated random parameter which is a factor of α_j.

$\alpha_{j/i}$ = generated parameter which is determined from dependent function of α_i and is a factor of α_j

α_m = modelling uncertainty factor

β = volumetric thermal expansion coefficient (K^{-1})

β = safety index = minimum distance from origin to hypersurface of failure function in standard normalised, n dimensional space

Δt = small finite time step (s)

Δx = small finite distance (m)

δ = deflection (m)

ε = emissivity

ϕ = an angle defined in Figure 2.3

η = error

κ = extinction coefficient (m^{-1})

λ = wavelength of radiation (μm)

μ = mean

$\tilde{\mu}$ = median

ν = kinematic viscosity of air ($m^2.s^{-1}$). Refer to equation (2.48)

π_g = proportion of total volume which is gaseous material

π_s = proportion of total volume which is solid material

π_w = proportion of total volume which is liquid water

θ = an angle defined in Figure 2.3

θ = direction cosine in standard normalised, n dimensional space.

ρ = density ($kg.m^{-3}$)

ρ = reflectance = 1- ε

ρ_s = bulk density of solid material (kg,m^{-3})

ρ_w = density of bound water (kg,m^{-3})

ρ_0 = oven dry density (kg,m^{-3})

σ = Stefan-Boltzmann constant ($W.m^{-2}.K^{-1}$)

σ = standard deviation

τ = transmissivity

ω = solid angle defined in Figure 2.3

ξ = interpolation factor in equation (2.42)

$\zeta(v)$ = joint probability sampling function of vector, v

Glossary

During the writing of this thesis, it was found that a number of terms were used with different meanings by different researchers. To clarify these terms, the following definitions are given:

Creep - Research into creep was not a main aim of the research for this thesis. It was deduced that some time dependent deformation occurs in light-timber frames exposed to fire. A variety of possible causes for this deformation were given - plastification, creep and stiffness reduction with temperature. These causes are collectively and briefly referred to, with the term, creep.

Convection - refers to heat transfer by the bulk movement of any material including gas and moisture.

Heat transfer - includes any mode of transfer - conduction, convection and radiation.

Load ratio - is the ratio of some applied action to the capacity relating to that action at ambient conditions. The action can be load or bending moment.

Mass transfer - refers to the movement of material alone.

Mass transfer of moisture - refers to the movement of moisture irrespective of any associated heat transfer

Melting point of glass fibres - refers to temperatures at which the gradual reduction in viscosity of glass causes it to lose its solid characteristics. It is realised that glass does not actually melt.

Moisture transfer - refers to the mass transfer of liquid water and vapour, and any consequential convective heat transfer.

Timber - refers to the wood plus growth characteristics which include knots, splits, gum pockets, veins and the like.

Validation - in the author's opinion, validation means that a model is shown to make predictions which are accurate in accordance with the aims in its development. Since models involve numerical methods and assumptions about phenomena (that is, assumptions about chemical and physical processes), then both the numerics and the phenomenological aspects should be checked and be collectively referred to as validation. Numerical checking should demonstrate that solutions are independent of mesh and time step, as well as demonstrating energy conservation. Checking of assumptions and modelling of phenomena requires good comparisons with experimental results. At the time of writing, it seemed that conventional

use of the word, "validation" related only to comparisons with experimental results. The conventional use of the word has been adopted in this thesis.

Wood - refers to the fibre in timber. In this thesis, it thus refers to clear wood.

1. Introduction

1.1 Background

Building regulations in Australia (BCA 1996) and throughout the world have, until recently, been prescriptive. Generally, prescriptive regulations specify "means" of compliance. In relation to fire safety and protection, building regulations have specified various details including the materials and construction of walls and floors, sprinkler layouts, alarms and the like. Since the inception of building regulations, fire safety requirements have been added often, particularly as new fire protection systems became available (NBFSS Project 1991) or when disasters occurred. Few of the requirements have ever been removed and the justification for the regulations was seldom documented. The prescriptive basis of the regulations did not facilitate removal of old superfluous requirements. The result of the prescriptive basis and the ever expanding regulations, was costly duplication of fire safety systems and inflexiblity of fire safety design procedures to meet the functional requirements for buildings.

Performance-based building fire safety regulations are at various stages of superceding prescriptive regulations in countries around the world (Bukowski and Babrauskas 1994, NAWPFRC 1997). Performance regulations specify goals rather than means. Examples of goals include the safe evacuation of people and property protection. No reference is made to materials and various hardware. Performance regulations allow economical safe engineering solutions and promote ingenuity. They enable fire engineers to maximise building function.

There are different bases for performance including:

1. Required levels of control of specified hazards; for example, the outbreak of fire.
2. Times of failure of fire protection systems to ensure safe egress and the level of property protection required by the building owner or authorities.
3. Risk of failure of fire protection systems to ensure acceptably safe egress and acceptable risk against large financial loss.

There are advantages and disadvantages with each basis. The first basis is simple and is most likely to be used in a consistent manner by different fire engineers. This basis, however, does not allow much scope for engineers to choose between alternative levels of protection from various fire protection systems; that is, trade-offs. The time of failure basis provides greater scope for trade-offs but would be used in a less consistent manner than the first basis. The risk of failure basis provides the greatest scope for trade-offs but would also be used least consistently among different fire engineers. Bukowski and Babrauskas (1994) explain that the risk of failure basis requires extensive analyses involving numerous scenarios, statistics and judgement which will involve some subjectivity. They also note that the first and second

bases are, however limited to only one fire scenario whereas in reality a number of fire scenarios may significantly influence risks to life and property. They recommend that performance codes will require a combination of all three bases of performance. Hence, bases for performance-based regulations should include time and risk of failures.

The introduction of performance-based regulations has allowed opportunities for a great range of flexibility, particularly for timber construction. To realise these opportunities, models must be developed for designing light-timber framed structures to achieve fire safety performance requirements. Although such models are technically feasible, prescriptive regulations have prohibited the use of timber in most types of buildings by greatly restricting the allowance of combustible building materials. Thus not only is there a need for models, but also the objection to combustible materials in the prescriptive regulations must be resolved. None of the performance requirements of the BCA (1996), namely "CP1-9", explicitly prohibit combustible materials.

It is understood, here, that risk relates to a consequence of failure such as cost and deaths. To estimate risks, the probability of failure must first be estimated. Hence it is important to develop design models to predict the time and probability of failure of timber structures in fire.

Performance-based design enables the consideration of the performance of elements of construction exposed to real fires rather than standard fires that are specified in prescriptive regulations. Generally, real fire models more closely simulate actual real fires and are potentially less conservative than standard fire equations (IEAust 1989). Thus, considerable economies should be realised by developing models for walls exposed to real fires.

The building element of interest in the research described in this thesis, is light-timber framed walls with hollow cavities and clad with gypsum board. Thus from the previous considerations, the general aim for the research should address the need to develop a model to aid the design of light-timber framed walls in real fire according to time and risk performance requirements.

Theoretical models for the thermal and structural behaviour of light-timber framed walls in fire have been developed by various researchers including Thomas (1997) and Gammon (1987). The general algorithm for these models is shown in Figure 1.1. These models simulate the behaviour of walls in fire, using small discrete time steps. At each time step, a series of separate models for fire severity, heat transfer and structural response were applied, and criteria for failure were checked. The fire severity submodel is used to predict the fire gas temperature at each time step. The heat transfer submodel is used to predict the temperature distribution at discrete nodes in sections through wall sections. The structural response submodel is used to predict the deflections and stresses at the discrete nodes.

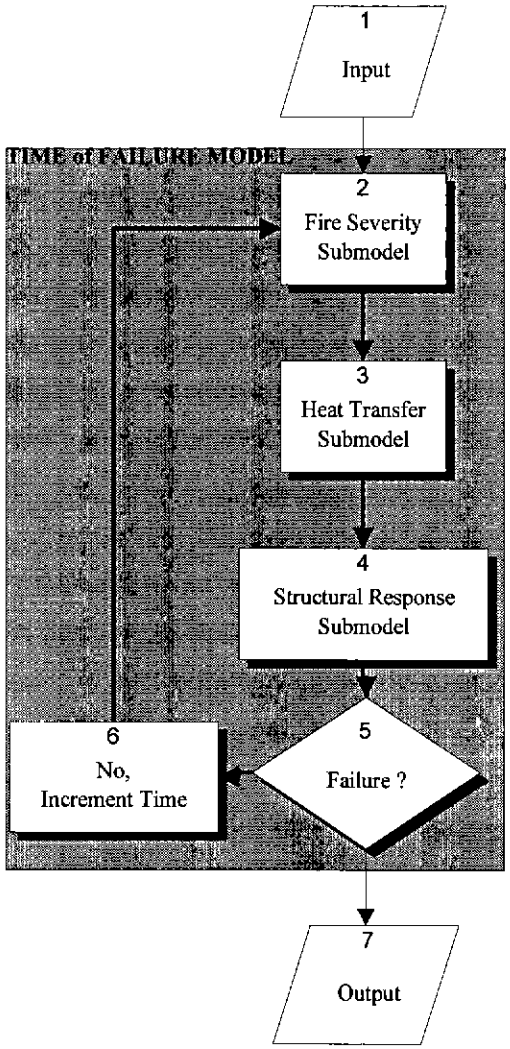

Figure 1.1. General Flowchart for Time of Failure Models.

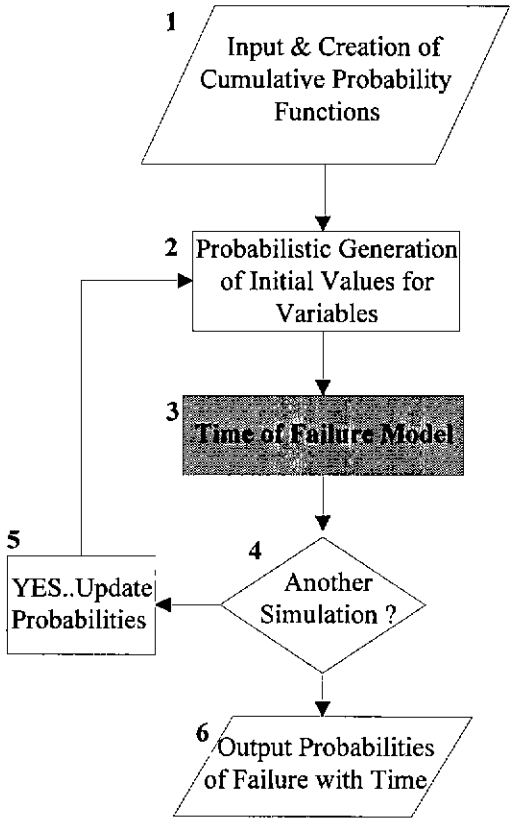

Figure 1.2. Probability of Failure Model.

Gammon described a conceptual framework for a probability of failure model similar to that shown in the flowchart in Figure 1.2, but did not complete its development. The probability of failure model is the time of failure model (box 3) incorporated into a Monte Carlo analysis. The Monte Carlo analysis commences each simulation of the time of failure model with the probabilistic generation of random variables. As failures (Figure 1.1- box 5) are encountered at the end of each simulation (Figure 1.2 - box 4), failure records are updated (Figure 1.2 - box 5) and further simulations are carried out until the number of simulations specified are completed.

Considering the background above, it was decided that the general aims for the research described in this thesis should address the needs for:

1. Significant advances in the modelling of time of failure of light-timber framed walls exposed to fire, by giving a more thorough consideration of thermal and structural phenomena than previous models for time of failure mentioned above, and by broadening the range of wall configurations modelled.
2. Development of what the author considers is the first time-dependent probability of failure model for timber framed walls in standard and real fires.

These general needs can be addressed with the general methodology shown in Figure 1.1 and Figure 1.2. Within these general needs, the research for this thesis focussed on more specific areas of focus. For this thesis, research into fire severity was excluded and the models for time and probability of failure were developed to link with most fire severity models that are currently available. In addition, research into structural response was also excluded from this thesis because, working in conjunction with the author, Young (2000) developed a structural response model to satisfy the aims of the time and probability of failure models. The research undertaken for this thesis generally focuses on the development of a heat transfer model that is well suited to heat transfer analysis for light timber framed structures. The research undertaken linked some well established fire severity models, Young's (2000) structural response model and the heat transfer model (developed by the author) to create a model for the time of failure. The model for time of failure was then incorporated into a framework to produce a model for the analysis the probability of failure (developed also by the author). The following sections will describe the research required in specific areas for the heat transfer model (§1.2) and the time and probability of failure (§1.4) models. An overview of Young's model and its suitability for analysing timber structures is given also (§1.3).

1.2 Research Required for the Heat Transfer Model

1.2.1 Recent Research in Models for Heat Transfer in Light Timber Framed Walls in Real Fires

Heat transfer modelling of light timber framed structures has been carried out by Gammon (1987), Mehaffey et al (1994) and Thomas (1997). Gammon seems to have been the first to have attempted such modelling. He adopted an existing general purpose finite element heat transfer program, FIRES-T3 and modified it by incorporating a model for heat transfer through cavities, based on the cross-string method (Hottel, 1954). He adopted values of all thermal properties from the literature. His results were mainly confined to sensitivity studies and comparisons of failure times.

Thomas (1997) used the heat transfer program, TASEF (Sterner and Wickstrom 1990). He compared his model predictions, not only with failure times observed in experiments, but also with plots of temperature versus time for various points throughout a wall. His comparisons allowed more critical appraisal of the adequacy of heat transfer modelling. In his conclusions he recommended further research into thermal properties since the values he obtained from calibrations were at the limits of published values. Further, Thomas (1997) had problems with over-prediction of temperatures above 400°C and under-prediction below 150°C in timber studs. Although the most crucial temperatures in relation to structural collapse involving charring are 200-300°C, temperatures outside this range can also be crucial. Studs larger than 90x45mm in section are more likely to reach surface temperatures higher than 400°C which will affect temperature gradients towards the core of the studs. Temperatures below 150°C cause vaporisation which dramatically reduces mechanical properties of timber and may cause collapse (Young 2000).

Mehaffey et al (1994) developed his model from first principles. He took into account more of the phenomena in heat transfer in light-timber framed walls. For example, he gave consideration to the effects of smoke, shrinkage of gypsum board and heats of reaction of charring wood. However, Mehaffey encountered similar problems to Thomas in over-predicting temperatures above 400°C, and under-predicting temperatures below 150°C in timber studs. He advised (NAWPFRC 1993) that there was some lack of confidence in the prediction of temperatures in timber sections.

Further research is required to resolve whether:

1. More accuracy in numerical analysis is required;
2. There is inadequacy in the knowledge of thermal properties; or
3. More knowledge of the phenomena which significantly influence heat transfer in light timber framed walls, is required.

To overcome these problems, areas requiring research are identified in Section, §1.2.2.

1.2.2 Further Research Required in Modelling Heat Transfer in Light Timber Framed Walls in Real Fires

TASEF (Sterner and Wickstrom 1990) and other explicit heat transfer programs are often beset with numerical stability problems arising from radiation analysis. These problems are common for explicit solution procedures. As temperatures increase, radiant heat transfer increases with the fourth power of absolute temperature. Explicit analysis simulates the transfer of discrete amounts of radiant energy to surface nodes. As surface temperatures rise, the discrete amounts of radiant heat greatly increase. Thermal diffusion analysis can only simulate the absorption of this heat if the nodes below the surface are

coarsely spaced or the time step is very small. Otherwise, temperatures gradients are generated towards the fire and numerical instability ensues. Coarse spacing leads to loss of numerical accuracy. Small time steps in the analysis lead to long computation times. Research is required to improve numerical stability without the loss of numerical accuracy or excessive computation times.

Numerical stability is particularly important in the probability of failure analysis that is shown in the model in Figure 1.2. Each execution of the loop (boxes 2-5) represents a random trial of a wall exposed to fire. Each trial randomly generates variables which affect numerical stability. Many trials are required to obtain failure probability as a function of time. Hence, some trials are likely to generate extreme values for variables which adversely affect stability. If, during the execution of any trial, stability is encountered, then the range of stable trials would be limited and not independent. Since probability analyses require independent trials, the probability of failure model would be invalid if numerical instability was encountered. Therefore, the heat transfer model must be numerically robust for a wide range of values for a number of variables.

There are considerable differences among values for material properties adopted by the researchers mentioned previously. For example, specific heats of gypsum board quoted from several researchers (Mehaffey et al 1994, Sultan 1996, and Hadjisophocleous 1996) range between 500-950 $J.kg^{-1}.K^{-1}$ for most temperatures. Values quoted for specific heat and conductivity of wood at elevated temperatures vary within a range of ±50% of average values (Janssens 1994, Fredlund 1988, Hadvig 1981, Knudson et al 1975). Assuming that there were no significant errors in their numerical analyses and that their good comparisons between model predictions and experimental results are valid, the reason for the large differences in material properties adopted is most likely due to differences in modelling heat transfer phenomena.. Given in the following is an identification of the modelling details that should be improved in order to clarify appropriate values for thermal properties.

Before the research for this thesis was undertaken, it was apparent that further modelling of heat transfer through cavities was required. Parker (1985, 88) and Mehaffey et al (1994) showed that wood, char and the thickness of gypsum board shrink during exposure to fires. Accordingly, shrinkage of these materials must create gaps between the studs and gypsum board on the fire side. It can be deduced from Fredlund's (1988) work on heat transfer through pores in wood and char, that gaps like pores, can substantially increase the rate of heat transfer at high temperatures (above 400°) by means of radiation. The gaps can transfer heat from the gypsum board immediately opposite the fire side of the studs, to the stud and the cavities (including their bounding surfaces) next to the gaps, as shown in Figure 1.3. The cavities and their bounding surfaces towards the ambient side of the wall would be cooler than the surface of the stud at the fire side, and thus the cavities and the cooler surfaces should draw significant radiant heat from the gaps. These gaps may be the reason for over-prediction of temperatures above 400°C by heat transfer

analyses which do not consider shrinkage of wood. Thus, research is required into heat transfer in cavities including gaps. The gaps create re-entrant corners; that is, corners where the angle subtended by an arc from one side of the corner to the other side, through the cavity is greater than 180°. Radiant heat transfer analyses of cavities in timber framed structures, to date, have only considered corners less than 180°C. They only consider cavities where each surface exchanges radiation with all other surfaces; that is, without obstructions. Since gaps create re-entrant corners, a more sophisticated cavity radiation analysis is required. The development of such an analysis capability would extend the application of heat transfer modelling to a greater scope of wall assemblies with built-in re-entrant corners irrespective of shrinkage gaps, including double-stud walls and staggered-stud walls as shown in Figure 1.4. These types of walls are commonly used to separate adjoining apartments in multi-residential accommodation in Australia.

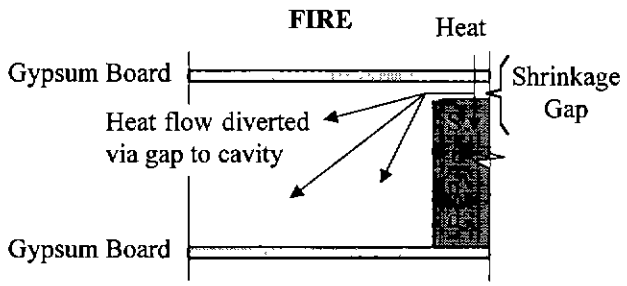

Figure 1.3. Part Horizontal Section through Ordinary Hollow Cavity Wall showing Diversion of Heat via Gap to Cavity.

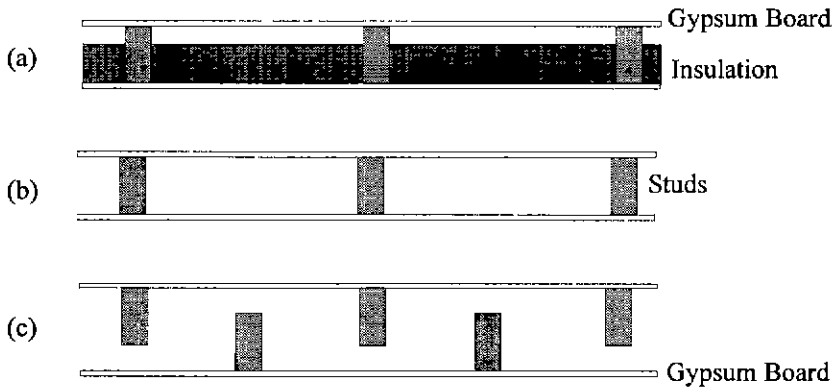

Figure 1.4. Range of Light-Timber Framed Wall Sections for Heat Transfer Modelling: (a) Ordinary Insulated Stud Wall. (b) Uninsulated Ordinary Stud Wall. (c) Uninsulated Staggered Stud Wall.

Mehaffey et al (1994) gave some consideration to the effects of smoke in cavities, on heat transfer. He assumed that the smoke absorbed all radiation from the cavity surfaces. He modelled the cavity simply as a single node and avoided complex radiation analysis. In a recent paper (Takeda and Mehaffey 1998), he has considered that radiant heat transfer through cavities is best modelled by ignoring smoke. However, due to the presence of wood, smoke is expected in cavities. Better results may be achieved by considering transmissivities intermediate between Mehaffey's two extremes of total absorbance and no absorbance of radiation through smoke.

Many light-timber framed walls have more than one layer of gypsum board on one or both sides. A model for progressive sloughing of boards needs to be developed.

One mode of failure which wall models must address is excessive temperature rise on the non-fire side; this is often referred to as "insulation failure" (AS1530.4). The temperature gradients and the plot of temperature versus time on the non-fire side is low. Every degree rise in temperature corresponds to a substantial period of time. Thus it is difficult to predict within, say, five minutes the time of insulation failure. Modelling for this mode of failure needs to be improved. Furthermore, the relevance of the mode needs to be evaluated as a viable cause of the spread of fire.

Although there is an awareness that studs permanently bend in fire tests and that the combination of fire, steam and mechano-sorptive creep can be used to bend wood for the manufacture of furniture and boats, no modelling to date has included these phenomena in respect of timber framed walls. It is a concern that the vaporisation of the moisture will create steam and mechano-sorptive creep and may cause structural collapse prior to charring. The under-prediction of temperatures by current models, in regions below 150°C in timber studs when vaporisation occurs, needs to be addressed.

Research into thermal conductivity of gypsum board is required. Mehaffey accurately measured conductivities for Canadian gypsum board (648-732 $kg.m^{-3}$) which is much lighter than Australian board (810 $kg.m^{-3}$, Boral 1997). Generally, conductivity depends on density (Fredlund 1988). Thus Mehaffey's conductivities for gypsum board are not universally applicable. Ways of transforming Mehaffey's independently measured properties to boards of other densities need to be investigated so that his conductivities can be used more universally. Mehaffey obtained the conductivity of gypsum board at temperatures above 400°C by calibration. He showed that radiation through cracks in gypsum board at these temperatures has a substantial influence on the rate of heat transfer. Tests by Goncalves et al (1996) showed that the crack widths and distributions varied greatly amongst boards from different manufacturers. Some boards had wider cracks spaced further apart than others which had fine close uniformly distributed cracks. Further tests at high temperatures, establishing rates of heat transfer through gypsum boards from different manufacturers is required.

Mechanical properties of wood typically vary several fold within batches of more than 10-20 samples (Leicester et al 1988). Intuition suggests that thermal properties could quite possibly vary by some similar large amount. The degree of variation is important to establish, not only for probability analyses, but also for establishing whether comparisons between model predictions and test results are within plausible limits. The measurement of conductivity involves expensive equipment and tedious time consuming procedures. Nonetheless, research is required to at least indicate the extent of variation in conductivities and other thermal properties of materials in walls.

1.3 Overview of Young's (2000) Structural Response Model

Young (2000) sought a model with detail to maximise understanding of the structural behaviour of timber framed walls in fire, and with robustness and speed for the wide range of generated input values that could be generated in the probability of failure model in Figure 1.2. Two approaches that have been developed for the detailed modelling of structural response models for light timber framed walls were those of Gammon (1987) and Thomas (1997).

Gammon (1987) determined the capacity of walls during fire exposure, from the capacity of the studs alone without the gypsum board. From a composite section analysis of stud cross-sections with elastic modulus varying with temperature and hence position, he determined the total flexural stiffness EI. He then used the Euler equation (1.1) to deduce the capacity of studs and the wall.

$$P_{cr} = \frac{\pi^2 EI}{L_e^2} \qquad (1.1)$$

where P_{cr} is the concentric vertical load concentric on the studs and L_e is the effective length; that is the length of stud with pinned supports each end and buckles at the same load as the actual studs. Gammon, lacked results of tests with well defined boundary conditions such as the degree of rotational restraint provided by end supports.

Thomas (1997) also determined the strength of timber framed walls in fire by only considering the studs. Instead of the Euler equation, they used the finite element program, ABAQUS. They reported problems with long computation times as the finite elements were refined. There was also some problem with stress reversal in some elements near the neutral axis. Many finite element programs define material properties identically for compression and tension. In timber, the compression properties degrade more than the tension properties with temperature. Stress reversal does not occur in many structural analyses and is

usually not a problem. They also had some problem with not having results from experiments with well defined supports for validation purposes.

Other research into the structural response of light-timber framed structures in fire is reported in §6.7. In the research for this thesis, the structural model was not related to the same grid used in heat transfer as was done by Gammon (1987) and Thomas (1997). Use of the same grid is desired in this research to aid detailed understanding.

Young (2000) favored the speed and robustness of the approach of using the total flexural stiffness, EI similar to Gammon (1987). He extended the concept further by deriving a model to determine the total flexural stiffness, EI for not only the studs but also including the partial composite stiffness contributed by gypsum boards and fasteners. Instead of the Euler equation (1.1), he adopted a second order direct stiffness analysis for large deflections. He allowed for rotational stiffness at the end supports ranging between pinned and fully fixed conditions. His model allowed for different non-linear mechanical properties for compression and tension, yielding, local failure of fibres, redistribution of stresses through sections and thermal expansion and shrinkage. He validated his model with a number of experiments with various end conditions, loads and stiffnesses of fasteners. He also validated his model with closed form solutions and results from three dimensional finite element analyses. His model which is accurate to within 0.1% compared with finite element and closed form solutions, is robust for a wide range of input values. It is fast, only taking a few seconds on a pentium 200 MHz personal computer and as such, it is most appropriate for the time and probability of failure models.

1.4 Research Required for the Time and Probability of Failure Models

Probability of failure analyses seldom require an accurate failure function (Melchers 1985) because usually there is not enough statistical data for accurate input of random variables. Often some engineering judgement is required for appropriate input values. Judgement is justified from Bayes' theorem (Melchers 1985) which shows that a probability analysis based on a mix of known data and judged data is better than pure guesswork or opinions. The failure function adopted in the model for the probability of failure is the time of failure model.

However, there was a lack of confidence in modelling the time of failure because as mentioned in §1.2.2, there is a wide range of values adopted for material properties by various researchers. It was apparent that better understanding of thermal and structural phenomena was required for the time of failure model before a probability of failure model could be developed.

To develop better understanding, the time of failure had to be detailed as well as robust and have reasonable speed of computation. Some loss of speed had to be tolerated to achieve the detail and confidence in the time of failure model.

The dominant variables affecting the time of failure have to be found in order to determine which variables are to be modelled as random variables in the probability of failure model. The usual procedure for finding dominant variables is to conduct sensitivity analyses and thus sensitivity analyses need to be undertaken and the dominant variables deduced. Furthermore, the sensitivities serve as a valuable guide to engineers designing light-timber framed walls for fire resistance.

From Figure 1.2 it is apparent that the potential large number of simulations in a probability analysis can be very time consuming. There are a number of general probability analysis methods (Melchers 1985, Benjamin and Cornell 1970, Leicester 1985) and it is necessary to evaluate which method offers optimum accuracy and computational efficiency.

It is also desirable to demonstrate the application of the time and probability of failure models for design purposes.

1.5 Aims of Research.

From the needs for research identified previously, it was decided that the general aim for the research described in this thesis, was to develop new models to advance the understanding of the behaviour, and the time and probability of failure light-timber framed walls in real fire. These models were to enable the design of light-timber framed walls in real fire according to time and risk based performance requirements.

This development involved:

1. Advances in heat transfer modelling of light-timber framed walls exposed to fire.
2. The review and adoption of a structural model.
3. The linkage of the heat transfer model and the structural model to produce a time of failure model.
4. The development of what appears to be the first probability of failure model for light-timber framed walls in real fire by incorporation of the time of failure model into a probability analysis.

The specific aims in the development of the heat transfer model were:

1. To analyse heat transfer in a wide range of walls including ordinary cavity walls, and walls with double and staggered studs as shown in Figure 1.4.
2. To consider a wide range of heat transfer phenomena and determine which are most dominant.
3. To develop heat transfer modelling of cavities, with the following capabilities:
    a) Analyse radiant heat transfer through cavities with re-entrant corners. The scope of application was to include gaps and to consider walls with built-in re-entrant corners such as double-stud and staggered-stud walls.
    b) Analyse radiant heat transfer including the absorption and re-emission of radiation through smoke, and thus determine whether more accurate modelling of radiant heat transfer through smoke should be carried out in future research.
4. Allow for progressive sloughing of sheets of gypsum board on the fire side of walls.
5. To independently determine and recommend thermal properties of gypsum board and wood using simple small scale tests and values published in the literature. These properties can then be used to obtain an independent comparison of model predictions with full scale wall furnace test results to establish whether all dominant heat transfer phenomena have been included in the model.
6. To have a model that has sufficient numerical robustness and computation speed for computing the probability of collapse by numerous simulations involving the generation of a wide range of values for random variables.
7. Following the successful achievement of the above aims, it was desired to establish the reasons why current heat transfer models over-predict temperatures above 400°C in wood on the fire side of studs.
8. To investigate a simple approach to moisture transfer modelling which would better predict temperatures less than 150°C in wood.
9. To make recommendations for improving the modelling for insulation failure.

The specific aims for the structural model were to:

1. Incorporate variables for a wide range of thermal and structural phenomena in light-timber framed walls exposed to standard and real fires to aid understanding of their effects on the time of failure.
2. Achieve fast and robust computations.
3. Be sufficiently accurate and enable design of walls according to time and risk based performance requirements.
4. Enable the production graphs for relationships between time of failure and major structural variables

The specific aims for the development of the time of failure model were to:

1. Reduce the need for wall furnace tests with a validated time of failure model.
2. Incorporate a wide range of thermal and structural phenomena in light timber walls exposed to standard and real fires to aid understanding of their effects on the time of failure.
3. Achieve fast and robust computations.
4. Have sufficient accuracy compared with test results and enable the design of walls according to time based performance requirements.
5. Demonstrate its use with one fire severity model.
6. Produce graphs for relationships between time of failure and major structural variables
7. Determine dominant variables required for the analysis of the probability of failure.

The specific aims for the development of a time dependent probability of failure model were to:

1. Enable design of light timber framed walls according to risk and time based performance requirements.
2. Achieve sufficient speed and robustness to obtain estimates of the probability of failure within a reasonable period of time, say one day.
3. Demonstrate its application with one fire severity model.
4. Demonstrate applications:
    a) The amount of variability of material properties and times of failure in tests.
    b) The variability of the times of failure for walls in standard and real fires, commonly built.
5. In the course of the above applications evaluate the variability of thermal properties in gypsum board and wood.

1.6 Significance of Research

The research for this thesis has made a number of significant advances in the modelling of heat transfer, and time and probability of failure of light-timber framed walls in real fire. As a result of these advances, the modelling will enable the rational design of light-timber framed walls to new performance based building regulations for which performance is a function of time alone or time and risk of failure. The models developed in the research will facilitate the use of timber in a much broader range of building types than has been permitted by traditional prescriptive based regulations.

Significant improvements in the numerical methods for heat transfer analysis of structures have been achieved. These improvements include the use of alternating direction implicit analysis (ADI) and

discrete radiation (DR) analysis of cavities containing absorbing-emitting media such as smoke. Compared with current explicit heat transfer analyses for structures, ADI analyses are more numerically stable without any significant loss of computational speed. These newly used methods of analysis for heat transfer in structures will establish the significance of smoke and shrinkage gaps on the temperature distribution in walls with time. The discrete radiation analysis will enable the heat transfer modelling of cavities with re-entrant corners and hence enable the analysis of a greater range of wall sections than has been possible in previous models. The expanded range will include double and staggered stud walls shown in Figure 1.4.

A wide range of thermal properties have been adopted by various researchers (§1.2.2). The research for this thesis will help to resolve typical values for thermal properties and the range of heat transfer phenomena which should be considered in modelling light-timber framed walls in fire. The research will be one of the first efforts to establish the variability of thermal properties of materials in walls.

The adoption of Young's (2000) structural response model will advance the modelling of the time of failure significantly by:

1. Incorporating modelling of a greater range of structural phenomena than previously modelled.
2. Improving numerical stability.
3. Ensuring fast computation times.

For apparently the first time, a particular range of walls for which moisture transfer substantially reduces mechanical properties, and hence the time of failure, will be established.

It does not appear that previous research to date has established relationships between the time of failure and a range of thermal and structural variables. Such relationships will be derived and will provide a useful aid for the design of light-timber framed walls in standard fire.

The probability of failure model will be the first such model for light-timber framed walls in real fire. It will be one of only a very few reliability studies involving time dependent degradation of structures. The applications of the probability of failure model in the research will also make significant advances. The research will, for the first time, provide some cumulative probability of failure plots with time for typical walls in standard and real fires. The amount of control that can be achieved over the variability of thermal properties in walls in tests, will be demonstrated. The research will also demonstrate the variability of times of failure for walls in standard and real fires, commonly built.

1.7 Methodology

A common traditional format for theses is a sequence of chapters similar to the following:

1. Introduction.
2. Literature review.
3. Methods - model and experiments.
4. Discussion.
5. Conclusions.

Although the author was aware of this format, it was thought to be too cumbersome for the wide range of topics covered in pursuing the aim of developing models for the prediction of the time and probability of failure of light-timber framed walls in fire. These topics included heat transfer, structural response, time of failure and probability of failure. A sequence of chapters similar to the above list would fragment these topics into each of the chapters and lead to disjointed description of each topic. It was thought that a more coherent format would be to structure the chapters according to the topics. Thus the chapters in this thesis describe the following sequence of topics:

1. Introduction, aims, overall methodology.
2. Heat Transfer:
    (a) Literature review.
    (b) Model.
    (c) Experiments.
    (d) Validation of model against experiments.
3. Structural response model.
4. Time of failure model.
5. Probability of failure model.
6. Conclusions.

Due to the wide range of topics, consideration was given to the appropriate level refinement of modelling to optimise the overall achievements from the research effort. Generally, all models linked within larger models, such as the time and probability of failure models, should be developed to a consistent level of refinement (Elms 1992, Beck 1986) to maximise the effectiveness of all model developments. Refinement refers to:

1. The level of knowledge of phenomena.
2. The level of detail to which phenomena are modelled.
3. The accuracy of numerical procedures.

Refinement of modelling of a limited range of phenomena which excludes phenomena that significantly affect time and probability of failure, would contribute little to achieving the general aim of the research.

To model a wide range of phenomena, the research for this thesis involved engineering methodologies rather than rigorous scientific methodologies such as computational fluid dynamics which could only be applied to the modelling of a limited number of phenomena within the research time available. The engineering methodologies included:

1. Scale considerations to eliminate those variables which did not have a dominant effect on the time and probability of failure.
2. Modelling latent thermal energy of vaporisation of moisture with the use of large specific heat values. Such modelling also increases computation speed and numerical stability which are aims of the research.
3. Engineering estimates of variables such as smoke density to determine whether smoke in wall cavities significantly affects the time of failure.

With this engineering approach, dominant variables and the effects of these, were determined. Areas of future research where more in-depth rigorous methodologies would be most fruitful, were thus identified.

2. Review of Research in Heat Transfer Relevant to Timber Walls in Fire

2.1 Introduction

The main aim of the review given in this chapter was to determine the most appropriate methodologies for modelling heat transfer through light-timber framed walls in fire, from the current state of knowledge. The review deduced which methodologies were most appropriate for adoption and which should be researched further in the development of the heat transfer model in accordance with the aims in §1.5.

The review commences with mainly a qualitative review of the basic behaviour of materials and associated phenomena (§2.2) which occur during the exposure of walls to fire. This qualitative review aims to identify the phenomena and consequently the types of heat transfer equations required in modelling (§2.3). From the equations, the required thermal properties are then identified and are reviewed in §2.4. Appropriate numerical methods for analysing the heat transfer equations are reviewed in §2.5. Literature on existing heat transfer models for light-timber framed walls in fire are then reviewed (§2.5.5) in light of the phenomena and methodologies reviewed earlier in the chapter. The chapter finishes (§2.6) by summarising key findings and areas of heat transfer modelling requiring further research.

2.2 Behaviour of Materials and Phenomena during Heat Transfer in Walls Exposed to Fire.

2.2.1 Gypsum Board

2.2.1.1 Basic Chemical Behaviour of Gypsum Board and the Effects on Heat Transfer

Gypsum board comprises more than 90% by mass of gypsum and has approximately 0.5% by mass of free water (Stray and Bates 1997). At ambient conditions, gypsum (Kelly et al 1941) is calcium sulphate dihydrate, $CaSO_4.2H_2O$. As its temperature rises, gypsum undergoes calcination - that is, dehydration - in two stages. Calcination affects density and specific heat (§2.4.2). The first stage of calcination occurs at approximately 100-120°C. It produces a hemi-hydrate and liberates water as shown in the following equation.

$$CaSO_4 . 2H_2O \rightarrow CaSO_4 . \tfrac{1}{2} H_2O + \tfrac{3}{2} H_2O \qquad (2.1)$$

This stage of calcination is endothermic. The liberated water and the initial free water leads to moisture transfer and the further absorption of heat as it is vaporised. Moisture transfer is a convective process; that is heat transfer by virtue of the bulk movement of material. In regions at temperatures less than 100°C, moisture transfer initially leads to higher heat transfer rates than can be explained by conduction (White et al 1981, Fredlund 1988). In regions at temperatures above 100°C, moisture transfer has a cooling effect and leads to lower heat transfer rates than can be explained by conduction. Moisture transfer has no net effect on heat transfer considered over the temperature range 0-200°C. It does cause temperatures to dwell at approximately 100°C longer than predicted with conductivity alone.

The remaining dehydration occurs in the second stage at approximately 600°C (Sultan 1996) in accordance with the equation,

$$CaSO_4.\tfrac{1}{2}H_2O \rightarrow CaSO_4 + \tfrac{1}{2}H_2O \qquad (2.2)$$

2.2.1.2 Manufactured Characteristics which Affect Heat Transfer

Gypsum board is manufactured in several ways. The board used in the research for this thesis, Boral Firestop (Boral 1997) is manufactured by pouring gypsum in paste form onto a thick sheet of paper. The paper is then folded to enclose the paste, and is passed through rollers from which the board emerges. The board then is passed through a drier which reduces the free water to less than 0.5% of the dry mass (Stray and Bates 1997), which is a small proportion and thus has little affect on the heat of vaporisation. The gypsum paste contains foaming agents which entrain air and enable the density of the board to be reduced to the desired value to reduce costs.

To maximise flexural strength to prevent the boards breaking when workers lift and place them in position during the construction of walls, some gypsum board manufacturers increase the density of gypsum near the surfaces of boards by firstly applying a non-foamed paste of gypsum on the paper prior to the placement of foamed gypsum. However, Stray and Bates (1997) advise that Boral Firestop has uniform density, and thus should have reasonably uniform thermal properties.

During the manufacture of fire rated gypsum board, glass fibres are added. Glass fibres hold together portions of board which crack during fire exposure and thus help to extend the fire resistance time.

The gypsum core in boards at ambient temperatures also comprises various fillers which include vermiculite and clays. Vermiculite is used in gypsum board intended for providing fire resistance. It reduces the shrinkage of gypsum board at high temperatures. Shrinkage effects are explained below.

2.2.1.3 Shrinkage, Crazing and Sloughing of Gypsum Board

Shrinkage is a mechanical characteristic which has significant effects on heat transfer through gypsum boards fastened to walls. Mehaffey et al (1994) has observed and measured the shrinkage in gypsum board thickness with temperature, shown in Figure 2.1. The upper two plots include the disappearance of surface paper between 200-400°C. Figure 2.1 indicates shrinkage of the thickness of gypsum boards. Presumably, shrinkage in the plane of the boards is similar. However, it is doubtful that shrinkage is the same in all in-plane directions since glass fibres in gypsum board can vary as much as 30% in concentration with direction (Goncalves et al 1996). Shrinkage has inconsistent effects on heat transfer. Shrinkage reduces thickness which reduces the resistance to heat transfer. However, shrinkage also increases density which increases the resistance to heat transfer.

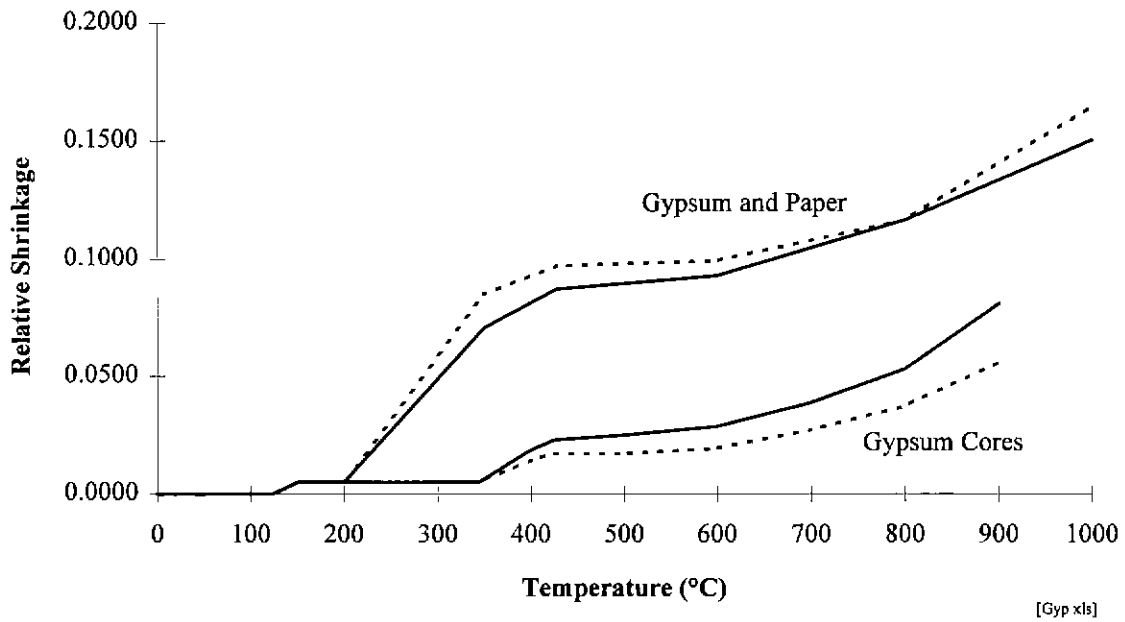

Figure 2.1 Linear Shrinkage of Gypsum Board Thickness with Temperature (Mehaffey et al 1994). (Continuous lines refer to Canadian type X boards 648 kg.m^{-3} and the dotted lines refer to Canadian type C boards 732 kg.m^{-3}.)

Figure 2.1 shows that some shrinkage commences at low fire temperatures, 200-400°C. The overall shrinkage of boards is prevented in the construction of walls because they are attached and restrained against movement with screw or nail fasteners. Thus local shrinkage occurs. It appears as a random pattern of fine cracks a few centimetres apart which is often referred to as crazing. Crazing and increasing dominance of radiant heat transfer increases the total rate of heat transfer, at 400°C and moreso at approximately 700°C. At 400°C shrinkage becomes more significant. Cracks begin to open and allow the ingress of radiation. Since radiant heat transfer through pores is significant at 400°C (Fredlund 1988), it is

expected that radiation through cracks would also be significant. Gypsum board is held together across the cracks by glass fibres (Carne 1995). These fibres do not have a precise melting point. As temperature rises, viscosity of the fibres reduces. The fibres stretch and flow to accommodate the shrinkage. Eventually, when the temperature reaches some value between 700-900°C (Carne 1995, Goncalves et al 1996) the viscosity and strength of the fibres reduces to such a low value that the fibres break. The cracks open to a depth where the temperatures are less than approximately 700°C. The widening of the cracks in this manner and the increased dominance of radiant heat transfer with temperature are the likely causes for the expected large increase in heat transfer rates through gypsum boards at temperatures greater than 700°C. When the minimum temperature through the thickness of vertical gypsum board rises above 700°C, it is expected that the cracks fully penetrate the board and pieces of gypsum board fall away. This phenomenon is known as sloughing. From the time when gypsum board sloughs and exposes light-timber framing to fire, the heat transfer into char and wood is so great that the frame structurally collapses within a matter of minutes (Collier 1991, 93).

Another consequence of shrinkage is the opening of joints between edges of adjacent boards of gypsum (Takeda 1998). The joints are located over some studs or across cavities. The opening of joints over studs would obviously accelerate heat transfer, charring and general degradation of the studs. The opening of joints over cavities would accelerate heat transfer into cavities and then to other parts of walls.

2.2.2 Timber

Jönsson and Pettersson (1985) gave a review of phenomena which occur as the temperature of wood increases. At temperatures less than 200°C there is a very slow pyrolysis and slow loss of density. Provided the wood is sound and without decay, the gases produced are not generated at a significant rate and are not ignitable. In the temperature range, 200°-280°C the pyrolysis gases are produced at a significant rate and are ignitable. Between 280°-500°C the density of wood reduces dramatically by some 70% due to volatisation. As wood material changes from solid to gas, the volume of the material expands approximately 500 times. At temperatures at the low end of this range, the gas contains CO_2 and water vapour which prevent spontaneous ignition. At the high end of this temperature range, if the volatiles mix with air with an oxygen concentration exceeding 11% (Tewarson and Pion 1976) there will be spontaneous ignition. The temperature of the flame is approximately 1100°C. The thickness of char continues to increase while volatiles are produced from the wood and shield the char from oxygen in the air. At 500°C, the char glows and begins to oxidize. When the surface temperature reaches 1100°C, char is consumed at the surface just as fast as it is produced at the interface between wood and char, provided heat transfer is one dimensional.

Heat transfer through charring wood depends on the position of the interface between char and wood. There are two processes which affect this position, kinetic processes and transport processes. Kinetic processes describe the rate at which chemical reactions take place as a function of temperature. They are often formulated as Arrhenius functions. Such a function for the reduction in density due to charring is,

$$\frac{d\rho}{dt} = -\rho \ .b.\exp\left(-\frac{E_A}{R.T}\right) \qquad (2.3)$$

where ρ = density at time, t ($kg.m^{-3}$)

b = rate constant (s^{-1})

E_A = activation energy ($J.mol^{-1}$)

R = universal gas constant = 8.314 ($J.mol^{-1}K^{-1}$)

T = temperature at time, t (K)

t = time (s)

Transport processes are those including the movement of gaseous and fluid reagents towards, and products away from the position where chemical reactions are taking place. The rate of chemical reaction is limited by the slower of the two processes. It is very difficult to determine the constants b and E_A from experiments. There is very little knowledge of the chemical reactions which take place as wood turns to char. Since much more is known about heat and mass transfer than about chemical processes, characteristic temperatures are usually sought to define the position of the interface between char and wood. Hadvig (1981) amongst many other researchers, chose the temperature criterion that wood chars at 300°C. He explained that the boundary between char and wood is insensitive to temperature due to the steepness of the temperature gradient in this vicinity. For example, if the actual temperature at the boundary between char and wood was 350°C or 250°C rather than 300°C, the differences in the positions where these temperatures occur would unlikely be more than a few millimetres.

Char receeds by two processes, contraction and surface recession. Contraction occurs as volatiles are released and char is formed. Contraction was investigated by Parker (1988) who explained that as char is formed by pyrolytic processes, it contracts and ultimately forms a graphitic structure. Douglas fir typically contracts 30% normal to the grain when the density has reduced to 20% of its virgin value. Contraction along the grain for such conditions is typically 25%. Surface recession occurs when the surface temperature reaches 1100°C.

As a consequence of contraction in the tangential and longitudinal directions, char cracks. The cracks widen due to oxidation and surface recession. The formation of cracks causes heat to penetrate to the wood at a faster rate via radiation and convective flows of gases (Jönsson and Pettersson 1985). It is difficult to model the geometrical changes due to char shrinkage and recession, and the consequential

affects on heat transfer. These phenomena may not greatly influence heat transfer prior to failure of timber structures in fire since they occur well after the onset of surface char and thus involve a small proportion of the time of exposure.

Fredlund (1988), White and Schaffer (1981) and Peralta and Skaar (1993), Maclean (1941) explain the relationships between heat transfer and the movement of moisture in wood. There are three causes for moisture movement - differential moisture concentrations, temperature gradients and vapor pressure. As wood is heated to approximately 50°C, temperature gradients cause moisture to flow towards cooler regions which takes many hours. As the temperature approaches the vaporisation point, at 100°C or above, wood dries out quickly. At the vaporisation point moisture is vaporised. Vapour pressure rises dramatically and vapour diffuses towards both cooler zones and hotter zones. The vapour in the hotter zones has a cooling affect. The vapour in the cooling zones has a heating effect and condenses thereby increasing the moisture content by as much as a factor of two or more. Vaporisation is often referred to as a dwell. The effects of vapour diffusion is to extend the dwell period and to increase the volume of wood exposed to steaming temperatures at any one time. Steam enables wood to be bent as is apparent from the manufacture of ships centuries ago and furniture today (Wood Handbook 1987). Despite moisture transfer having no net impact on the total heat influx it may critically affect mechanical properties and hence time of failure.

It is apparent from the movement of moisture with temperature and the long period of time to achieve a steady state temperature profile that it is very difficult to measure conductivities of wood at a set moisture content and temperature.

Lie (1992) reports that the heat of reaction of wood pyrolysis has been highly disputed. Roberts (1971) has found that published estimates range between 370 $kJ.kg^{-1}$ endothermic to 1700 $kJ.kg^{-1}$ exothermic. In their models for the fire resistance of timber structures, Gammon (1987) and Thomas (1997) assume no heat of reaction. Thomas (1997) based their assumption on reserch by Parker (1988). Mehaffey et al (1994) and Knudson and Schniewind (1975) assume endothermicity of 370 $kJ.kg^{-1}$.

2.2.3 Air within Cavities and next to External Surfaces

As heat transfers through external surfaces and cavities, air near surfaces is heated, becomes more bouyant and thus flows, stratifies and transfers heat by convection (Prakash, Turan and Thorpe 1999). Within wall cavities these air flows distribute the smoke observed by Collins (1992). At temperatures greater than 300°C, radiant heat transfer dominates over convective heat transfer and is affected by the smoke (Raithby and Chiu 1990).

2.2.4 Types of Equations Required to Model the Heat Transfer Phenomena Identified

From the above review in §2.2.1-§2.2.3, the phenomena which have been found to affect the heat transfer in light-timber framed walls in fire are as follows:

1. Conduction.
2. Rate reactions for phenomena such as moisture vaporisation and charring, and the subsequent production of volatiles and soot.
3. The transfer of moisture, volatiles and soot through porous media such as timber and gypsum board.
4. Natural convection of air, volatiles and smoke particles in cavities and next to external surfaces.
5. Radiation through an absorbing-emitting medium such as smoke.
6. Dimensional changes of gypsum board and timber

To model all of the above phenomena in detail would require a complex algorithm with many fundamental equations. Such an algorithm is technically feasible but would require an extremely large amount of research and development. Several researchers (Beck 1986, Elms 1992, Bejan 1984) have argued that efficient modelling research should not attempt to model all phenomena in detail. An aim of model development should be a consistent level of refinement amongst all submodels. Hence the only phenomena that should be modelled are those which have an effect on results which is significant according to the aims.

Researchers (Gammon 1987, Mehaffey et al 1994, Thomas 1997) have shown that radiant heat transfer at external surfaces and through cavities dominates over convective heat transfer through light-timber framed walls exposed to fire. It is more appropriate for efficient modelling research, to use detailed radiant heat transfer equations and simple convection equations. Hence, it is more appropriate to use simple convection equations which use average heat transfer rates across surfaces instead of convection equations which predict heat transfer at all points in a continuum.

There do not appear to be any records of walls collapsing due to moisture transfer during wall furnace experiments. Collier (1991, 93) observed that at the time of failure of walls he tested, temperatures in studs were well above the vaporisation point and the studs were substantially charred. Since moisture transfer has little effect on the time when charring temperatures are attained, moisture transfer equations will not be reviewed.

To achieve a consistent level of model refinement, rate reactions equations should be ignored. It is appropriate to use Hadvig's (1981) simple temperature criterion for determining the transition of timber to char. It is also appropriate to consider all moisture vaporisation to occur at 100°C since structural collapse of walls occurs when the temperatures in timber studs is much higher. Hence, equations for rate reactions will not be reviewed.

In accordance with the aim of achieving a consistent level of modelling refinement, it is appropriate to adopt thermal properties which account for the effects of dimensional changes of wall components on heat transfer.

Thus equations which will reviewed are those for thermal conduction, simple modelling of convective heat transfer and radiation through an absorbing emitting medium.

2.3 Fundamental Equations for Heat Transfer

The fundamental equations for the phenomena identified in §2.2.4 as governing the behaviour of light-timber framed walls in fire, have been obtained from Incropera and De Witt (1990), Siegel and Howell (1981), and Gray and Müller (1974). These references explain three modes of heat transfer; namely, conduction (§2.3.1), convection (§2.3.2) and radiation (§2.3.3).

The post-flashover stage of fires dominates over the other stages in their influence on time of failure of walls (Drysdale 1985). During this stage of fire development temperatures in the fire enclosure can be considered uniform. Consequently, temperatures in walls will not vary with height and thus temperature distributions in walls are two dimensional. Accordingly, the equations in this section, §2.3 are for two dimensional heat transfer.

2.3.1 Conduction

Heat is a form of kinetic energy of molecules, excluding bulk motion. Conductive heat transfer is the transfer of this energy from more energetic to less energetic molecules when they collide as a consequence of random molecular motion. Although the random motion occurs in three dimensions, the heat transfer is described as two dimensional when, at the macroscopic scale rather than at the molecular scale, there is no significant transfer of heat out of plane.

The fundamental equation for two dimensional conductive heat transfer is,

$$\frac{\partial}{\partial x}\left(k\frac{\partial T}{\partial x}\right)+\frac{\partial}{\partial y}\left(k\frac{\partial T}{\partial y}\right)+\dot{q}''' = \rho c\frac{\partial T}{\partial t} \qquad (2.4)$$

where k = thermal conductivity ($W.m^{-1}.K^{-1}$)

T = temperature (°C or K)

x = distance in the orthogonal "x" direction (m)

y = distance in the orthogonal "y" direction (m)

t = time (s)

$\dot{q}'''$ = source heat rate explained in §2.3.4, assumed positive for exothermic heating ($W.m^{-3}$)

ρ = density ($kg.m^{-3}$)

c = specific heat ($J.kg^{-1}.K^{-1}$)

For one dimensional heat transfer perpendicularly through an infinitesimal slice of solid material of thickness dx, equation (2.4) can be reduced to,

$$\dot{q}''_k + \dot{q}''_{source} = \dot{q}''_{stor} \qquad (2.5)$$

where $\dot{q}''_k = k_x \frac{\partial T}{\partial x}$

$\dot{q}''_{stor} = \rho c \frac{\partial T}{\partial t} dx$

If the thermal conductivity is constant and there is no source heat then equation (2.4) reduces to,

$$\alpha\frac{\partial^2 T}{\partial x^2} = \frac{\partial T}{\partial t} \qquad (2.6)$$

where α = thermal diffusivity ($m^2.s^{-1}$)

$= \frac{k}{\rho c}$

2.3.2 Convection

Convection comprises two fundamental modes of heat transfer - diffusion due to random molecular motion and advection which is heat transfer due to macroscopic fluid flow. The two applications of interest in the research for thesis are convection between a large volume of gas and an external vertical planar surface, and convection between an internal vertical surface and a small volume of air. The latter

application is for the transfer of heat between sheeting and cavities in cavity walls. The characteristics of convective temperature profiles are shown in Figure 2.2. The temperature profile in the air near the surface has a steep gradient through a boundary layer. The surface temperature is denoted as T_s (°C). In Figure 2.2(a) the body of air is assumed to have uniform temperature, T_∞ (°C). This assumption is reasonable because the type of fire, which is hazardous to the structure, is post-flashover fire which involves much mixing of the fire gases due to turbulence (Drysdale 1985). In Figure 2.2(b) the temperature profile through most of the cavity has a slight gradient. The average temperature is denoted as T_∞ (°C).

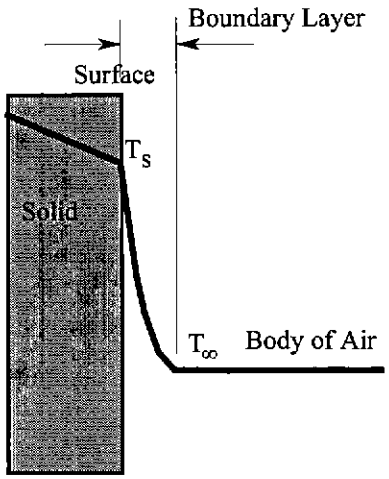

Figure 2.2 (a) Temperature Profile through External Surface of a Solid.

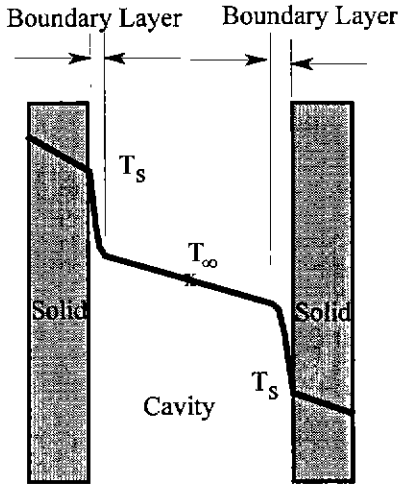

(b) Temperature Profile through Cavity Surfaces.

The simplest model for determining convective heat transfer per unit area, $\dot{q}''_c$ ($W.m^{-2}$) is Newton's Law of Cooling,

$$\dot{q}''_c = h(T_s - T_\infty) \qquad (2.7)$$

where h = convective heat transfer coefficient ($W.m^{-2}.K^{-1}$) which is found from Nusselt numbers, $\overline{Nu}_L$, defined in equation (2.8).

$$\overline{Nu}_L = \frac{h.L}{k} \qquad (2.8)$$

where L = characteristic length which is typically for an external wall surface is its height and for a cavity, its width.

k = thermal conductivity of air determined for the average temperature, T_f in the boundary layer.

$$T_f = \frac{T_s + T_\infty}{2} + 273 \quad (K) \tag{2.9}$$

Nusselt numbers are dimensionless measures of the temperature gradient through boundary layer air. They indicate the convective heat transfer rate. Convective heat transfer coefficients and Nusselt numbers vary with position over surfaces. Values at particular points are local values. To model overall heat transfer through surfaces, values averaged over the entire surfaces are required. Average values are used in the research for this thesis, as explained in §2.2.4.

2.3.3 Radiation

Radiation is heat transfer by electromagnetic waves. Unlike conduction and convection, it does not require matter to transfer heat. Conduction and convection modes of heat transfer are quantified as the flux of heat energy either through or from a unit area in a unit of time. The quantification of radiation is more complex. Since radiation comprises a spectrum of electromagnetic waves with different proportions of the total radiant heat flux for different unit ranges of wavelengths, the quantification of radiant heat must also be expressed in terms of unit ranges of wavelengths. Furthermore, radiation disperses as it moves away from its source and must be quantified in terms of solid angle. Thus radiation is quantified as $W.m^{-2}.sr^{-1}.\mu m^{-1}$, where sr is the abbreviation for steradian, the unit for solid angles. Radiation quantified with these units is referred to as radiation intensity, $I_{\lambda e}$ and can be expressed as follows,

$$I_{\lambda e}(\lambda,\theta,\phi) = \frac{d\dot{q}_r}{dA_1.\cos\theta.d\omega.d\lambda} \tag{2.10}$$

where $d\dot{q}_r$ = the rate at which radiation emitted from dA_1 passes through dA (W)

λ = wavelength of radiation (μm)

Other terms are defined in Figure 2.3.

Siegell and Howel (1981) explain that radiation intensity from an object is uniform in every direction and in every position. They demonstrate this characteristic of radiation by considering thermal radiation equilibrium inside a sphere surrounding an object.

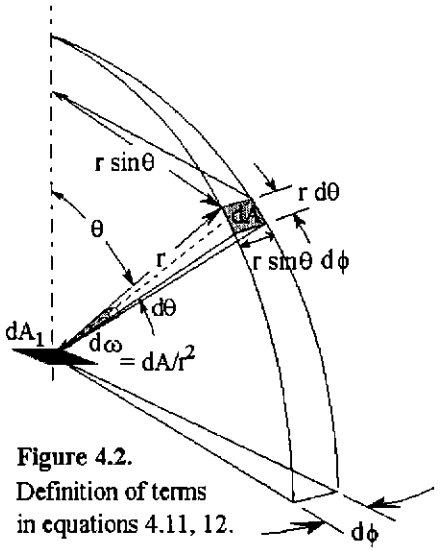

Figure 4.2.
Definition of terms
in equations 4.11, 12.

Figure 2.3. Definitions of Terms in Equations (2.10), (2.11).

Consideration of wavelengths is too detailed for the aims of the research for this thesis given in §1.5. Thus radiation intensity over the entire spectrum of wavelengths will be considered, $I_e(\theta,\phi)$; that is,

$$I_e(\theta,\phi) = \frac{d\dot{q}_r}{dA_1.\cos\theta.d\omega} \qquad (2.11)$$

Rearranging equation (2.11), the rate at which radiation emitted from dA_1 passes through dA can be expressed as,

$$d\dot{q}_r = I_e.dA_1.\cos\theta.d\omega \qquad (2.12)$$

From Figure 2.3, the radiation rate, $d\dot{q}$ emitted from a small area dA_1, can be expressed as,

$$d\dot{q}_r = I_e.dA_1.\cos\theta.\sin\theta.d\theta.d\phi \qquad (2.13)$$

The total rate radiation is emitted per unit of surface area, $\dot{q}''_r$ is thus,

$$\dot{q}''_r = \int_0^{2\pi}\int_0^{\pi/2} I_e.\cos\theta.\sin\theta.d\theta.d\phi \qquad (2.14)$$

A useful variable in radiant heat transfer analysis is emissive power, E. It is the rate at which radiation is emitted per unit surface area of a body. E differs from I_e which is the rate per unit surface area on some

hemisphere centred on the body and per unit of solid angle. Bodies at the same temperature do not necessarily have the same emissive power. The maximum emissive power, E_b is transferred by black bodies. In general,

$$E = \varepsilon . E_b \qquad (2.15)$$

where ε = surface emissivity

Surface emissivity, ε is 1.00 for a black body. E_b is thus in fact, $\dot{q}_r''$ in equation (2.14) ;that is,

$$E_b = \int_0^{2\pi} \int_0^{\pi/2} I_e . \cos\theta . \sin\theta . d\theta . d\phi = \pi . I_e \qquad (2.16)$$

In radiation analysis it is often useful to consider, ***e*** the emissive power per unit solid angle in a particular direction, θ. By the definitions of E and ***e***, the latter can be expressed as,

$$e(\theta) = \frac{dq}{dA_1 . d\omega} \qquad (2.17)$$

By comparing equations (2.10) and (2.15), it is apparent that,

$$e = I_e . \cos\theta \qquad (2.18)$$

Equation (2.18) is known as Lambert's cosine law.

E_b is a unique function of temperature and wavelength. This function is known as Planck's distribution. It is not quoted here because as mentioned above, consideration of wavelength is beyond the scope of this thesis. The integration of E_b for all wavelengths leads to the Stefan-Boltzmann Law; that is,

$$E_b = \sigma . T^4 \qquad (2.19)$$

From equation (2.15) the emissive power for surfaces in general is expressed as,

$$E = \varepsilon . \sigma . T^4 \qquad (2.20)$$

Equations (2.10)-(2.20) consider radiation emitted from a body. Radiation transfer analysis also involves incident radiation on a surface. The amount of incident radiation ***e*** from another body which is absorbed by a surface is,

$$G = \alpha . e \tag{2.21}$$

where α = surface absorptivity

From Kirchoff's Law the surface absorptivity is equal to the surface emissivity, ε. The radiation power reflected from a surface is,

$$R = \rho . e \tag{2.22}$$

where ρ is the reflectance of the surface. By equilibrium, radiation which is not absorbed must be reflected. Thus,

$$\rho = 1 - \varepsilon \tag{2.23}$$

Reflections can be considered to be of two types - diffuse and specular. Diffuse reflections are reflected radiation which is scattered. Specular reflections are those for which the angle of reflection equals the angle of incidence. Surfaces which produce diffuse reflections can be seen from any position. Surfaces which produce specular reflections can only be seen when the lines of vision and reflection are coincident. In reality, virtually all surfaces have diffuse and specular characteristics.

In radiant heat transfer analysis it is useful to know the proportion of radiant power emitted from a surface with area, say A_i shown in Figure 2.4, and is incident on surface with area, say A_j. This proportion is known as the view factor, F_{ij}. It is found as follows.

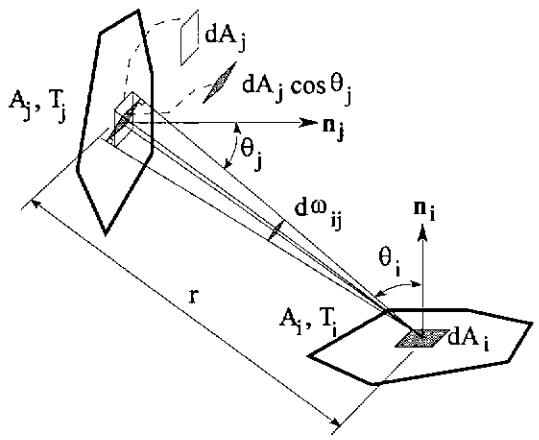

Figure 2.4.Variables Used for Determining View Factors.

The radiant power emitted from dA_i, incident on dA_j is,

$$dq_{ij} = e_{ij} . d\omega_{ij} \qquad (2.24)$$

From equations (2.15), (2.16) and (2.18),

$$e = \frac{E}{\pi} . \cos\theta \qquad (2.25)$$

$$d\dot{q}_{ij} = E.\frac{\cos\theta_i.\cos\theta_j}{\pi r^2} dA_i.dA_j \qquad (2.26)$$

Integrating over both areas, A_i and A_j, the radiant power emitted from A_i incident on A_j is found,

$$\dot{q}_{ij} = E\int_{A_i}\int_{A_j} \frac{\cos\theta_i.\cos\theta_j}{\pi r^2} dA_i.dA_j \qquad (2.27)$$

The proportion of radiant power emitted from A_i incident on A_j; that is the view factor F_{ij} is thus,

$$F_{ij} = \frac{1}{A_i}\int_{A_i}\int_{A_j} \frac{\cos\theta_i.\cos\theta_j}{\pi r^2} dA_i.dA_j \qquad (2.28)$$

Radiation heat transfer between fires and surfaces of walls can be modelled by considering the fire as a wall of heat. The heat transfer can then be modelled as the transfer between two large parallel plates each with a surface area, A. The heat transfer from plate 1 to plate 2 is,

$$\dot{q}_{12} = A.\varepsilon_{12}.\sigma.\left(T_1^4 - T_2^4\right) \qquad (2.29)$$

where

$$\varepsilon_{12} = \frac{1}{\frac{1}{\varepsilon_1} + \frac{1}{\varepsilon_2} - 1} \qquad (2.30)$$

As radiation passes through gases it can be absorbed. For uniform gas, the proportion absorbed per unit length along a radiation ray is the absorption coefficient, κ (m^{-1}); that is,

$$dI_e = -\kappa.I_e(x).dx \qquad (2.31)$$

Integrating equation (2.31) gives the remaining radiation, I(x) after some distance, x the ray passes through the gas.

$$I(x) = I(0).e^{-\kappa.x} \qquad (2.32)$$

The exponential term in equation (2.32) is the transmissivity, τ ; that is,

$$\tau(x) = e^{-\kappa.x} \qquad (2.33)$$

It follows that if a surface is the same temperature as adjacent gas, the portion of radiation from the surface absorbed by the gas is equal to the transmissivity and the portion of radiation emitted by the gas towards the surface is also equal to the transmissivity. Otherwise, uniform temperature could not be a state of equilibrium. Thus the emissivity of gas equals its transmissivity. The radiation transferred from gas is therefore,

$$E = \tau . \sigma . T^4 \qquad (2.34)$$

The physical nature of smoke is gas with particulate matter. The absorption and emission of radiation in the gaseous part of smoke can be modelled with equations (2.32)-(2.34). Fernando (1999) has undertaken research which shows that the specular and diffuse dispersion of radiation incident on smoke particles can be ignored for the heat transfer analysis of fire growth in a room. It is argued that smoke in a wall cavity is no more dense with smoke particulates in the hot ceiling layer of a growing fire. Thus the effects of specular and diffuse dispersion of heat due to smoke particulates is ignored and the radiation heat transfer theory for these phenomena is not covered here.

2.3.4 Thermal Energy Sources

Patankar (1980) described positions as sources where thermal energy is generated and subsequently flows as heat. Positions where thermal energy is absorbed, are described as negative sources or sinks. The generation of thermal energy is described as exothermic and the absorption of thermal energy is described as endothermic. Exothermic and endothermic energies are the result of physical or chemical processes.

2.3.5 Thermal Energy Balance

Temperature distributions with time are found from the above equations (2.3)-(2.34) by using the principle of conservation of energy. In the science of heat transfer, this principle is applied as a thermal energy balance; that is, the sum of all energy transfers and generation occurring as a result of conduction, convection, radiation, sources and sinks at all points and boundaries, during any time period must sum to zero (Incropera and De Witt, 1990). Commonly in fire engineering, thermal energy balances are referred to as, "heat balances" (Drysdale 1985). However, heat is energy in transit passing through some surface, and arises from some chemical or physical source.

2.4 Thermal Properties

2.4.1 Emissivities of Furnaces

The heat output, at the same gas temperatures varies among furnaces (Holm and Loikkanen 1981). These variations are due to different materials of furnace construction, different fuels and imperfections in monitoring the heat output. The materials and fuels have different thermal properties and consequently different thermal gradients. Heat output depends on these gradients, and temperature differences between the surfaces of furnaces and walls tested. Heat output is generally controlled by temperature measurements at several points in the furnace gas. These points are not sufficient to monitor all of the gradients and differences in surface temperatures – hence the variation in heat ouput of furnaces despite similar furnace gas temperatures. The dominant mode of heat transfer from furnaces is radiation. Furnaces and test walls are usually considered as infinite parallel plates, for which an equivalent emissivity is adopted in accordance with equation (2.30). Nordic furnaces are oil fired and have "Hiporos" brick walls. They have an emissivity (ε_1 in equation (2.30)) of 0.7-0.85. Australian (CSIRO Division of Building, Construction and Engineering, North Ryde, Sydney and Warrington Fire Research, Dandenong Melbourne) furnaces are lined with mineral fibre and are fired with gas. The mineral fibre has a lower density compared with bricks. Since temperature rises inversely with density (equation 2.6), brick surfaces rise to lower temperatures than the surfaces of mineral fibre, for similar monitored furnace gas temperatures. The lower temperatures lead to lower radiation from the furnace surface to the exposed wall surface. Hence, the apparent value for ε_1 for determining this radiation in terms of the furnace temperatures at the monitoring points, is lower. Conversely, emissivities greater than 0.85 are expected for Australian furnaces. Thomas (1997) used measurements from a furnace lined with refractory bricks for which he used an emissivity of 0.6; low values for refractory bricks are expected from Siegell and Howell (1981). Mehaffey et al (1994) used a concrete lined furnace for which they used an emissivity of 0.9. This value of 0.9 compares well with 0.94 given in Siegell and Howell (1981). However, according to the effect of high density of furnace lining material, explained above, a lower value is expected.

Effective furnace emissivity in equation (2.29) requires knowledge of the surface emissivity of the wall being tested. Emissivities for gypsum surfaces are given in §2.4.2.6.

2.4.2 Thermal Properties of Gypsum Board

2.4.2.1 General

The gypsum board used in the experiments described in §4, is Australian "Boral Firestop" (Boral 1997). As for all gypsum boards calcium sulphate dihydrate constitutes 90% of the gypsum core (Stray and Bates 1997). Mehaffey et al (1994) reports on two types of Canadian gypsum boards, namely Type X and Type C.

Stray and Bates (1997) advised that type X contains glass fibres but little or no vermiculite. Type C contains both. Vermiculite assists in resisting shrinkage of gypsum during fires. Boral Firestop is more like Type C. Thermal properties at ambient temperature published by manufacturers of gypsum boards around the world are shown in Table 2.1. Properties from this table are discussed in the sections below.

Table 2.1. Thermal Properties for Gypsum Board in Ambient Conditions, from a Range of Sources.

#	Reference (see §8)	Density $kg.m^{-3}$	Specific Heat $J.kg^{-1}.K^{-1}$	Conductivity $W.m^{-1}.K^{-1}$	Diffusivity $10^{-6}\ m^2.s^{-1}$
Aus	Boral (1997) Firestop	810		0.17	
Aus	CSR Gyprock			0.18	
NZ	Winstone Wallboards	880			
Can	Westrock Heavy, regular	578	600	0.20	0.577
Can	Mehaffey et al -Type C	732	950	0.24	0.345
	(1994) - Type X	648	950	0.24	0.390
Can	Sultan (1996) - Type X	698	1500	0.25	0.239
UK	British Gypsum Glasroc	1000		0.288	
UK	British Gypsum Fireline	800		0.20	
UK	Knauf Plasterboards	800		0.25	
USA	Gypsum Association			0.16	

Note: # Countries where gypsum board is manufactured; Aus - Australia, NZ - New Zealand, Can - Canada, UK - United Kingdom, USA - United States of America.

2.4.2.2 Density of Gypsum Board

The specific gravity of gypsum at ambient conditions is 2.32 (Dee Snell et al 1971); that is a density of 2320 $kg.m^{-3}$. Table 2.1 indicates that density of gypsum boards range between 578-1000 $kg.m^{-3}$ which is obviously much less. Thus gypsum board must be highly porous.

Values for the relative mass of gypsum at various temperatures, were measured by Mehaffey et al (1994) and are shown in Figure 2.5. To obtain densities at various temperatures, the relative mass values would have to be multiplied by mass at ambient conditions and divided by reduced board thickness relative to the initial board thickness. Figure 2.5 should be the same for all makes of gypsum board. Reductions in mass correspond to the stages of calcination at approximately 120°C and 600°C.

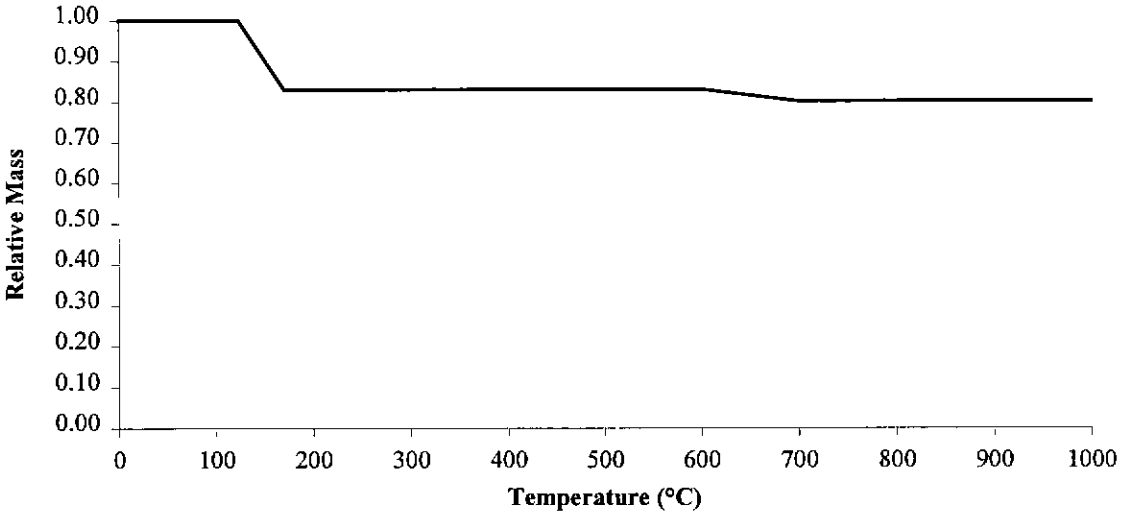

Figure 2.5. Mass of Gypsum versus Temperature, Relative to Mass at Ambient Conditions (Mehaffey et al 1994).

2.4.2.3 Specific Heat of Gypsum Board

Values for specific heat of gypsum board measured at ambient conditions are shown in Table 2.1. Measurements of the specific heat with temperature have been undertaken by Mehaffey (1991), Sultan (1996) and Hadjisophocleous (1996), and are shown in Figure 2.6. Since specific heat is expressed per unit of mass, it should be unaffected by the variations in initial densities at ambient conditions apparent in Table 2.1, and thus be similar for all makes of gypsum board. However, there is a large range of values published for specific heat at ambient conditions, 600-1500 $J.kg^{-1}.K^{-1}$. Values vary considerably at higher temperatures, too. Appropriate values for specific heat with temperature need to be resolved.

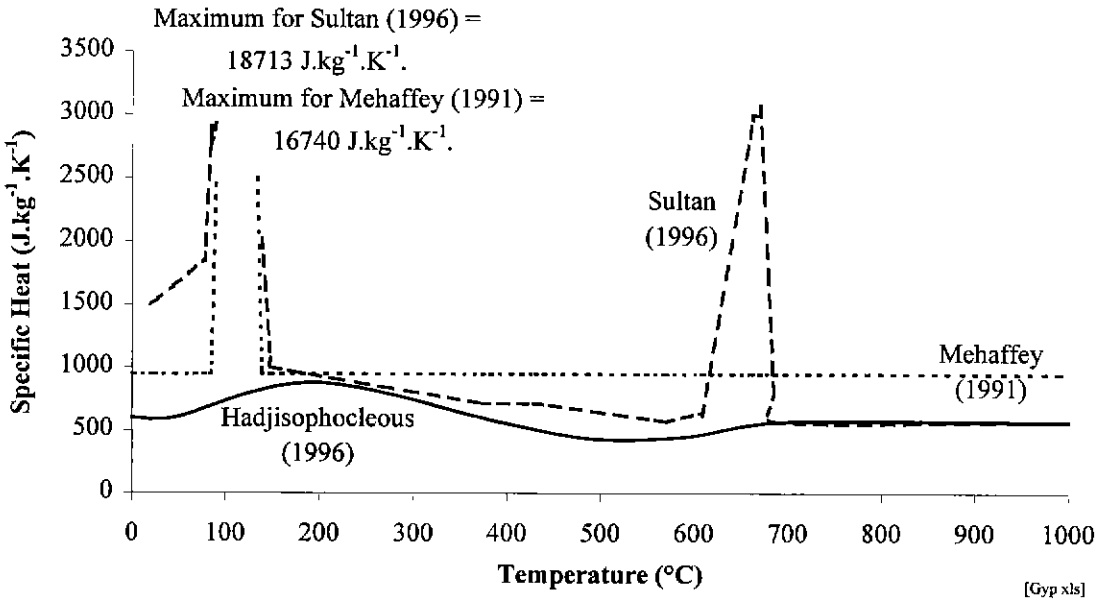

Figure 2.6. Variations in Values for Specific Heat of Canadian Gypsum Boards Measured by Mehaffey (1991), Sultan (1996) and Hadjisophocleous (1996).

The spikes in Figure 2.6 are due to the heat absorbed in calcination mentioned in §2.4.2.1. In heat transfer analysis, it is convenient to include heat absorbed during calcination in the relationship for specific heat with temperature. Alternatively, heat absorbed during calcination can be omitted from the specific heat relationship, and considered as heat sinks, that is negative sources. Values for heat absorbed are given in §2.4.2.5.

Sultan (1996) detected both stages of calcination; that is, the first stage when hemihydrate is formed at approximately 100-120°C (equation(2.1)), and the second stage when anhydrous calcium sulphate is formed at approximately 600°C (equation (2.2)). Mehaffey (1991) detected the first stage, but apparently not the second. Hadjisophocleous (1996) did not show any spikes for calcination.

2.4.2.4 Thermal Conductivity of Gypsum Board

Table 2.1 reveals some general increase in conductivity with density; although there are some values which contradict this trend. Since gypsum makes up more than 90% of gypsum boards from all manufacturers, conductivities should be similar for similar densities. Thus the inconsistencies reveal some errors in the published values which need to be addressed when seeking conductivity values for modelling the fire resistance of light-timber framed structures.

Plots of thermal conductivity with temperature are shown in Figure 2.7. The experimental results from which Mehaffey et al (1994) based his plot are shown in Figure 2.8. Mehaffey et al (1994) adopted significantly greater conductivities than those measured at temperatures greater than 400°C to allow for the inclusion of heat transfer through cracks in gypsum board on walls exposed to these high temperatures. Cracks are expected from the combined effects of shrinkage in core gypsum shown in Figure 2.1, and the restraint of gypsum board fastened to the supporting timber frame. The method of measuring conductivity involved the use of a lead weight which not only secured gypsum specimens but also restrained cracking.

Sultan's (1996) and Hadjisophoceous' (1996) plots for conductivity with temperature between 100°-400°C are similar to Mehaffey's. There is some difference at temperatures less than 100°C. However, conductivities at temperatures lower than 100°C would have little effect on heat transfer at high temperatures in gypsum board exposed to fire. Hadjisophocleous' conductivities at temperatures greater than 400°C are considerably different to Mehaffey's and Sultan's. This difference may be due to the variations in cracking in gypsum boards from different manufacturers as noted by Goncalves (1996). It seems that the distribution of cracking is dependent of the differences in additives in gypsum boards. It is thus desirable that some future research be carried out into measuring conductivities for these high temperatures amongst gypsum boards from a range of manufacturers. The measurements would have to simulate conditions of restraint and heat exposure suffered by gypsum boards exposed to fire. Until such measurements are carried out, fire resistance models for gypsum board cladded light-timber framed structures will require calibration to results from full scale wall furnace experiments. Alternatively, conservative conductivities leading to underestimates of fire resistance times will have to be adopted.

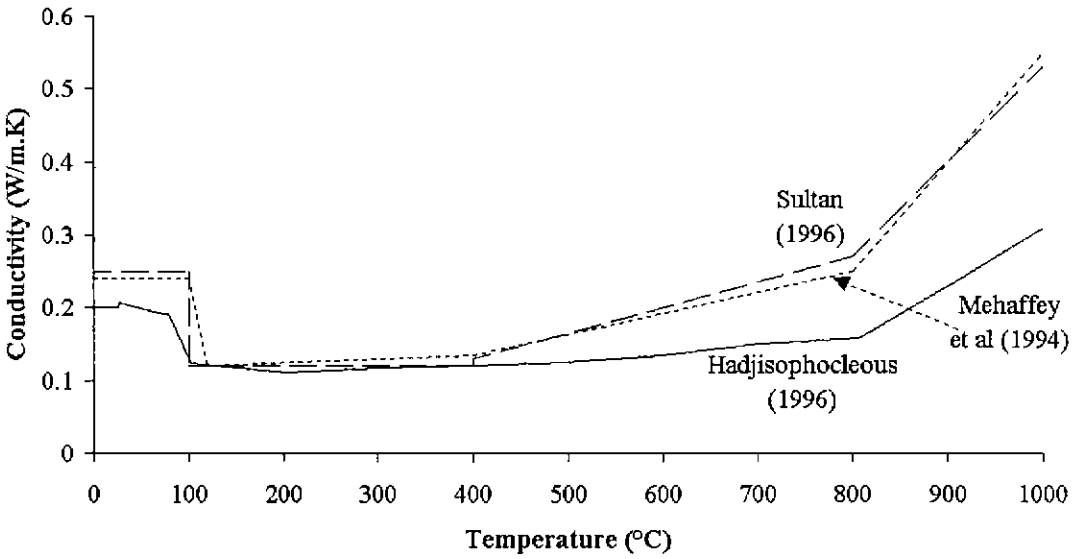

Figure 2.7. Conductivity versus Temperature for Gypsum Boards Obtained by Mehaffey et al (1994), Sultan (1996) and Hadjisophocleous (1996).

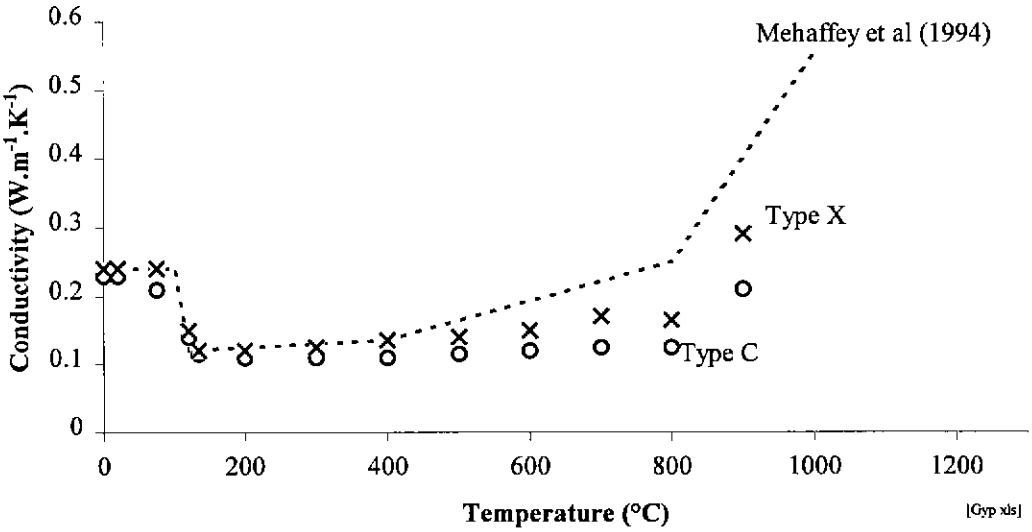

Figure 2.8. The Plot of Conductivity of Gypsum Board with Temperature Adopted by Mehaffey et al (1994) and the Measurements he Obtained from which he Derived the Plot.

2.4.2.5 Thermal Energy Sources

Mehaffey et al (1994) reported that at 80°C water dissociates from calcium sulphate dihydrate crystals to form calcium sulphate hemihydrate in accordance with equation (2.1). Stray and Bates (1997) advised that this process can occur at lower temperatures but is only significant over a longer time period than occurs during fires. The remaining water dissociates at temperatures generally between 100-120°C; the higher the influx of heat, the higher the temperature is at the final stage of calcination which forms the hemi-hydrate form. Mehaffey reports that the total amount of heat absorbed during calcination is 150 $J.kg^{-1}$ of gypsum. This heat excludes the heat of phase change from liquid to vapour. Mehaffey states that for Canadian board, the free moisture content, that is the moisture which is not chemically combined in crystal form at ambient temperatures is 0.5%. Stray and Bates (1997) concurred that for Boral Firestop the free moisture content is also 0.5%. The total water content of Boral Firestop is thus 21.5%. Since the heat of vaporisation of moisture is $2.26MJ.kg^{-1}$ (Mehaffey), the heat required to vaporise all moisture in Boral Firestop is 481 $kJ.kg^{-1}$ of gypsum. The total heat of calcination for Boral Firestop is thus 631 $kJ.kg^{-1}$ of gypsum; that is $3.02MJ.kg^{-1}$ of initial moisture.

2.4.2.6 Surface Emissivity

The surface emissivity of gypsum board should be dependent on the state of thermal degradation of its surface. For temperatures less than 100°C, moisture transfer can lead to some condensation on the surface of gypsum board away from the fire. The emissivity of this surface should be that for moist paper. Up until 200°C the surface paper would be uncharred and should have the same surface emissivity as dry paper. By the time the surface temperature is 300°C, the surface gradually chars; the emissivity of the surface should gradually become that for charred paper. At approximately 600°C anhydrous calcium sulphate forms. At temperatures less than 600°C the emissivity should be that for the hemihydrate. At greater temperatures, it should be that for anhydrous calcium sulphate. The emissivities of all of these constituents and other related materials are shown in Table 2.2.

Table 2.2. Emissivities of Some Constituents, or Materials Similar to Constituents, of Thermally Degraded Gypsum.

Material	Emissivity		Temperature (°C)	Reference
Gypsum	0.90-0.92	Hemi-spherical	23°C	Incropera et al (1990)
	0.93		20°C	Lide et al (1996)
	0.90		0-200°C	Raznjevic (1976)
$CaSO_4.½H_2O$	0.91		38°C	Rohsenow et al (1985)
Paper	0.92		95°C	Rohsenow et al (1985)
White Paper	0.92-0.97		23°C	Incropera et al (1990)
Carbon	0.83		500-1100 K	Rohsenow et (1985)
Coal	0.79		625°C	Raznjevic (1976)
Soot	0.96		20°C	Lide et al (1996)
Soot	0.95	Normal Total	100-260°C	Siegel et al (1981)
Water	0.96	Hemi-spherical	23°C	Incropera et (1990)
	0.96		38°C	Rohsenow et al (1985)
Deep Water	0.96	Normal Total	0-100°C	Siegel et al (1981)

Mehaffey et al (1994) adopted an emissivity of 0.90 for gypsum board for all temperatures. His value compares well with the values of 0.90-0.92 for dihydrate and hemi-hydrate in Table 2.2. Thomas (1997) adopted an emissivity of 0.60 constant with temperature. Unlike Mehaffey et al (1994), he did not consider any resistance to heat transfer due to smoke in wall cavities. Mehaffey et al (1994) assumed the smoke had an emissivity of 0.9 which is not sufficiently low to fully explain the different value of

gypsum emissivity adopted by Thomas (1997). Young (1998) has undertaken measurements of emissivity of gypsum board on the ambient side of walls exposed to fire. At temperatures below 200°C, he found that emissivity was 0.6-0.7. However, these measurements do not consider charring of paper at higher temperatures. From the literature, it is not clear what value should be adopted for emissivity for gypsum.

2.4.3 Thermal Properties of Timber and Char

2.4.3.1 Density of Timber and Char

Researchers involved in the structural response of timber in fire (Knudson 1975, Gammon 1987, Lie 1992, Mehaffey et al 1994, Thomas 1997) have adopted the relationship for relative oven dry mass versus temperature obtained by Tang (1967), shown in Figure 2.9. The samples he analysed were ponderosa pine sapwood, 0.14mm thick and with a mass of 100 mg; he did not specify further details. He employed thermogravimetric analysis (TGA). Tang only measured mass loss in the temperature range of 200-370°C. Thereafter, Knudson assumed that the residual percentage oven dry mass reduced linearly to 21% at 1000°C. Gammon, Mehaffey and Thomas have followed his practice since. Fredlund (1988) adopted a minimum residual of 27%, probably on the basis of calibration of model predictions to experimental results. He did not use Tang's measurements but rather adopted reaction kinetics modelling.

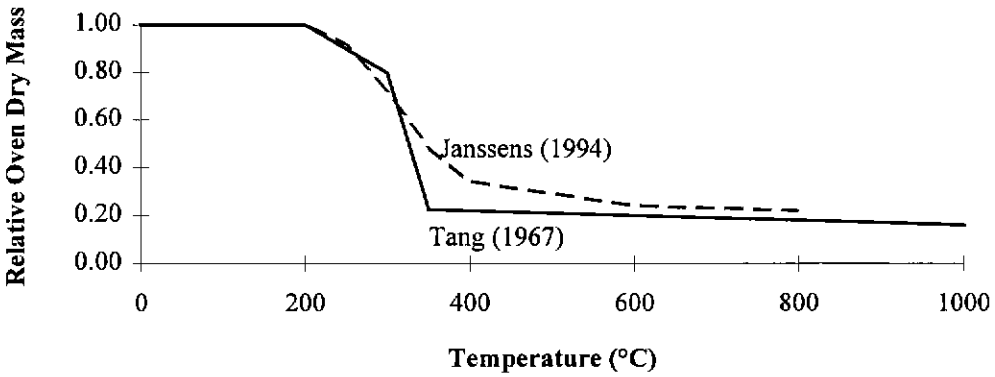

Figure 2.9. Relative Oven Dry Mass of Softwoods versus Temperature

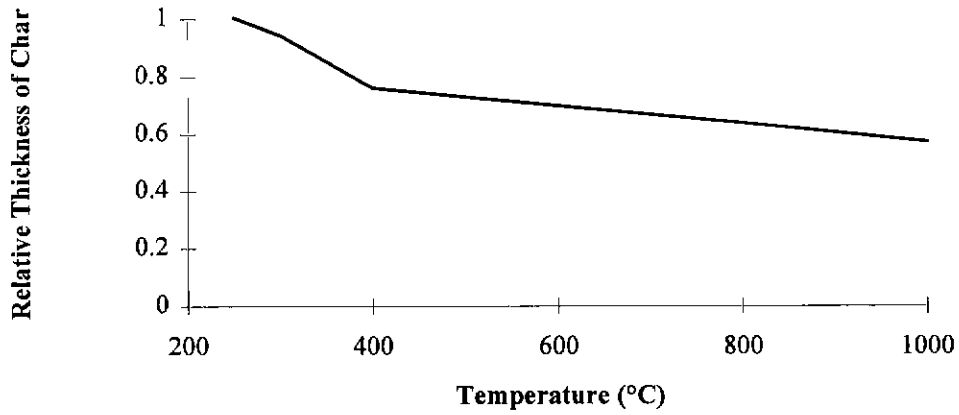

Figure 2.10. Char Shrinkage Perpendicular to the Grain Derived for Softwood from Janssens (1994).

Mehaffey et al (1994) explained that the density loss from 0-200°C is mainly due to vaporisation of moisture; from 200°-350°C is mainly due to loss of volatiles; and thereafter, oxidation of char.

Janssens (1994) developed a model for mass loss, and validated it against measurements made by White (1988). The model involved expressions for determining density from mass loss, allowing for shrinkage due to loss of moisture, thermal expansion and char shrinkage. An example of a plot from the model, based on average values for variables for timber used in the experiments carried out in the research for this thesis (§4), is shown in Figure 2.9. These values were - softwood, initial density of 470 $kg.m^{-3}$ and an initial moisture content of 12%. For a rise in temperature from 20-100°C, the increase in density due to moisture shrinkage is approximately 4%. The reduction in density due to thermal expansion is 0.5%. Char shrinkage perpendicular to the grain is approximately 20% at 400°C and 40% at 1000°C, as shown in Figure 2.10.

2.4.3.2 Specific Heat of Wood

Gammon (1987), Parker (1988) and Janssens (1994) found that alternative expressions for specific heat c_0 ($J.kg.K^{-1}$) of oven dry wood with temperature, T (°C) by Volbehr (1896), Koch (1969), McMillin (1969), Kuhlmann (1962), Geiger (1942) and Atreya (1983) for both softwoods and hardwoods were very consistent with Dunlap's (1912) below,

$$c_0 = 1110 + 4.84T \qquad (2.35)$$

Knudson et al (1975) derived the relationship shown in Figure 2.11. Between 0-100°C he adopted specific heat values which were the sum of those from Dunlap's (1912) expression (2.35) for dry wood

and the specific heat for 10% moisture content. Figure 2.11 shows Knudson's plot adjusted for 12% moisture content which was the moisture content of timber in experiments reported in §4. Between 100-105°C, he increased the specific heat to account for all latent heat of vaporisation. In the temperature range of 105-200°C he simply used Dunlap's expression (2.35) for dry wood. He found only one value for specific heat of char and decided not to vary it with temperature. Knudson's values for specific heat of wood and char have been widely adopted in recent research in the modelling of heat transfer in timber (Gammon 1987, Mehaffey et al 1994, Thomas 1997 and Fredlund 1988 to a large extent).

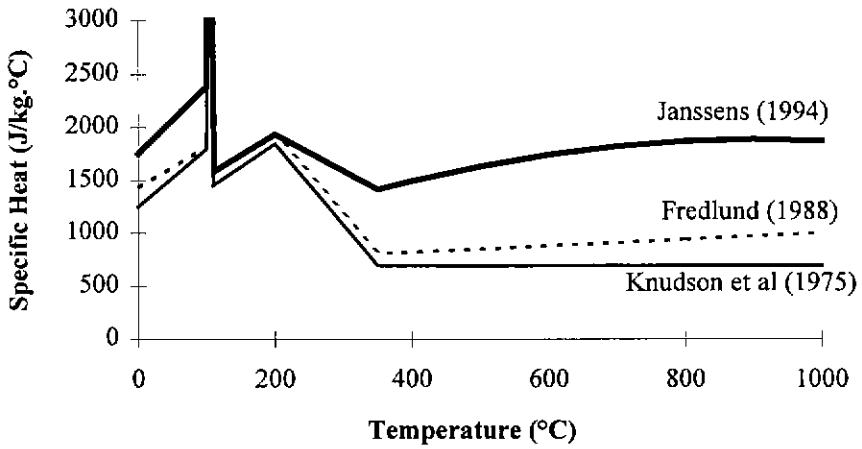

Figure 2.11. Specific Heat for Timber as a Function of Temperature.

Reputable text books such as Incropera and De Witt (1990) and Drysdale (1985) quote temperature-independent values for the specific heat of softwoods being in the vicinity of 2800 $J.kg^{-1}.K^{-1}$. This value is dramatically different to the average value of 1600-1700 $J.kg^{-1}.K^{-1}$ used by Fredlund and Knudson, for specific heat of wood in the temperature range of 20-300°C. Furthermore, both of these books show that there is a substantial difference in the temperature-independent specific heats for hardwoods and softwoods. The specific heat of hardwoods is quoted as being 500 $J.kg^{-1}.K^{-1}$ less than the specific heat of softwoods.

To a large extent the difference in specific heat for wood given by Knudson and the temperature independent specific heat quoted by the text books can be explained with the use of Janssens (1994) paper. He showed that water bound in the cell walls of wood has a higher specific heat than free water in cell cavities. All of the water in moisture contents to 30% is bound in cell walls. Janssens gave the following expression for specific heat of wood with temperature.

$$c_u = \frac{c_0 + 4187.u}{1+u} + \Delta c \qquad (2.36)$$

where c_0 = $1159 + 3.86T$

Δc = specific heat of water bound in cell walls, above specific heat of free water

= $(23.55T - 1326u + 2417)u$

Janssens adopted specific heat for char similar to that for graphite. Fredlund (1988) noted specific heat for graphite from tables given by Landolt-Börnestein (1961); these values are very similar to Janssens (but are not shown in Figure 2.11). From the calibration of thermal properties in his heat transfer model, Fredlund found better comparisons of predictions with experimental results when he adopted a relationship for the specific heat of char not very dissimilar to Knudson's. This calibration is shown in Figure 2.11.

2.4.3.3 Conductivity of Timber and Char

Values of conductivities of timber and char quoted in the literature should be interpretted with due regards to the difficulties and assumptions made in obtaining them. Some of the difficulties are as follows. It takes a long time to establish uniform raised temperatures in samples because of the low thermal conductivity of wood; for example, three hours for radiata pine samples 35 mm thick (Young 1996). Raising temperatures causes moisture movements (White and Schaffer 1981), the evaporation of moisture at surfaces and thus non-steady moisture contents. As well, there are difficulties in measuring the conductivity of char with temperature due to its non-steady shrinkage and cracking with a given charring temperature (Parker 1985, Hadvig 1981, Jonsson and Pettersson 1985). The relationships for conductivity of wood and char with temperature, developed by the researchers have involved theoretical extrapolations of some measurements.

Up until the 1980's most researchers measured conductivities for wood at ambient conditions at which steady states in temperature and moisture could be easily obtained. Conductivities at raised temperatures were derived by extrapolating on the basis of equation (2.37) (Maku 1954, Kollmann 1951, Nusselt 1908),

$$k(T_2) = \frac{T_2}{T_1} k(T_1) \qquad (2.37)$$

where $k(T_2)$ = conductivity of timber at absolute temperature, T_2 ($W.m^{-2}.K^{-1}$)

$k(T_1)$ = conductivity of timber at absolute temperature, T_1 ($W.m^{-2}.K^{-1}$)

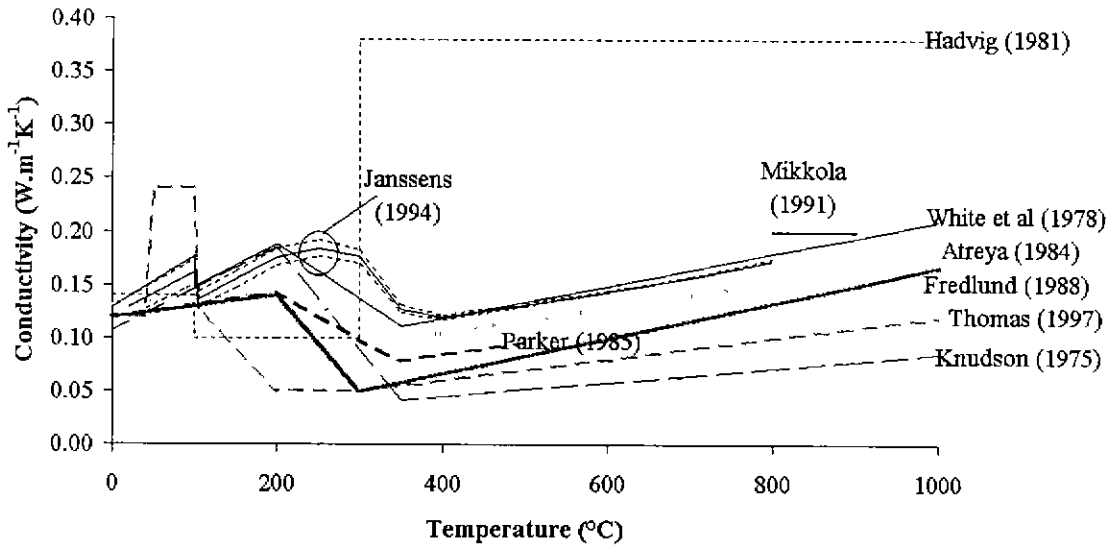

Note - Three plots are shown for Janssens (1994) - the lower plot for density of 420 $kg.m^{-3}$, the middle plot for 470 $kg.m^{-3}$ and the upper for 520 $kg.m^{-3}$. All are for softwood with a moisture content of 12%.

Figure 2.12. Conductivities for Heat Flow Normal to the Grain in Timber and Char, Plotted against Temperature.

That is, conductivity increases proportionally with absolute temperature. It seems that there have been no measurements of the conductivity of char since a steady state of heat transfer through samples cannot be established due to char shrinkage, cracking and oxidation. Researchers have derived conductivities for char at ambient temperature from measurements taken for carbon. Conductivities for char at raised temperatures were then extrapolated from equation (2.37). Various details on conductivities for wood at ambient temperature and extrapolations carried out by various researchers up until the 1980's are discussed below.

Relationships for the conductivity of wood at ambient conditions as a function of density and moisture content were established by Rowley (1933), Kollman (1934), Wangaard (1940), Maclean (1941). Maclean's, given in the following equation, is often quoted in the literature on models involving heat transfer through timber .

$$k_{amb} = 0.238 + S(0.2005 + 0.0040u) \qquad (2.38)$$

where k_{amb} = conductivity of timber at ambient conditions ($W.m^{-2}.K^{-1}$)

S = specific gravity

u = moisture content (%)

k_{amb} is the starting value for the plots for Knudson (1975), White et al (1978), Parker (1988) and Fredlund (1988) in Figure 2.12. The plots are for a specific gravity of approximately 0.450 and a moisture content of 12%.

Griffiths and Kay (1923) showed that anisotropy in timber causes k_{amb} to vary with direction. Conductivity in the tangential direction is usually 0.5-0.9 times that in the radial direction. In the longitudinal, that is in-grain, direction it is usually 1.75-2.25 times that in the radial direction. In a literature survey, Maku (1954) found data which also confirmed that conductivity in the direction of the grain was approximately double the conductivity across the grain. However, he did not find any significant difference in conductivities in the radial and tangential directions across the grain.

Knudson et al (1975) derived a relationship shown in Figure 2.12, for conductivity for Douglas Fir timber and char. Douglas Fir is a softwood with a density between 410-510 $kg.m^{-3}$ (MacLean 1941). The moisture contents for Knudson's Douglas Fir samples were 12%. He used Maclean's expression (2.38) to find the conductivity of Douglas Fir at ambient conditions. He applied Maku's expression (2.37) to extrapolate conductivities for temperatures between ambient conditions and the onset of significant volatisation at 200°C. He did not account for a drop in conductivity due to loss of moisture at vaporisation at approximately 100°C. Knudson obtained a value for conductivity of char at 350°C from the literature and then applied Maku's extrapolation method to obtain conductivities for char at higher temperatures. Knudson assumed that density of char was 20% of the density of the timber at ambient conditions in accordance with Tang's (1967) plot for timber density versus temperature in Figure 2.9. Conductivities for temperatures between 200-350°C were found by interpolation of conductivities found at the extremes of this range.

A plot of the conductivity of timber and char as a function of temperature determined similarly to the procedure given in White et al (1978) is shown in Figure 2.12. The plot is for timber with a density of 475 $kg.m^{-3}$ and a moisture content of 12% at ambient conditions. The conductivity for moist and dry timber at ambient conditions was determined in accordance with Maclean's expression (2.38). From these conductivities values were extrapolated in accordance with Maku's expression (2.37). The extrapolated values for moist timber were plotted for temperatures up to 100°C and for dry timber from 100-200°C. The conductivities for char exceeding a temperature of 350°C were determined by extrapolating from two values for char conductivity from the literature - 0.0581 $W.m^{-1}K^{-1}$ at 0°C and 0.0733 $W.m^{-1}K^{-1}$ at 100°C. Between 200-350°C conductivities were interpolated. Conductivities for char determined by White's relationship are approximately twice those of Knudson's. One reason for the larger char conductivities of White's is that he assumed the density of char was 215 $kg.m^{-3}$. This density compares with 20% of 475 $kg.m^{-3}$, that is approximately 100 $kg.m^{-3}$, assumed by Knudson. The large

difference in conductivities can be explained by considering Fredlund's study of the influence of porosity on conduction. At temperatures when heat transfer across pores is dominated by conduction rather than radiation, a difference in porosity from 90% to 80%, that is a doubling of density, will approximately double the conductivity. Further, Knudson assumed some exothermicity between the temperatures of 200-450°C which would have increased the heat transfer rate. Thus the total difference in heat transfer rates between rates predicted by White and Knudson are not as large as the conductivities alone would indicate. Their modelled rates of heat transfer are quite similar. Thus it seems that if it is to be assumed that there is no heat of reactions produced during pyrolysis, it is more appropriate to adopt conductivities in the region of White's plot.

Since the 1980's, more phenomena have been taken into consideration in deriving relationships for conductivity with temperature from limited measurements. Perhaps the most thorough consideration of phenomena was undertaken by Janssens (1994). He refers to the development of theory (Kollman and Malmquist 1956, Fredlund 1988) that heat transfer through the porous microstructure of wood and char comprises three components - conduction through solid fibre and conduction and radiation through pores.

The conductivity of porous wood, ignoring any heat transfer due to radiation across pores, was interpolated between two bounds. The upper bound conductivity could be theoretically deduced for a system of layers of materials in parallel to the direction of heat flow, as shown in equation (2.39). These materials are solid wood fibre, air and water.

$$k_{max} = \pi_g k_g + \pi_s k_s + \pi_w k_w \qquad (2.39)$$

where k_g = thermal conductivity of gas in cell cavities ($W.m^{-1}.K^{-1}$)

$= 0.024 + 7.05*10^{-5}*T - 1.59*10^{-8}*T^2$

k_s = thermal conductivity of solid material ($W.m^{-1}.K^{-1}$)

$= 0.42 + 1.3*10^{-3}*(T - T_{amb})$

k_w = thermal conductivity of bound water ($W.m^{-1}.K^{-1}$)

$= \left(0.66 + 2*10^{-3}*T - 8*10^{-6}*T^2\right)\frac{\rho_w}{1000}$

T = temperature of gas, solid and water (°C)

$\pi_s = \frac{\rho_0}{(1 + 0.00084\rho_0 u)\rho_s}$

$\pi_w = \frac{\rho_0 u}{(1 + 0.00084\rho_0 u)\rho_w}$

$\pi_g = 1 - \pi_s - \pi_w$

ρ_0 = oven dry density (kg,m^{-3})

ρ_s = bulk density of solid material (kg,m^{-3})

ρ_w = density of bound water (kg,m^{-3})
= $1298 - 1132u + 1766u^2$

The lower bound conductivity determined from a system of layers of air, solid wood fibre and water perpendicular to the flow of heat is theoretically deduced from,

$$k_{min} = \frac{k_g.k_s.k_w}{\pi_s\pi_w k_g + \pi_g\pi_w k_s + \pi_g\pi_s k_w} \qquad (2.40)$$

The conductivity producing equivalent heat transfer to the radiation across pores is found from,

$$k_r = \frac{4\pi_g\sigma(T+273)^3 d_p.F(d_p,\varepsilon)}{1-\pi_g} \qquad (2.41)$$

where d_p = diameter of pores; that is, cell cavities (m)
$F(d_p,\varepsilon)$ = function of geometry and emissivity of cell cavities. ($F \leq 1$)

Fredlund (1988) showed that k_r typically does not become significant until char is formed with a porosity exceeding 80% (that is, the proportion of voids in the overall volume) and the temperature exceeds 700°C. As porosity increases beyond 80%, k_r increases dramatically. It can increase the total conductivity, k_u below in equation (2.42) several fold. The importance of incorporating k_r into modelling conductivity is very apparent.

Janssens (1994) shows that the conductivity, k_u ($W.m^{-1}.K^{-1}$), for wood with a moisture content of u ($kg.kg^{-1}$) at a temperature of T (°C) is determined from interpolation between the above bounds and with the addition of the contribution due to radiation across pores is,

$$k_u = \xi.k_{max} + (1-\xi)k_{min} + k_r \qquad (2.42)$$

where ξ = interpolation factor
= $0.58 + 10^{-4}\rho_0 + 0.5u$

Janssens showed that wood begins to char at 200°C. Young (1996) also noticed that wood began to turn brown at this temperature. Thus equation (2.42) seems applicable in the temperature range of 20-200°C.

Very little has been published on the conductivity of char. Janssens found the following expression for the conductivity for the solid material in char.

$$k_s = 0.33 + 1.6*10^{-4}*T + 1.08*10^{-7}*T^2 \qquad (2.43)$$

From the information provided by Janssens, equation (2.43) seems to apply for char with a density for solid material of 1240 $kg.m^{-3}$. He also shows that the density of solid material in char reduces with temperature in accordance with Table 2.3. The value of 1240 $kg.m^{-3}$ seems to be a reasonably representative density for solid char in the temperature range of 400-1000°C. At the temperature of 400°C wood is fully carbonised (Schaffer 1982, Browne 1958). Thus equation (2.43) applies for the temperature range of 400-1000°C. The conductivity for char in its porous form is found by substituting k_s into equations (2.39), (2.40) and (2.42).

Table 2.3. Density of Solid Material in Charred Timber (Janssens 1994).

T (°C)	ρ_s of softwoods ($kg.m^{-3}$)	ρ_s of hardwoods ($kg.m^{-3}$)
200	1460	1460
250	1445	1445
300	1420	1405
350	1368	1340
400	1355	1320
600	1305	1270

For partially charred wood Janssens recommends that k_s be found by firstly obtaining ρ_s for each of the wood and char portions from Table 2.3. The conductivity, k_s for each of these portions can then be obtained from equation (2.43). By interpolation, k_s for partially charred wood can then be obtained. The appropriate temperature range for this approach for determining the conductivity for partially carbonised wood is apparently 200-400°C.

Atreya (1984) gave the following general expression for the conductivity of timber as a function of temperature,

$$k(T) = a_1 + a_2(T-20).10^{-4} \qquad (2.44)$$

where $k(T)$ = conductivity of timber at temperature, T in degrees Celcius ($W.m^{-1}.K^{-1}$)

a_1 = a factor which varies depending on the kind of wood, carbon, and direction of heat flow ($W.m^{-1}.K^{-1}$)

a_2 = temperature coefficient = 1.2 $W.m^{-1}.K^{-2}$

For heat flow parallel to the grain through pine, Atreya gave a_1 as 0.264 $W.m^{-1}.K^{-1}$ prior to char, and 0.059 $W.m^{-1}.K^{-1}$ thereafter. Considering, from the above (Griffiths et al 1923, Maku 1954) that conductivity normal to the grain is approximately half the conductivity parallel to the grain, the normal conductivity was obtained by halving values determined from equation (2.44) and plotted in Figure 2.12.

Parker (1985) gave expression (2.45) for conductivity which he obtained from experiments on 1 mm and 2 mm thick specimens of pine heated to 250°C in front of a radiant panel. Expression (2.45) is plotted in Figure 2.12.

$$k(T) = 0.12(1 + 0.0026(1.35 - Z)T)(0.71Z + 0.29) \qquad (2.45)$$

where $k(T)$ = conductivity of timber at temperature, T in degrees Celcius ($W.m^{-1}.K^{-1}$)

$$Z = \frac{\text{weight of specimen at temperature, T}}{\text{Initial weight of specimen at ambient conditions}}$$

Mikkola (1991) stated that from various experiments involving charring of timber, the conductivity of char at "high" temperatures averaged 0.20 $W.m^{-1}.K^{-1}$. This value compares well with the extrapolations of Janssens (1994), White(1978), Atreya (1984) and Fredlund (1988) and gives confidence in their relationships for char conductivity.

However, calibrations of thermal properties to achieve temperatures measured in larger scale experiments by Hadvig (1981) and Thomas (1997) show substantially different relationships. Hadvig calibrated conductivities in a model to achieve a good comparison with measured char rates for large timber sections (that is with minimum cross-sectional dimensions exceeding 80 mm). Thomas calibrated conductivities to achieve predicted times of failure of timber framed walls exposed to fire similar measured times of failure.

Hadvig (1981) considered conductivities for timber and char to be constant in three temperature ranges. For temperatures between 20-100°C, he adopted a conductivity for timber determined for a moisture content of 10% and density of 475 $kg.m^{-3}$, in accordance with Maclean's expression (2.38). For temperatures between 100-300°C he adopted a conductivity assuming that the timber was dry and again

applied Maclean's expression. For temperatures greater than 300°C he adopted a value of 0.38 $W.m^{-1}K^{-1}$. Hadvig's conductivity for char is 2-5 times larger than values from other researchers in Figure 2.12. A likely reason for this large difference is the nature of the charring each researcher considered. Knudson used results of char experiments on small dowels whereas Hadvig used results from experiments on from large timber sections defined as having cross-sectional dimensions not less than 80mm. Hadvig's experiments would have involved longer durations of charring and hence more extensive char cracking. The cracks would have allowed more heat transfer by radiation through the cracks. The cracks would have also allowed greater convective heat loss from volatiles escaping from charring tubular wood fibres directly to the cracks (Jönsson and Pettersson 1985). Hence, the heat transfer rates in Hadvig's experiments would have been larger and are relevant to large samples of timber.

Thomas (1997) found that to accurately model heat transfer in light-timber framed walls exposed to fire, the value of thermal conductivity had to be almost doubled at temperatures within 50°C of the vaporisation point. Contrary to Hadvig (1981), he found that values of the conductivity of char were midway between the relationships given by Fredlund and Knudson, but well below values measured by Janssen (1994), White (1978) and Atreya (1984). He did not estimate the large conductivity for char obtained by Hadvig (1981). His timber sections were small compared with Hadvig's and thus probably suffered less char cracking.

For the heat transfer in the various wall models which have been developed, the following conductivity relationships were adopted. Gammon (1987) adopted Knudson's conductivities for timber and a constant conductivity of 0.2206 $W.m^{-1}.K^{-1}$ for char. Mehaffey et al (1994) adopted Knudson's conductivities for timber and char. Both of these authors have assumed some exothermicity.

2.4.3.4 Thermal Energy Sources

There are three sources of thermal energy to consider in the heat transfer analysis in timber - the endothermic energy of the vaporisation of moisture, and the energies involved in pyrolysis and combustion. The heat absorbed in vaporising moisture is greater than 2.26 $MJ.kg^{-1}$ for the phase. Additional heat is required to draw the moisture from the wood fibre. The heat of reaction for vaporisation of moisture should thus be derived from equation (2.36). Many researchers such as Mehaffey et al (1994) include the heat absorbed during vaporisation as part of the specific heat.

Fredlund (1988a) reports from a literature review that estimates for heats of pyrolysis range between an endothermic value of 0.75 MJ.kg-1 and an exothermic value of 18.8 MJ.kg-1. Roberts (1971) explains that a large variation in the measurement of the heat of pyrolysis is due to rate of heating and size of

wood samples. He also explains that oxygen concentration has no effect since the rapid efflux of gases from zones of pyrolysis prevents any influx of oxygen. Parker (1988a) measured no net heat of pyrolysis reactions overall. His results showed that there could be some endothermicity between 400-500°C but this when aggregated with heat from exothermic processes produced no net heat change as temperatures increased from ambient values to 500°C. He commented that if heat of reaction is dependent on the relative proportions of cellulose which is endothermic and lignin which is exothermic, then the heat of reaction during pyrolysis would be sensitive to composition. Since the heat of reaction of pyrolysis is uncertain, a number of researchers have assumed it to be zero (Atreya 1984, Gammon 1987, Fredlund 1988, Parker 1988, Thomas 1997). Knudson (1975) and Mehaffey et al (1994) assumed some endothermicity.

Due to studs in cavities being isolated from fresh air, oxygen concentrations exceeding 11% cannot be sustained during combustion (Tewarson et al 1976). Thus combustion does not happen, the heat of combustion is not relevant and has not been reviewed.

2.4.3.5 Surface Emissivity of Wood and Char

Total hemispherical emissivities for surfaces of various species of wood with different moisture contents are quoted in Table 2.4. In a review of thermal properties of wood, Janssens (1991) quoted from Kollmann and Côté (1984) that emissivity is a maximum of 0.93 for wood with a moisture content, u at fibre saturation level; that is, approximately 30%. It reduces as moisture is lost, to as low as 0.60 when oven dry. These values are reasonably consistent with the following expression for the surface emissivity of wood, ε as a function of moisture content, u given by Kollman and Malmquist (1955),

$$\varepsilon = 0.013u + 0.65 \qquad (2.46)$$

but ε should not be taken greater than 0.96 which is the emissivity of water (Table 2.2).

To some extent the large reduction in emissivity of wood with reduction in moisture content is borne out by the emissivity quoted for sawdust. One would expect that the surface area to mass ratio of sawdust to be very high, the moisture content to be low especially at the surface, and consequently the emissivity to be low which is apparent in Table 2.4. Emissivity generally varies with temperature. From emissivity tables in Incropera and De Witt (1990a) it is apparent that there is no common relationship for emissivities of all materials with temperature which could be used to infer how the emissivity of wood changes with temperature. However, from Thomas (1997), it is apparent that the sensitivity of surface temperatures of studs in cavity walls to changes in emissivity of wood surfaces from 0.60-0.90 is less than 2%. Such a result is to be expected since thermal conduction is the slowest mode of transfer in cavity

walls and, thus is most dominant and reduces the significance of radiant heat transfer in cavities in affecting time of failure. Thus it is expected that accurate knowledge of emissivity of wood and char is not critical to modelling the time of failure of timber framed walls exposed to fire. It is thus not of great concern that Mehaffey and Gammon adopted substantially different constant values with temperature, of 0.9 and 0.6 respectively.

Janssens (1991) deduced that Kirchoff's law applies; that is, absorptivity equals emissivity. He also deduced that wood surfaces can be considered as grey diffuse emitters of radiation.

Emissivities for materials similar to char - soot, coal and carbon - are given in Table 2.2

Table 2.4. Total Emissivities for Hemispherical Radiation from Timber.

Reference	Species	Fibre saturation u ~ 30%	u= 10-20%	Oven Dry
Incropera and De Witt (1990, page A28)			0.82-0.92	
Gammon (1987)	Spruce pine fir		0.80	
Kollmann and Côté (1984)	Many species	0.93		0.60-0.72
Mehaffey et al (1994)	Spruce pine fir		0.90	
Siegell and Howell (1981a)	planed oak beech sawdust		0.90 0.94 0.75	
Thomas (1997)	Radiata Pine		0.60	0.60

Notes:

1. All at ambient temperature unless noted otherwise.
2. u = moisture content.

2.4.4 Convection Coefficients

2.4.4.1 Convection Coefficients for External Surfaces of Walls

As mentioned in §2.3.2, convection heat transfer coeffcients, h are determined from Nusselt numbers. An empirical expression derived by M^{c}Adams (1954), Warner and Arpaci (1968) and Bayley (1955) for determining Nusselt numbers for external wall surfaces is,

$$\overline{Nu}_H = C.Ra_H^n \qquad (2.47)$$

where C = 0.59 for laminar convection which occurs when Ra_H^n is less than 10^9.

= 0.10 for turbulent convection which occurs when Ra_H^n is greater than 10^9

n = 0.25 for laminar convection.

= 0.33 for turbulent convection.

Ra_H = Rayleigh number which is described below.

$$= \frac{g.\beta.(T_s - T_\infty).H^3}{\nu.\alpha} \qquad (2.48)$$

β = volumetric thermal expansion coefficient (K^{-1})

$$= \frac{1}{T_f} \qquad (2.49)$$

α = thermal diffusivity of air ($m^2.s^{-1}$)

ν = kinematic viscosity of air ($m^2.s^{-1}$)

g = gravitational acceleration = 9.81 ($m.s^{-2}$)

The Rayleigh number is dimensionless and is used to indicate whether the boundary layer is laminar or turbulent. The transition from laminar to turbulent flow occurs when the Rayleigh number exceeds approximately approximately 10^9. The Rayleigh number is the product of the Prandtl number and the Grashof number. The Prandtl number is a dimensionless ratio of the momentum and thermal diffusivities of gas. The Grashof number is the ratio of bouyancy to viscous forces.

After considering typical values for variables in equations (2.48)-(2.49) for structures exposed to fire, Sterner and Wickstrom (1990) found that the convective heat transfer coefficient for external vertical planar surfaces of structures can be approximated to,

$$h = F_{cv}.(T_s - T_\infty)^n \qquad (2.50)$$

where F_{cv} = a convective factor, usually 1.6 ($W.m^{-2}.K^{-1\,33}$) for free turbulent convection.

n = 0.25 for laminar convection, 0.33 for turbulent convection.

T_∞ = the temperature of gas outside of the boundary layer (°C).

T_s = the temperature of surface (°C).

They adopted equation (2.50) in TASEF, which has become a well used heat transfer program for structures.

A more recent method by Churchill and Chu (1975) of determining the Nusselt number for an external vertical surface and which is applicable for both laminar and turbulent convection is,

$$\overline{Nu}_H = \left\{ 0.825 + \frac{0.387 Ra_H^{1/6}}{\left[1 + (0.492/Pr)^{9/16}\right]^{8/27}} \right\}^2 \qquad (2.51)$$

where Pr = Prandtl number

$$= \frac{\nu}{\alpha} \qquad (2.52)$$

A summary of convective heat transfer coefficients for the furnace side and the ambient side of 3 metre high walls exposed to standard fire tests are given in Table 2.5. These have been obtained from Mehaffey et al (1994), Sterner and Wickstrom (1990), and Thomas (1997). Mehaffey obtained his values from recommendations in the Eurocode (1990). Thomas (1997) obtained values in the course of comparisons of their model predictions with test results.

Table 2.5. Coefficients for Convective Heat Transfer at External Vertical Surfaces of Walls.

	Convective Heat Transfer Coefficients ($W.m^{-2}.K^{-1}$)	
	Furnace Side	Ambient Side
Mehaffey et al (1994)	25	9
Thomas (1997)	Ignored	6 when (T_g-T_s) = 25°C 8 when (T_g-T_s) = 50°C 10 when (T_g-T_s) = 100°C 12.6 when (T_g-T_s) = 200°C
Sterner and Wickstrom (1990) equation (2.50)	4.6 when (T_g-T_s) = 25°C 5.8 when (T_g-T_s) = 50°C 7.3 when (T_g-T_s) = 100°C 9.2 when (T_g-T_s) = 200°C	4.6 when (T_g-T_s) = 25°C 5.8 when (T_g-T_s) = 50°C 7.3 when (T_g-T_s) = 100°C 9.2 when (T_g-T_s) = 200°C

2.4.4.2 Convection Coefficients for Wall Surfaces Bounding Cavities

MacGregor and Emery (1969) derived the following equation for Nusselt numbers for two dimensional natural convective heat transfer between vertical parallel cavity surfaces.

$$\overline{Nu}_H = 0.42 Ra_L^{0.25} Pr^{0.012} \left(\frac{H}{L}\right)^{-0.3} \qquad (2.53)$$

where H = the height of the cavity.

L = width of the cavity through the plane of the wall.

$Ra_L = \dfrac{g.\beta.(T_{s1} - T_{s2}).L^3}{\nu.\alpha}$

T_{s1} = temperature of one surface bounding the cavity

T_{s2} = temperature of opposite surface bounding the cavity.

Equation (2.53) is valid provided,

$$10 < \frac{H}{L} < 40$$

and $1 < Pr < 2 \times 10^4$

and $10^4 < Ra_L < 10^7$

Alternatively, the Nusselt numbers for two dimensional natural convection between parallel vertical cavity surfaces can be found from (MacGregor and Emery 1969, and Ince and Launder 1989),

$$\overline{Nu}_H = 0.046 Ra_L^{0.33} \qquad (2.54)$$

which is valid provided,

$$1 < \frac{H}{L} < 40$$

and $1 < Pr < 20$

and $10^6 < Ra_L < 10^9$

A summary of convective heat transfer coefficients for the furnace side and the ambient side of 3 metre high walls for standard fire tests are given in Table 2.6. The coefficients are for temperature differences between a surface and the centre of a cavity. These coefficients have been obtained from Mehaffey et al (1994), Thomas (1997), and Sterner and Wickstrom (1990)

Table 2.6. Coefficients for Convective Heat Transfer between Internal Surface of Sheeting and Centre of Cavity. (The coefficients are assumed to be the same for internal surfaces on the furnace and ambient sides.)

	Convective heat transfer coefficient. ($W.m^{-2}.K^{-1}$)
Mehaffey et al (1994)	9
Thomas (1997)	2.9 when (T_g-T_s) = 25°C 3.6 when (T_g-T_s) = 50°C 4.6 when (T_g-T_s) = 100°C 5.7 when (T_g-T_s) = 200°C
Sterner and Wickstrom (1990)	4.6 when (T_g-T_s) = 25°C 5.8 when (T_g-T_s) = 50°C 7.3 when (T_g-T_s) = 100°C 9.2 when (T_g-T_s) = 200°C

2.5 Methods of Heat Transfer Analysis

2.5.1 Overview of Methods Generally Practiced

El-Zafrany (1993) gave a brief overview of numerical analysis methods commonly used. These methods are the finite difference method, the finite element method and the boundary element method.

Finite difference methods are the most well established. Essentially the methods involve discretising the governing differential equations at a finite number of points. Finite difference methods involve a simple level of mathematics. The methods easily accommodate the incorporation of additional equations for phenomena in an established analysis. For example, chemical engineers who are interested in a wide range of phenomena, often use finite difference methods. The main disadvantage of finite difference methods is difficulties in applying the methods to irregular boundaries, such as curved boundaries. Over large domains, finite difference methods are numerically intensive and lead to slow computation times - as do finite element methods.

Finite element methods are also well established. They formulate the analysis in terms of a variational principle or some weighted-residual principle. Finite element analyses solve variables over a domain so that the integral of the formulation over the domain is zero. The integration is carried out with interpolation functions in discrete portions of the domain, referred to as finite elements. Finite element methods solve variables at boundaries with ease. For this reason, finite elements are often preferred in the structural analysis of complex shapes. Structural analysis is generally concerned with few phenomena - mainly stress and strain. The incorporation of new equations for phenomena, in an existing finite element analysis, is difficult but is not of great concern in structural analysis. Over large domains, finite element methods are numerically intensive and slow to compute. Xie (1995) advised that finite element and finite difference methods generally have comparable levels of accuracy and computational speed for similar grids of nodes, provided comparisons are for the same type of scheme whether explicit or implicit.

Boundary element methods offer computational advantages for large domains. They involve the application of the reciprocal theorem of which virtual work is one example. Thus boundary element methods enable the solution of variables at points a long way from the boundaries, without the need for extensive differentiation or integration through the domains, in contrast to finite difference and finite element methods. However, boundary element methods involve much more complex mathematics which defeats advantages of the methods when there are non-linearities in the domain. The complex mathematics does not lead to the sparse symmetrical matrices of equation coefficients characteristic of finite difference and finite element analyses. This complexity can slow down the solution time of boundary element methods.

Analytical solutions, that is closed formed solutions, have been developed by Carslaw and Jaeger (1959). The solutions usually involve a complex series of integrals of trigonmetric functions. Direct use of the solutions enables rapid analysis. However, manipulation of the solutions for application in problems with boundary condions different to those solved by Carslaw and Jaegar are very difficult. Analytical solutions generally tractable when there are uniform thermal properties and simple boundary conditions which do not occur in realistic problems.

As mentioned in §2.2.4, Bejan (1984) noted that heat transfer analysis is potentially very complex because of the many variables and phenomena involved. He explained that it is unlikely that all of these will have a dominant effect on heat transfer. Before undertaking a heat transfer analysis, he recommended that scale analysis be carried out to determine dominant and significant variables. Only these variables should be modelled accurately to ensure that the analysis is tractable and that computational effort is not excessive nor wasted.

2.5.2 Finite Difference Analyses for Conduction, Convection and Sources

The finite difference method was adopted for the heat transfer model in this thesis for reasons given in §3.2. It is thus reviewed in more detail below.

There are various text books such as Carnahan et al (1969) and Croft et al (1977), which describe a range of finite difference methods. The methods can be broadly categorised as either explicit, implicit or a combination such as Crank-Nicholson. All methods can be used to determine temperature distributions after successive small time steps.

Explicit methods derive equations for temperatures at the current time step from known heat transfer relationships between nodes at the previous time step. All of the equations have only one unknown temperature and thus can be solved quickly and simply. However, there is potential for numerical instabilities to occur during analysis. These instabilities can be prevented by controlling the time step and node spacing. In two dimensional thermal conduction problems, numerical stability is assured if the following is satisfied.

$$\frac{\alpha.\Delta t}{\Delta x^2} \leq 0.25 \qquad (2.55)$$

where α = thermal diffusivity

$$= \frac{k}{\rho.c}$$

k = conductivity ($W.m^{-1}.K^{-1}$)

ρ = density ($kg.m^{-3}$)

c = specific heat ($J.kg^{-1}.K^{-1}$)

Δx = distance to adjacent finite difference node (m)

Δt = discrete time step used in finite difference analysis (s)

The implicit method can be used to reduce numerical instabilities independent of time step and node spacing. These methods derive equations for temperatures at the current time step from heat transfer relationships between nodes at the current time. Each equation has several unknown temperatures. Applications of implicit methods have the potential to generate matrices which represent the equations, with large band widths and thus take considerable computation time to solve. Despite being able to obtain a stable answer with larger time steps, implicit methods must use a similar time step to explicit analyses to achieve comparable accuracy (Thorpe 1995).

The band widths of matrices used in implicit finite differences can be reduced to three if an alternating directing scheme is employed. In these schemes heat flows are analysed separately in each orthogonal direction in each time step. During the analysis in one orthogonal direction, the heat flows along each grid line are considered separately. The temperatures are solved at all nodes along a grid line implicitly. The solution leads to equations for heat flows from each node b to adjacent nodes a and c along grid lines, in terms of temperatures, T at the next time step. These equations are of the form,

$$a.T_a + b.T_b + c.T_c = d \qquad (2.56)$$

and hence lead to matrices of band width 3 as shown in the generalised expression (2.57) below.

$$\begin{bmatrix} & 0 & \\ a & b & c \\ 0 & & \end{bmatrix} \begin{bmatrix} \\ T \\ \\ \end{bmatrix} = \begin{bmatrix} \\ d \\ \\ \end{bmatrix} \qquad (2.57)$$

These systems of equations can be solved rapidly by back-substitution. Higher order analysis involving five or more adjacent nodes along a line is possible but leads to greater complexity of computation and longer computation times.

Combined methods employ equations from both explicit and implicit methods. A weighting, say w, is assigned to all implicit equations and a complimentary weighting (1-w) is assigned to all explicit equations. The method involving a 50% weighting for explicit equations and implicit equations is known

as mid-difference or the Crank-Nicholson method. Well used text books such as Carnahan et al (1969), and Croft et al (1977) advise that such methods have superior numerical accuracy over fully explicit and implicit methods. Croft et al (1977) refer to a minimum of truncation error as the reason for the superior accuracy. Another reason why the Crank-Nicholson method is most accurate is it applies heat transfer relationships based on average temperatures during each time step. Average temperatures at nodes are more representative of temperatures during a time step than temperatures at the beginning or the end of the time step. Explicit methods use temperatures only from the beginning of time steps and implicit methods only from the end, despite the temperature changing during the time step. Although mid-difference methods are numerically stable for w greater than 0.5, when these methods are applied to highly transient problems they can produce large oscillations in temperature solutions at successive time steps. To reduce oscillations, it is recommended to increase the weighting factor towards 1.0, that is make the solution scheme more implicit. Alternatively, numerical oscillations can be controlled by applying stability criteria such as that in expression (2.55) above.

Equations of the form in equation (2.56) above can be derived either by replacing the terms in governing differential equations with several terms of Taylors' series (Carnahan et al (1969) and Croft et al (1977)) or by considering energy balances of heat flows at nodes(Patankar 1980). The energy balance method concentrates on physics, whereas the PDE method is more mathematically focussed.

Irregular grids of nodes are desirable in several cases. Irregular grids minimise the computation effort over a large domain. Concentrations of grid lines are desirable where there are large variations in temperature gradients. Another case is the insertion of nodes off grid to model surfaces between materials. Croft et al (1977) show from the consideration of Taylor's series, first and second order differentials of some function, f at a node, "b" in a variable grid, where "b" is in a sequence of nodes, "a b c", are as follows,

$$\frac{df_b}{dx} \approx \frac{1}{\Delta x}\left[\frac{s_{ab}}{s_{bc}(s_{ab}+s_{bc})}f_a - \frac{s_{bc}-s_{ab}}{s_{ab}s_{bc}}f_b + \frac{s_{bc}}{s_{ab}(s_{ab}+s_{bc})}f_c\right] \qquad (2.58)$$

$$\left.\frac{d^2f}{dx^2}\right|_{x=x_b} \approx \frac{2}{\Delta x^2}\left[\frac{1}{s_{bc}(s_{ab}+s_{bc})}f_a - \frac{1}{s_{ab}s_{bc}}f_b + \frac{1}{s_{ab}(s_{ab}+s_{bc})}f_c\right] \qquad (2.59)$$

where f = the function such as temperature, over the domain
x = distance along the grid line through the domain (m)
Δx = perpendicular distance between adjacent grid lines (m)
$s_{ab}.\Delta x$ = distance between nodes "a" and "b" (m)
$s_{bc}.\Delta x$ = distance between nodes "b" and "c" (m)

2.5.3 Numerical Analyses for Two Dimensional Radiation

When radiant heat transfer is unaffected by smoke, absorption and scattering need not be considered. The cross-string method developed by Hottel (1954) can be used to determine view factors for surfaces inside cavities. The cross-string method can be applied not only between surfaces with clear views of each other but also, between surfaces with obstructed views. For example, the view factor, F_{12} for radiation from surface A_1 to surface A_2 shown in Figure 2.13 can be found from the equation,

$$F_{12} = \frac{A_{cf} + A_{ad} - A_{abc} - A_{def}}{2A_1} \qquad (2.60)$$

where A = the area formed by straight lines between the points indicated by the subscripts a-g or the area of the curved surface indicated by subscripts 1-4.

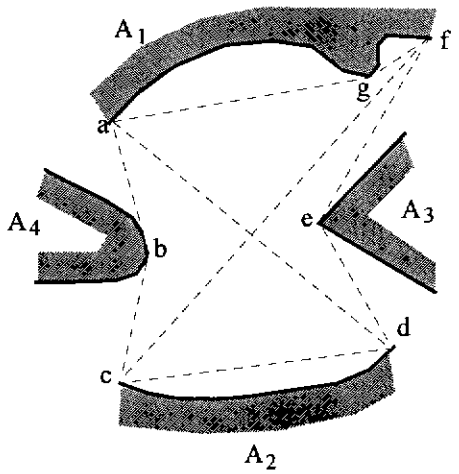

Figure 2.13. Surfaces A1 and A2 with Views of Each Other Obstructed by Surfaces A3 and A4.

Many researchers such as Maruyama and Aihara (1997) and Coelo and Carvalho (1997) showed that for computer modelling of radiant heat transfer in cavities with obstructing or re-entrant corners, it is convenient to use the discrete radiant heat transfer method. Surfaces can be discretised into small segments centred at nodes. Radiation from each surface node can be modelled as a large number of discrete rays emitted in all directions. By tracking each ray across a numerical grid, incident surface segments will eventually be encountered. The incident radiation can be aggregated for each surface node. After all emitted rays have been tracked from a surface node, one can determine the proportion of

radiation from the emitting surface node which is incident on every other surface node. These proportions are the view factors for the emitting surface node and should add to one to ensure conservation of energy. An advantage of discrete radiant heat transfer modelling is that surfaces do not have to be defined by the person using the model. Tedium and precision in defining surfaces as one modifies the grid are avoided.

When absorbing scattering media are present, then equation (2.33) can be applied to each discrete ray to determine the amount of emitted discrete radiation which arrives at an incident surface node. The amount that does not arrive can be allocated to the heat which is absorbed in the media. For conservation of energy, the sum of view factors and absorptivities must add to one.

Discrete heat transfer can be extended to the Monte Carlo method (Siegel and Howell 1981). There is virtually no theoretical limit to the range of radiation phenomena it can model. The method probabilistically generates a photon at some surface point. Further constraints are generated as the path of the photon is tracked. These constraints include angle of emission, wavelength of photon, position where a scattering particulate is encountered. By aggregating the data from numerous trial paths of photons, a complex array of radiation phenomena can be modelled. This method is too detailed for the heat transfer model in this thesis, but it does demonstrate the possibilities of discrete radiation transfer.

Having found view factors for each surface by one of the above methods, the radiation heat transfer can be solved by a system of simultaneous equations (Gray and Müller 1974). Each equation expresses the radiant heat balance between a particular surface and every other surface.

2.5.4 Linkage of Numerical Analysis for Radiation with Numerical Analysis for Conduction, Convection and Sources.

Patankar (1980) showed that radiant heat transfer analyses can be linked with analyses for conduction and convection by treating the radiant heat gains or losses at surface nodes as sources. However, this linkage described by Patankar can introduce numerical instabilities into an otherwise numerically stable heat transfer analysis. Instability occurs despite the use of implicit analysis for conduction. If the time step in a numerical analysis is too large, a local nodal source of heat from a radiant analysis may be so large as to momentarily predict that heat flows in the opposite direction to the overall heat flow and thereafter lead to numerical instability.

2.5.5 Methods of Analyses Adopted in Models with Heat Transfer Capabilities

General purpose and special purpose models with heat transfer capabilities which relate to the research in this thesis are discussed below.

TASEF was purposefully written for analysing heat transfer through sections of structural members exposed to fires. It has been used extensively (Thomas 1997, IEAust 1989). Its modelling capabilities include heat transfer through several materials, two dimensional radiation through cavities and lines of symmetry. For radiant transfer, TASEF employs the cross-string method but it does not consider re-entrant corners in cavities. For conduction (equation (2.4)) and simple convective (equation (2.7)) heat transfer, TASEF employs explicit analysis of finite elements of rectangular, quadrilateral and triangular shapes. As mentioned in §2.5.1, being a finite element model, it handles complex boundaries with ease but considers only a few heat transfer phenomena including thermal conduction, convection and radiation. TASEF does not consider the transfer of moisture and vapour during heating of wood. This transfer has no net effect on overall heat energy balances and hence should accurately predict temperatures substantially above the vaporisation point. Heated moisture and vapour do affect mechanical properties of wood.

TCD (1990) is similar to TASEF insofar as it uses rectangular finite elements. It differs in that it uses a Galerkin finite element scheme which leads to a non-diagonal system of implicit equations. TCD has more prepocessing to facilitate the input of nodes and more postprocessing facilities for making isothermal plots and designing structural members.

ANSYS (De Salvo and Gorman, 1989) is a general purpose finite element program mainly developed for applications in structures but also has thermal analysis capabilities. Its structural capabilities include analysis of stress, creep, plasticity, vibrations, large deflections, shells, stress stiffening and buckling. Its thermal capabilities include analysis of steady state, transience, conduction, radiation and convection in 1-3 dimensions. Boundary nodes can be nominated at which temperatures can be defined with time. Transfer of heat from these nodes modelled conduction, convection and radiation procedures. Thermal analysis can be coupled with fluid flow analysis if it is desired to model both heat and mass transfer. ANSYS uses a Houbolt implicit solution scheme which requires care with node numbering to minimise the bandwidth of implicit equations and hence minimise computation time. The user can choose whether to undertake a "hidden" or a "non-hidden" scheme for determining view factors for two-dimensional radiation analysis. The hidden scheme must be selected when there are re-entrant corners around a cavity; that is, some surfaces are obscured from view of other surfaces. This scheme seems to employ a ray tracking procedure mentioned in §2.5.3. The non-hidden scheme probably uses the cross-string method

without concern for obstructing surfaces. The radiation analysis does not consider aborption and scattering. Temperatures in the radiant heat transfer analysis are solved by a Newton Raphson scheme.

ABAQUS (1997) is general purpose finite element program which can analyse problems including creep, static and dynamic stress-displacement, heat and mass transfer. It has a range of solution procedures which basically involve explicit, implicit and combined methods. Fully implicit methods are recommended for highly transient problems. Commercial licences for ABAQUS are very expensive - prohibitive to most consulting engineers. It is mainly used by large research organisations.

PHEONICS (Spalding 1992) solves CFD, computational fluid dynamics, differential equations given by a user. Examples of problems which can be handled by PHEONICS include design of a heat exchanger, aerodynamic drag of a road vehicle, heat and mass transfer through porous solids and multi-phase flow in three dimensions. PHEONICS uses finite difference methods similar to Patankar's (1980) finite volume method (which is a finite difference method). The user can specify interpolation routines to define how functions vary over finite volumes attributable to finite difference nodes. The user can specify whether the solution is to be undertaken explicitly, implicitly or by a combination. Either an implicit or combined scheme is recommended for reliable stability and accuracy.

Strand 6 (G+D Computing 1993) is another general purpose finite element package developed mainly for application in structures but also has heat transfer capabilities. It is a popular well used structural analysis package in Australia. In additional to structural analyses, it analyses conductive heat transfer through solids, that is the structural material, as well as convective and radiant heat transfer at the surface of the structure. However, Strand 6 requires the temperatures of external surface nodes to be defined with time. It also does not model convective and radiant heat transfer through cavities. The user can choose a combination of explicit and implicit solution schemes. In Section 3.2.4.1 it was explained that combined schemes employed a weighting factor, w to the implicit part and (1-w) to the explicit part. In Strand 6 the user is free to choose any value for w. A value between 0.5 and 0.667 is recommended to achieve unconditional numerical stability and optimum accuracy. In the case of highly transient problems, a value for w approaching 1.00 is recommended to minimise oscillation in temperature solutions at successive time steps. The cost of Strand 6 is within reach of large consulting engineering practices.

There are difficulties in using general purpose programs in developing special fire engineering models. Providers of general purpose commercial computer programs such as ANSYS, PHEONICS, ABAQUS and Strand 6 restrict the use of their source code which can be a hindrance for researchers. Practising engineers do not use them sufficiently to justify the expense of acquiring them and consequently do not feel confidant in using them. However, they do provide a means of establishing simple empirical models

with limited scopes of application, which practising engineers would find useful. Further research in developing simple models is desirable.

The methods of analysis adopted in theoretically based models related to the fire resistance of timber framed walls reviewed throughout this section, §2 are summarised as follows. Existing general purpose heat transfer models were adopted by a number of researchers. Knudson and Schniewind (1975) adopted the finite element program written by Bizri (1973) for heat transfer in concrete structures. Gammon (1987) adopted an existing general purpose finite element heat transfer model, FIRES-T3 (Iding et al 1977) and modified it by incorporating radiant heat transfer for cavities based on the cross-string method. Thomas (1997) adopted TASEF. König (1997) adopted TCD. Special purpose analyses have also been developed. Mehaffey et al (1994) and Mehaffey (1997) describe the development of WALL2D which employs explicit finite differences. It seems likely that Mehaffey chose to develop a new heat transfer so that he would not be restricted in circulating his model rather than use a general purpose model which restricts circulation by copyright laws. Mehaffey would also have had more scope to modify the modelling of phenomena than would have been the case with general purpose models for which access to source code is restricted. Fredlund (1988) developed an explicit finite element model for one-dimensional heat, moisture and vapour transfer in various wood based boards, because he was concerned about fundamental modelling of phenomena and would have wanted access to source code.

2.6 Summary

In the introduction, §2.1 it was explained that this chapter began with a review of fundamentals including the behaviour of materials in fire and basic heat transfer equations. Based on this review, this section then evaluated literature on more applied heat transfer topics relevant to heat transfer in timber framed walls. The main findings which should be taken into consideration in the development of heat transfer models for light-timber framed walls in real fire are summarised below.

Behaviour of Gypsum Board During Thermal Degradation

The fire resistance of light-timber framed walls is highly dependent on gypsum board, and thus the thermal responses of gypsum board must be carefully considered. The modelling of heat transfer in gypsum board must account for:

1. Heat and density losses due to calcination (§2.2.1.1 and §2.4.2.2).
2. The effects of crazing caused by shrinkage at temperatures greater than 400°C (§2.2.1.3). Mehaffey et al (1994) showed that the additional heat transfer due to crazing is best

modelled with conduction which results in the same rate of heat transfer as actually occurs through the crazed gypsum board.

3. Sloughing due to glass fibres melting at temperatures between 700-900°C (§2.2.1.3).

Thermal Properties of Gypsum Board

There is a considerable range of properties published for gypsum board (§2.4.2). The range of densities of gypsum boards around the world widely varies between 578-1000 $kg.m^{-3}$ (§2.4.2.2). There is a wide range of specific heat values published for gypsum boards between 500-950 $J.kg^{-1}.K^{-1}$, excluding specific heats at calcination temperatures (§2.4.2.3). Specific heat should be independent of density and hence the range of values for specific heat should not be due to the range of densities. There is a significant range of published values for conductivity between 0-100°C and above 400°C (§2.4.2.4). Most of the properties published are for Canadian gypsum boards which are substantially less dense than Australian boards. Since conductivity is generally dependent on density (Fredlund 1988), it is apparent that thermal properties published for gypsum board cannot be used without some modification for variations in density. The variation in conductivities at temperatures greater than 400°C, is not only due to the variation in densities but also variations in the intensity of crazing which varies in boards from different manufacturers. Appropriate procedures for modifying conductivity for density should be investigated. Relative density with temperature should be consistent because the proportion of constituents is consistent among all boards.

Behaviour of Wood during Thermal Degradation.

The key behaviours of timber at various temperatures which should be considered in modelling are as follows (§2.2.2). Moisture vaporises between 100-150°C, depending on the moisture diffusivity of the wood. Vaporisation absorbs a substantial amount of heat (2.26 $MJ.kg^{-1}$). At 200°C wood turns brown, loses mass and gives off volatiles. By 300°C the wood is black in colour. It is reasonable to assume that at this temperature all wood suddenly changes to char. Little loss of mass occurs at temperatures greater than 400°C.

Shrinkage (Figure 2.10) is a phenomenon that significantly affects heat transfer. It ranges between a few percent during moisture vaporisation and 40% at 1000°C. Shrinkage not only occurs perpendicular to the grain but also along the grain, causing char cracking which greatly increases heat influx, particularly by radiation at temperatures above 400°C.

Smoke is an obvious product of the thermal degradation of wood and could significantly affect radiant heat transfer. (§2.2.2)

Studs in wall cavities do not burn because of lack of oxygen supply (§2.2.2), and hence, there is no heat produced from combustion before walls have failed. The formation of char involves pyrolysis reactions. The total heat of all pyrolysis reactions is quoted in the literatures between wide ranging values. (In the validation of the model in this thesis some indication of the heat of reaction of pyrolysis will be apparent).

Thermal Properties of Wood

Similarly to gypsum board, apart from density there is a considerable variation in published thermal properties for wood and char at elevated temperatures (§2.4.3). Appropriate values should be judged from consideration of the behaviour of the constituents of wood, and if possible, from independent experiments. For example, Janssens' (1994) specific heat for wood includes the heat required to remove water bound in wood fibres and is thus appropriate to adopt. The value adopted for the conductivity of char should be chosen with due regards to the likely degree of char cracking (§2.4.3.3).

Heat Transfer Modelling Equations

Since heat transfer in walls should be largely two dimensional, fundamental equations for two dimensional heat transfer were summarised (§2.3), including conduction, Newtonian convection, equation (2.7), and radiation. A broad range of convective heat transfer coefficients published in the literature were noted (§2.4.4). However, convection is not a dominant mode of heat transfer. Thermal conduction, moisture diffusion, and radiation should dominate.

Numerical Analysis Methods

It is apparent from published heat transfer models (§2.5.5) that finite difference methods are preferred when the modification of modelling of phenomena is a dominant consideration. When the modelling of boundary conditions is more important, finite element models are more advantageous and are preferred.

The cross-string method (§2.5.3) has been used for numerical analysis of radiation in heat transfer models for structures, to date. This method is difficult to apply to structures with cavities with re-entrant corners. It cannot be applied to problems involving absorbing emitting media such as smoke. Discrete radiation analysis could be applied to most types of cavities.

3. Heat Transfer Model - ADIDRAS

3.1 Introduction

This chapter gives a detailed explanation of the heat transfer model. It commences with an overview of the model (§3.2), giving justification for adopting a finite difference method. Since it is impractical to model most of the heat transfer phenomena in a wall exposed to fire, appropriate simplifications and assumptions about phenomena are justified in §3.3. The modelling of wall sections with the finite difference mesh is explained in §3.4-3.8. The modelling equations are then given in detail in §3.9. The modelling equations and numerical analyses are checked for convergence and conservation of energy at boundaries (§3.10). A comparison of model predictions with predictions from the well established heat transfer model, TASEF (Sterner and Wickstrom 1990) is given.

3.2 General Description of Model

The heat transfer model has been developed particularly for light-timber framed structures subjected to real fire. The structures may comprise sheeting, studs (or joists), insulation and cavities in a variety of arrangements. Only the heat transfer modes of thermal conduction in sheeting and studs, and radiation and convection at surfaces are considered. Detailed discussion on these assumptions and others are given in the next section, §3.3. The heat transfer analysis carries out two separate analyses in parallel:

1. Analysis of conduction in solids, surface convections and radiant heat transfer at external surfaces, and
2. Analysis of radiant heat transfer in cavities.

An alternating direction implicit (ADI) finite difference scheme has been adopted for the first analysis with the aims of maximising numerical stability and computational efficiency. The discrete radiation (DR) method has been adopted to analyse radiant heat transfer for a wide scope of cavity shapes with and without smoke. The model has been named, ADIDRAS which is an acronym for Alternating Direction Implicit and Discrete Radiation Analysis (of heat transfer) in Structures. More detailed reasons for adopting these methods of analysis are given below.

A finite difference method for conduction and surface convection was chosen for the reasons given in §2.5.1. The simplicity of finite difference equations was appealing and the method is well established. Techniques are available for finite difference modelling of heat transfer at boundaries as shown in equations (2.58)-(2.59). Finite differences facilitate any future refinements to the modelling of heat transfer phenomena. Finite difference solutions are of comparable accuracy to finite element solutions (Xie 1995).

An alternating direction implicit (ADI) finite difference method (§2.5.2) has been chosen for the following reasons. ADI is simple to apply because it enables solution based on one dimensional formulations. It leads to a set of simultaneous equations representing heat transfer at nodes along a grid line. The set can be expressed in terms of a tridiagonal matrix of coefficients (equation 2.57) which can be solved quickly and simply by back-substitution.

An implicit method was adopted because of its superior numerical stability compared with explicit and combined procedures. Numerical stability is potentially a problem with radiation transfer. The energy balance method of Patankar (1980) for deriving finite difference equations was adopted in preference to the use of Taylor's series approximations because it directly addresses the conservation of energy and thus should minimise the potential for errors in formulating equations. The formulation of energy terms for substitution in energy balance equations is detailed in §3.9.

For radiation analysis the discrete radiation heat transfer method (§2.5.3) was chosen in preference to the cross-string method because of its versatility in computing view factors without the need for defining surfaces as well as the arrangement of materials in the input. Input is faster, more convenient and less prone to user-input errors. Discrete radiation analysis facilitates further enhancements to radiation modelling in the future.

A flowchart for ADIDRAS is shown in Figure 3.1 (b). It has been developed to fit into a model for predicting the time of failure of walls in fire as shown in Figure 3.1 (a). The sequence of modelling operations shown in Figure 3.1 (b) is explained as follows. The temperature of a some specified or modelled fire at the current time step is an input into the model (box 1). The temperature distribution at the previous time step is used to determine the distribution of thermal properties (box 2). Source heat gains and losses at nodes on surfaces of an assembly, due to radiant transfer are determined on the basis of the temperature distribution and fire temperature at the previous time step (box 3). The conduction of heat gains and losses from radiation and convection from surfaces through solid materials is modelled with energy balance equations updated implicitly at each time step in box 4; implicit meaning for temperatures at the current time step. The equations are solved using an ADI method (box 5), giving the temperatures at the current time step, that is the output box. The current temperature distribution is used in the structural response model.

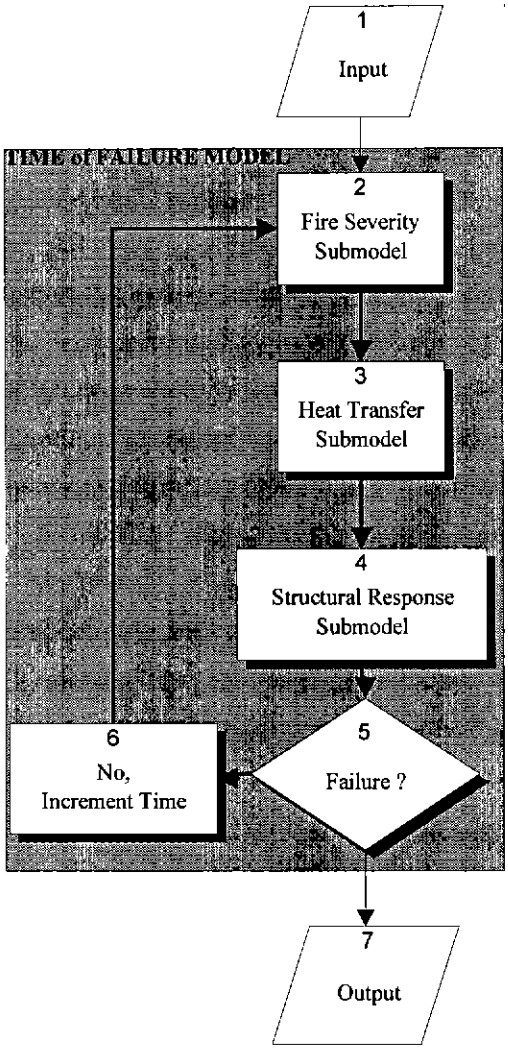

Figure 3.1. (a) General Flowchart for Time of Failure Models. (Figure 1.2 reproduced).

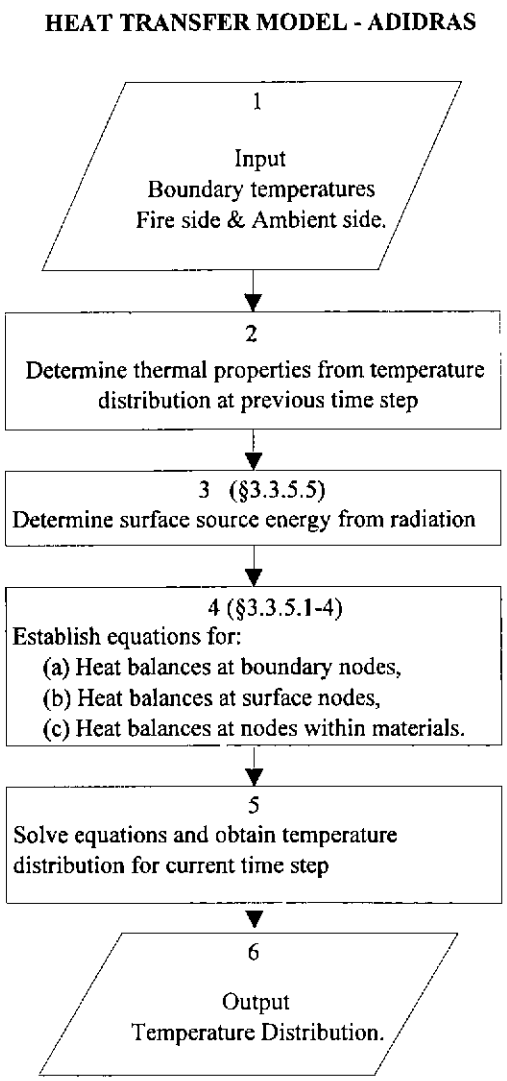

Figure 3.1 (b) Flowchart for ADIDRAS.

3.3 Modelling Assumptions

Various heat transfer phenomena affecting temperatures in light-timber framed structures were discussed throughout the literature review, §2. The most important assumptions on heat transfer phenomena made in ADIDRAS are as follows. Heat transfer is two dimensional. Heat is transferred through solid materials by thermal conduction. Through cavities heat transfer is modelled with equations for:

1. Radiation through absorbing-emitting media.
2. Convection based on simple heat transfer coefficients in accordance with equation (2.7).
3. Conduction, to avoid the inconvenience of having discontinuities in the finite difference analysis grid where there are cavities.

In external gaseous spaces, heat is assumed to be transferred similarly to the transfer of heat in cavities, except absorbing-emmitting media are ignored. More detailed assumptions on phenomena, made in ADIDRAS are discussed below.

It is assumed that gases in the fire are well mixed and conditions are uniform. These are pre-conditions necessary for two dimensional heat transfer.

In §2.2.1.2, it was explained that some gypsum boards are manufactured with greater density towards the surface. The model does not allow density to vary with position within the same material at the same temperature. Density can only be varied with position by specifying different materials and defining the appropriate material properties.

Several assumptions were made in relation to shrinkage of the thickness of gypsum board. Figure 2.1 showed that the thickness of gypsum board shrinks as much as 8% as the temperature of the board rises to 900°C (ignoring the reduction in thickness due to charring and ashing of surface paper). This shrinkage is not modelled with the movement of nodes. Thickness is assumed to stay constant with time and heat exposure. Thermal conduction properties must therefore be input so as to model the same rate of diffusive heat transfer as occurs during fire exposure. 8% is considered to be too small a movement to warrant the numerical difficulties with moving nodes in the analysis.

Unconstrained in-plane shrinkage of the gypsum board with temperature is assumed to be a similar percentage to that for the shrinkage of thickness. However, overall in-plane shrinkage is prevented by the fasteners which secure the board to the timber frame. In-plane shrinkage must occur locally. Local shrinkage causes the extensive crazing with cracks extending through the full thickness of the board §2.2.1.3. It is expected that the cracks created by crazing would increase the rate of heat flow through gypsum board by convection and radiation. ADIDRAS does not directly model increases in heat transfer through gypsum board due to cracking. It is necessary to employ the practice by Mehaffey et al (1994) of incorporating this additional heat flow with an increased conductivity similar to the way shown in Figure 2.8.

At 700°C, the glass fibres in the gypsum board, which hold gypsum board together during crazing, undergo a substantial reduction in viscosity and can no longer resist shrinkage stresses (§2.2.1.3). Sloughing of the board results. The model adopts this temperature criterion for predicting the sloughing of gypsum board but does not simulate heat transfer for the remaining wall section after sloughing occurs. Tests show that the period of time to collapse after sloughing is short compared with the total failure time. It is an excessive level of refinement to attempt to accurately predict this short period with a

model. Aan empirical estimate of the period should be added to the sloughing time to predict the time of collapse.

In §2.2.1.1 it was explained that heat transfers through gypsum board by conduction and moisture transfer. Since moisture transfer does not affect the net heat change as temperature rises from 0-200°C, it is not directly modelled. Gypsum is a secondary structural element after the timber framing. Structurally, it is not expected to be important. Any weakening due to moisture vaporisation is not a concern. Moisture transfer in gypsum board is thus ignored in ADIDRAS.

The use of heat sources to model the heat lost in calcination, vaporisation and possibly other processes is not as convenient as simply adjusting the input of specific heat to account for such losses. The model does not directly consider heat losses. These losses must be incorporated into specific heat input.

From §2.2.2 it is apparent that pyrolysis can be simply modelled as a transition of wood to char at a particular temperature, 300°C. The transition between char and wood is almost always insensitive to temperature because of the steepness of temperature gradients at the transition. The use of an Arrhenius function such as equation (2.3) is too refined for the aims of this research (§1.5). The practice of using a particular transition temperature has been adopted. Estimates of heats of pyrolysis reactions vary from 370 $kJ.kg^{-1}$ endothermic to 1700 $kJ.kg^{-1}$ exothermic (§2.4.3.4). An appropriate value will be proposed after making comparisons between model predictions and experimental results (§5.4).

From §2.2.2 it is apparent that charring involves surface recession and shrinkage. It is difficult to model these phenomena because in a numerical analysis it would involve the movement of nodes in the vicinity of wood surfaces. Recession occurs at 1100°C. Temperatures in wood in light-timber framed walls do reach such high values at times prior to collapse (Collier 1992). Thus recession can be ignored. However, shrinkage will occur. This phenomenon of shrinkage will be accounted for by modelling nodes in gradually shrinking char with fixed nodes but increased conductivity.

In §2.4.3.3 it was discussed that the conductivity of wood varies with direction. Considering the difficulty in modelling conductivity as a function of direction, and the small improvements gained in predicitons of temperatures and times-of-failure, modelling anisotropy is an excessive level of refinement. Consequently, the heat transfer model being developed will be does not allow for conductivity varying with direction; isotropy is assumed.

In §2.2.2 it was also explained that wood, like gypsum board, transfers heat not only by conduction but also convection of moisture and vapour. As for gypsum board, moisture and vapour transfer has no net effect on heat transfer after temperatures have risen from 20° to 200°C. However, moisture does

profoundly affect mechanical properties of timber, particularly at the vaporisation point (§6.3.5 and §6.3.6). Experimental results in Figure 4.34 show that moisture dispersion can extend through most of a 90x45mm timber section at a particular time. Figures 6.7 and 6.8 show that compression properties consequently degrade to a small proportion of values at ambient conditions. Section §4.5.4, refers to an experiment involving a very slender wall which failed when the temperature in studs reached approximately 100°C - well before studs charred. However, no report could be found in the literature, of walls exposed to fire, failing prior to substantial charring of the studs. Since walls are rarely ever as slender as the one tested, moisture transfer in studs has not been directly modelled in ADIDRAS.

Heat loss due to vaporisation of moisture in wood is modelled in a similar manner as for vaporisation of moisture in gypsum board; that is, by approriate allowance in the input of specific heat.

Vaporisation of moisture and volatisation which is the conversion of wood to gas during pyrolysis, involve a volumetric expansion of 500-1000 times which is apparent from comparing the density of wood and moisture with the density of gas and vapour. Such an expansion is expected to disperse volatiles and vapours soon after formation.

In §2.4.3.4 it was stated that fire could only be sustained if the oxygen concentration was greater than 11%. It will be assumed that oxygen in cavities is not replenished after any flaming combustion. Thus, heat from surface flame on timber framing will be ignored.

Transfer of moisture from gypsum board, and the transfer of moisture, volatiles and particulates from the combustion of studs (albeit in an oxygen starved cavity) must affect the density and other thermal properties of cavity gases. These properties are considered in §5.2.6.

3.4 Range of Light-Timber Framed Structures

The heat transfer model was developed to analyse a wide range of wall sections, in accordance with aims §1.5. One category of sections which ADIDRAS can analyse are those with orthogonal surfaces as shown in Figure 3.2. All surfaces are either parallel to the general plane of the wall (that is, "in-plane") or perpendicular to the general plane of the wall (that is, "out-of-plane"). Figure 3.2 (a) and (b) are ordinary stud walls, with and without insulation respectively. Figure 3.2 (c) is a staggered stud wall without insulation. Floors of similar sections to those in Figure 3.2 can also be analysed. To maximise the efficiency of computation, the model should be applied to a representative portion of the wall, as shown by the dashed rectangle in each of the examples shown.

ADIDRAS can also model heat transfer through sections with non-orthogonal surfaces such as the section shown in Figure 3.3. The non-orthogonal surfaces are the diagonal surfaces of the insulation. However, more effort is required with the input of data.

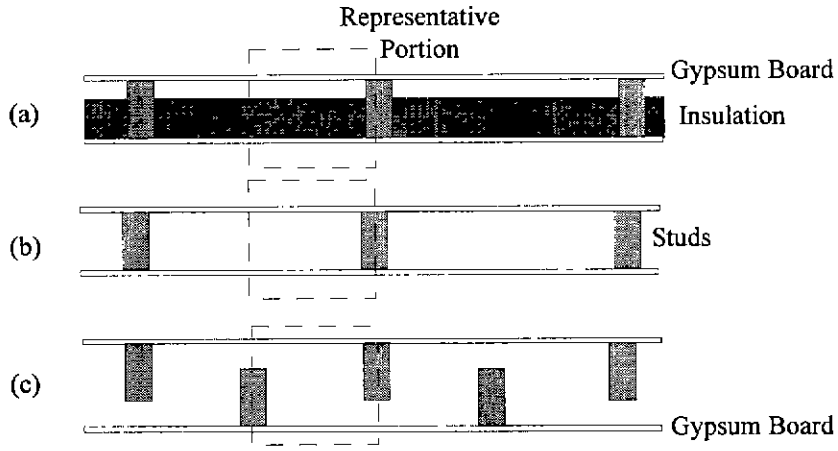

Figure 3.2. Range of Light-timber Framed Sections with Orthogonal Surfaces. (a) Ordinary Insulated Stud Wall. (b) Uninsulated Ordinary Stud Wall. (c) Uninsulated Staggered Stud Wall.

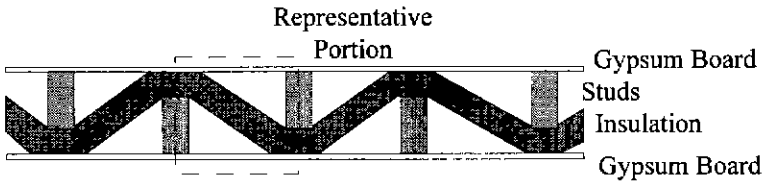

Figure 3.3. Example of Wall with Non-orthogonal Surfaces, a Staggered Stud Wall with Insulation.

3.5 Generation of Finite Difference Grid for Walls with Orthogonal Surfaces

The wall arrangement in Figure 3.2 (c) is used here as an example of how ADIDRAS generates a grid of nodes for the finite difference heat transfer analysis of wall sections with orthogonal surfaces.

The model, firstly subdivides an orthogonal wall section into bands from the key cross-sectional dimensions given for studs, gypsum board and insulation, as shown in Figure 3.4. Bands are generated in-plane and out-of-plane. Sufficient bands are created so that each surface is coincident with an edge of a band.

Gridlines are then generated within each band as shown in Figure 3.5. The lines are generated at close spacings near the edges of each band, and at increased spacings towards the centre of each band. This varied arrangement of lines, compared with uniform arrangements of lines, improves computational efficiency of transient heat transfer analysis of large sections by creating fewer grid lines and thus fewer computations, while at the same time improving numerical accuracy with closely spaced lines where transient temperature gradients are large near surfaces (§2.5.2). The spacing of gridlines is set with the input of spacing of the first line from the edge, the spacing between two gridlines closest the centre of the band and the ratio of adjacent spacings. The minimum spacings should be set at the edges. (The programming in the model does allow for the minimum spacings to be set at the centre of bands.)

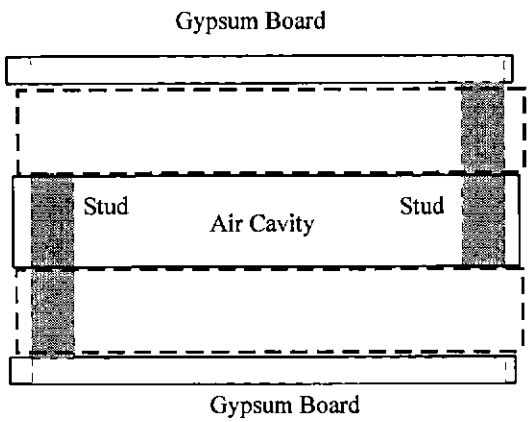

Figure 3.4 (a). Subdivision of Section into Bands in the Plane of the Wall

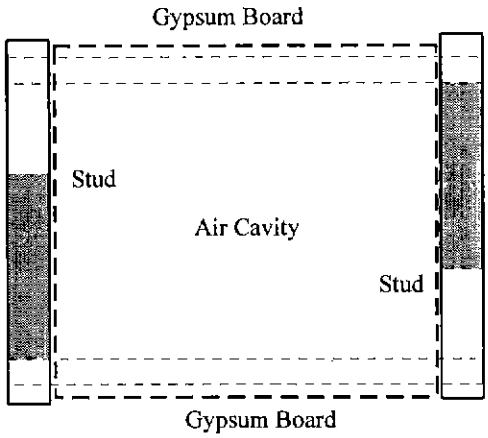

(b) Subdivision of Section into Bands Perpendicularly through the Wall

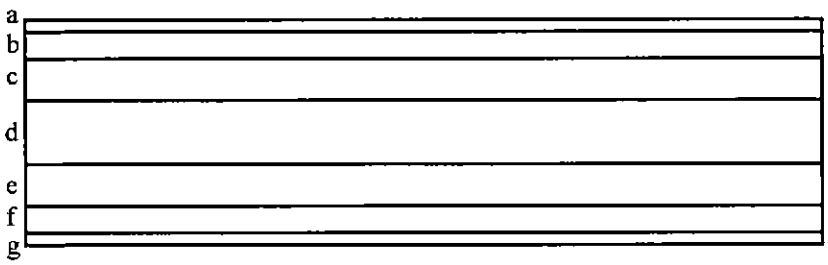

Figure 3.5. Generation of Grid Lines in Band.

After the generation of grid lines for each band in both the in-plane and out-of-plane directions, the nodes are created as shown in Figure 3.6. The intersection of gridlines become the major nodes. The major nodes outside the wall section become the fire and ambient boundary nodes. The major nodes along centre lines through studs and air cavities are adiabatic boundaries - they do not allow heat to escape and behave as perfect insulation.

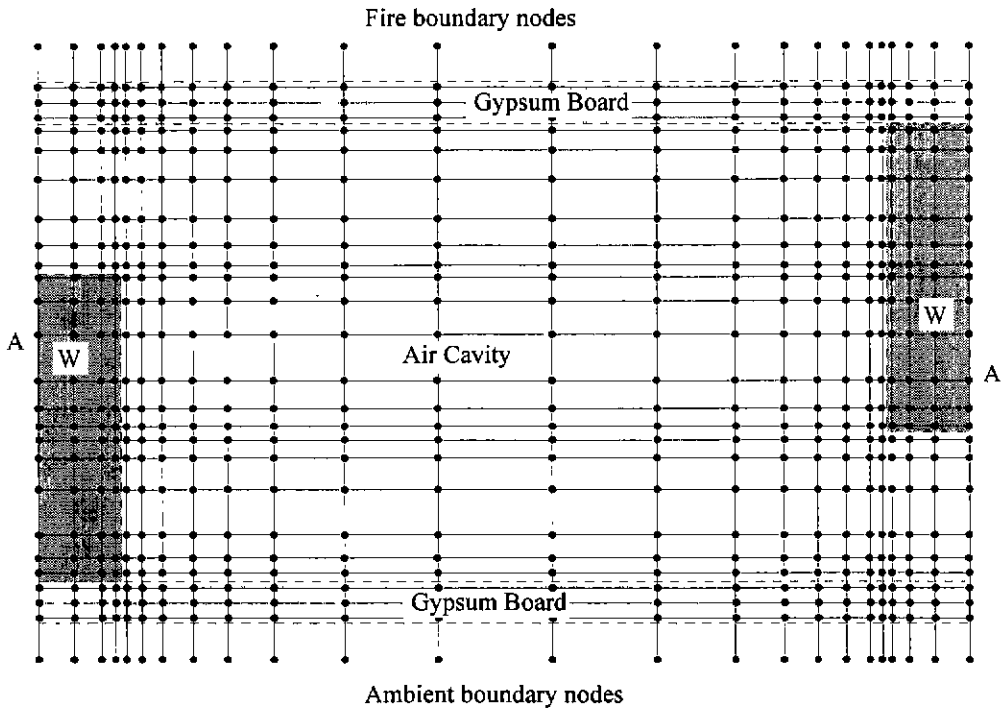

Note A - adiabatic boundary
W - wood stud section

Figure 3.6. Resulting Finite Difference Grid from Bands in Figure 3.4 and Generation of Lines in Figure 3.5.

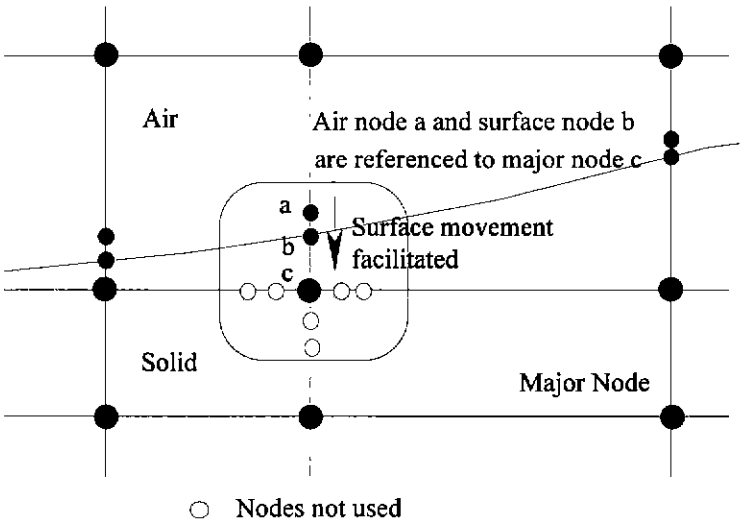

Figure 3.7. Surface Nodes.

Surface nodes are generated in pairs where the edge of a band actually coincides with a surface. No grid lines are generated along the edges of bands. Surface nodes only lie on one grid line. An example of pairs of nodes at a non-orthogonal surface are shown in Figure 3.3. Pairs of nodes for orthogonal surfaces are

similar. One node of a pair is on the surface, and the other node lies just in the gas next to the surface. The two nodes have an infinitesimal distance between them.

3.6 Generation of Finite Difference Grid for Walls with Non-orthogonal Surfaces

The positions of nodes generated in §3.5 are recorded in a coordinate file. For non-orthogonal sections, the coordinate file and the array for material types at nodes, have to be created manually.

3.7 Extent of Materials and Finite Volumes at Nodes

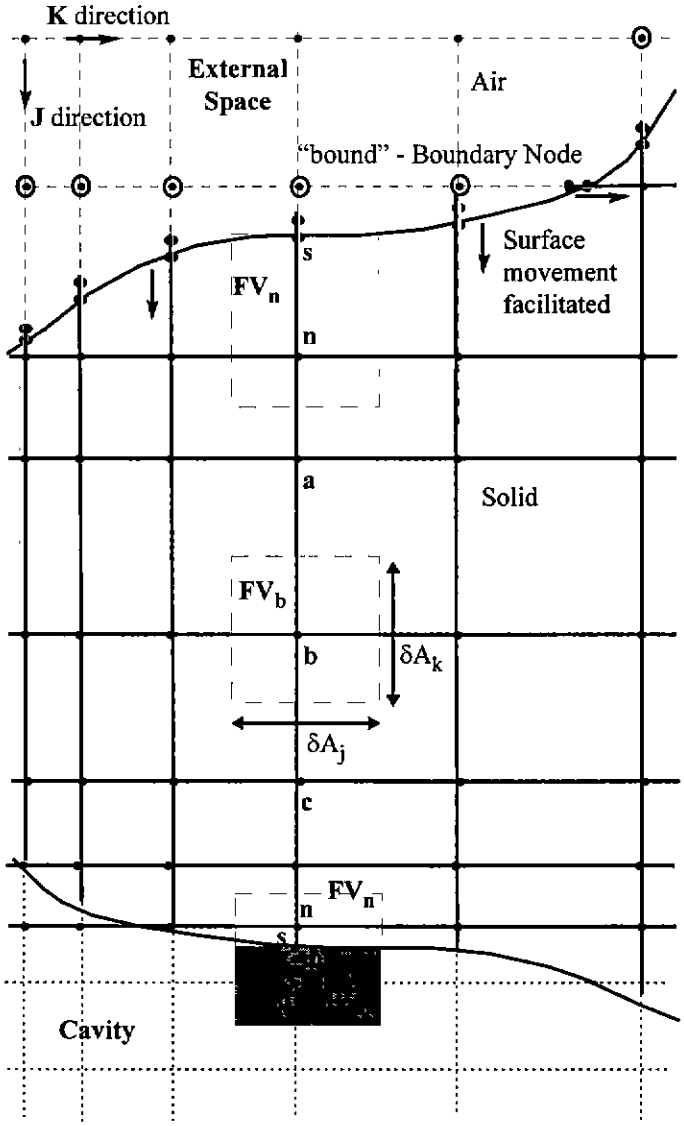

Figure 3.8. Nodes and Finite Volumes (FV).

In §3.2 it was mentioned that ADIDRAS adopts Patankar's (1980) method which establishes equations based on heat flows in and out of finite volumes centred on nodes. The range of finite volumes used in

ADIDRAS is illustrated in Figure 3.8. All finite volumes are centred on major nodes. Finite volumes such as "FV_b" centred on major nodes, "b" in Figure 3.8, cover a rectangular area extending half way to adjacent major nodes. Finite volumes such as "FV_g" and "FV_n", centred on major nodes near surfaces, extend all of the way to the surface and half way to adjacent major nodes.

A material type is allocated to each major node and is assumed to cover the entire finite volume surrounding the node.

3.8 Modelling for Sloughing of Gypsum Boards

In §2.2.1.3 it was explained that sloughing occurs at some temperature between 700-900°C. When the minimum temperature in a sheet of gypsum board reaches the designated sloughing temperature, the model transforms the gridlines as shown in Figure 3.9. Temperatures at nodes in the remaining sheeting are obtained by linear interpolation from temperatures at nodes prior to sloughing. Transformation in this manner avoids the need to modify the rest of the gridlines and the wall section. No other arrays of other variables need to be modified, either.

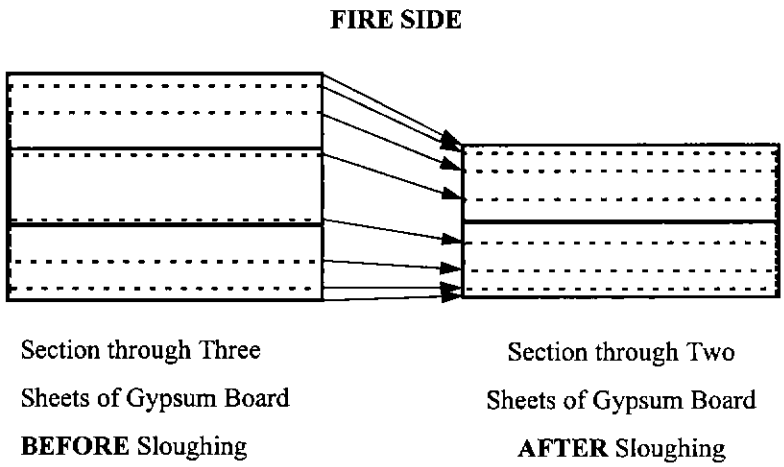

Figure 3.9. Movement of Gridlines at the Time of Sloughing of One Sheet of Gypsum Board Closest to the Fire.

3.9 Energy Balance Equations for ADIDRAS

In the general description of ADIDRAS in §3.2, it was mentioned that finite difference equations were obtained using the energy balance method of Patankar's (1980). This method requires that equations at each node be written in terms of heat flows. For major nodes, the equations establish the energy balance of heat flows into and out of the volume attributable to the node; that is, "finite volumes" (Figure 3.8). Boundary, surface and cavity air nodes next to surfaces have no finite volumes. Air nodes immediately next to external surfaces are ignored since heat exchanges between boundary nodes and surface nodes are considered directly. For boundary, surface and cavity air nodes the energy balance equations are written for heat flows into and out of the nodes. Thus there are four types of nodes and hence four types of equations; that is, equations for thermal boundary nodes, surface nodes, air nodes immediately next to surfaces and for major nodes. Since the solution procedure is the ADI method, ADIDRAS creates equations alternately in each orthogonal direction.

3.9.1 Energy Balance at Thermal Boundary Nodes

Thermal boundary nodes are in the space external to the structure being analysed for heat transfer. Only the nodes closest to the surface are considered; that is the circled nodes in Figure 3.8. The energy balance at a node at a boundary on the fire side or ambient side such as "bound" in Figure 3.8 is determined so that the conservation of energy can be checked (§3.10.3). Thermal boundary nodes exchange heat directly with surface nodes. The advantage of direct exchange is that the equation below for radiant heat, $\dot{q}''_{r_{bound}}$ can be linearised and be incorporated directly into the implicit equations to prevent numerical instabilities occurring at the surface. Otherwise, the high surface temperatures could make the finite difference solution prone to instability. Direct exchange means that nodes such as "a" in Figure 3.7 are ignored. The balance is found from,

$$\dot{q}''_{bound} + \dot{q}''_{c_{bound}} + \dot{q}''_{r_{bound}} = 0 \qquad (3.1)$$

where $\dot{q}''_{bound}$ = is the heat influx to achieve a given temperature at the boundary node at a given time. ($W.m^{-2}$)

$\dot{q}''_{c_{bound}}$ = the convective heat flux exchange between the boundary node and surface node, "s" ($W.m^{-2}$)

$= h_{c_{bound,s}} .(T_{s,p+1} - T_{bound,p+1})$ ... from equation (2.7)

$\dot{q}''_{r_{bound}}$ = the one dimensional radiant exchange between the boundary node and

surface node, "s". ($W.m^{-2}$)

$= h_{r_{bound,s}}.\left(T_{s,p+1} - T_{bound,p+1}\right)$ ... which is a linearised approximation of equation (2.29)

$$h_{r_{bound}} = \frac{\varepsilon_{bound,s}.\left(T_{s,p}^4 - T_{bound,p}^4\right)}{T_{s,p} - T_{bound,p}}$$

h = heat transfer coefficient ($W.m^{-2}.K^{-1}$)

T = temperature (K)

$$\varepsilon_{bound,s} = \frac{1}{\frac{1}{\varepsilon_{bound}} + \frac{1}{\varepsilon_s} - 1}$$ .... from equation (2.30).

superscript: · symbolises differentiation with respect to time

" symbolises that the quantity is per unit of area transverse to the grid line in question.

subscript: bound refers to boundary node

c refers to the convection heat transfer mode

p, p+1 refer to time steps p and p+1 respectively

r refers to radiant heat transfer mode

s refers to surface

$h_{bound,h}$ is set to some arbitrarily large value in accordance with the assumption that the air is well mixed.

3.9.2 Energy Balance at a Surface

The energy balances at surface nodes such as "s" in Figure 3.8 are found from,

$$\dot{q}_{k_{ns}} + \dot{q}_{c_{sh}} + \dot{q}_{r_s} = 0 \qquad (3.2)$$

where $\dot{q}_{k_{ns}}$ = the conductive heat flow to surface nodes, "s" from the first major node, "n" beneath the surface in Figure 3.8. (J)

$$= \frac{k_{ns}\left(T_{n,p+1} - T_{s,p+1}\right)}{x_{ns}}.\delta A.\left(t_{p+1} - t_p\right)$$

$\dot{q}_{c_{sh}}$ = the convective heat energy which flows into surface area δA centred on node "s", from an air node such as "h" immediately next to a surface. (J)

$$= h_{c_{sh}}\left(T_{h,p+1} - T_{s,p+1}\right)\delta A.\left(t_{p+1} - t_p\right)$$

δA = transverse area through which heat flows. Examples are given for the J and K orthogonal directions in Figure 3.8.

t = time (s)

For an external surface,

q_{r_s} = the one dimensional radiation heat energy which flows to δA centred on surface node "s", from a boundary node such as "bound" in Figure 3.8. (J)

$$= h_{r_{bound,s}} \cdot \left(T_{bound,p+1} - T_{s,p+1}\right) \delta A \cdot \left(t_{p+1} - t_p\right) \qquad (3.3)$$

... which is a linearised approximation of equation (2.29)

$$h_{r_{bound,s}} = \frac{\varepsilon_{bound,s} \cdot \left(T^4_{bound,p} - T^4_{s,p}\right)}{T_{bound,p} - T_{s,p}}$$

$$\varepsilon_{bound,s} = \frac{1}{\frac{1}{\varepsilon_{bound}} + \frac{1}{\varepsilon_s} - 1}$$

For an internal surface bounding a cavity,

q_{r_s} = is a source term for radiant heat from the cavity and bounding surfaces, obtained as shown in §3.9.5 (J). This term is inserted according to Patankar's (1980) method.

subscript: n refers to a major node in solid material.

h refers to an air node close to the surface.

The term, q_{r_s} is an explicit source term for surface nodes facing cavities. It is possible for Patankar's (1980) method to lead to numerical instabilities. For example, if the time step is too large, q_{r_s} will be so large as to cause heat at the surface bounding the cavity, to flow towards the fire and initiate numerical instability. No controls against this instability are in the ADIDRAS, but are recommended for further research. This instability has only occurred when the cavity attains temperatures of 600°C. At approximately 700°C sloughing of gypsum board occurs. Instability is only of concern if ADIDRAS is applied to non-loadbearing walls which collapse only when most of the sections through studs have charred. Thus it is felt that 600°C is sufficiently high not to be much of a practical limitation. If such an instability occurs, it can only be controlled by changing the time step and node spacing. Numerical accuracy is likely to be affected.

3.9.3 Energy Balance at a Cavity Air Node Immediately Next to a Surface

The energy balance at a cavity air node such as "**h**" immediately next to a surface node "**s**" in Figure 3.8 is found from,

$$\dot{q}''_{c_{hg}} + \dot{q}''_{c_{sh}} = 0 \qquad (3.4)$$

where $\dot{q}''_{c_{hg}}$ = the convective heat flow from the surface node "**s**" to an air node such as "**h**" immediately next to a surface in Figure 3.8. ($W.m^{-2}$)

= $h_{c_{sh}}\left(T_{s,p+1} - T_{g,p+1}\right)$ ... from equation (2.7)

$\dot{q}''_{c_{sh}}$ = the convective heat flow from the first major air node such as "**g**" to an air node such as "**h**" immediately next to a surface in Figure 3.8. ($W.m^{-2}$)

= $\dfrac{k_{sh}\left(T_{s,p+1} - T_{g,p+1}\right)}{x_{sh}}$ ... from equation (2.5)

k = conductivity ($W.m^{-1}.K^{-1}$)

k_{sh} = some arbitrarily large value which leads to a large convection coefficient, k_{sh}/x_{sh} consistent with the assumption (§3.3) that the air in the cavity is well mixed. ($W.m^{-1}.K^{-1}$)

x = distance (m)

subscript: g refers to a major node in air immediately next to a surface node.

3.9.4 Energy Balance at a Major Node

The energy balance for the heat flow into a finite volume FV_b centred on a major node such as "**b**" in Figure 3.8 is,

$$\dot{q}_{k_b} + \dot{q}_{v_b} + \dot{q}_{r_b} = \dot{q}_{stor_b} \qquad (3.5)$$

where $\dot{q}_{k_b}$ = the influx of conductive heat into the finite volume between times t_p and t_{p+1}. (J)

= $\left(\dfrac{k_{ab}\left(T_{a,p+1} - T_{b,p+1}\right)}{x_{ab}} + \dfrac{k_{bc}\left(T_{c,p+1} - T_{b,p+1}\right)}{x_{bc}}\right).\delta A.\left(t_{p+1} - t_p\right)$

... from the conductive terms in one orthogonal direction, of the left hand side of equation (2.4)

$\dot{q}_{stor_b}$ = the heat stored in the finite volume centred on node "**b**". (J)

$$= \left(\rho_b . c_b . x_b . \frac{(T_{p+1} - T_p)}{t_{p+1} - t_p} \right) . \delta A . (t_{p+1} - t_p)$$

... from the heat storage terms on the right hand side of equation (2.4)

x_b = the length of the finite volume in the direction of the grid line currently being analysed by the ADI method. (m)

$= 1.0 * x_{ab} + 0.5 * x_{bc}$ ... where node "**a**" is a surface node such as "**s**" in Figure 3.8.

$= 0.5 * x_{ab} + 0.5 * x_{bc}$ ... where neither node "**a**" nor "**c**" is a surface node

$= 0.5 * x_{ab} + 1.0 * x_{bc}$ ... where node "c" is a surface node such as "**s**" in Figure 3.8.

q_{r_b} = only applies if the node represents air in an internal cavity (J). It is a source term for the absorption of radiation by smoke; that is, the energy not transmitted according to equation (2.32). The method of computation is given in the next section, §3.9.5.

$\delta A.x_b$ = the finite volume centred on node "**b**" shown in Figure 3.8.

ρ = density. ($kg.m^{-3}$)

c = specific heat. ($J.kg^{-1}.K^{-1}$)

subscripts: a refers to node "**a**"
b refers to node "**b**"
c refers to node "**c**"

3.9.5 Sources of Radiative Thermal Energy, q_{r_s} at Surfaces around Cavities

The source of radiant thermal energy, q_{r_s} at surface nodes around cavities is derived from equations provided by Gray and Müller (1974) as follows. The radiated heat, W_i ($W.m^{-2}$) shown in Figure 3.10, emitted from each surface, i is,

$$W_i = \varepsilon_i . E_{b_i} + \rho_i . H_i \qquad (3.6)$$

where E_{b_i} = emissive black body power of surface, i, defined in equation (2.19). ($W.m^{-2}$)

H_i = radiation incident on surface, i from all other surfaces and any emissive smoke. ($W.m^{-2}$)

ε_i = emissivity of surface, i

ρ_i = reflectivity of surface, i = $1 - \varepsilon_i$

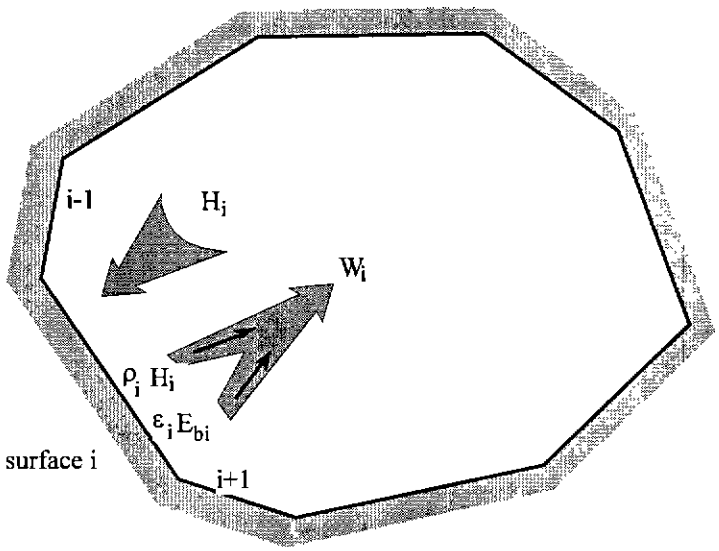

Figure 3.10. Radiant Heat Exchange Between the i.th Surface and All Other Surfaces in a Cavity.

The radiant heat, $\dot{q}_{r\,ji}$ (W) transferred from surface j to surface i through a cavity with smoke is,

$$\dot{q}_{r\,ji} = E_{b_j}\left(T_{s_j}\right) A_j . F_{ji} . \tau_{ji} \qquad (3.7)$$

where $E_{b_j}\left(T_{s_j}\right) = \sigma . T_{s_j}^4$ ($W.m^{-2}$) ... from equation (2.19)

A_j = area of surface j (m^2)

F_{ji} = view factor for emitted radiation from i, incident on j. Refer to equation (2.28).

T_{s_j} = temperature of surface j (K)

τ_{ji} = transmissivity defined in equation (2.33).

If the cavity and surrounding surfaces bounding the cavity are uniform in temperature, then there is a equal and opposite heat transfer between the smoke and the bounding surfaces. The rate that heat is absorbed by radiation passing through the smoke is the same as the rate heat is emitted by the smoke to the surfaces. Thus, assuming that the smoke in the cavity is well mixed and of uniform temperature, T_{sm}

the heat emitted, $\dot{q}_{r_{sm_{ji}}}$ (W) by smoke which travels along all ray lines which pass from surface j to surface i is,

$$\dot{q}_{r_{sm_{ji}}} = E_{b_{sm_j}}(T_{sm}).A_j.F_{ji}.(1-\tau_{ji}) \qquad (3.8)$$

The amount of radiation transmitted from any other surface, j incident on surface, i is $W_j.A_j.F_{ji}$ (W). The total incident radiation at surface, i is,

$$A_i.H_i = \sum_{j=1...i-1,i+1..n} W_j.A_j.F_{ji}.\tau_{ji} + E_{b_{sm}}(T_{sm}).A_j.F_{ji}.(1-\tau_{ji}) \qquad (3.9)$$

Since,

$$A_i.F_{ij} = A_j.F_{ji} \qquad (3.10)$$

and

$$\tau_{ij} = \tau_{ji} \qquad (3.11)$$

then,

$$A_i.H_i = \sum_{j=1...i-1,i+1...n} W_j.A_i.F_{ij}.\tau_{ij} + E_{b_{cav}}(T_{cav}).A_i.F_{ij}.(1-\tau_{ij}) \qquad (3.12)$$

$$H_i = \sum_{j=1...i-1,i+1...n} W_j.F_{ij}.\tau_{ij} + E_{b_{cav}}(T_{cav}).F_{ij}.(1-\tau_{ij}) \qquad (3.13)$$

$$W_i = \varepsilon_i.E_{b_i} + (1-\varepsilon_i).\sum_{j=1...i-1,i+1...n} W_j.F_{ij}.\tau_{ij} + E_{b_{cav}}(T_{cav}).F_{ij}.(1-\tau_{ij}) \qquad (3.14)$$

Hence for n cavity surfaces there are n simultaneous equations from which all W_i can be found. The radiant heat gains can be considered as heat sources, $\dot{q}''_{r_{si}}$ and can be found from,

$$\dot{q}''_{r_{si}} = \frac{\varepsilon_i(E_{b_i} - W_i)}{(1-\varepsilon_i)} \qquad (3.15)$$

In order to solve these terms, $\dot{q}''_{r_{si}}$ which are substituted into equation (3.2) for the energy balance at surface nodes bounding cavities, it remains to determine view factors F_{ij} and transmissivities τ_{ij}. From the aims (§1.5) these have to be determined for cavities with re-entrant corners and smoke. In §3.2 it was

explained that the cross-string method as used in other models such as TASEF is not able to determine F_{ij} and τ_{ij} for such cavities. Thus the discrete radiation method was selected as the most suitable method. The model scans for internal surfaces by sequentially considering every major node within external surfaces. At each major, a simple search for surface nodes shown Figure 3.7 is undertaken. As each surface node "i" is encountered, the radiation emitted from the surface is simulated as a large number of discrete rays, for example 100-1000, at evenly spaced angular intervals. They are sequentially tracked across the finite difference grid in cavities, until they encounter another surface, say j. The energy of each ray incident at surface j is added to the progressive sum of energies of all rays from i to j. The view factor, F_{ij} is the final sum divided by the sum of all energy radiated from surface i, assuming no absorbing medium such as smoke is present. If an absorbing-emitting medium is present, equation (2.33) is employed during the tracking of each discrete ray. The sum of radiant energy emitted at i and incident on j is the product of transmissivity and the view factor, $\tau_{ij}F_{ij}$. The mathematics of the procedure is outlined below. The ray tracking procedure allows for any arrangement of cavities such as those in Figure 3.11.

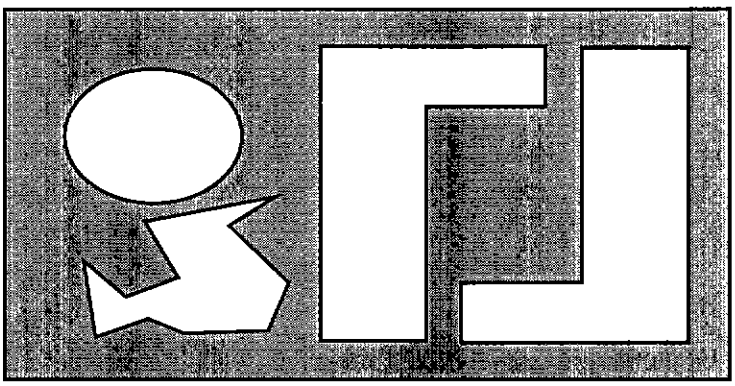

Figure 3.11. Example of an Assembly with Multiple Cavities with Re-entrant Corners of Various Shapes which can be Analysed with the Discrete Radiation Method.

Assuming that rays emitted from surface i can be approximated as emission from a single node without significantly affecting view factors, F_{ij}, and that each ray comprises all wavelengths, from equations (2.18) and (2.24), the intensity of each discrete ray emitted from surface i is,

$$r_i = e.d\theta = I_e.\cos\theta.d\theta \qquad (3.16)$$

where $d\theta = \frac{\pi}{n}$

n = total number of discrete radiation rays emitted from a surface.

Applying equation (2.16) in two dimensions, the emissive power is,

$$E = \int_{-\pi/2}^{\pi/2} I.\cos\theta.d\theta \qquad (3.17)$$

And hence the radiation intensity, I is,

$$I = \frac{E}{2} \qquad (3.18)$$

The discrete radiation emitted from i which is incident on j is thus,

$$\dot{q}''_{ij} = \int_{\substack{\text{integrated over ranges of q}\\ \text{in which rays}\\ \text{from i are incident on j}}} \frac{E}{2}\cos\theta.d\theta \approx \sum_{\substack{\text{summed for all rays}\\ \text{from i incident on j}}} \frac{E}{2}\cos\theta.\frac{\pi}{n} \approx F_{ij}.E \qquad (3.19)$$

Considering that the definition of F_{ij} is the proportion of radiation emitted from i which is incident on j, the view factor, F_{ij} can be approximately obtained from,

$$F_{ij} \approx \sum_{\substack{\text{summed for all rays}\\ \text{from i incident on j}}} \frac{\pi}{2n}\cos\theta \qquad (3.20)$$

From equations (3.20), (2.32) and (2.33), the transmissivity of radiation from surface i to surface j can be found as follows,

$$\tau_{ij} \approx \frac{1}{F_{ij}} . \sum_{\substack{\text{summed for all rays}\\ \text{from i incident on j}}} \frac{\pi}{2n}\cos\theta . e^{-\kappa . x_{ij}} \qquad (3.21)$$

Obviously, the greater the number of discrete rays used to model emission from a surface, the more accurately F_{ij} and τ_{ij} are estimated.

To minimise computation memory and execution time, it is desired to analyse the smallest repeatable portion of a wall. Specular divisions are used to reduce the size of a repeatable portion to a minimum as shown in Figure 3.12. The radiation emitted from h, i and k incident on j in Figure 3.12(a) can be simulated as shown in in Figure 3.12(b). The radiation from h to j can be simulated with specular reflection at e. Similarly, the radiation from k to j can be simulated with reflection at f. ADIDRAS takes

advantage of this simplification by modelling cavity boundaries at the edge of a finite difference grid as specular boundaries.

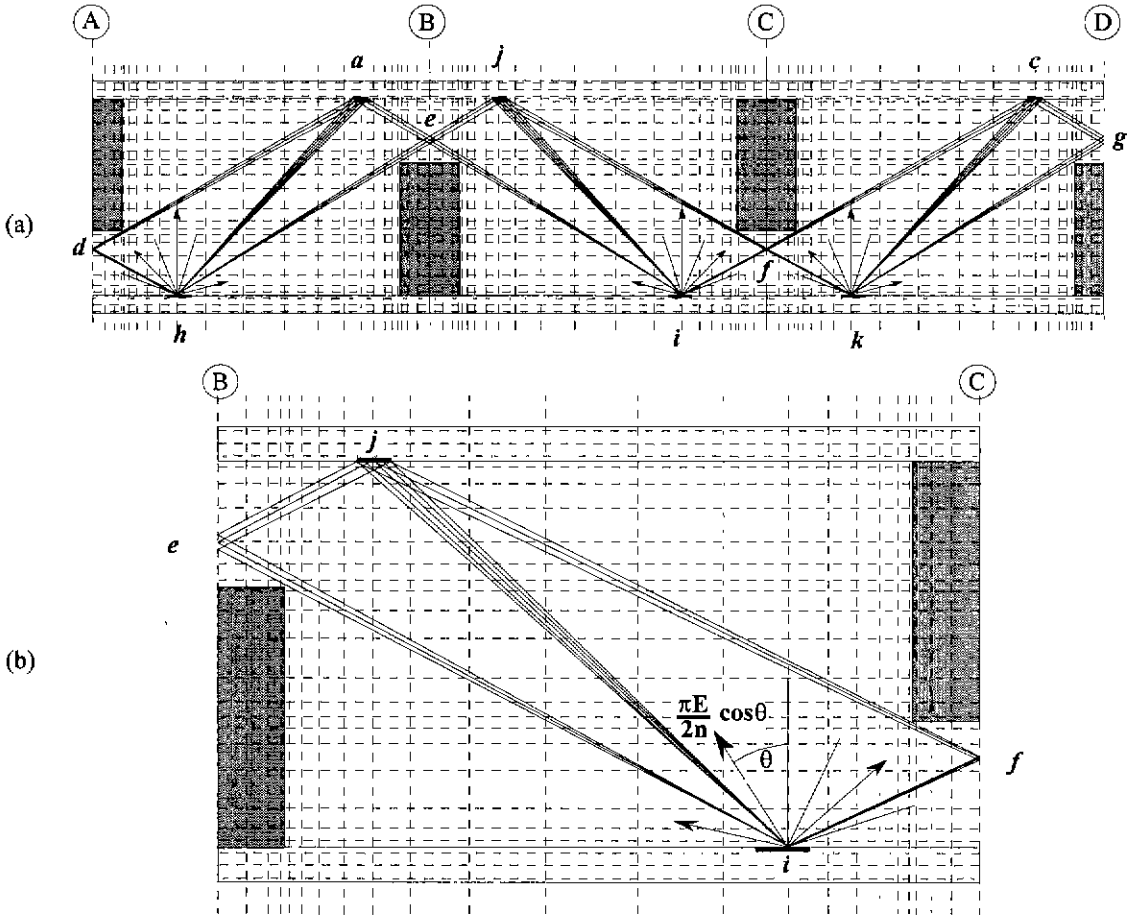

Figure 3.12. Tracking of Discrete Radiation Rays through Cavities, with the Heat Transfer Model, ADIDRAS:

(a) **Total Radiation Incident on j has Cumulative Radiation Contributions from h, i and k in Adjacent Cavity Spaces.**

(b) **Total Radiation Incident on j Found by Considering a Single Cavity Space with Specular Boundaries.**

3.10 Convergence and Conservation Checks of the Numerical Analyses in ADIDRAS

Modelling generally involves some degree of approximation in numerical analyses and assumptions about phenomena to achieve the desired degree of simplification and accuracy. The numerical analyses adopted in ADIDRAS, are validated in this section, §3.10 by checking convergence, energy conservation and by comparing results of ADIDRAS with results from a well used model, TASEF §3.10.4 (Sterner and Wickstrom 1990, Thomas 1997, IEAust 1989) using similar input. The validation of assumptions on

phenomena made in ADIDRAS, is carried out by comparing model predictions with wall furnace experimental results in chapter 5.

Convergence is checked in §3.10.1 by evaluating whether results, particularly temperature distributions with time, asymptote to unique values as discretisation of input variables is refined. The variables which have been discretised in ADIDRAS are distance and time; that is, grid and node spacings, and time steps. Convergence also involves some evaluation of whether the chosen time steps and grid spacings are sufficiently refined to give acceptable accuracy.

Since ADIDRAS is a heat transfer model, and heat is a form of energy, checking of boundary conditions is basically the checking of energy conservation. ADIDRAS involves two general heat transfer analyses – discrete radiation analysis in cavities; and an analysis of thermal conduction across the entire wall section, explicitly incorporating source heat terms from the radiation analysis. Conservation of energy for these analyses is checked in §3.10.2 and §3.10.3, respectively.

The material properties and wall arrangement used in validating the numerical analyses in this section, are those in §5.2, are those estimated for the walls in the experiments undertaken in the research for this thesis.

3.10.1 Convergence

Checking of convergence should demonstrate that the model predictions are independent of the size of the time steps and spacings of grid lines as both of these discretisations approach zero; that is, as the level of refinement is increased (Croft et al 1977). It is apparent from the equations for the model in §3.9 that the convergence of predictions with the level of refinement, is affected by thermal properties. From the properties reviewed in §2.4, it is apparent that the thermal properties of materials in light-timber framed walls vary by an order of magnitude with material type and temperature. Hence, to adequately demonstrate convergence of the model in the research, the checks for convergence should demonstrate independence of grid and time step for the following conditions:

1. A wall section with geometry similar to walls of interest.
2. Thermal properties similar to those of the walls of interest.
3. Points which are in key positions on the heat paths through the wall which critically affect the time of failure.

To satisfy these requirements, convergence was checked for the wall section shown in Figure 3.13. The geometry of this section is very similar to that for walls in the research documented in subsequent chapters in this thesis. The key points A-D are on the path along which most heat travels. This path is

perpendicular to the wall and passes through the cavity. Point E is a key point in the stud. Much less heat is expected to flow into the studs but this heat does critically affect the time of failure.

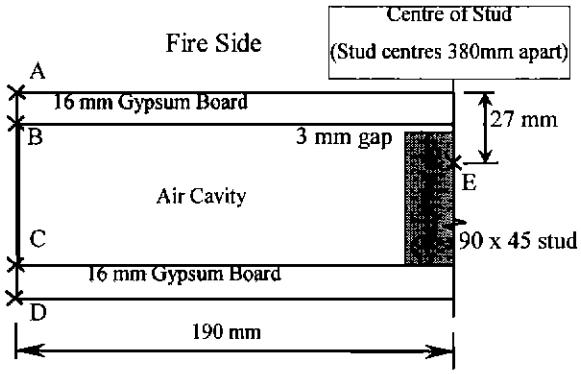

Figure 3.13. Part Horizontal Section through Wall Showing Positions A-E where Convergence of Temperatures is Checked. (Note, the gap is deduced from results in §5.4.3, and is likely due to shrinkage §2.4.3.1)

ADIDRAS was applied for several levels of refinement detailed in Table 3.1. Refinement involved the reductions of the following variables which were explained in detail in the description of the model in §3.5:

1. Time step.
2. The minimum spacing of nodes; that is the distance to the first node next to a surface.
3. The factor for increasing the distance between successive nodes beneath surfaces; that is, the "grid factor".

Croft et al (1977) explain that numerical accuracy of finite difference analysis depends on D/dt^2 where D is the grid spacing and dt is the discrete time step. Hence, successive levels of refinement should approximately reduce the grid spacing by a factor of two and reduce the time step by a factor of four. In the convergence checks undertaken, I, II and III, the grid spacing was reduced by a factor two and the time step was reduced by five. Much accuracy can be gained by close grid spacings near surfaces. Thus a check was also carried for a coarse level of refinement with close grid spacings near surfaces, Ia to optimise computation speed and accuracy.

It is apparent from the results in Table 3.2 that ADIDRAS does converge for the sections and thermal properties of the walls in the experiments for this thesis. It is also apparent from the results in Table 3.3 that the level of refinement, Ia used in the research is numerically accurate to generally within 2%.

Table 3.1. Levels of Refinement of Grids of Nodes Used to Check Convergence of the Heat Transfer Analysis with ADIDRAS, Applied to the Wall in Figure 3.13.

Level of Refinement	Grid N_j x N_k	Approximate Computation time for simulation of one hour of fire exposure (minutes)	Time Step (s)	Ratio between Adjacent Grid Spacings	Minimum Spacing between Grid Lines (mm)
I - coarse	32 x 17	2	5.00	1.50	2.00
Ia - coarse	40 x 20	5	5.00	1.50	1.00
II - medium	55 x 30	20	1.00	1.22	1.00
III - fine	95 x 55	500	0.20	1.10	0.60

Notes:

1. N_j is the number of nodes along a grid line in the plane of the wall.
2. N_k is the number of nodes along a grid line perpendicular through the wall.

Table 3.2. Convergence of Temperatures (°C) at Key Points A-E Shown in Figure 3.13.

time (min)		**10**			**20**			**30**	
refinement	**I**	**II**	**III**	**I**	**II**	**III**	**I**	**II**	**III**
A	516	528	533	705	708	710	798	801	801
B	69	69	69	96	99	101	318	327	332
C	28	28	28	41	42	42	102	105	108
D	21	21	21	29	29	29	44	48	50
E	29	30	30	53	56	56	91	94	95
time (min)		**40**			**50**			**60**	
refinement	**I**	**II**	**III**	**I**	**II**	**III**	**I**	**II**	**III**
A	851	851	851	883	883	884	915	915	916
B	380	385	386	420	426	428	467	471	474
C	162	172	176	237	250	255	316	325	332
D	74	75	76	84	85	85	90	90	91
E	196	199	200	262	272	274	336	346	350

Table 3.3. Table for Judging the Numerical Accuracy of Temperatures (°C) Predicted with ADIDRAS Using the Level of Refinement, Ia Adopted in the Research Described in this Thesis.

time (min)	10			20			30		
refinement	I	Ia	III	I	Ia	III	I	Ia	III
A	516	535	533	705	707	710	798	800	801
B	69	70	69	96	97	101	318	323	332
C	28	28	28	41	42	42	102	103	108
D	21	21	21	29	29	29	44	46	50
E	29	30	30	53	57	56	83	90	95
time (min)	40			50			60		
refinement	I	Ia	III	I	Ia	III	I	Ia	III
A	851	851	851	883	883	884	915	915	916
B	380	383	386	420	424	428	467	468	474
C	154	164	176	237	242	255	316	318	332
D	74	74	76	84	84	85	90	90	91
E	180	191	200	262	274	274	336	351	350

Note. Points A-E shown in Figure 3.13.

3.10.2 Conservation of Energy in Radiant Heat Transfer Across Cavity

The following checks were carried out to ensure conservation of heat energy in the radiation model (§3.9.5), and to ensure accuracy of the view factors determined:

1. The sum of all view factors for any surface node should be 1.00.
2. There were a sufficient number of discrete rays from each surface node, ensuring acceptable accuracy for the computed view factors.
3. The net overall radiant heat exchange among cavitiy surfaces, results in no net creation of heat.

These checks were carried out for the wall in Figure 3.13, thereby demonstrating the numerical efficacy of the model for analysing radiant heat transfer across walls with re-entrant cavities.

All view factors were summed for each cavity surface node. All sums equalled one, to at least 6 significant figures. The first check was satisifed.

The accuracy of view factors and the sufficiency of refinement of radiation discretisation was evaluated for the surface nodes indicated in Figure 3.14 which is another view of the wall in Figure 3.13. In particular, the view factors for radiation emitted from node 21 and incident on nodes 1-20 were considered. Three levels of refinement were considered in discretising the radiation emitted from node 21. Radiation from node 21 was discretised, for these levels, into 100, 500 and 1000 rays. The view factors determined by the radiation model, are shown in Table 3.4.

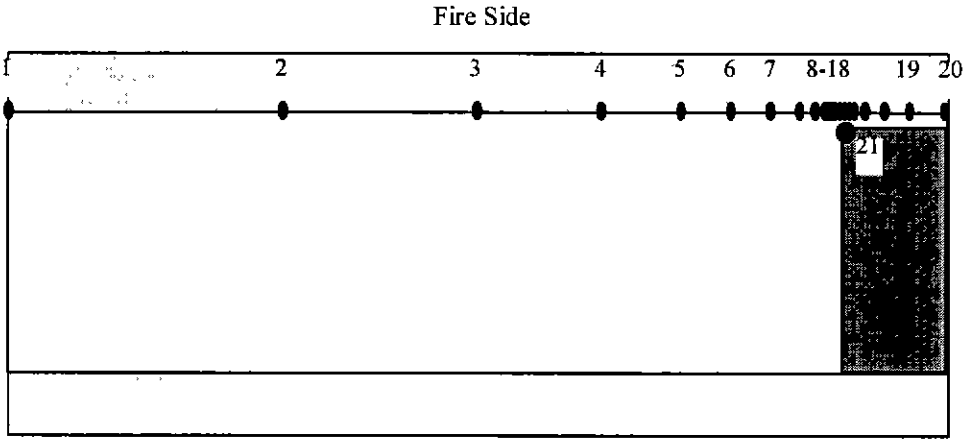

Figure 3.14. Surface Nodes Referenced in Table 3.4, for the Wall Section in Figure 3.13.
(Node 13 is immediately opposite node 21.)

In Table 3.4, as the number of discrete radiation rays increases from 100 to 500, the accuracy of view factors improves by approximately 10% on average. As the number of rays increases from 500 to 1000, the accuracy of view factors impoves by 1-2% on average. Convergence is apparent and at least 500 rays are required to achieve acceptable accuracy for the view factors. 1000 rays were adopted for the analyses by ADIDRAS in §5.

Analysis must not only converge to give a precise indication of view factors, but the matrix of view factors for all radiant exchanges between all surface nodes around a fully enclosed cavity, must also lead to no net heat gain after the exchange of radiation, irrespective of what the initial distribution of surface temperatures may be. The heat gains for several analyses of the wall in Figure 3.14 were determined for three levels of grid refinement at the 60^{th} minute of exposure to heat. Radiation emitted from each surface node was discretised into 1000 rays. The heat gains were compared with the summation of the absolute values of all radiant heat exchanges between surface nodes. This comparison is shown in Table 3.5. For the coarse grid the heat gain was approximately 2% of the sum of the absolute values of all radiant heat exchanges between the surface nodes. The fine grid led to a heat gain of 0.23%. Different levels of

discretisation were tried – 100, 500 and 1000 rays per node – but made no discernable difference to the heat gain. The heat gain was solely a function of the number of nodes around the surface of the cavity.

Table 3.4. View Factors for Different Total Numbers of Discrete Radiation Rays Emitted from Node 21 to Surface Nodes 1-20 Shown in Figure 3.14.

Surface Nodes	Distance (mm) from Node 1	View Factors for Radiation from Node 21 to Surface Nodes 1-20		
		Number of Discrete Rays Emitted from each Surface Node		
		100 File r100x0_O HT0	500 File r500x0_O HT0	1000 File r1000med1t_o ht0
1	0	0.0065	0.0037	0.0031
2	56	0.0000	0.0061	0.0074
3	94	0.0116	0.0075	0.0074
4	119	0.0069	0.0099	0.0099
5	136	0.0171	0.0157	0.0147
6	147	0.0238	0.0219	0.0238
7	154	0.0330	0.0356	0.0353
8	159	0.0590	0.0528	0.0504
9	162	0.0744	0.0789	0.0801
10	165	0.1130	0.1190	0.1210
11	166	0.1550	0.1420	0.1420
12	167	0.1240	0.1370	0.1370
13	168	0.1170	0.1160	0.1160
14	169	0.1130	0.1070	0.1060
15	170	0.0919	0.0919	0.0912
16	171	0.0456	0.0456	0.0461
17	173	0.0089	0.0089	0.0092
18	177	0.0000	0.0000	0.0000
19	182	0.0000	0.0000	0.0000
20	190	0.0000	0.0000	0.0000

Table 3.5. Effect of Refinement of Discretisation of Emission Around Cavity Surfaces, on Accuracy of Radiation Heat Balance at the 60th Minute of Fire Exposure.

Level of Refinement File (Detailed in Table 3.1)	Radiation Heat Balance / Sum of Absolute Values of all Radiation from Surface Nodes File numchk xls(sheet 2)
Coarse sy_t10_**	2.06%
Medium sy_t2_**	0.98%
Fine sy_t1_*.*	0.23%

The cause for heat gain varying inversely with the number of surface nodes can be explained with reference to Figure 3.15. The radiation heat transfer between surfaces is modelled in ADIDRAS as shown in Figure 3.15(a). The model is based on the simplifying assumption that the proportion of emitted radiation, from every point on a surface apportioned to a surface node, which is incident on surface j, is the same. The larger the surfaces, such as the surfaces apportioned to nodes 1, 2 and 3 in Figure 3.14, the larger will be the inaccuracies resulting from the simplification. A more precise discretisation is that shown in Figure 3.15(b) which involves the use of more emission nodes i_1-i_3.

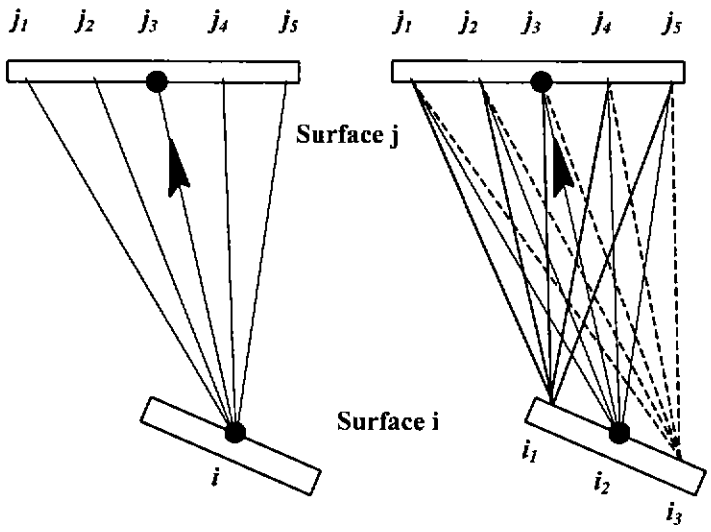

Figure 3.15. (a) Method of Radiation Discretisation Adopted in ADIDRAS. (b) More Accurate Method of Radiation Discretisation

3.10.3 Conservation of Energy Over Entire Wall Cross-Section

The conservation of energy was checked by comparing the total heat input at the boundaries, with the total enthalpy rise in the wall section. The heat input on the fire side boundary and the heat removed from the ambient side boundary are found from the terms, $\dot{q}''_{bound}$ solved from equation (3.1). The solved terms are summed over all boundary nodes and the time steps of interest. The total enthalpy is q_{stor_b} obtained from equation (3.5), summed over all major nodes. The percentage difference between total heat input at the boundaries with the total enthalpy rise is shown in Figure 3.16. Two plots are shown. One is for the difference determined for the current time step, and the other is for the difference over all time steps from the beginning of the fire. It is apparent that the difference is generally less than 0.5% which is acceptable compared with the uncertainties which would be expected for such variables as thermal properties, fire severity and others. Most of the difference is likely to be due to the small net heat gain in radiation transfer across the cavity, apparent in Table 3.5.

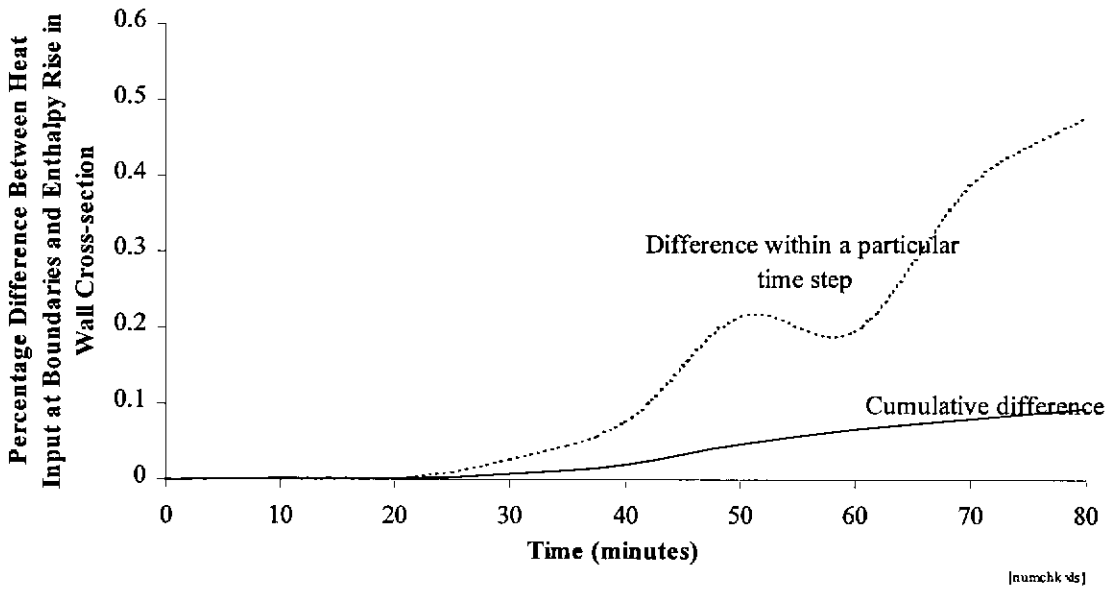

Figure 3.16. Heat Imbalance Across Entire Wall Section Measured as Percentage Difference between Total Rise in Enthalpy in Wall Cross-section and Heat Input at Boundaries.

3.10.4 Comparison with Results from TASEF

As part of the validation of numerical analyses in ADIDRAS, comparison of results with those from a well used model, TASEF (§2.5.5) were made.

Figure 3.17 shows temperature versus time results from TASEF (Sterner and Wickstrom 1990) and ADIDRAS, as well as results from experiments described in §4. The results are for temperatures at points C7X and S8 shown in the inset diagram of a wall section in the figure.

The upper lines of the figure are for C7X. Using a "coarse" grid (Table 3.1) TASEF compared with ADIDRAS makes a substantially greater overestimate of temperatures in relation to the experimental results. Use of a "medium" grid (Table 3.1) in ADIDRAS improves estimates of temperatures in relation to the experimental results. One plot is for the temperature on the surface of the gypsum board on the fire side of the gap, and lies just above the experimental results. The other plot is for temperature on the surface of the timber stud on the other side of the gap, and lies just below the experimental results. These two plots obtained by using ADIDRAS with a medium grid are in the positions expected with respect to the experimental results. The reason for the better predictions of ADIDRAS is its ability to analyse heat transfer across cavities with re-entrant corners. TASEF does not have such scope and thus does not model the substantial efflux of radiant heat from the gap to the cavity at temperatures above 350°C.

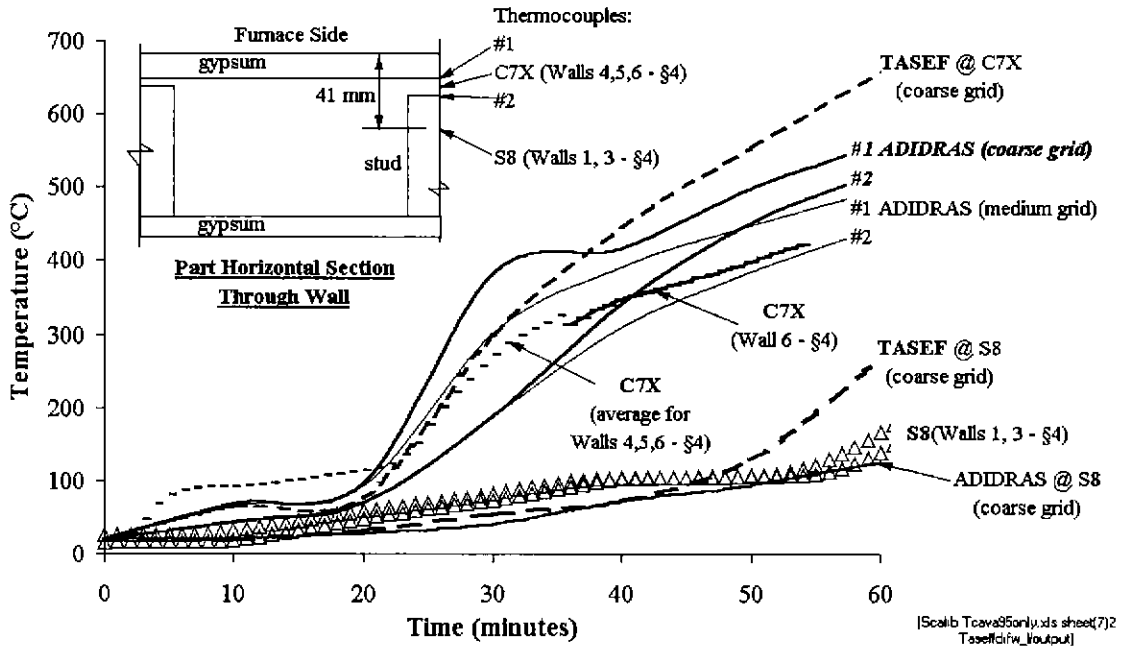

Figure 3.17. Comparison of Predictions with ADIDRAS (allowing for char shrinkage Figure 2.10) with Predictions with TASEF (Sterner and Wickstrom 1990) and Experimental Results at C7X and S8 Obtained from Experiments Described in §4. (Note that "coarse" and "medium" grids are defined in Table 3.1)

The lower lines are plots of temperature versus time in the stud at point S8. The overestimate of temperature predictions of TASEF is apparent from 50 minutes onwards. There is a good comparison between the results of ADIDRAS and experiments.

The above further checks whether the numerical analyses in ADIDRAS are consistent with convergence, conservation and have reasonable accuracy. Validation of whether the modelling of phenomena in ADIDRAS is satisfactory will be carried out in §5.

3.11 Summary

ADIDRAS, a heat transfer model for light-timber framed walls in fire, has been written and checked for conservation of energy and convergence. Validation against experimental results remains to be undertaken in the next chapters, §4 and §5. In the heat transfer model, thermal conduction is modelled with an alternating direction implicit finite difference method (§3.2) to achieve speed and robustness of computation. Radiant heat transfer at external surfaces is modelled implicitly with linearised equations for one-dimensional transfer of heat between surfaces and surrounding gas (§3.9.2). Radiant heat transfer across cavities is modelled two-dimensionally with the discrete radiant heat transfer method (§3.9.5). Convection is modelled simply with Newton's Law of Cooling (equation 2.7) which is appropriate since convection is not a dominant mode of heat transfer. The model has been written for a wide range of wall sections with and without re-entrant cavities including ordinary cavity walls, staggered and double stud walls and walls with any gaps between components of the wall.

4. Wall Furnace Experiments

4.1 General Overview and Aims of Experiments

Given in this chapter are the relevant details and records of a program of eight wall furnace experiments undertaken to provide data to validate models for heat transfer, structural response and time of failure. Extensive details and records of the experiments are documented in Clancy and Young (1996b) where Clancy's focus was on heat transfer and time of failure, and Young's focus was on structural response.

The aims of the experiments with regards to heat transfer were as follows:

1. To establish reproducible procedures for the measurement of temperatures in light-timber framed walls with time. The effects on measured temperatures due to any variations in the procedures must be insignificant compared with effects on temperatures due to variations in the thermal properties of materials in the walls.
2. To repeat experiments so that means and coefficients of variation of thermal properties of materials in walls can be deduced from a number of temperature measurements at similar positions.
3. To obtain data for checking modelling assumptions given in §3.2; namely that:
    (a) Heat transfer is two dimensional; that is, temperature does not vary in the vertical direction at any time.
    (b) Temperatures are the same at similar points in studs, sheeting and cavities, in horizontal sections through walls.
    (c) Evidence that convective in heat transfer through cavities and at the surface on the furnace side of walls is not a dominant mode of heat transfer.
    (d) Heat transfer through gypsum board and timber can be modelled with thermal conduction, without consideration given to the transfer of moisture or vapour.
4. Obtain data for the purpose of validating heat transfer models, including temperature measurements in the furnace, on the surface of gypsum boards, in cavities and in timber framing. As well as temperatures, the measurement of initial density and moisture contents of timber was desired.
5. Observe the thermal degradation of timber near supports compared with timber elsewhere in the frames to determine the requirements for heat transfer modelling of the timber frame in this region.
6. Observe characteristics of thermal degradation of walls, at the stage of structural collapse, so that modelling assumptions at this stage can be validated

The experimental work involved:

1. The assembly of light-timber wall frames at the laboratories of CSIRO, Division of Building Construction and Engineering, Graham Road, Highett, Melbourne.
2. The conduct of wall furnace experiments at BHP Research - Melbourne Laboratories. Engineering and Scientific Research. Mulgrave, Melbourne.

Given in Figure 4.1 to Figure 4.6 is an overview of the experimental work undertaken. The timber frames were similar to that shown in Figure 4.1. The gypsum boards were not nailed to the timber frames until they were transferred and mounted in steel frames at BHP-Research Laboratories. Figure 4.2 shows the placement of thermocouples prior to nailing on the final gypsum boards. Next, the completed walls in the steel frames were wheeled against the furnace at BHP as shown in Figure 4.3. After the walls were secured against the furnace, the thermocouple wires shown in Figure 4.4 were attached to data acquisition computers shown at the left in Figure 4.6. The typical condition of exposed surfaces of walls wheeled away from the furnace after experiments is shown in Figure 4.5. Further experimental details and results are given in the remainder of this chapter, §4.

Given in the remainder of this chapter are descriptions of the construction of walls (§4.2), temperature measurement apparatus (§4.3) and experimental procedures (§4.4). Observations are detailed in §4.5, and results for temperature versus time at key points are plotted in §4.6. Evaluation and conclusions obtained from the experiments are given in §4.7.

4.2 Construction of Walls

Details of the construction of each wall are shown in Figure 4.7. The walls were 3.00 metres high comprising five studs of kiln dried radiata pine 45 x 90 mm in cross-section, spaced at 380 mm between centres. The noggings were also radiata pine of the same cross-section and were placed at 1200 mm and 2400mm above the bottom of the walls. A single layer of 16mm thick Firestop gypsum board (Boral 1997) was placed on each side of the walls and nailed as detailed in Note 6 of Figure 4.7. All sheets of gypsum board were placed horizontally to minimise charring of studs if the gypsum boards shrank, and opened up gaps in butt-joints over studs. After placement of the sheets, the butted joints were covered with paper tape, gypsum paste and trowelled smooth as shown in Figure 4.8. This covering is referred to as stopping or caulking.

The reasons for the selection of these construction details are as follows. A maximum number of studs in each wall was desirable to promote load sharing and reproducibility of times of failure which was an aim

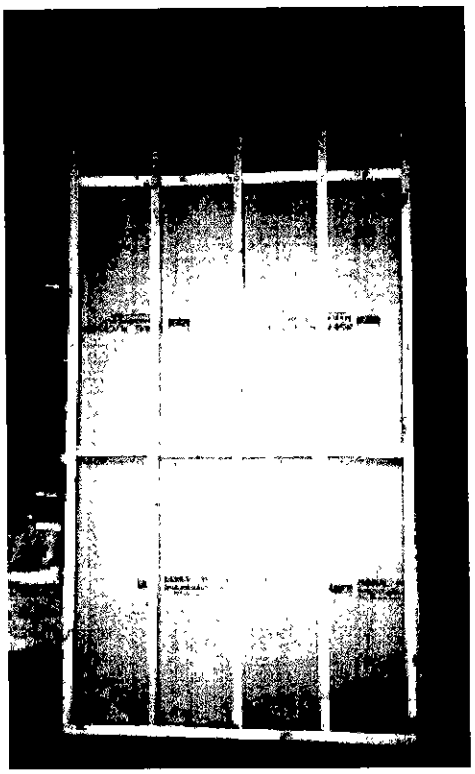

Figure 4.1. Timber Frame with Gypsum Board Fastened to One Side. (Outer studs not yet cut at mid-height and bottom as shown in Figure 4.7.)

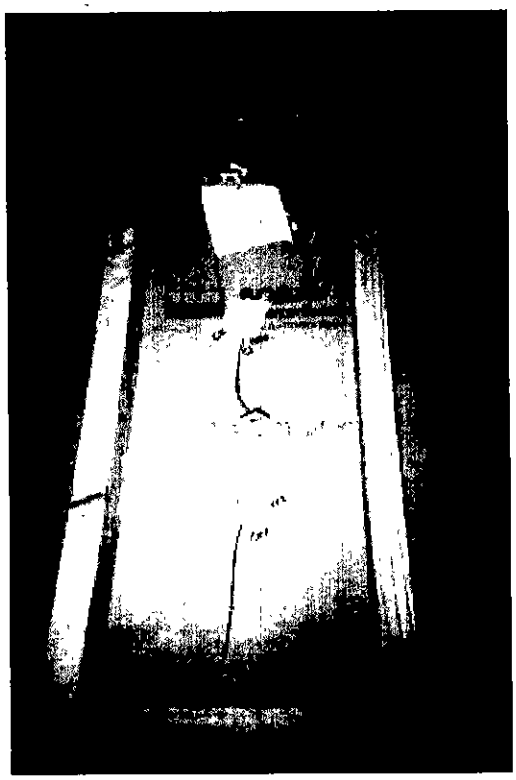

Figure 4.2. Thermocouples Placed in the Cavity while Gypsum Board on One Side Only. (Thermocouple shielded by tube at top.)

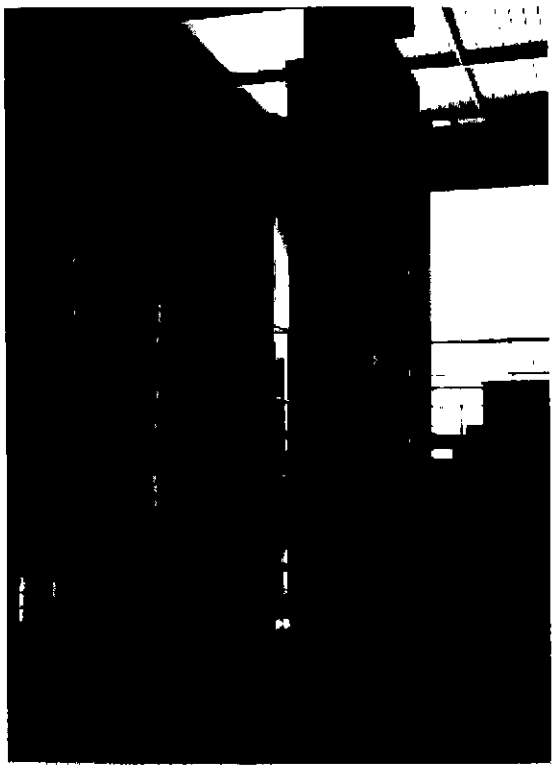

Figure 4.3. Wall in Steel Frame Being Wheeled to Face of Furnace.

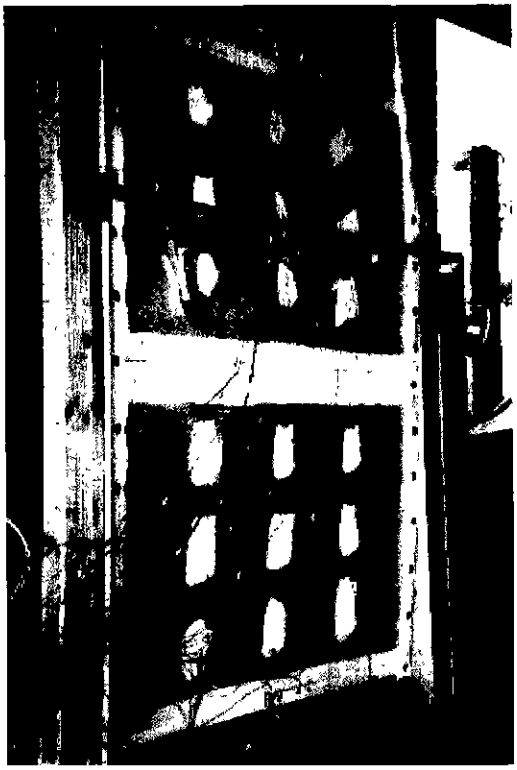

Figure 4.4. Wall Failing Structurally at the End of a Furnace Experiment.

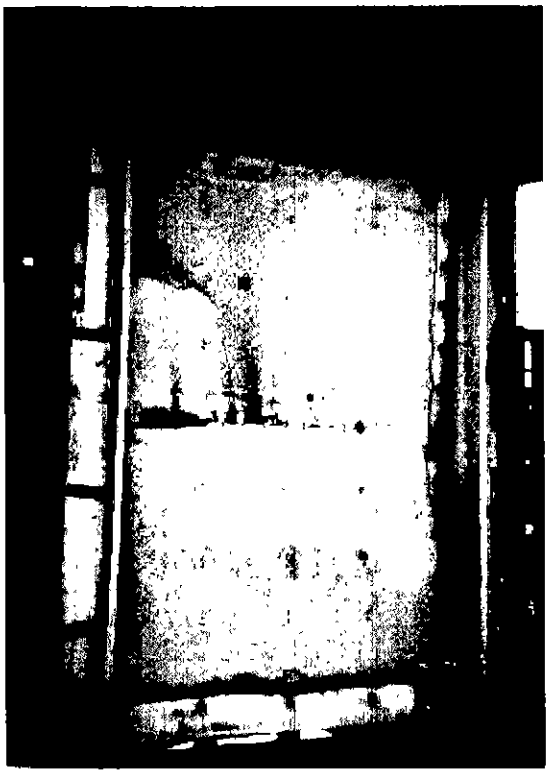

Figure 4.5. View of 16 mm Thick Gypsum Board on Fire Side Immediately after 60 minutes of Standard Fire Exposure.

Figure 4.6. View of Wall, Furnace and Data Aquisition Equipment in Laboratory .

of the experimental program (§4.1). It was also desirable that the spacing between studs be reasonably similar to spacings in conventional timber framed walls. The maximum total of five studs per wall seemed to be the best compromise. The 380 mm spacing between stud centres was somewhat less than conventional spacings of 450 and 600mm (Boral 1997), but led to three studs exposed to the furnace under similar heating conditions. The outer studs, 1 and 5 in Figure 4.7 experienced heat from a cavity on one side only, compared with the inner three studs, 2-4 which were heated from cavities on two sides. Since the heat conditions for outer studs was substantially less severe and thus not the same as that for the three inner studs, the outer studs were structurally isolated. Collier (1992) established the procedure of cutting the outer studs to achieve structural isolation. Young (1996c) showed that at least three cuts - top, middle and bottom are required to overcome lateral support from straight segments of outer studs to inner studs through the resistance of gypsum boards to double curvature.

Studs were chosen with the following details to achieve reproducible experimental results, in accordance with the first aim in §4.1. All studs were the same species, radiata pine. The selection was restricted to a minimum total density of 400 $kg.m^{-3}$ and lengths of timber with no machine grade markings indicating strength grades less than F8 (AS1720.1). F8 is a common building grade in Australia that has a short duration design elastic modulus of 9100 MPa - the dominant mechanical property determining the strength of walls. The average densities of the studs are shown in Table 4.1. Young obtained these by simply measuring weights of studs and dividing by their volume. The moisture content was measured with a moisture meter and was consistently $12 \pm 0.5\%$ among ten lengths of timber chosen randomly. Young (1996d) confirmed this measurement by comparing weights of samples before and after oven drying. A sufficiently large batch of timber studs, having the above characteristics, was gathered to build all of the walls in the experiments. With the aim of ensuring similar times of structural collapse for similar wall experiments, studs were chosen so that each wall had similar strength in resisting vertical loads. Similar strengths for each wall were obtained by selecting one of the studs 2, 3 or 4 in Figure 4.7 from the lower third of elasticities, one from the middle third and one from the upper third. The average densities recorded for each stud, 2, 3 and 4 is shown in Table 4.1.

The noggings were located so as to back and seal butt-joints between sheets of gypsum board. Sealing of the joints in this manner helped minimise the amount of heat transferred into cavities through joints - a mechanism of heat transer which is ignored in ADIDRAS (§3.2).

A thickness of 16mm for gypsum boards was chosen since this thickness is representative of walls currently rated (Boral 1997) for one hour fire resistance to AS1530.4.

Insulated cavities and alternative stud arrangements were excluded from the scope so as to provide experimental data for thorough validation of the heat transfer model and Young's (1999) structural

response model for ordinary cavity walls. Experiments on walls with insulated cavities and alternative stud arrangements is recommended for further research.

Table 4.1. Average Densities, ρ of Studs at Ambient Conditions Prior to Furnace Exposure.

Wall	ρ_2 ($kg.m^{-3}$)	ρ_3 ($kg.m^{-3}$)	ρ_4 ($kg.m^{-3}$)	$\rho_{2,3,4}$ ($kg.m^{-3}$)
1	507	454	510	490
2	477	421	467	455
3	494	501	487	494
4	431	467	488	462
5	484	496	405	461
6	434	437	486	452
7	513	488	463	488
8	484	438	504	475

Notes:

1. Densities are the average over the entire length and over all studs indicated by the subscripts.
2. Subscripts, 2 3 and 4, indicate stud numbers shown in Figure 4.7.
3. Densities are the measured weight of stud (including moisture) divided by the volume of the stud at the beginning of the experiment.

4.3 Experimental Apparatus

The main experimental apparatus was a furnace (Figure 4.3-Figure 4.6) and thermocouples which were attached to the surfaces of gypsum board, placed in cavities (Figure 4.2 and Figure 4.4) and placed within timber framing. Special attention was given to seals (Figure 4.4) placed around walls, to allow movement during thermal degradation without significant escape of heat through the seals.

The furnace was the full height but half the width of the standard size specified in AS1530.4. The internal clear dimensions were approximately a height of 3000 mm by a width of 1575 mm. The furnace was gas fired and lined with ceramic fibre insulation. It had a window at mid-height on one of its narrow sides perpendicular to the opening for exposing walls to furnace fire. For all experiments, temperatures were measured in the furnace at the positions F7-10 indicated in Figure 4.9. These were contained within protective metal sheaths protruding from the back of the furnace. To overcome the time lag for

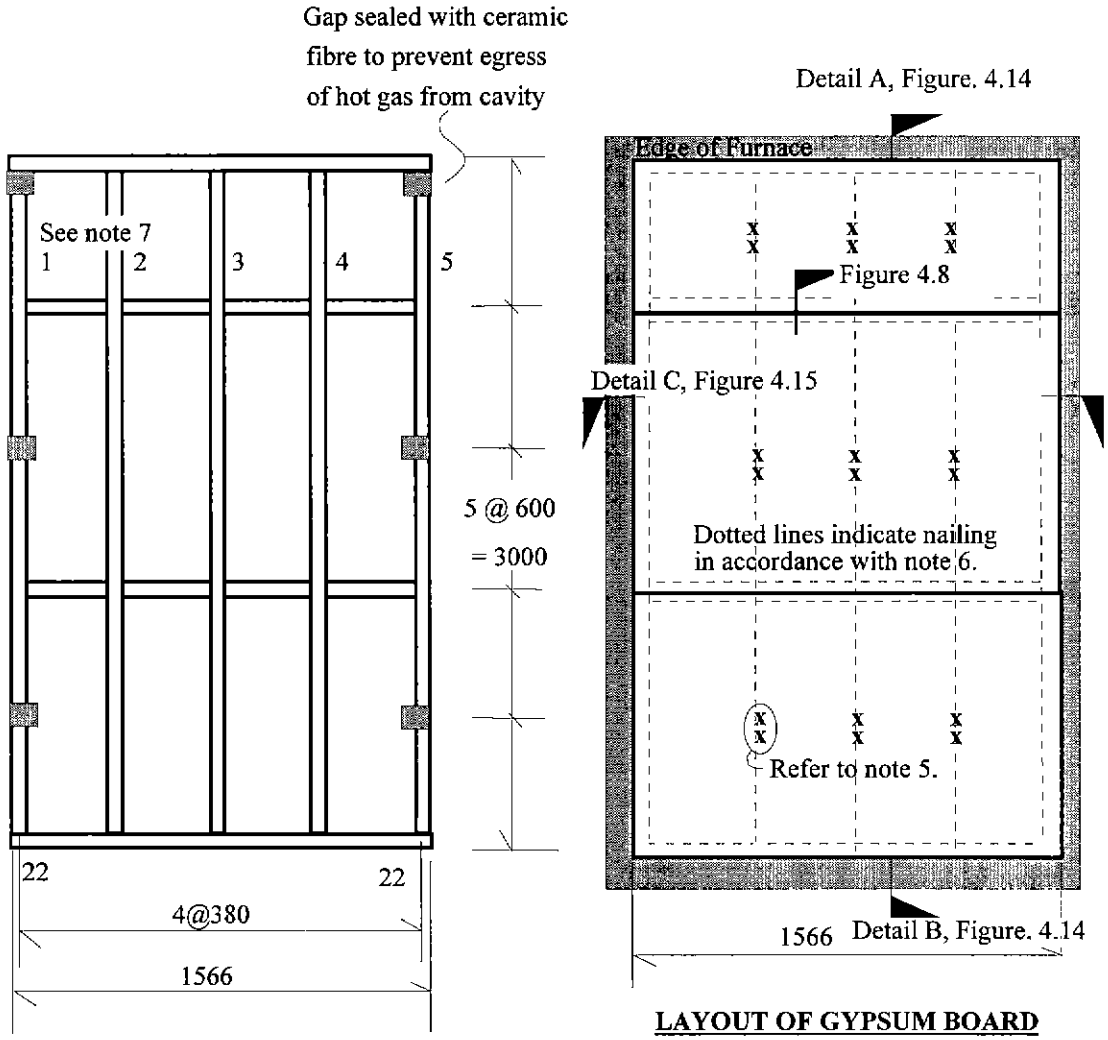

ELEVATION OF WALL FRAME

LAYOUT OF GYPSUM BOARD EACH SIDE OF WALL and references to DETAILS BETWEEN WALL & FURNACE

Notes:

1. All dimensions in millimetres.
2. All timber framing, 90x45 mm radiata pine of consistent stress grade F8 (refer to AS1748)
3. All joining of members in accordance with the Victorian Timber Framing Manual (1994)
4. All gypsum board 16mm thick manufactured for fire rated panels.
5. The perimeters of walls were caulked with gypsum paste.
6. Gypsum board fully fastened with 50x2.8mm nails @100mm around perimeter, and double nailed @300mm elsewhere along studs and noggings; except on ambient side for Walls 7 & 8, minimal fastening with pairs of nails at positions indicated, x x
7. Numbers 2-4 indicate stud numbers with respect to ambient side, in Table 4.1.

Figure 4.7. Elevations of Typical Light-Timber Framed Wall in Furnace Experiments.

thermocouples to measure furnace temperatures at the beginning of experiments when temperature changes were rapid, the tips of thermocouples were moved out beyond their protective sheaths. After ten minutes, the thermocouples were retracted into their protective sheaths. Additional thermocouples F1-6 were used in experiments 7 and 8 as shown in Figure 4.13 to more accurately evaluate the heat exposure of surfaces of walls in the experiments.

All thermocouples were K type and were constructed in accordance with the requirements of AS1530.4. Most installed thermocouples were 2.4-3.0 mm in diameter, and had fibreglass insulation sheathing over the wires. The thermocouple junctions at the ends of these fibreglass insulated wires were made after cutting off all wire exposed to elevated temperatures in previous experiments. From the experience of laboratory personnel, the glass insulated thermocouples, when exposed to elevated temperature for just one experiment, could reliably measure temperatures up to approximately 600°C without short-circuiting. Where lengths of thermocouple wire were expected to be directly exposed to furnace temperatures greater than 600°C, thermocouples with ceramic fibre insulation were used and could reliably withstand temperatures up to 1300°C. All thermocouple wires were made long enough to be connected directly to the data acquisition equipment and to allow re-use after heat affected lengths were cut off at the end of the each wall experiment.

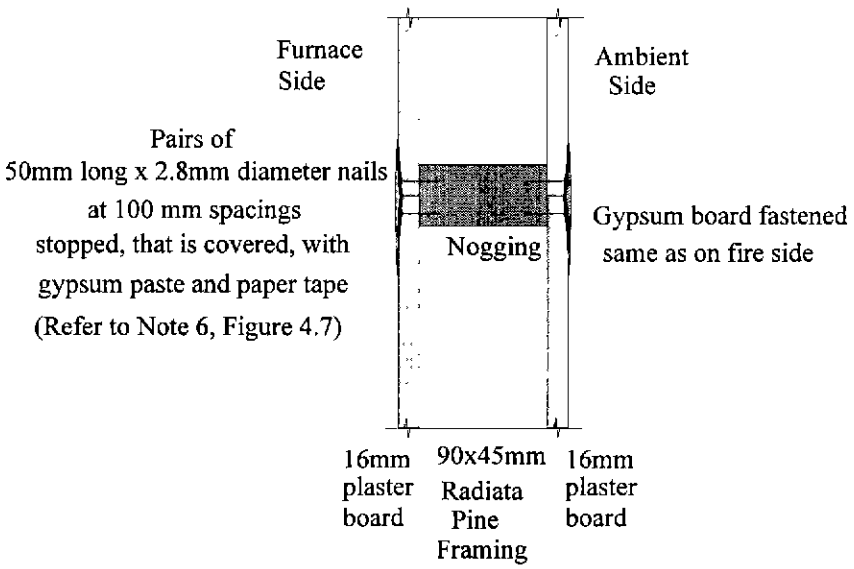

Figure 4.8. Nailing of Gypsum Board at Joints Between Sheets.

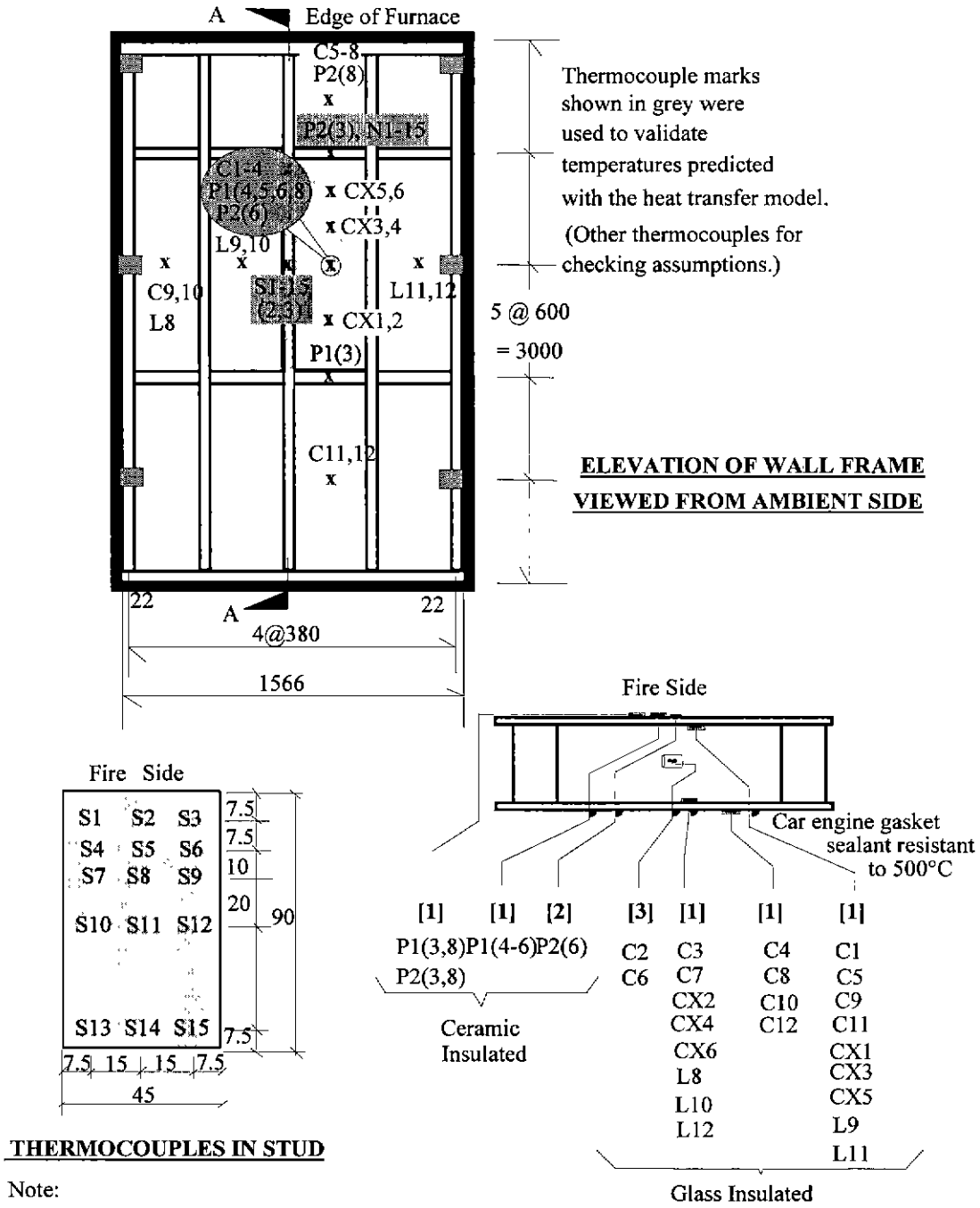

Note:

Further Details Shown in Figure 4.12.

Thermocouples N1-15 in noggings in the same position as S1-S15.

[1] Surface thermocouple with pad and copper disc (Figure 4.10)

[2] Surface thermocouple with copper disc, no calcium silicate pad

[3] Cavity thermocouple shielded in a tube (Figure 4.11).

Figure 4.9. Location of Thermocouples in Wall Experiments 1-8.

(Where thermocouples were limited to particular experiments, the numbers of these experiments are shown in brackets.)

Thermocouples were placed to provide an intensive distribution of readings in the centre of the wall to validate the heat transfer model, ADIDRAS in accordance with aims 2-4, §4.1. Temperatures were measured in the central cavity, and in a stud and nogging bounding the cavity shown shaded in grey in Figure 4.9. Thermocouples were arranged vertically within the central cavity to monitor any vertical variation in temperature possibly due to convection (thermocouples CX1-6 and C1,3 in Figure 4.24 and Figure 4.25). Thermocouples were placed in both the studs and noggings in two experiments which involved non-loadbearing walls. In subsequent wall experiments, most of which were loadbearing, thermocouples were placed in the noggings, but not in the studs, so as not to affect load capacity. Comparisons between the temperatures in the noggings and studs in the first three experiments enabled stud temperatures in subsequent experiments to be evaluated from the temperatures recorded in the noggings.

Thermocouples were also placed sparsely across the extent of walls to obtain temperature measurements to validate the assumptions in aim 2 §4.1, made in ADIDRAS. To validate these assumptions, thermocouples were arranged to monitor the temperature distribution vertically (C1,4,5,8,11 and 12 in Figure 4.18-p124) and horizontally (C9,1,3 and L9,11,8,10,12 in Figure 4.19-p124) across the walls in the experiments. Readings from all thermocouples were recorded with computer data aquisition equipment at one minute intervals.

Surface temperatures were measured with disc thermocouples (Figure 4.10). Copper discs were soldered to the ends of thermocouple wires. The discs were secured to wall surfaces with the insertion of small steel pins. The discs were covered with calcium silicate pads in accordance with AS1530.4. The edges of covers were glued to surfaces with calcium silicate. To gauge effects from the pads, thermocouple P2 in Wall 6 was mounted without one.

As shown in Figure 4.11, cavity temperatures were measured with thermocouples placed in open 50 mm diameter steel tubes wrapped in ceramic fibre to ensure that the thermocouples measured the temperature of the air in the cavity without additional incident heat of radiation on the thermocouple. It would have been desirable to have some device to move cavity air through the tube to ensure that the general temperature of the air in the cavity was being measured rather than possibly stagnant air in the tube. However, obtaining appropriate apparatus was not possible within time and budget constraints.

Temperatures in timber were measured in a similar manner established by Collier (1991,93), as shown in Figure 4.12. An alternative method is to insert a thermocouple in a hole drilled perpendicularly to the surface and secure it with glue (Gardner and Syme 1991). There are several advantages of Collier's method. The last 60mm of the thermocouple wire is parallel with isotherms. Consequently, there is no heat flow along the thermocouple wire and thus the temperature of the tip of the thermocouple is the

same as the wood in contact with it. Collier's method also allows much tolerance in the placement of a thermocouple, compared with the use of a perpendicular hole which is much more likely to have a considerable temperature gradient. In the presence of such a gradient, an error of just 1 mm in the placement of the tip of the thermocouple can lead to an error of 50°C or more.

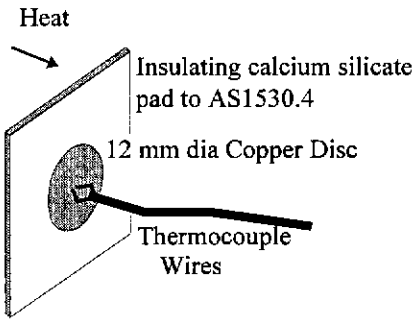

Figure 4.10. Surface Thermocouple Comprising Copper Disc and Pad.

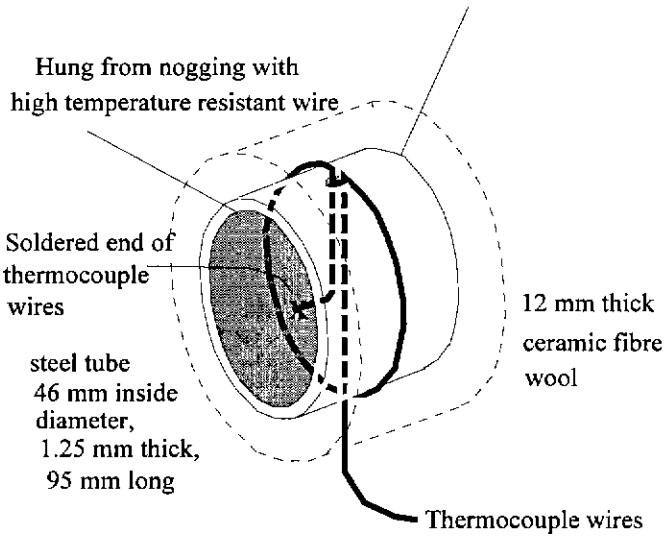

Figure 4.11. Thermocouple Shielded within Steel Tube.

Several modifications to Collier's method of measuring temperatures in timber were undertaken. Collier used isolated blocks of wood which contained the thermocouples. He referred to these as "dummy studs". He placed these vertically and centrally in cavities. This arrangement locally reduced the clear width of the cavity between wood surfaces but it is unlikely that it would have affected temperatures in timber because of large aspect ratio of his cavities; that is, 555/90 which is approximately, 6. The spacing between studs in these experiments (Table 4.2) was 380mm between centres (Figure 4.7) which was possibly close enough for dummy studs to affect temperatures of adjacent timber studs. It was decided to put thermocouples into the studs in the non-loadbearing walls 1 and 2, and into the noggings of all walls. The aim was to show that noggings had similar temperature distributions to studs and could be thermocoupled instead of dummy studs.

Another modification to Collier's arrangement for measuring temperatures in timber was to use calcium silicate glue instead of epoxy glue, because calcium silicate is more resistant to high temperatures. Collier (1994) advised that above 200°C, epoxy liquefies. From preliminary work, it was found that dried calcium silicate tends to be brittle, can be broken by hand and can dry with mud-cracking. To overcome

these shortcomings screws were used to reinforce and secure the connection between the faces cut at 60°. These screws were placed clear of thermocouple wire and on the ambient side where thermal gradients were low so as not to have a significant effect on the temperature distribution in the surrounding wood.

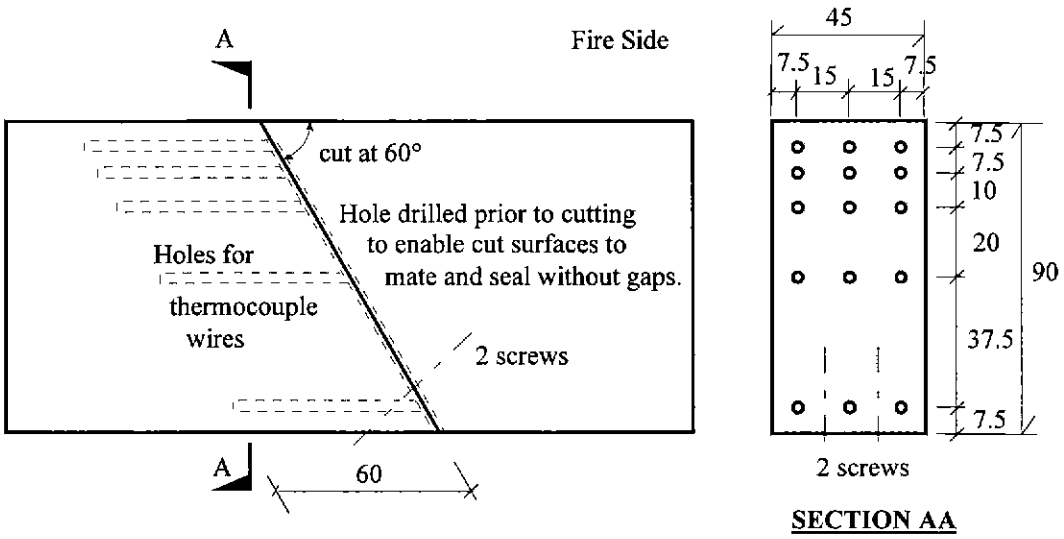

Figure 4.12. Typical Details of Timber Nogging used for Temperature Measurement.

The apparatus involved in mounting walls against the furnace is shown in Figure 4.14 and Figure 4.15. Figure 4.14 shows that walls were mounted in steel frames with sections comprising a composite pair of angles toe-to-toe. The light-timber framed walls in experiments were secured with coach screws connecting top and bottom plates to steel supporting plates. Grooves in the steel plates enabled these to be pinned into position with small angles welded to plates bolted to the steel frame. The bolts could be finely adjusted to set the vertical position of the steel plates and to accommodate the exact height of timber walls. The eccentricity of the pin supports was 10 mm towards the furnace. It was thought that this eccentricity would be similar to that imposed on timber framed walls in construction of several storeys. This eccentricity ensured that walls in experiments deflected away from the furnace, that is, in the same direction as timber framed walls usually fail when exposed to fire. Eccentricity away from the furnace would not have been desirable because it would initially lead to some deflection towards the furnace which may or may not be finally countered with deflection away from the furnace. Increased variability in times of structural collapse may have resulted. When full rotational fixity was desired at the top and bottom (Wall 6 - Table 4.2) rather than pinned supports, steel packing was inserted to prevent rotation of steel supporting plates. Sealing along top and bottom edges of walls against the furnace was achieved with 25 mm thick ceramic fibre wool. Figure 4.15 shows that the space between vertical edge of steel frame and the wall was packed with gypsum board covered timber framing "a-e". The side edges of the steel frame and furnace were sealed with ceramic fibre wool and 25 mm thick gypsum board. Ceramic

fibre wool was attached to both the furnace side and the ambient side of vertical wall edges to form "wiper" seals against the 25 mm thick gypsum board. The 25mm thick gypsum board extended 150 mm beyond the ambient face of the wall. The wiper seals and the 25mm thick gypsum board ensured that the seal to the vertical edges of the walls was maintained and prevented any significant egress of heat past the edges of the walls while they deflected.

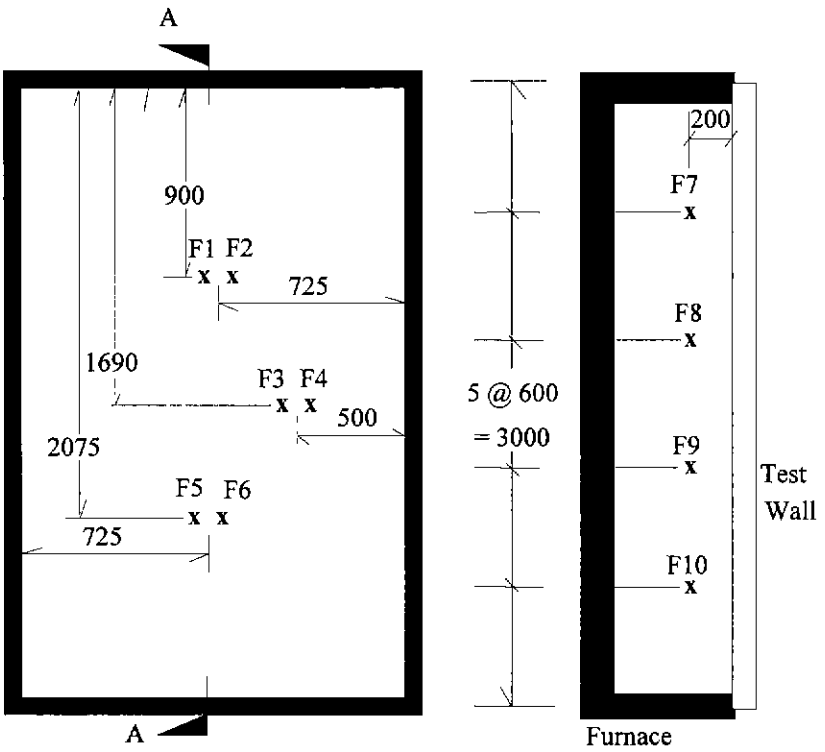

ELEVATION OF FURNACE SURFACE OPPOSITE EXPOSED WALL SURFACE

SECTION AA SHOWING POSITION OF FURNACE THERMOCOUPLES

Notes:

F1,3,5,6 - K type thermocouples with welded junctions at ends.(Tests 7 & 8)

F2,4 - K type thermocouples with soldered to copper disc without radiation shielding of mica pad shown in Figure 4.10. (Tests 7 & 8)

F7-10 - Large gauge thermocouples retractable inside sheathing.(All tests)

Figure 4.13. Location of Thermocouples in Furnace.

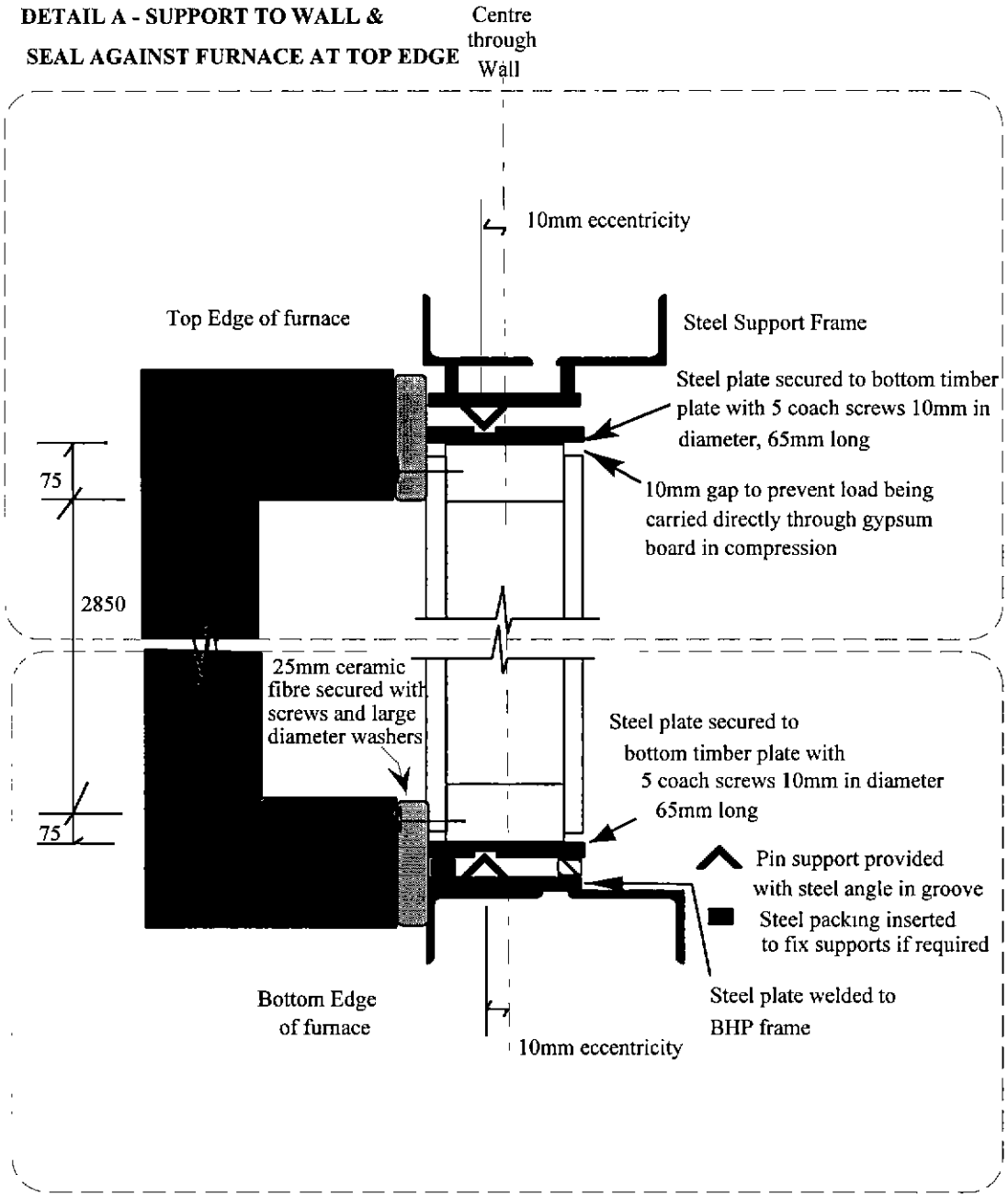

Figure 4.14. Support to Wall and Seal against Furnace at Top and Bottom Edges.

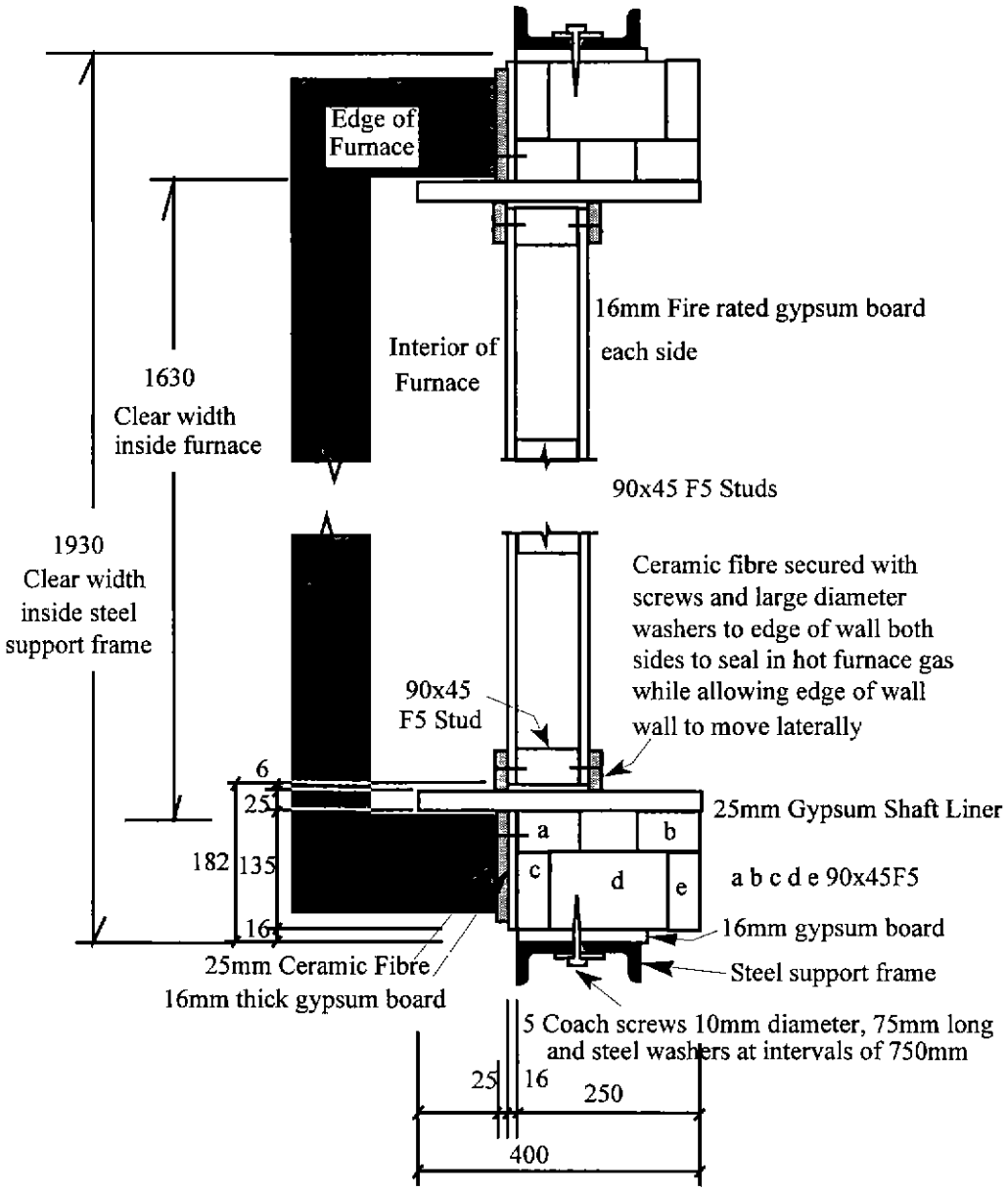

Note - F5 is a grade of timber defined in AS1720.1

Figure 4.15. Detail C -Horizontal Section through Vertical Edges of Wall.

4.4 Experimental Procedures

Due to the large weight of the walls, and to minimise possible damage of the walls when positioning them against the furnace, each wall was constructed in a mobile steel frame (Figure 4.3-Figure 4.6). The sequence of construction of each wall was as follows:

1. The construction of timber wall frames was undertaken at CSIRO laboratories (§4.1) in accordance with conventional practice. The ends of studs were T-butted and diagonally nailed to the top and bottom plates. Two flat headed 75 mm long x 2 mm diameter nails were driven through each wide side of the studs. Noggings were similarly connected to the studs. Nailing was carried out with a pneumatic nailing gun. At completion, the frames were transported to BHP-Research Laboratories (§4.1).
2. Each grooved steel plate shown in Figure 4.14 was secured to the top and bottom timber plates with five 65 mm long x 10 mm diameter coach screws.
3. Timber frames were hoisted into the steel support frame shown in Figure 4.3-Figure 4.6.
4. Timber framing lengths, "a-e" and the 25 mm thick gypsum board in Figure 4.15 were placed and secured in the steel supporting frame. The 25mm thick gypsum board was secured against the timber lengths. The dimensions of the timber lengths and gypsum left a 10 mm gap between the 25 mm thick gypsum board and the edge of the wall, to maintain unimpeded movement of the wall when deflecting during furnace exposure.
5. 16 mm thick gypsum board was placed on the ambient side of the wall frame and was fastened to the timber framing as shown in Figure 4.1.
6. Thermocouples were installed as shown in Figure 4.9-Figure 4.13. The gypsum board for the fire side was placed close to its final position and thermocouples on its surfaces were attached.
7. The gypsum board for the fire side was fastened to the timber frame.
8. Holes in the 16 mm thick gypsum board on the ambient side, where thermocouple wires penetrated, were sealed with a glue used for sealing gaskets in car engines. This glue was resistant to temperatures not exceeding 500°C.
9. Ceramic fibre wool seals around the edges of the wall and furnace were secured into positions shown in Figure 4.14 and Figure 4.15.

The wall furnace experiments involved the following sequence of steps:

1. The wall mounted in the steel support frame was wheeled to the face of the furnace (Figure 4.3). The elevation of the steel support frame was adjusted with hydraulic jacks and was bolted to the frame surrounding the furnace (Figure 4.6).
2. The thermocouple wires were connected to the computer data aquisition equipment. Calibration of thermocouple readings with temperatures had been previously carried out by laboratory personnel. Nonetheless, some simple validation of temperature measurements was

carried out. Insertion of some thermocouple tips into icy water confirmed correct measurement of 0°C. Use of a hand held electronic thermometer confirmed correct measurement of ambient temperatures.

3. The bar shown at approximately mid-height across the walls in Figure 4.4-Figure 4.6 was screwed onto timber framing "a-e" shown in Figure 4.15. The purpose of the bar was to assure safety by preventing the collapse of the wall onto laboratory personnel at structural collapse, as well as to prevent the costly loss of much thermocouple wire.
4. The sequence of wall furnace experiments proceeded in accordance with the schedule shown in Table 4.2. The furnace temperature was programmed to follow the standard fire curve. Initially a more narrow scope for the experimental program was planned because considerable variation was expected in the results due to the inherent variability of timber properties. However, as will be shown in §4.5 and §4.6, the results were much more consistent than expected. Consequently the scope was extended to consider pinned and fixed supports, as well as non-composite action. In Experiment 7 the furnace extinguished after 5 minutes from ignition and was restarted. Experiment 7 was repeated as Experiment 8 .

Table 4.2. Schedule of Experiments (Clancy and Young 1996b).

Wall experiment Number	BHP Results File	Fastening of Gypsum Board to Timber Frame (Refer to Note 6, Figure 4.7)	Applied Load per stud (kN)	Comments
1-2	BFT668 BFT669	Full fastening.	0.00	Thermocouples placed in one nogging and one stud in each experiment for correlation. Pin supported top and bottom.
3	BFT676	Full fastening.	0.00	No thermocouples in studs. Pin supported top and bottom.
4, 5	BFT679 BFT680	Full fastening.	8.00	No thermocouples in studs Pin supported top and bottom
6	BFT681	Full fastening.	8.00	No thermocouples in studs Fixed top and bottom
7	BFT682	Minimal fastening	8.00	No thermocouples in studs Pin supported top and bottom. Substantial seals at joint between sheets of gypsum board.
8	BFT683	Minimal fastening.	8.00	No thermocouples in studs Pin supported top and bottom. Normal joint detailing on fire side but substantial seals on the ambient side.

5. Observations of the ambient and the fire-exposed side of walls witnessed through the window at the side of the furnace were recorded. A summary is given in §4.5.
6. Recordings of all thermocouples shown in Figure 4.9 were taken at one minute intervals. Sufficiently short time (less than one second elapsed) between the first and last readings elapsed to assume that all readings were simultaneous.
7. Each experiment was finished when the wall was deemed to have collapsed; that is, when the wall deflected approximately 150 mm at mid-height, at which stage it rested against the restraining bar. Thermocouple wires were cut close to the wall. The wall was wheeled away from the furnace and final observations were recorded. A summary of the observations is given in §4.5.4. The wall was disassembled and cleaning and tidying was carried out.

4.5 Results - Observations

The following summarises the general observations noted during all experiments.

4.5.1 Smoke Emissions

Smoke emissions from the ambient side, were more significant in Experiments 1-3. In these experiments the wiper seals at the vertical edges of the walls were not as firm against the 25 mm thick gypsum board as was achieved in later experiments. The intensity of emitted steam and smoke from the seals increased during experiments 1-3. Vision through the furnace window became clouded. At 55.00 minutes after ignition the smoke changed from steamy white to a sooty grey. In all experiments smoke was emitted from the furnace exhaust approximately between the 3.00 and 8.00 minutes after furnace ignition.

4.5.2 Observations of Gypsum Board Exposed to the Furnace, During Experiments.

The window in the furnace, gave a clear view of the lower half of the wall. The upper half could only be seen at an acute angle and only by putting one's face very close to the glass which was unbearably hot 25-50 mm from the surface of the glass. Thus most observations were made of the lower half the walls. Times of structural collapse are given in §4.5.4.

Between 0-10 minutes after ignition, the paper charred to a black colour, then dark grey and gave the appearance of mud-cracking. At the corners of cracks the charred paper curled.

Between 10-20 minutes after ignition, 5-10% of stopping material covering joints between abutting sheets of gypsum board (Figure 4.4) had cracked, sloughed off and lifted leaving nail heads visible. Where nails were still covered by stopping material, the nail heads were evident from the appearance of black spots at the surface of the stopping material. No cracks in gypsum board were apparent. Sheathing around furnace thermocouples was dark red. The gypsum board was dull red. The paper appeared medium grey and fluffy indicating the formation of ash from 20-30% of gypsum board paper.

Between 20-30 minutes after ignition, the furnace was bright orange. Most of the stopping material over nails fell off during this period. Exposed nail heads were black. The sheets of gypsum board were flat; no out-of-plane warping of the gypsum board was apparent at this stage. The gypsum board paper was light grey and very fluffy in appearance.

Between 30-40 minutes after ignition, there was further sloughing of stopping tape and material. Cracking was evident in gypsum board either side of the lower joint (1200 mm above the bottom of the wall) at end of this time period. By visual estimation, the widths of cracks varied between hairline to 1mm thick.

Between 40-50 minutes after ignition there was further dislodgement of stopping tape. Cracking of the exposed face continued.

Between 50-60 minutes after ignition the gap in the lower joint appeared to open up to 2 mm in width. More than 80% of all stopping had sloughed off revealing nail heads which had turned black in colour. No warping of the gypsum board was apparent at this stage.

Between 60-70 minutes after ignition, there were several cracks apparent in addition to crazing across the exposed face. These cracks appeared to be several hundred millimetres long and 1 mm wide. There was intensive crazing about lower joint.

Between 70-80 minutes after ignition there was local cracking around nails. The exposed face was intact but nails in the field of boards (that is away from edges) had pulled through. Crazing was intense about the lower joint, across the full width of wall. The gap in the lower joint appeared to open up to 3mm in width. Cracks elsewhere in the wall had opened up to 3-4mm in width. The gypsum board was very warped.

Between 80-90 minutes after ignition, cracks appeared to open up to 5mm in width. The amplitude of warping increased and appeared to be as large as 50mm.

4.5.3 Observations of Gypsum Board on the Ambient Side, During Experiments

Between 0-10 minutes after ignition, the gypsum board on the ambient side was warmer to touch in areas towards the top of cavities. This observation indicates that convection was the dominant mode of heat transfer through cavities in the first 10 minutes of fire exposure.

Between 10-20 minutes after ignition, moisture formed on glass when placed within one centimetre of the unexposed surface. The surface was warm, comfortable to touch and the temperatures measured were 50-60°C.

Between 20-30 minutes after ignition steam was emitting from some holes in the unexposed face, where thermocouple wires penetrated. It was apparent that the gasket sealant described in Section 3.5.4 had not always been placed adequately. The temperature of the face was 60-70°C. Droplets of water fell from the lower corners of wall onto the floor.

Between 30-40 minutes after ignition, in pin-ended loaded wall experiments (walls 4 and 5), a horizontal crack formed in the lower joint in the ambient face (that is, 1200 mm from the bottom of the wall). The temperature was 70-75°C. Water continued to drip from the lower corners of the wall.

Between 40-50 minutes after ignition, the face was 75-80°C. Dripping water continued from the bottom corners of the walls, but became a black sooty colour.

Between 50-60 minutes after ignition, in the fixed-ended wall experiment (Wall 6), horizontal hairline cracks were observed about the mid-width of the unexposed face about lower horizontal joint.

Between 60-70 minutes after ignition, random cracking sounds came from inside the walls. There was a slight darkening of the face. The smell of burning timber was apparent.

Between 70-80 minutes after ignition, the cracking sounds coming from inside the wall were loud and audible at 6 metres away from it. The surface temperature was 95-110°C.

Between 80-90 minutes after ignition, water continued to pool below the corners of wall. The surface temperature was 110-120°C.

4.5.4 Observations Immediately after Experiments, and Failure Times

Failure of each of the walls was deemed to occur when they had deflected to the stage of touching the safety bar at mid-height; that is, approximately 150 mm of deflection. Integrity failure did not occur because gypsum board on the furnace side was observed not to slough off prior to the occurrence of deflections of 150 mm. Temperatures on the ambient facing wall surfaces rose less than 140°C and thus insulation failure, as defined by AS1530.4, did not occur. Failure times are summarised in Table 4.3.

It was apparent from close examination of all failed walls that vermiculite beads within gypsum boards had substantially expanded. Timber studs were permanently bent. There were no visual signs of degradation in the joints at the 60° cuts in studs and noggings in which thermocouples were inserted.

Timber at the top and bottom of walls, near the supports was less charred than the rest of the timber. The main reason for less charring would have been the insulation from the adjacent ceramic fibre seals between the furnace and the walls (Figure 4.14 and Figure 4.15). The connection between steel plates and timber wall plates remained rigid. Time of failure did not appear to be governed by degradation of the supports. Support conditions and eccentricities imposed by the steel plates in Figure 4.14 could be assumed to be maintained throughout the periods of exposure of walls to the furnace.

The following observations were made of Walls 7 and 8 soon after they failed, which was at approximately 28 minutes after ignition. For Wall 7, there was no char or browning of timber or gypsum board paper in the vicinity of the noggings. For Wall 8, the surface of the studs and noggings were black but the char was very superficial; less than one millimetre deep. The superficiality of the char accords with the observation that water dripping from the lower corners of the walls, did not turn black until after the 40th minute of exposure (§4.5.3). The black colour seems most likely due to smoke particulates from smoldering and charring of the studs, being caught in droplets of water which condensed during the transfer of steam to regions cooler than the vaporisation point.

Walls 4 and 5 failed at 34 and 35 minutes respectively. Observations similar to those for walls 7 and 8 were noted.

At 59 minutes after ignition, Wall 6 failed. The studs and the unexposed gypsum board broke one metre above the bottom of the wall. The size of uncharred stud sections was measured as 30x30mm. This size would have been much less than the size of the uncharred sections at the time of failure. However, the size of the uncharred sections at the tim of failure The gypsum board exposed to the furnace seemed to craze much more, immediately after the wall was moved away from the furnace when the exposed face came into contact with ambient air.

Walls 1-3 all failed between 89-91 minutes under self weight plus the weight of steel bars that were attached to the top and bottom of the walls with coach bolts. The gypsum board exposed to the furnace seemed to craze much more, immediately after the walls were moved away from the furnace and the exposed face came into contact with ambient air. No uncharred wood was found in these walls. It was apparent that only the gypsum board on the ambient side had been holding up the wall for a considerable time towards the end of the experiments. All of the exposed gypsum board was intact, but warped out-of-plane. Crazing was intense, extensive and to a depth of approxmately 2/3 of the thickness of the gypsum boards.

Table 4.3. Times of Failure Recorded for Walls in Experiments.
(Clancy and Young 1996b).

Wall Experiment Number	Time of Failure (minutes)
1	90
2	89
3	91
4	35
5	34
6	59
7	Refer to Note 2.
8	28

Notes:

1. All walls failed by collapsing. Integrity failure did not occur because gypsum board on the furnace side did not slough. Temperatures on the ambient facing wall surfaces rose to approximately 120°C which was a rise of less than 140°C. Thus insulation failure, as defined by AS1530.4, did not occur.
2. No failure for Wall 7 was recorded because of ignition problems which occurred with the furnace in this experiment.

4.6 Results and Discussion on Temperature Measurements

4.6.1 General

The discussion of experimental results in this section, §4.6 will address the aims listed in §4.1.

To appreciate the relationships between temperatures at different points in the walls during experiments, an overview of measured temperatures is shown in Figure 4.16. Due to the large number of measurements that were taken and to aid clarity, only average temperatures at similar points over all experiments are plotted. Variations in temperatures measured at similar points can be evaluated in later figures in this section, which give the plots for all temperatures in particular locations.

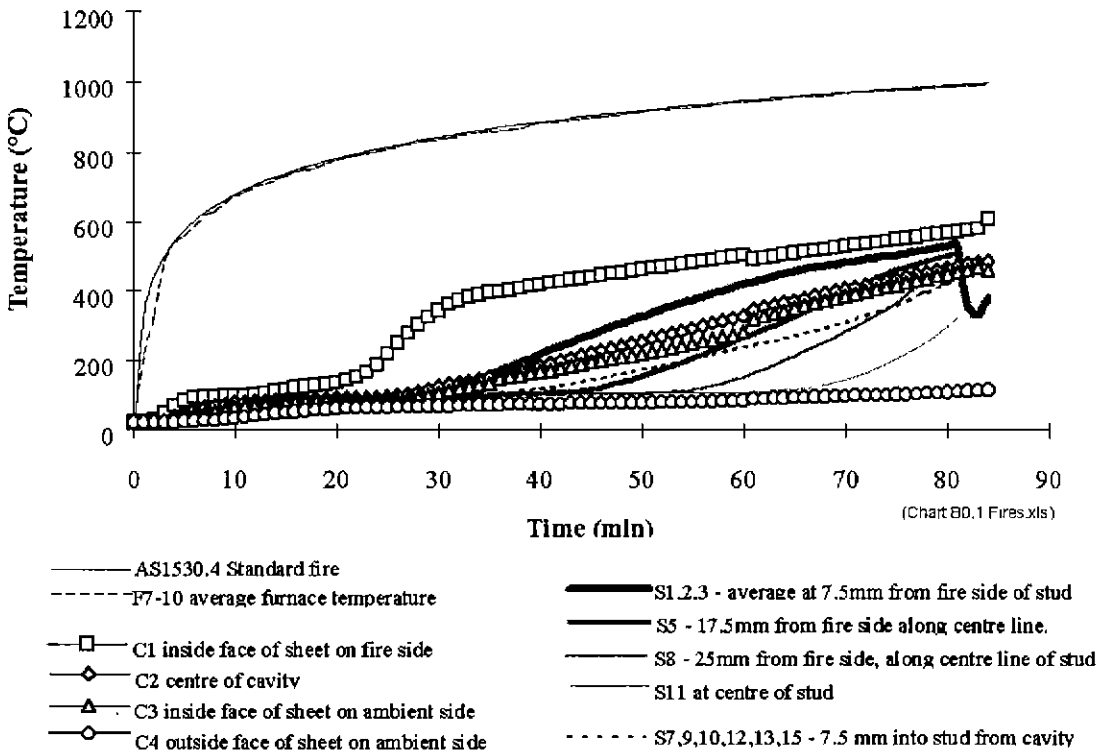

Figure 4.16. Temperature versus Time at various Points in Walls. (Temperatures outside of studs averaged over experiments 1-6 and 8. Temperatures in studs averaged for experiments 1 and 2.)

Figure 4.16 was produced to address the third aim in §4.1 to provide data for validating heat transfer models. The two uppermost plots are for the standard fire temperature - the smooth plot is for the standard fire temperatures specified in AS1530.4, and the other is for the average fire temperatures

recorded with all of the thermocouples in the furnace for all of the experiments. From the plots with square, diamond and triangular symbols, it is apparent that it takes 20 minutes before temperatures substantially rise in the cavity. When the temperatures do rise, the rise is quite sudden and can be likened to the arrival of a "wave of heat". The gypsum board always maintains temperatures in the cavity at least 400°C lower than in the fire. Its value as an insulator is apparent. The grey lines show that 40 minutes expire before the temperatures in the timber studs increase substantially. The plot with circular symbols shows that temperatures on the surface of gypsum board facing the ambient side remain low throughout. Dwells at 100°C are common to all plots. The points furthest from the fire experience the longest dwells which is to be expected since temperature gradients and heat flow reduce with distance from the surface facing the fire. Observations and discussions on the results at particular groups of points follow.

4.6.2 Furnace Temperatures

Regarding aim 3, §4.1, furnace temperatures were measured to evaluate the modelling of heat transfer from the furnace to the walls. As mentioned in §4.4, during Experiment 7 the furnace momentarily ceased burning at approximately five minutes after ignition. The results from Experiment 7 have, thus, not been considered in this section. Temperatures of interest, recorded in the furnace are shown in Figure 4.16 and Figure 4.17. After the 30th minute, many of the plots in Figure 4.17 are erratic, indicating that it was likely that the thermocouples had dislodged.

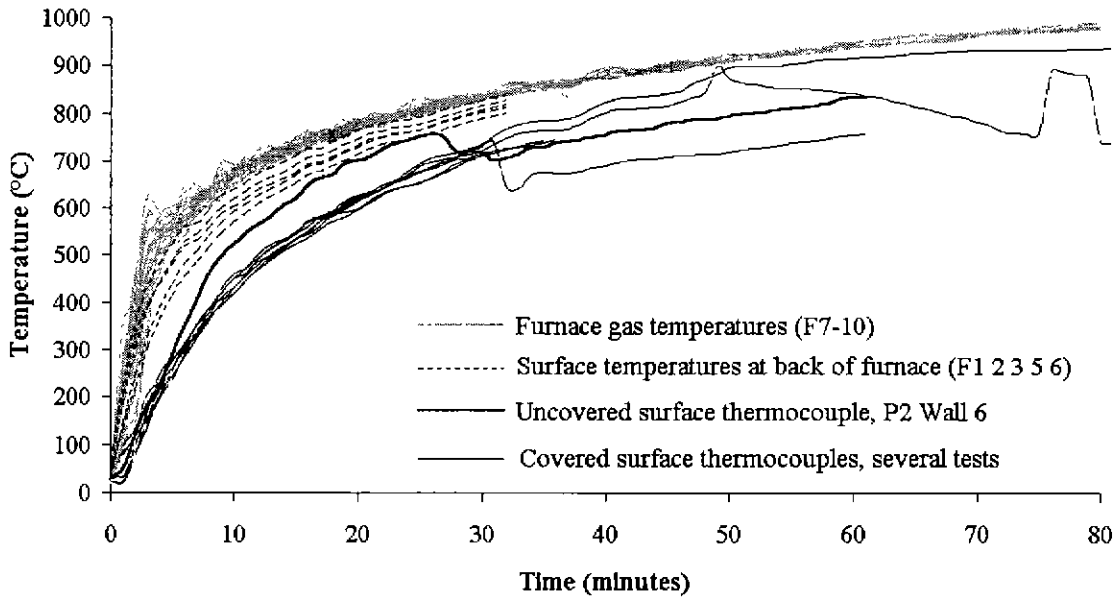

Figure 4.17. Temperature Measurements in Furnace Gas, and on Surfaces Bounding the Furnace.

A comparison between standard fire temperatures (AS1530.4) and the average furnace temperatures at F7-10, for experiments 1-6 and 8, can be made from the plots in Figure 4.16. It is apparent that the

average furnace gas temperatures closely followed the standard fire trajectory. The cluster of thin grey lines at the top of Figure 4.17 shows the actual recorded temperatures at F7-10 during Wall Experiments 1-6 and 8. These lines show that the variation in furnace temperatures was small (an observation important for aim 1 §4.1).

Figure 4.17 shows from the dotted lines, that the temperatures F1-6 on the surface of the back wall were as much as 100°C cooler than the furnace gas (grey lines, F7-10). The fact that the back wall was cooler than the furnace gas is expected since the gas supplies the heat and should be the hottest region in the furnace. There was considerable variation in temperatures, as much as 100°C, at the points F1-6 where temperatures were measured on the back wall. The variation was most likely due to the difficulty in placing the thermocouples F1-6 with precision on the rough woolly surface.

The uncovered thermocouple, P2 on the surface of Wall 6 was generally 100°C higher than conventionally covered thermocouples shown in Figure 4.10. This difference significantly affects the evaluation of surface emissivity, discussed further in the following model validation sections §5.2.2, §5.2.3.4 and §5.3.

The temperatures plotted as thin black lines in Figure 4.17 for the conventional covered wall surface thermocouples showed little variation. These results indicated that there must be little variance in surface emissivities of gypsum board and overall heat flow from the furnace to the walls during the experiments.

4.6.3 Distribution of Heat Flux Across Walls

Temperatures were measured at points at different heights to check assumption 3(a) in §4.1 that the heat flux is uniform with height, allowing two dimensional heat transfer analysis of the walls. Figure 4.18 shows the distribution of temperature with height up the walls, at 30 minutes after ignition. The positions for which these distributions were obtained, were along vertical centre lines through the furnace gas (F7-10), on the cavity facing surface of the gypsum board on the fire side (C5, 1, 11) and on the ambient gypsum board surface (C8, 4, 12). The three distributions in Figure 4.18 are reasonably uniform and support the assumption.

Temperatures were measured at points at different horizontal positions to check assumptions in 3(b) in §4.1. That is the heat flux was uniform across the walls and allowed heat transfer analysis of a representative portion involving studs and cavities as shown in Figure 3.2. Figure 4.19 shows the variation of temperatures at similar points in horizontally adjacent cavities, at the 30th minute of fire exposure. Points C9, L9, C1 and L11 show the variation at similar points on the cavity side of gypsum

board nearest the furnace. Points L8, L10, C3 and L12 show temperatures at points on the surface of gypum board on the ambient side. This little variation supports the efficient practice of limiting heat transfer analysis to a representative portion of wall.

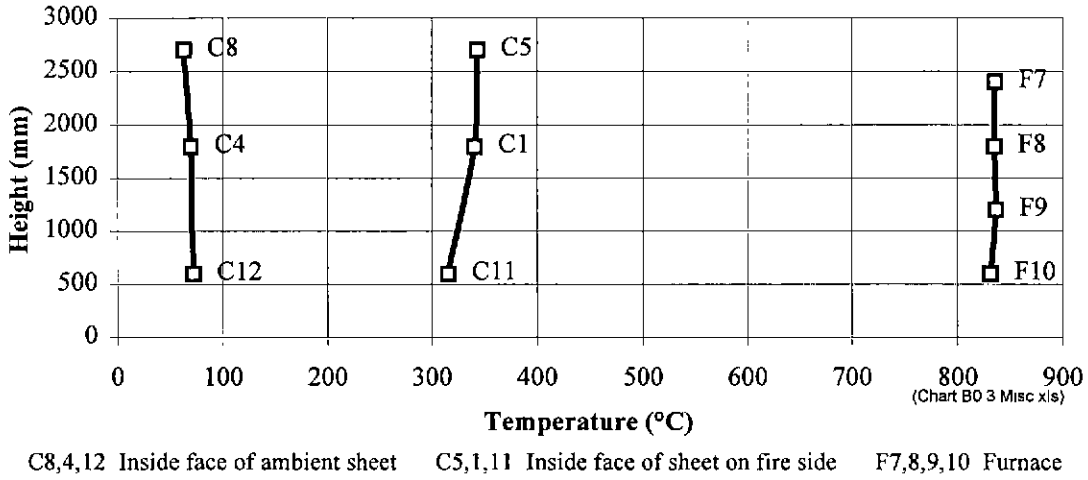

Figure 4.18. Temperature Distribution with Height at 30 Minutes Exposure Averaged over all Wall Experiments 1-6 and 8.

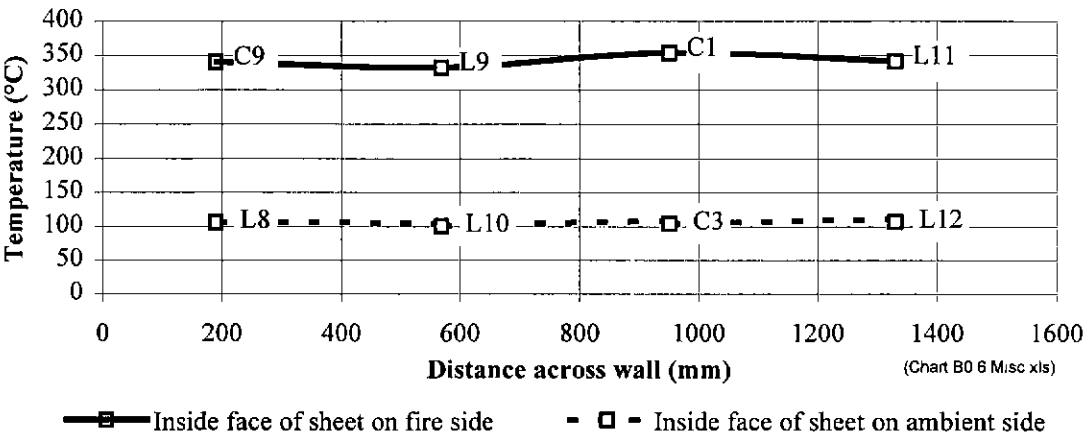

Figure 4.19. Temperature Distributions Horizontally across Wall at Midheight at the 30th Minute of Fire Exposure, Averaged over all Experiments 1-6 and 8.

4.6.4 Temperatures Along Heat Paths Through Cavities

Temperatures were measured over a vast array of points. It is convenient to separately consider points along two types of heat paths. The dominant heat paths are through the cavities. Temperatures at points

along these paths are considered in this section, §4.6.4. Other paths to consider are those that transfer heat to the studs and are considered in §4.6.5.

Figure 4.16 shows the relations between plots of temperature versus time at particular points along heat paths through cavities, averaged over Wall experiments 1-6 and 8. These plots are made with symbols; not lines. Plots of temperatures measured in individual experiments are given in Figure 4.20 - Figure 4.23. Evaluation of the experimental results in accordance with the aims in §4.1 is given below.

Figure 4.20 refers to the temperatures measured on the cavity facing surface of the gypsum board on the fire side. Plot A results from measurements taken in Wall Experiment 3, with a surface thermocouple similar to the one shown in Figure 4.10, except no calcium silicate pad was used. The purpose for this thermocouple was to evaluate the effects of pads on temperatures. Plot A is 50°C higher than other plots between 10-20 minutes. The lower temperatures shown in the other plots may be due to the effect of the pads in reducing the flow of water vapour from the gypsum board on the fire side, towards the cavity, thereby increasing the dwell time. After 30 minutes, plot A has a slightly lower gradient than the other plots. The uncovered thermocouple would have shed more heat by radiation into the cavity than was shed by the covered thermocouples, and hence the lower rate of heat build-up. Since it is apparent that pads significantly affect measured temperatures, these effects should be considered when validating heat transfer (Aim 4, §4.1). Future research should pay closer attention to the measurement of surface temperatures. The measurement of surface temperatures will always be difficult because surfaces theoretically have no thickness, no thermal inertia, are at locations where temperature gradients are very steep and where there are several dominant modes of heat flux. These modes include conduction of heat and diffusion of moisture in gypsum board, cavity radiation and boundary layer convection of cavity gas. Surface temperatures are thus very sensitive to many phenomena.

Plots B and C for temperature measurements in Wall Experiments 4 and 6, result from conventional surface thermocouples shown in Figure 4.10. Similar thermocouples were used to obtain the unmarked plots for temperatures measured in other experiments. Plots B and C are substantially higher compared with other plots after 30 minutes. No reason is apparent for the higher temperatures, unless cracks in the gypsum board formed near the thermocouples and let through more heat from the fire.

Figure 4.21 shows temperature versus time measured in the tube at the centre of the cavities. The plots are consistent except for D (Wall Experiment 6) which lags five minutes behind the other plots. Thermocouple D was similar to all others for which measured temperatures are plotted. Although the tube would have prevented the thermocouple being affected by radiation, it may have caused the temperature of the air in the tube to lag behind the temperature of the air in the cavity since air was not drawn through the tube. However, stagnation of air does not explain D lagging behind other plots which

were obtained with similar thermocouple details. Other plots for temperatures at points on the heat path through the cavity in Wall 6 are C in Figure 4.20, F in Figure 4.22 and G in Figure 4.23. Comparing all of these plots with plots for other walls, apparently, there were greater temperature gradients along the heat path through the cavity in Wall 6.

Figure 4.22 and Figure 4.23 show plots of temperature versus time measured on surfaces both sides of the gypsum board on the ambient side. If plots E (Wall 6) and F (Wall 4) are considered, the variation in temperatures with respect to average values is as much as ± 20-30%. The time lags between plots in Figure 4.23 for surface temperatures on the ambient side, are larger; more than 20 minutes in some cases. Even if plots E and F are ignored, the variations are considerable and the gradient is very low which indicates difficulties in predicting the times of insulation failures (AS1530.4). Unfortunately, the measured temperatures did not reach the range, 150-200°C in which insulation failure temperatures are specified in AS1530.4. The experiments did not provide the results for validating heat transfer models for this type of failure.

It is apparent from Figure 4.20-Figure 4.23, that the measured temperatures at similar points in heat paths through cavities in all of the wall experiments have reasonable consistency. Thus the experimental procedures adopted are reproducible (Aim 1 §4.1). There is a reasonable indication of variability (Aim 2 §4.1). The results are thus useful for validating heat transfer models (Aim 4, §4.1).

The significance of convection (Aim 3 c, §4.1) can be judged from Figure 4.24 and Figure 4.25 which show the distribution of temperatures with height on the surfaces of gypsum board bounding a cavity. There is a bulge at C3 and C1, which indicates that these thermocouples were placed too close to the steel tube. From the other thermocouples, a small increase in temperature with height can be observed in Figure 4.24 for 5 minutes of exposure but not in Figure 4.25 for 30 minutes of exposure. The increase in temperature with height is most likely caused by the convection of cavity gas. It is apparent that convection is significant at 5 minutes but insignificant at 30 minutes. Hence the modelling assumption that convection is a not a dominant mode of heat transfer in the cavity is valid.

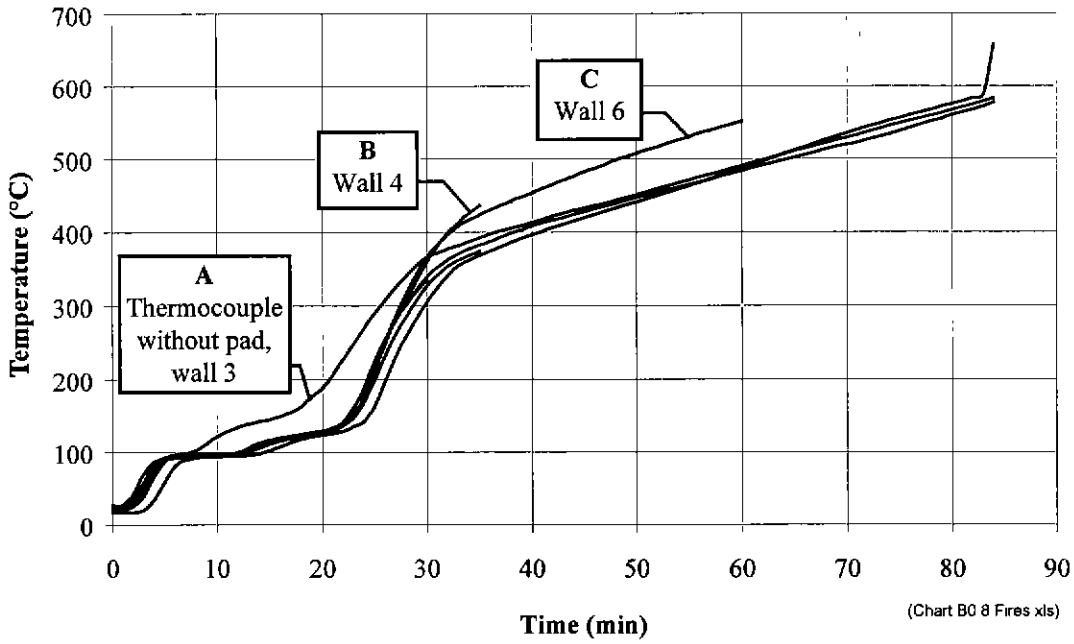

Figure 4.20. Temperatures Recorded at C1 (Figure 4.9), placed on Cavity Facing Surface of Gypsum Board on Fire Side. (Note, all surface thermocouples covered with pad as shown Figure 4.10 in except the one for plot A)

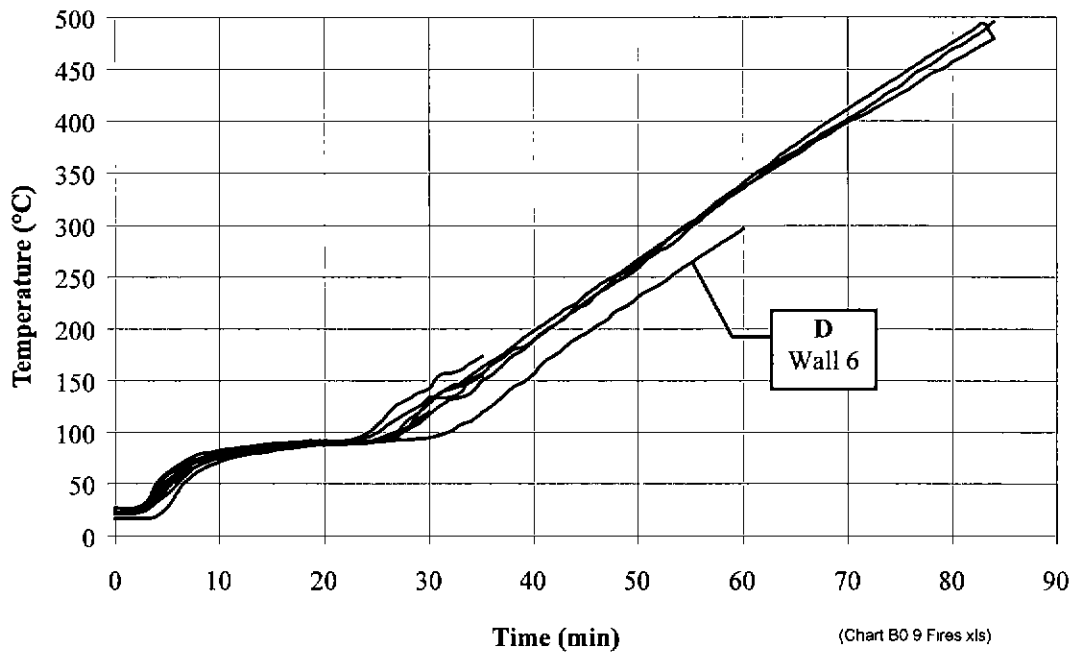

Figure 4.21. All Temperatures Recorded at C2 (Figure 4.9), at Centre of Cavity at Mid-height in Wall.

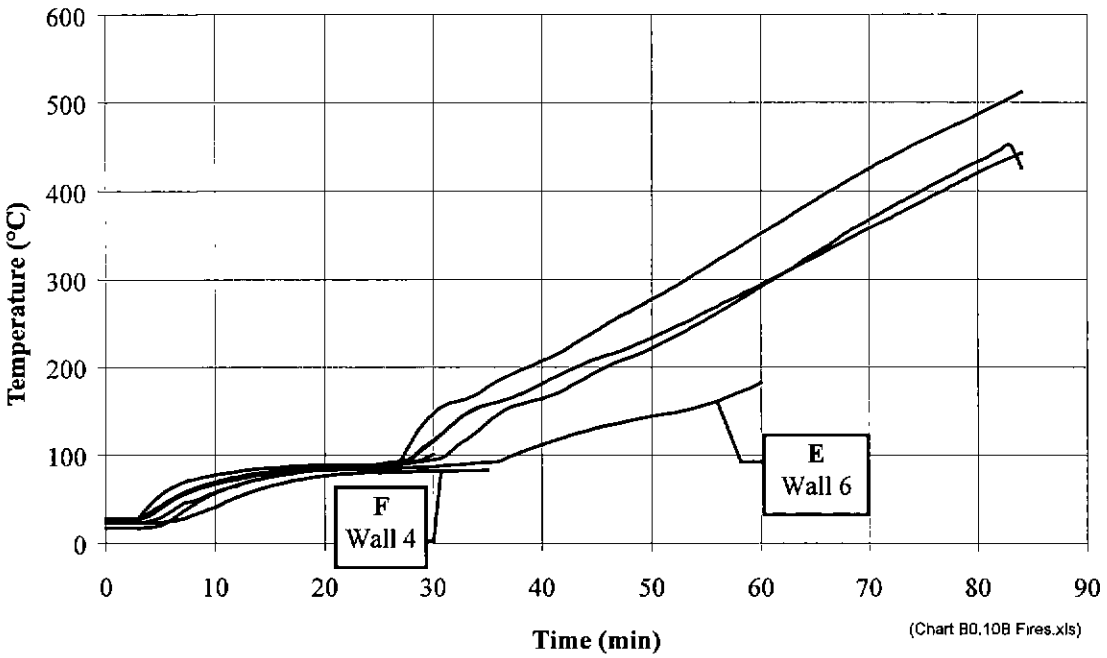

Figure 4.22. All Temperatures Recorded at C3 (Figure 4.9), on the Inside Surface of Gypsum Board Covering the Cavity at Mid-height.

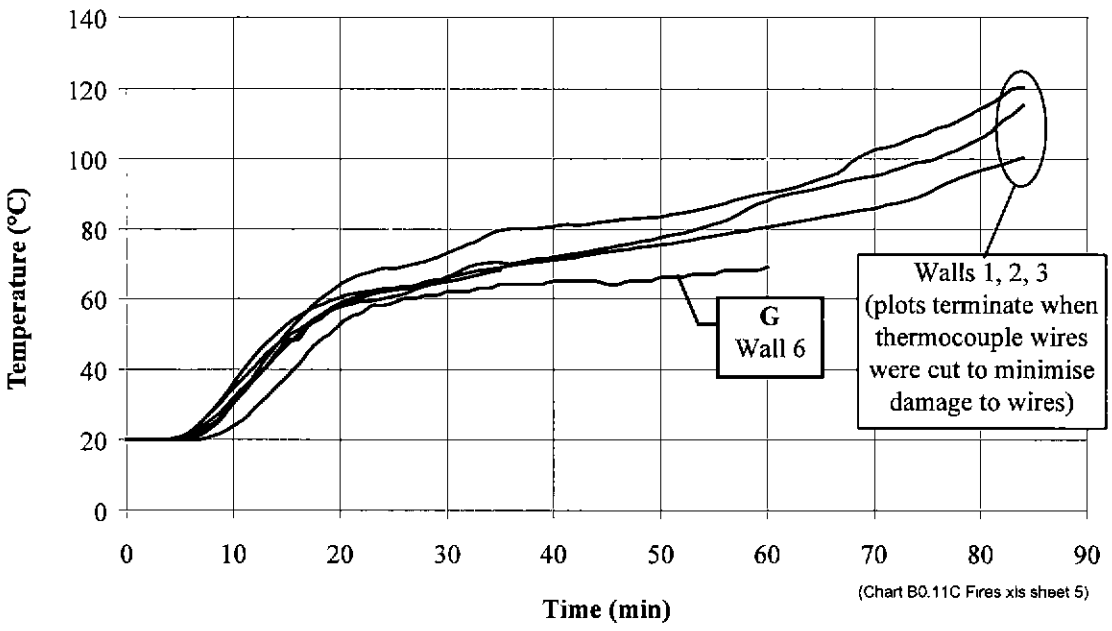

Figure 4.23. All Temperatures Recorded at C4 (Figure 4.9), on Outside Surface of Gypsum Board Covering Cavity at Mid-height.

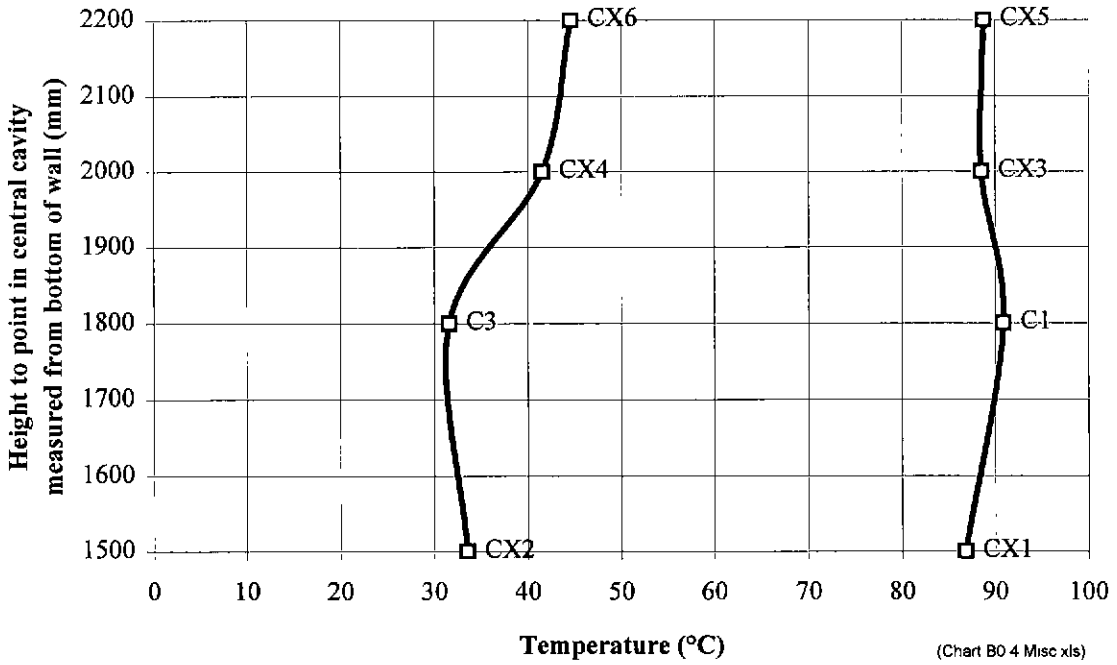

C3,CX2,4,6 Inside face of ambient sheet C1,CX1,3,5 Inside face of sheet on fire side

Figure 4.24 Temperature Distribution in Central Cavity with Height at 5 Minutes Exposure Averaged for Wall Experiments 4-6.

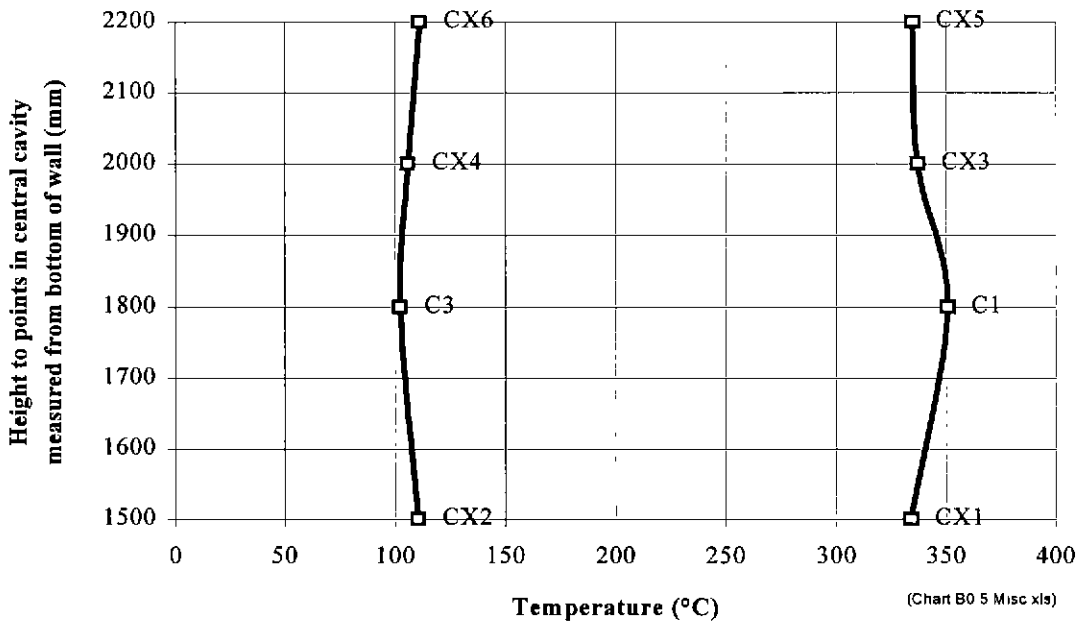

C3,CX2,4,6 Inside face of ambient sheet C1,CX1,3,5 Inside face of sheet on fire side

Figure 4.25. Temperature Distribution in Central Cavity with Height at 30 Minutes Exposure Averaged for Wall Experiments 4-6.

4.6.5 Temperatures in Timber Framing

Temperature versus Time Plots

Figure 4.16 showed the relation of temperatures in timber framing to temperatures of other key points in the wall with time (Aim 1, §4.1). As would be expected, there is generally a lag demonstrating the role of gypsum board and the insulation inherent in timber, in providing resistance to fire. There is a dwell at 100°C at all points in timber at various times. The fact that the dwells occurred at 100°C, rather than higher temperatures indicates that the timber was sufficiently diffusive and porous for vapour to readily diffuse out of the timber at atmospheric pressure. (White's, 1988 experiments showed dwells at higher temperatures, no doubt due to the build up of vapour pressure and lower diffusivity of his wood samples.)

Variations in recorded temperatures at similar points in timber framing (Aims 1 and 2, §4.1) in Walls 1 and 2 are shown in Figure 4.26 and Figure 4.27. The variations are generally within ±5-10% of averages, and are similar to the variations of temperatures at points along heat paths through cavities, discussed in the previous section, §4.6.4.

Since heat is distributed two dimensionally in the sections through timber framing members, temperature-time plots at points give a limited indication of heat flow and likely influential phenomena. Consequently, these plots give limited scope for evaluating modelling assumptions (Aim 2(d), §4.1). A more useful method of plotting results is desired. It was decided to plot temperature distributions in sections through timber framing members, as shown in Figure 4.29-Figure 4.36. These distribution are discussed below.

Temperature Distributions

Before evaluating modelling assumptions against the experimental temperature distributions plotted in this section of the thesis, it is easier to firstly plot the expected distribution from the assumptions adopted (§3.3.2) and then compare the plots from experiments with these expected plots. The degree of consistency between the two types of plots, and the relative influence of phenomena will then be more apparent.

The expected typical isotherms for the temperature distribution can be deduced as follows. The two main heat paths into a typical stud are:

1. The path from the cavity through the wide side face of the stud and into its core; and
2. The path from the fire, through the gypsum board, through the narrow face of the stud and into the core of the stud.

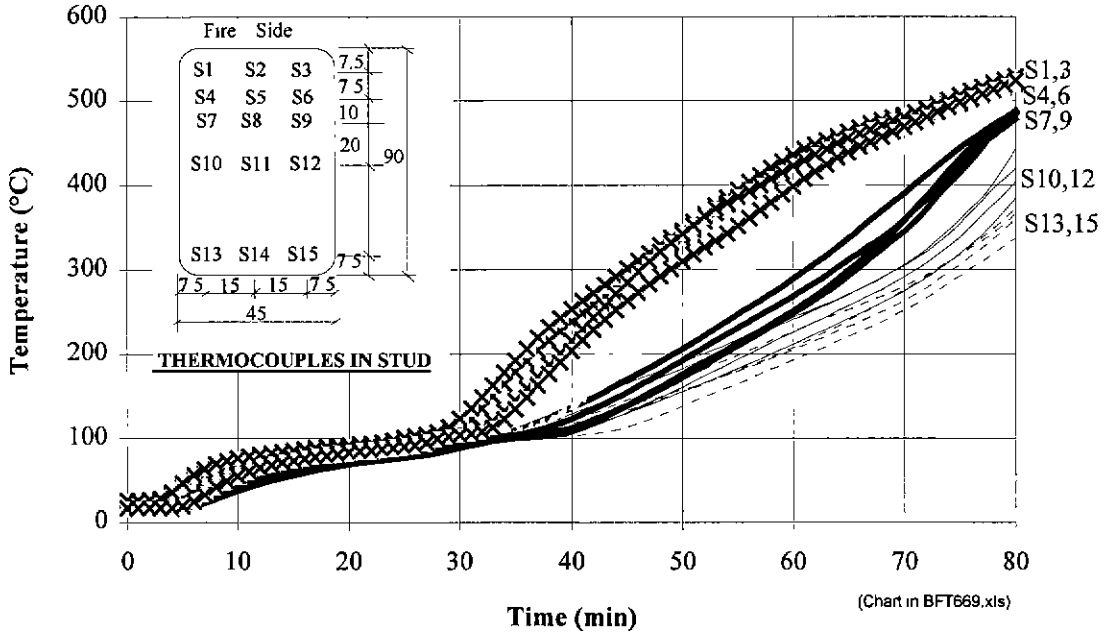

Figure 4.26. Temperatures at Points 7.5 mm below Surfaces of Studs Bounding Cavities, in Wall Experiments 2 and 3.

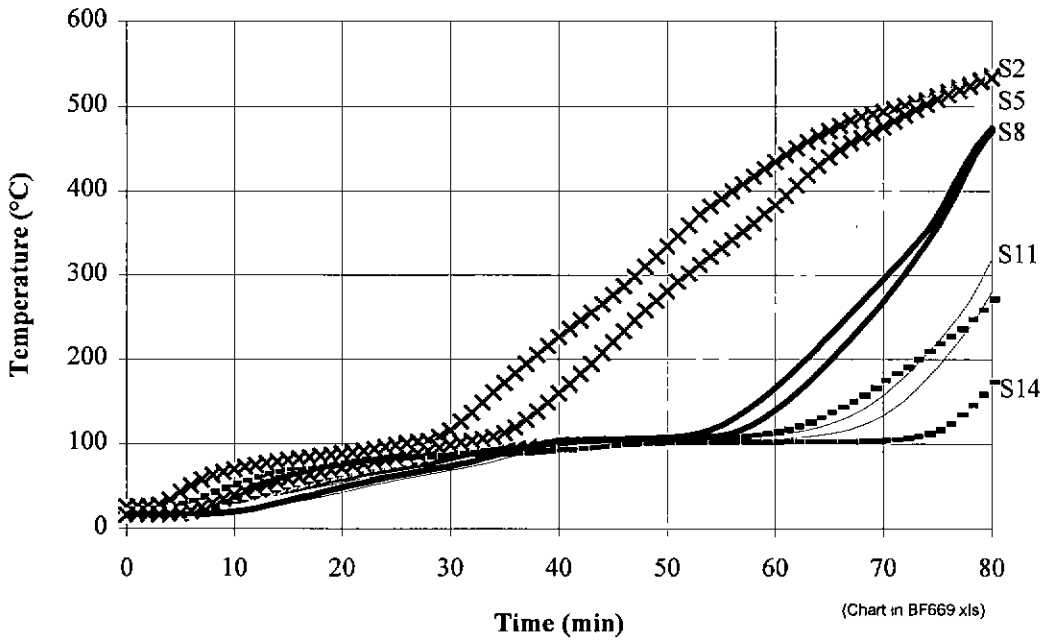

Figure 4.27. Temperatures at Points along Centre Lines through Studs and Perpendicular to Walls in Wall Experiments 2 and 3.

The first path would be expected to deliver a fairly uniform distribution of heat flux across the wide surface of the stud because the extreme aspect ratio of the cavity. The uniformity is expected irrespective of whether the main mode of heat transfer through the cavity is convection or radiation. The aspect ratio dominates the heat flux distribution on this face. Heat losses through ambient side of the stud and two dimensional effects of radiation would slightly skew the heat flux and normals to isotherms towards the ambient side. The second path would also transfer a fairly uniform distribution of heat flux through the narrow face of the stud on the fire side. It was assumed in the model (§3.2) that heat transfer could be solely modelled with thermal conduction through the stud. Since the wood in the stud has low thermal diffusivity and thus experinces low heat transfer rates compared with heat transfer rates through the cavity, steep temperature gradients at the edges of the stud are expected, as well as considerable curving in the isotherms at the corners near the fire side. The isothermal plot in Figure 4.28 is therefore expected.

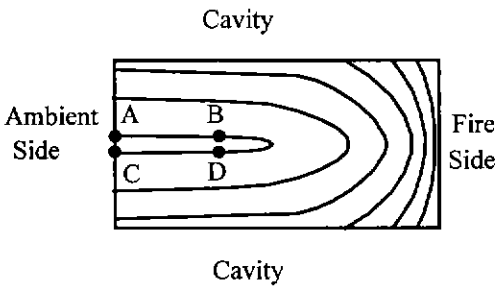

Figure 4.28. The Distribution of Isotherms in Sections through Studs and Noggings Expected from Assumptions made in the Heat Transfer Models in §3.2.

The expected distribution of isotherms in noggings is deduced as follows. In the early stages of heating, cavity temperatures would be ambient or slightly above. Convection would dominate (Figure 4.24 compared with Figure 4.25). Since convective heat rises, the underside of noggings should be hotter than the topside. After vaporisation of moisture, the cavity facing surface of the gypsum board on the fire side reaches temperatures greater than 300°C (Figure 4.20) and radiation dominates. The top and bottom sides of noggings have similar views of the inside face of the gypsum board on the fire side, and thus should have similar temperatures. The heat flow to the nogging rapidly increases at this stage, and within a short period of time the isotherms should be similar to isotherms in the studs.

The method of plotting the isotherms is also given here to aid the interpretation of the plots from the experiments. The method is called, kriging (ASCE et al 1994) which involves the following assumptions:

1. The distribution of temperature (or whatever variable is being plotted) is linearly related to temperatures at particular points.
2. The difference between the distribution and temperatures at the particular points is zero.
3. The covariance of the distribution with respect to these temperatures is a minimum.

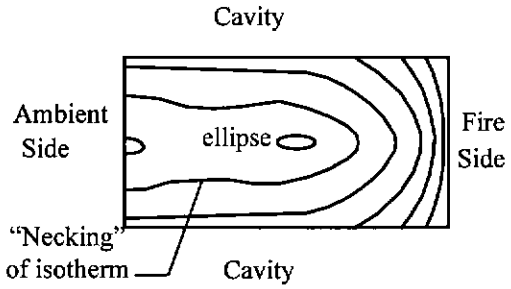

Figure 4.29. Character of Plots after 35 Minutes.
(Local depressions due to errors in kriging.)

The process of kriging did not maintain close long approximately parallel lines such as AB and CD in Figure 4.28 where there were few thermocouples in wood within 30 mm from the ambient facing side (Figure 4.12). Consequently, ellipses and necking of isotherms occurred as shown in Figure 4.29. However, kriging gave less erratic isotherms than alternative methods involving interpolations weighted to the inverse square (or other power) of the distance from points where temperatures were measured. These errors do not detract from deductions about the heat flow in the timber framing. Knowledge of the errors does help to avoid errors in deductions.

Temperature Distributions 0-35 minutes

Figure 4.30 and Figure 4.31 show temperature distributions derived from measurements obtained during the first 35 minutes. The temperature distributions are shown in bands of 10°C. Each temperature noted on the figures is the median temperature of the band. Temperatures are only noted in the white bands. The grey bands indicate temperatures in odd muliples of 10, intermediate between the median temperatures of the white bands. The temperature distribution within 7.5 mm from the outside surface was not drawn because of difficulties in extrapolation from the points where temperatures were measured (Figure 4.9 and Figure 4.12).

The temperature distributions plotted from the experiments for studs and noggings are quite similar during the first 35 minutes of fire exposure. The shape of temperature bands is similar and can be typified as shown in Figure 4.32. The time lag between temperature distributions is within a few minutes, that is the difference in times when two temperature distributions have maximum similarity. Thus thermal properties must have been consistent for temperatures up to 100°C.

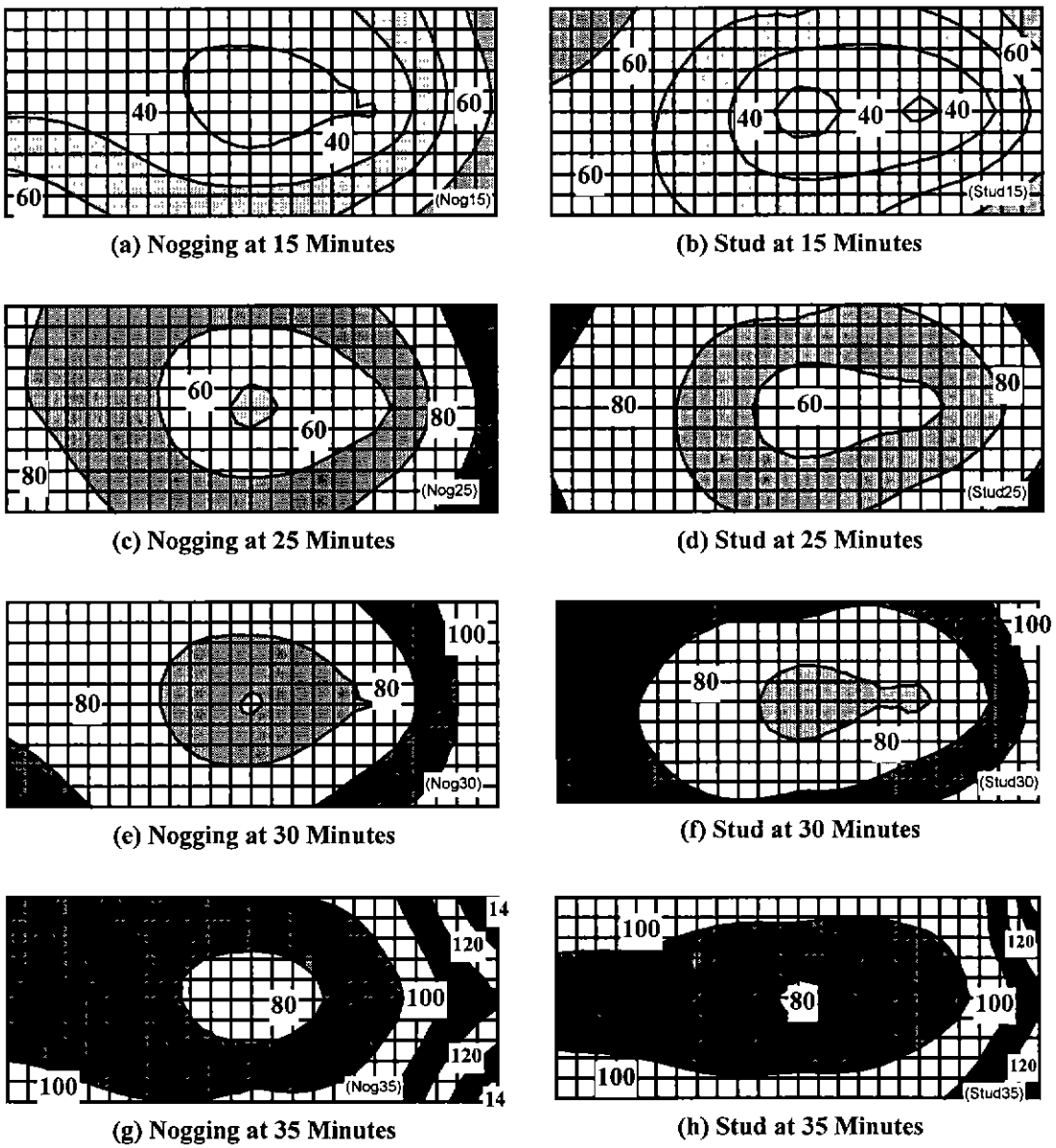

(a) Nogging at 15 Minutes

(b) Stud at 15 Minutes

(c) Nogging at 25 Minutes

(d) Stud at 25 Minutes

(e) Nogging at 30 Minutes

(f) Stud at 30 Minutes

(g) Nogging at 35 Minutes

(h) Stud at 35 Minutes

Figure 4.30. Development of Temperature Distributions (°C) in Timber Framing in Wall 1 during First 35 Minutes of Furnace Exposure. (Sections cropped 7.5 mm from edges; median temperatures ±5°C in white bands shown.)

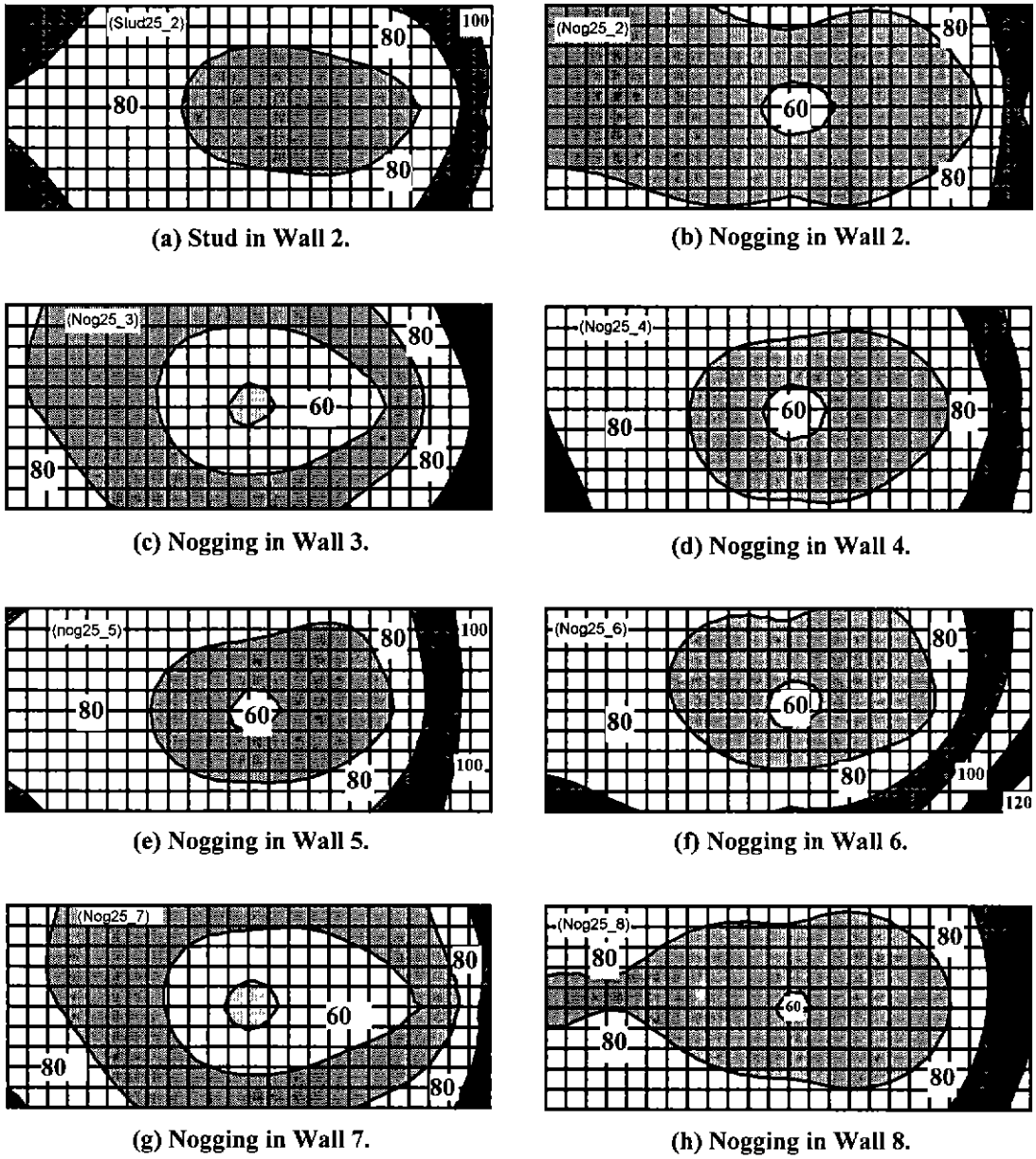

(a) Stud in Wall 2. **(b) Nogging in Wall 2.**

(c) Nogging in Wall 3. **(d) Nogging in Wall 4.**

(e) Nogging in Wall 5. **(f) Nogging in Wall 6.**

(g) Nogging in Wall 7. **(h) Nogging in Wall 8.**

Figure 4.31. Temperature Distributions (°C) in Sections through Noggings and Studs in Walls 2-8, and in the Central Stud in Wall 2, at 25 Minutes. (Sections cropped 7.5 mm from edges; median temperatures (±5°C) in white bands shown.)

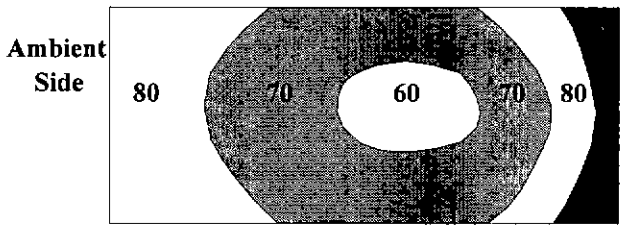

Figure 4.32. Typical Isothermal Plot in Noggings and Studs at 25 Minutes.

Comparing the expected distribution, shown in Figure 4.28, with the typical distribution in, shown in Figure 4.32, the isotherms expected from the model are similar to those in the typical plot on the fire side. However, the isotherms on the ambient side of the expected plot are strikingly different to those in the typical plot. The most striking difference is the isotherms in the experiments were not parallel to the wide surfaces of the studs; in fact the isotherms were elliptical. The elliptical shapes are not errors in kriging because temperatures were measured at S14 (Figure 4.9) which confirmed that temperatures in the middle of the ambient side of the studs and noggings were similar or only marginally less than temperatures at the nearest corners. More heat transferred to the ambient side of the timber sections than to the centre of timber sections. It does not seem that the elliptical nature of isotherms, when temperatures in studs are less than 100°C, has been previously reported.

Two reasons for the greater rate of heat transfer to the ambient side than to the centre of timber sections are possible. Firstly, there may have been some shrinkage of the timber on the ambient side of sections as generally discussed in §2.4.3.1. Thus, shrinkage gaps may have opened between the timber sections and gypsum board on the ambient side. These gaps would have allowed air and, hence convective heat, to flow from the cavity along the sides of the timber sections bounding these gaps.

However, from Figure 2.10, temperatures less than 100°C seem too low for shrinkage to open up gaps. A second reason related to convection in the cavities, as demonstrated in Figure 4.33, seems more likely. In §2.4.4.2 it was shown that convection for the first 20 minutes is expected to be laminar. The figure shows the laminar convection expected in a vertical section through a cavity. Air close to the surface of the gypsum board on the fire side would heat up to 100°-150°C (Figure 4.20), rise and circulate to A, B, D and on to C as shown. Further, as shown in Figure 4.20-Figure 4.22, this convective flow circulated around a relative cool centre at 100°C. Air in the corners of the cavity bounded by both the noggings and gypsum board would tend to stagnate and exchange little heat convectively with the relatively cool centre. The corners, A-D would thus be hot spots at 100-150°C, heating the corners of noggings on the ambient side as well as the fire side. The vertical corners of the cavity would also have stagnant air and heat the studs in a similar manner, causing the timber on the ambient side of studs to heat in a similar manner, resulting in elliptical isotherms similar to those indicated at the ambient in Figure 4.32.

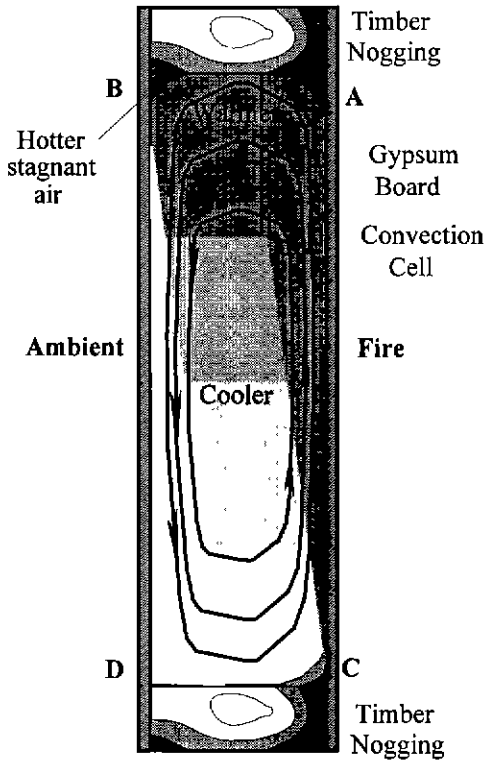

Figure 4.33. Convective Heat Transfer through Cavities. (Darker areas indicate higher temperatures.)

Another difference between the expected temperature distribution, as shown in Figure 4.28, and the typical distribution from experiments, as shown in Figure 4.32, is the low gradients of the temperature distribution on the ambient side. The most likely reason for the low gradients seems to be moisture transfer. Although some moisture would have transferred from the fire side of the stud to the ambient side, it could not have been the dominant source of moisture transfer because of the coolness of the core compared with the surrounding wood in the studs and noggings. It seems more likely that the moisture transfer was initiated from cavity heat. In the preceding paragraph it was explained that the corners of the cavities on the ambient side were likely to have temperatures of 100-150°C from five minutes onwards. The question arises as to whether the moisture came from the cavity or from within the wood. Moisture diffusion from gas to wood at less than 100°C would be too slow to explain the rapid rise in temperature on the ambient side of the noggings and studs. It seems more likely that the air in the hot corners of the cavity heated surface wood to 100°C. The moisture in the wood would have vaporised and flowed to the middle of the stud on the ambient side. The fact that the dwell in temperature rise in the wood was at 100°C, the boiling point of water at atmospheric pressure, means that the wood was quite porous so as not to raise the boiling point and readily accommodated the huge expansion involved as moisture changed to vapour - a volumetric expansion of the order of 1000 times.

Figure 4.34 shows the temperature distributions at 35 minutes, in studs and noggings in all walls during the experiments. This was approximately the time when pin-supported walls 4 and 5 (Table 4.2) structurally failed (§4.5.4). The temperature distributions are dominated by the 100°C band. Bands of temperatures less than or equal to 100°C are irregularly shaped. This sudden irregularity can be explained from the sudden volumetric expansion of vapour and dispersion of heat in many directions. Although some irregularity is due to kriging, this irregularity would only be minor compared with the irregularity caused by vapour diffusion.

Figure 4.34 thus reveals that there is a stage in heat transfer when vaporisation induces a rapid diffusion of steam throughout the timber sections. This diffusion is strongly driven by the approximate 1000 fold volumetric increase (under atmospheric pressure) as moisture is vaporised. Young et al (1998) explained that this rapid extensive diffusion of steam greatly reduced the of mechanical properties of timber in compression by as much as 80% and was the cause of the structural collapes of Walls 4 and 5. There were no temperature bands at 300°C and above; accordingly, no charring was present. It is thus apparent that failure of timber framed walls in fire must not only be checked for a charring mode, which reduces the net section of timber framing, but also a "steaming" mode caused by the rapid extensive diffusion of steam through the timber section before charring commences. Steam has been used for a long time as a means of bending timber; from centuries ago when timber gallions were built, to the present in the manufacture of furniture. The effects of steam in producing creep in experiments on loaded timber structures in fire can also be seen from the results of König et al (1991) and Olesen et al (1992).

By examination of Figure 4.30, Figure 4.31 and Figure 4.34 it is apparent that there was no more than 1-2 minutes difference in variation of temperature distributions in the timber sections with time. It seems that thermal properties of timber were very consistent.

Temperature Distributions after 35 Minutes Exposure

Temperature distributions at 60 minutes for sections in walls which had not failed by this time are shown in Figure 4.35. It was at approximately this time, 60 minutes that Wall 6 structurally failed (Table 4.3). The ends of Wall 6 were restrained against rotation. The temperature distributions shown in Figure 4.35 are more like those expected in Figure 4.28 for both studs and noggings, despite some ellipse and necking errors in kriging. It can thus be deduced that the modelling assumptions that heat transfer was dominated by thermal conduction in solid materials and radiation at surfaces were most applicable after 30 minutes. The time lag between the temperature distributions appears to be only a few minutes. Thus, the thermal properties should have been very consistent in all the walls in the experiments, for the temperatures in the range of 100-400°C.

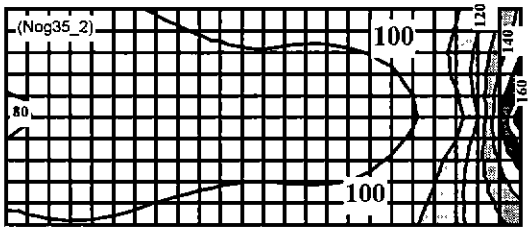

(a) Nogging in Wall 2 at 35 Minutes

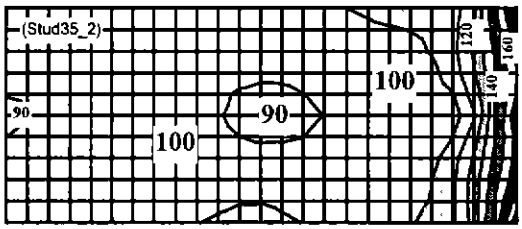

(b) Stud in Wall 2 at 35 Minutes.

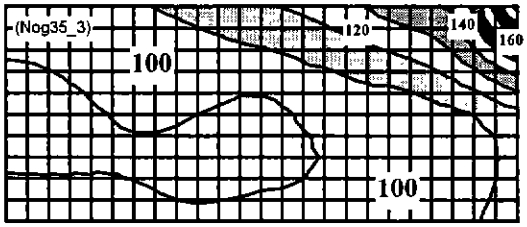

(c) Nogging in Wall 3 at 35 Minutes

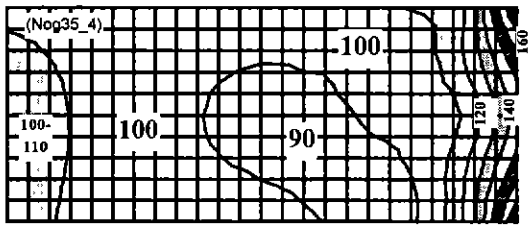

(d) Nogging in Wall 4 at 35 Minutes

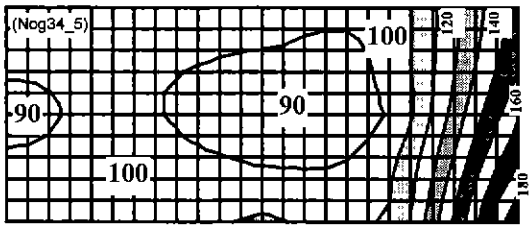

(e) Nogging in Wall 5 at 34 Minutes.

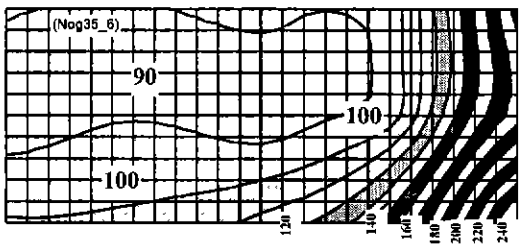

(f) Nogging in Wall 6 at 35 Minutes

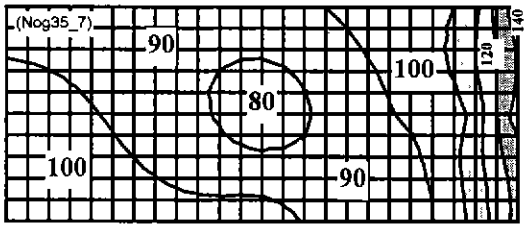

(g) Nogging in Wall 7 at 35 Minutes.

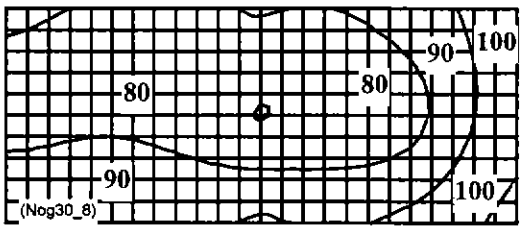

(h) Nogging in Wall 8 at 30 Minutes.

Figure 4.34. Temperature Distributions (°C) in Sections through Noggings and Studs in Walls 2-8, at Times close to 35 minutes. (Sections cropped 7.5 mm from edges; median temperatures ±5°C in white and some grey bands shown.)

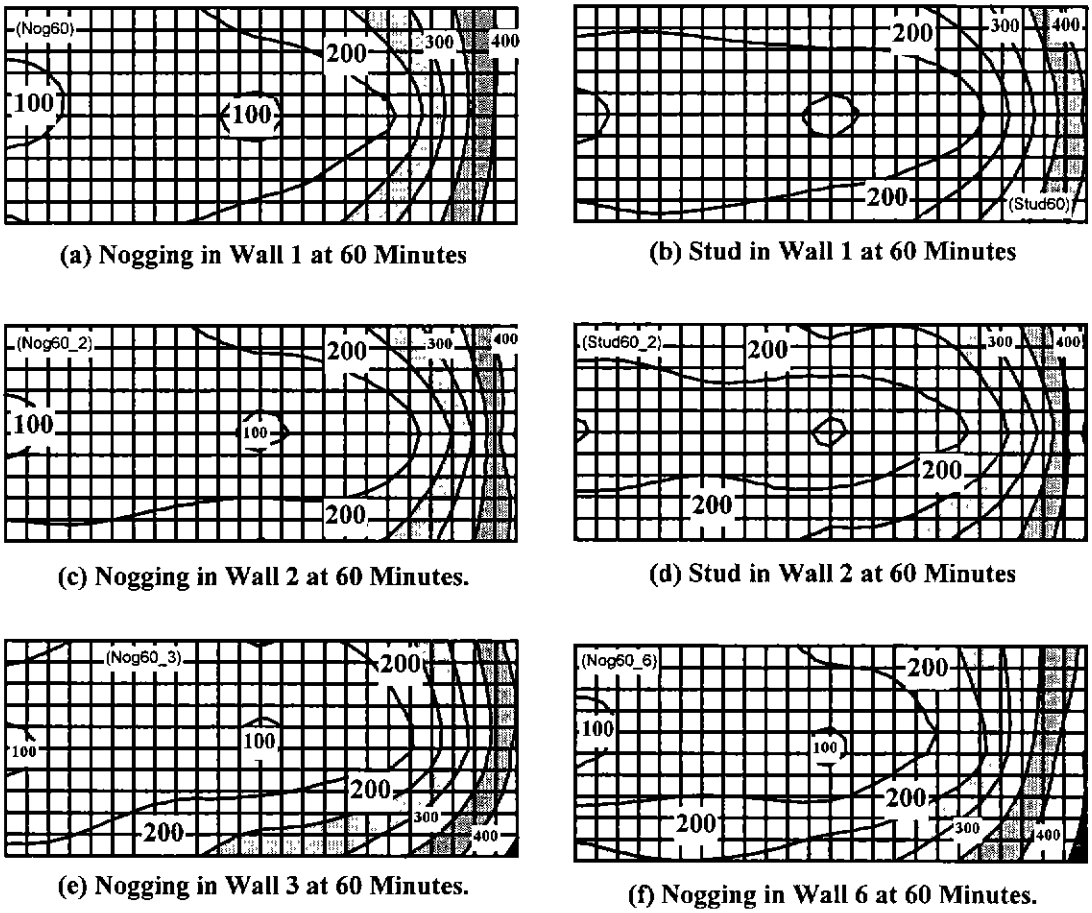

Figure 4.35. Temperature Distributions (°C) in Sections through Noggings and Studs at 80 Minutes. (Sections cropped 7.5 mm from edges. Median temperatures ±25°C in white bands shown.)

Figure 4.36 shows the temperature distributions at sections in studs and noggings in Walls 1-3 at 80 minutes. These walls all failed within a minute of each other. The average time of failure was 89 minutes (§4.5.4). The temperature distributions in Figure 4.36 are generally consistent. There is very little time lag between temperature distributions except at S14 in (d) which shows the temperature distribution in a stud in Wall 2. Figure 4.27 also shows the same inconsistency, evident from the diverging plots for thermocouple S14. No reason for the divergence is apparent from any of the data gathered. A possible reason may be separation of the stud from the gypsum board on the ambient side, thereby allowing cavity gas to heat the ambient facing side of the stud. All other results are consistent and hence it is reasonable to conclude that the thermal properties in noggings and studs in these walls at this time are also similar for the temperature range of 100-500°C.

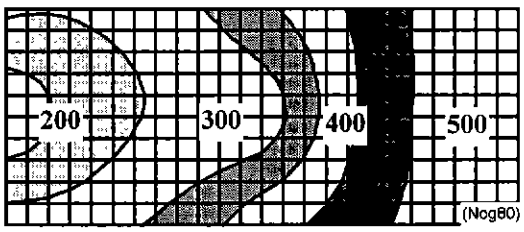

(a) Nogging in Wall 1.

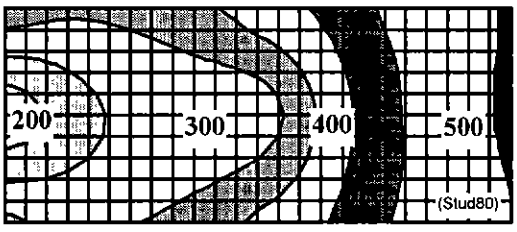

(b) Stud in Wall 1.

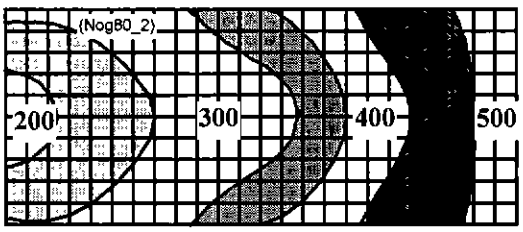

(c) Nogging in Wall 2

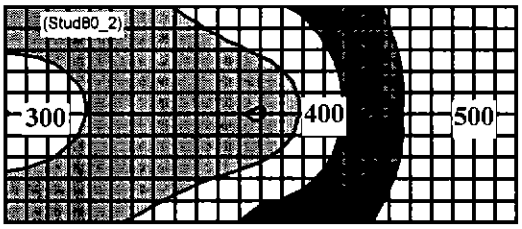

(d) Stud in Wall 2.

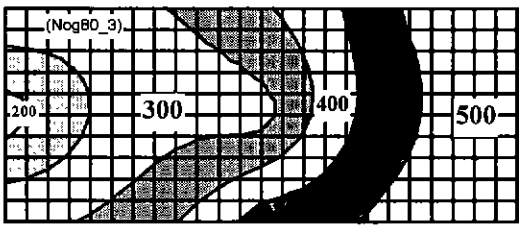

(e) Nogging in Wall 3.

Figure 4.36. Temperature Distributions (°C) in Sections through Noggings and Studs in Walls 1-3, at 80 Minutes. (Sections cropped 7.5 mm from edges. Median temperatures ±25°C in white bands shown.)

4.7 Conclusions from Experimental Program

The results in experiments 1-6 and 8 indicate that reproducible temperature distributions and times of structural collapse of walls can be achieved if:

1. The furnace, and the relationship for fire gas temperature with time are the same for all experiments.
2. Timber framing is chosen from a narrow range of elastic moduli and a narrow range of strength grades (§4.2).
3. Timber studs for each wall are systematically chosen to cover the same range of elastic moduli (Table 4.1).
4. Load and support conditions are the same.
5. Initial moisture content is consistent amongst all studs.

From the consistency in temperature distributions and times of collapse it seems that thermal properties of materials, surfaces and cavities are consistent. Consistency in gypsum board would be expected because of consistency in manufacturing processes. It is apparent that the selection of timber studs from the same species and with similar elastic moduli ensured consistency in the thermal properties of timber.

Temperatures in timber studs in walls are very similar to those in noggings after radiation becomes the dominant heat transfer mode in cavities. This similarity occurs when the gypsum board on the fire side has fully converted to dihydrate. Results in these experiments show that temperature distributions in noggings are reasonably similar to those in studs in the early stages as well. Hence thermocouples can be inserted into noggings rather than studs, so as not to affect the loadbearing capacity of walls. Dummy studs can be avoided so as not to affect the geometry of cavities and hence not affect heat transfer.

Modelling assumptions mentioned in Aim 3 (§4.1) were generally supported by the experiments. There was little variation of temperatures with height up walls indicating that modelling heat transfer in two dimensions is satisfactory (Figure 4.18, Figure 4.24 and Figure 4.25). There was little variation in temperatures at similar points in horizontal planes through walls (Figure 4.19). Thus heat transfer modelling based on representative portions of walls as shown in Figure 3.2, to improve computational efficiencies, is valid. In these experiments, radiation was the dominant mode of heat transfer in cavities when average temperatures of the surface of gypsum boards bounding the cavities on the fire side exceeded 300°C, after 30 minutes of fire exposure. Prior to this time, evidence of laminar convection is apparent in temperature distributions in cavities (Figure 4.24). It was apparent that convection and moisture transfer prior to 30 minutes (Figure 4.33) produced distributions of temperatures less than 100°C, in studs and noggings (Figure 4.30 and Figure 4.31) that were quite different to the temperature distributions expected from the modelling assumptions. After 30 minutes, studs and noggings charred and the shape of the temperature distributions in timber members was similar to shape of the temperature distrbutions expected from modelling assumptions. Since fire rated walls (Boral 1994) have not been known to fail before studs have substantially charred, in standard fire tests (AS1530.4) the modelling assumptions (Aim 2 §4.1) which neglect the transfer of heat by the movement of moisture and steam are appropriate.

However, walls in the Experiments 4 and 5 did collapse prior to any significant charring of the studs. At the time of collapse, it was apparent that temperatures were 100°±20°C across much of the sections through studs and noggings, and that the distributions of temperatures were quite random within this temperature range which indicated rapid diffusion of moisture and steam. The steam greatly reduced mechanical properties and caused the failure prior to charring.

The experiments provide adequate data to validate temperature distributions predicted by heat transfer submodels for ordinary timber framed cavity walls sheeted in gypsum board. However, temperatures on the ambient side of walls did not reach sufficiently high values to validate the insulation mode of failure specified in AS1530.4 (§4.6.4).

Thermal degradation of timber framing near supports was less than for other timber framing (§4.5.4). No special heat transfer modelling seems necessary at the supports. The support conditions imposed by attached steel plates can be assumed in structural submodels.

5. Validation of Heat Transfer Model

5.1 Introduction

The research described in this chapter generally aimed to validate the heat transfer model, ADIDRAS. Ideally, validation should be carried out by obtaining thermal properties from simple independent experiments, and using these properties to obtain model predictions for comparison with results from full scale experiments. Since the properties used in the model are functions of just one variable, temperature, ideally the simple experiments would vary just one property with temperature. In reality, properties may depend on several variables including temperature. For example, at elevated temperatures, properties of materials often change with time. To derive properties as a function of temperature alone, and to ensure they lead to good predictions of time of failure, all other properties and phenomena during the simple experiments should be controlled to similar values expected in the full scale wall experiments. This general approach involving simple independent experiments and full scale experiments to validate the heat transfer model was generally undertaken. Some properties were obtained from the literature and were used in faithful manner in the aim that model predictions were, as much as possible, independent of the results of the full scale experiments.

The methodology for validating the heat transfer model, ADIDRAS and for deducing the conclusions has is documented in this chapter, §5 as follows. This chapter commences by explaining how the values for most thermal properties were obtained from small scale independent experiments and from the literature (§5.2). It is convenient to consider the heat flow through the wall in two general paths - one perpendicularly through the wall at the location of wall cavities, the others, as paths to the studs. The evaluation of the heat transfer model for predicting temperatures along the cavity paths is carried out in §5.3. The evaluation of the heat transfer model for predicting temperatures along paths to the studs is carried out in §5.4. In the course of validation of temperatures along paths to studs, the need to consider shrinkage gaps between studs and gypsum board to improve temperature predictions at points at the fire side of studs will be demonstrated. Having established the efficacy of the model in respect of numerical checks in §3.10 and comparisons (§5.3, §5.4) with experimental results obtained in the research, it was desired to compare the efficacy of the models with the efficacy of other models that have been published. This comparison is undertaken in §5.5. To address the aim of modelling a wide scope of wall sections, the application of the model will then be demonstrated in §5.6, with a double stud wall, and comparisons will be made with available experimental results. Conclusions (§5.7) and recommendations for future research (§5.8) in heat transfer modelling will then be summarised.

5.2 Thermal Properties of Materials Adopted for Validation against Wall Furnace Experiments

5.2.1 General

In this section, §5.2 the best estimates are given for thermal properties of materials used in the wall furnace experiments described in §4. These estimates are made with reference to the literature in §2.4 and calibrations to temperature versus time plots obtained in simple independent experiments on individual materials. In §3.3 it was stated that ADIDRAS makes the simplifying assumption that geometry is constant with time to minimise numerical difficulties. It is known, however, that geometry of wall cross-sections does change due to shrinkage of gypsum board and charring. In this section, the thermal properties have been chosen with the aim that modelled heat transfer rates for constant geometry are similar to heat transfer rates in experiments in §4. The assumption is evaluated throughout this section.

5.2.2 Thermal Properties of Furnace

The modelling of the radiant heat flux from the furnace to the exposed surface of a test wall was given as the variable, $\dot{q}''_{r_{bound}}$ which was defined in §3.9.1 as shown below.

$$\dot{q}''_{r_{bound}} = h_{r_{bound,s}} \cdot \left(T_{s,p+1} - T_{bound,p+1}\right)$$

where

$$h_{r_{bound}} = \frac{\varepsilon_{bound,s} \cdot \left(T_{s,p}^4 - T_{bound,p}^4\right)}{T_{s,p} - T_{bound,p}}$$

$T_{s,p}$ = temperature of the surface of wall at time step, p.

$T_{bound,p}$ = fire temperature at time step, p.

$$\varepsilon_{bound,s} = \frac{1}{\frac{1}{\varepsilon_{bound}} + \frac{1}{\varepsilon_s} - 1}$$

ε_s = emissivity of the surface of wall at time step, p.

ε_{bound} = emissivity of the furnace at time step, p.

From the above equations, the radiant heat flux depends on the variables ε_{bound} $T_{bound,p}$ $T_{s,p}$ and ε_s. Values for these were deduced from the plots in Figure 5.1 as discussed below.

Alternative fire temperatures to adopt for, $T_{bound,p}$ are the temperatures measured on the back surface of the furnace (F1-6), and the gas temperatures (F7-10). The average back surface temperature was expected to dominate the heat flux to the wall, since the emissivity of the furnace gas was expected to be low (less than 0.10, from Gray and Muller 1974). However, Figure 5.1 shows a much larger variation in the back surface temperatures compared with the furnace gas temperatures. Since it was more difficult to choose an appropriate back surface temperatures with time, gas temperatures were chosen for $T_{bound,p}$.

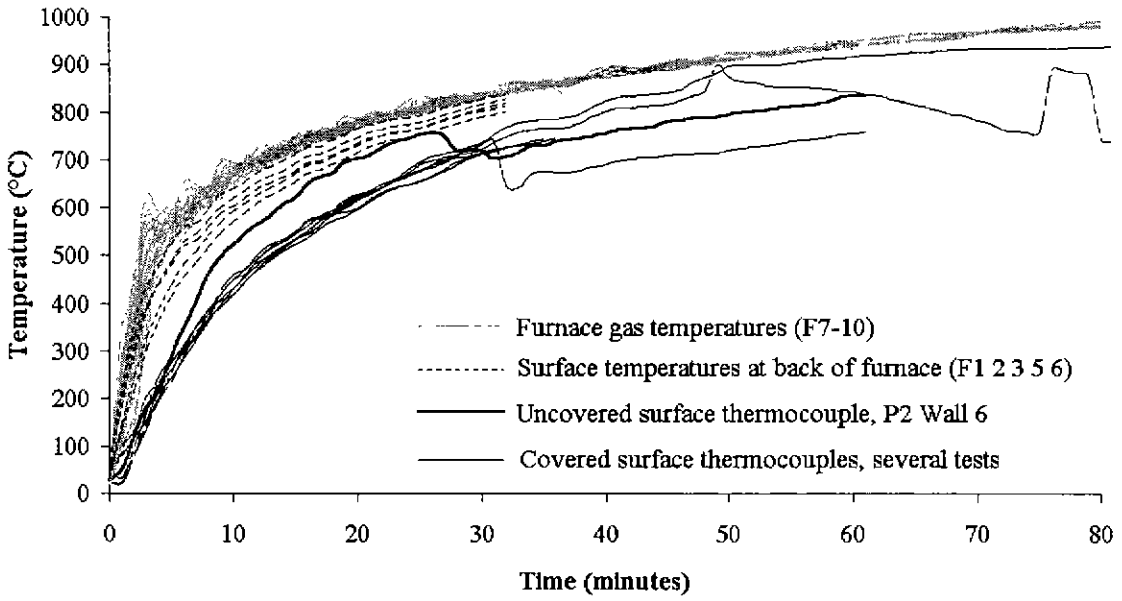

Figure 5.1 (Figure 4.17 repeated). Temperature Measurements in Furnace Gas, and on Surfaces Bounding the Furnace.

Alternative wall surface temperatures to adopt for $T_{s,p}$ in Figure 3.47 are those measured without a pad (continuous thick black line) and those measured with a pad (continuous thin black lines). It was explained that the use of pads is the standard procedure for measuring surface temperatures according to AS1530.4 (§4.3, Figure 4.10). However, the pads insulate the small copper disk in the surface thermocouple from direct heat exchange with the furnace, cooling it by 50-100°C. The uncovered copper discs were dull brown in appearance. Tables in Seigel and Howel (1981) suggest that for such copper, the emissivity would be 0.3-0.6, somewhat less than the emissivity of 0.6-0.9 for gypsum board (§5.2.3.4). Thus, the copper discs would not absorb more radiant heat than the gypsum board surface. Further, the conductivity of copper (460 $W.m^{-1}.K^{-1}$) is very much more than that of gypsum board (0.1-0.2 $W.m^{-1}.K^{-1}$) at high temperatures and thus conduction would greatly influence disc temperatures towards gypsum temperatures. Uncovered thermocouple temperatures thus appear to give a better indication of surface temperatures and have been adopted for $T_{s,p}$.

Surface emissivity, ε_s is a thermal property of gypsum board. The value adopted for ε_s is discussed in respect of thermal properties adopted for gypsum board in §5.2.3.4.

From the values adopted for $T_{bound,p}$ $T_{s,p}$ ε_s and other thermal properties chosen in the remainder of this chapter, §5, the emissivity for the furnace, ε_{bound} was deduced by the calibration of temperatures predicted with ADIDRAS against measured furnace temperatures. Wall surface temperatures predicted with ADIDRAS using emissivities of 0.3, 0.6 and 0.9 for ε_{bound} are plotted in relation to experimental results in Figure 5.2. Compared with the wall surface temperatures measured without pads, the predicted temperature using an emissivity of 0.6 gives the best calibration and has been adopted for the emissivity of the furnace, ε_{bound}. The value of 0.6 is conditional on the ways $T_{bound,p}$ and $T_{s,p}$ are obtained as explained above. From §2.4.1 it was expected that the emissivity should be greater than 0.85. However, since the wall surface temperatures are not very sensitive to furnace emissivities ranging between 0.6-0.9, the accuracy of the value should not be of great concern.

Properties for the convective heat transfer from the furnace gas to the surface of the wall are given in §5.2.5.

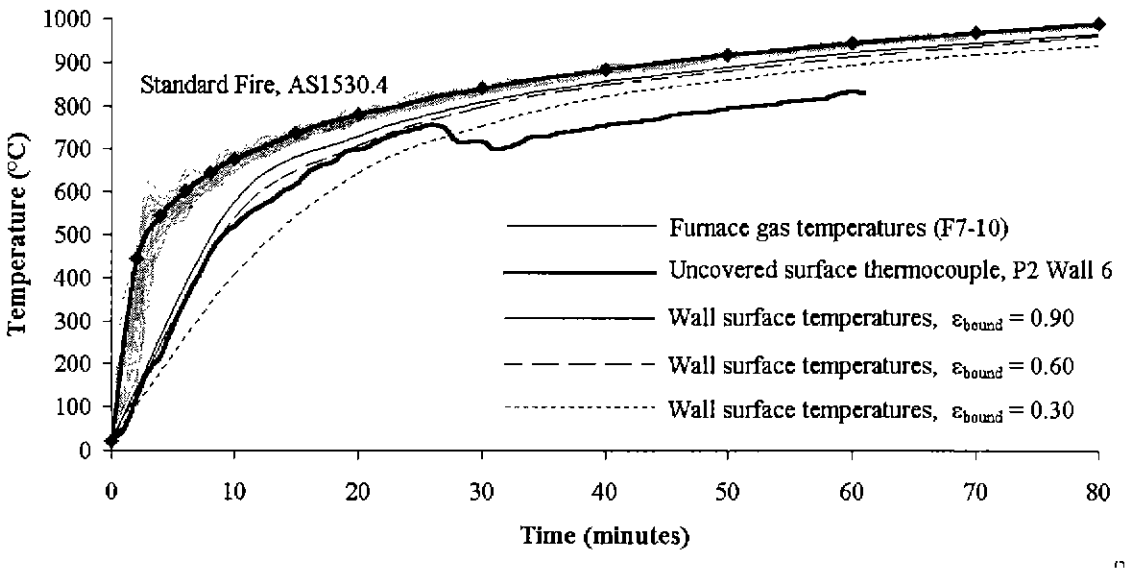

Figure 5.2. Calibration of Emissivity of the Furnace.

5.2.3 Thermal Properties of Gypsum Board

The values adopted for thermal properties in this section are for Boral Firestop (Boral 1997) which was the type of gypsum board used in experiments reported in §4. As mentioned in §5.2.1, thermal properties have been selected on the assumption that geometry is constant with time, and with the aim of modelling similar heat transfer rates as for the gypsum board in the wall experiments reported in §4.

5.2.3.1 Density of Gypsum Board

The mass resulting from exposure at some temperature can be easily measured accurately. Since all gypsum boards predominantly consist of gypsum with only a small amount of additives, published measurements of mass with temperature are relevant to generally all brands of gypsum board. Thus the mass measurements by Mehaffey et al (1994, §2.4.2.2) should accurately indicate the mass of boards with temperature, in the wall experiments in described in §4. Decreases in mass due to the loss of ¾ of moisture as gypsum changes to hemi-hydrate at approximately 100°C and the remaining moisture as hemi-hydrate changes to anhydrous calcium sulphate at 600°C, are apparent in Mehaffey's measurements. If geometry is constant, as is assumed in ADIDRAS (§3.3), then relative density equals relative mass. Thus the relationship for mass versus temperature published by Mehaffey has been adopted for modelling the density of gypsum board with temperature.

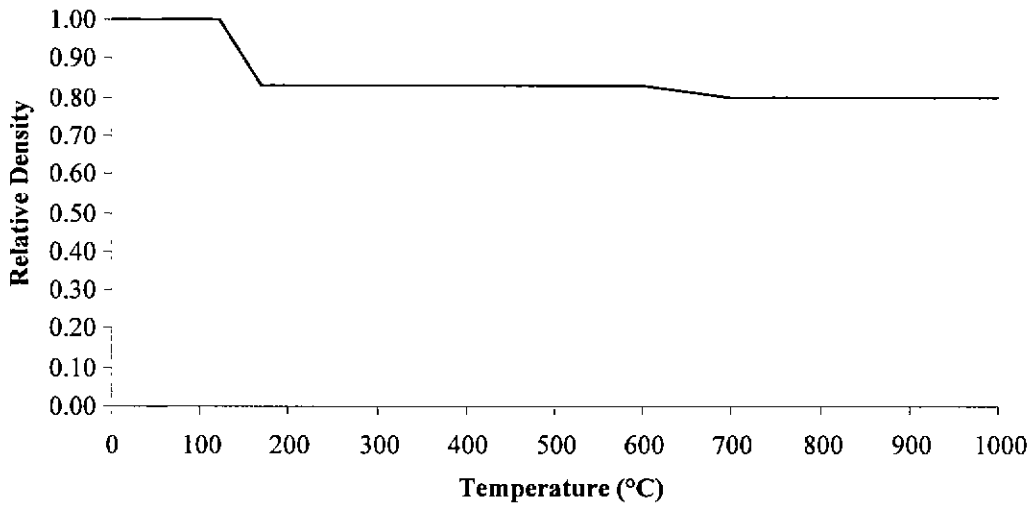

Figure 2.5. Relationship Adopted for Relative Density of Gypsum Board versus Temperature from Mehaffey et al (1994).

5.2.3.2 Conductivity of Gypsum Board

It is apparent in Table 2.1, assuming all things being equal, that conductivity is dependent on density. Since gypsum board was expected to be an important component affecting the time of failure, values for conductivity were carefully derived for Boral Firestop gypsum board (Boral 1997) in accordance with the following procedure:

1. The experimental values of Mehaffey et al (1994) for thermal conductivity of a Canadian gypsum board were adopted as a basis for deriving the thermal conductivity of Firestop.
2. These values for conductivity between the temperatures 20-400°C, were modified for the different density of Firestop compared with that of the Canadian board, in accordance with equations (2.39) and (2.40) which are reproduced further below. These equations basically give conductivity as a function of density. At higher temperatures when gypsum board cracks, these equations do not apply because the ADIDRAS models all heat transfer through solid materials with diffusion equations alone(§3.9.4). Thus values for conductivity used in ADIDRAS must allow for the increase in heat transfer due to the cracking.
3. The derivation of values for conductivities of Firestop was extended for temperatures up to 700°C by calibration against results from an independent small scale experiment involving a sandwich of four sheets of gypsum board exposed to the standard fire, AS1530.4.
4. Values for conductivity at temperatures higher than 700°C were calibrated against results from full scale wall experiments, so that the values not only represented the conductive heat transfer but also the radiant heat which transfers through the cracks. (Mehaffey et al 1994, §3.3). This last stage was the only stage that did not involve means of obtaining conductivity values independently of the full scale experiments described in §4.

Derivation of Conductivities for Temperatures between 20-400°C

Experimental values of Mehaffey et al (1994) used for deriving the expected conductivities of Boral Firestop gypsum board, are shown in Figure 5.3. Mehaffey measured conductivities for gypsum boards with densities of 732 $kg.m^{-3}$ (Canadian Type X) and 648 $kg.m^{-3}$ (Canadian Type C). His measurements were obtained while a lead weight was placed on the samples, thereby slightly crushing them at high temperatures (> 400°C). Presumably, his conductivities are based on the initial thickness of board. The Boral Firestop gypsum boards used in the experiments described in §4 had a density of 810 $kg.m^{-3}$.

Equations (2.39) and (2.40) show that the conductivity depends on the proportion of solid, π_s and hence density, irrespective of material type.

$$k_{max} = \pi_g k_g + \pi_s k_s + \pi_w k_w \qquad (2.39)$$

$$k_{min} = \frac{k_g.k_s.k_w}{\pi_s\pi_w k_g + \pi_g\pi_w k_s + \pi_g\pi_s k_w} \qquad (2.40)$$

Hence, these equations were used to derive the conductivities for temperatures between 20-400°C, before any significant cracking was observed (§4.5.2). As was explained in §2.4.3.3, equations (2.39) and (2.40) model constituents as thin parallel plates. Equation (2.39) models the plates being parallel to direction of the conducted heat flow and equation (2.40) models the plates perpendicular to the direction of the conducted heat flow.

Equations (2.39) and (2.40) can be simplified. As was mentioned in §2.2.1.1, Stray and Bates (1997) confirmed that Firestop like Canadian boards has a free moisture content of approximately 0.5%. Gypsum boards comprise small amounts of constituents, such as vermiculite ash as well as the free moisture, which are unlikely to significantly influence the conductivity of the gypsum board. These constituents were ignored. Ignoring the small amount of free moisture, the equations reduce to,

$$k_{max} = \pi_g k_g + \pi_s k_s \qquad (5.1)$$

$$k_{min} = \frac{k_g.k_s}{\pi_s k_g + \pi_g k_s} \qquad (5.2)$$

Theoretically, these equations can be used with Mehaffey's properties to deduce bounds for the conductivity of Boral Firestop. Equation (5.2) led to negative values for k_s, the conductivity of solid gypsum without voids. This is obviously impossible. Thus the conductivity of gypsum cannot be modelled as alternate plates of air and solid gypsum along the path of conductive heat transfer.

Equation (5.1) was applied to Mehaffey's data for Type X board to make theoretical deductions for conductivies for Type C and Boral board. For the temperature range, 0-90°C, the volumetric proportions of gypsum board comprising solid gypsum without voids, π_s and air voids π_g were deduced from the total densities and the density of solid gypsum without voids, ρ_s (=2320 kg.m^{-3} Dee Snell et al 1971). The deduced conductivities are shown in Table 5.1. For the temperature range, 130-400°C, π_s and π_g can be similarly computed, except the gypsum is in the hemi-hydrate form which has ¼ of the 21% of the bound moisture in ambient gypsum. The density of the hemi-hydrate solids, ρ_s is 1955 kg.m^{-3}. The conductivities derived for the temperature range, 130-400°C are shown in Table 5.2. The conductivities for Boral Firestop gypsum board that were derived from Mehaffey's values between 20-400°C are shown in Figure 5.3.

Table 5.1. Conductivities deduced for Gypsum Boards in the Temperature Range 0-90°C, from Equation (5.1)

Board	ρ_{total} ($kg.m^{-3}$)	ρ_s ($kg.m^{-3}$)	π_s	π_g	k_s ($W.m^{-1}.K^{-1}$)	k_g ($W.m^{-1}.K^{-1}$)	k_{total} ($W.m^{-1}.K^{-1}$)
Type X	732	2320	0.316	0.684	0.726	0.03	0.25
Type C	648	2320	0.279	0.721	0.726	0.03	0.22
Boral	810	2320	0.349	0.651	0.726	0.03	0.27

Table 5.2. Conductivities deduced for Gypsum Boards in the Temperature Range 130-400°C, from Equation (5.1)

Gypsum Board	ρ_{total} ($kg.m^{-3}$)	ρ_s ($kg.m^{-3}$)	π_s	π_g	k_s ($W.m^{-1}.K^{-1}$)	k_g ($W.m^{-1}.K^{-1}$)	k_{total} ($W.m^{-1}.K^{-1}$)
Type X	617	1955	0.316	0.684	0.272	0.05	0.12
Type C	546	1955	0.279	0.721	0.272	0.05	0.11
Boral	682	1955	0.349	0.651	0.272	0.05	0.13

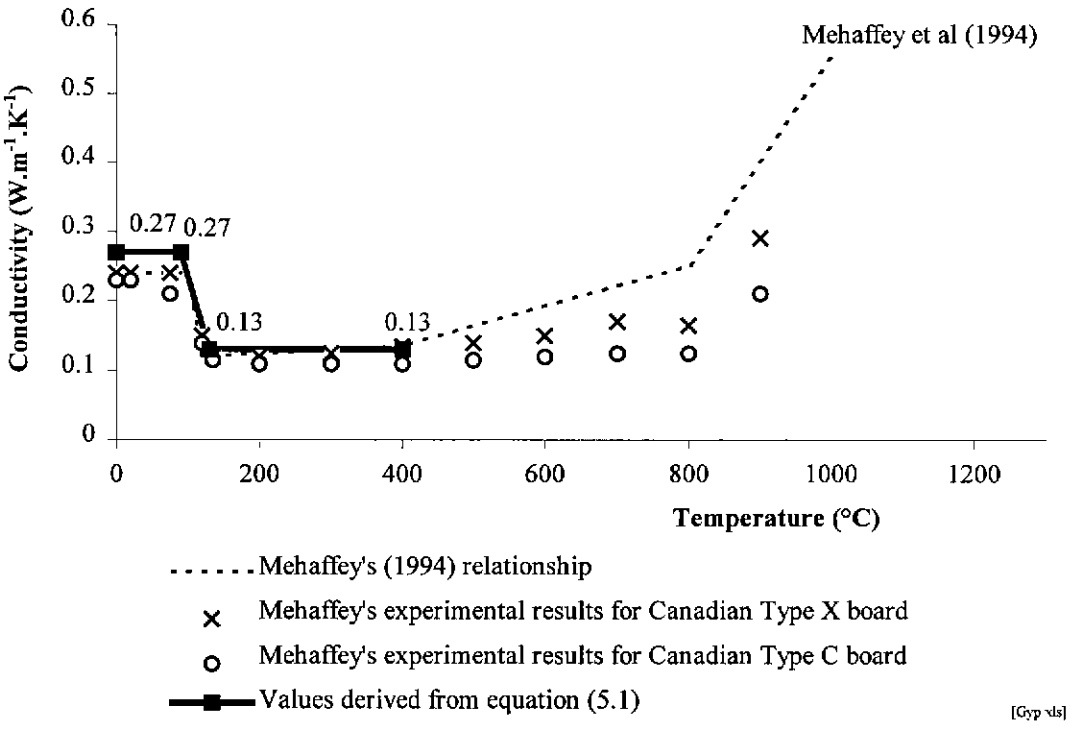

Figure 5.3. Conductivities of Boral Firestop Gypsum Board derived from values from Mehaffey et al (1994), in accordance with Equation (5.1).

Conductivities for Temperatures between 20-700°C

The derivation of conductivity values for Boral Firestop gypsum board as a function of temperature was extended to 700°C by undertaking calibrations with results of experiments that were obtained from Warrington (1998). Warrington's experiments involved a sandwich of four 13mm thick sheets 300x300mm square, placed in a window against a standard fire (AS1530.4). The edges of the window were well insulated. The sheets were sealed against the window, effectively preventing the influx of heat around the edges. The calibration of conductivity values was not carried out at temperatures higher than 700°C because it was believed that the restraint around the edges of the 300x300mm gypsum boards was insufficient to represent the restraint by nails in gypsum board in walls. Consequently, the cracks in the Warrington experiment would not have been as wide or extensive as in gypsum board in full scale wall experiments at temperatures higher than approximately 700°C, when shrinkage greatly increases (Figure 2.1). Calibration in this manner is generally consistent with the manner undertaken by Mehaffey et al (1994), Figure 5.2.

Temperatures were measured with time, at points A and B between sheets, and are plotted as dashed lines in Figure 5.4. The plots of temperatures, that were obtained from conductivity values calibrated with the use of ADIDRAS, are shown as continuous bold lines. The continuous line plots in Figure 5.4 compare well with the dashed line plots after 30 minutes which was approximately the time when the effects of heat transferred by the movement of moisture was reducing in significance. As was explained in §2.2.1.1 and §2.2.2, the vaporisation of moisture in materials such as gypsum board and timber, increases the heat transfer rate in regions where temperatures are less than the vaporisation point (approximately 100°), and reduces the heat transfer rate in regions where temperatures exceed the vaporisation point. These effects of moisture transfer are the reason for the dashed plots being approximately 50°C higher than the calibrated plots during the first 30 minutes. Hence the calibrated plots are the best that can be derived by ignoring the effects of moisture.

The calibrated values for conductivities are plotted as a continuous line in Figure 5.5. The results of Mehaffey et al (1994) are also shown in Figure 5.5 for comparison. The values for conductivities between 20-400°C, obtained from equation (5.1), were found to be suitable in the calibration. The values for conductivities calibrated between 400-700°C compared well with the experimental results of Mehaffey et al (1994), but were significantly less than his recommended conductivity values shown as a dotted line. Mehaffey recommended higher conductivity values to incorporate the heat transfer by radiation into cracks that begin to open at 400°C as a result of gypsum board attempting to shrink within the constraint of the light-timber frame(§2.2.1.3, §2.4.2.4).

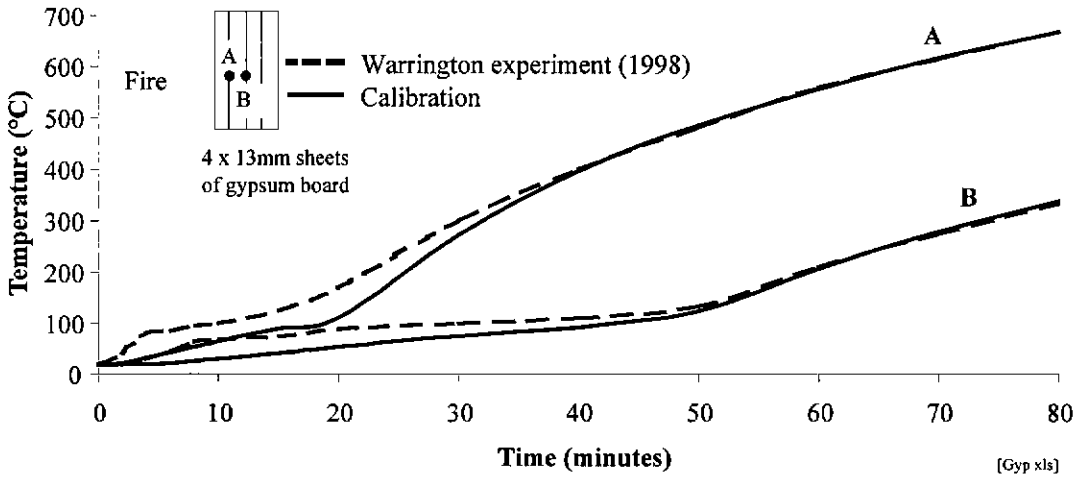

Figure 5.4. Temperature versus Time at Two Points in Four 13mm Thick Sheets of Boral Firestop Gypsum Board Exposed to Standard Fire (AS1530.4)

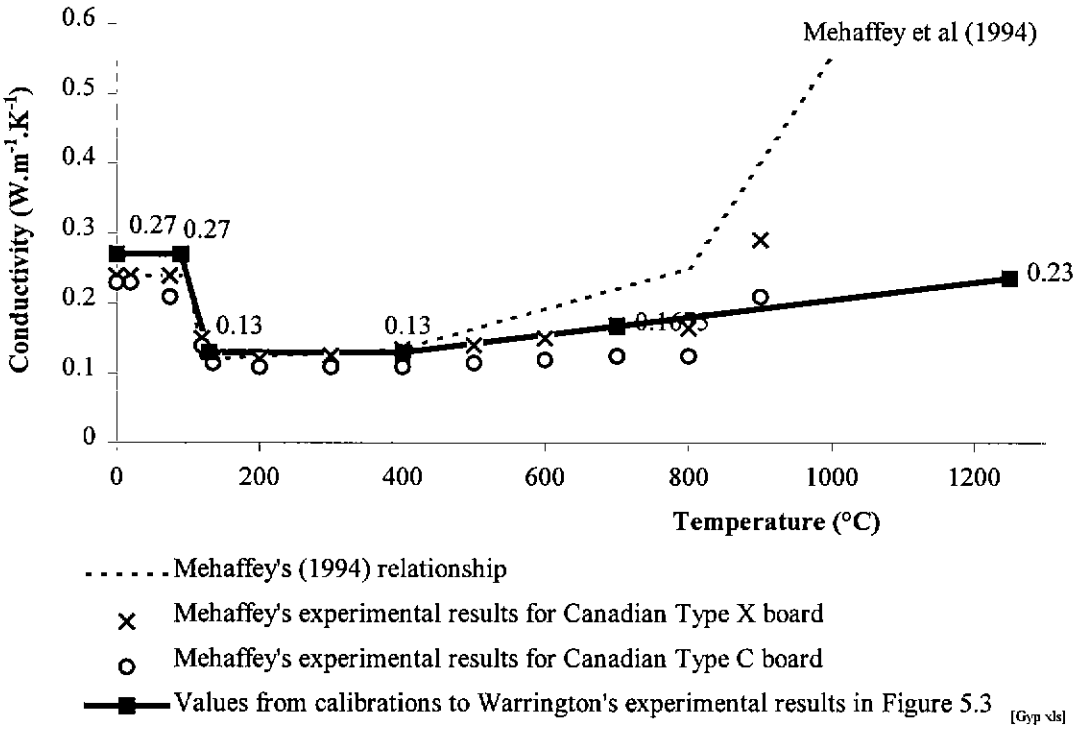

Figure 5.5. Conductivity values of Boral Firestop Gypsum Board derived from calibrations to Warrington's (1998) Experimental Results in Figure 5.4.

The accuracy of conductivity values required for obtaining good predictions of temperature in Boral Firestop gypsum board was evaluated with sensitivity analyses. Each analysis involved increasing the calibrated conductivity values, shown in Figure 5.5 and repeated in Figure 5.6, by 50% over a limited temperature range. The ranges considered were 0-90°C, 130-400°C and above 1000°C. The respective conductivity values are shown in Figure 5.6 as dotted, dashed and thin continuous lines. Rather than sudden step changes in the conductivity at the bounds of these ranges, the changes varied linearly over intervening temperature ranges. The predicted temperatures from these sensitivity analyses and the prediction based on calibrated conductivity values are shown in Figure 5.7. The dotted line shows that changes in gypsum board conductivity in the temperature range 0-90°C has virtually no effect on temperature relative to the prediction based on the calibrated value for conductivity (bold line). The conductivity of gypsum above 130°C most significantly affects temperatures; that is, by 100°C. Since a 50% change in conductivity values results in a 100°C change in temperature, a 10% change should result in a change of 20°C in temperature which is comparable to the variations of measured temperatures shown in Figures 4.20-4.23. Thus, accuracy within ±10% for the values adopted for the conductivity of Boral Firestop gypsum board appears to be acceptable.

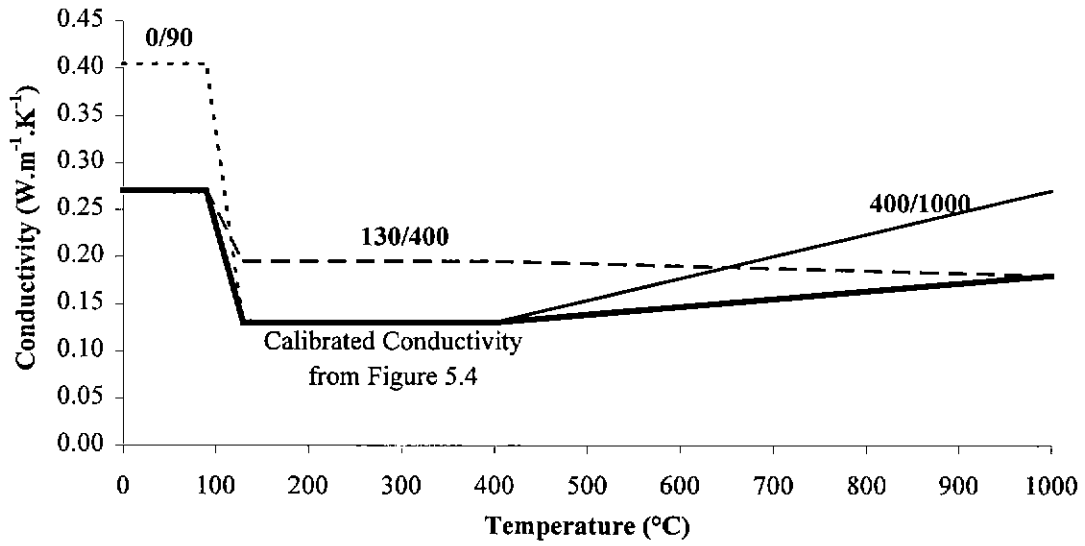

Figure 5.6. Conductivities considered in Evaluating Sensitivity of Temperature versus Time.

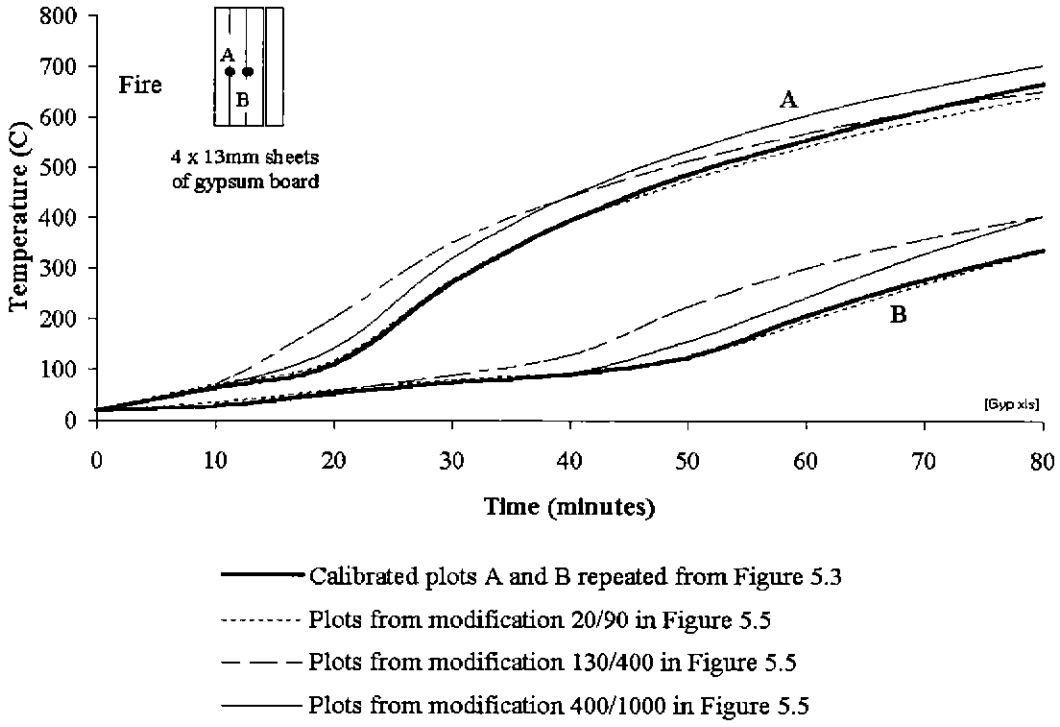

Figure 5.7. Sensitivity of Temperature versus Time in Gypsum Board, to 50% Increases in Conductivity. (Conductivities used to derive each plot are those with the same format as in Figure 5.6.)

Calibration of Conductivity Values for Temperatures Higher than 700°C

Above 700°C, glass fibres within gypsum board melt (§2.2.1.3) and consequently cracks should widen and penetrate to a depth where the temperatures are approximately 700°C. Gypsum board should stay intact until the minimum temperature through the thickness of the board exceeds 700°C. The increase in crack widths should lead to an increase in the rate of heat transfer, mainly by radiation which is the dominant mode of heat transfer at high temperatures. As mentioned in §3.3, the model requires that radiation through cracks in gypsum board at these high temperatures be modelled with conduction equations. Mehaffey et al (1994) showed this expected increase commencing at 800°C rather than at 700°C. Rationally, it is more likely that the increase would start at 700°C which is shown in Figure 5.8. The conductivity values at temperatures above 700°C were obtained by calibration against results from the wall furnace experiments described in §4. The walls had a single 16mm thick sheet of Boral Firestop gypsum board on each side. Calibration analyses with ADIDRAS showed that the 700°C isotherm in the boards directly exposed to the fire, was at the surface at 20 minutes, 8 mm beneath the surface at 60 minutes and 10 mm beneath the surface at 80 minutes. Thus, for a duration of 60 minutes, less than half the thickness of the fire exposed gypsum boards was at temperatures greater than 700°C. Thus, the

conductivity values used in ADIDRAS were largely obtained by means which were independent of the wall experiments described in §4.

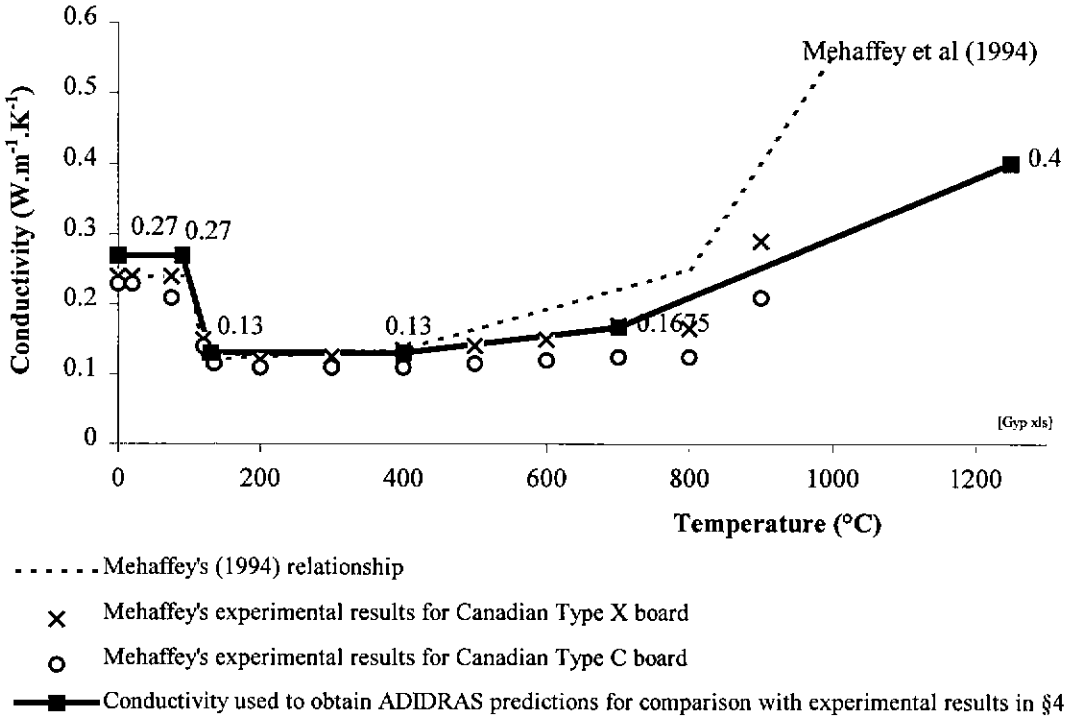

Figure 5.8. Conductivity of Gypsum Board Adopted for Validation of ADIDRAS against Results from Experiments in §4.

5.2.3.3 Specific Heat of Gypsum Board

The literature review in §2.4.2.3 discussed several relationships for the specific heat of gypsum board with temperature. Sultan's (1996) relationship accounts for the peaks in specific heat due to vaporisation during both the formation of hemihydrate (~100°C) and anhydrous calcium sulphate (~600°C). Except for these peaks, Sultan's specific heats are similar to those given by Hadjisophocleous (1996). Since specific heat is not dependent on density, it should be similar for all makes of gypsum board. Sultan's relationship for the specific heat of gypsum boards with temperature has been adopted in heat transfer modelling, and is shown again in Figure 5.9.

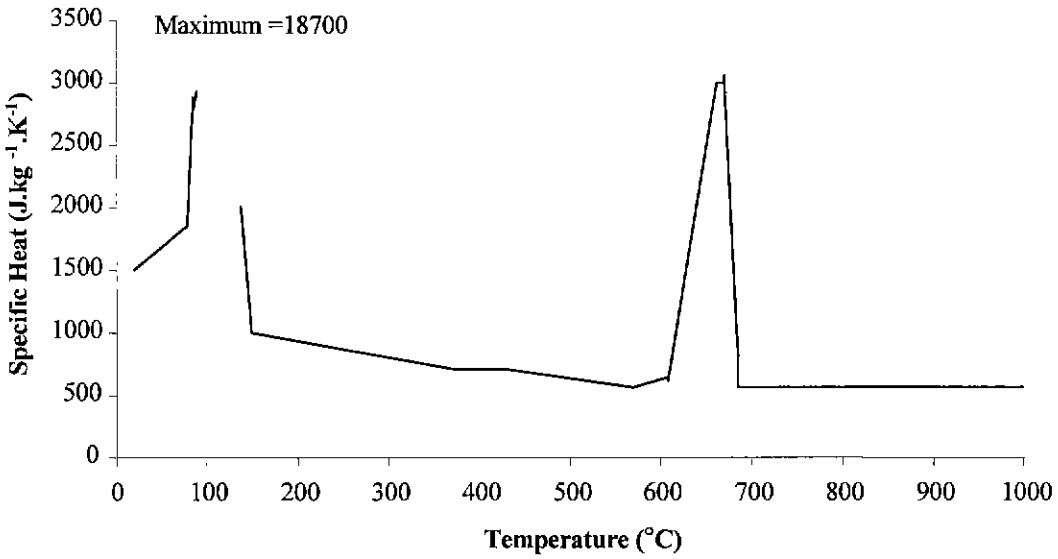

Figure 5.9. Specific Heat Adopted in Heat Transfer Models. (Sultan 1996)

5.2.3.4 Surface Emissivity

From the literature review in §2.4.2.6 it was found that emissivity of gypsum board is somewhere between 0.6 – 0.92. The lower values may result from calibrations ignoring smoke reflectivity and transmissivity, or from the methods used to measure surface temperatures. For example, the use of calcium silicate pads to cover surface thermocouples (Figure 4.10) is likely to increase the resistance to heat flow and indicate emissivity at the lower end of the range; that is, 0.6. Considering smoke and other phenomena, a value for emissivity is calibrated in §5.3 where the modelling of heat transfer through cavities is evaluated. Independent measurements of the surface emissivity of gypsum board were not available.

5.2.4 Thermal Properties Adopted for Timber and Char

Thermal property values of timber have been obtained from the literature in §2.4.3 and from calibrations shown in §5.2.4.4 of model predictions with independent experiments involving small samples of timber. As mentioned in §5.2.1, thermal property values have been adopted on the assumption that geometry does not change with time; for example, char shrinkage has been ignored. Some consequences of char shrinkage on the temperature distribution through a wall are discussed in the comparison of temperatures from models and experiments in §5.4.

The properties in the literature were adopted with due regards to the average characteristics of the timber used in the wall furnace experiments described in §4. The characteristics were - radiata pine species (softwood), an initial average density of 470 $kg.m^{-3}$ (Table 4.1) and a moisture content of 12%.

5.2.4.1 Density of Timber and Char

In §2.4.3.1 it was explained that a number of researchers have adopted relationships between relative dry mass and temperature, for relative dry density. Janssens (1994) gave a methodology for considering thermal expansion and char shrinkage from which the actual density can be determined. For constant geometry with time, which was assumed in the heat transfer model (§3.3), relative density equals relative mass. Janssen's (1994) relationship for relative mass with temperature in Figure 2.9 has been adopted for relative density and is shown again in Figure 5.10. The measurement, by Young (1996), of dry density of a sample at 275°C, relative to the initial ambient dry density supports Janssen's model for density.

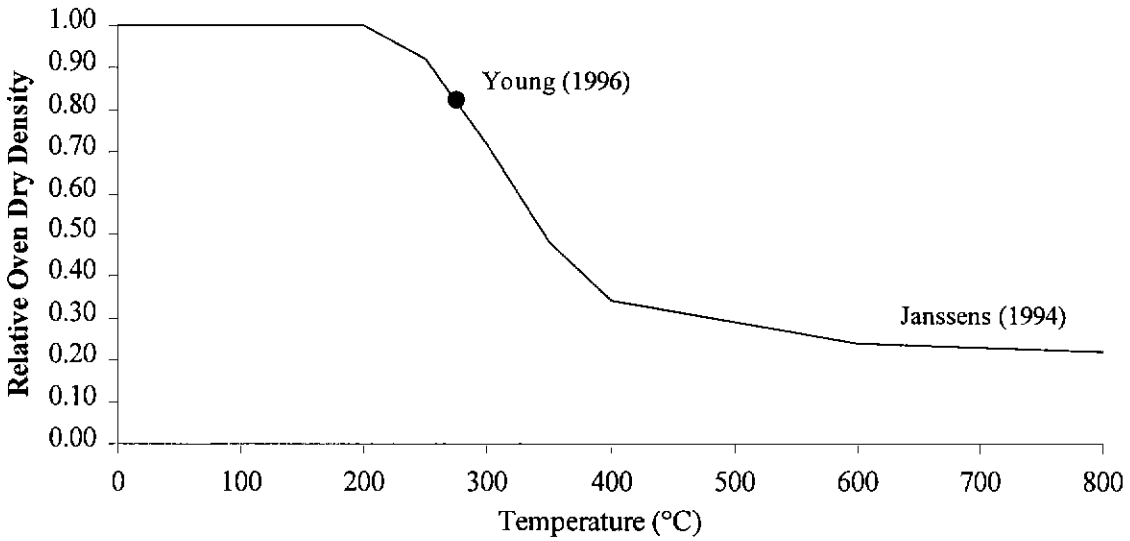

Figure 5.10. Relative Dry Density Adopted (after Janssens 1994).
(One data point plotted from results of experiments by Young, 1996).

5.2.4.2 Conductivity of Timber

In §2.4.3.3 it was shown that there was much consistency in conductivity values published for timber at ambient conditions. However, at elevated temperatures, there is considerable scatter in conductivity values published in the literature. Janssen's (1994) model for conductivity which referred to the work of

Kollman and Malmquist (1956) and Fredlund (1988) gave the most comprehensive treatment of phenomena affecting conductivity, including – porosity, moisture content, density of solid material, radiant heat transfer through pores, and char. His model also accounts for different effects of softwood and hardwood on conductivity. The comprehensive treatment of phenomena by Janssen's model, makes it a desirable one to adopt from the literature. From his model, the relationship for conductivity for the timber used in the wall experiments (§4) - that is, softwood, 470 $kg.m^{-3}$, 12% moisture content - is shown below in Figure 5.11.

Figure 5.11 also shows the conductivity values calibrated to Young's experimental results (§5.2.4.4). Calibration of conductivity values was carried out for a timber sample with a density of 401 $kg.m^{-3}$. The calibrated conductivity was then scaled by the proportional increase in conductivity computed from Janssen's model as density was increased from 401 to 470 $kg.m^{-3}$.

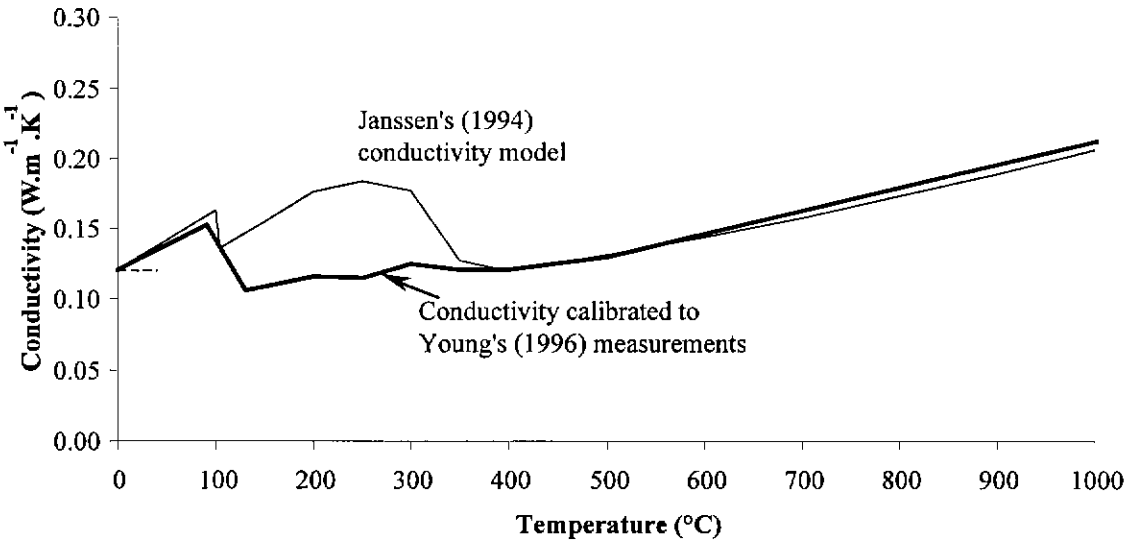

Figure 5.11. Conductivity Values of Timber Adopted in §5.4.

There is a good comparison between Janssen's conductivity values and those calibrated from Young's experimental results, except in the temperature range between 100-350°C. There may be some endothermic reactions during pyrolysis which would explain the lower conductivity values obtained from calibration. To obtain plots for the comparison of predicted and measured stud temperatures in §5.4-p173, both Janssen's model and the conductivity values calibrated from Young's experiments are to be used.

5.2.4.3 Specific Heat of Timber

Janssens' (1994 , equation 2.36) relationship for specific heat of wood with temperature has been adopted. He considers the heat content involved in binding water in wood cells, which does not appear to have been considered by other researchers reviewed in §2.4.3.2. Further, since Janssen's model for conductivity was adopted in the previous section it was desirable to be consistent and choose his model for specific heat. Consistent with a number of other modellers including Fredlund (1988), Gammon (1986), Thomas (1997), any heat of pyrolysis has been ignored. It was observed in §2.4.3.3, that researchers who adopted conductivities greater than 0.10 $W.m^{-1}.K^{-1}$ for char, ignored any heat of pyrolysis, while Knudson (1975) who used a low conductivity of 0.05-0.08 $W.m^{-1}.K^{-1}$ adopted some exothermicity, resulting in similar modelled rates of heat transfer.

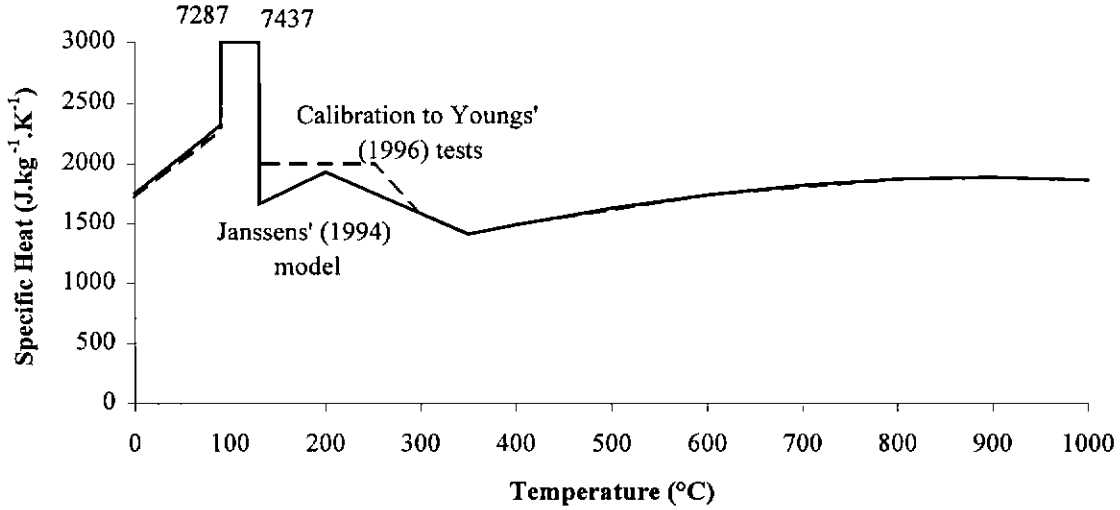

Figure 5.12. Relationships for Specific Heat of Timber with Temperature Adopted in Heat Transfer Models.

5.2.4.4 Comparison of Temperatures Predicted Using the Adopted Thermal Properties with Temperatures from a Simple Experiment on a Timber Section.

A simple experiment by Young (1996) enabled the property values given in §5.2.4.1-§5.2.4.3 to be evaluated. He measured temperatures at several points in timber which was the same species and had similar density and moisture content to the timber used in the experiments described in §4. The samples were 300x35x90mm in size and were heated on all surfaces along the grain, with steel plates of uniform temperature shown in Figure 5.13. Samples had an initial density of 401 $kg.m^{-3}$ and a moisture content of

11.4%. The experiments gave the times necessary to heat the samples to required uniform temperatures prior to measuring compression properties which are reported in §6.3.7.

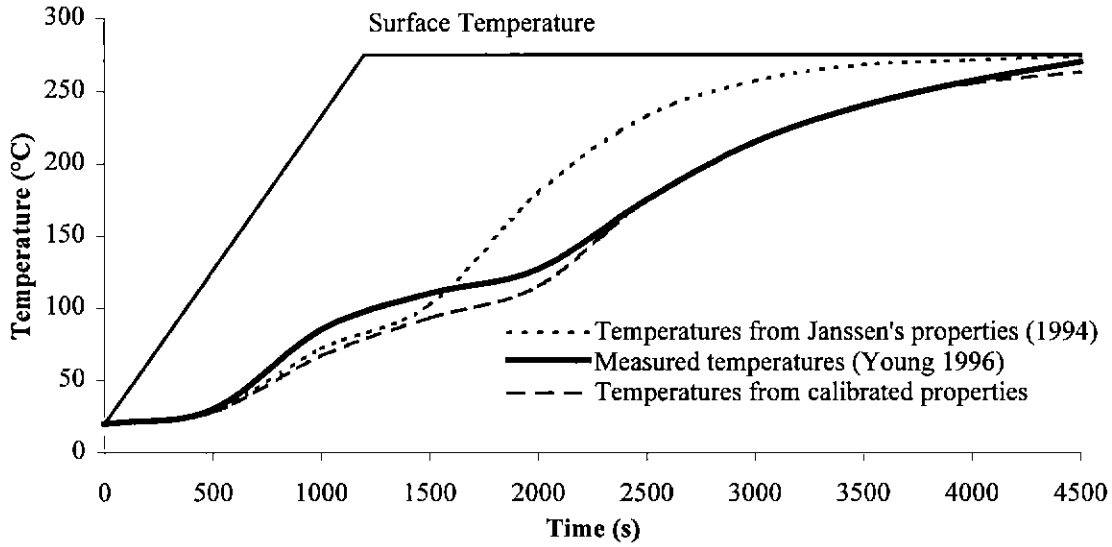

Figure 5.13. Comparison of Predicted Temperatures and Temperatures Measured at the Centre of 300x90x35mm Sample of Timber by Young (1996).

Figure 5.13 shows the measured temperatures at the centre of the sample and predictions with ADIDRAS using Janssens' thermal property models in §5.2.4.1-§5.2.4.3 and properties calibrated to the results of Young's (1996) experiments. Janssens' properties led to the dotted plot which is conservative. Temperatures predicted with his property values were 500 seconds earlier than occurred in Young's experiments after 1500 seconds. Alternatively, predicted temperatures were generally 75°C higher than temperatures measured above 150°C at the same time. The calibrated conductivity values in Figure 5.11 and the calibrated specific heat in Figure 5.12 led to the dashed line. The calibration matches experimental results for temperatures above 150°C. There is a slight difference for lower temperatures. However, calibration in this temperature range, using diffusion modelling, is hindered by moisture transfer. Imprecision in calibration at these lower temperatures is not as important as at higher temperatures because the heat flow from the fire must first transfer through high temperature regions.

Both Janssens' and the calibrated property values are considered in evaluating the modelling of heat transfer into studs with ADIDRAS, in §5.4.

5.2.4.5 Surface Emissivity of Timber

From the literature review in §2.4.3.5, a mid-range value of 0.65 for emissivity of dry timber was chosen (Kollman and Malmquist 1955). From their relationship, equation (2.46) for emissivity of timber versus moisture content, an emissivity of approximately 0.80 was adopted for the timber of 12% moisture content, used in the wall experiments described in §4. From §2.4.3.5 and Table 2.2, materials similar to char at temperatures greater than 200°C have an emissivity of 0.80 which was adopted in deriving the plots in §5.4. The adopted values for the surface emissivity of timber and char are summarised in Figure 5.13.

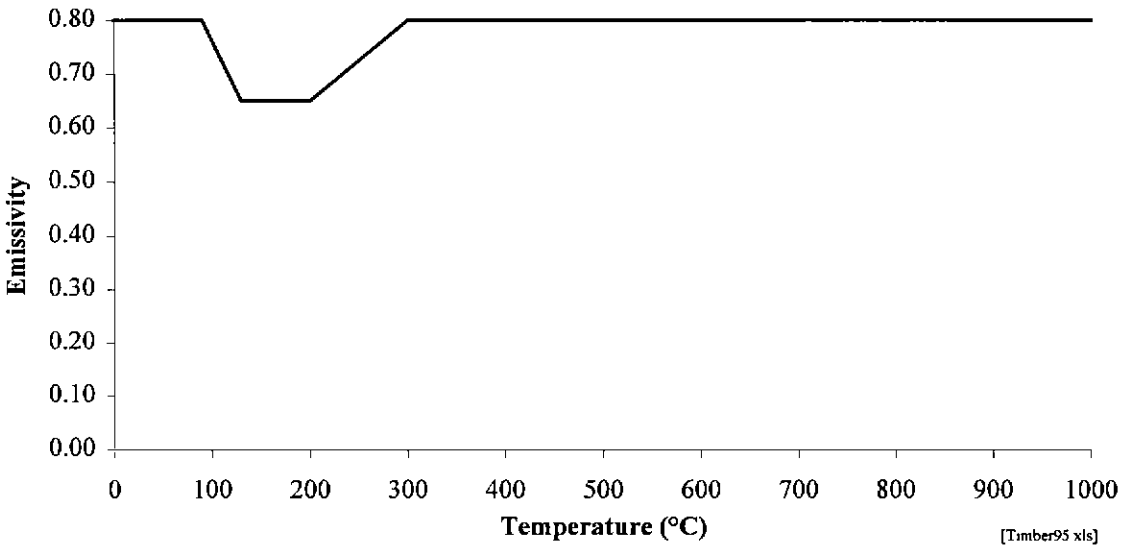

Figure 5.14. Emissivity Values Adopted for Timber and Char.

Heat transfer from the cavity into the stud involves radiation and convection in series with diffusion. Since the thermal diffusion is a much slower heat transfer mode than radiation and convection at temperatures above 300-400°C, then thermal diffusion in wood is the dominant heat transfer mode that controls degradation and the time of failure. Due to the lower dominance of radiation, great accuracy for the emissivity of timber is, thus, not necessary. An approximate constant value of 0.8 would be acceptable for all temperatures. However, allowance has been made for the smaller emissivity of 0.65 for hot dry wood (100°-300°C).

5.2.5 Convective Heat Transfer Coefficients

5.2.5.1 Convective Heat Transfer Coefficients for External Wall Faces

A summary of convective heat transfer coefficients for the external surfaces of walls, similar to those described in §4, are given in Table 5.3. Coefficients are given for both the ambient and furnace facing sides. The walls were 3.00 metres high and were exposed to standard fires (AS1530.4). Equations for coefficients and values adopted by various researchers were given in §2.4.4.1. Values derived from the equations are given below.

The convective heat transfer coefficients in Table 5.4 and Table 5.5 were deduced for the temperatures recorded during the experiments described in §4.6.2. The temperatures were substituted into equation (2.48) to obtain the Rayleigh numbers and into equation (2.49) to obtain bouyancies. The results of these two equations were substituted into equations (2.47) and (2.51) to obtain Nusselt numbers which were substituted into equation (2.8) to finally obtain the convective heat transfer coefficients listed. Values for thermal properties such as ν and α, were obtained from tables of thermal properties for air with temperature given in Incropera and De Witt (1990).

Table 5.3. Coefficients for Convective Heat Transfer between Gas and External Vertical Surfaces of Walls.

	Convective Heat Transfer Coefficients ($W.m^{-2}.K^{-1}$)	
	Furnace Side	Ambient Side
Mehaffey et al (1994)	25	9
Thomas (1997)	Ignored	6 when (T_g-T_s) = 25°C 8 when (T_g-T_s) = 50°C 10 when (T_g-T_s) = 100°C 12.6 when (T_g-T_s) = 200°C
Sterner and Wickstrom (1990) equation (2.50)	4.6 when (T_g-T_s) = 25°C 5.8 when (T_g-T_s) = 50°C 7.3 when (T_g-T_s) = 100°C 9.2 when (T_g-T_s) = 200°C	4.6 when (T_g-T_s) = 25°C 5.8 when (T_g-T_s) = 50°C 7.3 when (T_g-T_s) = 100°C 9.2 when (T_g-T_s) = 200°C
Typical values obtained in Table 5.4 and Table 5.5.	2	2

There are substantial differences in coefficients given by various researchers listed in Table 5.3. These differences are not expected to significantly affect the time of failure since the overall proportion of heat transferred by convection is much smaller than the proportion of heat transferred by radiation during the total furnace exposure time. Since a coefficient of 2 is theoretically rational, this value has been adopted.

Table 5.4. Temperatures from Experimental Results in §4 Substituted into Convection Equations and Resulting Coefficients for Convective Heat Transfer on Vertical Wall Surface Exposed to Furnace.

Time (min)	Difference in Temperatures T_s-T_g (°C)	Estimated Temperature of gas in boundary layers, T_f (°C)	T_f (K)	Ra_H equation (2.48)	h from equations (2.47), (2.48)		h from equations (2.51) & (2.8)
					Laminar	Turbulent	
10-20	200	550	823	1.42×10^9	2.40	2.11	2.93
30-40	150	800	1073	8.76×10^8	2.03	1.79	2.29
70-80	100	925	1198	4.38×10^8	1.79	1.58	1.92

Table 5.5. Temperatures from Experimental Results in §4 Substituted into Convection Equations and Resulting Coefficients for Convective Heat Transfer on Vertical Wall Surface on Ambient Side.

Temperature, T_s of Surface on Ambient Side (°C)	Difference in Temperatures T_s-T_g (°C) (T_g = 20°C)	Estimated Temperature of gas in boundary layers, T_f (°C)	T_f (K)	Ra_H equation (2.48)	h from equations (2.47) & (2.8)	h from equations (2.51) & (2.8)
25	5	23	298	1.42×10^{10}	1.86	2.34
50	30	40	313	8.76×10^9	1.80	2.26
100	80	80	353	4.38×10^9	1.62	2.07
150	130	130	403	2.46×10^9	1.50	1.93

5.2.5.2 Convective Heat Transfer Coefficients for Wall Surfaces Bounding Cavities

A summary of convective heat transfer coefficients for wall surfaces bounding cavities in 3 metre high walls, was given in §2.4.4.2. It is repeated below in Table 5.6. The coefficients are for temperature differences between a surface and the centre of a cavity. These coefficients have been obtained from Mehaffey et al (1994), Thomas (1997), Sterner and Wickstrom (1990). Coefficients were also obtained from equations (2.53) and (2.54) as explained below.

Table 5.7 details how coefficients from equations (2.53) and (2.54) were obtained from measured temperatures plotted in Figure 4.20. Values for thermal properties such as ν and α were obtained from tables of thermal properties for air with temperature given in Incropera and De Witt (1990).

Table 5.6. Coefficients for Convective Heat Transfer between Internal Surface of Sheeting and Centre of Cavity. (The coefficients are assumed to be the same for internal surfaces on the furnace and ambient sides.)

	Convective heat transfer coefficient. ($W.m^{-2}.K^{-1}$)
Mehaffey et al (1994)	9
Thomas (1997)	2.9 when (T_g-T_s) = 25°C 3.6 when (T_g-T_s) = 50°C 4.6 when (T_g-T_s) = 100°C 5.7 when (T_g-T_s) = 200°C
Sterner and Wickstrom (1990)	4.6 when (T_g-T_s) = 25°C 5.8 when (T_g-T_s) = 50°C 7.3 when (T_g-T_s) = 100°C 9.2 when (T_g-T_s) = 200°C
Coefficient deduced from Table 5.7	12

As in Table 5.3 there are substantial differences in coefficients given by various researchers listed in the Table 5.6. These differences are not expected to significantly affect the time of failure, due to the dominance of radiant heat transfer over convection. The value of 12 has been derived with some theoretical rigor and is thus adopted.

Table 5.7. Coefficients for Convective Heat Transfer determined from Equations (2.53)and (2.54).

Time (min)	Difference in Temperatures of Surfaces T_{s1}-T_{s2}	Estimated Temperature of gas in boundary layers (K)	h_{12} from Equation (2.53) ($W.m^{-2}.K^{-1}$)	h_{12} from Equation (2.54) ($W.m^{-2}.K^{-1}$)	h_1, h_2 ($W.m^{-2}.K^{-1}$)
10-20	50	400	6.85	5.02	11.9
30-40	300	600	7.15	5.30	12.5
70-80	150	800	4.16	2.60	6.8

Notes:

T_{s1} is the temperature of surface 1, that is the internal surface of sheet on the furnace side.

T_{s2} is the temperature of surface 2, that is the internal surface of sheet on the ambient side.

h_{12} is the coefficient for convective heat transfer from surface 1 to surface 2.

$$= \left(\frac{1}{h_1} + \frac{1}{h_2}\right)^{-1}$$

h_1 is the coefficient for convective heat transfer from surface 1 to the centre of the cavity.

h_2 is the coefficient for convective heat transfer from surface 2 to the centre of the cavity, and is assumed to equal h_1.

5.2.6 Thermal Properties of Air and Smoke in Cavities

One of the aims in §1.5 was to, "analyse radiant heat transfer including the absorption and re-emission of radiation through smoke, and thus determine whether more accurate modelling of radiant heat transfer through smoke should be carried out". To achieve this aim it is sufficient to undertake an approximate analysis to determine the range over which temperatures vary due to the effects of smoke. Thus it is sufficient to obtain approximate values for thermal properties to estimate this range and thence deduce the level of significance of smoke in its effects on heat transfer. Accordingly, approximate values for thermal properties of smoke are estimated below.

The thermal properties of clean air are given in Table 5.8. However, from observations in §4.5 it is apparent that during fire exposure, air in cavities is infused with moisture, vapour, volatiles, and solid smoke particulates- all of which will collectively be referred to as smoke. The thermal properties of the smoke in the cavities will be influenced by the thermal properties of moisture and other constituents of smoke. The influence of these other constituents are considered below.

In the walls in the experiments described in §4, the initial mass of moisture in the walls would have been approximately 21% (§2.4.2.5) of the mass of gypsum board; that is,

Initial moisture
$= 0.21 \times 810 \text{ kg.m}^{-3} \times 2 \text{ sheets} \times 0.016 \text{ mm}$
$= 5.4 \text{ kg per square metre of wall}$

If half of all the initial moisture in the walls transferred outside the walls and half to the cavities during fire exposure, the density of this moisture portion of smoke would be.

$= 0.5 \times 5.4 \text{ kg.m}^{-2} / 0.090 \text{ m}$
$\approx 30 \text{ kg.m}^{-3}$

where 0.090m is the width of the cavity. Moisture has four times the specific heat of air at temperatures less than 100°C and vapour above this temperature has twice the specific heat of air (Incropera and DeWitt 1990). Since the mass of moisture and vapour could be much larger than that of air, these constituents could double the specific heat as air turned to smoke.

Figure 5.10 shows the density of wood reduces by 80% when it chars. Figure 4.35 shows that at 60 minutes, approximately half of the stud sections have charred. Thus, approximately 40% of wood changes to smoke and volatises during charring. The density of volatiles would therefore be approximately,

$\approx$ 0.40 x mass of stud / volume of cavity
$= 0.40 \times 470 \text{ kg.m}^{-3} \times (90 \text{ mm} \times 45 \text{ mm}) / (380 \text{ mm} \times 90 \text{ mm})$
$\approx 20 \text{ kg.m}^{-3}$

From Figure 5.12, it is apparent that particulates from charring would have a specific heat of approximately 1500 $\text{J.kg}^{-1}.\text{K}^{-1}$ compared with approximately 1000 $\text{J.kg}^{-1}.\text{K}^{-1}$ for air at the same temperature. Since the density of air reduces to 0.28 kg.m^{-3}, the density of particulates could be very much larger. The addition of char particulates to clean air could increase the specific heat by 50%.

Table 5.8. Thermal Properties of Air (Incropera and DeWitt 1990).

Temperature (°C)	Density ($kg.m^{-3}$)	Specific Heat ($J.kg^{-1}.K^{-1}$)	Conductivity ($W.m^{-1}.K^{-1}$)
27	1.1614	1007.	0.0263
1027	0.2679	1189.	0.0820

It is plausible that the total density of smoke in the cavities could reach a maximum of 50 $kg.m^{-3}$. However, the observations documented in §4.5.3 showed that water condensed in the cavities and dripped with a sooty colour, from the bottom of the walls mounted in steel frames onto the floor. Some proportion of the particulates and moisture appears likely to have fallen out of suspension in the cavities.

The above considers effects of smoke to the thermal diffusion properties of density and specific heat. Unlike the smoke in room enclosures (Jun di Li, 1998), the smoke in wall cavities may significantly affect radiant heat transfer. Since wall cavities are much smaller than room enclosures experiencing flaming combustion, it is plausible that smoke may be more concentrated and thus significantly increase resistance to radiant heat transfer by both absorption and reflection. Reflection of radiant heat by particulates is commonly referred to as back scattering (Siegel and Howell 1981). Since cavities are enclosed and flaming combustion cannot be sustained at an oxygen concentration less than 11% (Tewarson and Pion 1976), then timber studs must char by smoldering. Smoldering produces much larger smoke particles than flaming combustion (Weimert 1998, Bohren and Huffman 1983). The large size of the smoke particles may increase the absorption and back scattering of radiant heat to significant levels.

No measurement of thermal properties of the gas mixture in cavities in light-timber framed walls has been made during the research for this thesis. There is a need to evaluate the resistance to heat transfer caused by smoke and moisture in cavities. The evaluation should consider resistance due to increases in gas density, specific heat, and resistance due to absorption and back scattering of radiation through smoke. The values for thermal properties for air and smoke in
Table **5.9** were adopted as likely typical values within ranges discussed above. The sensitivity of predicted temperatures to these values as well as the sensitivities to absorption and back scattering of radiation were evaluated in §5.3.3 and §5.3.4. The conductivity of 10 $W.m^{-1}.K^{-1}$ was selected to ensure reasonably uniform modelled temperatures in the air and to ensure that modelled convection and radiation dominated heat transfer through the cavity.

Table 5.9. Thermal Properties Adopted for Air and Smoke.

Temperature (°C)	Density ($kg.m^{-3}$)	Specific Heat ($J.kg^{-1}.K^{-1}$)	Conductivity ($W.m^{-1}.K^{-1}$)
0	1	1000	10
100	1	1000	10
105	2	1500	10
250	2	1500	10
300	25	1700	10
1500	25	1700	10

The transmissivity of air and smoke only significantly affects heat transfer when the temperature exceeds 300°C; that is, when smoke forms and radiant heat transfer becomes dominant. The value of transmissivity will have no effect on temperatures less than 300°C. The density of the smoke given in Table 5.9 is 25 $kg.m^{-3}$, approximately 25 times that of clean air. It was assumed that the density for air and smoke was so large as to obscure all direct radiation through the cavities. Unless otherwise mentioned, an arbitrarily large extinction coefficient of 50 was assumed. The effect of the extinction coefficient on temperature distribution is evaluated in the next section, §5.3.

5.3 Evaluation of ADIDRAS for Modelling Heat Transfer through Cavities

5.3.1 Introduction

As explained in §4.6.4, heat transfer through light-timber framed walls can be categorised into two main types - heat transfer through cavities and heat transfer into studs. The heat transfer through cavities involves a path from the fire through gypsum board on the fire side, the cavity, gypsum board on the ambient side and finally to ambient space; that is ABCD in Figure 5.15. The heat transfer into studs involves two heat paths. One path is in the plane of the wall, transferring some heat from the cavity path to the stud. The other path involves heat transferring along a direct line from the fire, through the gypsum board and into a stud. Evaluation of the detailed heat transfer model for heat transfer through the wall cavity is carried out below. Evaluation for heat paths to the studs is carried out in the next section, §5.4.

5.3.2 Heat Flow through Cavities and Surface Emissivity of Gypsum Board.

Figure 5.15 shows plots of temperature versus time at points, A-D on surfaces along heat paths through cavities of walls exposed to standard fire (AS1530.4). The grey lines indicate the results from experiments described in §4. The black lines indicate predictions with the heat transfer model, ADIDRAS; in particular, a continuous line for gypsum emissivity of 0.9, a dashed line for an emissivity of 0.6 and a dotted line for an emissivity of 0.3. The comparison of temperature predictions with ADIDRAS, to temperatures measured in experiments, shows that provided the emissivity of gypsum is between 0.6-0.9, the model generally performs well. A surface emissivity of 0.6 for gypsum board gave the best overall predictions of temperature. This value is lower than most values given in text books such as Incropera and De Witt (1990), but the same as Thomas (1997). The insulation pads placed over the surface thermocouples (Figure 4.10) may have caused the greater apparent resistance to radiant heat transfer and thus explain calibrations indicating an emissivity of 0.6 rather than the common published value of 0.9. Young (1998) measured the emissivity of Boral Firestop gypsum board (Boral 1997) and found it to be 0.7. Further measurements are obviously desired in future research. For the research described in this thesis, a value of 0.6 was adopted for the emissivity of gypsum board.

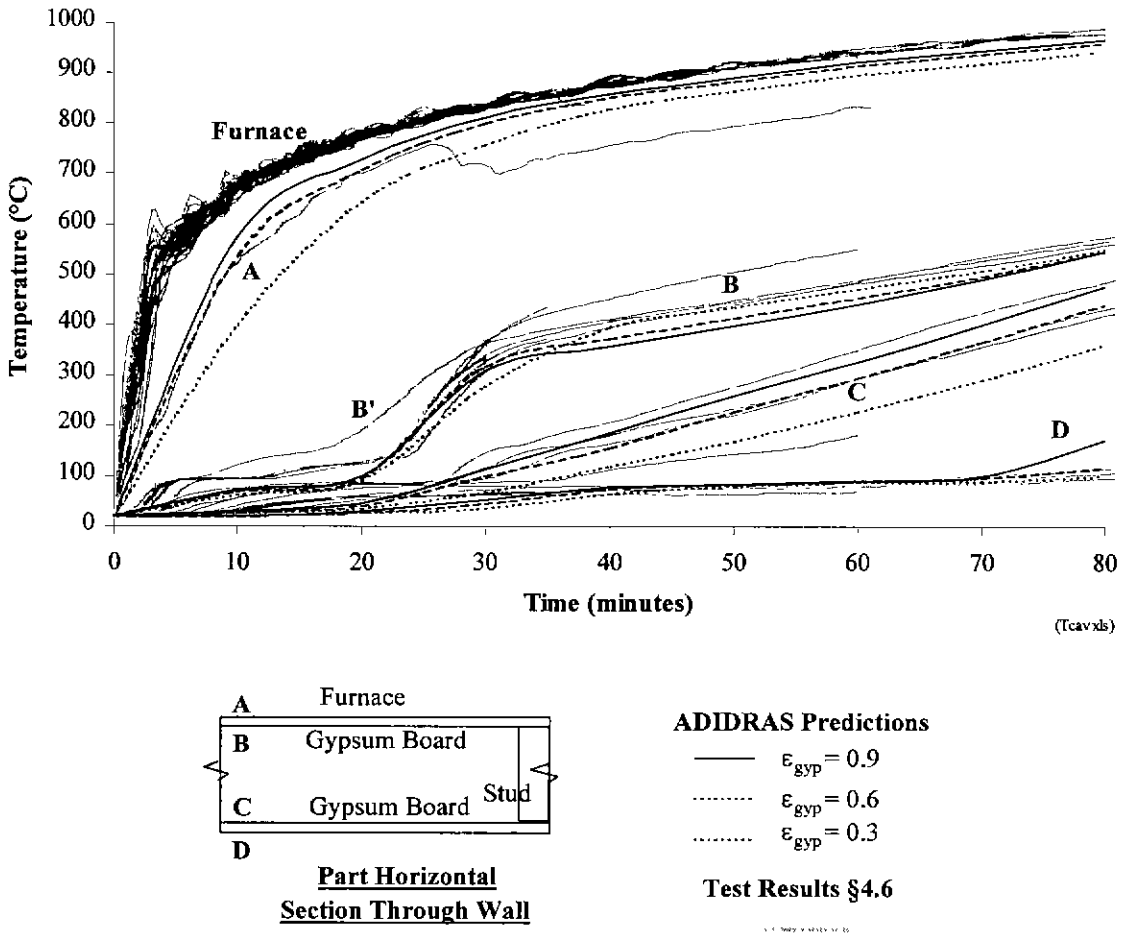

Figure 5.15. Temperature versus Time at Surface Nodes, A-D along Heat Paths through Cavities.

The above comparisons ignore the possible effects of back scattering on calibrated surface emissivites. It is expected that significant back scattering would reduce the apparent calibrated value of the surface emissivity of gypsum boards. However, the temperatures are insensitive to emissivities in the range of 0.6-0.9. Thus, if backscattering does affect calibrations of emissivity within that range, its effect does not appear to significantly affect temperatures.

There is an inconsistency in the temperature plots in Figure 5.15. Although the experimental results for an uncovered thermocouple on the surface facing the furnace gave better comparisons with model predictions than were given by covered thermocouples (Figure 5.1), the same cannot be claimed for the uncovered thermocouple, **B'** on the cavity facing surface of the gypsum board on the furnace side of the wall. Temperatures measured with this thermocouple were as much as 100°C greater than the temperatures measured by the covered thermocouples and the temperatures predicted by the model. Difficulties in measuring surface temperatures due to the presence of steep temperature gradients in the convective boundary layer and surface radiant heat fluxes are apparent. In future research it desirable that the emissivity of gypsum be obtained by direct measurements. Further research is also required into methods for the measuring of surface temperatures.

It is important to evaluate the efficacy of the heat transfer model in predicting the times of failure by insulation and integrity. Insulation failure (AS1530.4) occurs when temperatures on the ambient facing side reach between 150-200°C. The experiments did not encounter these temperatures on the ambient facing external surface. Since model predictions of temperatures plotted as B and C in Figure 5.15, on the surfaces of gypsum boards bounding the cavity compare well with experimental results, it is likely that the model does predict gypsum board temperatures accurately and can be used to predict the time of insulation failure. However, there is some doubt that ADIDRAS and heat transfer models in general can predict the time of insulation failure accurately. The temperature gradients on the ambient side are low and thus greatly increase the variability of times at which a defined insulation failure temperature occur.

Integrity failure occurs when the minimum temperature throughout gypsum board attains some value between 700-950°C (§2.2.1.3). It is virtually impossible for complete integrity failure to occur through a timber framed wall. The timber frame will char and collapse as temperatures rise above 300°C before the gypsum board on the ambient side rises above 700°C and sloughs. The mode of integrity failure which is of concern in timber framed walls is integrity failure of gypsum board on the fire side followed by charring and collapse of the timber frame. In this mode of integrity failure, it is critical that the model accurately predicts when curve B reaches some nominated sloughing temperature - conservatively 700°C. By the time the inside face of gypsum board reaches the sloughing temperature, the low gradient of the temperature-time plot is likely to restrict the accuracy of prediction to ± 5minutes.

5.3.3 Effect of Transmissivity of Smoke on Heat Flux through Cavities

The effect of smoke transmissivity is further examined with the aid of Figure 5.16. The continuous lines in the figure show temperatures predicted with the heat transfer model, ADIDRAS assuming an extinction coefficient of 50. For this value of extinction coefficient, virtually no radiation would be directly transferred through the cavities. The dashed lines show the temperatures when the extinction coefficient is zero resulting in clear transmission of radiant heat between surfaces bounding the cavities. A surface emissivity of 0.6 was assumed for gypsum board. The densities in
Table 5.9 were assumed for the air and smoke in the cavities. There is little difference between corresponding continuous and dashed lines in Figure 5.16. The presence of smoke may greatly affect transmissivity but it does not significantly affect overall heat transfer.

The fact that overall heat transfer is insensitive to transmissivity suggests that modelling heat transfer through cavities represented with just a single node would work well compared with sophisticated radiation models. Simplified modelling of heat transfer through cavities has been undertaken by Mehaffey et al (1994) and Clancy et al (1995). At the time these simplified models were developed, there was less known about thermal properties. Simplified heat transfer models for cavities should be revisited. Temperatures in the cavity predicted by models was uniform within 20°C. This result further suggests that heat transfer through cavities can be modelled with a single node.

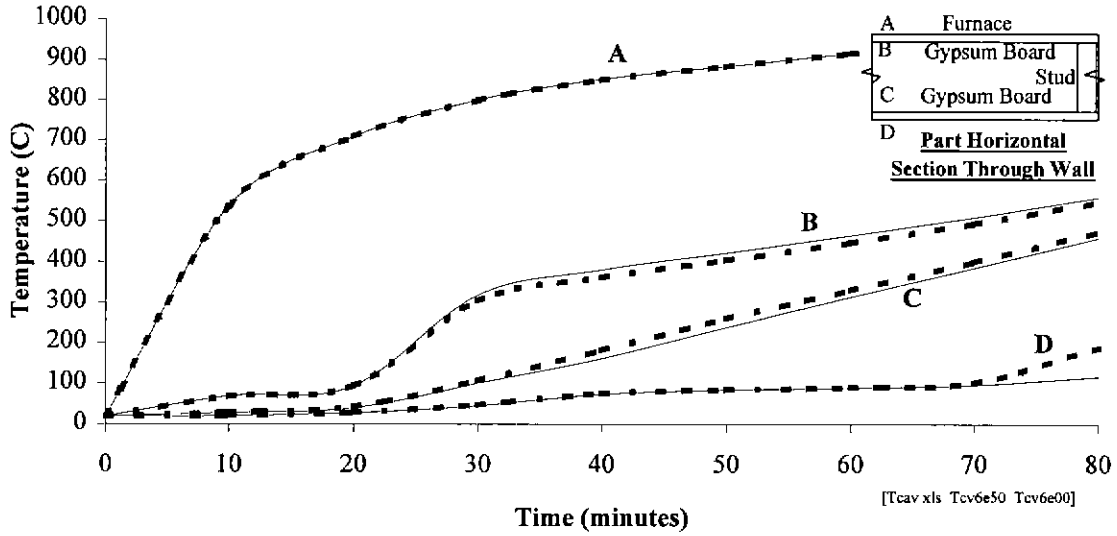

Figure 5.16. Comparison of Temperatures Predicted with the Heat Transfer Model, ADIDRAS for Two Extreme Cases of Transmissivity of Radiant Heat through a Wall Cavity.

5.3.4 Effect of Smoke Density on Heat Flux through Cavities

Another variable which may significantly affect heat transfer through cavities and for which the effects are not known, is the density of air and smoke. Estimates of the density were given in Table **5.9** and were adopted. Figure 5.17 shows the temperatures predicted with ADIDRAS using these densities, plotted as continuous lines. These lines are the same as those continuous plots in Figure 5.16 and the dashed lines for emissivity of 0.6 in Figure 5.15. The temperatures resulting for an extreme lower bound estimate of the density of air and smoke of 1 $kg.m^{-3}$ are plotted in Figure 5.17 as dashed lines. It is apparent that smoke density has little effect on heat transfer.

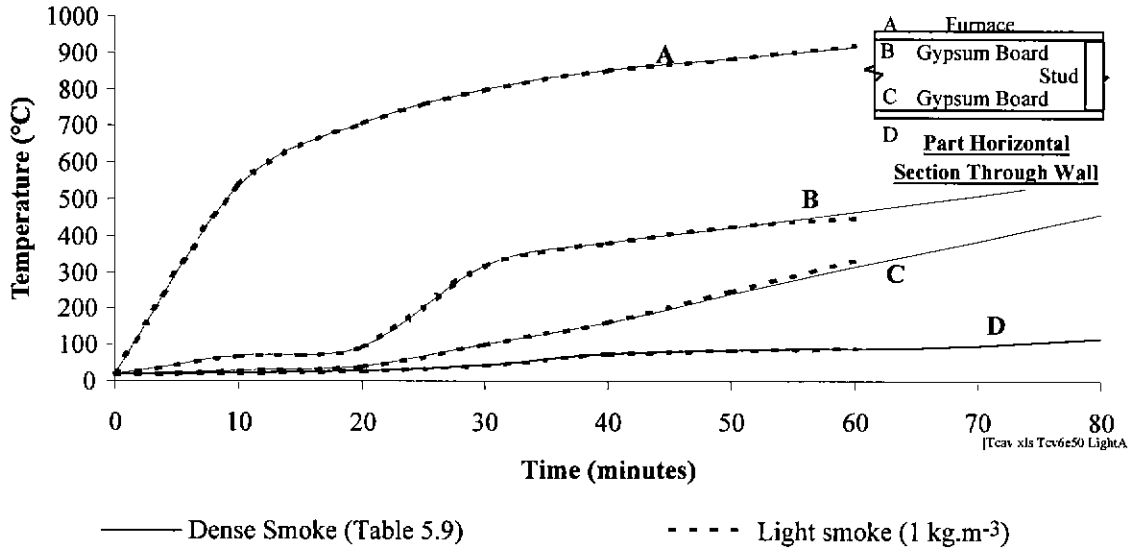

Figure 5.17. The Effects of Smoke Density on Heat Transfer through a Wall Cavity Predicted with the Heat Transfer Model, ADIDRAS.

5.4 Evaluation of ADIDRAS for Modeling Heat Transfer into Studs

5.4.1 Introduction

In this section §5.4, predictions of temperatures in studs obtained with the heat transfer model, ADIDRAS are compared with the measured temperatures plotted in Figures 4.26 and 4.27. In the following section, §5.4.2, evaluation is undertaken for the predictions based on the properties adopted in §5.2 and based on the assumption that gypsum boards stay in contact with the studs during the course of fire exposure. Although most comparisons between model predictions and experimental results are found to be good, there some inconsistencies. These inconsistencies are resolved in §5.4.3 and §5.4.4.

5.4.2 Evaluation of Model Predictions Based on the Assumption that Gypsum Boards Stay in Contact with Studs for the Entire Duration of Fire Exposure.

Results from the application of ADIDRAS assuming that gypsum boards stay in contact with studs for the entire duration of fire exposure, are plotted together with experimental results in Figure 5.18 and Figure 5.19. The experimental results are reproduced as grey symbols from Figures 4.26 and 4.27. The assumption was similarly made by Mehaffey et al (1994) and Thomas (1997) when they compared their heat transfer model predictions with experimental results. Figure 5.18 shows temperatures at 7.5 mm below the stud surfaces facing cavities in Walls 1 and 2. Figure 5.19 shows temperatures along centre lines through studs in these walls. The thermal properties adopted in the application of ADIDRAS were those given in §5.2. Two sets of thermal properties of studs were obtained in §5.2.4 from Janssen's (1994) models and by some further calibration to results of an independent experiment by Young (1996). ADIDRAS predictions with Janssens' (1994) properties are shown as black continuous lines and predictions with properties calibrated to results from Young's (1996) experiment are shown as black dotted lines.

The evaluation of ADIDRAS for modelling the transfer of heat into studs will subsequently be carried out for the following comparisons between predictions and experimental measurements:

1. Comparisons of temperatures at the time when structural failure coincides with moisture vaporisation which was noted in §4.5.4.
2. Comparisons of temperatures at the time when structural failure is caused by charring of studs.
3. Comparisons of the effects of cavity smoke on temperatures in studs.
4. Comparisons where temperatures reached high values greater than 400°C.

These comparisons are discussed below.

Comparisons of Temperatures at the Time when Structural failure Coincides with Moisture Vaporisation.

It was noted in §4.5.4 that the experiments demonstrated that light-timber framed walls can fail prior to charring, when much of the stud sections experience the vaporisation of moisture. Thus there is a need for heat transfer models to approximately predict temperatures at the stage of moisture vaporisation.

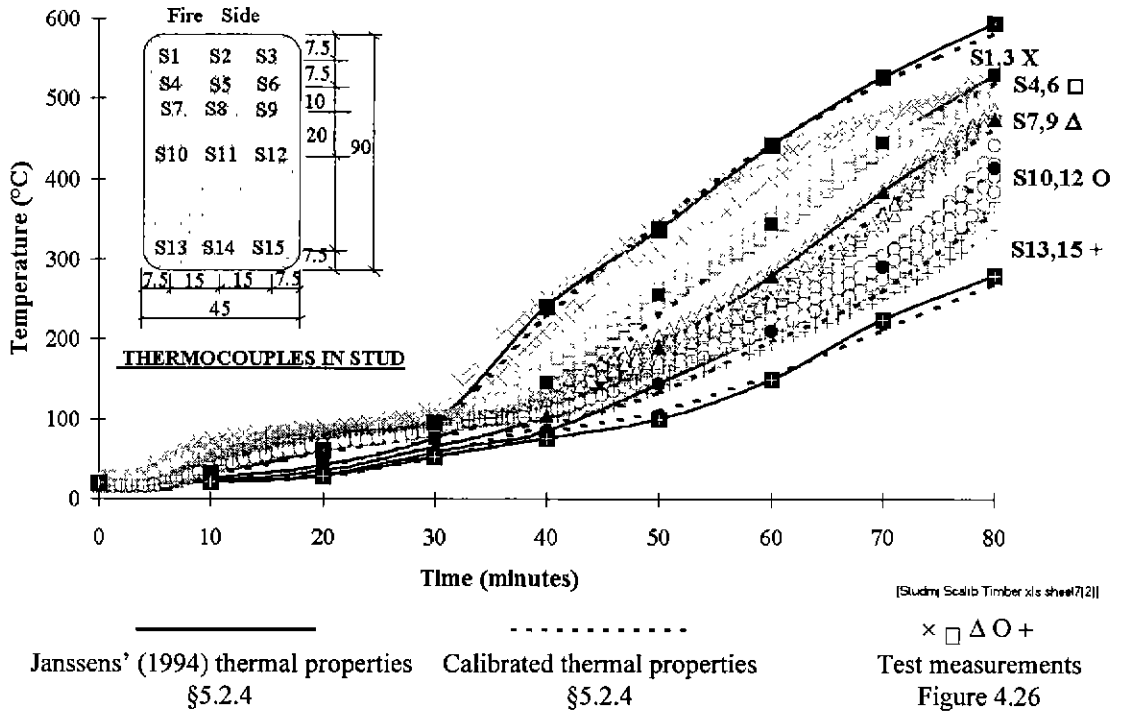

Figure 5.18. Comparison of ADIDRAS Predictions, with Experimental Results for Temperatures at Points 7.5 mm beneath the Cavity Facing Surfaces of Studs in Wall Experiments 1 and 2, based on the Assumption that Studs and Gypsum Board remain in Contact. (Heat transfer coefficient gypsum board to stud =500 $W.m^{-2}.K^{-1}$)

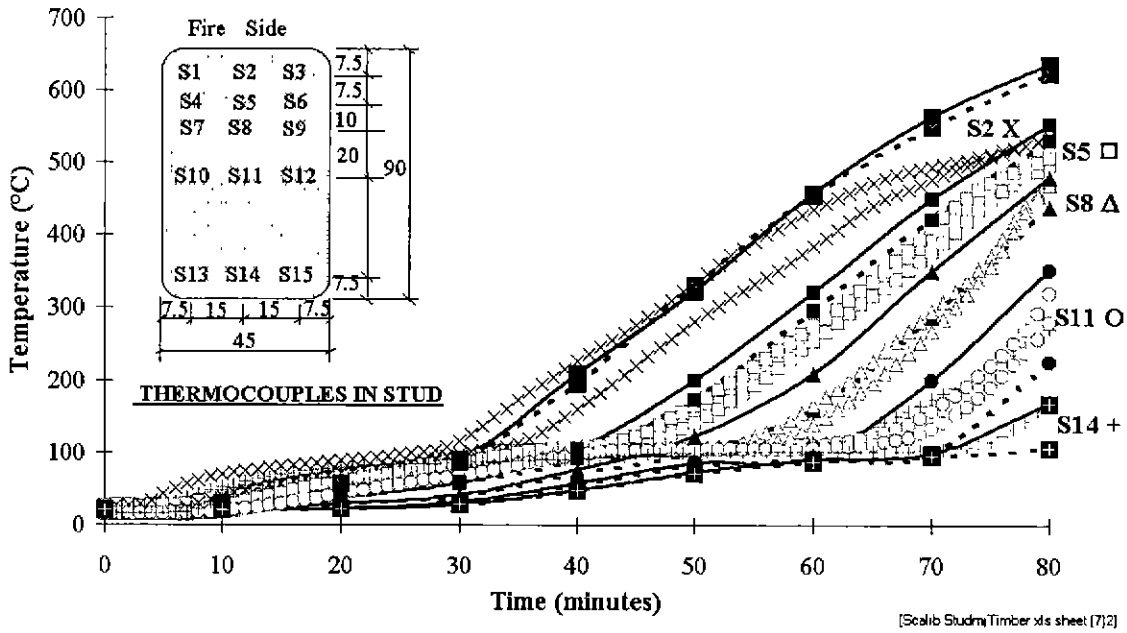

Figure 5.19. Comparison of ADIDRAS Predictions, with Experimental Results for Temperatures at Points along a Centre Line through Studs in Wall Experiments 1 and 2, based on the Assumption that Studs and Gypsum Board remain in Contact. (Heat transfer coefficient gypsum board to stud =500 $W.m^{-2}.K^{-1}$). Refer to legend in Figure 5.18.

Figure 5.18 and Figure 5.19 show that temperatures predicted with the model in the first 30 minutes lagged measured temperatures by some 50°C. This difference in temperatures is small, particularly considering the effect of such a change in temperature on mechanical properties in the range of 20-90°C. The effect would be less than 10% (§6.3.4-6.3.7). However, the fact that in terms of time, the lag is approximately 20 minutes, and that timber framed walls structurally collapsed at 34 minutes when timber was at approximately 100°C and moisture was vaporising (Wall Experiments 4, 5, 7 and 8 in §4.5.4 and Figure 4.3.4), raises concern about the heat transfer model (and others such as Mehaffey et al 1994 and Thomas 1997 developed to date). The low gradient of the temperature-time plots in this vicinity also suggests that even if heat transfer models incorporated mass transfer analysis allowing for the convective movement of moisture and vapour, it would be very difficult to refine the models to accurately predict some specific time when temperatures were critical and collapse was most likely. The distinct mode of structural collapse due to moisture vaporisation, well before charring was not anticipated at the beginning of the research for this thesis. Although the use of steam to bend was known, no known wall furnace tests had recorded failure prior to the charring of studs.

Further research into this mode of failure is recommended. The first stage of this research should establish the range of slendernesses and load ratios over which this mode of failure is critical. If this range encompasses a significant proportion of walls in practice, then this mode of failure should be researched further. Some preliminary investigation of into these critical ranges has been undertaken and is described in chapter §7 of this thesis. A simple method for accounting for the heat transferred by moisture movement, that is convection, is evaluated in §5.4.4. More detailed research into this mode of failure is being undertaken by Jong (1999).

Comparisons of Temperatures at the Time when Structural Failure is Caused by Charring of Studs

It was noted in Table 4.3 that Wall 6 failed at 59 minutes. Amongst all of the walls tested, it was the one most similar to walls in common building construction. It had similar loading and support conditions. It can be deduced from Figure 5.18 and Figure 5.19 that at the time of failure, approximately one third of stud sections had charred (>300°C) and that temperatures in another third had exceeded 200°C which the temperature when mechanical properties substantially degrade (§6.3.4-§6.3.7). Hence, the most dominant cause for failure was charring. For this cause of failure, it is important for the model to accurately predict temperatures between 45-65 minutes.

In Figure 5.18, good comparisons are evident between predictions and experimental results from all thermocouples and property values from both Janssens (1994) and the calibrations except at S13 and S15. Temperatures predicted at these points lagged the results by 5-10 minutes. This lag is most likely due to

heat influx into the stud not only from the cavity but also from the rounded corners of the stud which would have enabled some heat to enter from the interface between the stud and the gypsum board on the ambient side.

In Figure 5.18, the plots derived with properties obtained from calibrations to Young's (1996) independent experiment, gave better predictions at all points except S14. Nonetheless, Janssens' properties gave good, slightly conservative results and the comparisons support the use Janssens' models for thermal properties of wood when independent experimental results are not available to obtain calibrated thermal property values.

Overall, the comparisons are good and support the use ADIDRAS and the assumptions in §3.3 for accurately predicting temperatures when charring causes failure.

Comparisons of the Effects of Cavity Smoke on Temperatures in Studs.

It was shown in §5.3.3 that the transmissivity of smoke had little effect on heat transfer along heat paths through wall cavities. This conclusion indicated the possibility of simplifying modelling of the cavity with a single node. It could thus be assumed that the temperature in the cavity is approximately uniform and that radiant heat flow between cavity surfaces and the node is one dimensional. These assumptions appear to be reasonable since the dimensions of cavities in the plane of walls is much greater than the thickness of the wall itself.

The feasibility of using this simplification for modelling the heat flow into studs is not so readily apparent. In the case of clear cavities, the radiant heat flow to the stud surface bounding the cavity may vary on the surface in the direction of the stud depth. This heat influx to the stud would promote two dimensional heat flow within the stud. In contrast, the uniformity of heat flow from a very smokey cavity with virtually no transmissivity, would be expected to promote one dimensional heat flow in the stud. It was desired to see how different the temperatures in the stud would be in the two extreme cases - a clear cavity and a very smokey cavity - and hence, whether it is feasible to simplify the heat transfer through cavities by using a single node without the use of a complex two dimensional radiation model.

To test the feasibility of this simplification, the surface temperatures of the stud were compared for the two extreme cases. If the surface temperatures are similar, then the temperatures inside the studs should be similar at similar points and times. A plot of predicted temperatures at 60 minutes of fire exposure, along this surface is shown in Figure 5.20. It is readily apparent from the figure that the temperatures along surfaces, and hence temperatures within studs, are little affected by smoke. The use of a single node

to model cavities, as was used by Mehaffey et al (1994), is a model simplification which should be developed further in future research.

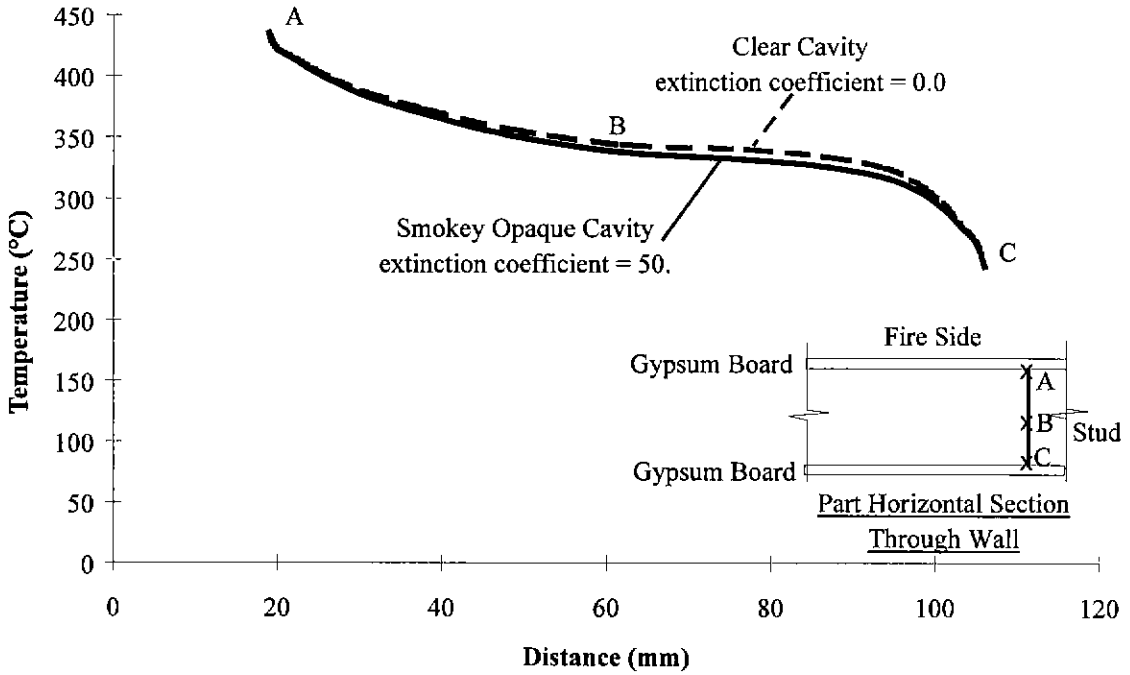

Figure 5.20. Predicted Temperatures of Stud Surface Facing the Cavity, at 60 Minutes of Fire Exposure.

Comparisons where Temperatures Reached High Values Exceeding 400°C.

Figure 5.18 and Figure 5.19 show that at S1, S2 and S3 the temperatures predicted with the model compare well with measured temperatures up to 60 minutes when the temperatures at these points reach approximately 400°C. Thereafter, the predicted temperatures increase more than the measured temperatures, until at 80 minutes the predictions are 150°C greater. It was shown in §4.5.4 that the wall failed at 59 minutes for typical practical conditions which involve fixed ends and a 30% load ratio. Thus the greater increase in predicted temperatures is only of practical concern when loads are less than a 30% load ratio. Walls with lower loads can char more before failing and have the potential to resist standard fire for more than 60 minutes. As well as desiring to accurately model high temperatures to predict the time of failure of lightly loaded walls, it is also desirable to know the reason for the greater increase to gain a better understanding of the phenomena which occur in the thermal degradation of light-timber framed walls.

There are two possible causes for the greater increase - errors in thermal property values or omission in modelling some significant phenomena. Many trials with thermal property values did not reveal any possible errors in thermal property values that could explain the lower temperatures. The phenomena which could possibly cause the lower temperatures are endothermicity in char commencing at 400°C or some other phenomenon. At 400°C all volatiles have been released and thus char at this temperature does not seem to be a source of endothermicity. Evidence of another phenomenon was sought from the experimental observations.

Figure 5.21 shows plots for temperatures recorded at the cavity facing surface of gypsum board on the fire side (C13, C1, C1X and C5X), and in the interface between the gypsum board and studs on the fire side (C7X). The dashed plot for C7X shows that if the stud and the gypsum board stayed in contact, the temperature at C7X should have risen substantially above the temperature at the cavity facing thermocouples. The most important observations to make from Figure 5.21 are that the temperature in the interface is similar to the temperature of the cavity facing surface of the gypsum board on the fire side and that this similarity does appear possible if the gypsum board remains in contact with the studs.

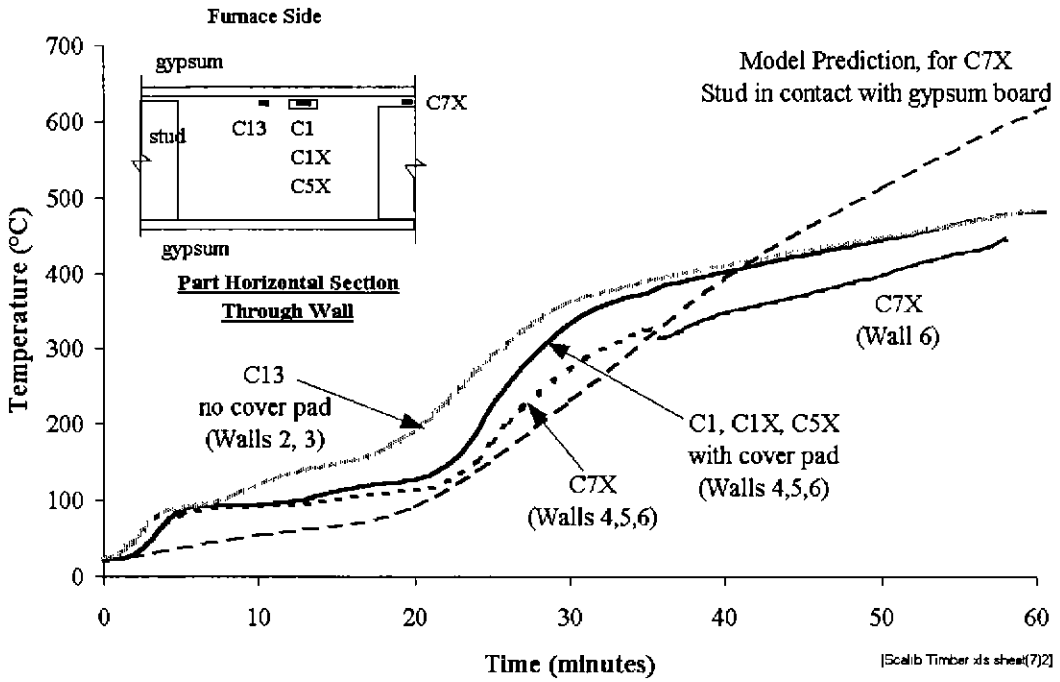

Figure 5.21. Comparison of Temperatures Recorded Centrally on the Cavity Face of Gypsum Board on the Fire Side and Recorded at the Interface between the Board and Stud on the Fire Side.

From Figure 2.10 it is apparent that several millimetres of shrinkage of wood and char must have occurred. From the observations in §4.5.2, it was apparent that the heads of nails stayed flush with the surface of the gypsum board exposed to the fire. It is thus apparent that a gap between the gypsum board and the studs opened up between the 30-40th minutes of fire exposure. The gap would have allowed heat

to divert to the cavity by some means discussed in §5.4.3 below, ensuring that the temperature at C7X did not rise above the temperatures on the gypsum board surface bounding the cavity. Thermocouple C7X was not firmly attached to either the gypsum board surface or the surface of the stud. It appears that thermocouple C7X must have moved towards the stud where temperatures were marginally lower.

In the course of recent experiments (Pohl and Young 1999), measurements to confirm the presence of gaps were considered but were thought to be extremely difficult to directly measure. Smoke in the cavity would have prevented any form of visual measurement. Use of some metal probe would have disturbed the soft surfaces of char and gypsum board in the vicinity of the gap. Further research is required to to measure the widths of gaps and hence confirm their presence. However, the evidence of char recession and timber shrinkage (Figure 2.10) and the similarity of measured temperatures in the expected gap and at the cavity facing surface of gypsum board on the fire side, are strong indications of the presence of such gaps.

5.4.3 Evaluation Allowing for Gaps between Studs and Gypsum Board, Created by Shrinkage of Timber and Char

In the previous section, §5.4.2 it was shown that it was most likely that a gap opened between the stud and the gypsum board on the fire side, and that this gap transferred heat to the cavity after approximately 30 minutes of fire exposure. It remains to determine how the heat flux was actually transferred through the gap. The answer is not immediately obvious. On one hand, high temperatures in the gap indicate that radiation should be the main mode. However, the gap was likely to be small (a few millimetres) and the angles for radiation to divert heat to the cavity appear too acute to have a significant effect on heat flow. Alternative means of heat transfer are discussed below, in order to assess the relative effects of different one and two dimensional modes of heat transfer through the gap. The results are presented in Figure 5.22.

The alternative modes of heat transfer considered were as follows:

(a) Gap modelled as an interface; h across gap constantly 500 $W.m^{-2}.K^{-1}$; one dimensional heat transfer across gap.

The simplest method of modelling heat transfer across the gap is to model all of the heat transfer with a heat transfer coefficient and otherwise ignore the gap. Ignoring radiation and assuming a gap width, $\delta x_{interface}$ of 0.1 mm which is the width of a hairline crack, a heat transfer coefficient is found as follows:

$$h_{across\ interface} = \frac{k_{air}}{\delta x_{interface}}$$

$$\approx \frac{0.05 W.m^{-1}.K^{-1}}{10^{-4} m}$$

$$= 500 W.m^{-2}.K^{-1}$$

The temperatures at S2 and S8 resulting from this heat transfer coefficient are shown as a thin dashed line in Figure 5.22.

(b) Gap modelled as an interface; h across gap varying from 500 $W.m^{-2}.K^{-1}$ at the early stages in the experiment, to 20 $W.m^{-2}.K^{-1}$ as the gap widens towards the end of the experiment; one dimensional heat transfer across gap.

The char towards the fire side has an average temperature of approximately 400°C between 30-80 minutes. From Figure 2.10 there is no appreciable shrinkage below 300°C. The average depth of the char with temperatures greater than 300°C is approximately 10 mm during this time period. Assuming that tips of nails are stationary, the gap will be equal to the shrinkage of the char. From Figure 3.10, the gap is expected to be 25% of 10 mm; that is, 2.5 mm. Following the equations in (a) above, the heat transfer coefficient should be approximately 20 $W.m^{-2}.K^{-1}$. Thus more refined modelling of heat transfer across the interface, compared with (a) would be to adopt a heat transfer coefficient which varied from 500 $W.m^{-2}.K^{-1}$ to 20 $W.m^{-2}.K^{-1}$ during the experiment. The predicted temperatures resulting from this varying heat transfer coefficient are shown as the bold dotted lines in Figure 5.22.

(c) Gap 3 mm wide; conductivity of air and smoke in gap equal to 0.05 $W.m^{-1}.K^{-1}$; two dimensional heat transfer in gap.

For this alternative a 3 mm gap was considered. Two dimensional conduction through stagnant air was the only mode of heat transfer to be considered. This alternative differs from (b) in that it involves the exchange of heat between the cavity and the gap. The predicted temperatures are shown as the continuous thin black lines in Figure 5.22.

(d) Gap 3 mm wide; conductivity of air and smoke in gap equal to 10.0 $W.m^{-2}.K^{-1}$; two dimensional heat transfer in gap.

This alternative examined the possibility that the air moved in the gap, creating a larger heat transfer coefficient than in (c). This possiblility of convection through the gap being

a dominant mode of heat transfer was considered by adopting a large value for air conductivity; namely, 10.0 $W.m^{-2}.K^{-1}$. The predicted temperatures are shown as the continuous thick grey lines in Figure 5.22.

(e) Gap 10 mm wide; conductivity of air and smoke in gap equal to 10.0 $W.m^{-1}.K^{-1}$; two dimensional heat transfer in gap.

This alternative was similar to (d) except it examined the possibility that the shrinkage may have been quite large. Radiation was ignored as with all alternatives (a-d) above. The predicted temperatures are shown as the continuous thin grey lines in Figure 5.22.

(f) Gap 3 mm wide; two-dimensional radiation in gap.

This was the only alternative to involve two dimensional radiation in the gap. All other variables were assumed to have values given in §5.2. An extinction coefficient of 50 was adopted for any smoke that may have been present. The predicted temperatures are shown as the continuous thick black lines in Figure 5.22.

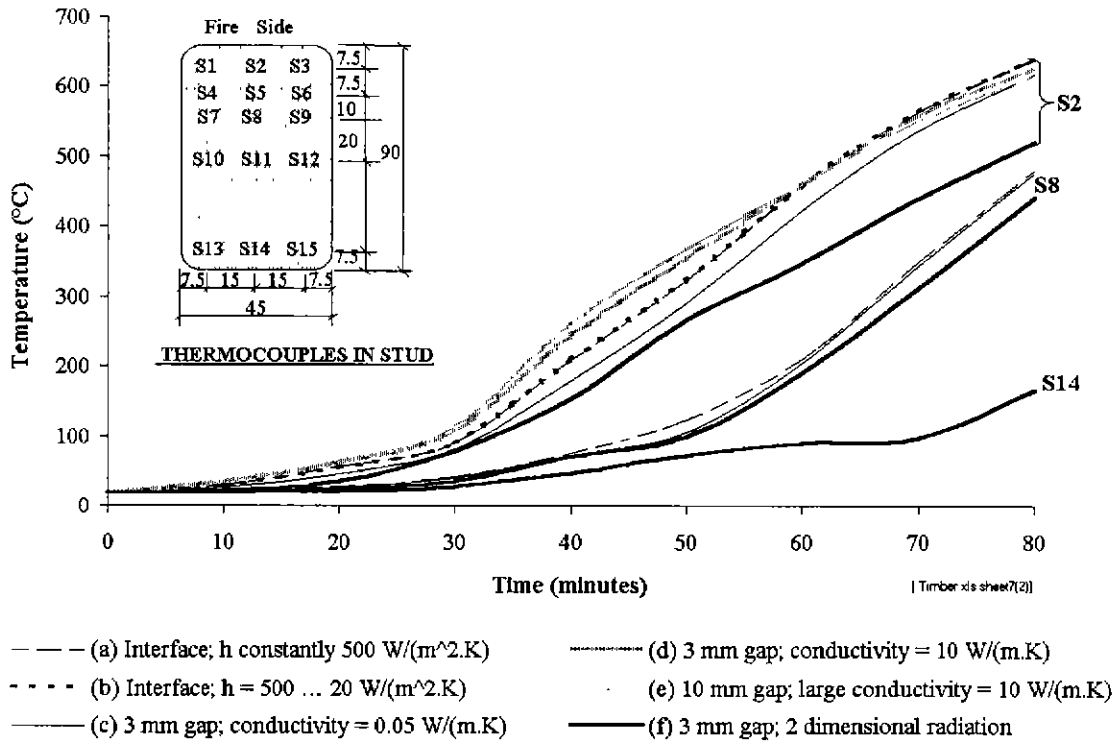

Figure 5.22. Temperature Predictions for Alternative Modes of Heat Transfer across the Gap between the Stud and Gypsum Board on the Fire Side.

The most noticeable comparison in Figure 5.22 is that the temperatures resulting from two dimensional radiation in the gap are substantially lower than other temperatures, especially towards 80 minutes at S2. At this time the temperature is some 150°C less and is similar to experimental results in Figure 5.19.

The maximum reduction in temperature that could be attributed to conductive and convective means of heat transfer was sought with alternatives (d) and (e) which resulted in the grey line plots in Figure 5.22. The grey plots show that high conductivity and convective heat transfer in the gap actually caused temperatures to increase in the fire side of the stud relative to temperatures shown in Figure 5.19. It appears that the high conductivities caused more heat to transfer to the stud than to the cavity.

The effects of the width of the gap on temperatures determined with alternative (f) above, can be evaluated from Figure 5.23 and Figure 5.24. Figure 5.23 shows a part horizontal section through the wall. It aids the comparison of typical predicted temperatures in the cavity, at the centre of the gap and at the edge of the gap for gap widths of 1mm, 3mm and 5mm, at 80 minutes. The figure shows that the temperatures are insensitive to gap width, and that the temperatures in the gap are not substantially greater those in the cavity. Figure 5.24 shows the variation of temperatures in the gap with time for the same gap widths in Figure 5.23. Figure 5.24 also shows that the temperature in the gap is insensitive to gap width. The presence of even small gaps as thin as 1 mm diverts a substantial amount of heat away from studs. It appears that radiation in the gap at temperatures above 400°C will quickly disperse heat to achieve fairly uniform temperatures between the gap and the cavity.

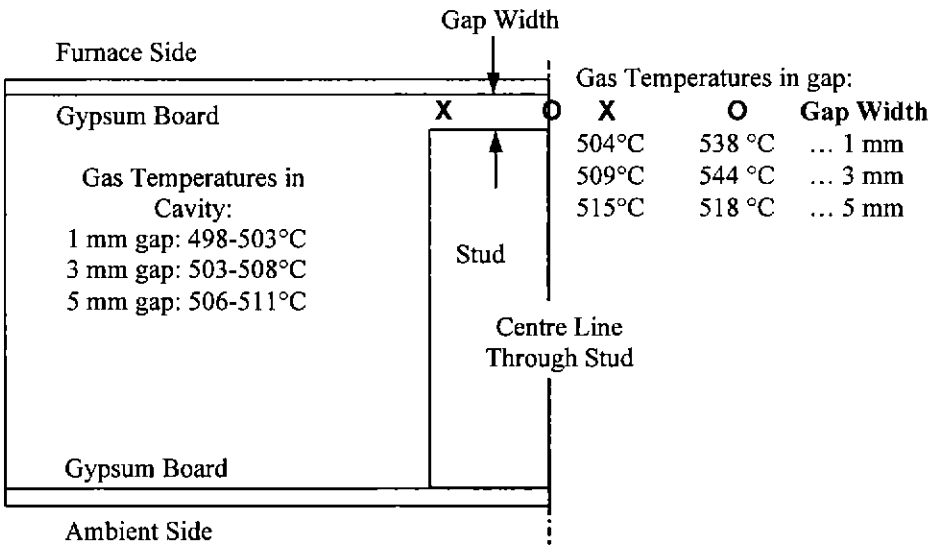

Figure 5.23. Predicted Temperatures in the Gap and Cavity for Different Gap Widths, at 80 Minutes of Exposure. (Predictions based on alternative (f), that is, modelling of two dimensional radiant heat transfer in the gap.)

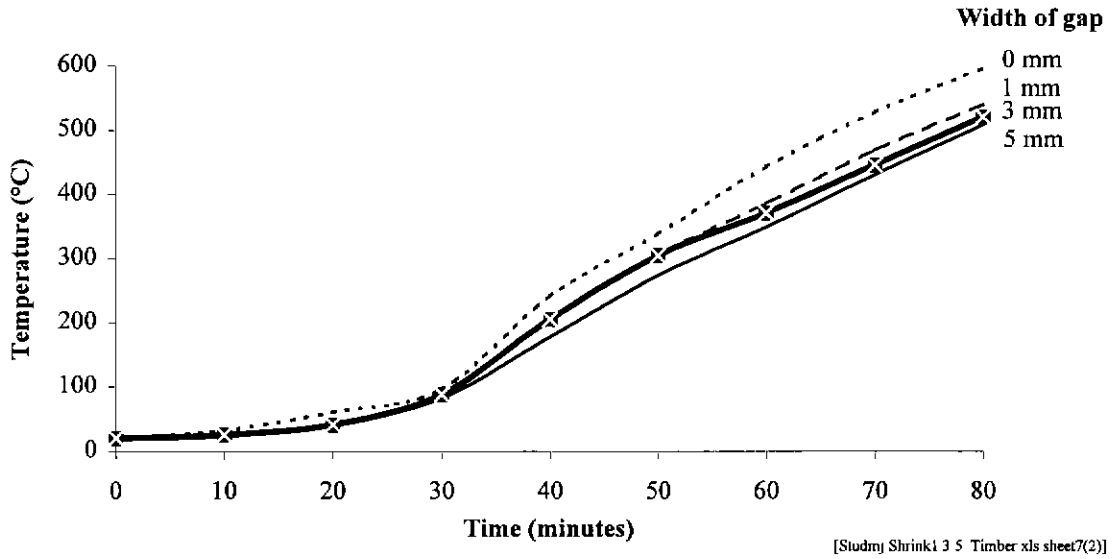

Figure 5.24. Effect of Gap Width on the Average of Temperatures Predicted at S1 and S3 by ADIDRAS. (Predictions based on Janssens', 1994 thermal properties in §5.2.4)

Use of large conductivities such as in (d) and (e) above could only produce a similar reduction in temperatures in the gap as two dimensional radiation, if much larger conductivity was adopted in air in the direction parallel to the gap compared with conductivity across the gap. Hence the use of large isotropic conductivities such those in (d) and (e) cannot be used as a simple replacement for two dimensional radiation in the gap. Use of anisotropic conductivities in air in the gap would not be practical. Two dimensional radiation in the gap should be included in the heat transfer analysis to avoid over-prediction of temperatures by as much 150°C between 60-80 minutes.

Predictions of stud temperatures which ignored the opening of gaps between the studs and gypsum board on the fire side, were shown in Figure 5.18 and Figure 5.19. In the light of the effects of gaps discussed above, predictions based on the modelling of two dimensional radiation through gaps, have been obtained and are shown in Figure 5.25 and Figure 5.26. The width of gaps was assumed to be 3.0 mm. Better comparisons between model predictions of temperatures at S1 and S3, and experimental measurements are apparent at the 80^{th} minute. The predicted temperatures at S13 and S15 are lower than the experimental results. The small re-entrant spaces due to the rounded corners of the stud may have had similar effects on heat transfer as cracks, and thus enabled some additional heat from the cavity through ambient facing edges within 10 mm of the corners of the stud. In Figure 5.26, Janssen's properties appear to have led to better temperature predictions than properties calibrated from Young's (1996) experiment, particularly at S8 and S11. Since Janssens' conductivities are greater than the calibrated conductivities, the predictions at S8 and S11 do not require inclusion of endothermicity of pyrolysis in the model. The predictions support the use of zero heat of reaction during pyrolysis. The

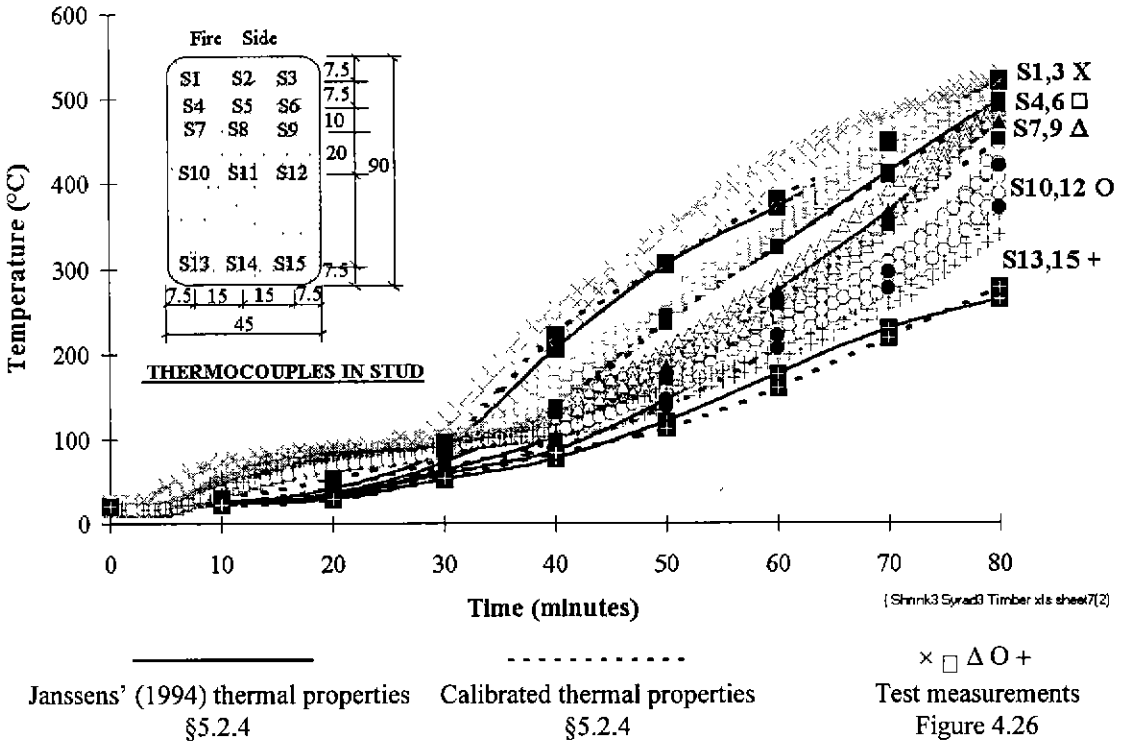

Figure 5.25. Comparison of ADIDRAS Predictions, with Temperatures (§4.6.5) Measured at Points 7.5 mm Beneath Cavity Facing Surfaces of Studs in Wall Tests 1 and 2, Based on the Assumption of there being a Constant Gap of 3 mm between Studs and Gypsum Board on the Fire Side.

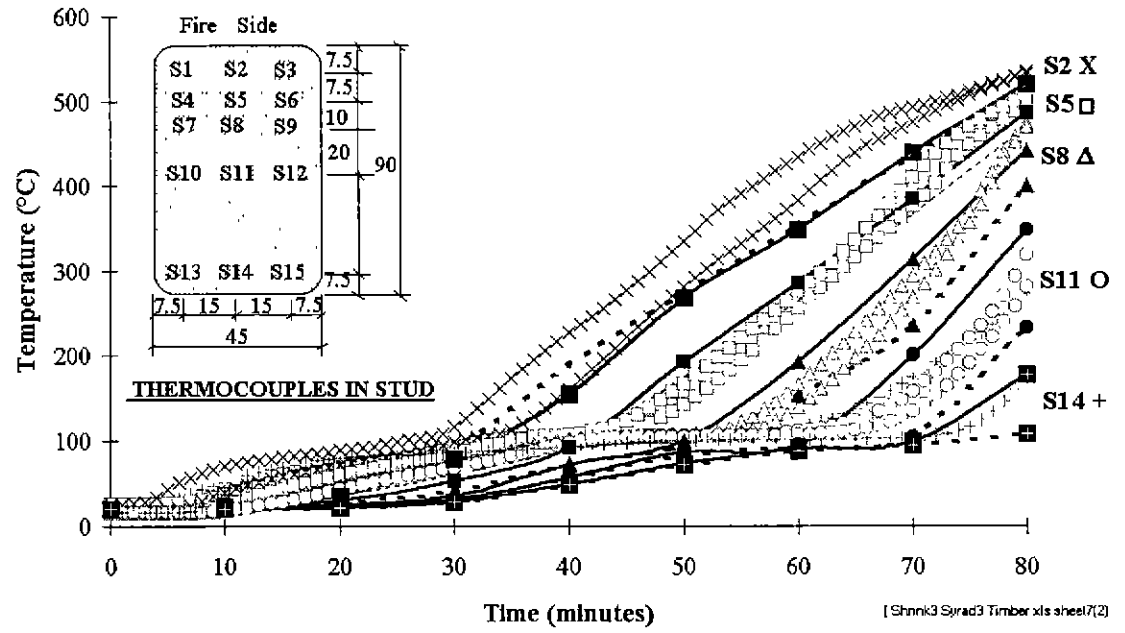

Figure 5.26. Comparison of ADIDRAS Predictions, with Temperatures (§4.6.5) Measured at Points along Centre Line through Studs in Wall Experiments 1 and 2, Assuming a Constant Gap of 3 mm between Studs and Gypsum Board on the Fire Side. (Refer to legend in Figure 5.25.)

model does not predict temperatures below 150°C well because it omits analysis for moisture transfer which affects temperatures in this range. A simple method for allowing for moisture transfer is evaluated in the next section, §5.4.4.

It is recommended that gaps of constant width (of approximately 3.0 mm) with time, between the studs and gypsum board on the fire side be modelled if timber fibres in this region are expected to reach temperatures higher than 400°C.

5.4.4 Evaluation of Simple Approach to Modelling Moisture Transfer.

It was explained in the discussion in reference to Figure 4.34 that transfer of heat by the movement of moisture apparently had a large role in the structural collapse of walls in Experiments 4, 5 and 8. It was thus desired to develop a simple approach to model moisture transfer in porous solids such as timber and gypsum board until a more rigorous model is developed in future research in light-timber framed walls in fire.

The only mode of heat transfer in solids that ADIDRAS models is thermal conduction. Thus, a simple approach, involving the modification of conductivities, was sought. It was explained in §2.2.1.1 and §2.2.2 that moisture transfer increases heat transfer rates in regions where the temperatures are less than the vaporisation point, and reduces the heat transfer rates in regions where the temperature is above the vaporisation point. Good comparisons between measured temperatures and temperatures predicted above 200°C in Figure 5.15, Figure 5.25 and Figure 5.26, ignoring the modelling of moisture transfer, demonstrate that the effects of moisture transfer on heat transfer rates are not significant at temperatures greater than 200°C.

Possible simplified approaches to modelling moisture transfer can be deduced from Thomas's (1997) calibrated values for thermal conductivities of timber. His values were approximately double the values published by other researchers in the temperature range 20-100°C, and half of the other published values in the range 100-300°C (Figure 2.12). It was decided to try simple formalised approaches for modelling moisture transfer that involved the modification of the values for conductivities with constant factors in temperature ranges which corresponded to the movement of moisture, whether in liquid or vapour form. These approaches are demonstrated in Figure 5.27 and Figure 5.28 in which the values for conductivities are modified for gypsum board and timber. Plots A are the unmodified values for the conductivities. Plots B involve the following modifications with respect to plots A:

(a) Increasing the values for conductivities by a constant factor in the temperature range 20-90°C.

(b) No modification over the temperature range 90-130°C in which vaporisation was assumed to occur.

(c) Reducing the values for conductivities by the same constant factor as in (a), within a temperature range of the same extent as in (a), above vaporisation temperatures; that is, 130-200°C.

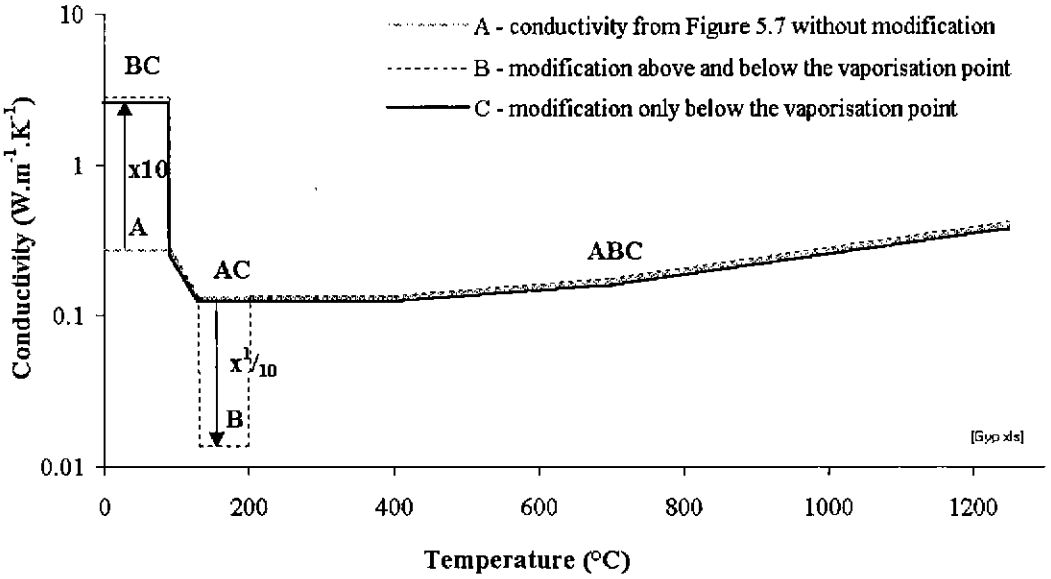

Figure 5.27. Modifications to Conductivities of Gypsum Board with Simple Approach to Moisture Transfer.

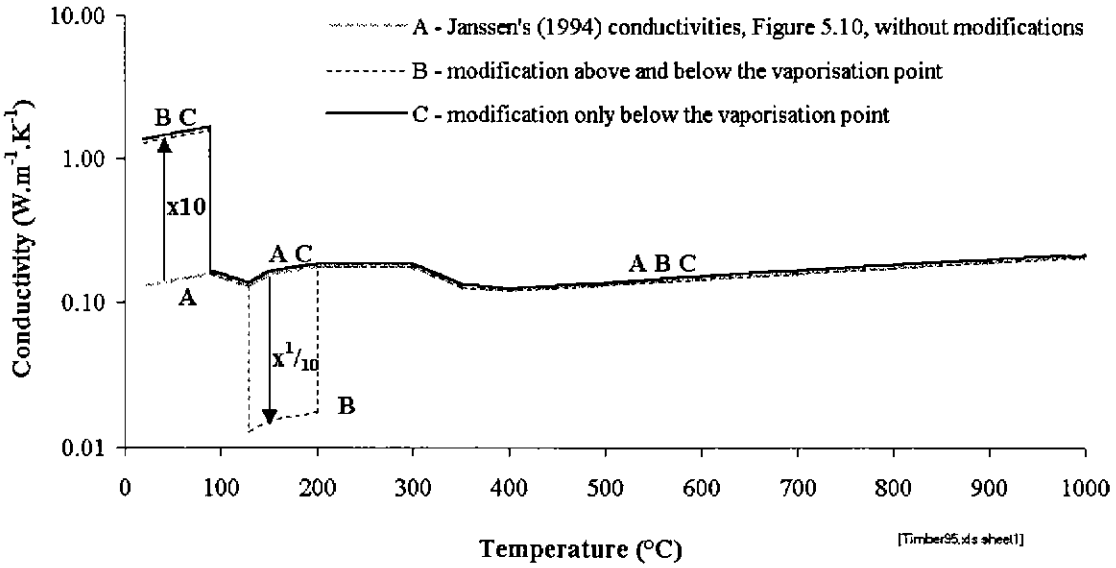

Figure 5.28. Modifications to Janssens' (1994) Values for Thermal Conductivities of Timber, with Simple Approach to Moisture Transfer.

Plots C involve only the modification in item (a) in the above list.

The temperatures in points (a)-(b) above were chosen for several reasons. As mentioned previously, the temperature, 200°C was used because the effects of moisture transfer, are not noticeable at temperatures greater than 200°C. Temperatures of 90°C and 130°C were chosen because these were the bounding temperatures used for modelling the endothermic energy of moisture vaporisation in the relationships for specific heat of gypsum board (Figure 5.9) and timber (Figure 5.12). The modifications, B and C were extended to temperatures to as low as 20°C because, as was apparent from plots of the measured temperatures in Figure 5.15, Figure 5.25 and Figure 5.26, the heat transfer was much greater than predictions which ignored moisture transfer. Initially, there was some concern that this modification would simulate much more heat influx through the fire-exposed surface of the wall, than would actually occur. However, the temperatures in the vicinity of the surface quickly rise to temperatures at which there are no modifications to the values of conductivity. Thus, the modifications in item (a) led to only a small increase in the modelled heat influx. This increase would lead to a small conservative reduction in the estimate of the time of failure.

The aim of modification B was to balance this overestimate of the heat influx due to the modification in item (a) with reductions in the values of conductivities in regions at temperatures between 130-200°C (item c). The results of this modification are discussed further below.

Simple scale analysis (Bejan 1984) of the general thermal diffusion equation (2.4) indicates that the order of magnitude of conductivity is proportional to the time for heat to penetrate to some chosen depth. (Scale analysis necessarily involves choosing dimensions such as a depth of penetration.) Thus, the increase in the rate of heat transfer due to the moisture transfer, that is the movement of moisture, should be approximately equal to the ratio of the time to reach the vaporisation temperature predicted by thermal diffusion alone, say t_{diff}, to the time to reach vaporisation measured in experiments, say t_{exp}. At outer points (7.5 mm below the stud surface) shown in Figure 5.25 t_{diff} is approximately 10 minutes and t_{exp} is approximately 30 minutes. At inner points (along the centre line of studs) shown in Figure 5.26, t_{diff} and t_{exp} vary but the ratio, t_{exp} / t_{diff} is also close to 3. Thus, scale analysis indicates that the factor should be approximately 3. However, calibration of the simplified approach used in producing Figure 5.30, indicated that the factor should be approximately 10. A factor of 20 was attempted and led to results similar to those for a factor 10. It is thus apparent that the simplified moisture transfer model is insensitive to large conduction modification factors. A factor of 100 was attempted but led to numerical instabilities.

Figure 5.29 shows the results from the heat transfer model using the simplified approach for moisture transfer, for the case of a constant 3 mm gap between studs and gypsum board on the fire side. Two dimensional radiant heat transfer in the gap was modelled. The simplified moisture transfer model did not significantly change the predicted temperature plots, despite the conduction modification factor being increased from 3 to 10 as a result of the calibrations previously mentioned. Apparently, modelling a gap with a constant width with time, including the first 30 minutes of fire exposure when moisture transfer occurred, hindered the modelled flow heat in the process of moisture transfer. To model the flow of moist heat across gaps and cavities, equations for convective heat transfer are required.

Temperature predictions based on the assumption that the gap does not open, are shown in Figure 5.30. Plots of temperature versus time are shown in Figure 5.30 (a) for all thermocouples along the centre line through the stud - S2, S5, S8, S11 and S14. For clarity, plots for each thermocouple are shown separately in Figure 5.30 (b)-(f). The simplified approaches to modelling moisture transfer, shown with modifications B and C in Figure 5.27 and Figure 5.28, generally give better results in comparison with measured temperatures than predictions which ignore moisture transfer. The exception to these comparisons is Figure 5.30 (f) which shows that while modification C gave better results, modification B led to unsafe under-estimation of the temperatures following vaporisation. Figure 5.30 (f) indicates that moisture transfer at S14 at the ambient facing portion of the stud, was greater than elsewhere. This greater rate of moisture transfer was discussed in relation to Figure 4.32, in explaining why the isotherms in timber in the vicinity of S14 close to make elliptical shapes, rather than being parallel as would be expected as shown in Figure 4.28. It was explained that the expected stagnant air in the corners of cavities was at higher temperatures than the air close to the mid-face of the stud facing the cavity. The hotter corners led to moisture transfer occurring sooner in the ambient facing portion of studs than at the centre of studs.

The good comparisons in Figure 5.30 would only be possible if a large proportion of the moisture initially in the gypsum board flowed to the stud instead of leaking through the interface to the cavities. It appears that not much pressure is required to drive the moisture into the wood, otherwise, high pressures expected as moisture changed state and greatly expanded from liquid at 1000 $kg.m^{-3}$ to vapour at approximately 1 $kg.m^{-3}$, would have caused virtually all of the vapour to leak through the interface into the adjacent cavities.

It is thus concluded that a simple approach for modelling heat flows in moisture transfer, is the use of modifications C in Figure 5.27 and Figure 5.28 and the assumption that no gap opens between studs and gypsum board during the transfer. This simple approach provides a useful method for predicting temperatures below 200°C until a phenomenologically rigorous model for moisture transfer is developed.

It is recommended that the simple moisture transfer model be used when it is expected that walls will fail while the temperature at any position in the studs or gypsum board on the fire side, is in the range of temperatures affected by moisture transfer - that is, 20 to 200°C. In other cases, moisture transfer should be ignored. As previously concluded in §5.4.3, it is recommended that gaps of constant width with time, (approximately 3.0 mm) between the studs and gypsum board on the fire side be modelled if timber fibres in this region are expected to reach temperatures higher than 400°C.

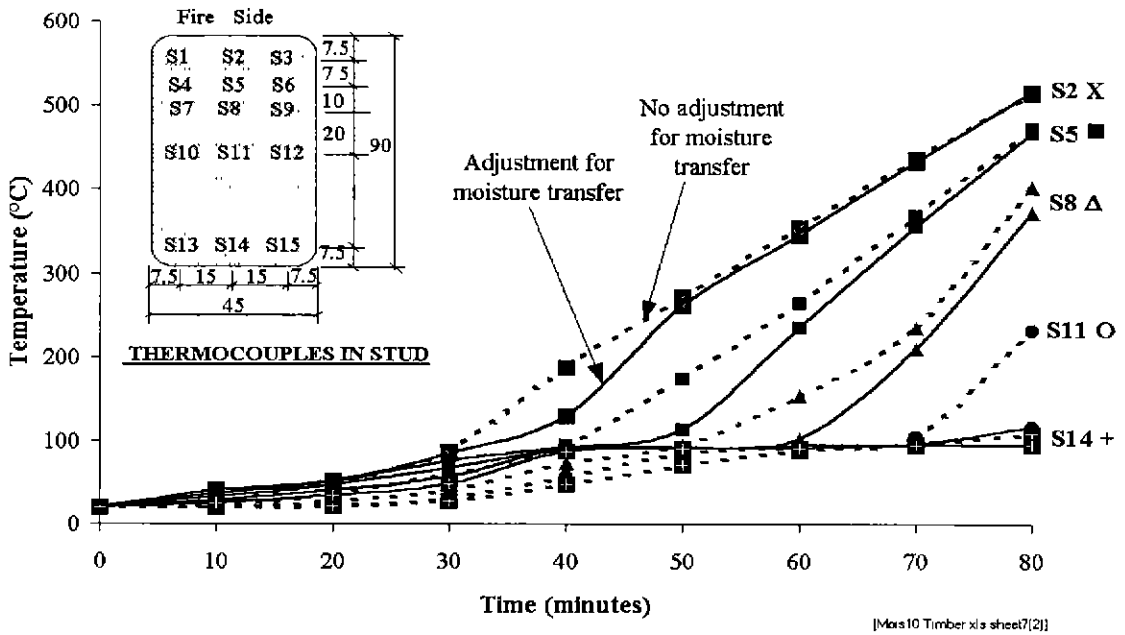

Figure 5.29. Comparison of Temperatures Predicted with the Heat Transfer Model, with and without the Simplified Approach for Moisture transfer, for the Case of a Constant 3 mm Gap between Studs and Gypsum Board on the Fire Side.

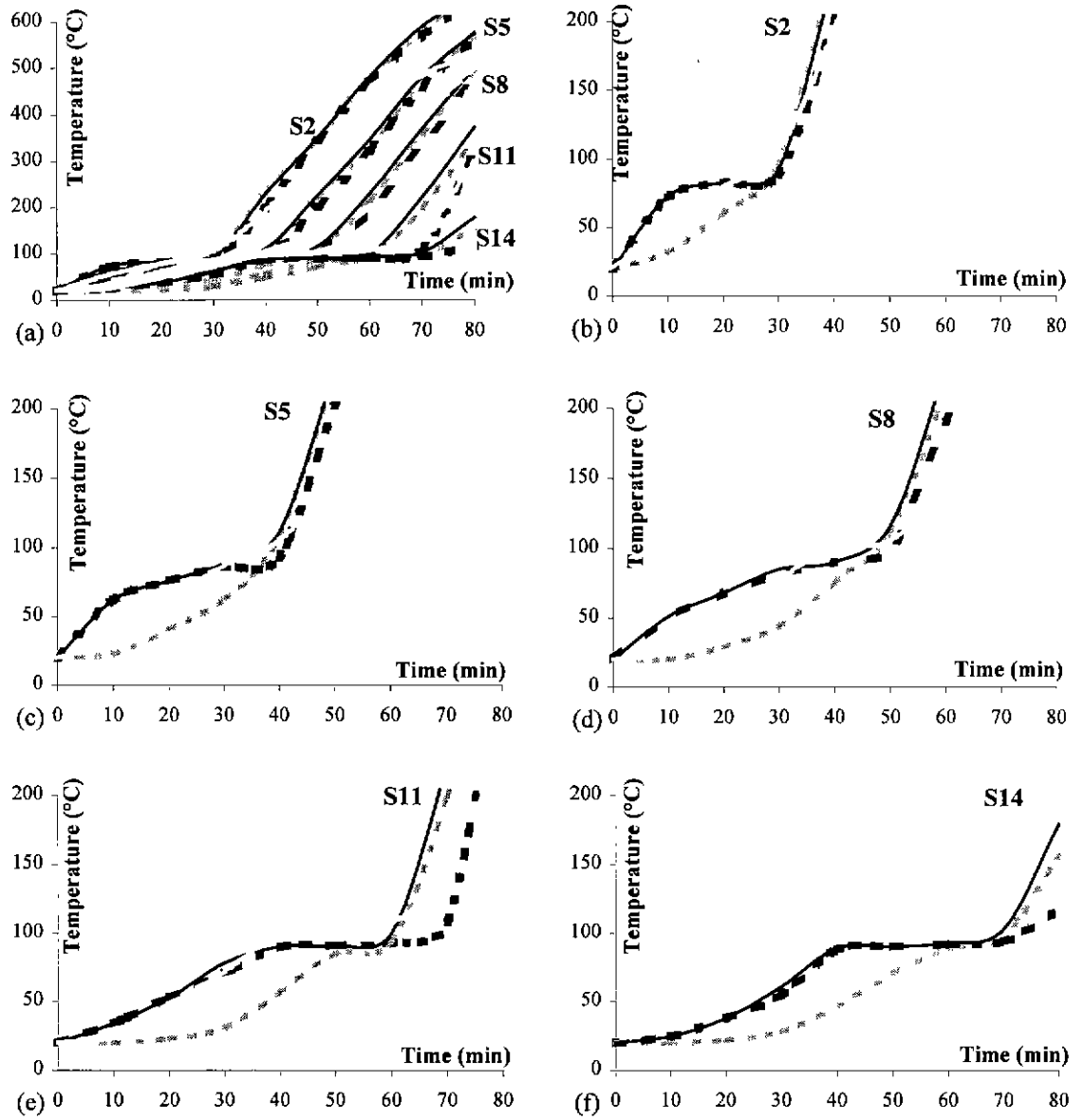

1. ——— Measured temperatures shown in Figure 4.27.
2. . . . . Predicted temperatures ignoring moisture transfer, that is, from input of plots A in Figures 5.26, 5.27.
3. - - - - Predicted temperatures resulting from modification B in Figures 5.26, 5.27.
4. ——— Predicted temperatures resulting from modification C in Figures 5.26, 5.27.
5. Marks S2, S5, S8, S11 and S14 refer to thermocouples shown in Figure 5.28.

Figure 5.30. Temperature-time Plots Demonstrating the Results of the Simplified Approach to Modelling the Heat Transferred by the Movement of Moisture, for the Case of there being No Gap between Studs and Gypsum Board on the Fire Side.

5.5 Comparisons of Predictions made with ADIDRAS, against Results from other Models and Experiments

The aim of this section, §5.5 is to appraise the efficacy of advances made in ADIDRAS in comparison with other models and experimental results. One such model is that described in Takeda and Mehaffey (1998); namely, WALL2D. Another model that preceded WALL2D is one described in Mehaffey et al (1994), The appraisal will focus on:

1. The consistency of numerical results between ADIDRAS, WALL2D and the model of Mehaffey et al (1994).
2. The improvements in predictions as a result of new assumptions and the adoption of recent models for thermal properties such as Janssen's (1994).

Consistency of numerical results will be appraised by comparing model predictions based on similar assumptions, so that any differences in predictions can be attributed solely to differences in numerical solution procedures. The second focus of appraisal will be addressed by comparing predictions of ADIDRAS resulting from the assumptions described in this thesis and the assumptions made by Takeda and Mehaffey (1998) and Mehaffey et al(1994). Basing this comparison on the predictions of ADIDRAS alone ensures that only the effects of the assumptions and not the effects of numerical methods will be apparent.

It was intended to use only the results of Takeda and Mehaffey (1998). However, after finding some anomalies, it was also decided to make comparisons with the results of the earlier research described in Mehaffey et al (1994). The results in this earlier paper are based on property values with characteristics which compare better with characteristics of heat transfer phenomena in gypsum board and timber.

Thermal Properties and Assumptions by Mehaffey et al (1994)

Values of the thermal properties that Mehaffey et al (1994) adopted for gypsum board were appraised at length in §2.4.2. These properties are briefly summarised here. It appears that Mehaffey et al (1994) adopted the relative mass, shown in Figure 5.31, for relative density. Values for the specific heat effectively used by Mehaffey et al (1994) are shown in Figure 5.32 and were deduced from enthalpy curves given by Mehaffey et al (1994). These values differ a little compared with the directly measured values (Mehaffey, 1991) for specific heat in §2.4.2. By direct measurement and some calibrations at temperatures higher than 400°C, Mehaffey et al (1994) deduced the values for conductivity of gypsum board shown in Figure 5.34. Mehaffey et al (1994) adopted a value of 0.90 for the surface emissivity of gypsum board, constant with temperature.

For the values of the density of timber, Mehaffey et al (1994) adopted measurements of relative mass shown in Figure 5.31 which he obtained from Tang (1967) (§2.4.3.1). Values for specific heat that Mehaffey et al (1994) effectively used, are shown in Figure 5.32 and have been deduced from the relationship Mehaffey et al (1994) adopted for enthalpy versus temperature. He deduced much of this plot from Lie (1992) who obtained the plot from Knudson et al (1975). Knudson's et al (1975) plot was discussed in §2.4.3.2. Mehaffey et al (1994) assumed considerable endothermic heat energy absorbed during pyrolysis which is apparent from the elevated values for specific heat between 200-350°C shown in Figure 5.32. Mehaffey et al (1994) adopted the plot for conductivity shown in Figure 5.35 which is similar to the values given by White et al (1978) and Atreya (1984) which were discussed in §2.4.3.3. Mehaffey et al (1994) adopted a value of 0.90 for the surface emissivity of timber and char, constant with temperature.

In addition to the properties summarised above, the main assumptions made by Mehaffey et al (1994) were that:

1. He did not consider the opening of shrinkage gaps between studs and gypsum board on the fire side (Figure 5.23).
2. He ignored moisture transfer.
3. He assumed that during fire exposure, wall cavities filled with thick smoke which completely prevented the direct transmission of radiant heat between surfaces bounding the cavity.

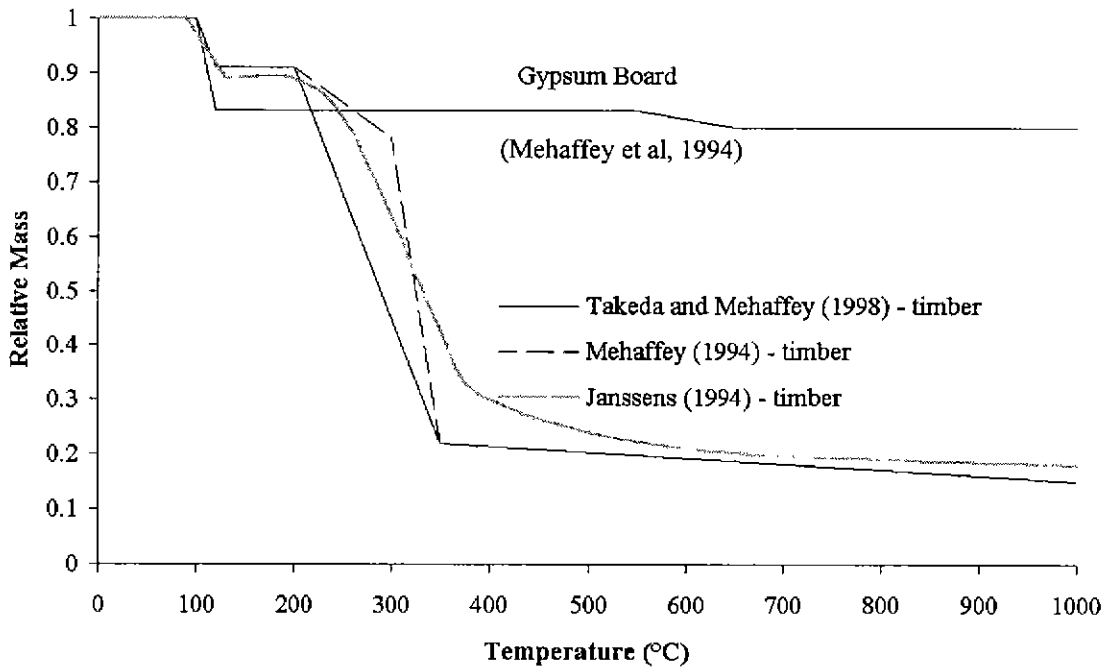

Figure 5.31. Relative Mass of Gypsum Board (Mehaffey et al 1994 and, Takeda and Mehaffey 1998) and of Timber (Janssens 1994).

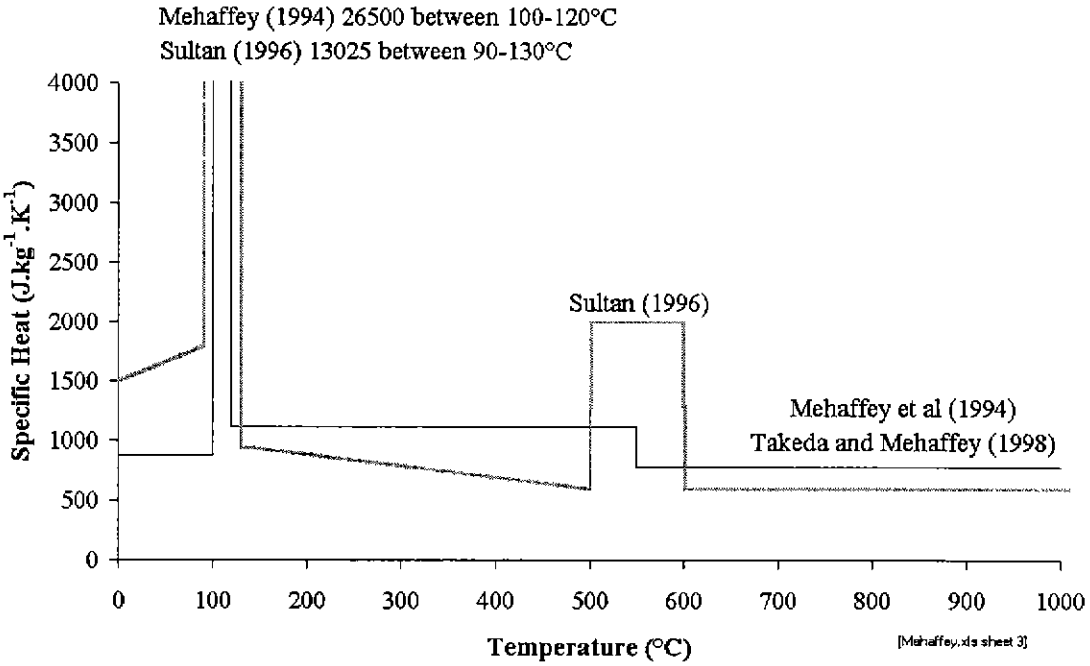

Figure 5.32. Specific Heat for Gypsum Board Derived from Enthalpy Plots published by Mehaffey et al (1994) and Takeda and Mehaffey (1998).

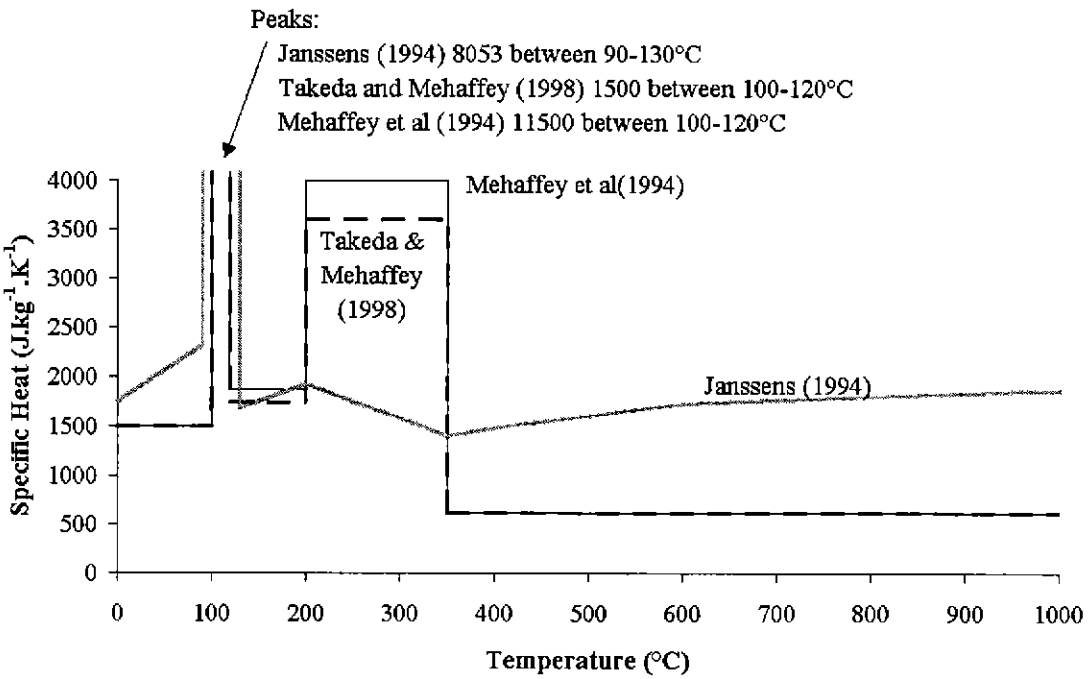

Figure 5.33. Specific heat for timber obtained from Janssens (1994) models and specific heats for timber derived from enthalpy plots published by Mehaffey et al (1994) and Takeda and Mehaffey (1998).

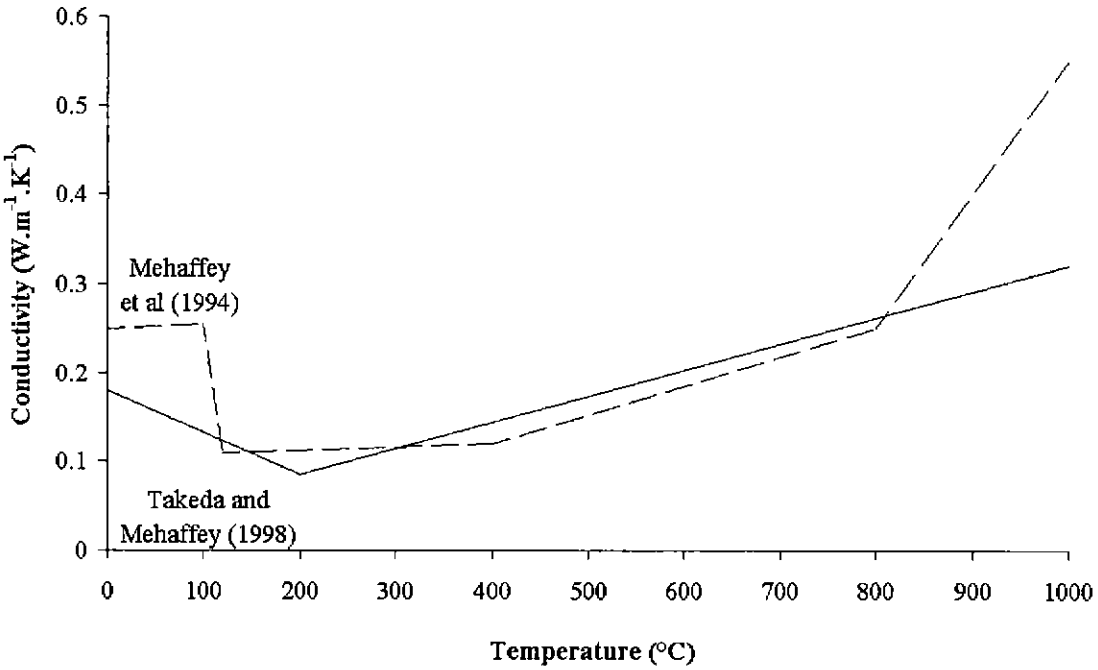

Figure 5.34. Conductivities Adopted by Mehaffey et al (1994) for Canadian Type X Gypsum Board and by Takeda and Mehaffey (1998) for Canadian Type C Gypsum Board.

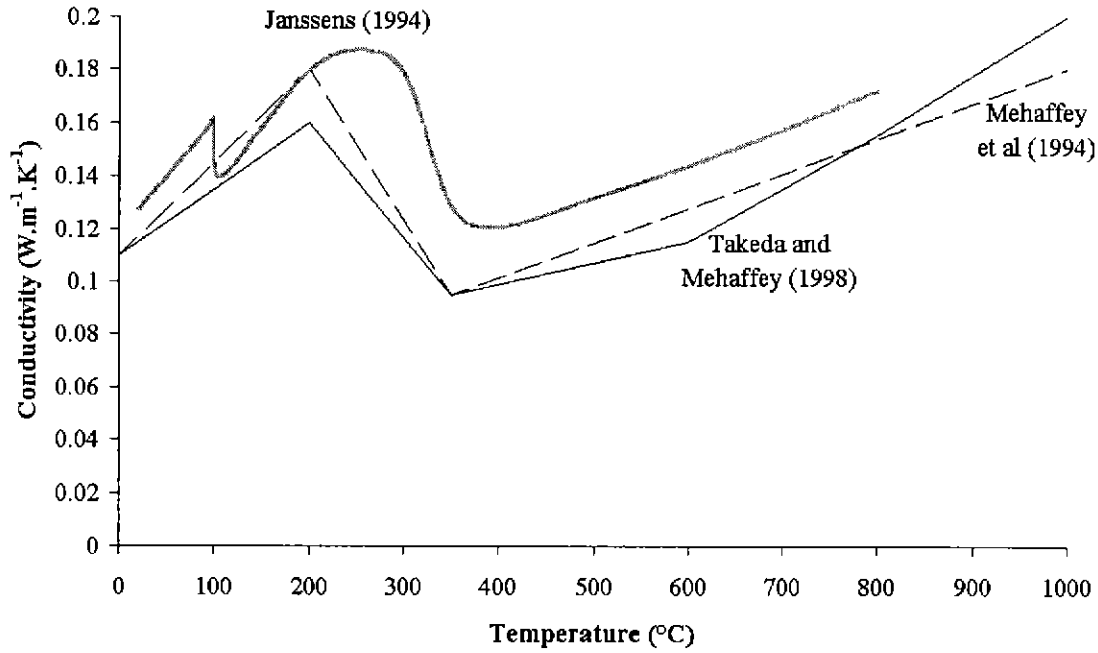

Figure 5.35. Conductivities of Timber Modelled by Mehaffey et al (1994) and Takeda and Mehaffey (1998). Comparative Values for Similar Timber Derived with Janssens (1994) Model Thermal Conductivity.

Thermal Properties and Assumptions by Takeda and Mehaffey (1998)

Takeda and Mehaffey (1998) used the same values for density, specific heat and surface emissivity of gypsum board as were used in Mehaffey et al (1994). The relationship they adopted for conductivity was simplified as shown in Figure 5.34. The simplifications, however, do not correspond to the characteristics of phenomena as well as the relationship given by Mehaffey et al (1994) does; for example, the increase in heat transfer as glass fibres, within gypsum board, fail at temperatures greater than 700-800°C (§2.2.1.3). The differences between the two plots for conductivity, at temperatures less than 120°C and greater than 800°C were not significant since little of the gypsum lies within regions at these temperatures during fire exposure.

Takeda and Mehaffey (1998) used the values for density of timber and char shown in Figure 5.31. These values are similar to those used in Mehaffey et al (1994). They also used similar values for specific heat and conductivity shown in Figure 5.33 with some minor modifications, presumably resulting from calibrations of model predictions to experimental results. They used the same value of 0.90 as Mehaffey et al (1994) for the surface emissivity of timber and char, constant with temperature.

Takeda and Mehaffey (1998) made similar assumptions to those of Mehaffey et al (1994), except that they assumed that smoke permits the transmission of all radiation between cavity surfaces.

Summary of Thermal Properties and Assumptions Described in this Thesis

In the research described in this thesis, Mehaffey's et al (1994) values for the density of gypsum board shown in Figure 5.31 were adopted (§5.2.3.1). Sultan's (1996) values for specific heat (§5.2.3.3) were adopted (Figure 5.32). Mehaffey's et al (1994) values for conductivity were used as a basis for deriving conductivities for gypsum board as a function of density at ambient conditions (§5.2.3.2). His values shown in Figure 5.34 are thus used in the evaluation of ADIDRAS in this section, §5.5. A value of 0.60 was used for the surface emissivity of gypsum board, constant with temperature (§5.3.2).

Janssen's (1994) models for density, specific heat and conductivity of timber were adopted (§5.2.4). The thermal properties derived with his models, for the same timber modelled and tested by Mehaffey et al (1994) and Takeda and Mehaffey (1998) are shown in Figure 5.31, Figure 5.33 and Figure 5.35, respectively. The surface emissivities adopted for timber and char were given in Figure 5.14. The initial characteristics of the timber were:

1. Density of 470 $kg.m^{-3}$.
2. Moisture content of 9.5%.
3. Spruce Pine Fir species.

Most of the assumptions made by Mehaffey et al (1994) and Takeda and Mehaffey (1998) can be modelled with ADIDRAS. The node generation routine in ADIDRAS (§3.5) and the numerical solution algorithm, however, do not lead to stable numerical solutions for the node spacings they used. They used node spacings of approximately 3.0 mm in regions of high thermal gradients. They also assumed that some gypsum or timber/char material is lumped at each surface node. The lump of material at each node was a small finite volume extending half the distance to adjacent nodes in solid material. Theoretically, surfaces have no mass, and were modelled accordingly in ADIDRAS (§3.9.2). Finite difference methods assume that the temperature at a node in a finite volume is the average temperature of that volume. Since surface temperatures are the temperatures at the boundary of a finite volume, they do not represent the average temperature of the finite volume, and thus apportionment of finite volume to surface nodes introduces numerical errors. These errors can be significant where there are steep temperature gradients near surfaces.

There are advantages and disadvantages in the numerical methods used in the models - that is, ADIDRAS which attributes no mass to the surface nodes, and the models of Mehaffey et al (1994) and Takeda and Mehaffey (1998) which does attribute mass to the surface nodes. The method in ADIDRAS is more rigorous. However, in having surface nodes without any finite volume to absorb the radiant source energy (§2.3.4), accurate modelling of the steep temperature gradients near surfaces is essential for transferring heat away from surface nodes to prevent radiant source energy accumulating at surfaces and causing numerical instability. To model steep temperature gradients, the spacing of nodes near surfaces must be kept small. The numerical method in WALL2D, simulates absorption of radiant source energy by the finite volumes at surface nodes and is thus less dependent on the accurate modelling of steep temperature gradients with small node spacings to maintain numerical stability. Hence WALL2D can maintain numerical stability with a coarser grid of nodes than ADIDRAS can. The consequences of the different methods used in the models for modelling heat transfer through surfaces is discussed in the comparisons given subsequently in this section, §5.5.

The assumption of there being a shrinkage gap (Figure 5.23) between studs and gypsum board on the fire side was included in the comparions in this section, §5.5. Shrinkage gaps of 1.0 mm and 3.0 mm have been considered.

ADIDRAS can model varying smoke transmissivities (§3.9.5). The cases of complete transmissivity (extinction coefficient, κ=0.00 m^{-1}) and virtually no transmissivity (κ=50 m^{-1}) have been considered.

The simple method, modification type C, for moisture transfer modelling described in §5.4.4 has been used for predicting temperatures prior to the post-dwell temperature rises. It was shown in §5.4.4 that the modelling of moisture transfer is only effective when there are no gaps between gypsum board and the

studs on the fire side. Thus, to incorporate the simplified modelling of moisture transfer and the modelling of gaps, ADIDRAS was run separately for each type of modelling. Predictions of pre-dwell temperatures were taken from the runs with moisture modelling, and predictions of post-dwell temperatures were taken from the runs with gap modelling.

Comparison of ADIDRAS Predictions with Takeda's and Mehaffey's (1998)

A typical horizontal section through walls, that were tested and modelled by Takeda and Mehaffey (1998), is shown in Figure 5.36. The figure shows the points A, B, C, D, E, F and G where temperatures were measured with time. Details of their experiments are summarised in Table 5.10.

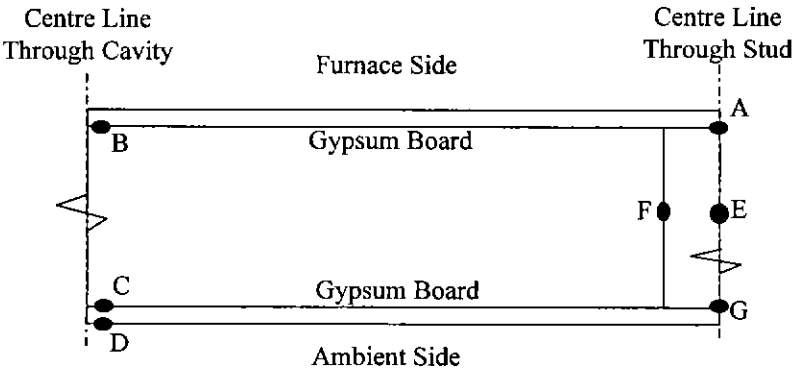

Part Horizontal Section Through Wall

Figure 5.36. Location of Thermocouples, A B C D E F G referred to in Figure 5.38 - Figure 5.44.

Table 5.10. Descriptions of Wall Experiments by Mehaffey et al (1994) and Takeda and Mehaffey (1998).

Wall Experiment	Description
2	Small scale experiment on a wall comprising a single sheet of 12.7mm thick Type C Canadian gypsum board each side of spruce pine fir studs, 89x38mm in cross-section spaced at 200mm between centres; wall exposed to ASTM E119 fire.
3	Small scale experiment on a wall comprising a single sheet of 15.9mm thick Type X Canadian gypsum board each side of spruce pine fir studs, 89x38mm in cross-section spaced at 200mm between centres; wall exposed to ASTM E119 fire.

The comparisons between the predictions of ADIDRAS and the results of Takeda and Mehaffey (1998) are carried out in a similar manner to the comparisons between modelling and experimental results in §5.3 and §5.4. The comparisons of temperatures in studs (at points A, E, F and G) are separated from the comparisons of temperatures at points along heat paths through cavities (at B, C and D).

To evaluate the consistency in numerical results from ADIDRAS and WALL2D for heat transfer through cavities, plots with the two models, based on the assumptions of Takeda and Mehaffey (1998), are given in Figure 5.37. Experimental results are also shown to evaluate the efficacy of the assumptions.

There are good comparisons between the predictions with ADIDRAS and WALL2D, of temperatures at points F and G. The differences in the predicted temperatures can be attributed to the differences in the numerical modelling of the heat transfer at surface nodes. There is also a good comparison between the model predictions and the experimental measurements, and thus there is some support for the assumptions.

The predictions of temperatures at point A with ADIDRAS, after the 15th minute, are 100-200°C higher than those with WALL2D, despite the use of the same thermal property values given by Takeda and Mehaffey (1998). In a personal communication, Mehaffey (1999) advised that the under-estimation of temperatures with WALL2D was due to calibration of their cavity radiant heat transfer sub-model. This sub-model uses the same emissivity for timber and gypsum board. To allow for the emissivities being different for the two materials, they introduced a model calibration factor to over-estimate radiant heat transfer from the exposed gypsum board and assumed that emissivities of all materials are 1.00. Apparently, the modelling involving the calibration factor in WALL2D requires some correction.

The temperatures predicted at A with ADIDRAS, compared with the experimental results, are approximately 100°C higher between 15-35 minutes and increase to 200°C higher by the 50th minute. It was explained in §5.4.3 that this increase is expected when assumptions ignore the presence of a shrinkage gap between studs and gypsum board on the fire side. Through these shrinkage gaps, much radiant heat transfers to the cavity instead of the stud and leads to lower temperatures in the char near the gap.

There is a good comparison between the predicted temperatures at E given with the models. However, the experimental measurements for temperatures at E are significantly different to the results of both models. The rise in the experimental temperatures at E above the dwell temperature, was gradual. Anomalies in

the measurements are apparent. It could be expected that when the dwell ceases, there would be a sudden rise in the temperature gradient because of the sudden absence of moisture to absorb thermal energy. The sudden absence of moisture is modelled as a sharp step-down in the specific heat at 120-130°C shown in Figure 5.33. A sudden rise occurs in the experimental measurements of temperatures shown in Figure 4.27 at S11 which is a position similar to E; that is, at the centre of a stud. The anomalous results from Experiment 2 (Table 5.10) may have been due to problems with the placement of thermocouples. Presumably, Mehaffey et al (1994) installed thermocouple, E in a hole drilled perpendicularly into the ambient facing side of the stud. This installation is prone to several problems:

1. Heat flow along the hole by either a gap due to the hole diameter being significantly larger than the diameter of the thermocouple wiring, or by conduction along the thermocouple wire in the presence of a steep temperature gradient. Both of these causes of heat flow would mean that the temperature measurement was representative of some small region rather than the point at the tip of the thermocouple wires.
2. Accidental tugging and partial withdrawal of the wire from the hole.

The advantages of Collier's (1991, 1993) method (Figure 4.12) of inserting thermocouples into timber studs, which was used in the research described in this thesis (§4), is apparent. His method secures thermocouples firmly. It positions thermocouple wires parallel to isotherms and thus prevents the influence of heat flow along the hole or along the wires. His method thus provides much tolerance in placement without significantly affecting temperature measurements.

Overall, the comparisons between the predictions of ADIDRAS and Takeda's and Mehaffey's (1998) are good except at point A, and thus support the validity of numerical analyses in ADIDRAS. Because of the anomalous results at A, comparisons of results for a similar point reported in Mehaffey et al (1994) are carried out further below.

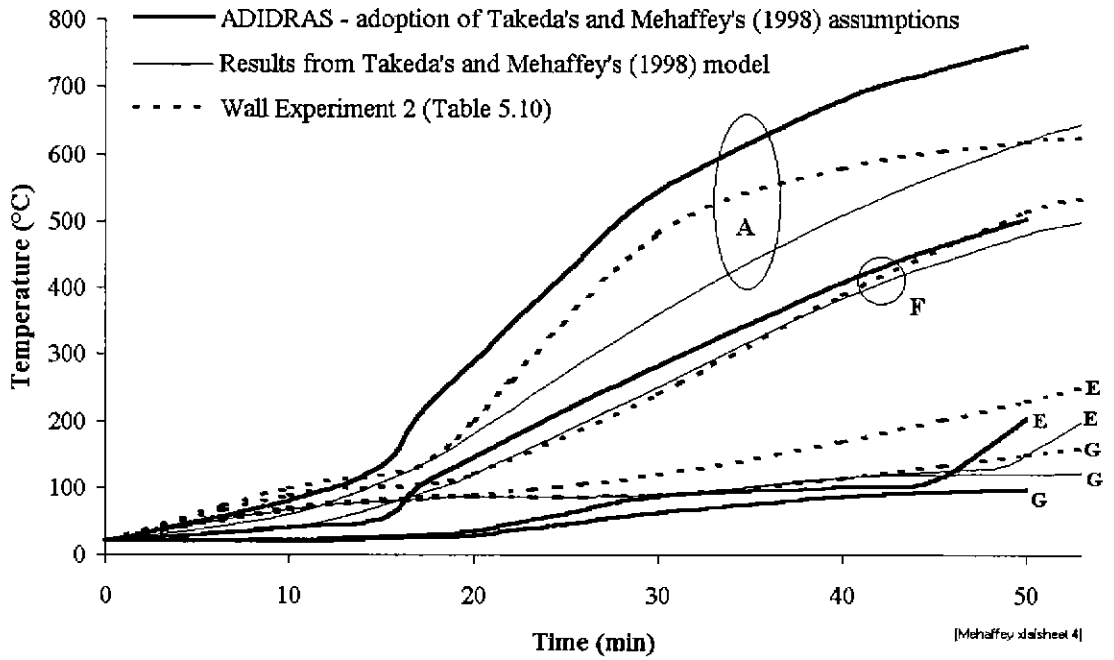

Figure 5.37. Plots for Evaluating the Consistency of the Numerical Results for Stud Temperatures Predicted with ADIDRAS and WALL2D. (All Model Predictions are based on the assumptions given by Takeda and Mehaffey, 1998.)

Comparisons of the efficacy of assumptions made in the research (as described in this thesis) to obtain stud temperatures, and the efficacy of assumptions in WALL2D, can be evaluated from Figure 5.38. The plots in the figure are based on the different assumptions of the models but the same numerical procedure; that is, ADIDRAS. The ADIDRAS plots, based on the assumptions described in this thesis, are shown as grey lines. ADIDRAS plots, based assumptions by Takeda and Mehaffey (1998), are shown as the continuous black lines. Plots of experimental results are shown as dotted lines.

The assumptions adopted in this research led to substantial improvements in the predictions of temperatures at A, compared with the predicted temperatures based on the assumptions of Takeda's and Mehaffey's (1998). Temperature predictions resulting from different assumed constant gap widths are shown in Figure 5.38. The figure indicates that the gaps opened at approximately 33 minutes and widened to a width of 1.0 mm at 50 minutes. It is apparent that the assumption of gaps opening between studs and gypsum board on the fire side is the main assumption that greatly improves the predictions of temperatures at A.

The assumptions adopted in this research and the assumptions of Takeda's and Mehaffey's (1998) led to similar predictions of temperatures at points F, E and G. Thus plots of predicted temperatures at these

points, based on alternative gap widths, are not shown in Figure 5.38. The gaps had little effect on temperatures at these points.

The plots of predicted temperatures at E show that Janssen's (1994) thermal properties for timber led to a slightly more conservative predictions, some 3-5 minutes ahead of predictions by Takeda and Mehaffey (1998).

The closer proximity of the grey lines than the black lines to the experimental results, plotted as dotted lines, shows that the modification (C in Figure 5.27 and Figure 5.28) of conductivities to allow for moisture transfer did improve temperature predictions prior to post-dwell rises. Despite the improvements, some temperature predictions lagged experimental measurements by as much as 10 minutes. That is, heat transferred by moisture movement was much more than 10 times the heat transferred by conduction.

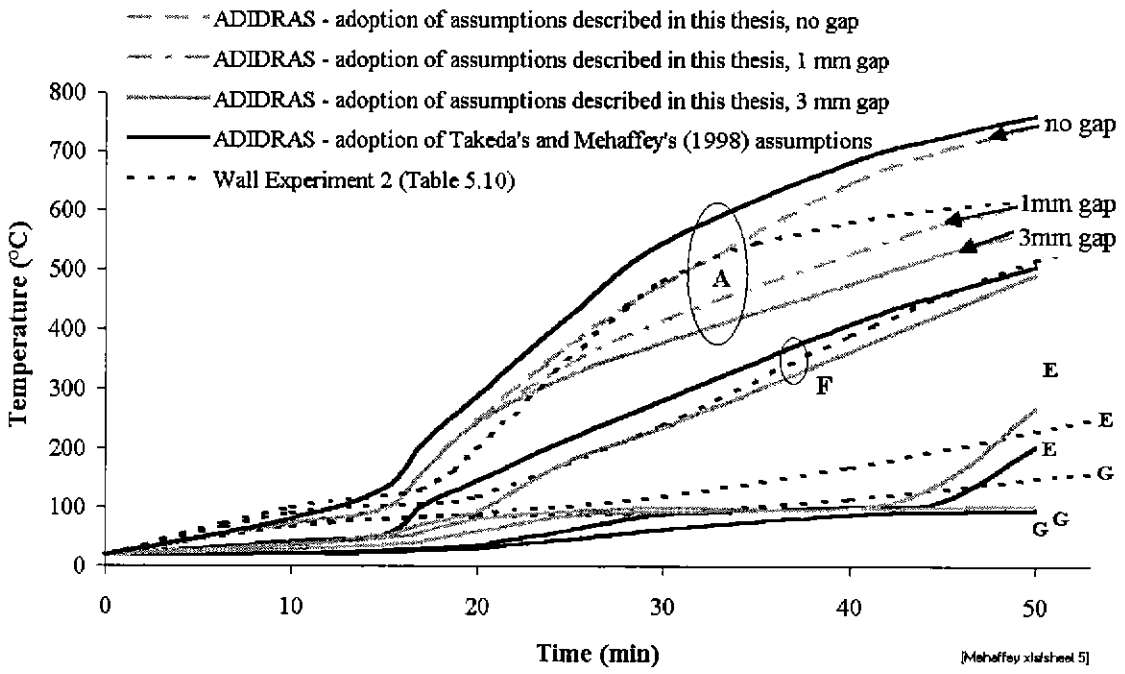

Figure 5.38. Plots of Stud Temperatures for Evaluating the Efficacy of the Assumptions described in this Thesis and of the Assumptions by Takeda and Mehaffey (1998).

Plots for evaluating the consistency of numerical results of the models, and the efficacy of Takeda's and Mehaffey's (1998) assumptions to predict temperatures at points along heat paths through cavities, are given in Figure 5.39. The plots have been produced with ADIDRAS using similar assumptions and values of thermal properties adopted by Takeda and Mehaffey (1998) in their model, WALL2D.

There are good comparisons between the predictions of the two models except for point B. The post-dwell rise in temperature at B, predicted with ADIDRAS is approximately 3 minutes ahead of the predictions with WALL2D. This difference can be attributed to the modelling of heat transfer at surfaces. The steep temperature gradients at surfaces are modelled more accurately in ADIDRAS. Greater rates of heat transfer are modelled and hence an earlier post-dwell rise is predicted with ADIDRAS. The gradients of the temperature-time plots predicted with the models between 15-18 minutes is similar.

The experimental results show evidence of the post-dwell rise in temperatures at B commencing barely noticeably at approximately 13 minutes. The post-dwell rise is firmly established by 18 minutes. These times compare favorably with the predictions of ADIDRAS and WALL2D and thus give some support for the efficacy of Takeda's and Mehaffey's assumptions for modelling the time the post-dwell rise begins. However, the prediction of the rate of the rise is greater than is apparent in the experimental results. The lower rate in the experiment indicates that the following phenomena may significantly affect the post-dwell rise:

1. The rate of vaporisation of moisture.
2. The dispersion of heat by moisture transfer into regions close to areas of vaporisation.

Improved modelling would require the application of the rate reaction equation for moisture vaporisation similar to equation (2.3), or moisture transfer equations.

At point D, in Figure 5.39, there is a good comparison between predictions with WALL2D and ADIDRAS. However, both models significantly underestimate the temperatures at D compared with the experimental measurements. These higher measured temperatures were most likely due to moisture transfer across the wall cavity which cannot be modelled with the use of modification C in Figure 5.27 and Figure 5.28.

Overall, the predictions made with ADIDRAS and Takeda's and Mehaffey's (1998) model are numerically consistent except for significant differences for points B and D. The comparisons generally support the validity of the numerical methods in ADIDRAS. Because of the significant differences between the results of the models at B, comparisons of results for similar points reported in Mehaffey et al (1994) are carried out further below.

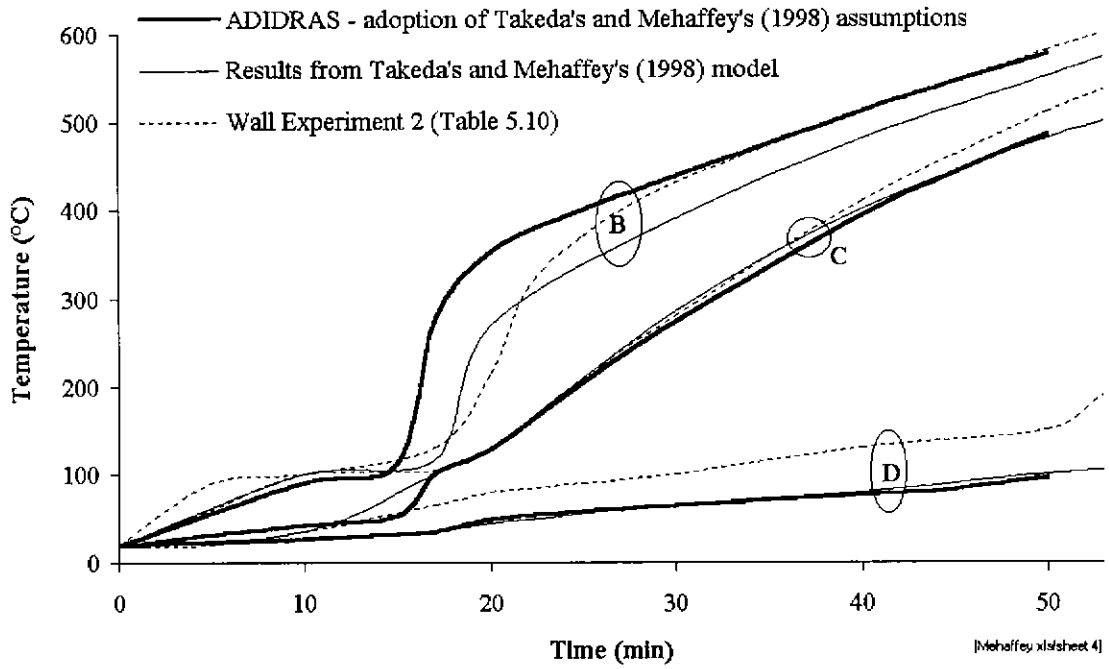

Figure 5.39. Plots for Evaluating the Consistency of the Numerical Results for Temperatures Predicted with ADIDRAS and WALL2D, for Points along a Heat Path through the Cavity. (All model predictions are based on the assumptions given by Takeda and Mehaffey, 1998.)

Comparisons of the efficacy of assumptions made in the research (as described in this thesis) to obtain temperatures at points along heat paths through cavities, and the efficacy of assumptions in WALL2D can be evaluated from Figure 5.40. As for Figure 5.38, the plots in Figure 5.40 are based on the different assumptions of the models but the same numerical procedure; that is, ADIDRAS. The ADIDRAS plots are based on the assumptions described in this thesis, and are shown as grey lines. ADIDRAS plots, based on assumptions by Takeda and Mehaffey (1998), are shown as the continuous black lines. The experimental results are shown as dotted lines.

The post-dwell temperatures predicted with ADIDRAS with both sets of assumptions are similar at B but are significantly different at C. The lower temperatures at C predicted as a result of assumptions in the research described in this thesis are most likely due to the lower values assumed for the emissivity of gypsum board (0.6 compared with 0.9 in Takeda and Mehaffey, 1998). The estimate of 0.6 for emissivity most likely resulted from the use of pads, shown in Figure 4.10, to cover surface thermocouples. The pads would have shielded the thermocouples and increased the resistance of the flow of heat in the vicinity of the thermocouples. Hence, the apparent emissivity was reduced.

The simple moisture transfer model gives good predictions of pre-dwell temperatures at B but not at C, in Figure 5.40. To improve predictions of pre-dwell temperatures at C modelling of moisture transfer across cavities is apparently necessary.

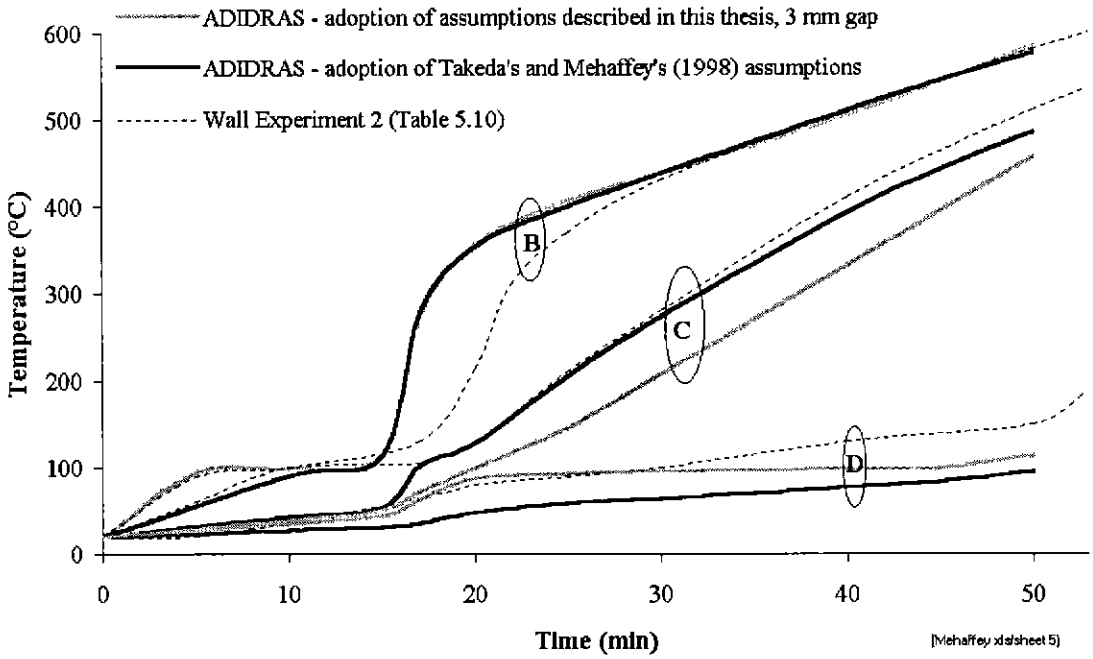

Figure 5.40. Plots for Evaluating the Efficacy of the Assumptions described in this Thesis and of the Assumptions by Takeda and Mehaffey (1998) for Predicting Temperatures at Points along Heat Paths through Cavities.

Comparison of ADIDRAS Predictions with Mehaffey's et al (1994) Results

As mentioned above, there were inconsistencies in the comparisons of temperatures predicted with ADIDRAS and WALL2D at A, B and E in Experiment 2 (Table 5.10), despite using similar assumptions and values for thermal properties. Further comparisons with the results of another model - namely, Mehaffey's et al (1994) - are thus carried out below to confirm the validity of numerical methods and assumptions used in the research described in this thesis.

Figure 5.41 shows plots of temperatures in studs predicted with ADIDRAS based on the assumptions of Mehaffey et al (1994). The results of his model and experiments are also shown for comparison. There are good comparisons between the predictions with ADIDRAS and Mehaffey's et al (1994) model at all points E, F and A. These comparisons support the validity of the numerical analyses of both models

which were developed independently. The comparison of temperatures predicted with the models is much better than the similar comparison of temperatures at A in Figure 5.37. The temperatures predicted at A by Takeda and Mehaffey (1998) appear to be in error and the predictions of ADIDRAS and Mehaffey et al (1994) appear to be more valid. As previously explained for errors in predictions by Takeda and Mehaffey (1998), in reference to Figure 5.37, this error was most likely due to a mistake in a calibration factor used in modelling radiant heat transfer across the cavity.

The results from both models compare well with the experimental measurements of temperatures at all points E, F and up until 40 minutes at A. This comparison supports the validity of Mehaffey's et al (1994) modelling of phenomena except in the region of the interface between the studs and gypsum board on the fire side after the 40th minute. It will be demonstrated below that the modelling with ADIDRAS, in the research described within this thesis, can more effectively model the temperatures at A after the 40th minute.

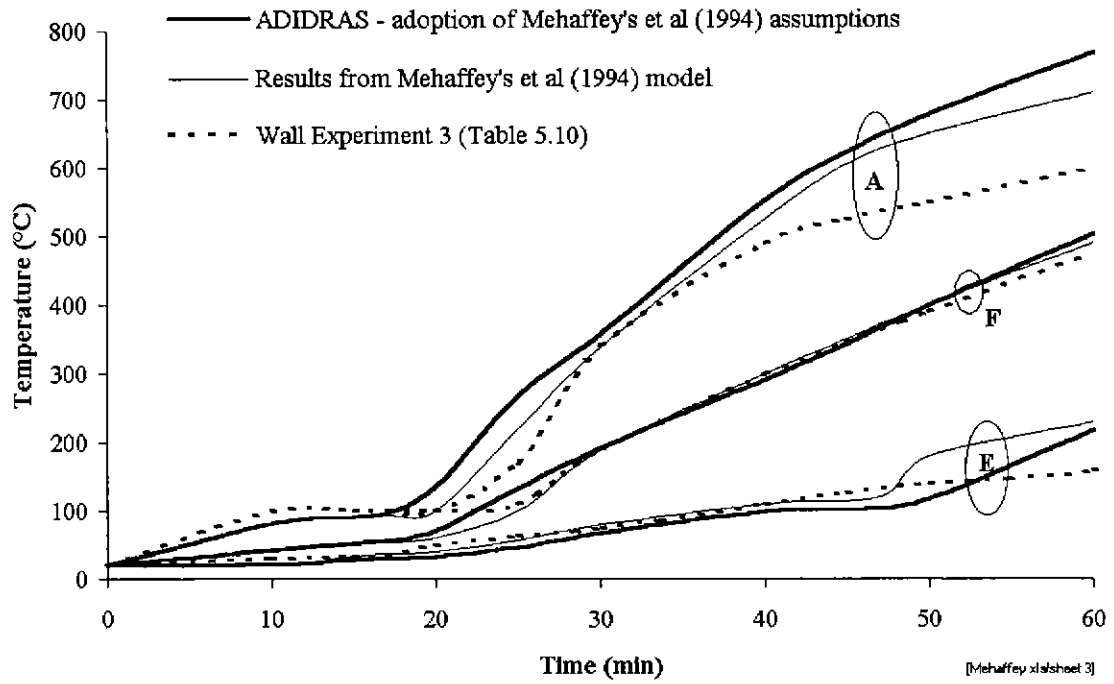

Figure 5.41. Plots for Evaluating the Consistency of the Numerical Results for Stud Temperatures Predicted with ADIDRAS and by Mehaffey et al (1994). (All model predictions are based on the assumptions given by Mehaffey et al, 1994).

Plots are shown in Figure 5.42 to demonstrate improvements in the efficacy of assumptions for predicting stud temperatures in the research described in this thesis. These plots have been obtained with ADIDRAS based on assumptions described in this thesis and the assumptions of Mehaffey et al (1994). It can be

seen that the assumption of a shrinkage gap greatly improves predictions at A. The modelling indicates that the gap began to open at 30 minutes, increasing to 1.0 mm at 53 minutes. Comparisons of temperatures at F are good. Comparisons at E show that the adoption of Janssen's (1994) thermal properties for timber in the research described in this thesis led to conservative overestimation of temperature at the centre of studs for times greater than 45 minutes.

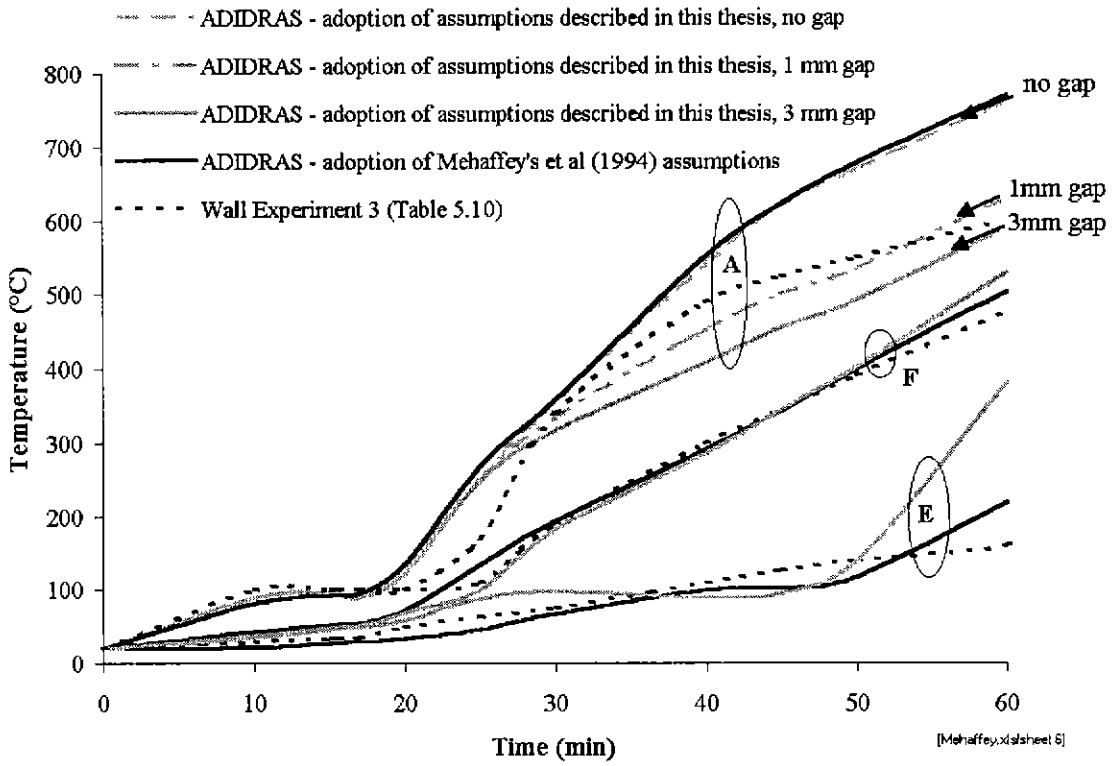

Figure 5.42. Plots of Stud Temperatures for Evaluating the Efficacy of the Assumptions described in this Thesis and of the Assumptions by Mehaffey et al (1994).

Plots for evaluating the consistency of numerical results of the models, and the efficacy of Mehaffey's et al (1994) assumptions to predict temperatures at points along heat paths through cavities, are given in Figure 5.43. The plots have been produced with ADIDRAS using similar assumptions and values of thermal properties adopted by Mehaffey et al (1994). Comparisons discussed in relation to Figure 5.39 are similar in Figure 5.43, except for plots B and C after 25 minutes. The plots for ADIDRAS in Figure 5.43 show a smaller temperature difference across the cavity than the plots in Figure 5.39. The mean cavity temperatures predicted with ADIDRAS and Mehaffey et al (1994) and the temperatures measured in experiments are similar. The differences in the three sets of plots of temperatures at B and C in Figure 5.43 may be due to the following reasons:

1. Difficulty in measuring surface temperatures as discussed in relation to Figure 5.40 above.

2. Mehaffey's et al (1994) numerical method of lumping finite volumes of mass at surface nodes may have led to greater apparent resistance to radiant heat transfer across the cavity.

Overall, the comparisons that can be made from Figure 5.43 support the validity of numerical analyses in ADIDRAS.

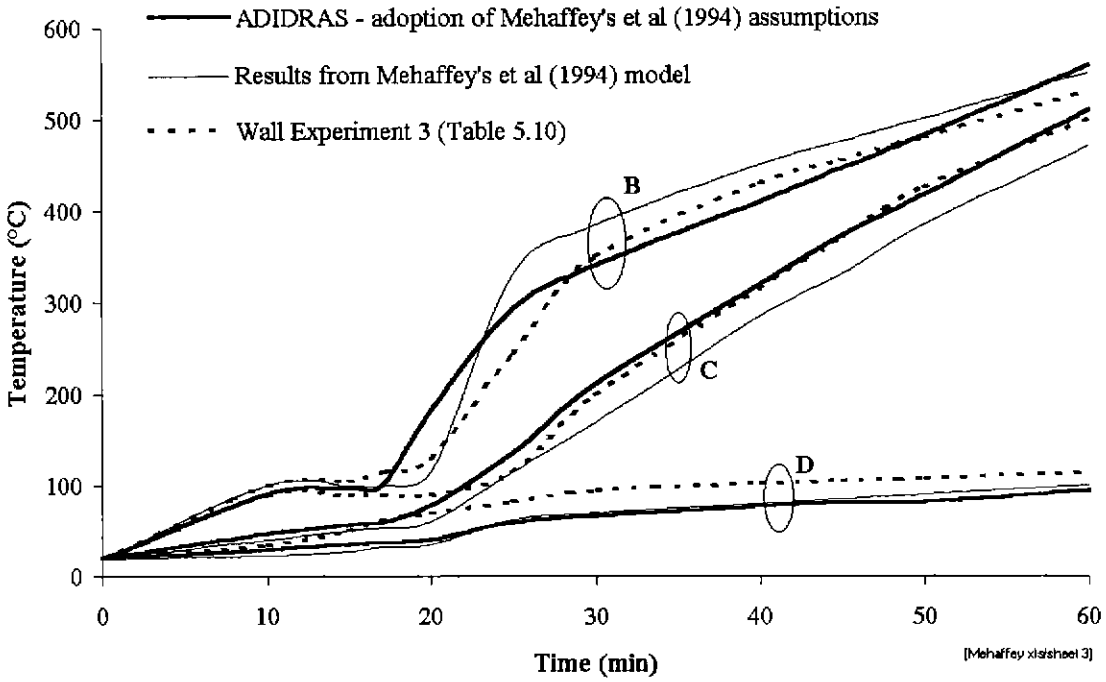

Figure 5.43. Plots for Evaluating the Consistency of the Numerical Results for Temperatures Predicted with ADIDRAS and by Mehaffey et al (1994), for Points along a Heat Path through the Cavity. (All model predictions are based on the assumptions given by Mehaffey et al, 1994.)

The effects on the predicted temperatures at points along heat paths through cavities, due to assumptions made in the research described in this thesis, and made by Takeda and Mehaffey (1998) can be deduced from the plots in Figure 5.44.

It is possible to compare the results given in Figure 5.40 and Figure 5.44. The plots of predicted temperatures in Figure 5.44 are better than than plots of predicted temperatures in Figure 5.40 in the following respects. The mean temperatures between model and experimental plots B and C in Figure 5.44 are similar which is not the case in Figure 5.40. These comparisons indicate that the only difference of significance in the assumptions is the values of surface emissitivity of gypsum board. As mentioned previously, there is difficulty in measuring surface temperatures and deducing surface emissivities. The mean cavity temperature appears to be insensitive to the emissivity and hence the heat transfer from cavities to the sides of studs is also insensitive to the surface emissivity of gypsum board.

As mentioned in the discussion in relation to Figure 5.40, the simple model for moisture transfer improves the ADIDRAS predictions of pre-dwell temperatures at B and D. To improve predictions at C it is apparent that a free convection model for the cavity is required.

To improve the predictions of temperature during the ten minutes following the dwells, either a reaction rate model in the form of equation (2.3), or moisture transfer equations are required.

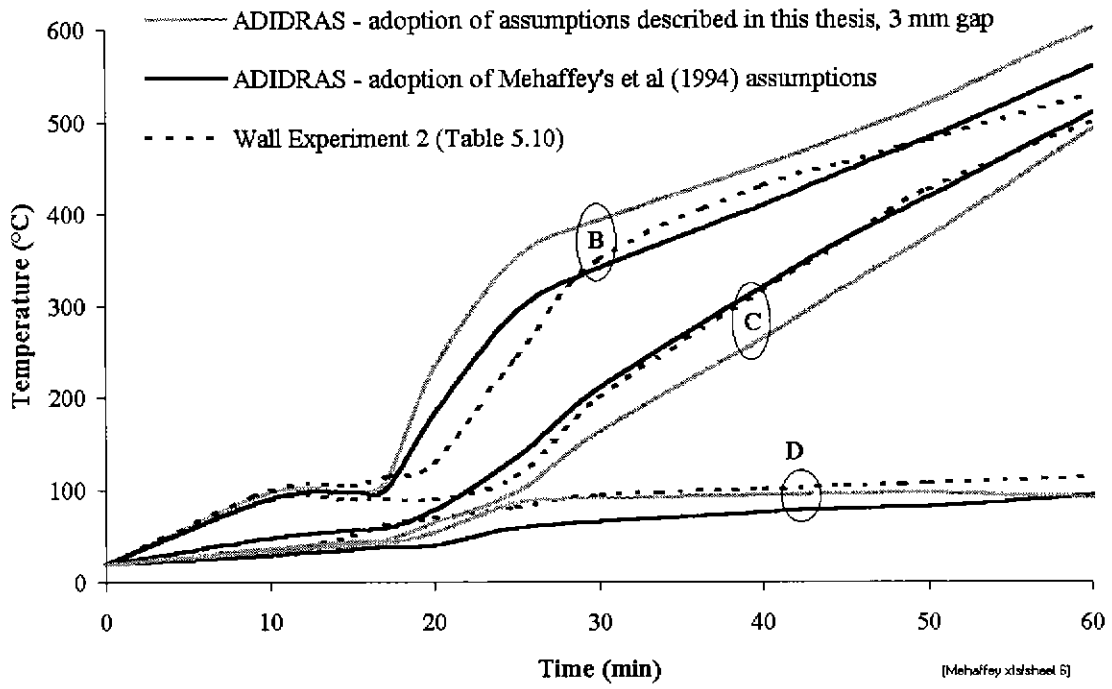

Figure 5.44. Plots for Evaluating the Efficacy of the Assumptions described in this Thesis and of the Assumptions by Mehaffey et al (1994) for Predicting Temperatures at Points along Heat Paths through Cavities.

Summary of Comparisons

The good comparisons between temperatures predicted with Mehaffey's et al (1994) model and with ADIDRAS based on similar assumptions used by Mehaffey et al (1994) indicate that the numerical methods in ADIDRAS have been carried out correctly and are satisfactorily accurate. Inconsistencies in comparisons between temperatures predicted by Takeda and Mehaffey (1998) and with ADIDRAS using similar assumptions, indicate that their radiant cavity heat transfer submodel requires some correction.

The assumptions adopted in the research described in this thesis have improved the predictions of pre-dwell temperatures and have also improved predictions of temperatures between studs and gypsum boards on the fire side by as much as 150°C. These assumptions are, therefore, recommended for modelling heat transfer in light timber framed walls in fire. As previously given at the conclusion of §5.4.4 it is recommended that the simple moisture transfer model be used when it is expected that walls will fail while the average temperature in the uncharred wood in studs is in the range of temperatures affected by moisture transfer - that is, 20 to 150°C. In other cases, moisture transfer should be ignored. It is recommended that gaps of constant width with time, between the studs and gypsum board on the fire side be modelled if timber fibres in this region are expected to reach temperatures higher than 400°C. From the results in this section, §5.5, a gap width of 1.0 mm appears most appropriate for adoption. However, after a gap is formed, temperatures are not sensitive to the width of the gap. It is more important to model a gap of some small width than to model the width of the gap accurately.

ADIDRAS more accurately models the heat transfer through surfaces, but WALL2D is more numerically robust for fast heat transfer rates which particularly occur through thin gypsum boards such as the 12.7 mm board used in Experiment 2 (Table 5.10).

Difficulty in accurately measuring the surface temperatures of gypsum board has led to different values of emissivity being adopted in this research compared with the value adopted by Mehaffey. Mehaffey's et al (1994) value is consistent with published values (Table 2.2). The value adopted in this research is more consistent with measurements taken by Young (1998). The value of emissivity does not appear to significantly affect temperatures in the cavity and, hence, the heat transferred to studs does not appear to be sensitive to the surface emissivity of gypsum board.

Further improvements to modelling may be made by incorporating into WALL2D and ADIDRAS, sub-models for:

1. The transfer of moisture through cavities by free convection.
2. Rate equation for moisture vaporisation similar to equation (2.3).
3. Equations for moisture transfer through porous materials.

5.6 Demonstration of the Wide Range of Applications of ADIDRAS by Application to a Double Stud Wall

In sections, §5.3 and §5.4 the efficacy of ADIDRAS was demonstrated in modelling heat transfer through a particular wall arrangement subjected to a particular fire - the standard fire (AS1530.4). To fulfill the aims of the research (§1.5), the range of walls for which ADIDRAS could be used, is evaluated in this section, §5.6. The model was applied to a double stud wall shown in Figure 5.45 for which test results were available from NAFI (1993). Double-stud framed walls are used for separating adjoining multi-storey houses in Australia. An advantage of this application is that the versatility of the discrete radiation analysis in ADIDRAS can be demonstrated on cavities with re-entrant corners. Radiant heat transfer around re-entrant corners formed by the pairs of studs could not be modelled by other heat transfer models (§2.5.5) commonly used for light-timber framed assemblies.

Another advantage of this application is that the sloughing modelling in ADIDRAS can be demonstrated. Since the test results for the double-stud wall were for a standard fire (AS1530.4), validation of ADIDRAS and indeed other models for timber framing exposed to non-standard fires is recommended for further research.

Additional thermal properties to those in §5.2 were required. Surface heat transfer coefficients shown in Figure 5.45 were adopted. These values are similar to those used in §5.3 and §5.4 except for the coefficient for convective heat transfer at the surfaces bounding the gap between the double studs. A coefficient of 6 ($W.m^{-1}.K^{-2}$), the same as for the sides of the studs was adopted.

A specification for the 50 mm thick glass fibre insulation used in the tests could not be found. Properties for glass fibre insulation, typically used in separation walls for multi-storey housing in Australia, were recently recommended by Davis (1998). He quoted the following properties independent of temperature:

1. Density = 10.8 $kg.m^{-3}$
2. Conductivity = 0.05 $W.m^{-1}.K^{-1}$
3. Specific Heat = 880. $J.kg^{-1}.K^{-1}$
4. Surface Emissivity = 0.95

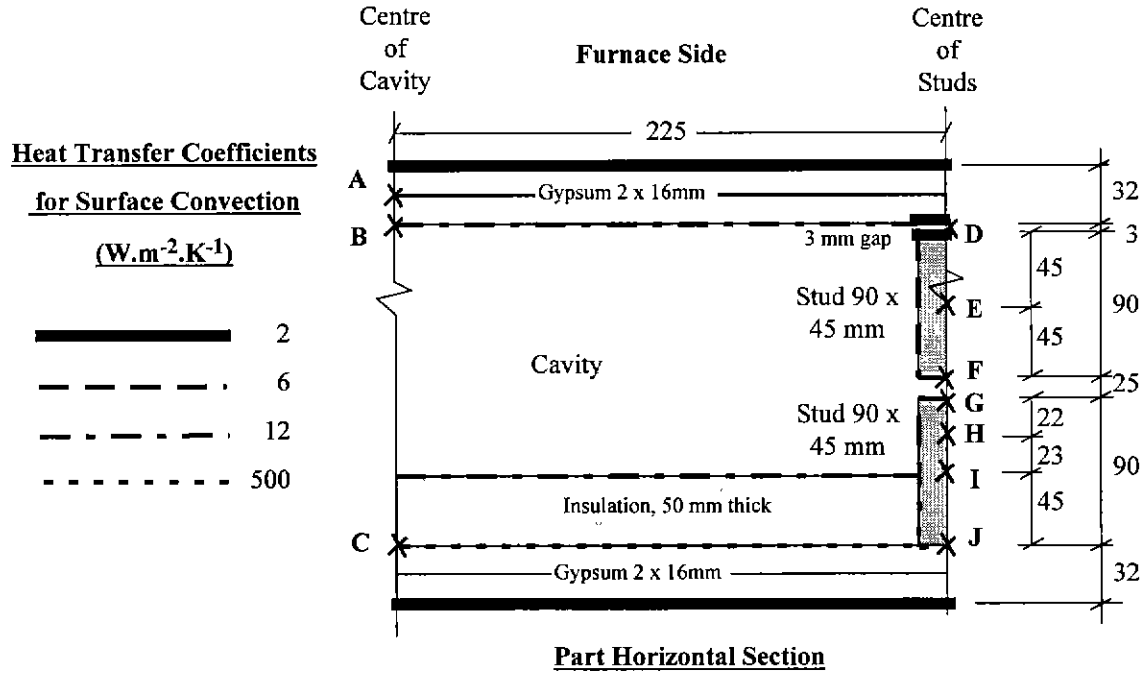

Figure 5.45. Part Horizontal Section showing Points A-K in Double Stud Wall Tested by NAFI (1993), for the Plots of Temperature versus Time in Figure 5.46 - Figure 5.48. (Note that no resistance to heat transfer was assumed between sheets of gypsum board in contact.)

Another property adopted was "sloughing temperature". Previously (§2.2.1.3) it was explained that sloughing is caused by the melting of glass fibres - more precisely, the reduction in viscosity of glass fibres within the gypsum board. Carne (1995) quoted typical temperatures in the range of 700-750°C. Goncalves et al (1996) showed with experiments that vertically hung strips of gypsum board sloughed at temperatures ranging between 700-1000°C, but mostly by about 800°C. Figure 5.46 shows plots for temperature versus times at several points at surfaces of gypsum boards in the double-stud wall tested. Sloughing occurred when the minimum temperature in the boards was approximately 700°C. This value was adopted for the sloughing temperature of gypsum board and is a reasonable conservative value compared with values measured by Carne and Goncalves.

For particular times, it was desired to compare predicted temperatures with test temperatures in the range of 200-300°C which largely determine the strength capacity and hence time of structural collapse by charring. At these temperatures shrinkage will occur (§5.4.3) and gaps will form between the studs and the gypsum board on the furnace side. Gaps with a constant width of 3.0 mm were assumed. Gaps hinder the simplified moisture transfer modelling discussed in §5.4.4, and thus simplified moisture transfer modelling (modification C in Figure 5.27 and Figure 5.28) was not applied.

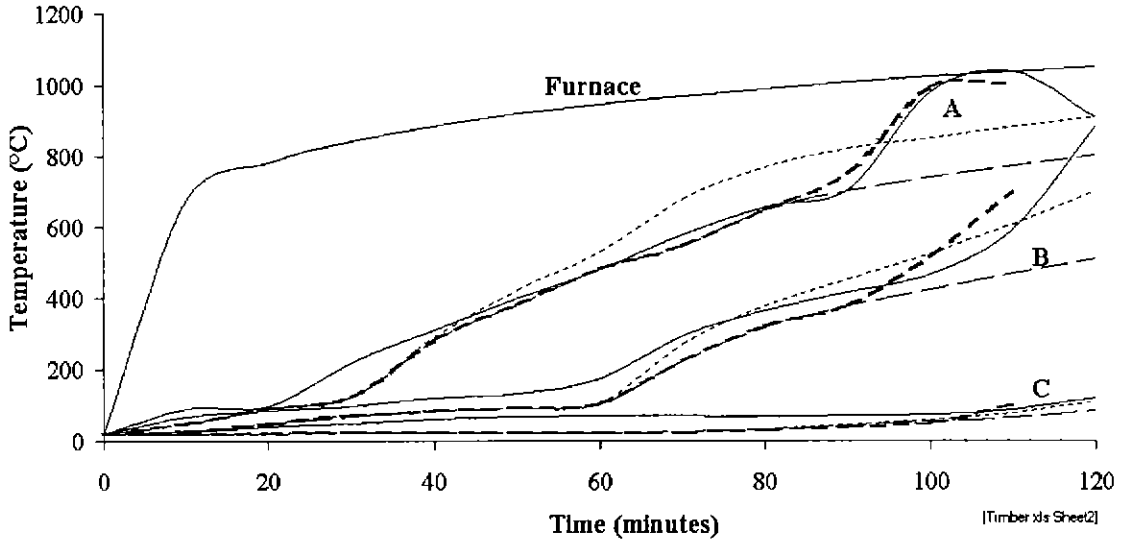

1. ——— Test results.
2. ------- Gypsum board conductivities in Figure 5.7, adopted in the research described in this thesis. No sloughing.
3. - — - — As for (2), except sloughing when minimum temperature in gypsum board = 700°C.
4. ····· Gypsum board conductivities in Figure 5.7, from Mehaffey. No sloughing.

Figure 5.46. Temperatures Predicted with ADIDRAS at Points through the Cavity of a Double Stud Wall and Results from Tests (NAFI 1993). (The location of points A, B and C are shown in Figure 5.45.)

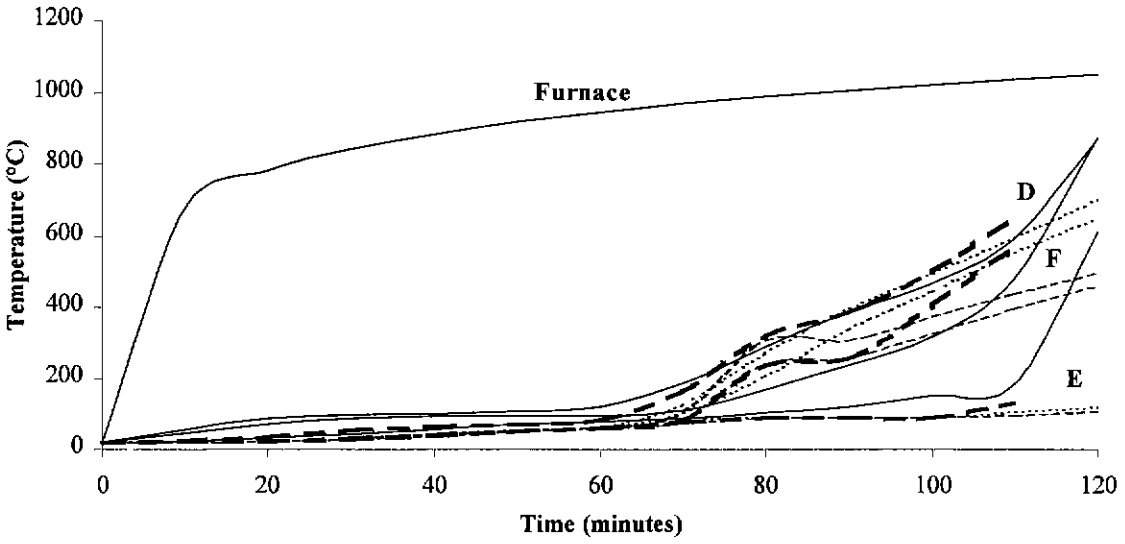

Figure 5.47. Temperatures predicted with ADIDRAS, in Stud on Furnace Side of Double Stud Wall and Results from Tests (NAFI 1993). (The location of points D, E and F are shown in Figure 5.45, and the definition of plotted lines is given in Figure 5.46.)

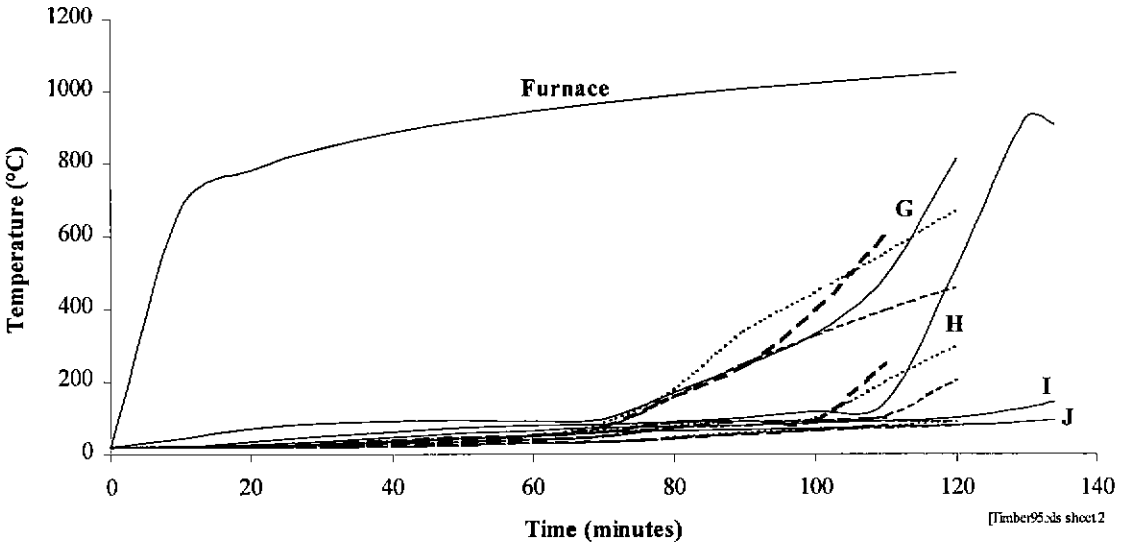

Figure 5.48. Temperatures in stud on ambient side of double stud wall, predicted with ADIDRAS and results from tests (NAFI 1993). (The location of points G, H, I and J are shown in Figure 5.45, and the definition of plotted lines is given in Figure 5.46.)

Temperatures were plotted for three groups of points. The group of points A, B and C in Figure 5.45 led to plots in Figure 5.46 indicating heat transfer through the cavity. Points D, E and F led to the plots in Figure 5.47 indicating heat transfer into the stud on the furnace side. Points G, H, I and J led to the plots in Figure 5.48 indicating heat transfer into the stud on the ambient side of the wall. For each point, four plots have been produced, which have been defined in the legend in Figure 5.46. The test results are indicated with the continuous black lines. The thin dashed lines indicate the model predictions resulting from material properties adopted in §5.2, assuming that no sloughing occurs. The thick dashed lines result from a similar procedure as for the thin dashed lines, except sloughing was assumed to occur when the minimum temperature in the gypsum board exceeded 700°C. The dotted lines result from an attempt to indirectly allow for sloughing of gypsum board by trebling the adopted conductivities for gypsum at temperatures above 700°C, without any reduction in the thickness of gypsum board on the fire side.

The model gives good predictions of temperatures between 200-300°C in timber compared with the test results. Since accurate prediction of these temperatures is necessary for accurate prediction of time of structural collapse, the heat transfer model could be adopted as one of the submodels in a time of failure model for double framed walls.

Both types of dashed lines compare well with test results up until the temperature at A reaches approximately 700°C. Thereafter, the thick dashed line, directly allowing for sloughing in the modelling, gave the best comparison. The attempt to model sloughing with higher conductivities in the gypsum board, did not give a satisfactory comparison with test results.

Hence, the results in Figure 5.46-Figure 5.48 generally indicate the versatility of the heat transfer model in modelling a wide range of wall sections and sloughing, which was an aim given in §1.5.

5.7 Conclusions on the Heat Transfer Model, ADIDRAS

Conclusions in relation to the aims in §1.5 and on other findings in the heat transfer research are given in this section §5.7. The conclusions on the main outcomes of research are given in general conclusions (§5.7.1). Other specific conclusions are given for phenomena (§5.7.2), thermal properties (§5.7.3) and methods of numerical analysis (§5.7.4).

5.7.1 General Conclusions

A new heat transfer model ADIDRAS, described in chapter 3 has been developed for a wide range of applications shown in Figure 5.49. This range includes walls with re-entrant cavities such as the staggered stud wall shown in Figure 5.49(c). The model has been validated for a number of applications. Validation remains to be carried out for walls with insulation and exposure to real fires (§5.8). The model was checked for conservation of energy and numerical convergence (that is, independence of mesh and time step) in §3.10. The assumptions and independently derived thermal properties used in the application of ADIDRAS led to predictions which compared well with results from wall furnace experiments undertaken in the research. The performance of the model has been compared with the performance of other recent models (Takeda and Mehaffey 1998, and Mehaffey et al 1994). This comparison revealed a number of achievements:

1. The comparison provided further confirmation on the validity of the numerical methods in ADIDRAS.
2. The assumptions used with ADIDRAS gave improved predictions of temperatures compared with the predictions with the other recent models.
3. The comparison clarified the efficacy of some assumptions in the recent models. For example, the assumption that smoke in the cavity is opaque to radiant heat transfer can be used to simplify modelling without a significant reduction in the accuracy of predicted temperatures.

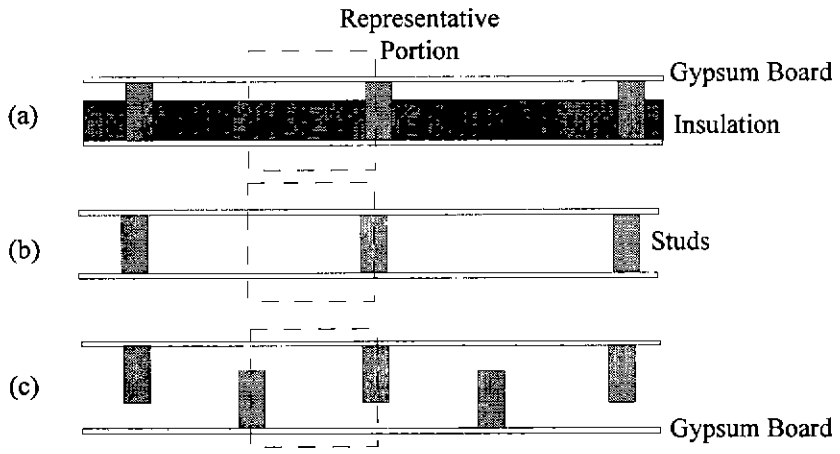

Figure 5.49. (Figure 3.2 repeated.) Range of Light Timber Framed Sections for which ADIDRAS has been Developed. (a) Ordinary Insulated Stud Wall. (b) Uninsulated Ordinary Stud Wall. (c) Uninsulated Staggered Stud Wall.

5.7.2 Conclusions for Assumptions on Heat Transfer Phenomena

Good comparisons between model predictions and experimental results were found in §5.3-5.6. These comparisons support the following conclusions about heat transfer phenomena (§3.3):

1. Heat transfer in light-timber framed walls is mainly two dimensional; that is with little variation vertically through the wall.
2. Modelling of heat transfer in gypsum board and timber can be satisfactorily carried out with thermal conduction analysis without moisture transfer in regions where temperatures are between 150-400°C. In positions where temperatures are less than 100°C, moisture transfer greatly increases heat transfer rates. In those positions where temperatures are between 100-150°C, moisture transfer reduces heat transfer rates. If a wall is expected to fail when the average temperature in the uncharred wood in the studs is less than 150°C, then moisture transfer critically affects the time of failure and should be modelled.
3. Studs shrink with heat and it is expected that gaps (§5.4.3) open up between the studs and gypsum board. The heat that transfers from the gypsum board on the fire side into the gap, transfers to the stud and to the cavity. The proportion of this heat that transfers to the cavity, when the temperatures in the gaps are greater than 400°C, is substantial and is insensitive to the width of the gap, even for gaps as narrow as 1mm (Figure 5.24). This substantial proportion of heat transferred to the cavity from the gaps, is the reason for observed temperatures in the fire side of studs being as much as 150°C less than temperatures predicted with heat transfer modelling which ignores the gaps. At gap temperatures above 400°C, the heat transfer across gaps can only be modelled accurately with two dimensional

radiation analysis. Thermal diffusion modelling cannot be manipulated to give predicted temperatures that are similar to predictions with two dimensional radiation analysis.

4. Despite movement of surfaces at temperatures higher than 150°C, due to shrinkage and recession of materials in light-timber framed walls, satisfactory modelling of heat transfer can be achieved with a constant grid; that is, without moving nodes. Shrinkage can be modelled using gaps of constant width for the entire duration of fire exposure (§5.4.3). Thermal properties should be chosen so as to lead to the same rate of heat transfer as actual shrunken wall components (studs and gypsum boards) and actual properties.
5. Evidence of some endothermicity during pyrolysis was observed in §5.2.4.3. However, good predictions of temperatures in timber were obtained without the need to consider heats of reaction during pyrolysis. Heat of reaction during pyrolysis does not appear to be significant. This conclusion is apparent from the discussion of results on temperature predictions in studs in Figure 5.25 and Figure 5.26; and the good comparisons between model predictions and experimental results generally throughout §5.4 and §5.6. This conclusion supports the assumption of no net heat of pyrolysis adopted by Fredlund (1988), Gammon (1986), and Thomas (1997)
6. Results of the research indicate that gypsum boards slough off when the minimum temperature of the board is 700°C. Sloughing at this temperature was reported in the full scale experiments discussed in §5.6. This temperature is within the range of temperatures in which glass gradually melts (§2.2.1.3).
7. Smoke transmissivity and density provide little resistance to heat transfer. Since smoke is buoyant it has low density. Since, in general, materials of low density provide little resistance to heat flow, this conclusion is expected. However, it is more valuable to note that whether cavities are assumed to be either clear or opaque to radiation, the predicted temperature distributions in a wall are similar (Figure 5.16 and Figure 5.21). It will be discussed in the next section, §5.8.2.2, that this conclusion potentially provides the basis for great simplification of heat transfer analyses in cavities.

5.7.3 Recommendations on Thermal Properties

Thermal properties that were adopted in the heat transfer analyses were based on studies reported in the literature, and on simple independent experiments. The results of this research support the use of the following property relationships and models published in the literature:

1. Relative density, specific heat and conductivity for wood by Janssens (1994).
2. Relative density of gypsum board by Mehaffey et al (1994).

3. Conductivity of gypsum board below 400°C by Mehaffey et al (1994) modified for variations in density in accordance with equation (5.1). Above 400°C, the effective conductivity (for which the aim is to predict the same rate of heat transfer as the actual conduction together with the radiation through shrinkage cracks in the gypsum board) should be obtained by independent experiments since the distribution of cracking varies substantially amongst boards produced by different manufacturers (Goncalves and Jong 1996). These experiments should mimic the restraints on the gypsum board of walls exposed to fire.
4. Specific heat of gypsum board by Sultan (1996).

5.7.4 Conclusions on Methods of Numerical Analysis Used in ADIDRAS

As was mentioned in §5.7.1, the use of ADIDRAS to model of walls similar to those in the experiments described in §4, was shown in §3.10 to be independent of mesh size and time step.

The speed of computation was sufficiently fast for the model to be incorporated into a probability modelling framework using many simulations such as, the Monte Carlo method. Speed was enhanced with the use of two methods. Firstly, the alternating direct implicit method of numerical analysis enabled the use of larger time steps than can be used with explicit methods. Numerical stability was not affected until radiant heat transfer in the cavity became dominant; this radiation was analysed explicitly. Unlike other models, radiation at external surfaces has been numerically stabilised for any time step by linearising radiant heat and incorporating it into implicit modelling. Although implicit methods are no more accurate than explicit methods, they enable the choice of faster computation speed, until radiation in the cavities becomes dominant. Secondly, the number of nodes in regions of low temperature was minimised by generating wider grid spacings with distance beneath surfaces. Executions (Table 3.1) of the model using a 2.5 second time step and a 20x40 grid of nodes to produce the predictions for an hour of fire exposure, were carried out in 5 minutes on a personal computer with an Intel Pentium 2, 200MHz chip. The numerical accuracy was generally within ±2% of the temperature rise above ambient conditions.

The numerical method of discrete radiant heat transfer in the model can be used to analyse more complex cavities than can other heat transfer models for light-timber framed structures. Furthermore, the input required to define the cavities is much more simple than for alternative crossed-string approaches. As a result, additional complexities can be modelled; these complexities include re-entrant corners, narrow shrinkage gaps and, absorption and emission of radiation through smoke. The narrow shrinkage gaps form between gypsum board and studs on the fire side of walls during fire exposure (§5.4.3). The

numerical accuracy of the discrete radiant heat transfer cavity model is within 1% for a medium level of refinement of mesh and time step, as defined in Table 3.2. The capability of the model to analyse radiation through cavities with re-entrant corners enables the model to analyse heat transfer in a larger range of walls than can be achieved with other models. The model can analyse double-stud and staggered stud walls as mentioned above. The discrete radiation analysis is numerically intensive but it is completed in about 10 seconds on the personal computer mentioned above, and the analysis need only be carried out once if surfaces are assumed to be stationary.

Other simple numerical models have been established during this research. One model is to represent the sloughing of gypsum boards at some nominated minimum temperature (§3.8 and §5.6). Another was developed and it adopted a simple approach to predicting temperatures below 150°C affected by moisture transfer (§5.4.4). This approach involved increasing the values of conductivities of porous solids such as timber and gypsum board by a factor of 10 for temperatures below the vaporisation point. This approach also involved the assumption that shrinkage gaps between gypsum board and studs did not occur until vaporisation was finished.

5.8 Further Research

Further research is required in a number of areas. Simple experiments need to be undertaken to derive values or develop models for several thermal properties (§5.8.1) that are critical in predicting temperatures and times of failure. Further modelling needs to be developed in a number of areas including radiant heat transfer at high temperatures with reduced tendency for numerical instabilities(§5.8.2, §5.8.2.1). Model simplifications are apparent (§5.8.2.2). More wall experiments are required to confirm shrinkage gaps, validate the model for real fires exposure and to develop improved methods of measuring surface temperatures (§5.8.3). There are benefits in further research on the effects of gaps in other applications (§5.8.4). All of these areas mentioned are discussed in more detail below.

5.8.1 Thermal Properties

The conductivities of gypsum board from a range of manufacturers should be determined from simple experiments at temperatures greater than 400°C. In this temperature range, Goncalves et al (1996) showed that there was considerable variation in the distributions of cracks in gypsum board and variations in the temperatures when these cracks occurred amongst boards from the different manufacturers. There is thus considerable uncertainty in the effective conductivity of gypsum board at high temperatures; that is, conductivity which approximately models heat transferred by both thermal diffusion and the radiant heat transfer through cracks. Since gypsum board is crucial in providing fire

resistance to timber framing, these experiments are crucial to the accurate prediction of temperatures and thence the prediction of the time of failure of light-timber framed walls, generally. These experiments should not be property tests involving the guarded plate (Mehaffey et al 1994) or hot wire methods (Ouchi 1988). The guarded plate sandwiches a sheet specimen between two metal plates at different elevated until steady state conditions are achieved. The conductivity of the specimen can thus be determined from the gradient of temperature through it. The hot wire method sandwiches a wire between two brick-like specimen halves. Conductivity is determined by the attenuation of a pulse of heat flux in the wire. Both of these methods involve time during which the conductivities of the specimens are changing and thus definitive values for conductivity are difficult be determined with temperature. Instead of these two methods, small scale tests should be undertaken; these tests should involve similar conditions to gypsum board in walls exposed to fire. That is, the gypsum board in the proposed small scale conductivity tests, should be restrained against shrinkage provided by fasteners and be tested in a vertical position.

From §5.3.2, further testing is required to confidently establish the surface emissivity of gypsum boards with temperatures as high as 1200°C.

The conductivity of char needs to be obtained from experiments. As mentioned in §2.4.3.3 there have been few if any experiments to determine the conductivity of char. The use of conductivity to model all of the heat flow through char is complicated by the presence of shrinkage cracks. These allow the convective efflux of heat in volatiles and oxidised gases. The cracks also allow the influx of substantial radiant heat as shown for gaps in §5.4.3. These fluxes are usually modelled with an effective conductivity which approximately models all of the heat fluxes through the material. Simple experiments need to be undertaken with particular controlled conditions. As with any property measurements, the aim should be to limit variations with time to a minimum number of variables to isolate the effect of the property, conductivity and allow simple calibration. Since one would expect char cracks to vary with time and rate of heat transfer, the experiments should represent similar heat transfer conditions as would be typically experienced by light-timber framing in walls cladded with gypsum board on both sides.

5.8.2 Further Model Development

5.8.2.1 Enhancement of ADIDRAS

Further research is required to develop modelling methods to predict insulation failure. In the wall furnace experiments undertaken in the research, temperatures measured (Figure 4.23) on the ambient side of the wall, reached 100-120°C. These temperatures were less than the temperatures, 150-200°C for insulation failure specified in AS1530.4. Thus, experimental validation of model predictions of the time

of insulation failure remains to be undertaken to show whether ADIDRAS requires further enhancement to predict the time of insulation failure. The low thermal gradients and the flatness of the slope of the temperature-time plot on the ambient side of walls causes considerable sensitivity for time of failure to some nominated temperature rise for failure (AS1530.4). Furthermore, the temperatures for defining insulation failure (rises of 140-180°C, AS1530.4), are not reliable criteria for determining insulation failure causing the spread of flame to items in contact with the non-fire side. Jönsson and Pettersson (1985) state that piloted ignition typically occurs at 350°C which is much higher than temperatures specified as criteria for insulation failure.

Further work is required to stabilise numerical computations for radiation in cavities at high temperatures. Some method of linearisation needs to be developed.

A second cause of structural collapse other than charring, was described in §5.4.2. The cause was termed, "steaming" failure and was due to the reduction in stiffness of timber during the vaporisation of moisture in timber. There are a number of possible causes for the loss of stiffness, including:

1. The doubling of moisture content in timber as moisture transfers from regions of vaporisation to cooler regions.
2. Creep induced by the movement of moisture (mechano-sorptive creep)
3. The combined effects of temperature and moisture as vaporisation occurs.

If either of the first two possible causes are verified in future research, then a moisture transfer model will be required to accurately predict the time of steaming failure. Although a simplified model for moisture transfer was formalised, a more rigorous model would be required for predicting heat and moisture transfer in porous solids and cavities.

The modelling of thermal diffusion through insulation in cavities should be validated against existing or new experiments. The scope of experiments should include simple experiments to obtain thermal properties independently, and experiments with large wall panels to validate that thermal diffusion alone is sufficient to model the heat transfer through insulation.

There is some need to enable ADIDRAS to model surface movements caused by the shrinkage of wood and char. This modelling would enable the simple approach to moisture modelling in §5.4.4 to be used in conjunction with the modelling of heat transfer through gaps §5.4.3. Currently, ADIDRAS can only effectively use the simple moisture transfer model when gaps are not present. To apply both models requires the model to be executed twice. ADIDRAS already has the data structures (Figures 3.20 and 3.21) for which simple modifications would enable heat transfer analysis for moving surfaces.

5.8.2.2 Development of a Simplified Model

Mehaffey's et al (1994) method of modelling heat transfer in a cavity with a single node needs to be re-visited. His model did not use a complex radiation model to analyse the simultaneous radiant heat transfer amongst all cavity surfaces. It was assumed that smoke in cavities is opaque to all radiant heat. As mentioned in §5.3.3 and §5.4.2, predicted temperatures throughout the wall were much the same irrespective of whether the smoke was assumed to be perfectly clear or opaque. The replacement of a complex radiation model with heat transfer through a single node appears possible. Similar simplified analysis of heat transfer through cavity spaces is commonly used in the modelling of protected steel sections in fire. The complexity of cavity spaces surrounding protected steel sections is ignored in these simplified analyses. Simplification of heat transfer analysis in steel, compared with timber, is further aided by its large conductivity. Large conductivity tends to ensure uniform temperatures in steel despite the complexity of cavities.

5.8.3 Wall Experiments

The gaps deduced in §5.4.2 should be confirmed with wire probes or devices to directly detect and measure gaps which are expected to open between studs and gypsum board on the fire side, during shrinkage of materials. Experiments to confirm the existence of gaps would, however, be difficult because of the softness of char and gypsum surfaces at high temperatures, as well as problems with smoke which would hinder means of visual observation.

Validation in the research for this thesis has considered mathematical checks of energy conservation and convergence. The use of standard fires (AS1530.4) has been used to check the adequacy of modelled phenomena. This validation is sufficient to demonstrate that the model can at least carry out the numerical analyses correctly for real fires. Experiments and validation should be carried out for real fires to check that the model adequately considers all appropriate phenomena in heat transfer in walls exposed to real fires.

In §5.3.2 it was shown that there are inadequacies in current procedures in measuring surface temperatures with surface thermocouples. To prevent distortion of temperature measurements due to radiant heat, surface thermocouples are covered with insulative pads (AS1530.4). However, these pads also distort measured surface temperatures. Improvements in measuring surface temperatures are desired.

5.8.4 Further Research on the Effects of Shrinkage Gaps

Future research should apply the model to research undertaken by others. For example, it is desirable to investigate how predictions with the model compare with König's (1991, 97) experimental results for insulated cavity filled panels exposed to "parametric" fires. Theoretically, at least, the discrete cavity radiation model should, for the first time enable accurate analysis of the radiation flux into shrinkage gaps which open up between the insulation and studs. An example of influx of radiation is the continuous zig-zag line between the insulation and wood section in Figure 5.50.

The modelling of gaps should be applied also to the opening of joints between abutting sheets of gypsum board to determine whether there is a significant transfer of radiant heat from fires to cavities via paths such as the dotted path in Figure 5.50. Such paths are a concern of Takeda's (1998).

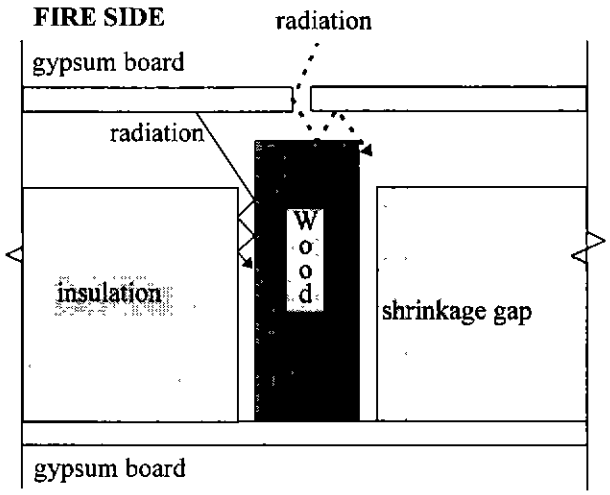

Figure 5.50. Shrinkage Gaps to be Analysed with Heat Transfer Model in Future Work

6. Structural Response Model

6.1 Introduction

Given in this chapter is an evaluation of existing structural models and justification of the most appropriate one for adoption in the models for time and probability of failure in accordance with the following relevant aims given in the introduction (§1.5):

1. Incorporate variables for a wide range of thermal and structural phenomena in light timber framed walls exposed to standard and real fires to aid understanding of their effects on the time of failure.
2. Achieve fast and robust computations.
3. Be sufficiently accurate and enable the design of walls according to time and risk based performance requirements.
4. Enable the production of graphs for relationships between time of failure and major structural variables, to general aid fire engineering design of light-timber framed wall barriers.

The evaluation is carried out by firstly considering an overview of the responses of timber framed walls in fire and the scope of structural actions and mechanical properties required for the model (§6.2). In the sections following, literature on mechanical properties is reviewed to establish the specific requirements for a structural response model. For example, it will be shown that the compression properties of timber vary non-linearly with strain and that properties in tension and compression are not equal and opposite. It will therefore be apparent that commonly used structural models which require equal and opposite linear properties in tension and compression, are not appropriate. In §6.3 alternative relationships for mechanical properties of timber studs with temperature are discussed. The adoption of relationships of Young et al (1998) is justified from experiments conducted and from the consideration of phenomena and constituents affecting the relationships. Section §6.4 justifies the use of the mechanical properties adopted by Young for gypsum board. Section §6.5 considers the properties for fasteners. Reviews of various structural models and the justification for adopting one is given in §6.7. Conclusions are given in §6.8.

6.2 Overview of Responses that Affect the Structural Behaviour of Walls in Fire, and that should be within the Scope of the Model

Young(2000), Collier (1991, 93), Collins (1992) and Carne (1995) discussed the degradation of gypsum board and light timber framed walls, in full scale wall furnace experiments. The apparent responses which affected the mechanical properties and the structural behaviour of walls (such as walls in the experiments described in §4) are discussed below. The modelling requirements are thus identified.

The general response of gypsum board to increasing temperatures was described in §2.2.1. It was explained that as the temperature of the gypsum board increases above 400°C, shrinkage becomes significant and a random pattern of cracks emerge. This pattern of cracking is referred to as crazing. Despite the large number of cracks in crazing, the board maintains integrity due to the presence of glass fibres in the gypsum core, which hold uncracked portions together. Crazed board viewed through windows in furnace walls, appears to almost drape like a curtain (Carne 1995) after prolonged fire exposure. Gypsum board at this stage provides no structural resistance and is thus ignored in Figure 6.1 which shows how the components of walls exposed to fire, contribute to structural resistance. Since gypsum board on the fire side does attain temperatures above 400°C, it is a component which can be ignored in structural modelling, apart from the consideration of self weight.

However, it was observed in §4.5.3 that for most of the duration of wall experiments, gypsum board on the ambient side was sound and was likely to contribute to structural resistance. The contribution can be judged by comparing the time of failure of Wall Experiment 8 with the time of failure of Wall Experiments 4 and 5. These three experiments were similar except in Wall Experiment 8 gypsum board on the ambient side was free to slip against the studs as they bent during the experiment. In Wall Experiments 4 and 5 (see Table 4.3) gypsum boards on the ambient side were nailed to studs in a conventional manner. The nailed fastening would have prevented some slip and created some degree of composite action between the studs and boards. This stiffness depends on the resistance to movement of the fasteners within the gypsum board, shear movement of the fasteners themselves and movement of the parts of the fasteners embedded in the studs. Wall Experiment 8 structurally failed at 28 minutes, compared with Wall Experiments 4 and 5 which structurally failed at 34-35 minutes. Considering that all similar experiments (4 similar to 5 and 1-3 all similar) failed within a minute of each other, the difference in failure times of approximately 7 minutes is a significant difference which results from the increase in structural resistance due to the composite or partial composite action of the ambient facing gypsum board with the studs. Hence it is desirable that the structural model analyse any degree of composite action

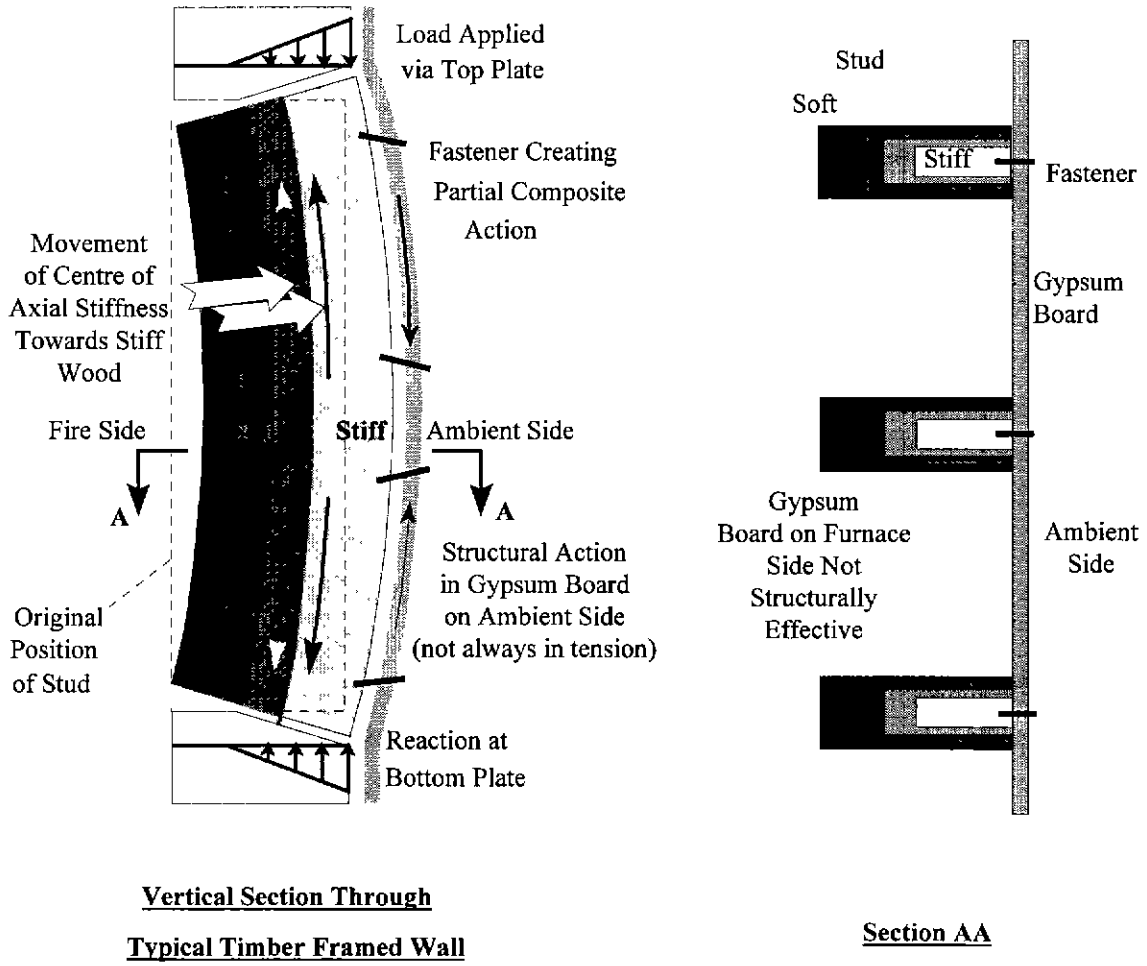

Figure 6.1. Components and Actions Affecting the Structural Response of Timber Framed Walls in Fire.

Thermally induced movements within materials are generally caused by expansion with temperature, and shrinkage with loss of moisture. Thermal expansion and non-uniform temperatures in timber studs would cause deflection towards fire. However, deflections towards the fire, of less than one-thousandth of the wall height occur only in the early stages of fire exposure (Clancy and Young 1996, Collier 1993). At later stages, walls deflect away from fires. Thus thermal expansion is not significant. Shrinkage in the direction parallel to the grain, is usually less than 1% (Wood Handbook 1987) and is also not significant. Furthermore, the ductility of wood in compression (Buchanan 1986) would alleviate adverse stresses by redistribution. Thus, thermal expansion and shrinkage along the length of studs need not be considered in the structural model.

Generally, the variation of mechanical properties with position in cross-sections, associated with variation in the temperature distribution, needs to be considered in predicting the response of structures to fire.

Often, it is possible to adapt conventional structural analyses which are limited to uniform temperatures and mechanical properties, to analyses for fire conditions. In some cases steel structures can be assumed to have uniform temperatures and, hence have uniform mechanical properties due to the high thermal conductivity of steel (Lie 1992). The strength of reinforced concrete is controlled by the small percentage of steel reinforcement which is often in a single layer of uniform distance from the tensile face of the concrete section. The temperatures in each steel reinforcement bar is approximately the same, and hence each bar has the similar mechanical properties and conventional analyses can be adopted. However, the low thermal diffusivity of wood, and the involvement of entire wood sections in resisting structural actions, necessitate structural response modelling which can carry out analysis of structures with mechanical properties varying with position.

Analysis should simulate the movement of timber framed walls away from fires. The movement is due to charring and softening on the fire side of studs. As shown in Figure 6.1, the centroid of stiffness thus moves towards the stiffer part of the timber sections and creates eccentricity and moments, P.e which cause the deflection away from the fire. The wall remains stable for some time, partly because the square ends of studs resist rotation and generate a reaction moment. This reaction is enhanced by the slower degradation rates in the vicinity of the top and bottom plates compared with the degradation rate of the studs. The degradation rates of the top and bottom plates are slowed by the greater concentration of floor and wall material in the vicinity of the plates.

Eventually during fire exposure, one would expect that the ends of studs, and the top and bottom plates would thermally degrade. Some rotation of the ends is possible and end fixity is likely to be variable with time. Thus, it is required that the structural model analyse structures with varying degrees of end fixity.

At the beginning of this research project, it was not clear whether a small or large deflection analysis was required of the structural model. The deflection of timber framed walls away from fire is approximately only 25 mm for a 3.00 metre high wall 10 minutes prior to structural collapse (Young 2000). This small deflection suggests that for timber walls, second order large deflection analysis is not required. However, the mode of structural failure of vertically loaded walls is usually buckling which does require analysis of large deflections for accurate predictions of load capacity. If heat travels through the framing quickly, then a first order analysis will be sufficient. If the heat travels slowly, second order analysis is necessary. Until the order of analysis required is established, a structural response model with second order analysis is desired.

It is useful to consider the overall structural actions when choosing mechanical properties. As mentioned above, for most of the period of exposure of timber framed walls to fire, deflections are less than 25mm. Thus the line of action of loads will mostly be within the middle third of stud sections and tensile stresses

will not be significant. Furthermore, the large slenderness of walls ensures that they will fail by buckling rather than crushing. Since buckling resistance is a function of the elastic modulus in compression, this property should be the most important mechanical property affecting the time of failure.

It was observed in experiments (Clancy and Young 1996) that some walls failed when the timber was close to 100°C and little or no charring had occurred. These walls were pin-ended, and hence much more slender than walls commonly built, which have considerable resistance to rotation at the top and bottom supports. There does not seem to be any record of wall furnace experiments on common walls which have structurally failed when the wood in studs was predominantly 100°. Nonetheless, the possibility of failure prior to charring is a concern. It seems that steam from vaporisation of moisture causes sudden reductions in mechanical properties which accords with the explanation of bending of wood with steam described in the Wood Handbook (1987). Little is known about the amounts of these reductions in stiffness which potentially cause failure well before studs start to char. Research is required in quantifying the effects of steam on mechanical properties, particulary the elastic modulus in compression and any plastification and creep. Research is required to determine the scope of walls for which moisture vaporisation causes failure prior to charring of studs. In the meantime, modelling of walls which are more slender than common walls must carefully appraise the consequences of moisture vaporistion.

The wall components for which mechanical properties need to be reviewed are timber studs, gypsum boards and fasteners. Since gypsum board on the ambient side is in tension when the walls fail, only its tensile properties will be considered. The forces and moments to consider are shown in Figure 6.1.

6.3 Mechanical Properties of Timber

This section, §6.3 will show that there are a range of relationships for mechanical properties as functions of temperature. It should be helpful to first consider how the degradation of the constituents of timber affects mechanical properties.

6.3.1 Constituents and Phenomena which Affect the Mechanical Properties of Timber in Fire Conditions.

The constituents of wood are explained in Dinwoodie (1989), Desch et al (1990) and Panshin and de Zeeuw (1980) as follows.

The primary constituents of wood which make up its microstructure and hence affect its mechanical properties are celluloses, hemicelluloses and lignin. There is a fourth primary group of constituents of

wood, termed extractives which do not contribute the mechanical properties except to blunt sharp tools. The relative proportions of each constituent are listed in Table 6.1.

Cellulose in wood is a natural polymer, in particular a polysaccharide, occuring in the form of long slender chains $(C_6H_{10}O_5)_n$ built up in cell walls from the saccharide (sugar), β-D-glucose monomer $C_6H_{10}O_6$. The chains are referred to as filaments and have an average length of 5 microns. The filaments have crystalline segments alternating with amorphous segments, as shown in Figure 6.2(a). Approximately, 70% of a filament is crystalline.

Table 6.1. Relative Proportions of the Constituents in Wood.

Primary Constituent	Percentage based on mass	
	Softwoods	Hardwoods
Cellulose	40-45	45-50
Hemicelluloses	25-30	21-35
Lignin	26-34	22-30
Extractives	0-5	0-10

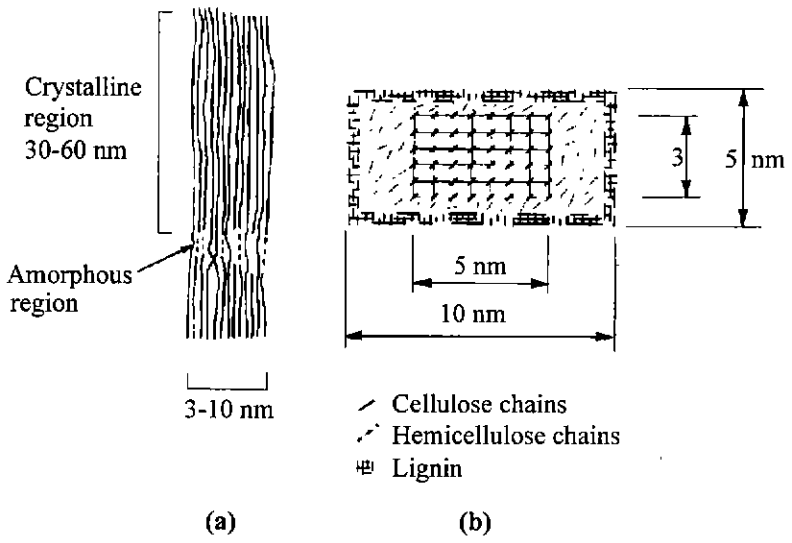

Figure 6.2. Composition of a Microfibril:

(a) Crystalline Core in Longitudinal Section.

(b) Transverse Section of Core and Surrounding Matrix. (Dinwoodie 1989)

Hemicellulose, shown in Figure 6.2(b) is also a polysaccharide comprising saccharide monomers other than β-D-glucose. It is less crystalline than cellulose, and has much less polymerisation and consequently has much shorter chains.

The molecules of lignin (Figure 6.2 b) are large and comprise hydroxy- and methoxy-substituted phenylpropane units.

The main microstructures which make up the walls of cells in wood are microfibrils shown in Figure 6.2. Microfibrils comprise a core of bundled cellulose filaments surrounded by a matrix with an inner layer of cellulose and hemicellulose filaments, and an outer layer of lignin. Microfibrils are very much longer than they are wide. Within individual microfibrils, the filaments are aligned in the same direction. Microfibrils make up layers of tubular cell walls as shown in Figure 6.3. In each layer the microfibrils run in a common direction. However, the directions differ among the layers. Lignin also makes a microstructure called middle lamella which surrounds each cell and secures all cells together.

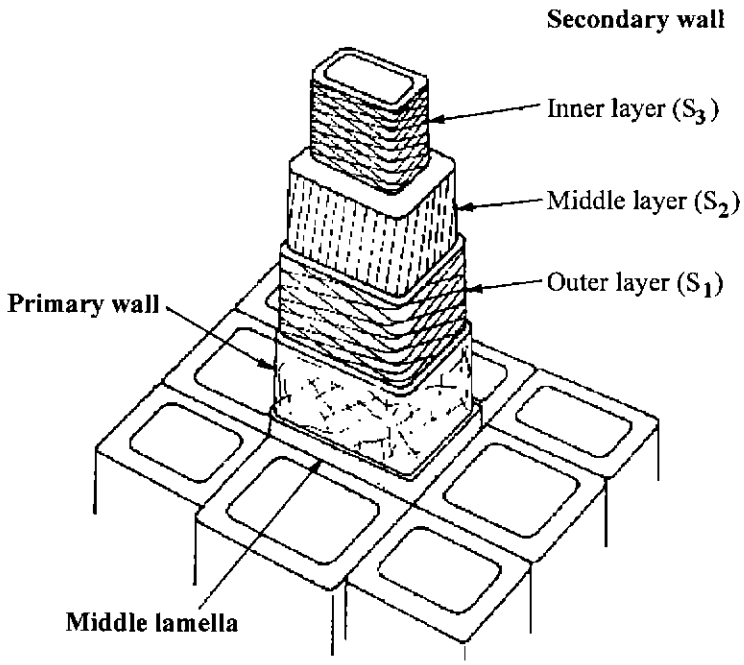

Figure 6.3. Simplified Stripped-back View of Cell Wall showing Orientation of Microfibrils shown as Lines in each of the Major Wall Layers. (Dinwoodie 1989)

The cellulose filaments are responsible for the tensile strength of wood. The amorphous segments of the cellulose filaments and the hemicellulose are weakened by water. Lignin provides some protection against water. Structurally, lignin provides in-grain stiffness and strength in compression and shear, by enabling the composite action between microfibrils, layers within cell walls and cells across the entire timber section.

The changes to the primary constituents of microstructures with temperature are listed in Table 6.2.

Table 6.2. Thermally Induced Changes in Dry Wood in an Inert Atmosphere (Schaffer 1973, 1982)

T (°C)	Changes to Constituents with Temperature
55	Hemicelluloses begin to soften. (Goring 1963)
70	Transverse shrinkage of wood begins (Kollmann and Fengel 1965)
70-120	Lignin softens and slowly begins weight loss (Goring 1963, Stamm 1956, Levin & Belikova 1968) At a temperature between 80-100°C , visco-elastic behaviour undergoes a transition from a glass to rubber type behaviour. (Schaffer 1982)
140	Bound water is freed (Amy 1961)
160	Melting of lignin is complete but begins to re-harden. (Levin and Belikova 1968)
180	Rapid weight loss of hemicelluloses (Davis and Thompson 1964; Kollmann and Fengel 1965)
200	Wood begins to lose weight rapidly (Tang 1967) Cellulose dehydrates (Davis and Thompson 1964, Harkin 1969)
210	Lignin hardens to resemble coke. Cellulose softens and depolymerises. (Back et al 1967)
280	Lignin has reached 10% weight loss (Browne and Tang 1962). Cellulose begins to lose weight.
288	Often quoted wood charring temperature (550°F)
300	Charring temperature given by Hadvig (1981), see page 21.
320	Hemicelluloses completely degraded (Beall 1968)
370	83% loss of cellulose. (Brown and Tang 1962).
400	Wood is completely carbonised. (Brown 1958)

6.3.2 Difficulties in Measuring Mechanical Properties of Timber at Raised Temperatures

Published mechanical properties of timber at raised temperatures should not only be evaluated in terms of the behaviour of constituents but also in terms of the difficulties in measuring the properties. Generally, it is desirable to measure a mechanical property while all other variables are uniform in the sample. For all

measurements, it is desirable that temperature is the only variable, other than the property of interest which changes. However, it is difficult to undertake such measurements for a number of reasons given below.

A representative sample of timber should be large enough to contain growth characteristics such as knots and be of a scale which will account for all thermo-structural phenomena in timber framing in walls exposed to fire. Thus samples should have a cross-section similar to the sections of framing members, and a length long enough to have similar mechanical property statistics as timber framing members. Such a sample will be referred to as a structural scale sample.

Due to the insulative qualities of timber, structural scale samples are slow to heat. However, mechanical properties degrade with time (Cramer et al 1996). To obtain similar degradation as wood in wall furnace experiments, the period of heating should be similar to the period of fire exposure. It is impossible to heat structural wood samples to uniform distributions of temperatures which occur in wall studs during fire exposure.

Heat applied to wood samples during the measurement of mechanical properties, increases the rate of moisture vaporisation. Hence, the moisture content of samples reduces with time. To maintain a constant known moisture content in an experiment, the humidity of air surrounding the sample would have to be controlled at a sufficiently high enough level.

Another difficulty arises from the high variability of mechanical properties of wood at ambient conditions (Leicester et al 1988, Doyle et al 1966, 67). Many experiments on structural scale samples are necessary to obtain representative statistical data for mechanical properties.

Due to the difficulties mentioned above, researchers discussed in the following sections §6.3.4-6.3.7, investigating the mechanical properties of wood or timber at temperatures between 20°-300°C, have had to make some simplifications to their procedures for measurement and evaluation of mechanical properties of timber in fire. The simplifications adopted have depended on the main focus of the application of the properties. A number researchers chose to conduct experiments on small samples for which uniform known values of temperature and moisture content can be achieved. Such samples do not contain knots, have little variability and thus minimise the number of experiments required. They assumed that the results on small samples are applicable to large samples. Other researchers have attempted measurements involving realistic conditions but have contended with non-uniform temperatures or long periods of heating, and hence some variation of mechanical properties with position in sample cross-sections, or with time.

6.3.3 Stress-Strain Behaviour of Timber

Stress-strain behaviour of timber in ambient conditions was well researched by Buchanan (1986). He recommended the relationship in Figure 6.4. The figure shows that wood is ductile in compression and stiffer and more brittle in tension. The elastic modulus in tension is clear. However, tangent and secant moduli need to be considered in compression. A structural model should take into account non-linearity of compression stiffness with strain.

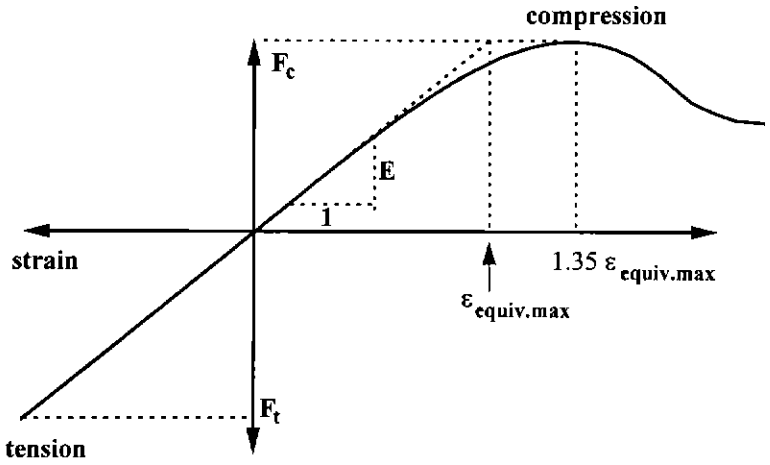

Figure 6.4. Stress-Strain Behaviour of Timber (Buchanan 1986).

6.3.4 Tensile Strength of Timber

The relative tensile strength of wood dependent on temperature and initial moisture content obtained by a number of researchers is shown in Figure 6.5.

Expected features of the relationship for relative tensile strength with temperature can be deduced from the review of constituents in §6.3.1. It was discussed that cellulose fibrils are responsible for the tensile properties in timber. Table 6.1 showed that cellulose makes up approximately 70% of timber. Table 6.2 showed that cellulose changed little until at 200°C, timber loses weight rapidly and the cellulose microfibrils which are responsible for tensile strength suddenly weaken. It is well known (as is apparent from codes such as AS1720.1) that moisture reduces strength. Thus, from consideration of constituents, one would expect that there would be an increase in strength as timber dried between 100°-150°C followed by a substantial loss above 200°C.

Knudson's (1975) relative tensile strengths are shown as "K 0-12%" in Figure 6.5. He carried out experiments on small samples of Douglas-fir, 4.76x4.76mm in cross-section. This size was sufficiently small to heat samples to uniform temperatures within 30 seconds at which time he measured the tensile strengths. The small size of the samples and the short time period would have been advantageous in minimising loss of moisture content which was initially 12%. Since some moisture would have been lost, Figure 6.5 denotes the moisture content between 0-12%. He concluded that relative tensile strength decreased linearly from 100% at ambient temperature to approximately 30% immediately prior to charring at 300°C. However, his relationship overlooks the increase in strength expected as moisture is driven off above 100°C followed by a sudden decrease above 200°C. The cause for these details missing from his relationship may have been that the fast heating rate did not enable samples to dry out.

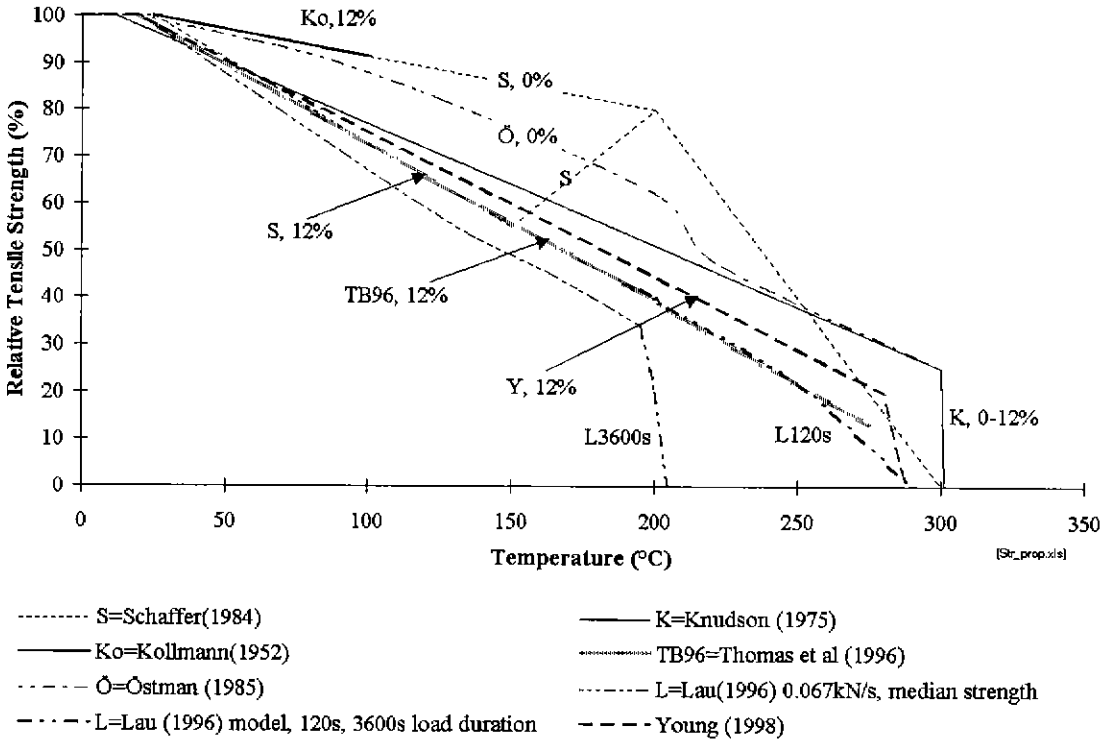

Figure 6.5. Tensile Strength of Wood as a Percentage of Initial Ambient Strength, as a Function of Temperature.

Schaffer's (1984) relative tensile strengths are shown as "S" in Figure 6.5. His experiments were also conducted on small samples but he did notice the details of the relationship expected from the behaviour of constituents described above. He conducted experiments on samples with an initial moisture content of 12% (S,12%), as well as samples which were initially dry (S,0%). He found that the moist samples had a greater reduction in tensile strength for temperatures up to 150°C. As the moist samples were heated from 150°C to 200°C, the tensile strength increased along line, S and met the plot for S,0%. Thereafter, the reduction for all samples was similar. Schaffer's results confirm earlier results obtained by Kollmann

(1952). Schaffer does not mention the load rate he used. His plot for moist timber is similar to Lau's, and thus it seems he adopted a similarly low loading rate to Lau. Schaffer's plots at ambient conditions do not show the relativity between tensile strengths for moist and dry samples.

Östman (1985) conducted experiments on small samples of Scandinavian spruce pine fir. She adopted a procedure, used for testing paper materials with a wide range of moisture contents (0-30%). The samples were tested while immersed in silicone oil which not only controlled the moisture content but also provided a non-oxidative environment which closely represents the environment of wood burning in fire (Parker 1988). She obtained a bilinear relationship with a sudden decrease in relative tensile strength at approximately 200°C. Her results were greater than Knudson's K,0-12%(1975) probably because of the fast rate with which she loaded her samples. She loaded them to full tensile strength in approximately 10 seconds. She chose a fast load rate to minimise effects of oil on strength.

Thomas et al (1996) relationship is shown as "TB96, 12%" in Figure 6.5. They deduced relationships for mechanical properties including relative tensile strength, compression strength and elastic moduli in tension and compression. They obtained the properties by calibration of finite element analyses against experimental results of König (1991) and Collier (1993). König's(1991) experiments involved timber framed panels subjected to bending over a pilot floor furnace. The timber was spruce pine fir at 12% moisture content. Collier carried out full scale wall furnace experiments on walls framed with radiata pine studs, also with approximately 12% moisture content. Thomas assumed that stress-strain relationships for wood at raised temperatures were similar in shape compared with the relationship at ambient conditions (Buchanan 1986). Unlike relationships derived above, their relationship applied to structural scale samples and were for a load rate experienced by light timber framed structures in fires. This load rate arises from the increase in load ratio, that is the ratio between load and load capacity as properties degrade in fires. The tensile strengths with temperature deduced from these calibrations is plotted in Figure 6.5.

Lau (1996) attempted to measure tensile strength of structural timber as realistically as possible. His samples were spruce pine fir, approximately 2440mm long, 90 mm wide and 35 mm thick. This species group is the most common in Canada. The samples were structural scale and had a moisture content of 10%. Essentially, the samples were randomly selected, and thus faithfully represented the statistical properties of structural timber typically used in construction. He subjected his samples to times of heat exposure experienced by light timber framed buildings in the event of fire. As explained in §6.3.2, he was not able to achieve uniform or steady state conditions in his samples. He applied the mathematics of damage accumulation theory to deduce relative tensile strengths. His relative tensile strengths are shown in Figure 6.5 as:

1. "L120s" for samples with load increased gradually at a constant rate for a period of 120 seconds after maintaining a nominated surface temperature for 1500 seconds; and
2. "L3600s" for samples with load increased gradually at a constant rate for a period of 3600 seconds after maintaining a nominated surface temperature for 1500 seconds.

The plot, L3600s compared with L120s shows the importance of time as a variable which affects tensile strength at temperatures at approximately 200°C and above. In this temperature range cellulose which is the constituent responsible for tensile strength (Table 6.2) depolymerises, resulting the gradual loss of all tensile strength. Figure 6.6 shows that as temperature increases, the variability of tensile strengths amongst samples reduces. This observation is important in evaluating whether variability of properties is as critical to the estimation of capacity at elevated temperatures, as it is at ambient temperatures. Figure 6.6 provides evidence for low variability in time of failure of loaded light framed timber structures in fire.

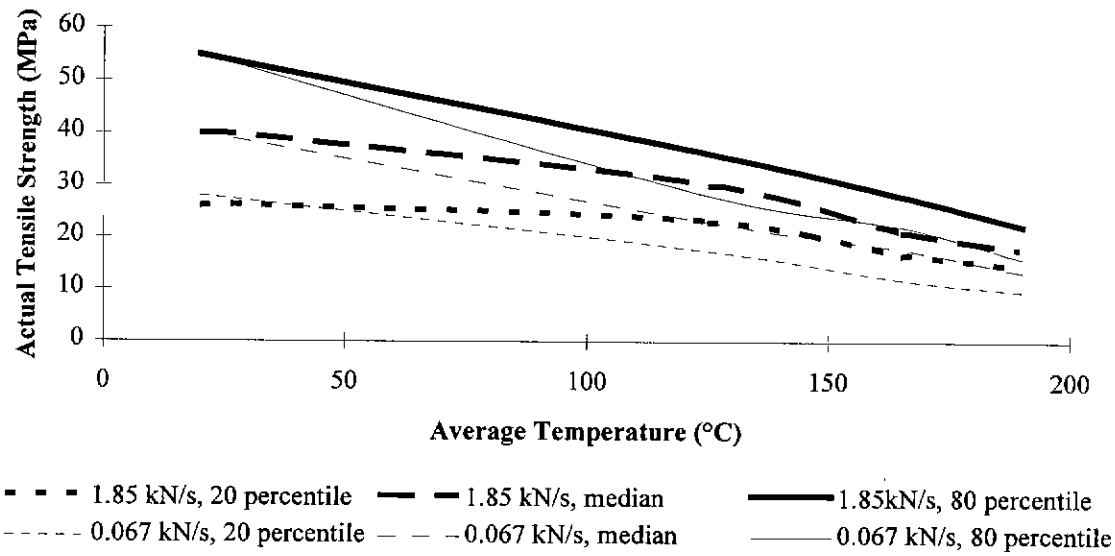

Figure 6.6. Effect of Loading Rate and Grade of Wood on the Reduction of Relative Tensile Strength with Temperature. (Lau 1996)

Young (2000) adopted a relationship which was similar to TB96 and L120s in Figure 6.5. He found that the time of failure of walls exposed to fire was insensitive to tensile strength of timber, and thus any of Lau's plots was acceptable.

6.3.5 Compressive Strength of Timber

From §6.3.1, lignin is the constituent which provides most of the compression strength. The following changes to lignin were noted in Table 6.2:

1. At 70-120°C, lignin softens from glass to rubber type behaviour.
2. At 160°C lignin begins to reharden at 160°C.
3. At 210°C lignin is hard and resembles coke.
4. At 280°C only 10% of lignin is lost (by weight).
5. At 288°C wood chars and has no strength.

The review of constituents reveals information on "hardness" and "softening" which relate to stiffness, but not strength. The best deduction that can be made from the above is that compression strength reduces at 70-120°C; increases between 120-200°C; then decreases to 280°C; and finally reduces to zero at 288°C.

Table 6.1 shows that lignin is approximately 30% of the mass of wood. Since the other 70% is mainly celluloses, one would expect that celluloses would contribute substantially to compression strength as well. Perhaps reinforced concrete is an appropriate analogy in which cellulose behaves as reinforcement and lignin as the concrete. If cellulose contributes to compression strength, then one would expect a substantial decrease in strength as temperature rises from 200 to 288°C.

Relationships for relative compressive strength dependent on temperature and moisture, obtained by a number of researchers are shown in Figure 6.7.

Knudson et al(1975) obtained compressive strength of small samples of wood in a similar manner to the way he obtained tensile strengths described in §6.3.4. The moisture contents of his compression samples were similar to the moisture content of samples in his tensile tests, that is 0-12%. He found that compressive strength decreased linearly as temperature rose from 20 to 300°C. His relationship is generally consistent with the behaviour of constituents identified above. Knudson's relationship confirmed an earlier one established over the temperature range 20-175°C by Kollmann (1940).

Schaffer (1984) obtained compressive strength for wood from small samples. He did not find much of a difference (less than 10%) between the relative compression strengths for dry wood and wood with a moisture content of 12%. This small difference is surprising because it would be expected that moisture would substantially reduce compression strength as is apparent from the relationships in Figure 6.7, from other researchers. Both of Schaffer's relationships are very similar to Knudson's.

As described in §6.3.4, Thomas et al (1995, 96) derived a number of mechanical properties, including compression strength. They found widely varying relationships for relative compression strength versus temperature. Some agreed well with the low results of Sulzberger (1953) and Sano (1961). Other results were more similar to Knudson's, Kollman's and Schaffer's results, all of which were discussed above. As explained in §6.2, failure of walls, such as in Collier's experiments, would have been due to buckling. So it is more important to know the modulus of elasticity in compression. The buckling load of a pin-ended column is given by,

$$P_{cr} = \frac{\pi^2 EI}{L_e^2} \qquad (6.1)$$

where P_{cr} is the buckling load and L_e is the effective length; that is the length of stud with pin supports each end and buckles at the same load as the actual stud. For Thomas' research in predicting the time of failure of walls in fire, compression strength properties were therefore not important.

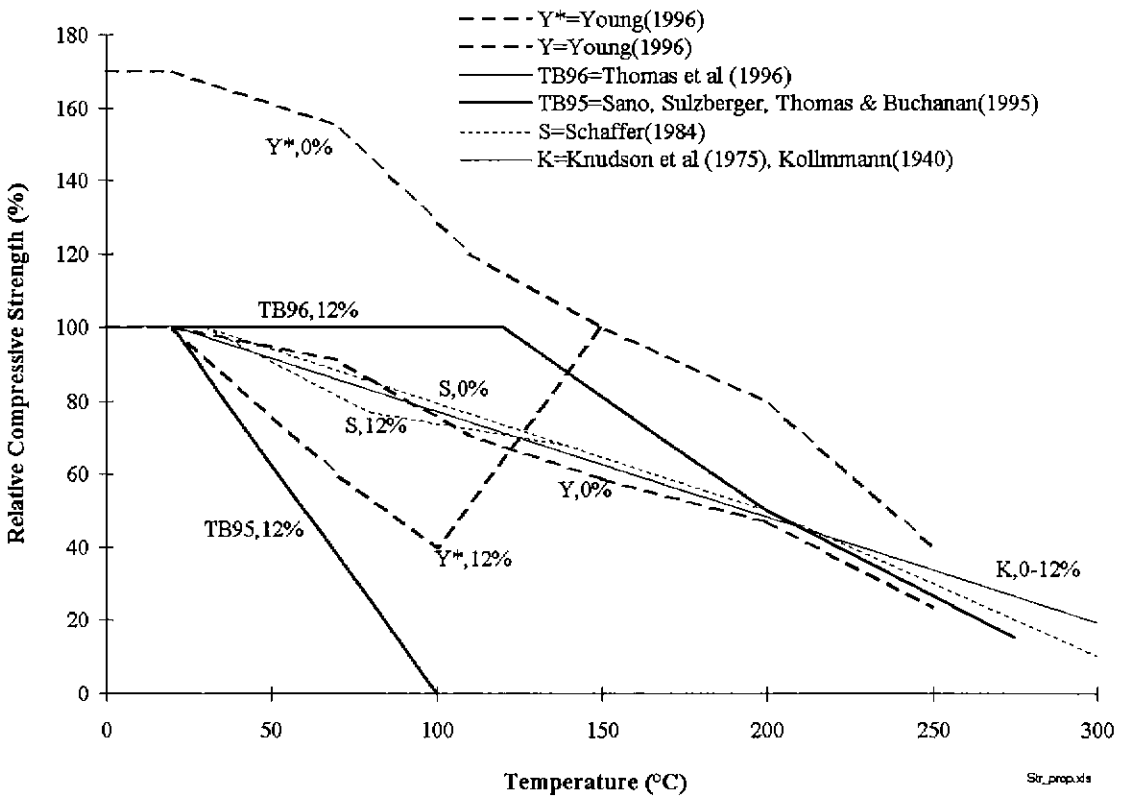

Figure 6.7. Relative Compression Strength versus Temperature.

(Moisture contents indicated in percentages.)

Young (1996) obtained relative compression strengths from radiata pine which is a common softwood used in timber construction in Australia. He generally aimed to obtain measurements for conditions typical for timber framing in fires. He encountered many of the problems in undertaking measurements mentioned in §6.3.2 and was not able to simulate all of the typical conditions. He chose samples with a cross-section of 90x38mm by a length of 400mm. To reduce variability of strengths to avoid doing a large number of experiments, he chose clear wood and employed split sampling. He produced the samples by splitting larger samples with 90x90mm square cross-sections. One split sample in each pair was tested to obtain compression strength at ambient conditions, and the other at elevated temperature so as to obtain relative strength. He adopted a loading rate which corresponded to a strain rate of 0.001 /min ± 25% in accordance with ASTM D1989 §12-§19. The duration of load application was 3-5 minutes. His rate was faster than the rates employed by Lau (1996) in §6.3.4.

Young not only showed compressions strengths at elevated temperatures relative to strengths at ambient conditions, but also strengths of dry samples (Y*,0%) relative to strengths (Y,12%) of samples with 12% moisture content. Figure 6.7 also shows (Y,0%) which is the compression strength of dry samples at elevated temperatures, relative to the strength of dry samples at ambient conditions. (Y,0%) compares well with the results of Schaffer, Knudson and Kollmann.

As mentioned above, timber framed walls are slender and fail under vertical load by buckling. As well, timber is ductile in compression and can redistribute stresses. Thus, accurate values for compression strengths with temperature, obtained in a similar manner to the tensile strengths by Lau(1996), are not necessary in predicting capacities and times of failure of walls in fire. Thus Young's properties are suitable for adopting in the time and probability of failure models in this research project..

6.3.6 Elastic Modulus for Tension Parallel to Grain

As explained in §6.3.1, the elastic modulus in tension is not expected to be a critical mechanical property governing the time of failure of walls. However, a reasonably sensible elastic moduli in tension should be adopted from the literature available, as explained below.

From the discussion at the beginning of §6.3.4, the sensibility of relationships for tensile elastic moduli with temperature, in the literature can be evaluated from the behaviour of constituents at elevated temperatures. It is expected that there should be some gain in the elastic modulus in tension as moisture dried out between 100°-150°C. Above 200°C, cellulose which is responsible for tensile properties, chemically degrades and elastic modulus should substantially reduce. One would expect that the chemical degradation would depend on reaction rates which were functions of temperature and time. Thus tensile

elastic modulus should not only depend on temperature but also time. From the consideration of constituents, one would expect the relationship between relative tensile modulus and temperature to be similar to the one shown as "C" in Figure 6.8. The steepness of the fall above 200°C may increase with load duration.

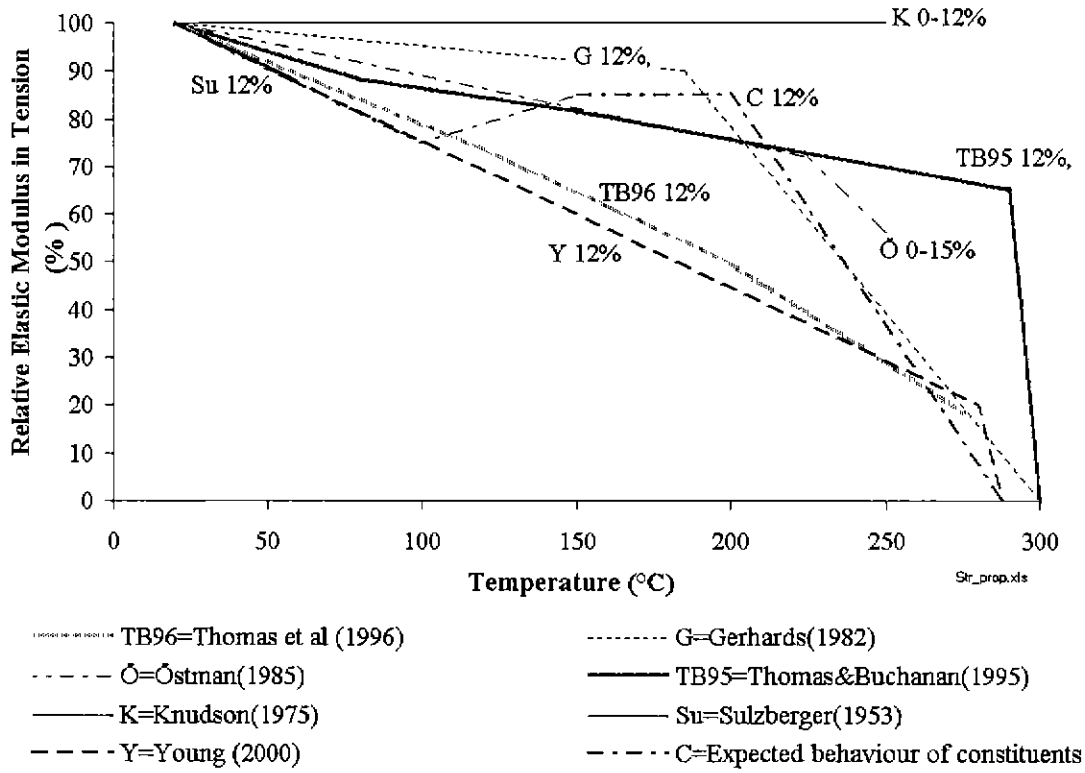

Figure 6.8. Relationships for Elastic Modulus of Timber in Tension Parallel to the Grain.
(Percentages indicate moisture contents of wood.)

A steep fall in elastic modulus in tension above 200°C was obtained in results of Gerhards (1982) and Östman(1985), shown in Figure 6.8. Gerhards reviewed literature which reported a steep fall commencing at 200°C and Östman measured a steep fall commencing at 225°C. Gerhards does not clarify whether his results are for tension or compression; however, when compared with results in Figure 6.8, it seems most likely he obtained his results from tension experiments. Östman showed that there is almost a 20% drop in the elastic modulus in tension as moisture content is increased from 15 to 20%. Gerhards also states that the elastic modulus decreases 22% as the moisture content increases from 6 to 20%.

Knudson (1975) measured no fall in the elastic modulus in tension. However he determined elastic moduli indirectly from measured natural frequencies of vibration. He must have made assumptions about

constraints, integrity of samples (that is, wholeness without cracks and voids), assumptions about appropriate equations for natural frequency as a function of the elastic modulus amongst other variables, all of which perhaps masked the expected fall at 200°C.

Sulzberger (1953) indicates that some fall in the elastic modulus is expected as soon as temperatures rise above ambient conditions.

König (1991) reported very little movement of the neutral axis in joists in bending, with the tension side exposed to fire. His results indicated that creep or plastification of wood in tension, heated to 250°C is not significant and thus the elastic moduli tension should not greatly reduce with time for given temperatures, during fire exposure.

As described in §6.3.4, Thomas et al (1995, 96) derived a number of mechanical properties, including elastic modulus in tension. There is a wide variation in their relationships for relative elastic moduli in tension, no doubt due to the insensitivity of the failure times and deflections measured in experiments which they used to calibrate the moduli. Variation of elastic modulus in tension is not a concern in the accurate prediction of the time of failure.

Young (2000) found that any rise in modulus would mean a reduction in mid-height deflections. However, such reduction does not occur. He concluded that either plastification or creep occurred. He found that it was practical to adopt the relationship shown in Figure 6.8 because it was conservative and that time of failure was expected to be insensitive to tensile modulus. Young's relationship for tensile modulus with temperature is appropriate for adoption.

6.3.7 Elastic Modulus for Compression Parallel to Grain

From the overview of responses affecting structural behaviour of walls exposed to fire in §6.2 and the discussion on constituents in §6.3.1, one would expect the following characteristcs of the elastic modulus of timber in compression applied parallel to the grain:

1. A steep fall in the elastic modulus in compression between 50-100°C due to steaming in timber with significant moisture content;
2. A fall in the elastic modulus in compression between 80-150 due to the transition of lignin from a glass to a rubber level of stiffness, irrespective of moisture content;
3. Some stabilisation between 150°-200°C as lignin re-hardens; and
4. A steep fall as temperatures rise above 200°C when wood material volatises and dissipates.

Young's (1996) experimental results compare well with these expectations; refer to Figure 6.9. However, the rise in stiffness at 100°-125°C did not correspond to a reduction in deflection of walls at mid-height. He suspected that creep or some plastification of wood occurred as explained in §6.2. Until some model is developed which can account for this apparent creep or plastification, Young recommended the adopted relative elastic modulus in compression at 100°C not be increased but be assumed constant until the temperature is 200°C. Thereafter, the elastic modulus in compression should be assumed to linearly reduce with temperature to zero at 288°C. That is, overall, the relationship shown as "Y00 12% case B" should be adopted. Thomas et al (1996) found that a similar relationship gave good predictions of times of failure compared with results from Collier's (1993) experiments. However, Young (2000) found that his case B relationship led to significant overestimates of times of failure of walls in fire. The deflections of the walls tested were greater than predicted by case B. This greater deflection seems most likely due to creep or some degree of plastic behaviour. For the particular case of walls reported in experiments in §4 in this thesis, he found that the relationship, "Y00 12% case A" gave the best prediction of times of failure. For structural response models which assume that the elastic modulus in compression is related to temperature, without consideration of time, case A is the best relationship to adopt.

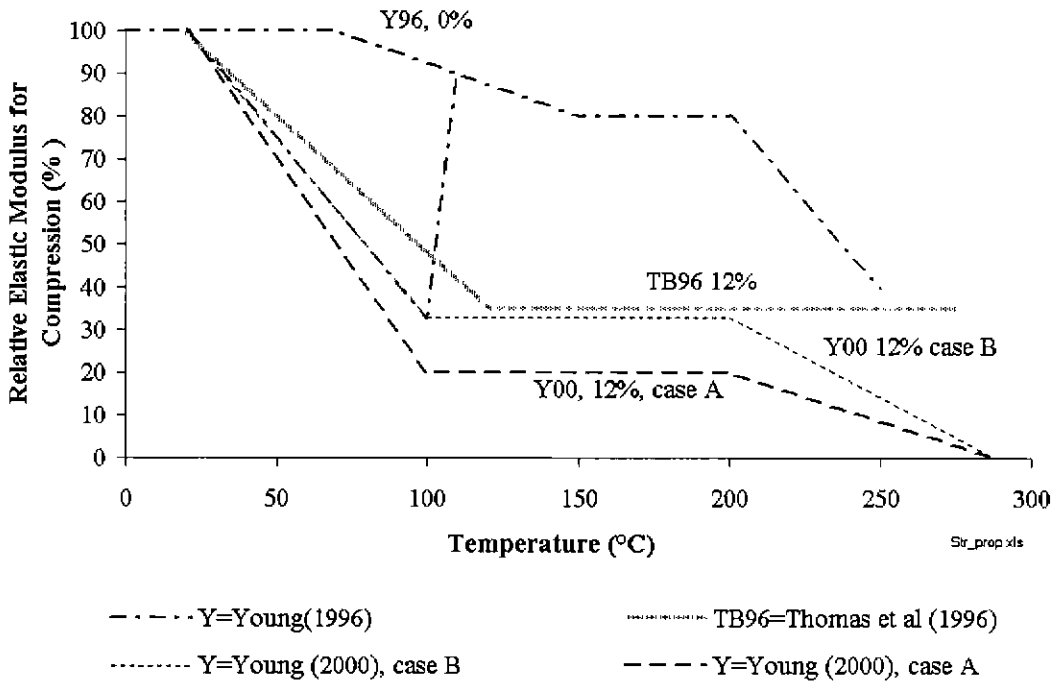

Figure 6.9. Relationships for Relative Elastic Modulus of Timber in Compression.

(Percentages indicate moisture contents of timber.)

6.4 Mechanical Properties of Gypsum Board at Raised Temperatures

For similar reasons given in §6.3.1, brief consideration is given below, to the behaviour of constituents for evaluating the mechanical properties of gypsum board. The discussion in this section refers to fire rated gypsum board which contains glass fibres; not regular board without glass fibres. Subsequently, the mechanical properties of interest - tensile strength, the elastic modulus in tension, expansion and shrinkage - are reviewed. Compressive mechanical properties of gypsum board are not of interest because, as explained in §6.2 gypsum board in compression is on the fire side of walls. Compression board is thus greatly degraded at an early stage during fire exposure, and although it remains intact, it contributes little to the structural resistance of the wall.

Constituents and Their Influence on Mechanical Properties

The constituents of gypsum board were reviewed in §2.2.1. Gypsum board comprises more than 90% by weight of gypsum dihydrate crystals and a few percent by weight of fillers, glass fibres and air entrainment agents. By volume, gypsum board is 25-40% gypsum and the remainder is mainly pores. At approximately 120°C the gypsum dihydrate crystals decompose to a hemi-hydrate, and as argued by Young (2000) should correspond to a large loss of strength and stiffness. At 400°C, shrinkage of gypsum hemi-hydrate becomes significant. Cracks form but the board is held together by the glass fibres. At 700°-900°C the glass fibres have been observed to gradually melt. Glass is a viscous substance and has no distinct melting point like ice.

Tensile Strength

Collins (1989) carried out tension experiments at ambient conditions on strips of gypsum board of various thicknesses. The board was Winstones Fyrestop which was made in New Zealand and contained pumice. The formulation of this board has changed since 1989. The tensile stress at failure for most samples was in the range of 2.00-2.25 MPa with no significant correlation to thickness.

Goncalves and Jong (1996) and Walker et al (1995) carried out ambient tension experiments on strips of 13 mm thick fire rated gypsum board from three Australian Manufacturers - Boral, Gyprock and Pioneer. The paper was scored repeatedly with a knife over a 75 mm wide band across the middle of the strips to remove the tensile resistance of the paper. Care was taken not to cut into the gypsum to initiate cracks. A plot of the typical shape of load versus extension is shown in Figure 6.10. Segment AB was linear. At some extension, B, the strips cracked but were held together by the glass fibres at some substantially reduced tensile resistance, C. Further extension, CD gradually caused the glass fibres to break and the resistance to reduce. The average strengths for strips cut parallel to the long direction of boards from each

brand varied between 0.89-1.09 MPa, respectively. Strips cut parallel to the width of boards were both 10-30% weaker, indicating that glass fibres were significantly biased towards the long direction.

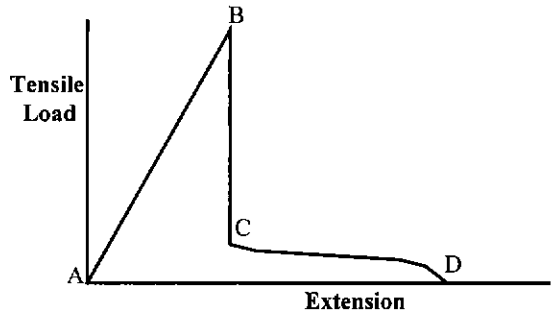

Figure 6.10. Typical Shape for Tensile Load versus Extension for Gypsum Board without Paper.
(Goncalves and Jong 1996, Walker and Lightfoot 1995)

Goncalves and Jong (1996) tested strips in a furnace, similar to the strips they tested at ambient conditions. Unloaded samples failed repeatedly in the temperature range 800-900°C. They also conducted pilot scale furnace experiments on loaded samples. There was a dramatic loss of strength below 320°C; only 10% of the strength remained at this temperature. The temperature of the furnace could not be lowered below this temperature to determine at what temperatures significant losses of strength occurred.

Young (2000) considered the results of Goncalves and Jong (1996) and Walker et al (1995), and considered the fact that gypsum dihydrate crystals dehydrate at approximately 120°. He argued that the substantial drop in strength of gypsum occurs at 120°C, which seems appropriate. He adopted the conservative value of 1.0 MPa for tensile strength at ambient conditions which ignores the strength of the paper.

Elastic Modulus in Tension

Collins (1989) found that the secant modulus- that is, the modulus of the chord between AB in Figure 6.10 - decreased substantially with strain as shown in Table 6.3.

Goncalves and Jong (1996) and Walker et al (1995) found that the secant modulus corresponding to segment AB in Figure 6.10, for 13mm thick fire rated boards from three Australian Manufacturers, Boral, Gyprock and Pioneer, varied between 0.49-0.53 GPa. Their measurements involved the removal of surface paper as mentioned above. Their results are reasonably similar to those for 12.5 mm thick board tested by Collins (1989).

Young (2000) adopted a value of 0.48 GPa which seems appropriate in light of the above experimental results.

Table 6.3. Secant Modulus for Winstone's Fyrestop Gypsum Board (Collins 1989)

Thickness (mm)	Secant Modulus (GPa) for various strains				
	0.0005 strain	0.001 strain	0.002 strain	0.004 strain	0.0061 strain
9.5	1.37	0.93	0.58	0.37	0.29
12.5	0.53	0.51	0.45	0.35	0.28
14.5	1.28	0.87	0.59	0.41	0.33
16	2.06	1.34	0.80	0.47	0.37
19	1.85	1.25	0.71	0.38	0.29

Shrinkage and Expansion

As discussed in §2.2.1 gypsum board shrinks with temperature as shown by Mehaffey et al (1994) in Figure 6.11. The two lower plots are more relevant. The top two plots allow for the burning away of paper. All of the plots show shrinkage in the thickness of gypsum board. Presumably, shrinkage along a line in the plane of a board is the same as it is through the thickness. The figure shows that shrinkage is not significant until the temperature is approximately 400°C. Considering the behaviour of constituents discussed above, one would expect that shrinkage would be significant at the stage of dehydration of dihydrate crystals. Figure 3.2 does show a small amount of shrinkage commencing soon after dehydration but not significant compared with shrinkage at temperatures greater than 400°C. However, shrinkage at temperatures greater than 120°C is not expected to cause significant distress since the elastic modulus is expected to greatly reduce at this temperature.

Prior to any moisture loss, some expansion is expected at very low temps (20°-50°C). Young adopted an expansion of 0.1% at these temperatures, and shrinkage along any line in the plane of gypsum board the same as given by Mehaffey et al (1994) for type C board in Figure 2.1 which is reproduced below.

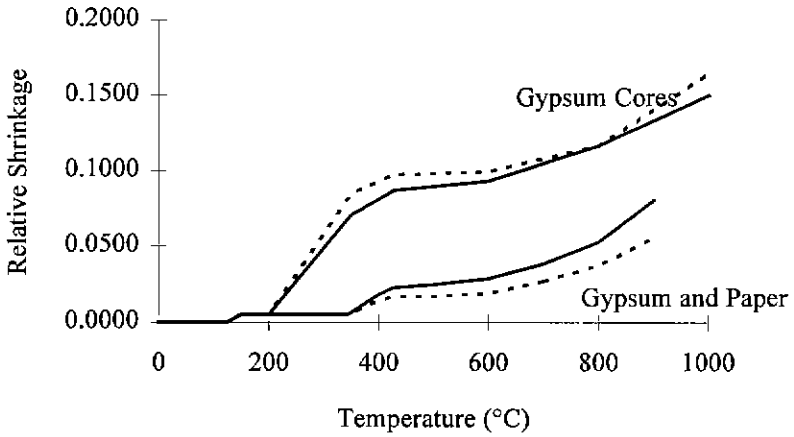

Figure 6.11. (Figure 2.1 repeated). Linear Shrinkage of Gypsum Board Thickness with Temperature (Mehaffey et al 1994). [Continuous lines refer to Canadian type X boards (648 kg.m^{-3}) and the dotted lines refer to Canadian type C boards (732 kg.m-^{3})]

6.5 Mechanical Properties of Fasteners

Fasteners can be screws or nails. Nails were used in the experiments described in §4 and will be discussed here.

Modelling the stiffness of fasteners realistically is complex for several reasons. As explained in §6.2, the fastener stiffness is a function of the stiffnesses of three components - wood, the fastener and gypsum board. In each component, the structural behaviour of the fastener is complex. Stiffnesses are non-linear with strains, as will be shown below. During fire exposure, all of these stiffnesses vary with temperature.

To minimise complexities in modelling the structural response of fasteners, dominant responses should be considered. Modelling of the function of the three component stiffnesses should be limited to the minimum of the stiffnesses. Young (2000) argued that fastener stiffness is only significant when the temperature in gypsum board is less than 120°C. Thereafter, much of the dihydrate crystals have dehydrated and the stiffness of board is insignificant and thence fastener stiffness can be ignored. The contribution of the wood stiffness to the overall fastener stiffness can be evaluated for the elastic modulus of wood in compression perpendicular to the grain. Gerhards (1982) found that this elastic modulus of wood decreases linearly to virtually zero in the temperature range 20-100°C; somewhat like Y00 in Figure 6.9. The timber frame influences wall strength more than the gypsum board. It seems reasonable to adopt stiffnesses obtained from measurements at ambient conditions and assume that they decrease

linearly with temperature in the gypsum board around nails near wood surfaces. When this temperature is 120°C, fastener stiffness should be taken as zero.

A number of researchers, Collins (1989), Aloysius (1996) and Polensek (1976) have determined shear stiffnesses of nails fastening gypsum board in establishing models for timber framed walls at ambient conditions; refer to Table 6.4. Collin's results show that the shear stiffness of nails fastening gypsum board to timber framing is independent of timber density over the range 350-420 $kg.m^{-3}$. Both Collins and Polensek show that nail stiffness is very non-linear, reducing dramatically with slip.

Table 6.4. Shear Stiffnesses Established by Collins (1989), Aloysius (1996) and Polensek (1976) for Nails Fastening Gypsum Board to Timber Framing.

Researcher	th_{board} (mm)	Board (Density)	Nail length x dia.	Stiffness ($kN.mm^{-1}$) for various amounts of : (i) Fastener slip of gypsum board wrt timber, 0.25 mm slip	1 mm slip	2 mm slip	3 mm slip
Collins	12.5	Winstones (§10)		1.17	.43	.24	.16
(1989)	16	Winstones (§10)		1.20	.48	.28	.19
Alloysius (1996)	16	Boral Firestop (810 kg.m-3)	50 x 2.8mm	na	na	na	.22
				(ii) Out-of-plane load (kPa) 0-0.14	0.14-0.38	0.38-0.958	0.958-
Polensek (1976)	13	na	39 x 2.23mm	1750 $kN.mm^{-1}$	12.25 $kN.mm^{-1}$	1.365 $kN.mm^{-1}$	0.21 $kN.mm^{-1}$

Notes: na = not available.
th_{board} = thickness of gypsum board
wrt = with respect to
dia = diameter

Young (2000) found that in experiments on walls similar to those described in §4 but carried out in ambient conditions, the fastener stiffness calibrated to achieve the best comparison between measured and predicted failure loads was approximately 2 $kN.mm^{-1}$ per nail. He defined the term, degree of fixity, d_{fix} which is:

$$d_{fix} = \frac{\delta - \delta_0}{\delta_1 - \delta_0} \qquad (6.2)$$

where δ = deflection of wall

δ_0 = deflection of wall if fastener stiffness was zero

δ_1 = deflection of wall if fastener stiffness was infinite.

If the load applied was less than 90% of the failure load, he found that the degree of fixity was approximately, 1.00. At failure, he found that the degree of fixity of the fasteners was 0.8. Considering the high degree of fixity of fasteners, there would have been little slip, and thus his result of 2 $kN.mm^{-1}$ per nail compares favorably with those of Collins and Aloysius.

Young also showed that the degree of fixity did not significantly affect mid-height deflections until the load exceeded 90% of the failure load. Thus, there is no need to model gradual degradation of the degree of fixity.

From the above, it can be seen that the structural response model need only consider partial composite action between gypsum board and timber framing on the ambient side when the temperature in gypsum board in the vicinity of nails is less than 120°C. It is appropriate to model the shear stiffness of nail fasteners linearly with the average temperature along the fasteners, between a maximum stiffness of 2 $kN.mm^{-1}$ at ambient conditions, to zero at 120°C.

6.6 Summary of Requirements of Structural Response Model

The aims given in §6.1, gave the following requirements for the structural response model:

1. It must be numerically robust; that is, stable for a large range of input values;
2. The computation speed must be sufficiently fast to be incorporated into a probability of failure analysis involving many simulations;
3. The model must be numerically accurate to within 5% of solutions produced from validated models and closed form solutions; and
4. The model must facilitate incorporation into the time of failure and probability of failure models described in §1.

Further to the above, the following analysis requirements for the structural response model have been found in this chapter:

5. The model must be able to analyse the structural response of materials which have the following mechanical properties:

(a) Non-linear stress-strain behaviour (§6.3.3),
(b) Yielding in compression (§6.3.3),
(c) Different elasticitie moduli in compression and tension (§6.3.6, §6.3.7).

6. Determine local failure of fibres and redistribute stresses, since it is unlikely that all fibres in timber cross-sections will reach failure strains at the same time, given the mechanical properties in 1 (a-c) above and the variation of strengths with temperature given in §6.3.4 and §6.3.5.
7. Consider variation of mechanical properties with position across sections through members; this variation results from variation in temperature distributions with temperature (§6.2).
8. Analyse partial composite action between timber framing and gypsum board (§6.2, §6.5).
9. Consider varying degrees of end fixity with temperature (§6.2).
10. Undertake large deflection analysis (§6.2).

In §6.2 and §6.3.7, it was revealed that compression stress-strain behaviour for timber is not only a function of temperature but also a function of time or is limited by some plastification in flexure. As was explained, this behaviour requires further research. For the time being, it can only be best modelled as a function of temperature alone in accordance with Young's (2000) relationships in §6.3.7.

6.7 Review of Models

This section gives a brief review of models which have been developed by Knudson (1975), Gammon (1987), Wright (1995), Collier (1993), Thomas et al (1996), Cramer and White(1996) and Young (2000). The most appropriate model for adoption in the time and probability of failure models will thus be deduced.

Gammon's (1987) model considered the strength of the wall to be dependent on the studs alone. He ignored partial composite action with gypsum board. This action was not significant for the scope of application he was considering, which involved the minimum temperatures in gypsum boards being above 120°C. His structural analysis considered a typical stud. The vertical load capacity of the wall was the product of the number of studs and the capacity of an individual stud. Like Knudson (1975) who modelled timber columns in fire, he obtained bending stiffness, EI by composite analysis of sections discretised into elements. Each element had a different elastic modulus determined from a relationship with temperature alone (§6.3.7). They substituted EI into the Euler equation (6.1), to obtain axial load capacity, P_{cr} for each wall stud. Euler's equation can be used because walls are slender, that is they fail by buckling, and the eccentricity of axial load is small, that is within the width of the top plate. Euler's equation is effectively equivalent to a simple large deflection analysis and offers the advantage of fast

stable computation. However, Euler's equation does not consider eccentricity and non-linear elastic modulus.

Wright (1995) developed three structural models of varying levels of complexity:

1. Single stud model
2. Composite stud model
3. A wall model

All three models determine the flexural stiffness, EI of wall frame members in a similar manner to the models of Knudson and Gammon. The single stud model, as the title implies, considered a typical single stud for the wall frame members. The vertical load capacity of the wall was obtained by multiplying the vertical load capacity of the single stud by the number of studs in the wall. The composite stud model is similar to the single stud model except it assumed full composite action between wall studs and gypsum board on the ambient side. Young's (2000) research supports this assumption. For both the single stud and composite stud models, load capacity is determined from the input of EI into the closed form expressions for the moment amplication factor, U (6.3) and horizontal deflection at the mid-height of a wall, δ as follows,

$$U = \frac{1}{1 - \frac{P}{P_{cr}}} \qquad (6.3)$$

$$\delta \propto U \frac{P.(e_c - e_p)}{EI.(kL)^2} \qquad (6.4)$$

where P = Vertical load applied to each wall stud (N)

e_c = Eccentricity of centre of charred stud section measured from centre of initial stud section prior to fire exposure (mm).

e_p = Eccentricity of centre of applied vertical wall load, P measured from centre of initial stud section prior to fire exposure (mm).

k.L = L_e, the effective length of pin ended column which buckles at the same concentric load as the column of actual length, L. (mm).

Although expression (6.4) is a proportionality, it can be used for modelling the structural response of walls. Some constant would have to be multiplied into the right hand side to make expression an equation. Although the constant is not known, a coarse approximation of the constant is acceptable because as the time of failure is approached, deflection δ increases very rapidly (Young 2000, Collier 1993). The time of failure is insensitive to the constant. The advantage of using expressions (6.3) and (6.4) is that they do account for eccentricity. Further, any initial crookedness could be approximately modelled by including it in the total initial eccentricity. Trahair et al (1994, p261) showed that there is a

good comparison of buckling loads between the above expressions (6.3), (6.4) and the deflection form of the secant equation (6.5) which is a closed-form solution for buckling capacity of columns with equal and opposite eccentric moments, M applied at each end. The deflection is given by,

$$\delta = \delta_0 \frac{8/\pi^2}{P/P_{cr}}\left[\sec\left(\frac{\pi}{2}\sqrt{P/P_{cr}}\right)-1\right] \qquad (6.5)$$

where $\delta_0 = \frac{M.L^2}{8EI}$

$M = P.(e_c-e_p)$

Wright compared his model predictions with results of experiments he carried out. These experiments involved ordinary cavity walls comprising 3050 mm long 89x38mm spruce pine fir studs with 12% moisture content, spaced approximately 400mm between centres, sheeted with a single 12.7mm thick type C Canadian gypsum board each side. The elastic modulus of timber in both tension and compression at ambient conditions, was assumed to be 11,000 MPa. He assumed that the moduli decreased with temperature in accordance with Gerhards (1982) plot in Figure 6.8. The average load on each stud was 8500 N. He supported the ends of walls with pinned supports. The times of failure predicted with the single stud and composite stud models were 39 and 41 minutes respectively, compared with the failure time of a wall furnace experiment of 50 minutes. Wright concluded that the difference was due to vertical flexural resistance of the top plate spanning between the outer studs which charred less than the inner studs. The outer studs charred less because they were exposed to heat from one cavity, whereas the inner studs were exposed to heat from a cavity on two sides of the studs. studs are bounded only by one cavity, compared with inner studs which have a cavity on two sides. From this conclusion, he decided to develop the wall model which included the resistances of the top plate and outer studs. These inclusions necesssarily required three dimensional modelling of the wall - a two dimensional planar structure which can deflect out of its plane.

The wall model involves a simple adaptation of any two dimensional structural frame analysis computer program, for the three dimensional structural behaviour of a wall. The adaptation modifies the analysis by considering the studs rotated 90° to constrain all actions and deflections in analysis to two dimensions. The wall model predicted a time of failure of 45 minutes which was significantly less than the time of 50 minutes in a wall furnace experiment.

There were two likely causes for underprediction of times of failure for all three of Wright's models. Both causes involved inadequate knowledge of the boundary conditions of the wall furnace experiment used for validation. The first cause appears to be lack of rotation of the pin-supports. His diagrams showing deflection versus wall height clearly show double curvature. Hence, he could not have modelled the support conditions with any certainty. The second cause was lack of knowledge of the resistance

provided by the top plate and the outer studs in his experiments. The boundary conditions of the top plate and outer studs can be controlled by cutting the outer studs as shown in Figure 4.7. It appears that this practice was initiated by Collier (1991, 1993). Without the cuts, the gypsum board on the ambient side would be restrained against horizontal movement along the outer studs. The gypsum board would then span horizontally and provide lateral support to the inner studs.

For the aims of adopting a structural response model given in §6.6, Wright's models similarly, do not meet the requirements unfulfilled by Gammon's and Knudson's models, except his models can consider eccentricity and initial crookedness, and have potential for future development of a simplified model of the structural response of light timber framed walls in fire.

Collier (1991, 1993) developed the "Char Factor Method" for predicting the time of failure of walls exposed to standard fire (AS1530.4). The method is based on the premise that conservative estimates - that is, extrapolations - can be made of required stud sizes of walls to achieve the same period of fire resistance as a wall that is shorter or more lightly loaded. The method is based on the fundamental assumptions that for the same surface heating conditions:

1. The depths of char around larger timber sections are the same or less than the depths around smaller timber sections.
2. The flexural stiffnesses, EI of larger timber sections are the same or less than the stiffnesses of smaller timber sections.

Collier's prerequisite for these assumptions is that the larger timber sections must have the same or greater densities than the densities of the smaller timber sections. The surface heating conditions are the same or less severe if:

1. The arrangement of gypsum boards on similar sides (that is fire sides and ambient sides) is similar for different walls.
2. The density of gypsum boards in the walls with the larger studs is the same or greater than the density of gypsum board either side of the smaller studs.

Collier used the secant equation (6.5) for carrying out the extrapolations. His method necessarily requires a furnace test on a prototype wall. He deduced the average elastic modulus, E for the studs at the time of failure with the use of the secant equation, the known load per stud and the measured uncharred stud sections. For larger stud sections, he then deduced the dimensions of the uncharred timber at the time equal to the time of failure by subtracting the same depth of char as there was in the smaller studs in the prototype wall. With the average elastic modulus, the uncharred section and the secant equation, he deduced the load capacity. Collier's method is appealing because of its simplicity and its reproducibility by different users. It is reproducible because it leaves little to interpretation and opinion. However, the extrapolations do not allow for creep or the plastification of wood which can cause failure prior to

charring in slender walls - as discussed in chapter 4. Further, for the purposes of the research in this thesis (§6.6), Collier's model, similarly, does not meet the requirements unfulfilled by Wright's model.

Thomas et al (1996) used the general purpose finite element program, ABAQUS to model the response of timber framed walls in fire. Each finite element had an elastic modulus dependent on temperature. At the time Thomas et al used ABAQUS because it met all of the requirements in §6.6 except that ABAQUS took considerable time to execute. There was concern it would not be readily incorporated into the time of failure model in §7.

Other general purpose finite element programs which have been well used are ANSYS and STRAND6. However, during the course of this thesis they did not meet requirements similar to those not met by ABAQUS. Further, they could not model materials with elastic moduli that were not equal and opposite in compression and tension.

Cramer and White (1996) developed a structural model for predicting the response of timber floor truss systems with decking and ceilings subjected to fire. The model requires the input of the maximum temperature at the core of each truss member from which the average mechanical properties for the member section are determined based on an empirical method. As mentioned in §6.6, it was desired to model mechanical properties varying with position through stud sections.

Young (1996) developed the structural model summarised in Figure 6.12. He substantially advanced the method of line members adopted by Knudson, Gammon and Wright - that is, the subdivision of wall sections into discrete elements, and the use of discrete time steps. The most significant advances of his model were:

1. The incorporation of the line members into a second order frame analysis.
2. Simple procedures for incorporating not only the decreases in stiffness and strength of materials with temperature but also:
    2.1 The redistribution of stresses when wood fibres rupture or yield.
    2.2 Thermal expansion and shrinkage.
    2.3 Creep (although this advance is yet to be validated).

His advanced model not only has the speed and numerical stability of frame analyses for line members but also has accuracy and scope exceeding that for three dimensional finite element analyses such as STRAND. It was purposefully developed for the time and probability of failure models described in this thesis in §7 and §8. His model well satisfied requirements in §6.6. Further details of his model are explained below.

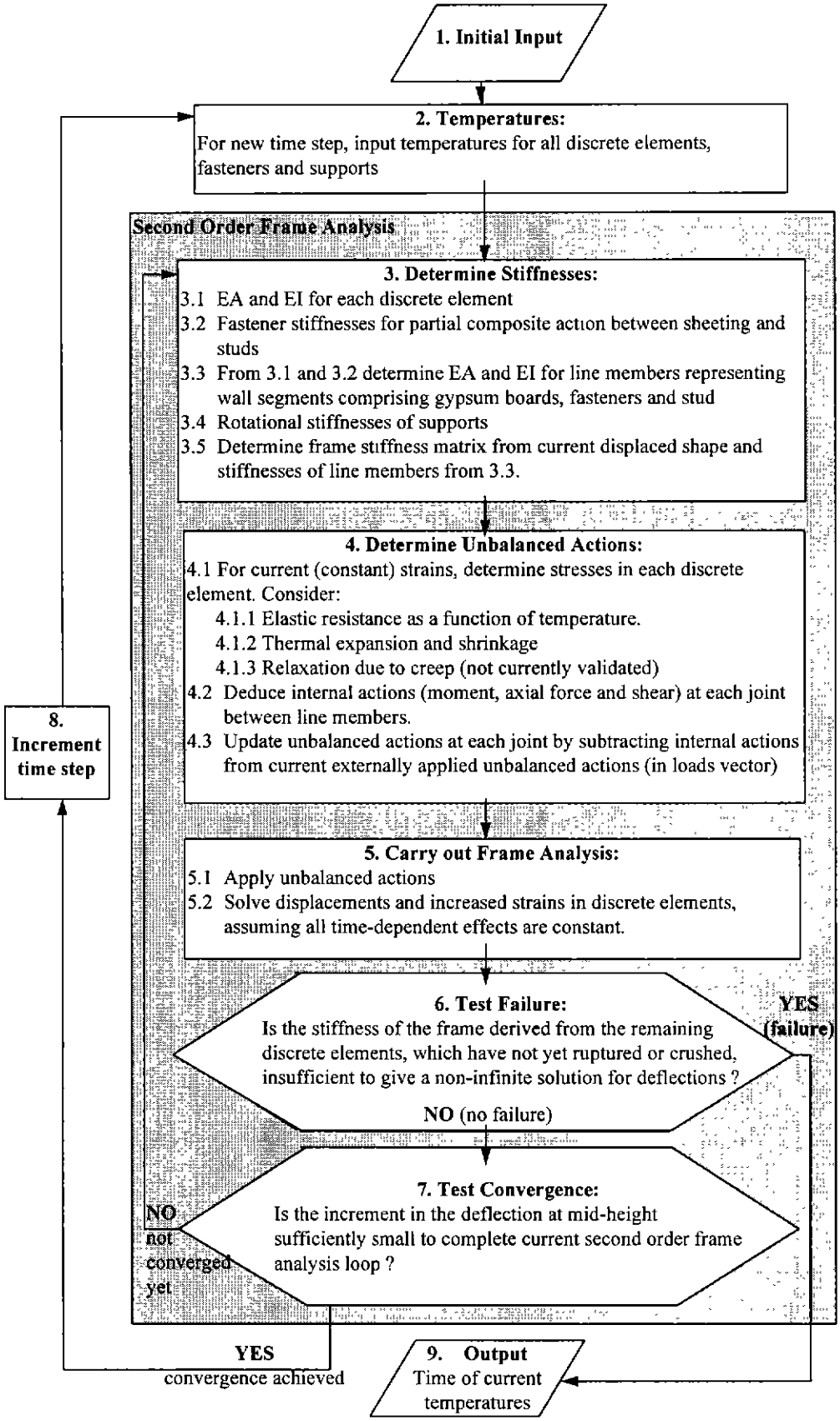

Figure 6.12. Flowchart giving Overview of Young's (2000) Model for Structural Response.

Young's (2000) model, shown in Figure 6.12, analyses a considerable number of structural phenomena which, potentially, are complex to analyse. The main fundamental procedure which he developed to greatly simplify the analysis was an iterative procedure in which each iteration was separated into two separate stages:

1. Analysis of time-dependent processes while all deflections are assumed to remain constant.
2. Deflection movements which are assumed to occur instaneously between time steps.

In the first stage of the iteration, during a time step of approximately 1.0 minute, the processes which were considered to be time dependent, were rises in temperature (box 2), the degradation of stiffnesses (box 3) in accordance with §6.3.4-6.3.7, thermal expansion and shrinkage, and creep (although creep modelling was not validated, box 4). He obtained temperatures at the end of a time step from a file. This file was either measured temperatures or predicted temperatures from some heat transfer model. Since deflections and strains were considered to be constant during the time step, he then deduced stresses of individual discrete elements from the product of known strains and elastic moduli (§6.3.6, §6.3.7). From these stresses, the internal actions (moments, axial forces and shears) were determined at joints (box 4) between line members. Due to creep, and hence relaxation, these actions would not be equal and opposite to the applied loads. That is, during the time step, the constraint of constant deflection led to an imbalance between the internal actions and the applied loads. This imbalance was deduced from the difference between the internal actions and the applied loads and is referred to as "unbalanced actions".

In the second stage of the iterations, the unbalanced actions were applied to the wall structure. At this stage (box 5), time was constant, the unbalanced actions were applied and the new deflected shape of the wall was determined.

As the wall degrades, its stiffness, EI decreases and hence its slenderness increases. The structural response of the wall would eventually be significantly influenced by moments created by the vertical load and the deflected shape. That is, buckling would become imminent. Hence second order analysis was carried out by iteration with the loop of boxes 3-7.

The wall section stiffnesses EA and EI were not only a function of temperature but also a function of stress and strain. Young's model ignores discrete elements as they rupture or crush. The iteration loop of boxes 3-7 thence redistributes stresses following the elimination of failed elements. That is, Young's model is not only a buckling model but also a strength model.

The frame analysis written by Young included rotational stiffnesses of the supports. These stiffnesses can be defined as a function of temperature.

Young checked whether all of the gypsum board engaged in partial composite actions was effective, or if some was ineffective due to shear lag. He found that shear lag was very minor for stud spacings up to 600mm. Young conducted a number of wall furnace experiments to validate his model.

Young achieved the modelling detail of three dimensional finite element analyses by not only discretising wall sections but also subdividing the height of walls into segments. He typically subdivided the wall height into ten segments. He demonstrated the numerical accuracy of his model by comparing predictions against those from a finite element program, STRAND6. His comparisons were well within 1%. However, the scope of Young's model exceeded the scope of finite element analyses, including STRAND6 and ANSYS, at the time of development in the following ways:

1. Partial composite action between gypsum board and studs. He found that it was very difficult, if not impossible to model slip stiffness between sheeting and studs with finite elements. Ill-conditioning of the structural stiffness matrix was created by extreme ratios between dimensions of finite elements modelling the fasteners and the finite elements modelling sheeting and studs.
2. Elastic moduli of different magnitudes in compression and tension. Young found that STRAND6 could only consider one relationship between the magnitude of the elastic modulus and strain for a material. The elastic modulus was positive for tension and negative for compression.
3. Redistribution of stresses as any element failed. STRAND6 cannot remove finite elements (which represent bundles of wood fibres), that is redefine geometry, if a finite element fails.
4. Elastic moduli non-linear with strain. STRAND has trouble destressing elements which are at strains greater than the strain corresponding to maximum stress resistance; for example, $1.35\varepsilon_{equiv.max}$, in Figure 6.4.

Validation showed that the numerical accuracy of his model was well within 1% of closed form solutions and solutions for particular cases obtained from finite element analyses.

Young rigorously validated his model against results from the following experiments in which measurements were obtained for dominant variables and boundary conditions:

1. Small scale axial compression experiments which established the compression properties of the timber studs in his walls.
2. Full scale wall furnace experiments with and without gypsum board sheeting to establish:
    (a) The vertical load capacity of walls prior to the experiments. This capacity enabled the load ratios (ratio of load to ambient load capacity) to be established prior to fire exposure. It does not seem that load ratios have been established in wall furnace

experiments to date. Young's experiments appear to be the first that enable the amount of degradation relative to ambient conditions to be evaluated.

(b) The degree of composite action between gypsum board and studs at ambient conditions.

3. Full scale wall furnace experiments under a variety of conditions:
   (a) No vertical load;
   (b) Vertical load similar to that required in design codes (AS1720.4);
   (c) Pinned supports;
   (d) Fixed supports; and
   (e) Ambient facing gypsum board sheeting with and without composite fastening to the timber studs.

In his full scale wall furnace experiments, the outer studs were cut to prevent them from providing any signifcant structural resistance. Outer studs degrade at a slower rate because they char on only one cavity facing side compared with inner studs. The outer studs thus unconservatively increase the time of failure, compared walls wider than those in standard tests.

6.8 Conclusions

From the review of models in §6.7, adoption of Young's (2000) structural response model meets the requirements listed in §6.6 and is justified for adoption in the time of failure model in §7 and the probability of failure model in §8.

The mechanical properties adopted by Young (2000) in §6.3.3-§6.5 have been shown to give satisfactory predictions of time of failure and are justified for adoption.

The following further research is required in the development of models for predicting the structural response of light-timber framed walls:

1. A model for creep or plastification of timber in compression in regions affected by moisture vaporisation, should be developed. Such a model would include variables for compression stress, strain, elastic modulus, temperature, moisture content and time.
2. Further, the above relationship for compression elastic modulus, should eventually consider structural scale timber; that is with knots and other growth characteristics as well as dimensions similar to those in walls.
3. It seems that no structural models consider the accelarated charring around nails (Collier 1993, and Fuller et al 1992). Such charring can treble the charring rate in the vicinity of nails, reducing wood fibre stiffness and strength, and thus effectively create large notches.

Future models should evaluate the significance of these notches on the time of failure and consider these, if shown to be significant.

4. Although creep in dry timber at temperatures above 200°C (Schaffer 1982) is not expected to significantly affect the time of failure of timber framed walls in fire, since studs of minimum temperatures exceeding 200°C should be close to failure, it does not seem that any modelling has been undertaken to justify this expectation. Such modelling should be undertaken in the future.

7. Time of Failure Model

7.1 Introduction

An overview of the time of failure model was given in chapter one (§1). It was illustrated in Figure 1.1 which is reproduced as Figure 7.1 below. The figure generally shows that the time of failure model is a linkage of several other models to simulate the physical degradation of a wall exposed to fire, in successive discrete time steps (box 6). The model commences with ambient conditions and defined loads. Each time step involves models for fire severity (box 2), heat transfer (box 3) and structural response (box 4).

The time of failure model can incorporate any fire severity model which gives single representative values of fire temperature with time. (It has recently been shown - Thomas and Bennetts, 1999 - that the temperatures of fire gases and surfaces of walls in enclosures are not uniform, as has been assumed in virtually all barrier models such as Gammon 1987, Mehaffey et al 1994, Thomas 1997, and Takeda and Mehaffey 1998. Until further research is undertaken, fire gases will have to be modelled with single single representative temperatures in fire resistance models of barriers.) It is assumed that the fire is only on one side of the light-timber framed wall being analysed by the time of failure model. The results described in this chapter, were derived using the standard fire defined in AS1530.4 which is very similar to the ISO standard fire.

The heat transfer model adopted was ADIDRAS which was described in §3, and subsequently validated in §4 and §5.

As mentioned in §6, the model adopted for simulating structural response was Young's (1998) which he extensively validated.

The simulation continues until one of the following modes of failure is determined (Figure 7.1, box 5):

1. "Insulation, average temperature" mode; that is, when the average temperature rise on the ambient side of the wall exceeds some nominated value. In AS1530.4, this value is 140°C.
2. "Insulation, maximum temperature" mode; that is, when the maximum temperature rise on the ambient side of the wall exceeds some nominated value. In AS1530.4, this value is 180°C.
3. "Integrity initiated failure" mode. As explained in §2.2.1.3, gypsum boards begin to crack in areas where the temperature rises above 400°C. Since this temperature exceeds insulation failure temperatures (150°-200°C, AS1530.4), failure due to integrity alone will never happen. However, pieces of gypsum board on the fire side, formed by the cracking, will

slough off when the minimum temperature those pieces exceed 700°C (§2.2.1.3). The fire then directly impinges on the studs and destroys them in a matter of minutes. Failure in this manner is referred to as, "integrity initiated failure."

4. Structural collapse.

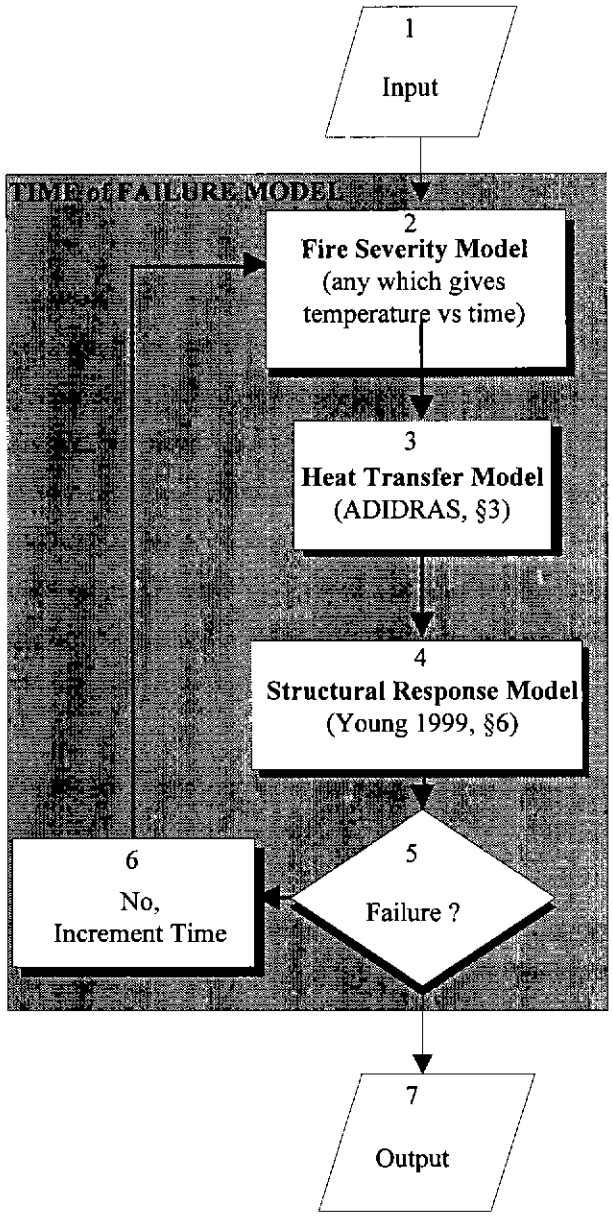

Figure 7.1. Time of Failure Model.

Given in this chapter are comparisons of model predictions of the time of failure with the failure times observed in several wall experiments described in §4. Many comparisons are made with Wall 6 because, among all of the walls tested, it was the wall that was most similar to walls in common building practice.

The top and bottom plates in Wall 6 were secured with coach bolts in the steel supporting frame. The top and bottom plates were therefore fixed against rotation, whereas the ends of other walls were free to rotate. The ends of the studs in Wall 6 were nailed to the plates in a conventional manner. If the ends of the wall developed a tendency to rotate during fire exposure, the nails would not have significantly resisted pull-out. It is thus argued that the resistance to rotation at the ends of the studs in Wall 6, despite the restraint of coach bolts in the top and bottom plates, was similar to the resistance to rotation at the ends of walls in common building construction.

It was apparent from the wall experiments described in §4 that the temperatures in gypsum board for periods up to 90 minutes were not high enough to cause either insulation or integrity initiated failure. Failure was caused by structural collapse, in particular, buckling. Thus, failure in this chapter mainly refers to buckling. Failure caused by inadequate strength is checked with the structural model (Young 1999, §6.7), and thus has not been ignored. Young's (1999) model analyses strength by iteration involving the determination of stresses in discrete elements in wall sections and ignoring those elements which either exceed their stress capacity or some maximum strain at rupture as defined by the user. The discrete elements represent bundles of wood fibres in the studs or discrete portions of gypsum board. The stress capacity and maximum strain at rupture are modelled as functions of temperature.

Having established the time of failure model, the aim (§1.5) of developing graphs of failure time as functions of a number of variables can be developed.

The aims of the research described in this chapter were to:

1. Develop a model to theoretically predict the time of failure of light-timber framed walls exposed to real fires. Validation was carried out for the standard fire, AS1530.4.
2. Indicate the effects of major variables on the time of failure of ordinary cavity walls in the standard fire.
3. On the basis of sensitivity of the time of failure to variables with values typically encountered in engineering practice, determine the variables which should be modelled probabilistically in the probability of failure model described in chapter 8.
4. Generally provide information to aid engineers in the design of light-timber framed walls to achieve required times of resistance to the standard fire, AS1530.4.

This chapter commences with a summary of most of the input used in the validation and applications of the time of failure model described throughout the chapter. Subsequently, the sequence of sections within this chapter generally follows the sequence of aims 1-3, above. Most sections of this chapter give graphs to address aim 4. Validation of the time of failure model is carried out by comparing model predictions with experimental results in §7.3. It is assumed in §7.3 that the individual models within the time of

failure model are valid, and thus, no further validation of the individual models is undertaken in this chapter. In relation to aim 2, discussion of the effects of major variables on the time of failure is carried out in sections on the following groupings of variables:

1. Load.
2. Mechanical properties of timber - stiffness and strength.
3. Arrangement of timber framing - wall height, support conditions, stud depth, stud breadth, stud spacing, initial crookedness.
4. Arrangement of gypsum board - thickness and number of sheets of gypsum board.
5. Thermal properties of materials - conductivity, density, specific heat and emissivity.
6. Fire temperature.

The effects of the variables on the time of failure are shown graphically to aid the evaluation of the dominance of variables (aim 3) and to provide valuable design aids (aim 4). Towards the end of the chapter the sensitivities of variables are summarised and dominant variables are deduced. Finally, conclusions on the time of failure model are summarised.

7.2 Summary of Input

Unless otherwise noted, the results in this chapter mainly relate to Wall Experiment 6 for reasons given in §7.1. A vertical load of 8kN was applied at the top of each stud. A detailed explanation of input for the heat transfer model, ADIDRAS was given in §5. Shrinkage gaps between studs and gypsum board on the fire side, mentioned in §5.4.3 were not included in the input to ADIDRAS unless otherwise mentioned. The reason for generally ignoring gaps was that times of failure were mainly less than 60 minutes during which time heat transfer from gaps does not significantly affect the temperature distribution in studs, as is apparent from §5.4.3. Explanation of the main input for Young's (1998) structural response model was given in §6. Particular values of all input for Young's model in this chapter is given in Appendix C.

7.3 Comparison of Predictions of Time of Failure Model with Results of Wall Experiments Described in §4.

Although the individual models within the time of failure model have been validated, it remains to validate the overall time of failure model (aim 1, §7.1). Young (2000) validated his structural response model for use in a time of failure model without using a model for heat transfer. He undertook this validation procedure (amongst a number of other validation procedures) by obtaining predictions of the time of failure with the input of temperature values measured in wall experiments described in §4. It is desirable to find out the level of accuracy of the overall time of failure model which involves the input of

temperatures from ADIDRAS into Young's model. This level of accuracy can be gauged from Table 7.1 which gives the times of failure of the walls in the experiments and the predicted failure times from both Young's(2000) validation procedure and the time of failure model. The level of accuracy of the time of failure model, apparent from Table 7.1, is discussed below.

Table 7.1. Summary of Times of Failure for Walls Described in §4, from Young (2000) and Predictions with the Time of Failure Model.

Supports	Nailing of Gypsum Board	Load per Stud (kN)	Wall	Times of Failure - structural collapse (min)			
				Exp't (§4.5.4)	Young (2000)	ToF Model k_C adopted	ToF Model k_A adopted
Fixed	Conventional	8.00	6	59	59 (A) 61 (B)	59 (A) 62 (B)	59 (A)
Pinned	Conventional	8.00	4,5	35	 35 (A) 41 (B)	36 (A1) 40 (A) 44 (B)	41 (A1) 43 (A) 46 (B)
Pinned	Minimal	8.00	8	28	 26 (A) 32 (B)	32 (A1) 35 (A)	 43 (A)

Notes:

1. A1, A and B refer to relationships for relative elastic modulus for compression in timber shown in Figure 7.2.
2. Exp't is an abbreviation for "experiment".
3. k_A k_C refer to the values for the thermal conductivity of gypsum board and timber, modified as shown in Figure 7.3. Plot C shows the simple allowance for moisture transfer (§5.4.4). Plot A is for the case ignoring moisture transfer.
4. Load is load per stud.
5. ToF means time of failure.

Pin Supported, Non-composite Wall 8

The wall for which conditions were best known, was the wall in Experiment 8. The supports were free to rotate and hence the rotational restraint at the supports was clearly known to be of zero stiffness (kN.m per radian). These supports are referred to as, "pinned" supports in Table 7.1. Conventional supports involving top and bottom plates may gradually degrade during fire exposure. Thus the rotational stiffness

of conventional supports during a fire are not clearly known. Results of experiments involving conventional supports would not enable clear comparisons with model predictions.

Another condition that was clearly controlled in Wall Experiment 8 was the degree of composite action of studs and gypsum board. The gypsum boards were secured against the studs but were free to slip. There was clearly no composite action of the studs and gypsum board in flexure, and thus the degree of composite action could be clearly quantified as zero. It would have been difficult to measure the degree of composite action provided by conventional nailing (Figures 4.7 and 4.8), during fire exposure.

The wall failed in the experiment by buckling at 28 minutes.

Young (2000) found that his structural model predicted a failure time of 32 minutes when he adopted relationship, B for the elastic modulus for compression of timber in Figure 7.2. This relationship was the one he obtained (§6.3.7) from independent compression experiments involving small samples of timber that were similar to the timber in the studs in all wall experiments (§4). Young (2000) explained that the difference between his model prediction, and the time of failure measured in the experiments was due to creep or some plastification of wood during the vaporisation of moisture. He concluded that one must be wary of predictions of models for walls which collapse prior to charring of the studs, until the models employ some creep or plastification sub-model for timber in compression during moisture vaporisation. He then accounted for creep in a simple manner as shown in relationship A in Figure 7.2 for the elastic modulus for compression of timber. With this relationship, he predicted structural collapse at 26 minutes which compares well with the failure time of 28 minutes in Wall Experiment 8.

From the comparison of Young's (2000) predictions of the time of failure at 26 minutes, allowing for creep, and at 32 minutes, ignoring creep, it is apparent that creep and plastification of timber in regions, at or near the vapour point of moisture, reduced the time of failure by approximately 6 minutes. Compared with the observed time of failure of 28 minutes, it is apparent that creep reduced the time of failure by at least 20%.

The time of failure model predicted structural collapse at 43 minutes, as a result of the input of thermal conductivity without any adjustments for the effects of moisture transfer (k_A adopted) and the input of Young's (2000) relationship, (A), for relative elastic modulus of timber in compression in Figure 7.2. Modification of thermal conductivities of gypsum board and timber in accordance with relationship C in Figure 7.3 (k_C adopted), led to the model prediction that structural collapse occurred at 35 minutes. (The appropriateness of modification C in preference to modification B was explained in §5.4.4.) Assuming a greater reduction in elasticity due to creep and plastification as shown for relationship, A1 in Figure 7.2,

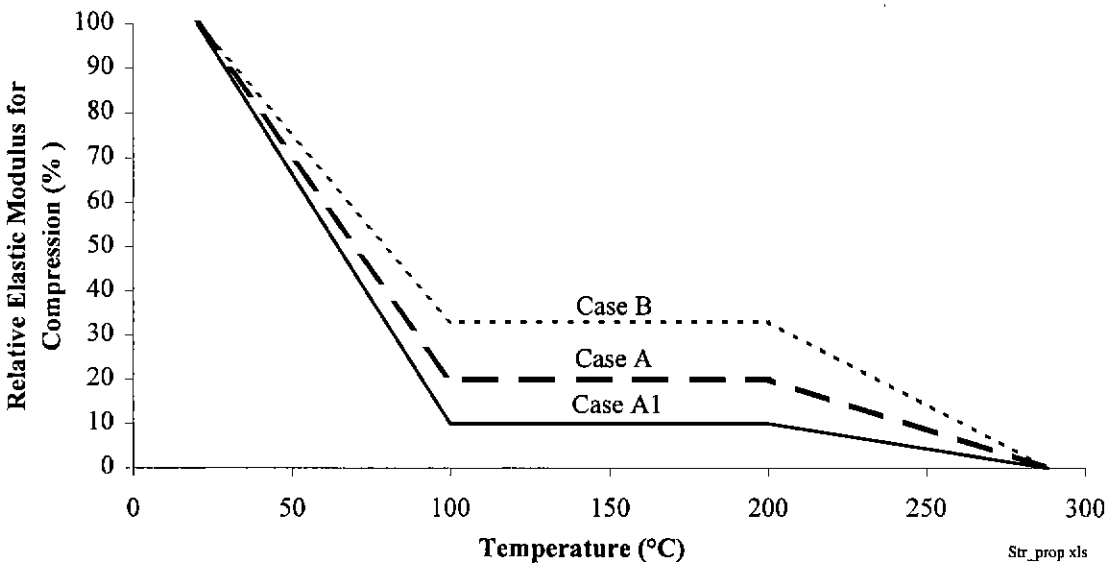

Figure 7.2. Young's (2000) Values for Relative Compression Elastic Modulus, Cases A and B (from Figure 6.9), and the Definition of another, Case A1.

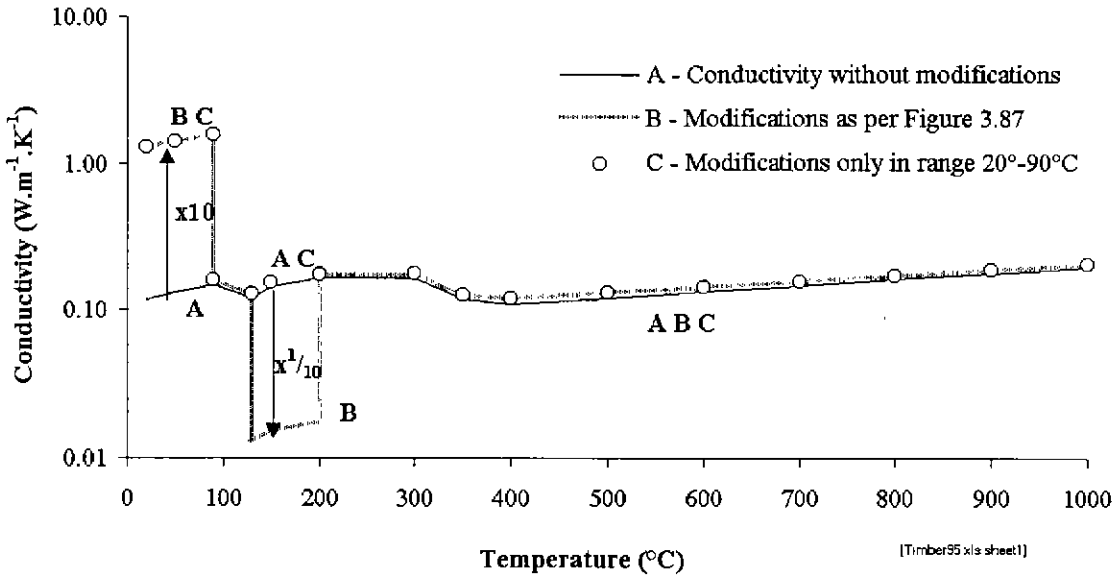

Figure 7.3. Modifications to Conductivity for Simple Modelling of Moisture Transfer.

led to a model prediction of 32 minutes. The comparisons of the predicted times of failure of 43, 35 and 32 minutes with the experimental value of 28 minutes, demonstrate limited success in modelling the effects of moisture transfer with:

1. Modification C in Figure 7.3 to allow for the heat transferred by moisture movement, and
2. Plot B in Figure 7.2 to allow for the loss of stiffness associated with behaviour of moisture.

It is apparent that to model the structural response of Wall 8, particularly at the time of failure, further research is required in developing more fundamentally based models of moisture transfer and creep than is given in modification C and plot B.

Pin Supported, Partially-composite Walls 4 and 5 in §4

Wall Experiments 4 and 5 described in §4, were similar to Wall Experiment 8 except the gypsum board sheets were nailed to the light-timber frames in the conventional manner referred to in Figures 4.7 and 4.8. The shear stiffness provided by partial-composite action of gypsum board, nails and framing was deduced from independent full scale load-deflection wall experiments at ambient conditions by Young (2000). In summary, he found that there was actually full composite action during the ambient experiments. He assumed for the full scale wall furnace experiments that there was full composite action until all composite action suddenly ceased at approximately 100°C in the gypsum board, when the gypsum underwent calcination to a hemi-hydrate.

With his model, Young (2000) obtained predictions for time of failure of 41 minutes, assuming no creep in the studs (plot B in Figure 7.2 for relative elastic modulus in compression), and 35 minutes assuming some creep in accordance with plot A in Figure 7.2. It is apparent that creep in the studs reduced the time of failure by 15-20%.

The prediction of the failure time with the time of failure model, ignoring moisture transfer and creep was 46 minutes. Modification of the thermal conductivities of materials in accordance with plot C in Figure 7.3, led to only a slightly reduced predicted failure time of 44 minutes. The small size of the reduction is due to several reasons. Modification C leads to a rapid transfer of heat through regions at less than 90°C. If failure occurs when temperatures in much of the stud section is approximately 100°C, then moisture movement greatly reduces failure time. However, if failure occurs when much of the stud section has temperatures which are substantially greater that 100°C, then considerably greater heat ingress from the fire into the wall must take place. This modelled ingress of heat is not greatly increased by modification C because the temperature at the surface of the gypsum board facing the fire quickly rises above 90°C when the conductivity is assumed to return to unmodified values. Hence, a substantial period of time must pass

before there is sufficient ingress of heat from the fire to cause failure, and thus modification C has little effect on failure times which occur after vaporisation.

Adoption of modification C and relationships A and A1 in Figure 7.2, to allow for creep, reduced model predictions of the failure times to 40 (A) and 36 (A1) minutes. It is apparent that the time of failure of Walls 4 and 5 is sensitive to the effects of creep. The sensitivity is greatly increased when the time of failure reduces to approximately 30 minutes when moisture vaporises and increases the total rate of heat transfer as well as promoting creep. As for Wall 8, the comparisons forWalls 4 and 5 indicate the need for more fundamental modelling of moisture transfer and creep.

Wall 6, a Common Type of Wall in Building Construction

As explained in §7.1, the wall that was most similar to common walls in building construction was the wall in Experiment 6 described in §4. Trahair et al (1994) showed that only a small lateral restraining force of the order of 1% of the axial compression force is sufficient to prevent buckling at the position of the lateral force. Young (2000) found that the rotational stiffness of the supports of Wall 6 closely approximated fixed supports at the time of failure. Hence, the supports for this wall are referred to as "fixed" in Table 7.1.

The gypsum boards were fastened in the conventional manner specified in Figures 4.7 and 4.8. The load applied was 8 kN per stud which, as shown in Appendix B, is a typical stud load. The wall failed in the experiment by structural collapse at 59 minutes.

Young (2000) found that his structural model predicted failure times of 59 and 61 minutes for respective relationships, A and B (Figure 7.2) for the elastic modulus for compression in timber. The time of failure model gave similar predictions indicating that:

1. Heat transferred by the movement moisture and,
2. The effects on the mechanical properties of wood due to moisture; that is, a reduction in the elastic modulus for compression, creep and/or some degree of plastification,

had little effect on the time of failure, when the studs were observed to have substantially charred.

Conclusions

From comparisons between model predictions and experimental results, the time of failure model is valid for walls which fail when the temperatures in the studs are higher than the vaporisation point. Such temperatures are expected in typical fire rated walls (AS1530.4) in common building construction. It is expected also that substantial charring of the studs is occurring at the time of failure. The model is less accurate for predicting the time of failure of walls for slender walls like Walls 4,5 and 8 which are slender due to having pinned rather than fixed supports. It is believed that the times of failure of these walls is affected by moisture transfer which increases the rate of heat transfer and reduces stiffness by a some mechanism including creep, plastification and reduction of elastic modulus of timber in compression. Hereafter, this mechanism will simply be referred to as creep. This creep can be approximately modelled with reduced elastic modulus in compression (plot A, Figure 7.2). The transfer of heat by moisture movement can be approximately modelled by magnifying the thermal conductivity in accordance with modification C in Figure 7.3. Further research is required to develop more theoretically sound models for the creep and the transfer of heat by moisture movement.

7.4 Effect of Load on the Time of Failure

It was desired to appraise the validity of the time of failure model for various load ratios (that is, the ratio of applied load to ambient strength), and hence deduce the effects of load on the time of failure. As indicated in §7.1, the appraisal has been carried out using results from Wall 6 (§4), which had rotationally restrained supports, as a basis for comparisons.

The effects of vertical loads on the predicted time of failure for walls similar to Wall 6 (§4) are shown in Figure 7.4. The top three plots (1-3) in the Figure 7.4 result from using ADIDRAS without allowance for heat transferred by the movement of moisture; that is using neither modifications, B or C, to thermal conductivity shown in Figure 7.3. Each of the three plots corresponds to a different compression elastic modulus between 100°-200°C, shown in Figure 7.2. The dotted line is for Case B, a modulus of 0.33 times the modulus at ambient conditions. The dashed line is for Case A for the relative modulus of 0.20 in the same temperature range. Both Cases A and B are the same as in Figure 6.9. The continuous thin line is for Case A1 for which the relative modulus in the same temperature range is 0.10. Plots (1-3) are coincident along segment AB in Figure 7.4.

The bottom two plots (4 and 5) in Figure 7.4 - the continuous thick line and the small circles without a line - were computed from temperatures resulting from the transfer of heat by thermal conduction and the movement of moisture. The continuous thick black line results from using temperatures measured in the

experiments in §4 instead of temperatures predicted with ADIDRAS. The points plotted as small circles result from temperatures computed with ADIDRAS using thermal conductivities modified for heat transfer due to the movement of moisture, according to plot C in Figure 7.3.

Plot 6 is a point plotted for the average failure time for the three non-loadbearing walls (Walls 1-3 in §4).

The observed failure time and the load for Wall 6 (§4) is plotted as plot 7.

To enable comparisons of model predictions with the experimental results for walls similar to Wall 6 over a wide range of load ratios, results from experiments on walls with pin supports, were adjusted in accordance with equation (7.1).

$$P_{ef} = \frac{P_{ep}}{P_{mp}} P_{mf} \qquad (7.1)$$

where P_{ef} is the extrapolated failure load to cause a wall with fixed ends to fail at the same time as the pin-ended wall in the experiment (N).

P_{ep} is the failure load for the pin-ended wall in the experiment (N).

P_{mp} is the failure load deduced with the model to lead to the same failure time as observed for the experiment on the pin-ended wall (N).

P_{mf} is the failure load predicted with the model to cause a wall with fixed ends to fail at the same time as the pin-ended wall in the experiment (N).

The other results plotted in accordance with equation (7.1), were the results for pin-ended Walls 4 and 5 (point-plot 8) and the average of the capacities (point-plot 9) measured by Young (1996) for ten walls, similar to Walls 1-8 in §4, in ambient conditions.

The following comparisons can be made between predicted failure times and experimental results plotted in Figure 7.4, for different load ratios:

1. *Comparisons for low load ratios (0-5%).* All model predictions (plots 1-5) for the time of failure for non-loadbearing walls, were approximately 80 minutes which compares reasonably well with the failure time of 90 minutes observed in Wall Experiments 1-3 (point plot 6). The reason for the difference can be explained from the strength and stiffness of materials assumed for temperatures computed with the model at 80 minutes. It is apparent from Figures 4.36, 6.7 and 7.2 that compression stiffness and strength of the uncharred wood section remaining at 80 minutes is small. After 80 minutes the walls would have been mainly supported by the gypsum board on the ambient side. Apparently the mechanical

properties adopted for gypsum board (§6.4 and Appendix C) were conservative and led to the under-estimation of the failure time.

2. *Comparisons for typical load ratios (5-15%).* There is a good comparison between the time of failure recorded for Wall 6 (with 8 kN load/stud - plot 7) and the time of failure predicted with the model using the elastic modulus for timber in compression, Case A recommended by Young (2000). The comparison is good irrespective of whether heat transfer due to the movement of moisture is considered (plots 4 and 5) or is ignored (plot 2). This comparison supports the validity of the time of failure model without any modifications for moisture transfer, at low load ratios (that is, within the range of loads normally permitted by AS1720.1).
3. *Comparisons for load ratios that are higher than normally used (20-80%).* These comparisons are made with respect to Wall Experiments 4 and 5 which involved pinned supports (§4). Point-plot 8, which was derived from extrapolation of experimental results in accordance with equation (7.1), shows that the load capacity at a failure time of 35 minutes was 10% less than that predicted with models - plot 4 (Young 2000) and plot 5 (time of failure model using ADIDRAS). These comparisons further demonstrate the need to consider the effects of moisture transfer on heat transfer and stiffness when modelling the time of failure for load ratios which are greater than those normally permitted in timber engineering codes such as AS1720.1.
4. *Comparisons for high load ratios (approaching 100%).* Plots 1-5 all run through point A which corresponds to the strength of the walls at ambient conditions (Young 1996). This comparison confirms the validity of Young's (1996) structural model for light-timber framed walls, including its assumptions and methods of analyses listed in §6.7. Furthermore, since all of the plots 1-5 approach point A, this comparison supports the validity of the model for very high load ratios approaching 100%. At these ratios, moisture transfer and creep have an insignificant role in the structural collapse of walls.

It can be generally concluded from the above comparisons that there is support for the validity of the model to predict the time of failure for given loads. The simple methods adopted for modelling heat transferred by the movement of moisture (modification C in Figure 7.3) and for modelling creep (plot A in Figure 7.2) improve model predictions. However, further rigorous modelling of these two phenomena is required.

Predictions with the model show that Large variations, say ±20%, in design loads (typically, 8kN/stud Appendix B) lead to a change of ±7 minutes (±12%) in the time of failure. That is, the time of failure is fairly insensitive to changes in design loads, and hence is insensitive to mechanical properties in typical building construction. This insensitivity is apparent, despite the fact that the slopes of the plots are

steepest in the region of typical design loads. This paradox can be explained from the low loads permitted by codes which are concerned with the large variability of mechanical properties. A large percentage change in low load values will not have a similarly large percentage effect on the time of failure.

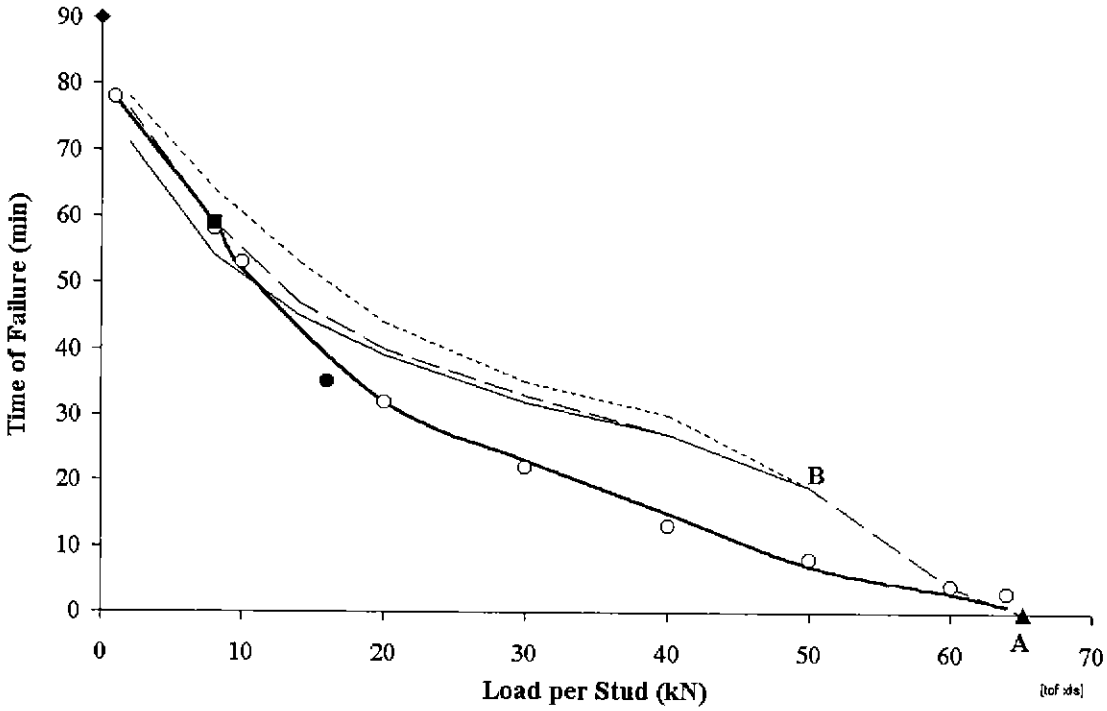

--------- 1. Temperatures from ADIDRAS, ignoring moisture transfer. E from plot B in Fig 7.2.
— — — 2. Same temperatures as above. E from plot A in Fig 7.2.
——— 3. Same temperatures as above. E from plot A1 in Fig 7.2.
——— 4. Temperatures from tests in §4, E from plot A in Fig 7.2 (Young 1999).
○ 5. Temperatures from ADIDRAS allowing for moisture transfer (C-Fig 7.3), E from plot B in Fig 7.2.
◆ 6. Average result for Non-loadbearing Wall Furnace Experiments 1-3
■ 7. Result for Fixed-End Wall Furnace Experiment 6
● 8. Capacity of fixed-end wall deduced from pinned Walls 4 and 5.
▲ 9. Capacity of fixed-end wall deduced from ambient experiments on 10 pin-ended walls.

Figure 7.4. Time-of-failure versus Load Ratio for Walls Similar in Cross-section to Wall 6 in §4, for Various Assumed Temperature Distributions and Compression Elastic Moduli, E for Timber Studs.

7.5 Mechanical Properties of Timber - Stiffness and Strength

The effects of the initial elastic modulus of timber on the time of failure can be deduced from model predictions given Figure 7.5.

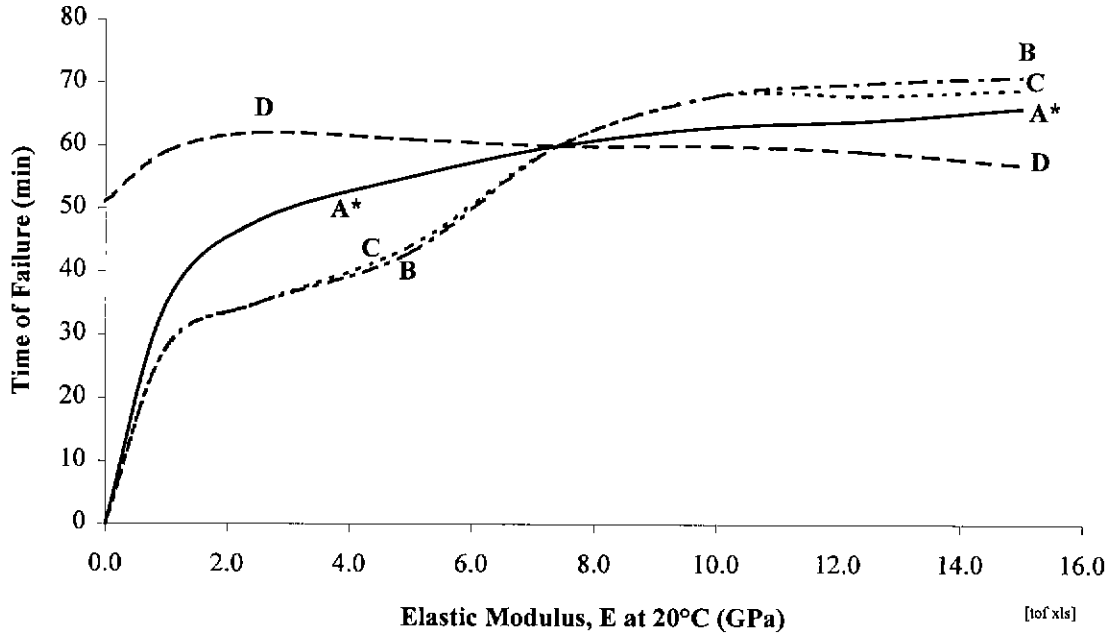

——— A* - Same E for compression & tension, temperatures from ADIDRAS, moisture transfer ignored.

— - — - B - Same E for compression & tension, temperatures from tests in §4.

- - - - - - C - Variation in E for compression only, temperatures from tests in §4.

— — — D - Variation in E for tension only, temperatures from tests in §4.

Figure 7.5. Predicted Times of Failure versus Elastic modulus, E at 20°C.

Figure 7.5 shows time of failure as a function of elastic moduli, E for timber studs and temperature distributions obtained in several ways. As explained in §7.4, moisture transfer can substantially affect the temperatures and mechanical properties (particularly the elastic modulus in compression), and hence affect the time of failure. Plots were thus obtained for failure times from temperature distributions resulting from moisture transfer (**B C D**) and no moisture transfer (**A***). Since E, the elastic modulus can be different for compression (§6.3.7) and tension (§6.3.6) at raised temperatures, the effects of each type of modulus is considered. Plot **C** considers E to change in compression only. Plot **D** considers E to change in tension only. Plot **B** considers the same changes in E for tension and compression.

Plot **D** shows that the elastic modulus of timber in tension has little effect on the time of failure. This result is expected since the wall is actually loaded in compression; tension is not a significant action. Tension only occurs during the large buckling deflections just prior to collapse.

Plots **A***, **B** and **C** show that the time of failure is more sensitive to initial elastic modulus in compression than in tension. There is substantial sensitivity at low values of elasticity less than 2 GPa. However, this sensitivity is of little practical importance since the elasticity for the design of timber structures of the lowest commonly used strength grade (F5 in AS1720.1, TPC 1994) is 6.9 GPa.

The close similarity of plots **B** and **C** further demonstrates that elastic modulus for compression dominates over the modulus for tension.

The comparison of plot **A*** with plots **B** and **C** shows that moisture transfer, which increases the rate of heat transfer and reduces the elastic modulus, substantially affects the time of failure of walls with studs having ambient elastic moduli less than 7 GPa.

Figure 7.6 shows the effects of timber strength on the time of failure. The strength is denoted as, F_{ct} (MPa). F_{ct} is simply approximated to be the same for tension and compression because the walls are loaded in compression and thus tensile properties need not be modelled accurately. As explained above, tension will not be significant until structural collapse by buckling is imminent. The average measured strengths of studs in walls in §4 was 24 MPa. The measurements of strengths of radiata pine by Leicester et al(1988) gave 15 MPa for the 5 percentile value of flexural strength of the lowest grade of radiata pine timber used in common building construction (F5 in AS1720.1). Compression strength would be expected to be similar. Figure 7.6 shows that ambient compression strengths as low as 7 MPa have little effect on the time of failure. Since the strength of more than 95% timber in common building grades exceeds 15MPa, timber strength has no discernable effect on the time of failure. The large extent of the independence of the time of failure to strength is expected, since the walls failed by buckling rather than by inadequate strength (crushing or rupture).

This section, §7.6 determines the effects of variables, defining the arrangement of the timber frame, on the time of failure. The variables considered in this section are wall height, depth and breadth of stud sections, spacing of studs and the initial crookedness.

Wall Height and Support Conditions

The effects of support conditions on the time of failure can be deduced from the effects of wall height in accordance with k_e in equations (6.2) and (6.5). For example, for perfectly straight walls with concentric

load at ambient conditions, changing the pinned supports to fully fixed at both ends, changes k_e from 1.0 to 0.5 and has the same effect on capacity as halving the height. The following discussion refers mainly to heights of walls with fixed ends similar to Wall 6 (§4) and walls in common building construction. Plots of time of failure versus wall height are shown in Figure 7.7.

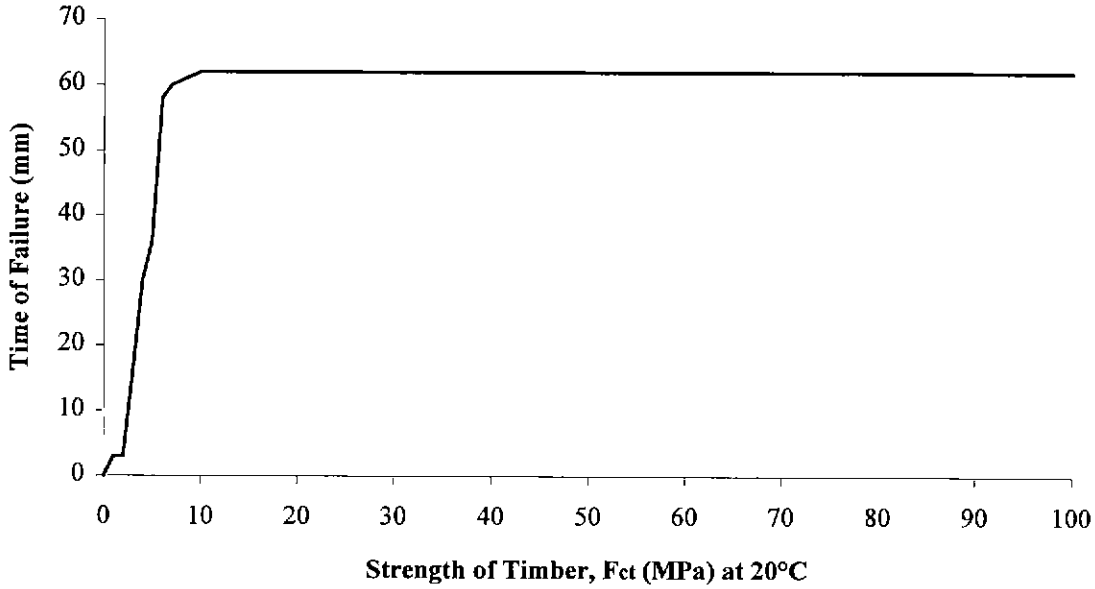

Figure 7.6. Time of Failure versus Strength of Timber, F_{ct} at 20°C.

7.6 Arrangement of Timber Framing - Wall Height, Support Conditions, Stud Depth, Stud Breadth, Stud Spacing and Initial Crookedness

Plot 1 (top continuous dashed line) was obtained with the time of failure model, ignoring any effects of moisture transfer.

As with any model validation, experimental results are desired. However, wall height was not varied in the experiments (§4) and thus a plot of observed failure times versus height could not be made for comparison with the plot predicted with the model. Nonetheless, the wall experiments involved different support conditions, from which the effects of wall height on the time of failure could be deduced. The height of the wall with fixed ends which would buckle at the same load as the pin-ended walls, was deduced as 6.0 metres from both the simple Euler equation (6.2) and the time of failure model. Hence, the middle dotted plot (2) through A (from fixed-ended Wall 6) and B (from pin-ended Walls 4 and 5) shown in Figure 7.7 was obtained.

Plot 3 was obtained by inputting measured temperatures into Young's (2000) structural model. The temperatures input, naturally incorporate the heat transfer due to the movement of moisture. The effect of moisture on stiffness was input in accordance with plot A in Figure 7.2.

Plot 4 was obtained with the time of failure model with allowance for the effects of moisture transfer including the increased rate of heat transfer (modification C , Figure 7.3) and the reduction in stiffness (plot A, Figure 7.2).

It can be concluded from Figure 7.7, that:

1. There is a good comparison between model predictions (plots 3 and 4) and experimentally based results (plot 2), and hence the figure gives confidence in the validity of the models for structural response (Young 2000) and for time of failure, for predicting failure time as a function of wall height.
2. By comparison of plot 1 with the other plots (2-4), it is apparent that the effects of moisture transfer on heat and stiffness should be considered for walls with heights exceeding 4 metres.

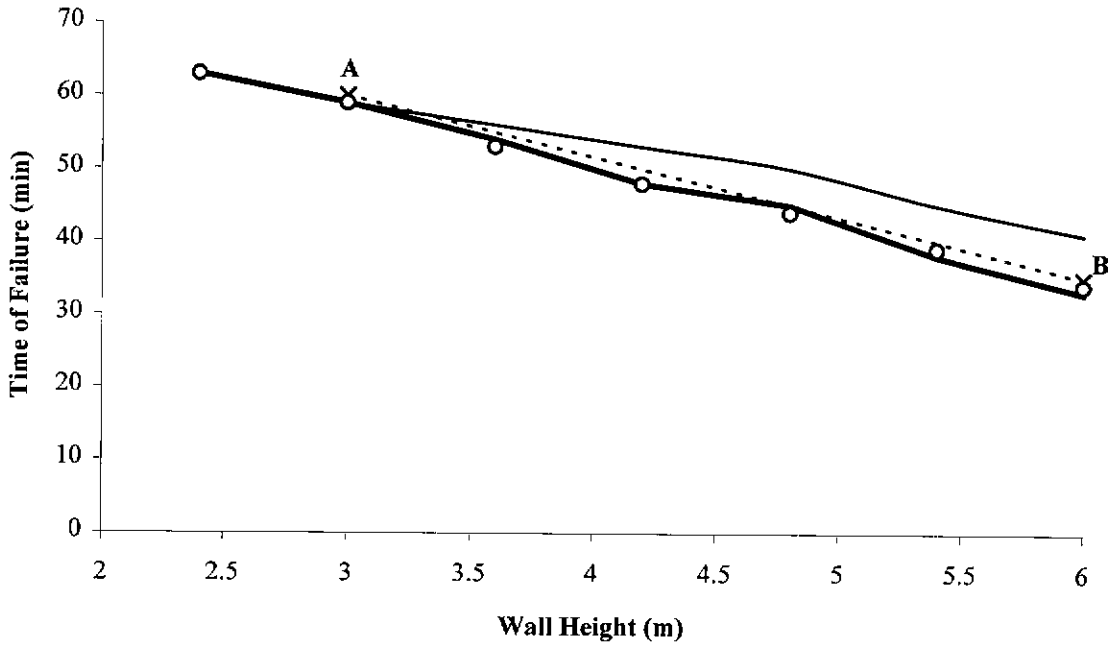

——— 1. Temperatures from ADIDRAS, moisture transfer ignored.

- - ✕ - - 2. Plot deduced from experimental results for Walls 4-6 (§4).

——— 3. Temperatures from tests in §4.

o 4. Temperatures input from ADIDRAS allowing for moisture transfer.

Figure 7.7. Effects of Wall Height on Time of Failure; that is for Walls with Top and Bottom Plates Fixed against Rotation, similar to Wall 6 (§4).

Stud Spacing

Figure 7.8 shows the effects of stud spacing on the time of failure. Practical spacings range between 300-600 mm (TPC 1994). Over this range, the time of failure is insensitive to the spacing of studs, particularly when the load per stud is constant. Another important observation is that studs must be very close, with gaps between studs less than 10 mm before the studs begin to behave as a slab of wood with predominantly one dimensional heat transfer. The reason for the insensitivity of time of failure to stud spacing must be the dominance of heat transfer through the cavity compared with heat transfer into timber.

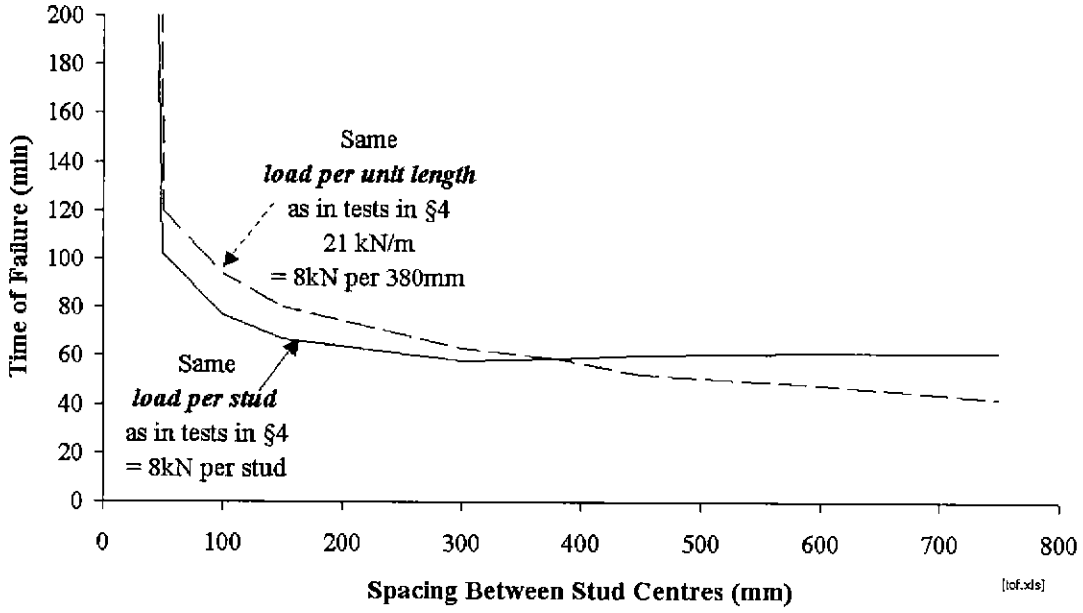

Figure 7.8. Effects of Stud Spacing on the Time of Failure.

Stud Size

Figure 7.9 and Figure 7.10 show the relative merits in increasing the depth and breadth of stud sections to achieve greater times of failure. Two factors determine the relative effects of depth and breadth. Firstly, from the two dimensional nature of heat transfer in studs, it would be expected that increasing stud breadth rather than depth would be more effective in increasing the time of failure. The second factor that counters the first, is stiffness, EI which controls buckling strength. Stiffness, EI increases with the cube of depth. It is thus not immediately obvious whether increasing the breadth or the depth, by the same proportion, is the more effective in increasing the failure time. The evidence in Figure 7.10 shows that for a 90x45mm stud section, a 50% increase in stud breadth (90x70mm) increases the time of failure the

same amount as shown in Figure 7.9 for a 50% increase in depth (140x45mm). For walls similar to Wall 6 (§4), it is apparent that the time of failure is similarly affected by similar percentage changes in breadth and depth of stud sections.

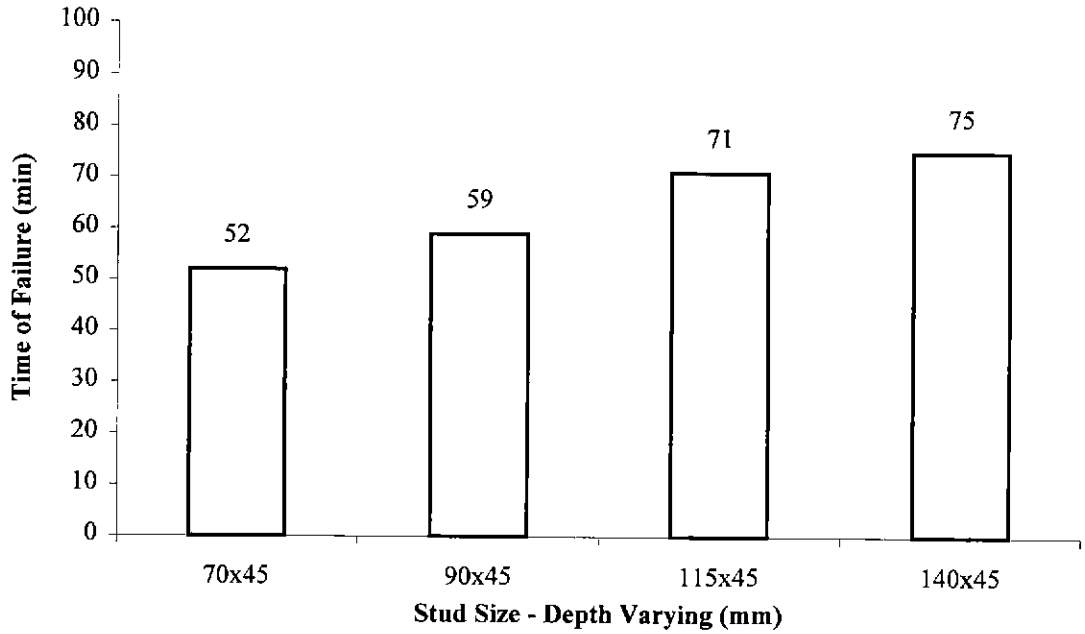

Figure 7.9. Increases in Time of Failure with Stud Depth.

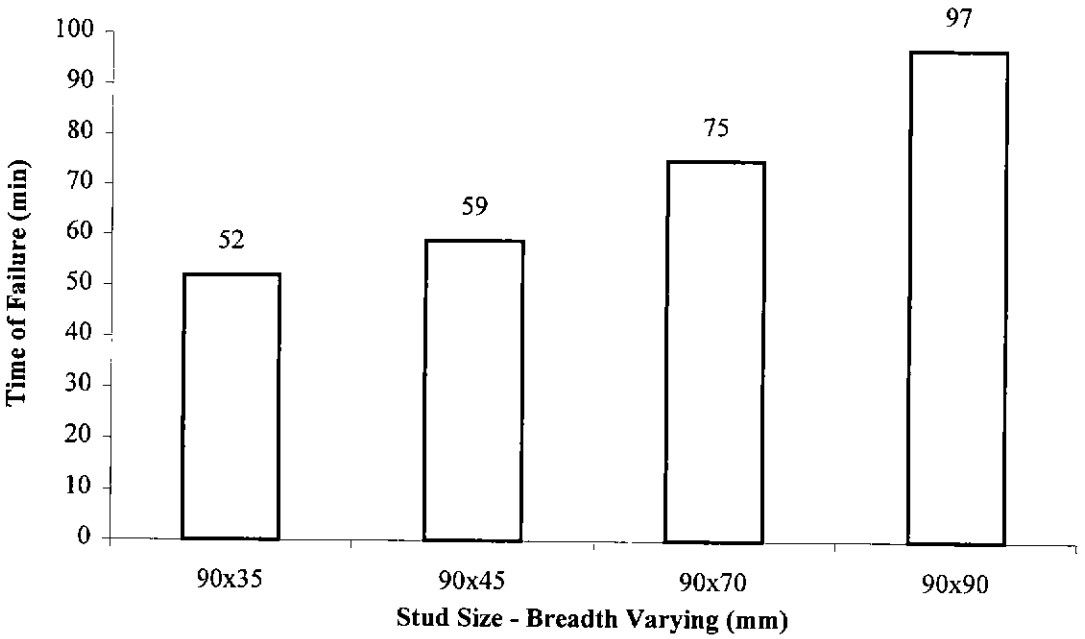

Figure 7.10. Increases in Time of Failure with Stud Breadth.

Initial Crookedness

No wall can be built perfectly straight, as a consequence of shrinkage, seasonal moisture movements, and limits to construction quality. Figure 7.11 shows the effects of initial crookedness on the time of failure of Wall 6 (§4). Crookedness is defined here as the amplitude of a bow which is assumed to be a half-sinusoid, with zero values at the top and bottom of a wall, and is a maximum at mid-height.

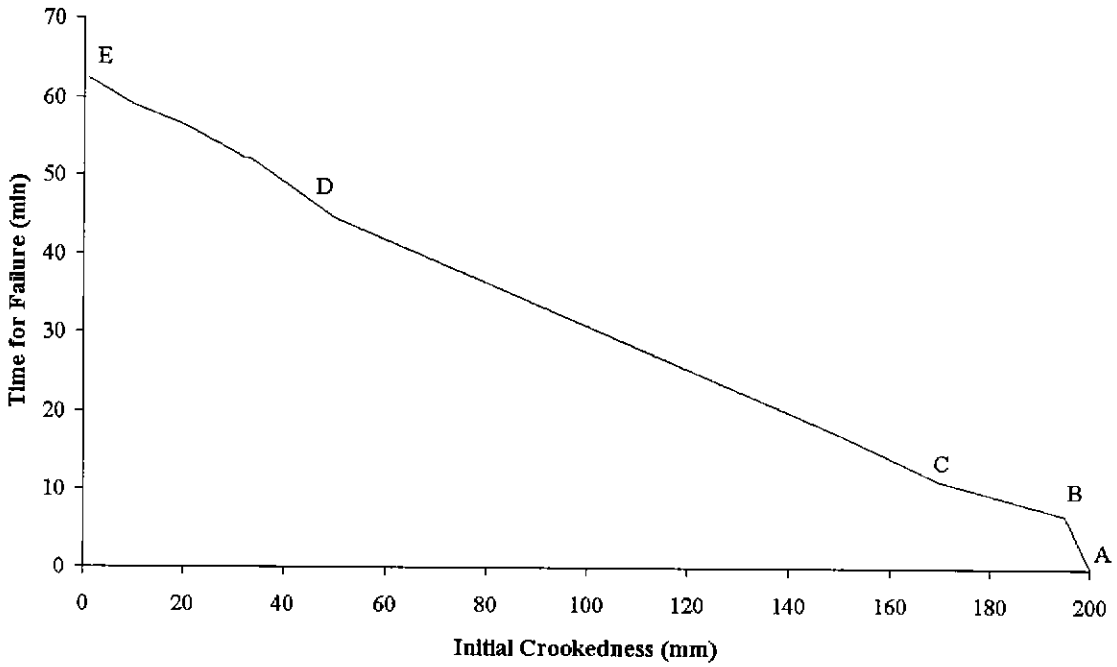

Figure 7.11. Effects of Initial Crookedness on the Time of Failure.

The effect of initial crookedness on the time of failure can be evaluated from Figure 7.11. As one would expect, the time of failure is generally inversely related to initial crookedness. The absence of noticeable changes in gradient along the plot AE, apart from that of segment AB, suggests that only one process is causing steady degradation. However, different processes must control the plot at different times.

Segment AB is controlled by the sudden degradation of mechanical properties of gypsum board on the fire side. At A, the effective structural wall section would have been a series of "I" sections comprising studs as the webs and gypsum boards as the flanges. At B the effective wall section would be a series of "T" sections comprising ambient facing gypsum board and studs. The contribution of gypsum boards on the fire side would have disappeared when the minimum temperature in the board reached approximately 100°C which was attained at 5 minutes (Figure 4.20).

From the rapid rise in temperatures from 20°-100°C in the stud shown in Figures 4.26 and 4.27, and the corresponding rapid fall in elastic modulus in compression for wood shown in Figure 7.2, it is apparent that segment BC is controlled by the effects of moisture movement on both heat transfer and stiffness reduction.

Segment CD would be controlled by moisture induced creep or plastification which results in the relationship for the elastic modulus of wood in compresssion following plot Y98 instead of Y96, 12% in Figure 6.9.

Finally, from Figure 4.26, it is expected that charring dominates the time of failure from approximately 45 minutes onwards as shown with segment DE.

7.7 Arrangement of Gypsum Board - Thickness and Number of Sheets of Gypsum Board

The effects of thickness and the number of sheets of gypsum board on the time of failure were computed with the model and are shown in Figure 7.12. Since times of exposure exceeded 60 minutes and cavity temperatures rose above 400°C (Figure 5.18), shrinkage gaps would be likely to open between the studs and the gypsum board on the fire side, and significantly affect the transfer of heat into the studs (§5.4.3). From the discussion in reference to Figure 5.20 a gap width of 3 mm was input into ADIDRAS. The model was also applied for the case of no gaps to evaluate the effects of gaps. Since load ratios were low (applied load /ambient strength = 8kN/96kN=2MPa/24MPa), much thermal degradation of the studs would occur prior to failure and the timber would thoroughly dry prior to collapse. Thus, moisture transfer was ignored.

The following observations can be made from Figure 7.12:

1. A small increase in the thickness of gypsum board significantly increases the time of failure. For example, an increase in thickness from 13mm to 16mm (that is, 23%) increased the failure time by 10 minutes (20%). An increase from 29mm to 32mm (10%) increased the time of failure by 12 minutes (11%).
2. The component additive method (White 1988a) for the fire resistance design of walls and floors assumes that the total fire resistance is conservatively the sum of the fire resistances of the components such as gypsum boards and studs in a wall. This method can be proven to be theoretically correct from equation (2.6). However, the predicted fire resistances for walls with total sheet thicknesses of 25, 29 and 32 mm, were marginally less than found by adding the fire resistances of the individual sheets. The main reason for the time of failure being less than expected was sloughing of the first layer of gypsum board. Sloughing occurs when the minimum

temperature in gypsum board exceeds 700°C (§5.5) which is approximately the melting point of glass fibres (Carne 1995) which hold the board together at high temperatures. If sloughing could be prevented until 800°C or higher, the time of failure would be greatly increased. If one attributes, say 5 minutes to the resistance of the studs and deducts the same amount from the fire resistance attributed to the gypsum boards, then the evidence in Figure 7.12 is that the component additive method is indeed safe, accurate and is not excessively conservative.

3. Shrinkage gaps significantly increase the time of failure by as much as 10 minutes in walls with a total thickness of gypsum board on each side greater than 25 mm. These walls have higher cavity and gap temperatures at failure and hence a greater proportion of the total heat in the gaps in these walls is transferred by radiation. As was discussed in reference to Figures 5.20-5.22, when the gaps reach temperatures greater than 400°C, radiation via the gaps transfers a significant proportion heat from the gaps to the cavities. At lower temperatures, when interfaces rather than the gaps are present, the dominant mode of heat transfer, thermal conduction, would have transferred virtually all of the heat flux at the interfaces to the studs and none to the cavities.

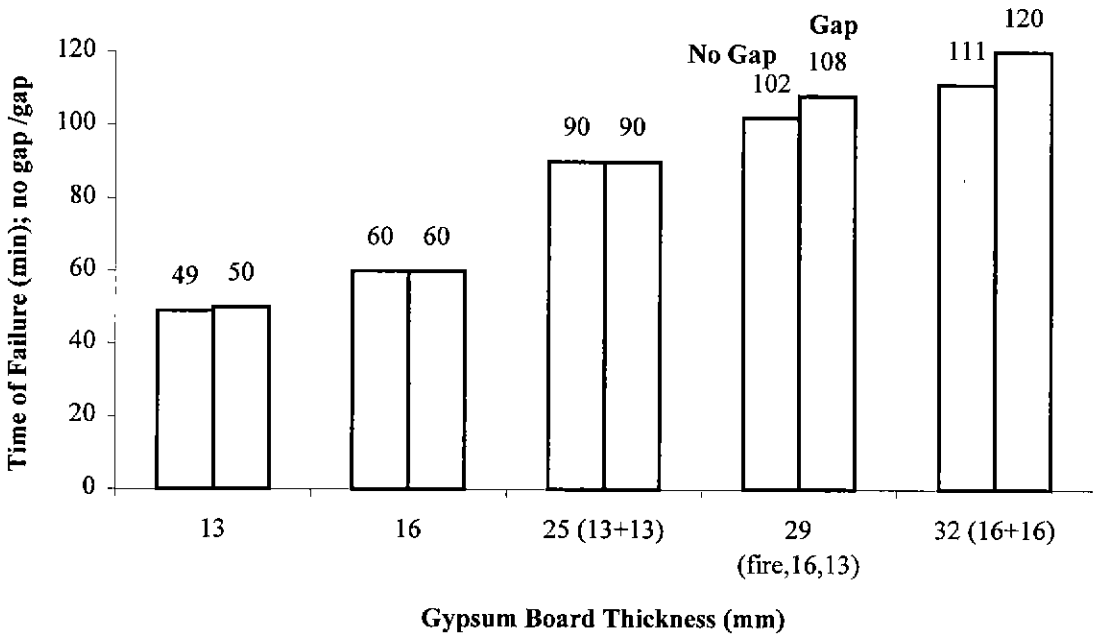

Figure 7.12. Effects of the Thickness of Gypsum Board on the Time of Failure. (Note that the numbers in brackets indicate the thicknesses of individual boards making up the total thickness. The first number refers to the board closest to the fire.)

7.8 Thermal Properties of Materials - Conductivity, Density, Specific Heat and Emissivity

Figure 7.13 shows the effects of a 20% change in thermal properties which reduce the time of failure. The two bars at the right are the known failure times from the wall experiments described in §4. It is apparent from the figure that reductions in the conductivities of materials have little effect on the time of failure, except for gypsum for which the time of failure reduced from 59 to 55 minutes. Even for gypsum, the reduction in the time of failure is 6% which is approximately 1/3 of the change in conductivity.

The product of density and specific heat, referred to here as enthalpy, had a larger effect on the time of failure. Enthalpy is defined here as the amount of heat absorbed by a material per degree rise in temperature. Low enthalpy leads to larger temperatures, larger temperature gradients and faster heat transfer. The reduction in the time of failure due to a 20% decrease in the enthalpy of gypsum, was 8 minutes or 14%. Thus significant improvements to the time of failure can be achieved by increasing the density of gypsum board. Changes in the enthalpy of char, and hence changes in the density of char have no discernable effect on the time of failure. A 20% decrease in the enthalpy of uncharred timber reduces the time of failure 5 minutes or 8%.

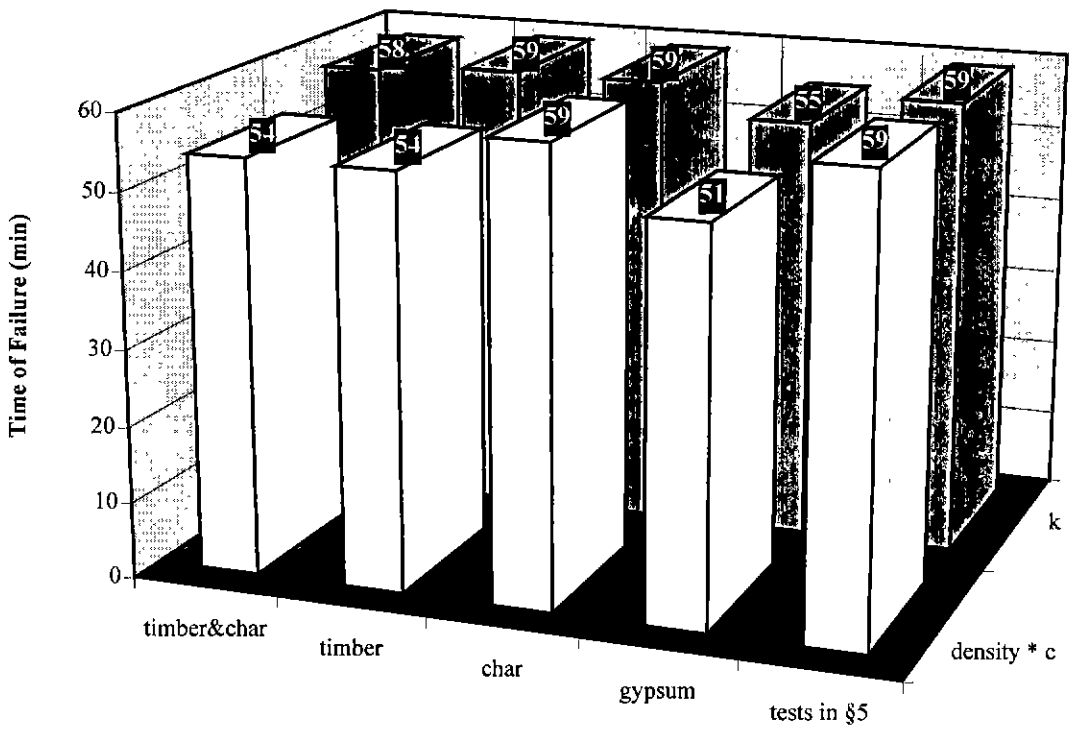

Figure 7.13. Effects of 20% Changes in Thermal Properties which Reduce the Time of Failure.

The effects of increased emissivity on time of failure were considered separately for the emissivities of fire, gypsum board and timber/char. The increases were a uniform amount of 0.2 above the values given in §5.2.2 for fire, §5.2.3.4 for gypsum board and §5.2.4.5 for timber/char, for all temperatures. There was no discernable change in the time of failure except when the emissivity of gypsum was increased. For this case, the time of failure reduced from 59 to 58 minutes. Thus emissivities increased by as much as 0.2 (~30%) above those given in §3.6.2, §3.6.3.4 and §3.6.4.5, reduce time of failure less than 2%. This result confirms that radiant heat transfer is a minor mode of heat transfer controlling the time of failure and hence, thermal conduction is the dominant mode of heat transfer through walls determining their time of failure.

From the above, it is apparent that variations in time of failure are no greater than 1/4-1/2 of the variations in thermal properties.

7.9 Fire temperature

The model predicted that a 20% increase in the fire temperatures for all times of exposure, in §4, would cause the time of failure to reduce from 59 to 48 minutes; that is a 19% reduction. Fire temperature is obviously the most dominant variable affecting the time of failure.

7.10 Conclusions

A time of failure model for the light timber framed walls in fire has been developed and can be used to replace much furnace testing. The time of failure model links particular models for heat transfer and structural response, and can be linked with any fire severity model which gives representative fire gas temperature with time, and gives emissivities. In this chapter, the standard fire relationship(AS1530.4) was adopted for the fire severity model. The heat transfer and structural response models have been validated by their authors. The model generally predicts times of failure consistent with experimental results in §4. All of the results in this chapter have been justified in discussions. Thus the linkage of the models within the time of failure model is generally validated within the limitations described below.

It was shown for Wall 8 (§7.3) that time of failure model had limited success in modelling the heat transferred by moisture movement and the consequential reduction in elastic modulus. However, for other walls which were of standard dimensions (3.00 metres high, 90x45mm studs) and in which gypsum board was conventionally fastened, the model was quite satisfactory. The sub-model used for including the heat transferred by moisture movement was modification C in Figure 7.3. The sub-model for including the

effects of creep was plot A in Figure 7.2. The comparisons with Wall 8 show that further research is required in modelling the effects of moisture movement.

Another limitation, is that the model has only been validated for structural collapse, in particular, buckling. The model does analyse the strength of walls and theoretically should accurately predict the time of failure when caused by inadequate strength. However, as shown in §7.5, strength seldom affects the time of failure.

The model has not been validated against experiments in which there were insulation and integrity failures. However, good general comparisons between temperature predictions of the heat transfer model, ADIDRAS and measurements from experiments (§4) give confidence that the time of failure model can be used to predict failure times for these modes failure.

As well as demonstrating the validity of the model, this chapter has demonstrated the efficacy of the model by determining the effects of a number of variables on the time of failure. This chapter thus provides valuable information for modellers and engineers with interests in fire resistant timber framed walls. This information includes the following conclusions:

1. The dominant mode of failure for many light-timber framed walls is structural collapse by buckling, and hence, the mechanical property of timber affecting the time of failure is the elastic modulus for compression. The strength of timber is unlikely to affect the time of failure (Figure 7.6).
2. For un-common walls which are taller than 4.0 metres or more heavliy loaded than is permitted in timber engineering codes such as AS1720.1, the effects of moisture transfer should be considered. These effects occur in the vicinity of moisture vaporisation and include the heat transferred by the movement of moisture and the reduction in the elastic modulus.
3. The time of failure is controlled more by heat transferred through solid material than by radiation through cavities and at external surfaces. The dominant modes of heat transfer through solid material are thermal conduction, conduction of moisture and vapour through pores, and as Fredlund (1988) showed for temperatures greater than 400°C, radiation inside pores.
4. For the wall studied and discussed in this chapter, similar percentage changes in depth and breadth of stud sections have similar effects on the time of failure (Figure 7.9 and Figure 7.10)
5. For the wall studied, the time of failure was inversely related to initial crookedness (Figure 7.11).

6. Time of failure is sensitive to the sloughing temperature of gypsum board. Time of failure would be increased if glass fibres or fibres made from other materials to maintain the integrity of gypsum board at high temperatures, could withstand temperatures greater than 700°C (§7.7).
7. If heat transfer analysis shows that cavity temperatures exceed 400°C for a significant period of time, modelling of small gaps (1-5mm) formed between timber and gypsum board due to char shrinkage, will lead to improved accuracy and significant (approximately 10 minutes) increases in predicted times of failure (Figure 7.12).
8. For the wall studied (§7.7), predictions with the component additive method were reasonably accurate and safe.

From the figures throughout this chapter, the sensitivities of the time of failure to a 20% change in a number of variables have been obtained and are summarised in Table 7.2. On the basis of these sensitivities, the following variables should be modelled probabilistically in the probability of failure model in chapter 8:

1. Fire temperature
2. Vertical load
3. Elastic modulus of timber in compression
4. Density of timber
5. Specific heat of timber

Failure time is also sensitive to stud depth, breadth, gypsum board thickness and height of wall. However, construction practices would not allow a random 20% variation of these variables. Control processes in the manufacture of gypsum board should prevent random 20% variations in its thermal properties Thus, these variables are not listed here.

Table 7.2. Changes in the Time of Failure (ToF) of Wall 6 in §4, Predicted with the Model for a 20% Change in the Variables Listed.

Variable changed by 20%	Change in ToF		Reference
	min	%	
Fire temperatures	11	19	§7.9
Vertical load	7	12	Figure 7.4
Elastic modulus of timber in tension	1	2	Figure 7.5 - D
Elastic modulus of timber in compression	10	17	Figure 7.5 - B
Compression strength of timber	0	0	
Height	1	2	Figure 7.7
Stud spacing	0	0	Figure 7.8 - dotted line
Stud depth	12	20	Figure 7.9 - 115x45
Stud breadth	7	12	Figure 7.10 - between 90x45 & 90x70
Initial crookedness	1	2	Figure 7.11 - 10 to 12mm
Gypsum board thickness	10	17	Figure 7.12- 13 to 16 mm
Conductivities:			
Gypsum	4	6	
Timber	0.7	1	Figure 7.13
Char	0.3	0.5	
Density x specific heat:			
Gypsum	8	13	
Timber	5	8	Figure 7.13
Char	0	0	
Emissivity:			
Gypsum	1	2	
Timber	0	0	Figure 7.13
Char	0	0	

8. Probability of Failure Model

8.1 Introduction

Background

In the introduction to this thesis, §1.1 it was explained that countries around the world are at various stages of introducing performance based regulations in their building fire safety codes. It was explained that two bases for performance are time of failure and risk of failure. Risk relates to some consequence such as death or property loss. To estimate risk, the probability of failure must be found. The focus of the research described in this chapter was on the development and application of a time dependent probability of failure model - that is, a model which estimates the probability of failure of light-timber framed walls with time of exposure to fire.

As well as the obvious purpose of a time dependent probability of failure model being used for design in accordance with risk based regulations, it would also be useful for determining times of failure which ensure adequate safety. For example, the use of standard fire tests, AS1530.4 is based on some implicit assumption that similar walls in similar fires fail at much the same time. A time-dependent probability of failure model will justify whether such an assumption is valid. It will not be valid if the coefficient of variation of the time of failure is different as shown in Figure 8.1. The figure shows probability density for the time of failure of two walls 1 and 2. Both walls have the same mean failure time. However, the times of exposure, t_1 and t_2, for which at least 95% walls can endure, are substantially different. The probability of failure model will enable the estimation of the time of failure required to ensure that a certain percentage of walls will not fail.

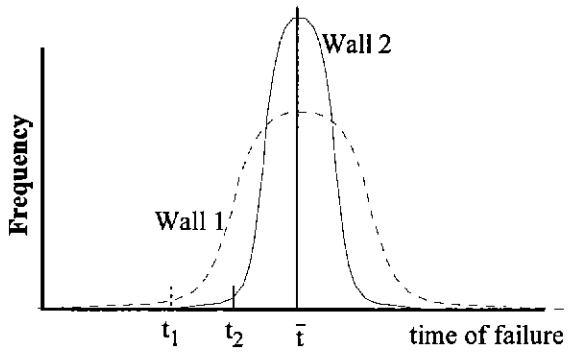

Figure 8.1. Demonstration of Inadequacy of Time of Failure Specification - Two Walls with Same mean Failure Time but Different Times, t1 and t2 at which 95% of Similar Walls Fail.

A further advantage of analysing probabilities of failure, is that such analysis gives a better indication of variations in the time of failure, than sensitivities to individual variables.

Aims

The general aim of the research described in this chapter, §7 was to advance the understanding of the probability of failure with time for timber framed walls in standard and real fires. The results of this section will thus give a better insight to rational design of timber framed walls for fire resistance. The particular aims of were to:

1. Develop a time-dependent probability of failure model. In the process, deduce the most appropriate method of analysing the probability of failure.
2. Deduce typical coefficients of variation, CoV's of thermal properties. CoV's are generally published for mechanical properties (§8.4) but not for thermal properties which are expensive and difficult to measure.
3. Show some typical plots of the probability of failure with time.
4. Obtain typical CoV's of time of failure for walls in standard and real fires.

Methodology

The uniqueness of the problem of estimating the probability of failure of walls in fire will be explained (§8.2.1). Consequently, a range of methods for the analysis of the probability of failure will be reviewed (§8.2.3 - §8.2.5) including reliability models for structures in fire (§8.2.7). The appropriate method of analysis will be selected (§8.3.1) and the overall probability of failure model explained (§8.3.2). Details of the probability of failure model will be given, including failure criteria(§8.3.2), random variables (§8.3.3), method of generation (§8.3.4). Finally, the efficacy of the model will be demonstrated with several applications (§8.4), and conclusions will be drawn (§8.5).

8.2 Literature Review

8.2.1 General

A review of papers published in the last 10-15 years in leading journals and monographs on the probability of failure, including Structural Safety, Reliability and Systems Engineering, Melchers (1987), Civil Engineering Transactions (1986), ASCE Journals of Structural Engineering, and Engineering Mechanics, revealed that there were only a few types of analysis with any relevance to the problem of estimating the probability of failure of structures in fire with time. These analyses were concerned with:

1. Fatigue.
2. Extreme stochastic events.
3. Service life of structures (de Kraker et al 1982, Geidl 1987, Sentler 1983).

Hasofer (1996) concurred with this finding. The loads for these analyses are stationary and ergodic; that is, they are random with time without having any trend which changes their statistical properties such as the mean and coefficient of variation. Compared with these three types of analysis, the analysis of time dependent probability of collapse of structures in fire is different in several respects. The load for structures in fire is not only the applied dead and live loads which the structure supports, but also the fire to which the structure is exposed. Fire is not a stationary ergodic process. It involves a period of increasing deterioration but eventually ceases. Fire exposure is a much more complex process than the application of dead and live loads. Very little research has been undertaken for structures that detriorate with time except for de Kraker who mentioned that the deterioration of structural resistance during the life of a structure could be approximated with some simple function. Currently, no such simple functions for the deterioration of structures in fire, particularly real fires, exist.

Two reports were found, Woeste et al (1981) and Bender et al (1985) (§8.2.7) which document models for estimating the probability of failure of timber beams and floor trusses in standard fire with time. However, these models used simple time of failure equations derived from constant char rates for large timber sections for which the following assumptions are made:

1. Heat transfer is approximately one dimensional.
2. Strength can be estimated assuming that uncharred wood does not have thermally reduced mechanical properties.

They did not consider the detailed phenomena and complex numerical analysis for light framed timber structures in real fire, for which these assumptions are not valid.

It is thus appropriate to review a range of methods for analysing the probability of failure of walls in fire with time, in order to deduce the most appropriate method to adopt for the probability of failure model. The methods reviewed in §8.2.2 - 8.2.5 were obtained from Leicester (1985), Melchers (1987), Melchers (1985) and Benjamin and Cornell (1970), all of whom provide a good introduction to reliability analysis of structures.

8.2.2 Description of Problem of Evaluating the Probability of Failure with Time.

Failure occurs when applied actions, S exceed the resistance, R. In structures S and R are expressed in terms of actions including external forces and bending moments. For barriers in fires, S and R also include temperatures used to define modes of failure such as insulation and integrity. Temperatures here will also be considered under the general term, actions. The same actions are used to define both S and R. S and R have probability distributions, $f_S(x)$ and $f_R(x)$ respectively which are functions of the actions

represented by the vector, x. Examples of these distributions when x is a single variable, are shown in Figure 8.2. For example, x could be compression. The action would be the applied compression load, x_S and the resistance would be the compression load capacity, x_R.

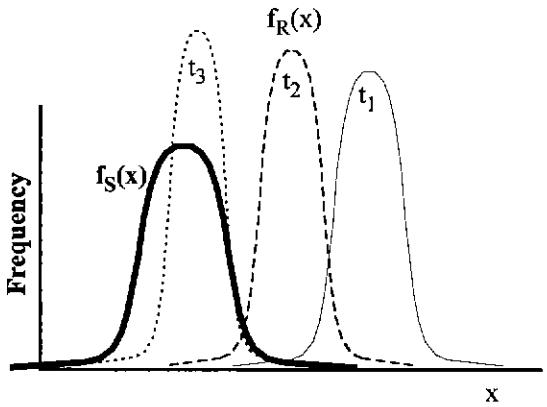

Figure 8.2. Probability Density Distributions for the Action on, and the Resistance of a Structure at Successive Times t_1, t_2 and t_3.
(The distributions are a function of one variable.)

Generally x_R is greater than x_S and the structure is stable. In fire, the structure degrades and the resistance, R moves to the left, with time. The mean reduces and the variance changes. If heat penetrates the structure quickly, the variance reduces with time. The probability of failure increases until failure occurs or the fire decays and the failure probability reaches some time-independent maximum less than 1.00. The probability of failure, p_f at any time can be expressed as,

$$p_f = P(R - S \leq 0) \qquad (8.1)$$

Methods for solving equation (8.1) can be categorised into:

1. Convolution methods
2. Transformation methods
3. Simulation methods

These methods are discussed in more detail in the following sections.

8.2.3 Convolution

The probability of failure for a particular value of x_S can be deduced from Figure 8.3. Failure occurs if x_R is less than x_S. The probability that x_R is less than x_S is the cumulative probability for R from $-\infty$ to x_S.

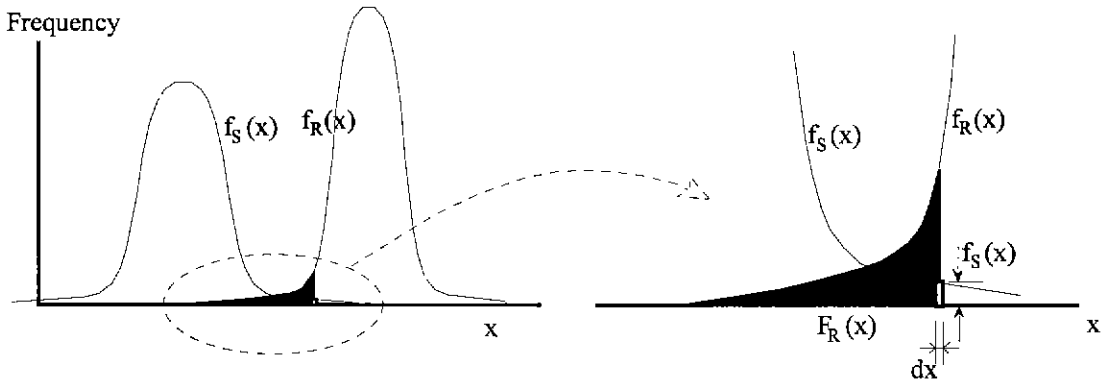

Figure 8.3. Probabilities Involved for a Case when Resistance, x_R is Less than a Particular Applied Action, x_S.

The probability that the applied actions equal x_S is $f_S(x_S).dx_S$. Thus the probability of failure for a particular value of x_S is,

$$dp_f = F_R(x_S).f_S(x_S)dx_S \qquad (8.2)$$

The total probability of failure for all possible values of x_S is thus

$$p_f = \int_{-\infty}^{\infty} F_R(x_S).f_S(x_S)dx_S \qquad (8.3)$$

Equation (8.3) is a convolution integral for one variable. These integrals are usually too intractable for closed form solutions and are thus usually solved numerically. To determine the probability of failure with time, convolution would have to be repeated at successive times as R moves to the left.

An example of the probability distributions for S and R for a vector, $\boldsymbol{x}$ comprising two variables, x_1 and x_2 is shown in Figure 8.4. It can be appreciated from the figure that as the number of variables increases in the vector $\boldsymbol{x}$, the complexity of integration greatly increases. Furthermore, as the number of variables increases, there is more chance that some variables will be related. For example, conductivity usually increases with density (equations 2.39 and 2.40). Variables which depend of each other are referred to as dependent variables. Melchers (1987) advises that convolution can be applied for a practical maximum of five variables in $\boldsymbol{x}$. All variables should be either independent or normally distributed which is often not realistic.

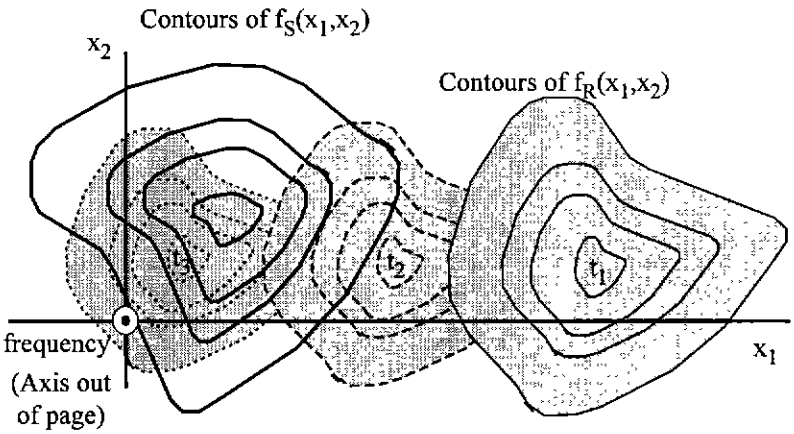

Figure 8.4. Probability Density Distributions for the Applied Actions, and the Resistance of a Structure at Successive Times t_1, t_2 and t_3.

(The distributions are a function of a vector, x comprising two variables, x_1 and x_2.)

Considering the complexity of convolution and the necessity to repeat it at different times to obtain the probability of failure with time, convolution, although direct, is not a practical method to adopt for the probability of failure model. Convolution is less practical considering the need to repeat it with time, such as for successive times t_1, t_2 and t_3 in Figure 8.4 as the resistance distribution moves to the left as the wall degrades in the fire.

8.2.4 First Order Second Moment Methods (FOSM)

Benjamin and Cornell (1970) described an early approach to first order second moment relaibility analysis (FOSM). It involved the estimation of the convolution integral for the probability of failure by combining the probability distributions for variables in accordance with well established rules for finding means and variances given in equations (8.4)-(8.7) below.

$$E(a.x_1 + b.x_2) = a.\bar{x}_1 + b.\bar{x}_2 \quad (8.4)$$

$$E(x_1 * x_2) = \bar{x}_1 * \bar{x}_2 \quad (8.5)$$

$$Var(a.x_1 + b.x_2) = a^2.Var(x_1) + b^2.Var(x_2) \quad (8.6)$$

$$\mathrm{Var}(x_1.x_2) \approx \bar{x}_1^2\mathrm{Var}(x_1)+\bar{x}_2^2.\mathrm{Var}(x_2) \quad (8.7)$$

Since then, FOSM has been advanced, and involves the transformation of variables. The transformation FOSM method is introduced here for independent normal and lognormal random variables, to give a simple overview of the method. Following this overview, the application of this method for realistic variables which may not be distributed normally or lognormally, and may have dependencies on other variables will be discussed. Considerations in using the transformation method for the probability of failure model will then be given.

A graphical overview of the transformation method for independent normal and lognormal variables is given in Figure 8.5. Figure 8.5 (a) shows that there is some joint probability density function, g(x) for all the variables which are needed to estimate whether failure occurs. The figure is for a vector x with two variables, x_1 and x_2. Failure occurs when some function, G is less than zero. An example of a failure function, G for a slender wall loaded vertically and concentrically by a load, W (N) is,

$$G = \frac{\pi^2 EI}{L_e^2} - W \quad (8.8)$$

where E = elastic modulus of structural material (Pa)
I = second moment of area of structural section (mm^4)
L_e = effective length (m)
W = load (N)

The stochastic variables are E and W. Equation (8.49) simplifies to,

$$G = K.E - W \quad (8.9)$$

where K = constant relating elastic modulus to wall buckling strength (mm^2)

Variables E and W can be replaced with the notation, x_1 and x_2 respectively as follows,

$$G(x) = K.x_1 - x_2 \quad (8.10)$$

The aim of the transformation method is to estimate the probability of failure which is the volume under g(x) in the region where G is negative - the shaded region in Figure 8.5(a). The method greatly simplifies the computation of this volume by transforming x or the logarithms of x to standard normal variables, y in accordance with the following equation,

$$y_i = \frac{x_i - \mu_{x_i}}{\sigma_{x_i}} \qquad (8.11)$$

where μ_{x_i} = mean value for variable, x_i.

σ_{x_i} = standard deviation of variable, x_i.

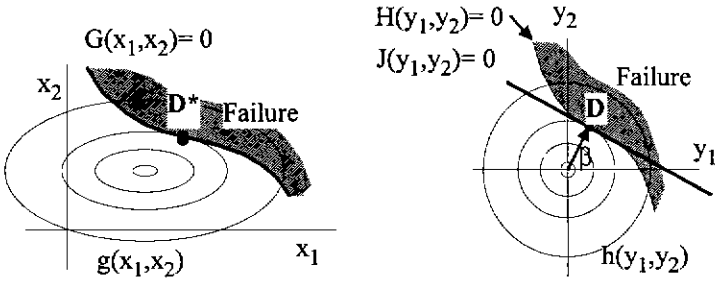

Figure 8.5.

(a) Joint Probability Distribution, g for Two Independent Variables, x_1 and x_2.

(b)Transformation of g(x) to h(y) in accordance with Standardised Normal Probability.

The transformation produces the probability distribution, h(y) and the failure function, H(y) shown in Figure 8.5(b). The probability of failure is thus the volume under h(y) where H(y) is negative. Since the probability density reduces rapidly with distance from the origin, the volume is closely approximated by the volume beyond the tangent J(y) at the point D on the hyperplane, H(y) equal zero, which is closest to the origin. This property of D, being closest to the origin, enables a simple fast search routine. The distance between the origin and D, in terms of the number of standard deviations, is β. The probability of failure, p_f beyond J into the main body of the failure region is thus,

$$p_f = 1 - F_h(\beta) \qquad (8.12)$$

where $F_h(\beta)$ = the cumulative probability in the safe domain

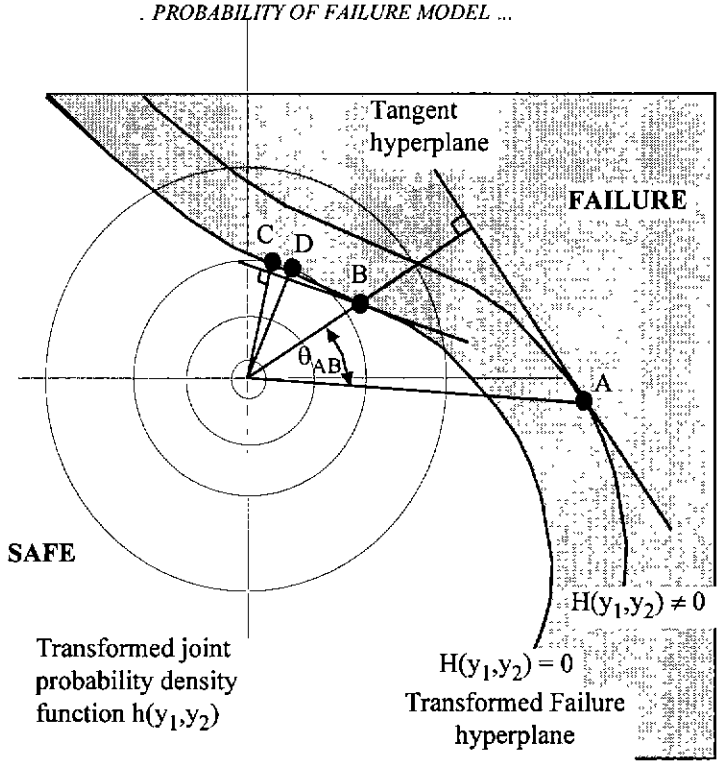

Figure 8.6. Simple Fast Search Routine for Finding β.

The transformation method finds the shortest distance, β between the origin and H, by the following iterative steps which are shown graphically in Figure 8.6.

1. Some initial arbitrary, reasonably sensible, guess of the values for *y* is made, such as point A in Figure 8.6.
2. These values are sufficient to determine a value for H. At this stage, H will likely have a non-zero value. However, the hyperplane for H with this value should be reasonably parallel to the hyperplane for H equal to zero, and will enable the iteration to proceed towards the point closest to the origin.
3. The equation for H enables the direction cosines of $\theta_{AB}(y_i)$ to be obtained for the line through the origin, normal to the hyperplane tangential to H at A. The distance, that is equal to β, is found by iteration of alternative points along this line until H equal to zero is obtained.
4. Steps 2-3 are repeated until no smaller value for the distance from the origin to the hyperplane for H equals zero, can be obtained. In Figure 8.6, this point is D.

The above description of the transformation method neglects some features of realistic variables. Such variables have dependencies amongst each other, and do not necessarily have normal or lognormal distributions. The probability density functions for realistic variables can show characteristics in Figure 8.8(a). Ridges in the density function, which are not parallel to one of the axes for the variables, result from dependencies between variables. The transformation method requires a set of independent variables

which can be used to fully define the probability density function, f(x) in Figure 8.8(a). The method also requires that marginal probability density functions for all of the variables be expressed as normal or lognormal functions. The marginal functions, $f_i(x_i)$ which are not, are changed to normal or lognormal functions $g_i(x_i)$ so as to have the same area under the tail beyond point D as shown in Figure 8.7. However, the position of point D is not apparent until after the standardising transformation from Figure 8.8(b) to (c). The position of D and the value of β can be solved either by iteration between Figure 8.8 (a), (b) and (c), or by finding D from Figure 8.8 (a) by searching for the maximum ordinate of f(x) along the hyperplane, G(x) equals zero.

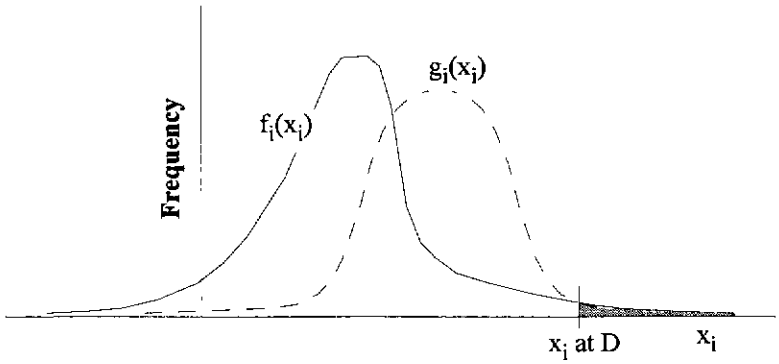

Figure 8.7. Normal Distribution, $g_i(x_i)$ with Area Under Tail Beyond x_i at D (Figure 8.6), the Same as for the Actual Probability Distribution, $f_i(x_i)$.

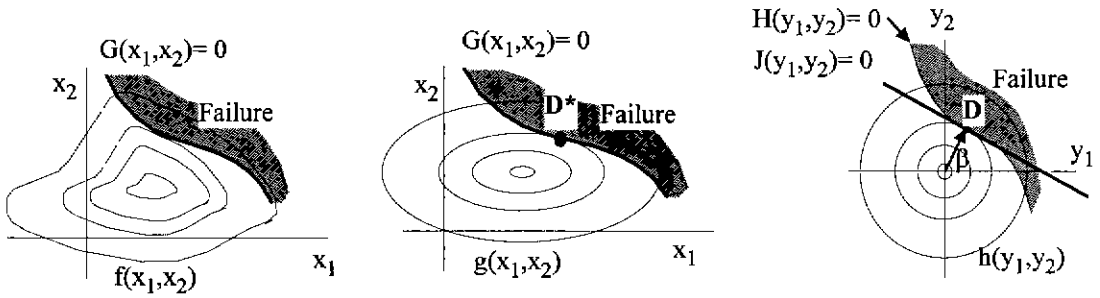

Figure 8.8.

(a) Joint Probability Density Distribution, f (x) and Limit State Function, G for Realistic Variables, x.

(b) Transformation Resulting in all Variables Normalised and Independent with Similar Volume in Shaded Region to that in (a).

(c) Transformation of g(x) to h(y) in accordance with Standardised Normal Probability Equation (8.11).

The following considerations are relevant to whether the transformation method should be adopted in the probability of failure model:

1. The transformation method is a fast method for solving the probability of failure.
2. The method can have numerical instabilities if the failure function, G is highly non-linear.
3. The method can only be applied for a particular time, and therefore must be repeated to obtain the probability of failure with time.
4. Without undertaking simulations, it is difficult to obtain marginal probability distributions with time for variables which are affected by fire.
5. Formulation of a failure function, G which represents the complex numerical analyses in the fire severity, heat transfer and structural response models is impractically difficult.

8.2.5 Monte Carlo Methods

8.2.5.1 Basic Monte Carlo Method

Monte Carlo methods are alternatively known as simulation methods. These methods are well known. A simple example for which the method can be used, is the determination of the bias in a die. Repeated throwing of the die will eventually determine the probabilities of throwing each of the numbers 1-6. The likening of these simulation methods to gambling has obviously led to the naming of the method, Monte Carlo. In reliability problems, simulations are more complex than the throwing of a die. They involve the generation of stochastic variables, the execution of a model and the recording of outcomes. Those variables which are random, have to be identified (§8.2.6). Each simulation involves the random generation of these variables in accordance with their probability distributions (§8.2.5.2). Usually there are more than six possible outcomes. Monte Carlo methods usually require many simulations. The number required is discussed in §8.2.5.3. Each simulation can take considerable computation time. To carry out a Monte Carlo reliability analysis in a reasonable period of time - within an hour or a day - either the modelling may have to be simplified (§8.2.5.4) or the number of simulations reduced (§8.2.5.5).

Following the completion of a Monte Carlo analysis, the probability of failure, p_f is simply determined from,

$$p_f \approx \frac{1}{N}\sum_{i=1}^{N} I[G(x_i) \le 0] \qquad (8.13)$$

where N = the number of simulations

I[ ] = an indicator function which has a value of 1.00 when the contents of the brackets is true and 0.00 when the contents are false.

x_i = is the generation of vector x for the i'th simulation.

8.2.5.2 Generation of Random Variables.

Generally, two types of random variables are generated - independent and dependent random variables. The generation of independent random variables, x_i is carried out as shown in Figure 8.9. The probability density functions, $f_i(x_i)$, shown in Figure 8.9(a), should preferably be obtained from many tests or surveys, for example, tests by Lau (1996). If tests or surveys cannot be undertaken, recommendations for $f_i(x_i)$ from the literature such as Pham (1985) should be sought. The literature usually gives the mean and the second moment, often in the form of the coefficient of variation, CoV. The CoV is the quotient of the standard deviation and the mean. If recommendations are not available in the literature, Bayes' theorem (Melchers 1987) shows that engineering judgement can be used to obtain $f_i(x_i)$; some reliability analysis provides a better basis for decision making than pure intuition. The cumulative probability ditribution, $F_i(x_i)$ is then created from $f_i(x_i)$ as follows,

$$F_i(x_i) = \int_{-\infty}^{x_i} f_i(\chi)d\chi \qquad (8.14)$$

$F_i(x_i)$ cannot always be expressed as a closed-form equation, in which case it must be an array of values coupled with x_i values. Generation is carried out by assigning a value for $F_i(x_i)$ from a number, R generated randomly between 0 and 1, that is,

$$F_i(x_i) = R \qquad (8.15)$$

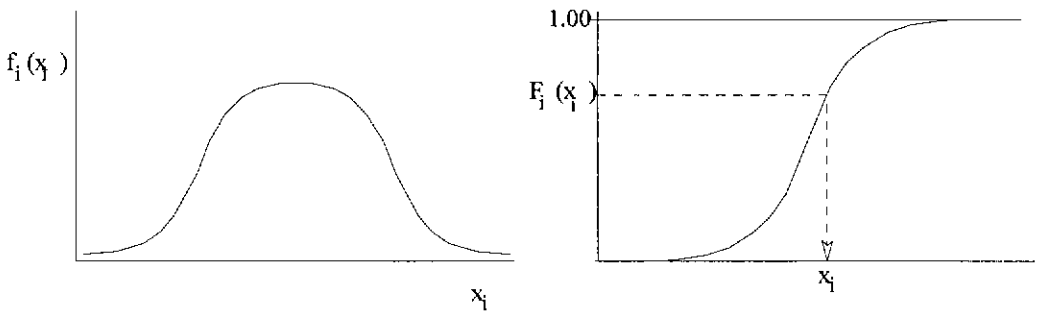

Figure 8.9. (a) Marginal Probability Density Function, f_i for Random Variable, x_i. (b) Generation of Random Variable, x_i from its Cumulative Probability Function, F_i.

Finally, from the inversion of the relationship in equation (8.15), x_i can be obtained from $F_i(x_i)$. This procedure is shown in Figure 8.9(b).

Random number generation is available through algorithms in the literature or more conveniently, in computer languages. Care must be taken in random number generation. It should be applied a large number of times to generate a histogram of generated numbers between 0 and 1 to ensure there is no bias towards any particular ranges of values. Random number generators have a cycle after which they repeat the numbers generated. The number of generations per cycle must exceed the number of Monte Carlo simulations required to ensure the accuracy required (§8.2.5.3).

There are a number of methods for generating dependent random variables. Normally distributed dependent random variables can be directly generated if their covariances are known (Melchers 1987, pp367-371). However, the covariances and correlations only indicate whether there is linear dependence between variables. They do not indicate relationships (Melchers 1987, p 350).

Another method is the use of a random parameter (Lehoczky 1990). This method involves the adoption of some deterministic relationship, $\xi(x_{ind})$ for the mean of the deemed dependent variable, x_{dep} in terms of the deemed independent variable, x_{ind}. The random parameter, α has a mean of 1 and an appropriate probability distribution. After generating the random parameter and the independent variable, the dependent variable is found from,

$$x_{dep} = \alpha.\xi(x_{ind}) \qquad (8.16)$$

In §8.2.5.5, importance sampling which is a method for reducing the number of simulations required, is reviewed. If importance sampling is adopted, the need to generate dependent random variables can be avoided by creating an importance sampling function, $\zeta(v)$ with all independent variables. Apart from avoiding the direct generation of dependent random variables, importance sampling has the additional attraction of being able to indirectly generate non-linear dependencies.

8.2.5.3 Number of Simulations Required

The number of simulations must be sufficiently large to ensure that the scope of error is within acceptable confidence limits. Melchers (1987, p93) deduced on the basis of the Central Limit Theorem, the probability density of predictions of failure by the Monte Carlo method is approximately normal irrespective of whatever the probability density function $f_i(x_i)$ (Figure 8.9 a) is for the prediction of failure. Thus, given that for any N simulations, the predicted probability of failure is p_f and the standard deviation for the prediction is σ, the confidence level that the prediction of the probability of failure from Monte Carlo analysis will be within a range of $\pm k.\sigma$ of actual probability of failure, μ can be found from,

$$C = P(-k.\sigma < p_f - \mu < +k.\sigma) \quad (8.17)$$

where C is the confidence level. Shooman (1968) showed that σ can be estimated from binomial theory as follows,

$$\sigma = \left(\frac{(1-p_f).p_f}{N}\right)^{0.5} \quad (8.18)$$

from which it can be shown that for a particular sequence of N Monte Carlo simulations, the error will be $\pm\eta$ for confidence level, C. The error, η is found from,

$$\eta = k.\left(\frac{1-p_f}{N.p_f}\right)^{0.5} \quad (8.19)$$

An example demonstrating the relationship between the number of simulations, confidence level and error is as follows. From equations (8.17) and (8.19), 10^5 simulations, a probability of failure of 10^{-3} and a confidence level of 95%, the error in the predicted probability of failure is within ±20%. Many more simulations are required to reduce this likely maximum error because error reduces inversely proportional to the square root of N.

Broding et al (1964) suggested that the minimum number of trials should be,

$$N > \frac{-\ln(1-C)}{p_f} \quad (8.20)$$

for which the anticipated probability of failure is substituted for p_f. For a confidence level of 95%, equation (8.20) suggests that the minimum number of trials should be $3/p_f$; for example 3000 for a p_f of 10^{-3}. Other authors (Mann et al 1974) have suggested that N must be in the range of $(10/p_f)$-$(20/p_f)$.

8.2.5.4 Response Surface Method

Application of the response surface method (Rajashekhar and Ellingwood 1993, Bucher and Bourgund 1990) would involve the development of an empirical model for G(x) obtained from a number of simulations to obtain times of failure. Only the dominant variables should be used in formulating G(x). The number of simulations would have to be sufficient to allow G to be determined from the empirical model for the great range of possible randomly generated vectors, x. The method is limited to G functions for which the number of basic variables in x is small and G is reasonably regular; that is, it does not have

extreme non-linearities. The empirical model can then be used in FOSM, transformation or Monte Carlo reliability analyses.

8.2.5.5 Importance Sampling

The number of simulations can be greatly reduced with importance sampling. This method basically employs the principle of conditional probability. Instead of generating data from f(x), data is generated from a joint probability sampling function, $\zeta(v)$, shown in Figure 8.10. In loose terms, the actual probability of failure for any simulation generated by a sampling function is the product of the proportion of simulations by the sampling function which lead to failure, multiplied by the conditional probability of the simulations being generated from f(x) in the region of the sampling function. In rigorous terms, the probability of failure for any v_i generated by a sampling function is,

$$p_f = \int \cdots \int I[G(v) \le 0] \frac{f(v)}{\zeta(v)} . \zeta(v) dx \qquad (8.21)$$

where I[ ] is an indicator function with a value of 1 for failure and 0 for success. In discrete terms for Monte Carlo simulations, equation (8.22) can be approximately solved numerically with the expression,

$$p_f \approx \frac{1}{N} \sum_{i=1}^{N} \left\{ I[G(v_i) \le 0] \frac{f(v_i)}{\zeta(v_i)} \right\} \qquad (8.22)$$

Importance sampling can reduce the number of simulations required to just 10-100, to estimate the probability of failure of 10^{-3}, with a confidence level of 95% and within an error of ±20%, provided the sampling function is chosen carefully. Otherwise, the sampling function can actually increase the number of simulations required. Ideally the importance sampling function should be centred on the point, D (Figure 8.6 and Figure 8.8) along the failure plane (G=0) where f(x) is a maximum which, Melchers (1987) advises, can be found with existing numerical maximisation computer programs. He also recommends that the sampling function be chosen with variances for the variables similar to those in f(x), but without any dependencies between them to simplify the generation of values (§8.2.5.2). Such an importance function would have the shape of a hyper-elliptoid with all axes of symmetry parallel to axes representing variables.

To estimate the probability of failure with time, the importance sampling function would have to have sufficient variance to cover the range of failure times within the range of failure probabilities which are of concern. Alternatively importance sampling analyses would have to be repeated with different sampling functions to cover the time range required.

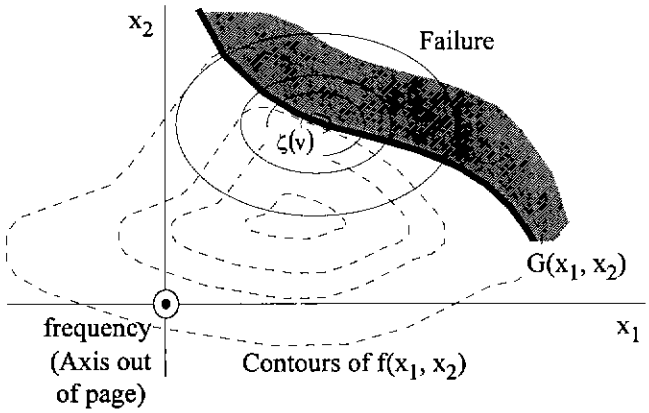

Figure 8.10. Importance Sampling Function, $\zeta(v)$.

8.2.6 Selection of Variables to be Modelled as Random

As indicated in §8.2.3 and §8.2.4, to prevent reliability analyses becoming excessively complex, only dominant variables should be modelled as random variables. The dominant variables are determined by sensitivity analyses such as those in §7. A variable is dominant when the object of the reliability analysis - the time of failure - is significantly affected by changes in the variable. One should take care to judge how large these affects and changes should be, when deeming them significant. One should also consider the appropriate level of refinement (§7.1) which should be generally consistent across all models in the probability of failure model.

As well as sensitivity, one should consider the variability of variables. If time of failure is sensitive to a variable, but that variable has little variance, it should not be modelled as a random variable. Conversely, if the variance of a variable is large enough to significantly affect the time of failure despite it being one of the less dominant variables, it should be modelled as a random variable.

Variables recommended by various researchers, to be modelled as random variables are given below. Their recommendations are based on sensitivity and variability.

Jönsson and Pettersson (1985) outlined the following which should be considered as random variables in a probability of failure model of light timber framed walls:

(a) Regarding fire severity - fire load, ventilation and thermal properties of wall components;
(b) Regarding structural response - structural geometry and imperfections, mechanical properties of components and structural load; and
(c) A factor accounting for the level of crudity of the model.

Melchers (1987 pp52-65) discusses in some detail a number of other uncertainties for which random variables should be considered including uncertainties with phenomena, decisions, predictions based on information that may change in the future, adoption of idealised probability functions to represent real statistics and human factors.

No literature seems to make reference to the uncertainty in heat transfer rates through walls as a result of service penetrations.

8.2.7 Probability Models Developed in Fire Research

Some of the earliest research into time dependent probability of failure of timber structures in fire seems to be a model for floors developed by Woeste and Schaffer (1981). The scope of the model includes light timber truss floors with continuous chords and concentric connections which induce bending and tension in the members of the truss. The model applies for standard fires (ASTM E 119). The failure function, G was derived from basic structural mechanics in terms of time of failure, net cross-sectional area of member sections, applied load, bending moment, tension and ambient mechanical properties. An empirical model based on experiments by Schaffer was used to determine net sections. No reduction of mechanical properties with temperature was adopted. Time of failure was conservatively predicted due to omission of any modelling for load sharing in the failure function. The probability of failure was estimated at various stages in time in accordance with a method similar to the FOSM described by Benjamin and Cornell (1970).

Bender et al (1985) developed a model to estimate the probability of failure with time for glulam beams in standard fire. They derived a failure function assuming a constant char rate. They incorporated the failure function into a Monte Carlo analysis.

Jönsson et al (1985) gave a review of methods for designing load bearing structures according to First Order Second Moment (FOSM) probabilistic methods. This review included the research of Magnusson et al (1976), Petterson et al (1978), Magnusson et al (1977), DIN 18230, Magnusson et al (1981), Petterson (1981), CIB W14, Brozetti et al (1983) and Petterson et al (1983). As pointed out in §8.2.4, the main problem with FOSM methods is the lack of knowledge of marginal probability distributions for random variables.

Beck (1986) developed a model for assessing the risk to life, from building fire safety systems comprising passive systems such as barriers and active systems such as sprinklers, smoke control, occupant response. He estimated the maximum cumulative risk by the stage the fire had extinguished. He referred to this risk as, time-independent risk. His failure function was a stochastic state transition model

which is a tree of all possible events. The base of the tree corresponds to the commencement of the fire and the ends of the branches corresponds to the end of alternative fire scenarios and sequences of events. He applied FOSM to his failure function.

Hasofer (1995) developed a stochastic model for real fires. The model did not aim to predict failure but rather stochasticly generate a gas temperature-time relationship for a real fire in a building enclosure. He based his model on the NRCC single zone real fire model (Takeda and Yung 1992). The NRCC model simulates a wide range of real fire phenomena including, fuel quantity, burn rate, the creation of toxic gases and their concentrations, fire growth, flashover, smouldering and a wide range of ventilation conditions (doors and windows closed and open). Hasofer sought the dominant variables and the basic form of the equations. He reduced the equations to their most simple forms and calibrated them. He incorporated these equations into a Monte Carlo analysis. His model is suited for adoption into larger models such as smoke spread models.

Lau (1996) developed a model for estimating the probability of failure of timber members in tension as a function of time, temperature, load and initial ambient strength. His failure function was a damage accumulation model which predicted the time of failure directly without simulation. He calibrated his model against the results of many tension experiments. He incorporated his failure function into a Monte Carlo analysis.

Law J (1997) developed a model for estimating the probability of failure of steel beams in real fire. His failure function was a series of models for fire severity, heat transfer and structural response. All of these models were reasonably simple, each reduced to a single equation. He incorporated his failure function into a Monte Carlo analysis.

The Fire Code Reform Project 4 (1993), II Part 1.5 has developed time dependent probability of failure models. The failure functions are simplified models for heat transfer and structural response for steel, reinforced concrete and timber structural systems. All of the failure functions are incorporated into Monte Carlo Analyses.

It seems that the earlier research of Woeste et al (1981) and Beck's (1986) adopted FOSM because the computers of the time were not as fast nor as convenient for programming. Since that time, researchers listed above have opted for Monte Carlo analyses. Melchers (1987), a leader in risk engineering in Australia shows much interest in Monte Carlo. He advocates the use of importance sampling. The appealing aspects of Monte Carlo analyses are the simplicity of concepts, the ease with which it analyses complexities in failure functions, and the accuracy that can be achieved with a sufficient number of simulations.

8.2.8 Commonly used Probability Distributions for Variables for Structural Response and Heat Transfer

The probability distributions commonly used by researchers mentioned in §8.2.7 as well as by Pham (1985) and Leicester (1985) who undertook substantial roles in converting Australian structural engineering codes to limit state format, were the normal, lognormal and Weibull probability distributions. Benjamin and Cornell (1970) explained that normal distributions result from the sum of a large number of independent influences. For example, the length of a queue of cars is normally distributed. The length of each car is independent of the lengths of other cars. Irrespective of whether the length of individual cars is normally distributed, the total length of a queue is normally distributed; that is the Central Limit Theorem. If a stochastic variable results from a product of a large number of influences, that variable will be lognormal. There is little difference between normal and lognormal distributions provided the coefficient of variation is small (less than 0.3-0.4). Benjamin and Cornell give the example of the sizes of stones in a stream being the outcome of a large number of collisions and other processes; the size is lognormal. Weibull distributions are distributions of extreme values.

8.3 Probability of Failure Model

8.3.1 Selection of Modelling Method

From the literature review in §8.2, the alternative methods of analysis to choose for the probability of failure model are convolution, FOSM and Monte Carlo methods. The non-Monte Carlo methods have a number of disadvantages listed in §8.2.3 and §8.2.4. The principle disadvantages are:

1. They can only estimate the probability of failure at a particular time and thus must be repeated to give the probability of failure continuously with time.
2. Without simulations, it is difficult to choose appropriate probability distributions for the random variables because the distributions change with time.
3. They can only estimate reliability for simple failure functions. The functions must have a limited number of random variables with little or no dependencies. The random variables usually have to be modelled with normal or lognormal distributions with similar tails (Figure 8.6) to the actual probability distributions for the variables.
4. Due to the restrictions of the simple failure functions, the non-Monte Carlo methods cannot model the range of phenomena necessary for modelling light-timber framed structures in fire.
5. They approximate the probability distributions for random variables with means and second moments. Monte Carlo methods can accurately estimate probability of failure for random

variables with virtually any probability distributions. In particular, Monte Carlo methods can directly utilise probability distributions obtained from surveys.

As explained in §8.2.7, fire researchers who have developed models for probability of failure in the last decade or so, have shown a distinct preference for Monte Carlo methods, no doubt for the above reasons. In recent times, the use of Monte Carlo methods has become more feasible due to the large increase in the speed and ease of access to personal computers. An advantage of Monte Carlo methods is the simplicity of the algorithm. Speed can be enhanced with importance sampling. The probability model described in §8.3.2, carried out 100 simulations of a wall exposed to a fire, in 6-8 hours on a 200MHz pentium personal computer. The speed was sufficiently fast for the requirements of the research without an importance sampling function. The inclusion of an importance sampling function in the probability of failure model would greatly improve computation speed and is recommended for future research.

8.3.2 General Description of Model

The probability of failure model incorporates the time of failure model shown in Figure 8.11 (repeated from Figure 7.1) into the basic Monte Carlo method as shown in Figure 8.12 (repeated from Figure 1.2). The development of modelling for importance sampling (§8.2.5.5) could not be carried out within the time period for the research for this thesis, but it is recommended for future research and development of the probability of failure model. The probability of failure model involved the development of modelling for boxes 1, 2, 5 and 6 in Figure 8.12. In relation to box 1, the model has an input routine for which the user must specify whether variables are random, and if so, specify their random properties including types of probability distribution, means and coefficients of variation. As part of the initialisation, cumulative probability arrays are established for subsequent probabilistic generation of variables for each Monte Carlo simulation similar to the method shown in Figure 8.9. The model proceeds to box 2, where Monte Carlo simulations commence by generating the random variables. In box 3, the time of failure model is then executed until all of the modes of failure, listed below, are obtained. Box 4 directs ongoing simulations, via boxes 5 and 2, until the total number of simulations required by the user have been executed. The user may desire to look at intermediate results before execution is completed. Box 5 updates files for the user to peruse during execution of the model. Upon completion of the number of simulations specified, box 6, finalises all output files.

In accordance with the aims in §1.5 and consistent with the time of failure model in §7, the probability of failure model estimates probabilities for the following modes and combinations of modes of failure:

1. "Insulation, average temperature" mode; that is, when the average temperature rise on the ambient side of the wall exceeds some nominated value. In AS1530.4, this value is 140°C.

2. "Insulation, maximum temperature" mode; that is, when the maximum temperature rise on the ambient side of the wall exceeds some nominated value. In AS1530.4, this value is 180°C.
3. Either insulation mode, whichever happens first.
4. "Integrity initiated failure" mode (§7.1).
5. Structural collapse.
6. The first occurrence of any mode of failure.

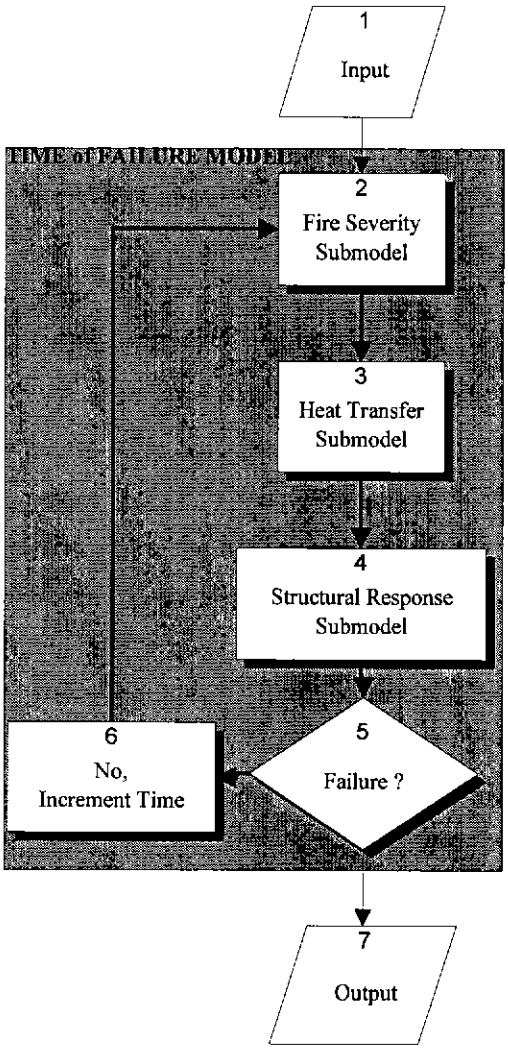

Figure 8.11. General Flowchart for Time of Failure Models. (Repeated from Figure 7.1)

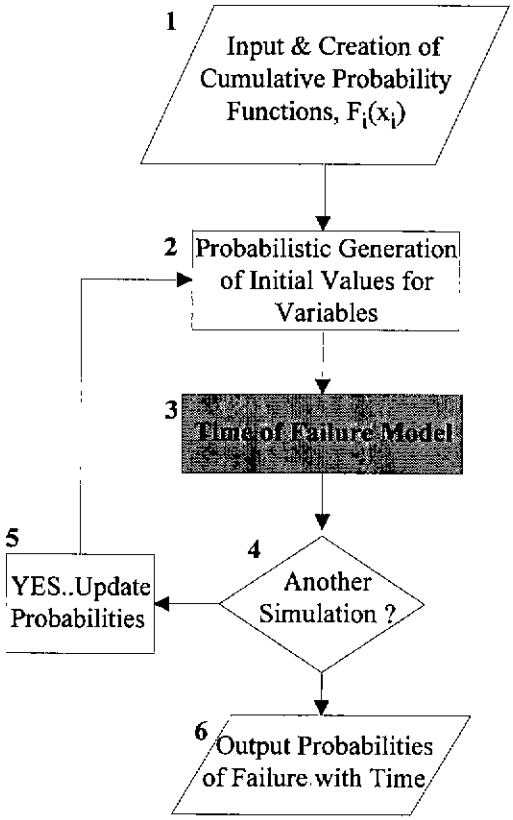

Figure 8.12. Probability of Failure Model. (Repeated from Figure 1.2)

The criterion for ending simulations in the time of failure model, when executed by the probability of failure model, differs to the criterion for ending simulations carried out by the time of failure model alone. The time of failure model, when used alone, ends each simulation when the first mode of failure is

encountered. The probability of failure model ends each simulation when all modes of failure have occurred. Failure in all modes must be simulated because all modes contribute to the total probability of failure, p_f as shown in equation (8.23) for the case involving a maximum of three possible modes of failure 1-3.

$$p_f = 1 - (1-p_1).(1-p_2).(1-p_3) \qquad (8.23)$$

where p_1, p_2 and p_3 are the probabilities of failure for modes 1-3 respectively. The terms in equation (8.23) are illustrated in Figure 8.13.

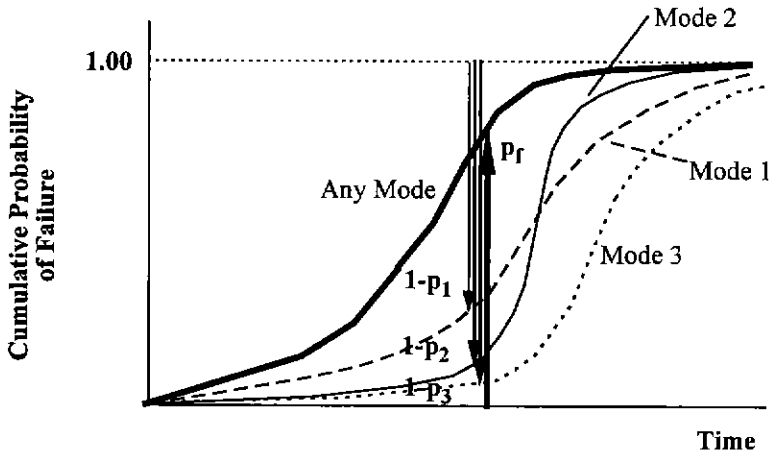

Figure 8.13. Total Probability of Failure from Several Modes.

8.3.3 Random Variables Adopted

Most variables in the time of failure model, including many of those recommended by Jönsson and Pettersson (1985) (§8.2.6), were modelled as random variables in the probability of failure model. The generation of a wide scope of variables was simplified by developing a generalised generation model which could be applied to any variable (§8.3.4). The provision of a wide scope of random variables does not mean that all of these variables have to be adopted by the user as random variables. It is therefore the user's responsibility to choose the variables to be modelled as random variables. In this chapter, the following variables were selected as random variables.

Regarding fire severity, allowance has been made for modelling fire load as a random variable. Ventilation is not considered as random because, unlike fire load, it does not vary for a particular enclosure. The aim was to analyse time and probability of failure for particular enclosures, rather than a group of enclosures.

Regarding heat transfer, all of the thermal properties of wall components - conductivity, specific heat, density and surface emissivity for gypsum board and timber studs - were selected as random variables.

Regarding structural response, structural load and all mechanical properties of studs and gypsum board sheeting were selected as random variables. Jönsson and Pettersson (1985) recommended that structural geometry be considered as a random variable. However, as mentioned above, the probability of faiure model was developed for application for a particular enclosure rather than a group of enclosures. Thus wall geometry variables were not modelled as random variables.

The dependent variables in the model are conductivity and mechanical properties of timber. They are considered as dependent on the density of timber.

A modelling uncertainty factor, α_m is included (§8.2.6) as a random variable to allow for the crudity of the time of failure model. The factor should be given a mean of 1.00 if the time of failure predicted by the model using mean values of the random variables, is the same as in experiments. Otherwise, the mean should be some scaling factor which when multiplied with the predicted time of failure should give the time of failure measured in experiments. The modelling factor should be given a CoV appropriate for the level of crudity of the time of failure model and input data. A trial value for the actual time of failure, t_{fa} is thus estimated from time of failure, t_{fm} determined by the time of failure model as follows,

$$t_{fa} = \alpha_m . t_{fm} \qquad (8.24)$$

8.3.4 Method of Generation of Random Variables for each Simulation

The random variables were generated with random parameters similar to the methods shown in equations (8.16). The use of random parameters has several advantages:

1. Random parameters facilitate the development of the probability of failure model as a separate module to the time of failure model. The probability of failure model assumed that the variables input in the time of failure were mean values. The input files for the probability of failure model only provided the data to generate the random parameters.
2. Random parameters provide a convenient non-dimensional method for comparing the variation of variables and judging the sensibility of generated values. These comparisons and sensibility checks aided validation.

Independent Variables

Independent random variables in the probability of failure model, $x_{pof.i.20}$, for each simulation, were obtained for ambient conditions, by multiplying a generated random parameter, α_i into the value of the variable, $x_{tof\,i\,20}$ input for the time of failure model, as shown in equation (8.25).

$$x_{pof.i.20} = \alpha_i . x_{tof.i.20} \qquad (8.25)$$

It is assumed that for the random variables which are functions of temperature, the functions are deterministic. Any randomness in the function should be allowed for in the CoV for α_i. Modelling the functions as random functions was thought to be too refined for the current stage of the development of the probability of failure model.

The random parameters, α_i are defined in terms of some probability distribution; for example, a normal distribution with a mean and coefficient of variation, CoV. The random parameters, are generated in a manner similar to the conventional method shown in Figure 8.9 (b) which is modified in Figure 8.14. The random numbers were generated with a library function in Fortran 90 (Lahey 1995).

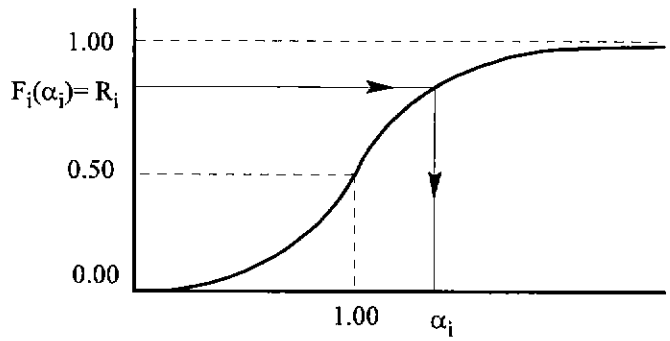

Figure 8.14. Generation of Random Factor α_i from Random Number, R_i and Cumulative Probability of Failure $F_i(x_i)$.

The probability distributions used for deriving appropriate load factors for limit state design in Australian structural engineering codes (§8.2.8) were the normal, lognormal and Weibull distributions. These distributions were adopted in the probability of failure model for the generation of random parameters. Since no closed form equation is available for normal cumulative probability, an array of cumulative probabilities was obtained by numerical integration of the standard density function h(y) which has a mean of 0.00 and a standard deviation of 1.00.

$$h(y) = \frac{1}{\sqrt{2\pi}} \exp\left[-\frac{y^2}{2}\right] \qquad (8.26)$$

Numerical integration was carried out by applying Simpson's Rule for an increment in y of 0.005, between the limits of 0.00 and 10.00; that is, between the mean and 10 standard deviations away from the mean. A simple search routine through the array found the standard random parameter, y from R. The graphical equivalent of the search is shown in Figure 8.15.

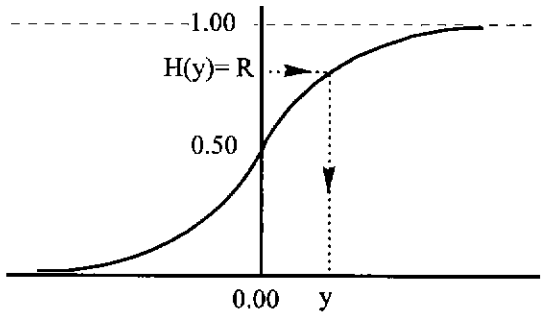

Figure 8.15. Generation of Standard Normal Random Parameter, y from Random Number, R and Standard Normal Cumulative Probability of Failure H(y).

The normal random parameter, α_n was thus obtained in terms of y, the mean, μ_{α_n} (usually 1.00) and standard deviation, σ_{α_n} as follows,

$$\alpha_n = y.\sigma_{\alpha_n} + \mu_{\alpha_n} \qquad (8.27)$$

The generation of lognormal random parameters was carried out by making use of the fact that cumulative lognormal probability, $F_\ell(\alpha_\ell)$ is equal to the cumulative normal probability of the logarithm of the parameter, $F_n(\ln(\alpha_\ell))$. $F_\ell(\alpha_\ell)$ can then be expressed in terms of cumulative standard normal probability, H(y) as follows,

$$F_\ell(\alpha_\ell) = H(y) \qquad (8.28)$$

where

$$y = \frac{\ln(\alpha_\ell) - \mu_{\ln(\alpha_\ell)}}{\sigma_{\ln(\alpha_\ell)}} \qquad (8.29)$$

Lognormal random parameters, α_ℓ were thus deduced in accordance with equations (8.28) and (8.29) after having generated a standard random parameter, y (Figure 8.15).

$$\alpha_\ell = \exp\left(y.\sigma_{\ln(\alpha_\ell)} + \mu_{\ln(\alpha_\ell)}\right) \quad (8.30)$$

Benjamin and Cornell (1970) show that,

$$\sigma_{\ln(\alpha_\ell)} = \sqrt{\ln\left(CoV_\ell^2 + 1\right)} \quad (8.31)$$

$$\mu_{\ln(\alpha_\ell)} = \ln\left(\tilde{\mu}_{\alpha_\ell}\right) \quad (8.32)$$

where $\tilde{\mu}$ = the median

The generation of Weibull random parameters, α_W was carried out from following equation for the cumulative Weibull probability, $F_W(\alpha_W)$,

$$F_W(\alpha_W) = 1 - \exp\left(-\left(\frac{\alpha_W}{B}\right)^C\right) \quad (8.33)$$

where B and C are Weibull probability variables. Equation (8.33) was rearranged and the random number generated, R was substituted for $F_W(\alpha_W)$ to give the Weibull random parameter, α_W as follows,

$$\alpha_W = B.\left[-\ln(1-R)\right]^{1/C} \quad (8.34)$$

The probability of failure model adds the random parameters as shown in equation (8.35), should the user wish to model random parameters with a combination of probability distributions.

$$\alpha = \alpha_n + \alpha_\ell + \alpha_W \quad (8.35)$$

Usually the means of α_n, α_ℓ and α_W are chosen so that they sum to 1.00, unless some scaling is desired.

Dependent Variables

Dependent random variables in the probability of failure model, $x_{pof,j}$, for each simulation, were obtained by expanding the equation (8.36).

$$x_{pof.j} = \alpha_j . x_{tof.j} \qquad (8.36)$$

where $x_{tof.j}$ = the value input for the variable, x_j in the time of failure model

α_j = random parameter with some dependency on α_i in equation (8.25)

to,

$$x_{pof.j} = \alpha'_j . \alpha_{j/i} . x_{tof.j} \qquad (8.37)$$

where α'_j = the parameter for the random variation in $x_{pof.j}$, which is independent of all other variables.

$\alpha_{j/i}$ = a parameter accounting for the dependency of x_j on x_i.

Equation (8.37) could have been extended to some more general form allowing for non-linear dependencies on several independent variables. However, such refinement is not warranted for the aims of this research (§1.5). The dependency parameter, $\alpha_{j/i}$ was defined by some reasonably simple general polynomial as follows,

$$\alpha_{j/i} = \sum_{n=1}^{3} a_{j/i_n} . \alpha_i^{b_{j/i_n}} \qquad (8.38)$$

where a_{j/i_n} and b_{j/i_n} are the respective coefficients and the powers of the polynomial.

The independent random parameter α'_j and dependent parameter $\alpha_{j/i}$ are illustrated in Figure 8.16. The dependent parameter, $\alpha_{j/i}$ define some specific relationship between variables x_j and x_i. The relationship is a line of "best-fit" for the data available. The random parameter α'_j is the randomness about this line.

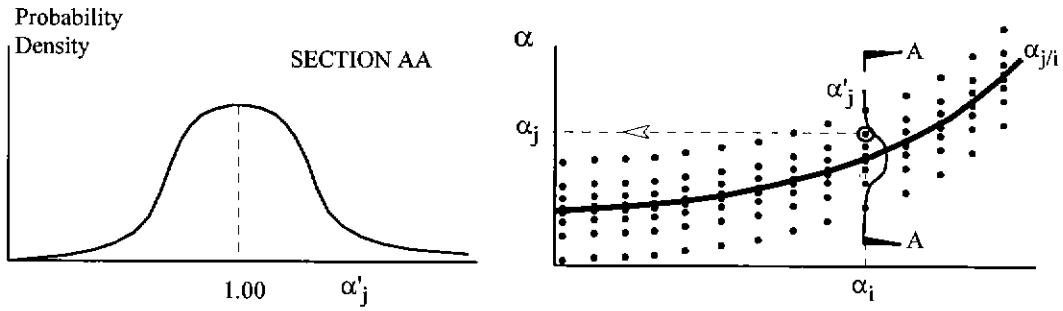

(a)Probability Density for Random Parameter, α'_j. **(b) Parameters α_j α'_j and $\alpha_{j/i}$.**

Figure 8.16. Generation of a Parameters α_j α'_j and $\alpha_{j/i}$ in Equations (8.37) and (8.38).

8.3.5 Method of Calculation of Probability of each Mode of Failure with Time.

The model updates the cumulative probability of each mode of failure with time after each discrete time step of each simulation, at box 5 Figure 8.12. It does this with arrays representing histograms of the cumulative number of failures with time, for each mode of failure.

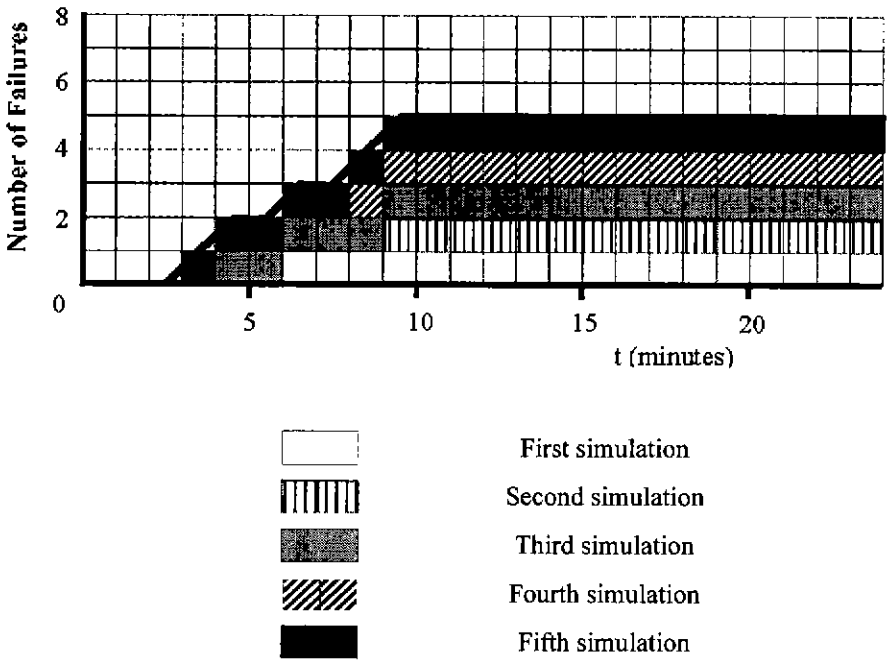

Figure 8.17. Example Showing Creation of Histogram of Number of Failures with Time, t for Particular Mode of Failure, from a Sequence of Several Monte Carlo Simulations.

An example of how the cumulative number of failures with time, for a particular mode of failure, is determined from a sequence of several simulations of a Monte Carlo analysis, is shown in Figure 8.17. Results from the first simulation are shown as, ☐. Failure for this simulation occurs some time between 6 and 7 minutes, but is conservatively rounded down to the nearest minute and is recorded as having occurred at 6 minutes. The cumulative number of failures is recorded as zero for times less than 6 minutes, and 1.00 at times greater than or equal to 6 minutes. The incremented number of failures with

time at the end of the second simulation is shown as  . During the second simulation, failure was determined between 4 and 5 minutes and recorded for the time rounded down to the nearest minute; that is, 4 minutes. The number of failures with time is then incremented by 1.00 for all times greater than or equal to 4 minutes. This procedure is repeated for successive simulations indicated with  ,  and  respectively. The cumulative probability of failure with time is computed in the model as the cumulative number of failures with time divided by the total number of simulations.

The model carries out the above procedures for each mode of failure and combination of modes of failure listed in §8.3.2. For the combinations of modes, the model deems that the time of failure is the earliest one for all of the modes in the combination. The cumulative probability of failure with time for a combination of modes is not the sum of cumulative probabilities for all modes in the combination.

8.3.6 Validation of Model

It was obviously impractical to validate the probability of failure model against failure statistics for a multitude of wall experiments because such a large number of repeated experiments does not exist and would be too expensive to undertake. However, parts of the model could be validated. The validity of the time of failure model was established in §7. The computations for cumulative probability distributions - normal, lognormal and Weibull - were validated against spreadsheet functions. The random number generation function in the model is checked below. All random numbers and parameters generated for all of the random variables in all of the simulations were filed and perused for sensibility. An example of all of the random numbers and parameters generated and recorded for a particular simulation, is shown in Table 8.1.

Table 8.1. Example of Random Numbers and Parameters, α Recorded for a Range of Variables in a Simulation (N=1). (Where α equals 1.00, the variable has been set as, deterministic.)

N = 1	Sheet A	Air	Insulation	Stud/Joist	Sheet B
Density	0.594794	0.878576	0.968479	0.086145	0.627846
α	1.000000	1.000000	1.000000	0.918132	1.000000
Spec Heat	0.710294	0.037758	0.705872	0.732582	0.435933
α	1.000000	1.000000	1.000000	1.012080	1.000000
Conductivity	0.704388	0.060184	0.326569	0.281089	0.154468
α	1.010390	1.000000	1.000000	0.988081	1.000000
Emissivity	0.811035	0.483756	0.076147	0.629143	0.331455
α	1.000000	0.000000	1.000000	1.000000	1.000000
Ext.n coeff				0.853429	
α				1.000000	
Mech Sheet				0.536795	
α				1.000000	
Mech Stud				0.407324	
α				0.978946	
Kspring1				0.063680	
α				1.000000	
Kspring2				0.161712	
α				1.000000	
Dead Load				0.338196	
α				0.976917	
Live Load				0.052138	
α				0.240600	
Epsmxc0_shee				0.750377	
α				1.000000	
Epsmxt0_shee				0.011420	
α				1.000000	
Epsmxc0_stud				0.984174	
α				1.000000	
Epsmxt0_stud				0.350040	
α				1.000000	
Kss0..sheet1				0.106213	
α				1.000000	
Kss0..sheet2				0.195890	
α				1.000000	
Alpha0_sheet				0.001721	
α				1.000000	
Alpha0_stud				0.855705	
α				1.000000	

Random numbers were generated in the probability of failure model with a library function in Fortran 90 (Lahey 1995). The function was checked for its capability to generate a sufficiently large number of independent random numbers to ensure accurate estimates of failure probabilities and that all Monte carlo simulations are independent. It was envisaged that the maximum likely number of simulations ever likely to be carried out with the model would be 10^4-10^5. The function was checked by generating 10^8 random numbers which should be sufficient to achieve the accuracy required for estimates of failure probabilities. No repetition of generated numbers was found and hence all numbers were independent.

A plot of the frequency of random numbers versus percentile values ranging between 0-100%, is shown in Figure 8.18. The generation of 10^8 random numbers produced a very uniform plot with a mean precentile of 50.0 and a standard deviation of 28.9. 100 generations produced a distribution reasonably uniform by observation, with a mean percentile of 50.07 and a standard deviation of 27.0. Thus the random number function produces random numbers with the desired uniformity.

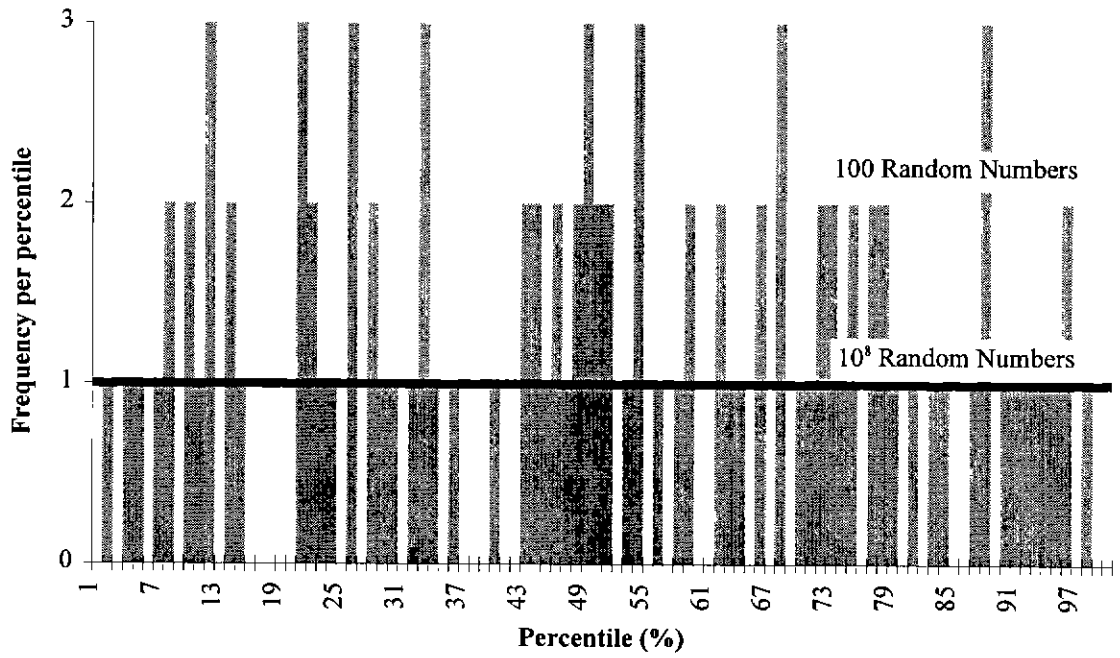

Figure 8.18. Validation of Random Number Function (Lahey 1995).

8.4 Applications of Model to Estimate Probability of Failure and Variability of Time of Failure

8.4.1 General

In this section, §8.4 the probability of failure model will be demonstrated in the predictions of the following:

1. The reproducibility of results for time of failure of Wall 6 in §4.
2. The distribution of times of failure of walls similar to Wall 6 but with typical mechanical properties of graded timber and realistic loads, subjected to standard fire.
3. As for (2) except subjected to real fire.

Wall 6 was considered in preference to other walls in §4 because it was the one most similar to walls in common building construction (§7.1). Considerations general to all of these applications are given below.

When applying the probability of failure model, the variables which are to be modelled probabilistically, must be chosen (§8.3.2, §8.3.3). The model allows most variables to be modelled probabilistically. The variables to be chosen must be those which have greatest effect on the time of failure judged from sensitivity and large variability (§8.2.6). In §7 it was shown that the time of failure is most sensitive to the following variables:

1. Fire variables
2. Density, specific heat and conductivity of gypsum board
3. Density and specific heat of wood
4. Elastic modulus of wood
5. Vertical load.

These variables are thus considered as random variables in §8.4.2-§8.4.4.

It is evident in Table 8.2 that compression and tensile strength of timber is highly variable. However, (Figure 7.6) showed the time of failure was so insensitive that the large variabilities would not significantly affect the time of failure. Hence these variables need not be modelled probabilistically with much accuracy.

In §8.3.3 it was explained that when estimating the probability of failure for design, it is necessary to account for the crudity of the model. The time of failure for each simulation should be multiplied by a random factor, α_m for model uncertainty, as shown in equation (8.24). In all of the applications below, a mean of 1.02 was adopted for α_m. The time of failure predictions in §7 compared with the experimental results given in §4 were no more than one minute less. This does not mean that the time of failure model is accurate to within one minute. As shown in the numerical checks for the heat transfer model in §3.10, the times for temperatures to occur at particular points can vary by several minutes depending on grid

spacing and time step. For the particular grid spacing and time step adopted, it so happens that only a very small adjustment of 1.02 is required for α_m. The CoV adopted for α_m was 0.00 for several reasons. There was little variability in the properties and experimental results in §4. No other uncertainties seemed to be significant. Furthermore, the aim in this section, was to give the best faithful estimate of failure probability and give the clearest indication of the effects of variables on failure probability, rather than to give conservative estimates of failure probability.

Broding (1964) equation (21) indicates that 100 simulations will give 95% confidence in the estimation of the 3rd and 97th percentile times of failure. Mann et al (1974) suggest that 100 simulations will give confidence in times of failure as extreme as the 10th and 90th percentiles. The application of equations (8.17) - (8.19) give similar results to those from Mann's. These extremes are sufficient to demonstrate the application of the probability of failure model. Hence, the number of simulations carried out was 100 for each application.

Table 8.2. Measured Mechanical Properties of Structural Scale Specimens of Radiata Pine 90 x 35 mm in Cross-section (Leicester et al 1988).

Mechanical Property	Stress Grade	Sample Size	AS1720.1 Basic Working Stress (MPa)	Mean Value (MPa)	Five Percentile Value (MPa)	Coefficient of Variation
Bending Strength	F5	153	5.5	42.3	14.5	0.44
	F8	151	8.6	57.4	29.5	0.35
	F11	154	11.0	71.4	38.2	0.30
Tensile Strength*	F5	150	3.3	16.8	7.0	0.41
	F8	153	5.2	25.9	13.2	0.38
	F11	151	6.6	35.3	18.2	0.36
Modulus of Elasticity	F5	152	6900	9800	6900	0.20
	F8	151	9100	12400	9600	0.15
	F11	154	10500	15100	12200	0.12

Note * Tensile strength parallel to grain.

It was explained in §7 that specific heat and density of gypsum board should have low variability since gypsum board is manufactured to specifications. These variables are thus modelled deterministically.

Wood has consistent proportions of constituents (Table 6.1) and thus the variability of thermal properties should be small. However, wood is a natural material which cannot be produced to specifications as tightly as gypsum board can. Thus some variability is considered for properties in (3) and (4) above. These assumptions on the small variability of thermal properties are evaluated in the next section, §8.4.2.

8.4.2 The Reproducibility of Results for Time of Failure of Wall 6 in §4

In §4.4 the procedures for ensuring the reproducibility of experimental results were explained. This section, §8.4.2 will evaluate the reproducibility of the experimental results and the control of the variability of variables by experimental procedures. It is expected that variability was low and reproducibility was good since the failure times of all repeated experiments were within a few percent of each other.

The estimated values for the coefficients of variation, CoV's and the dependencies between random variables for wall 6 in §4 are given below. Variables not listed below were considered as deterministic. Values for means and for deterministic variables were the same as those adopted in §5.2 and in Appendix C. The mean conductivities were modified for moisture transfer in accordance with plot C in Figure 7.3. A 3 mm shrinkage gap was assumed between the studs and the gypsum board on the fire side (§5.4.3).

Fire Variables

The mean fire temperature, T_f (°C) as a function of time, t (s) adopted was the standard fire (AS1530.4) in equation (8.39).

$$T_f = T_{f0} + 345.\log_{10}\left(\frac{8t}{60}+1\right) \qquad (8.39)$$

where T_{f0} (°C) is initial ambient temperature. Figure 4.17 shows variations in temperatures of the surface of gypsum board facing the fire. However, it is considered that these variations were due to the oscillations in the computer control of furnace gas temperature in the narrow range between set maximum and minimum temperatures. It is not expected that the furnace gas temperatures averaged over small time intervals would have been significantly different to the standard fire temperature, $T_f(t)$. Thus, despite fire temperature being a dominant variable, a coefficient of variation of 0.00 was adopted for both the furnace gas temperature and the emissivity ε_{fire}.

Thermal Properties of Gypsum Board

The coefficient of variation, CoV of density was obtained in consultation with Poynter (1999), an engineering advisor at Boral Plasterboard. He advised that the density of most board was expected to vary within 2-3% of the mean density. "Most board" essentially means a range of two standard deviations each side of the mean. Hence a CoV of 0.02 was chosen for the density of gypsum board.

In §5.2.3.2 it was argued that the thermal conductivity of gypsum board depends on density in accordance with equation (5.1) which is repeated below.

$$k_{max} = \pi_g k_g + \pi_s k_s \qquad (5.1)$$

Considering a CoV of 0.02 for density and the values given in Table 5.1, it can be deduced from equation (5.1) that the dependency of conductivity of gypsum board on density, in the form expressed in equation (8.38) is,

$$\alpha_{k/\rho} = 0.1 + 0.9\alpha_\rho \qquad (8.40)$$

Since specific heat is a property expressed in terms of per unit mass, it should not be dependent on density.

One would expect that the independent random parameters for conductivity and specific heat to be primarily a function of the variability of constituents within gypsum board. Since gypsum board is manufactured to specifications, the proportions of constituents should be consistent and hence the CoV of random parameters for conductivity and specific heat for gypsum board should be small. Figure 8.19 shows plots of temperature versus time for a point on the cavity facing surface of gypsum board on the fire side, as well as plots for other points in the stud. Figure 8.19 (c) and (d) show measurements from all of the wall furnace experiments (§4) plotted as continuous lines, and predictions of the probability of failure model for 10 independent simulations plotted as dotted lines. Only 10 simulations have been plotted because the variability of the simulations can only be meaningfully compared with the variability of temperatures measured in a similar number of wall experiments. Figure 8.19 (c) shows the plots for a CoV of 0.02 for the random parameters for specific heat and conductivity. Figure 8.19 (d) shows the plots for a CoV of 0.10 for the random parameters. Except for three continuous line plots, the variations among the plots with continuous lines and dotted lines are similar, although, the variation of dotted line plots from CoV's of 0.10 is marginally greater than the variation of dotted line plots from CoV's of 0.02. Continuous line plot A was obtained from measurements which were carried out with a surface

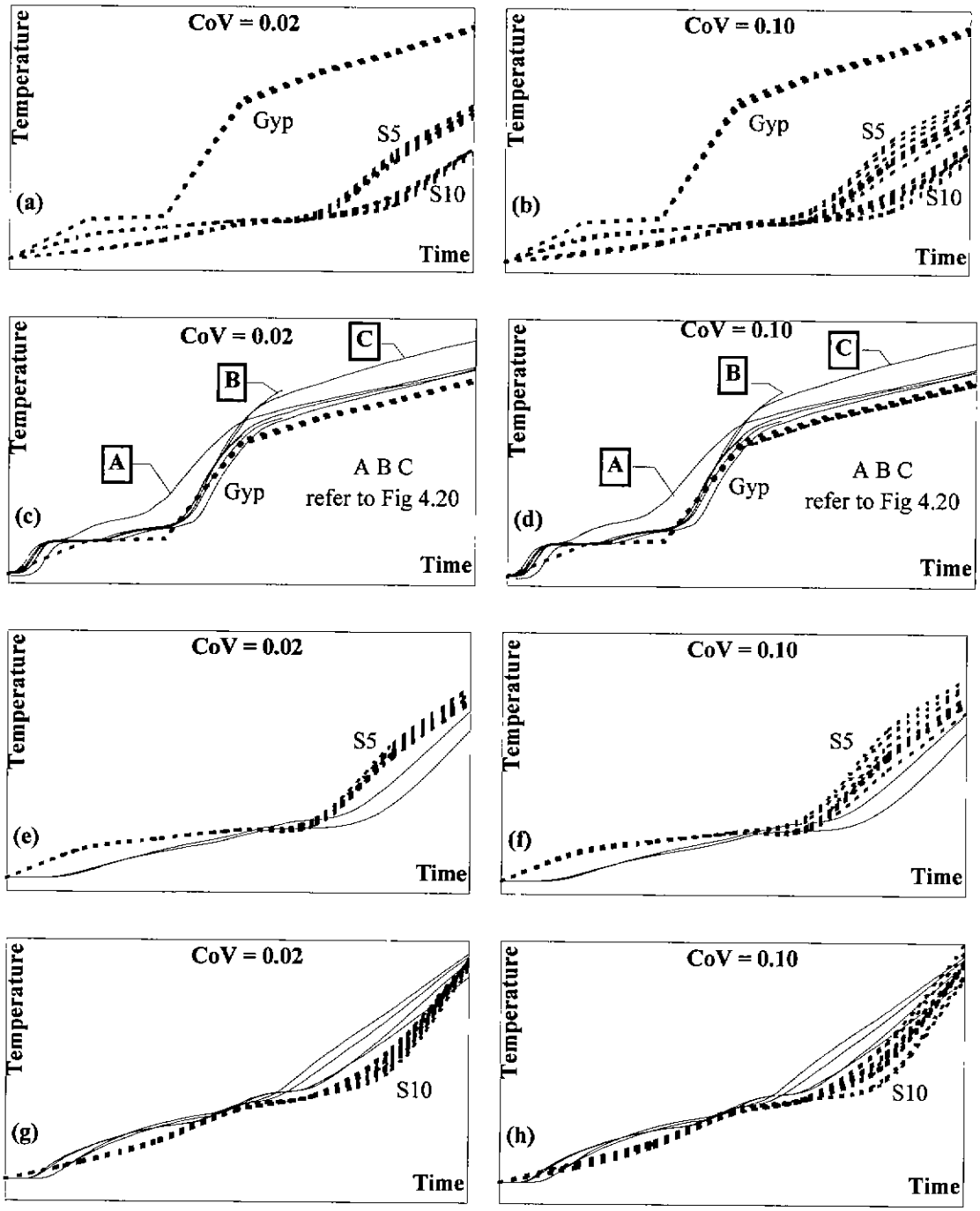

Notes:

1. Gyp, refers to temperatures measured on the cavity facing surface of gypsum board on the fire side.
2. S5 and S10 refer to thermocouples in the studs and the positions for which are shown in Figure xx.
3. CoV refers to the coefficient of variation of the random parameters for the specific heat and thermal conductivity of timber,
4. Dotted lines refer to model predictions and continuous lines refer to measured temperatures.

Figure 8.19. Variations in Temperatures at Several Key Points in Wall.

thermocouple not covered with a pad (Figure 4.10), unlike other surface thermocouples which were covered with pads. Plots B and C seem to be anomalous and may have resulted from calcium silicate glue smeared over the pads, thereby creating greater thermal energy build-up behind the pads. The essential considerations are that the experiments did indicate some variability in the random parameters for specific heat and conductivity. The failure times for Wall Experiments 1-3 were within one minute of each other (Tables 4.2 and 4.3). It was apparent from the observations noted in §4.5 that just prior to failure, the studs were completely charred and hence the gypsum board on the ambient side provided all of the support. The similarity of the failure times thus indicates similar thermal and mechanical properties of gypsum boards. Hence, CoV's of 0.02 have been adopted for the independent parameters for specific heat and conductivity of gypsum board, for ambient conditions.

In §8.3.4 it was mentioned that for the random variables which are functions of temperature, the functions are deterministic. Any randomness in the function should be allowed for in the CoV for α'_i which is the random parameter for variable $x_{tof.i.20}$, that is, at ambient conditions. It has been assumed that the CoV's for the random parameters for specific heat and conductivity do not increase with temperature. This assumption is supported by the closeness of failure times for similar wall experiments in §4.

Thermal Properties for Timber

In deciding what timber properties to adopt, it is necessary to consider whether the studs behave individually or together. An individual stud can either initiate failure or it can share and redistribute load to adjacent studs. Thus the appropriate properties to adopt are either for the least fire resistant stud or the properties averaged for a number of studs involved in load sharing. From the following considerations it is apparent that some sharing of loads amongst studs should occur. As one stud buckles perpendicular to the plane of the wall, the gypsum board on the ambient side would provide some lateral support (Young 2000) by resisting double curvature (that is, horizontal curvature as well as vertical curvature). Only a small amount of lateral support (less than 1% of the axial force Trahair and Bradford 1994) is required to substantially increase (double or more) the buckling resistance and enable the adjacent studs to give some support and share load. The buckling could be due to low elasticity or degradation of the stud section. Each of these causes is dependent on density. Since load sharing seems apparent, it is appropriate to use properties averaged for the three studs in the wall.

Young (2000) measured the densities and dynamic elastic moduli of all studs in the walls tested (§4). He chose those studs which were closest to the average elastic modulus. The average of the densities was adopted as the mean, 470 $kg.m^{-3}$. He also calculated the average density for the studs in each wall. The coefficient of variation of the averages for all walls was 0.03. This procedure for obtaining averages ignored those studs which had a density of less than 400 $kg.m^{-3}$ and were rejected during selection.

However, because of Young's selection procedure based on elastic modulus, only a very small proportion of studs had densities less than 400 kg.m^{-3} before final rejection as shown in Table 8.3. Thus, ignoring studs with densities less than 400 kg.m^{-3} would not have significantly affected the calculation of the mean and coefficient of variation of the probability distributions of material properties. In the probability of failure model, the generation of average density for all studs in a wall could be less than 400 kg.m^{-3}. The model was programmed to reject repeated generations until a density greater than 400 kg.m^{-3} was obtained.

Table 8.3. Distribution of Stud Densities.

Range of Densities	Number of Studs
>500	2
480-499	4
460-479	11
440-459	6
420-439	4
400-419	1

Janssens (1994) conductivities in Figure 5.8 for a timber density of 470 kg.m^{-3} were adopted for mean values. From Janssen's model for conductivity of timber, it was found that a 10% change in density led to a 6% change in conductivity. Thus, the dependency factor, $\alpha_{k/\rho}$ was determined from the random factor, α_ρ for density as follows,

$$\alpha_{k/\rho} = 0.4 + 0.6\alpha_\rho \qquad (8.41)$$

The random factor for the conductivity of timber was thus found (refer to equations (8.36) and (8.37)) as follows,

$$\alpha_k = \alpha_{k/\rho}.\alpha'_k \qquad (8.42)$$

where α'_k = the random factor in the conductivity of timber independent of all other variables.

The random factor for conductivity, α_k should not be dependent on variations in growth characteristics such as knots. Rather, it should depend on the variability of constituents which is small (Table 6.1) and thus a small coefficient of variation is expected. Specific heat should also only depend on constituents and hence its CoV should be small.

Two sets of trials for estimating the CoV's for independent random factors for conductivity and specific heat were undertaken. The CoV's for conductivity and specific heat were assumed to be the same. In one set of trials, 0.02 was adopted for the CoV's and in the other set 0.10 was adopted. Plots of temperature versus time predicted with the probability of failure model using these CoV's are shown as dotted lines in Figure 8.19 for two key points, S5 and S10 in the stud shown in Figure 4.9. Plots obtained from measurements in the wall experiments are shown as continuous lines. There are only two plots for S5 in Figure 8.19 (e) and (f) because there were only two thermocouples at such a position in studs in the wall experiments. There were four thermocouples in positions similar to that for S10 and hence four plots are shown. Ten random plots from the probability of failure model are shown in each Figure 8.19 e-h. From these figures it appears that the CoV's were between 0.02 and 0.10. However, these figures alone are not sufficient to deduce the CoV's since the measured temperatures would have been very sensitive to the positions of thermocouples. As can be seen from Figure 4.35, a 1.0 mm misplacement of the thermocouple tip could result in as much as ±30°C difference in the temperature measured. A small misplacement would have been quite possible due to some slight diversion of the long thin thermocouple holes as the drill bit was drilled through stiffer oblique late wood grain in the timber. To obtain a clearer indication of these CoV's, plots of the cumulative probability of failure with time were obtained with the model using both sets of CoV's. These plots are shown in Figure 8.23 and the appropriate values for the CoV's are discussed further below.

As for the thermal properties of gypsum board, there is no apparent reason for considering randomness of the function relating thermal properties of timber to temperature.

Mechanical Properties of Timber

Elastic moduli for studs in compression, for a series of wall experiments (Young 2000), are shown in Series I in Figure 8.20. Each point plotted corresponds to average density for all studs in a wall and average elastic modulus deduced by loading the entire wall in compression. The studs in Series I were from the same batch of timber used for walls in the experiments described in §4. However, the average density of the studs in Series I was 460 $kg.m^{-3}$ which differed slightly from the average density of 470 $kg.m^{-3}$ for the studs in the experiments. Points are shown for another series (II) of wall experiments by Young (2000) from a different batch of timber but having several similarities to the timber in series I. The timber was of the same species (radiata pine), similar moisture content, similar densities and from a

similar geographical location. The mean elastic modulus adopted from series I was 7.4 GPa. Dependency of elastic modulus on density is expected. Some dependency seems apparent in series I but no discernable dependency is apparent in series II. It is apparent in Figure 8.20 that the range of elastic moduli among groups of wall studs is narrow; that is, low variability. This low variability reduces the significance of any dependency of elasticity on density. Thus the simplifying assumptions were made that the elasticities for studs in a wall were the same and independent of density. The coefficient of variation of elastic moduli in series I was 0.013. This coefficient is much less than the coefficient of 0.15 for F8 grade radiata pine measured by Leicester et al (1988) in Table 8.2.

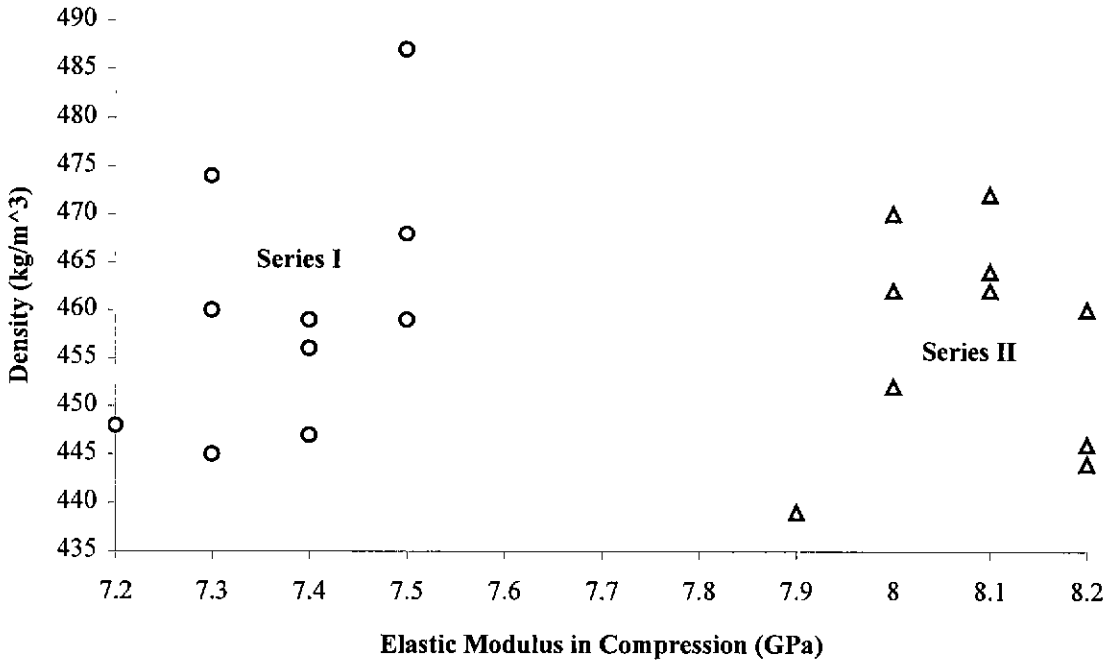

Figure 8.20. Average Density of Load Bearing Studs in each Wall, versus the Average Elastic Modulus in Compression for the Studs in each Wall. (Each point corresponds to a wall tested, Young 2000)

In §8.3.4 it was mentioned that for the random variables, which are functions of temperature, the functions are assumed to be deterministic in the probability of failure model. Any randomness in the function should be allowed for in the CoV for α_i which is the random parameter for variable $x_{tof.i.20}$, that is, at ambient conditions. Appropriate allowance for the randomness of the function for the mechanical properties of timber can be evaluated from Figure 8.21 and Figure 8.22 below.

For ambient conditions, alone, the CoV of 0.03 for the elastic modulus of timber in compression requires further comment in the light of experimental results in Figure 8.21. This figure shows the measurements obtained by Young (2000) in deducing his relationship for the relative elastic modulus of small samples

(90x35mm in section x 300mm in length) of radiata pine in compression. The CoV for ambient conditions is obviously greater than 0.03. However, the experiments were carried out for timber which was similar to timber in the studs in the wall experiments. The greater variation in Figure 8.21 is attributed to size effects. Apparently, the elastic modulus in small samples is more sensitive to variations in the growth characteristics in timber, such as the spacing of growth rings - the greater the spacing, the lower would be the percentage of late wood which is less stiff compared with early wood. The randomness of elastic modulus apparent in Figure 8.21 is thus discounted and is assumed to be 0.013 as deduced above.

Since the randomness for ambient conditions shown in Figure 8.21 has been discounted, randomness shown in Figure 8.21, for the higher temperatures, is also discounted.

As mentioned in §8.3.3, many variables can be represented probabilistically in the probability of failure model. However, compression and tensile strength of wood have been given the same random factor as for elasticity since time of failure is insensitive to timber strengths (Figure 7.6). Thus the model assumed a coefficient of variation of 0.013 for tensile and compression strengths. The mean values adopted for compression and tensile strengths were both 24 MPa (Appendix C).

The randomness of compression strengths with temperature can be evaluated from Figure 8.22. The variations at ambient conditions and at 250°C are both approximately 25% of mean values of the relative compression strengths for ten measurements. Hence the randomness does not change with temperature and can be ignored.

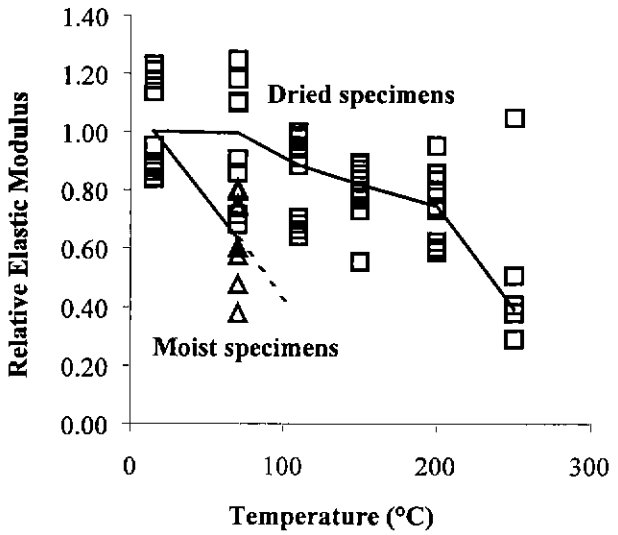

Figure 8.21. Relative Elastic Modulus of Radiata Pine in Compression versus Temperature

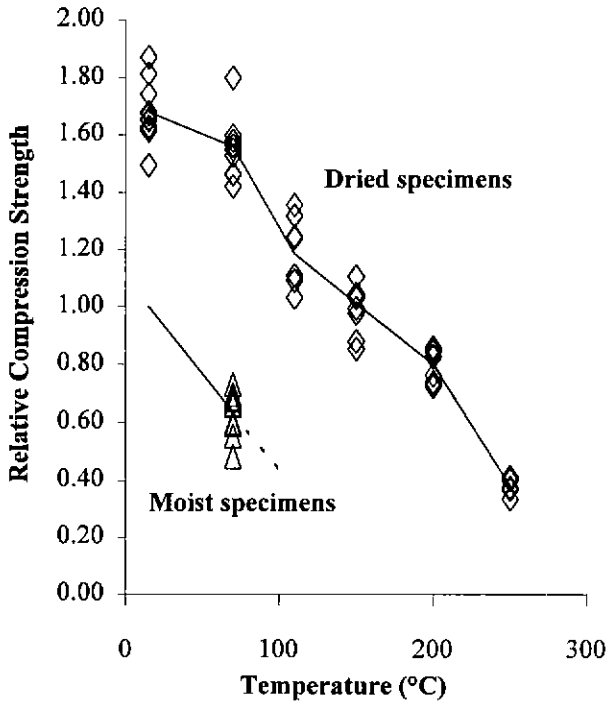

Figure 8.22. Relative Compression Strength of Radiata Pine versus Temperature.

Structural Load

Since load can be controlled under experimental conditions, vertical load was modelled as a deterministic variable; that is, 8kN per stud with zero variability.

Estimate of Cumulative Probability of Failure with Time

The reproducibility of results for the time of failure of Wall 6, from the input data above (summarised in Table 8.4) and the procedures given in §4, is shown in Figure 8.23. Two plots are shown resulting from different CoV's for the random parameters for the conductivity and specific heat of timber. A continuous line is plotted for the CoV's equal to 0.02 for both variables. A dotted line is plotted for the CoV's of both variables equal to 0.10. The number of simulations was 100 and took approximately 6 hours to compute on a personal computer with a 200 MHz pentium chip. No smoothing was used to produce the plots. The results in Table 4.3 showed that similar walls failed within one minute of each other. The continuous line plotted in Figure 8.23 is more closely consistent with experimental results than the dotted line is. Thus it is apparent that the independent random parameters for conductivity and specific heat

were approximately 0.02 which is very small. Hence the evidence shows that the experimental procedures were successful in controlling the variability of material properties.

Since it is apparent from Table 6.1 that the proportions of constituents in timber do not vary much, and that thermal properties of each of the particular constituents of timber should not vary much, it is apparent that the thermal properties of timber are much less variable than the mechanical properties which are sensitive to knots and other growth characteristics.

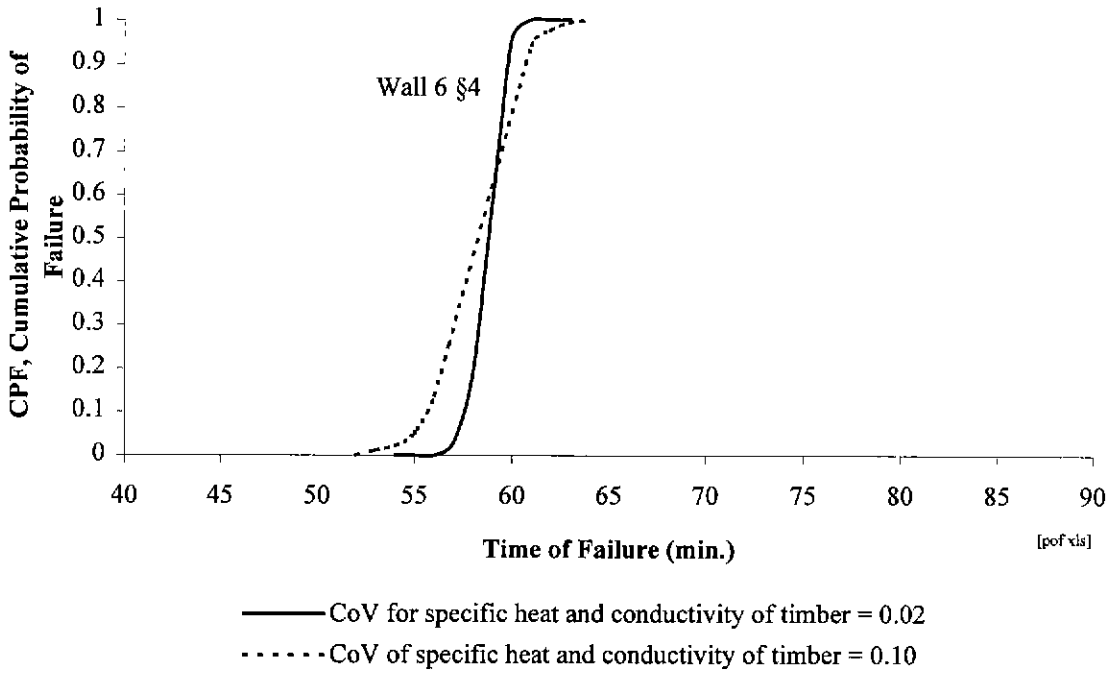

Figure 8.23. Cumulative Probability of Failure with Time for Wall 6 Tested in accordance with all of the Procedures in §4.

8.4.3 The Distribution of Times of Failure of Walls Similar to Wall 6 but with Typical Mechanical Properties of Graded Timber and Realistic Loads, Subjected to Standard Fire.

Means and coefficients of variation of many variables should be the same as in §8.4.2. The fire variables in §8.4.2 were for a standard furnace, and thus should be the same. The gypsum board should be similar and its constituents are consistent, thus the variables for the thermal properties of gypsum board should be the same. The consistency of the constituents of timber should ensure that the variables for specific heat and conductivity should be the same. The density and mechanical properties of typical graded timber would be more variable than the timber used in studs in Wall 6 in §4. These properties are deduced below.

From the discussion on thermal properties for timber in §8.4.2, it is appropriate to adopt average property values for timber. It is doubtful that an external load would be shared by more than three adjacent studs. Thus properties were obtained for the average of any three typical F8 grade (AS1720.4) radiata pine studs. Assuming that all studs have the same statistical properties, and are otherwise independent of each other, then mean properties for all groups of three studs is the same as for individual studs. The variance, $\mathrm{Var}(\bar{S})$ of a material property averaged, for groups of three studs with particular properties, S_1 S_2 and S_3 respectively, can be expressed as,

$$\mathrm{Var}(\bar{S}) = \mathrm{Var}((S_1 + S_2 + S_3)/3) \qquad (8.43)$$

Equation (8.43) can be solved with the expression (8.44) from Benjamin and Cornell (1970), for the variance of the combination of two independent random variables, X_1 and X_2 as follows,

$$\mathrm{Var}(a.X_1 + b.X_2) = a^2.\mathrm{Var}(X_1) + b^2.\mathrm{Var}(X_2) \qquad (8.44)$$

where a and b are combination factors. Substituting equation (8.43) into equation (8.44), the following is obtained,

$$\mathrm{Var}(\bar{S}) = \frac{1}{3^2}\mathrm{Var}(S_1) + \frac{1}{3^2}\mathrm{Var}(S_2) + \frac{1}{3^2}\mathrm{Var}(S_3) \qquad (8.45)$$

The statistics for the property is the same for each stud; that is,

$$S = S_1 = S_2 = S_3 \qquad (8.46)$$

and therefore, the variance of the property averaged for all groups of three studs is,

$$\mathrm{Var}(\bar{S}) = \frac{1}{3}\mathrm{Var}(S) \qquad (8.47)$$

Since, the random factors have means of unity, their standard deviations are the CoV's, and their variances are the square of the CoV's. Therefore, the CoV for the average property for any three studs is,

$$\begin{aligned} \mathrm{CoV}(\bar{S}) &= \frac{1}{\sqrt{3}}\ \mathrm{CoV}(S) \\ &= 0.57\,\mathrm{CoV}(S) \\ &\approx 0.6\ \ \mathrm{CoV}(S) \end{aligned} \qquad (8.48)$$

Thus the coefficient of variation for properties averaged over three studs is approximately 0.6 times that for individual studs.

The author could not find the CoV for density of F8 (AS1720.1) radiata pine. Considering that the average density was 470 $kg.m^{-3}$ and that most samples should be approximately within 100 $kg.m^{-3}$ of this value; that is two standard deviations, a CoV of 0.10 seemed reasonable. Applying equation (8.48), the CoV adopted for density averaged for three studs was 0.06.

Leicester et al (1988) found that the CoV for the elastic modulus for individual lengths of F8 radiata pine was 0.15. The CoV for elastic modulus, E averaged over three studs would, from equation (8.48) be 0.09. This CoV enables probabilistic generation of E with a random parameter, α_E. This parameter is the product of a parameter, $\alpha_{E/\rho}$ for the dependence of the elastic modulus on density, and an independent random parameter, α'_E. The relationship between these factors is thus,

$$\alpha_E = \alpha_{E/\rho}.\alpha'_E \qquad (8.49)$$

König (1991) showed that the elastic modulus is approximately proportional to density. Thus the variance of density will be the variance for $\alpha_{E/\rho}$, and hence the CoV for $\alpha_{E/\rho}$ can be obtained. To approximately obtain the CoV for α'_E, the following expression from Benjamin and Cornell (1970) can be used,

$$Var(X_1.X_2) \approx \overline{X}_1^2 Var(X_1) + \overline{X}_2^2.Var(X_2) \qquad (8.50)$$

provided the CoV's are sufficiently small, say, less than 0.30.

Substituting equation (8.49) into (8.50), and allowing for the fact that by definition of the α parameters their means are 1.00, the following expression is obtained,

$$Var(\alpha_E) \approx 1.Var(\alpha_{E/\rho}) + 1.Var(\alpha'_E) \qquad (8.51)$$

Rearranging.

$$Var(\alpha'_E) \approx Var(\alpha_E) - Var(\alpha_{E/\rho}) \qquad (8.52)$$

Substituting CoV values obtained above,

$$\begin{aligned} \mathrm{Var}(\alpha'_E) &\approx 0.09^2 - 0.06^2 \\ &= 0.07^2 \end{aligned} \qquad (8.53)$$

Thus the CoV for the independent parameter, α'_E is 0.07.

The random factor, α_E was therefore obtained from the generated values for $\alpha_{E/\rho}$ and α'_E. The factor accounting for dependence, $\alpha_{E/\rho}$ was equated to the generated value for α_ρ (from a mean of 1.0 and a CoV of 0.06). The independent factor, α'_E was generated from a mean of 1.0 and a CoV of 0.07.

As mentioned in the introduction to §8.4, tensile and compressive strengths of timber were not as dominant as elasticity (Figure 7.6). These properties were simply obtained by multiplying their means with the random parameter, α_E.

Computations in Appendix B show that for strength design, the live load is approximately equal to the dead load. This computation assumed a nominal live load of 2 kPa. Pham (1985) recommended that arbitrary point in time live loads should be one quarter of nominal live loads. One quarter of 2 kPa, is unrealistically small. It seems that Pham was referring to typical nominal design live loads for offices and the like of 4 kPa (AS1170.1). An arbitrary point in time live load of 1.0kPa has been considered. This value would lead to live load being one half the dead load. To enable a comparison of the cumulative probability results in this section, §7 with the results in Figure 8.23, the mean total load of 8.00 kN per stud was adopted. The mean live load adopted per stud was 2.33 kN and the mean dead load per stud was 5.67 kN. The CoV's adopted were 0.7 for live load and 0.1 for dead load (Pham 1985).

The cumulative probability of failure versus time generated by the probability of failure model for a wall similar to Wall 6 (§4), with the realistic properties and loads in Table 8.4, is given in Figure 8.24. The plot for wall 6 in Figure 8.23, is repeated for comparison. It can be seen that realistic properties and loads significantly increase the variability of the time of failure. By comparing the dashed plot with standard cumulative normal probability tables, it is apparent that the CoV for the time of failure is approximately 0.12 which is comparable to the CoV of the elastic modulus of timber (Table 8.2). The compression elastic modulus is the dominant mechanical property affecting the load capacity of the wall.

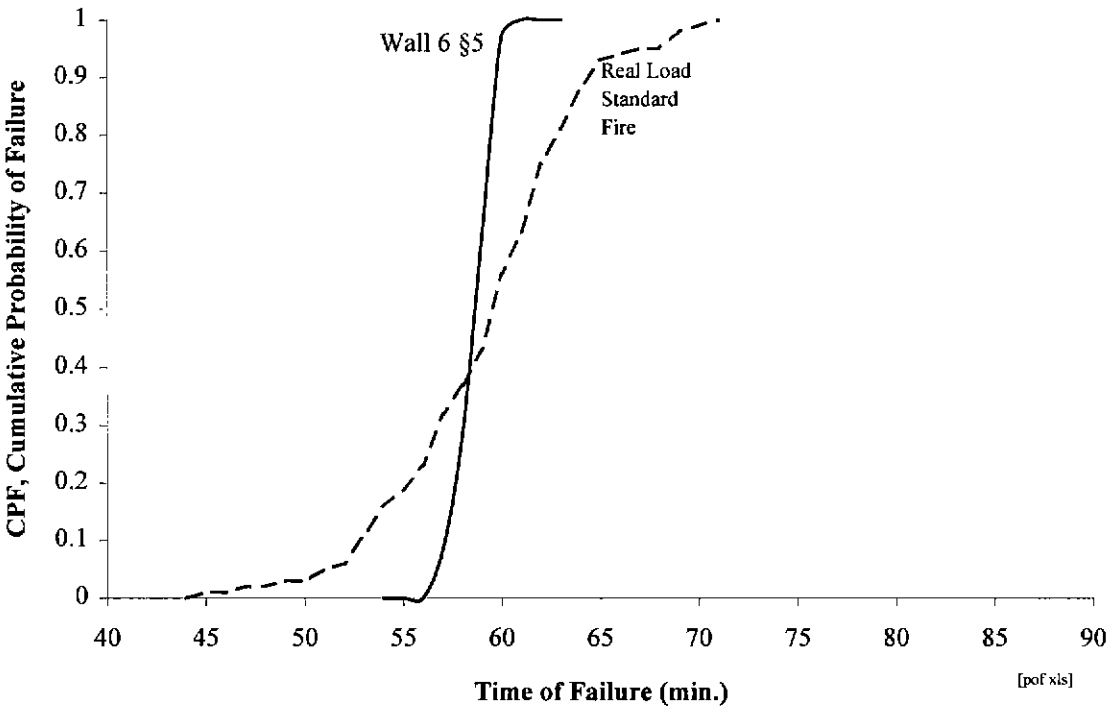

Figure 8.24. Comparison of the Cumulative Probabilities of Failure with Time for Wall 6 (§4) and a Similar Wall with a Realistic Variation in Mechanical Properties and Loads, subjected to Standard Fire.

8.4.4 The Distribution of Failure Times for Walls Similar to Wall 6 but with Typical Variations in Mechanical Properties, Real Arbitrary Loads and Subjected to Real Fires

To demonstrate that the probability of failure model can be linked with any post-flashover fire severity model in which the heat output can be defined in terms of gas temperature and emissivity, the probability of failure model was linked with the well established fire severity model of Kawagoe and Lie's (Lie 1992).

The model is based on the balance of all heat flows into an enclosure including:

1. Radiation lost through openings
2. Heat content of air flowing in through openings
3. Heat content of smoke flowing out through openings
4. Heat absorbed by boundaries
5. Heat absorbed by gases as the gases rise in temperature
6. Heat produced by combustion

The heat balance produces expressions in terms of fire gas temperature, T_f. The solution was closely fitted with the empirical expression (Lie 1992),

$$T_f = 250.(10F)^{0.1F^{-0.3}} e^{-F^2 t}\left[3.\left(1-e^{-0.6t}\right)-\left(1-e^{-3t}\right)+4.\left(1-e^{-12t}\right)\right]+C\left(\frac{600}{F}\right)^{0.5} \quad (8.54)$$

where F = Opening factor

$$= \frac{A\sqrt{H}}{A_T}$$

A = Area of openings (m^2)

A_T = Total internal surface area of enclosure with no deductions for openings (m^2)

H = Average height of openings (m)

t = Time (hr)

$$= \text{minimum}\left[\text{time since start of fire}, \frac{0.08}{F}+1\right]$$

C = A factor allowing for heat loss through boundaries (walls, floor and ceiling)

= 0 ... for heavy materials

= 1 ... for light materials

The duration of the fire until decay starts is, τ (hours),

$$\tau = \frac{Q}{330F} \quad (8.55)$$

where Q = Fuel (kg of wood per square metre of total internal surface area)

Examples of plots of T_f versus time are given in Figure 8.25 for an opening factor of $0.05m^{0.5}$. The plots show that the model accounts for the basic features of a real fire including - rapid growth (flashover), sustained gradual increase in gas temperatures (post-flashover) and decay after the combustion of most fuel. The model can simulate fuel controlled fires ($Q = 5$ kg.m^{-2} in Figure 8.25) which behave as a fire in the open, are independent of the enclosure, are controlled by the fuel quantity rather than the supply of oxygen. The model can also simulate ventilation controlled fires ($Q > 5$ kg.m^{-2} in Figure 8.25) which are dependent on the enclosure geometry, the supply of oxygen and are independent of fuel. The model does not account for a number of features such as concentrations of toxic gases and combustion efficiency in more recent models, for example, NRCC (Takeda and Yung 1992) and CFAST (Jones and Forney 1990). However, features such as concentrations of toxic gases are not of interest in fire resistance of structures. The Kawagoe-Lie model is simple to apply and understand. It is easy to accommodate engineering

judgements and adjust the inputs to the model. For example, combustion efficiency could be modelled by reducing the fuel load in accordance with available statistics or engineering judgement. Hence, use of the Kawagoe-Lie (1992) real fire model is justified for demonstrating the application of the probability of failure model for real fires.

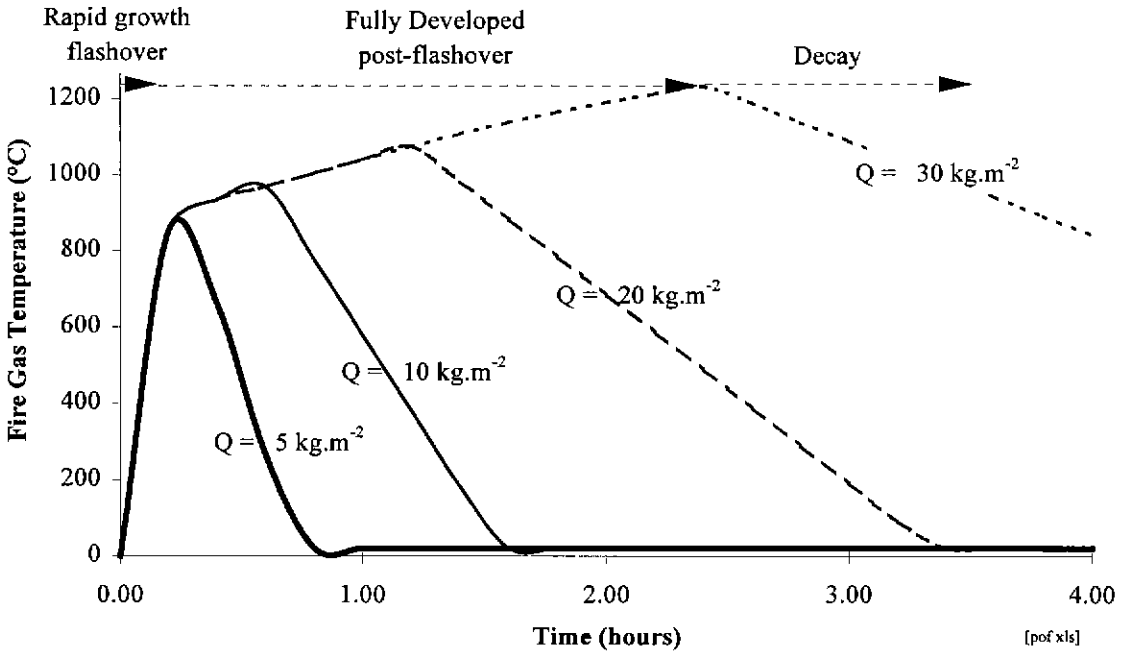

Figure 8.25. Fire Gas Temperature versus Time for Various Fire Loads, Q. (Opening factor, F = 0.05 $m^{0.5}$, heavy bounding material, Lie 1992).

The size of enclosure adopted was 3.00 metres height by a floor plan of 5.00 metres breadth and 4.00 metres depth. The opening adopted was 1.20 metres high by 2.00 metres wide. To enable comparison of the cumulative probability of failure estimated in this application with the probabilities estimated in §8.4.2 and §8.4.3, the same live load was adopted. All of the live load was assumed to be fuel with same heat content as a mass of wood which would lead to the same load as the live load. Kilograms of wood is a traditional unit in fire science because wood fuel was convenient and led to reproducible fire test results (Drysdale 1985). A mean arbitrary live load of 1.0 kPa thus equates to 100 kg per square metre of floor which is approximately 20% of the total surface area bounding the enclosure. Hence the mass of wood fuel per unit area of boundary surface is approximately 20 kg (of wood) per square metre. Not all fuel is burnt during the course of a fire because much of it tends to be isolated from oxygen; for example, pages in books. A burning efficiency of 50% was assumed. Thus the actual burnt fuel adopted was 10 $kg.m^{-2}$. All other variables were adopted with the same values as in §8.4.3. A summary of values adopted for variables is shown in Table 8.4.

The cumulative probability of failure with time estimated by the probability of failure model is shown in Figure 8.26. A characteristic of real fires is that there is some chance that the wall will not burn down; that is, a maximum time independent probability of collapse, less than 1.00. In Figure 8.26, this time independent probability of collapse is 0.61. For the particular real in this application, the variance of the time of failure, given that failure does occur, is similar to the variance for standard fires; that is 0.12 (§8.4.3). This result is a coincidence. The temperature of the real fire with time was similar to that for the standard fire, until decay occurred.

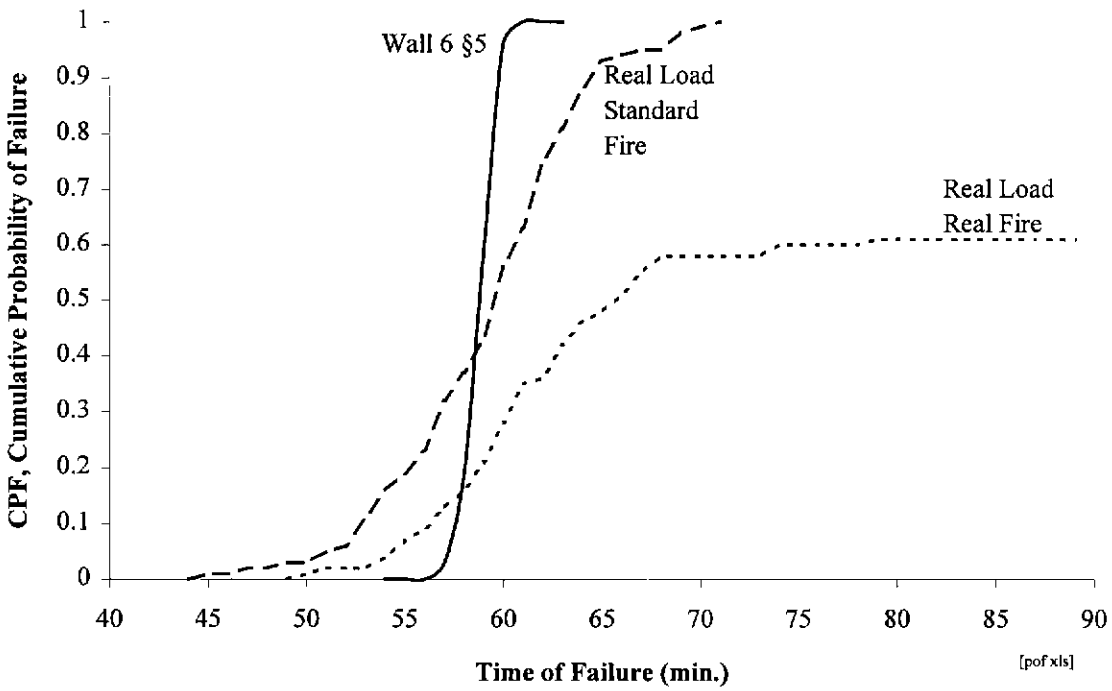

Figure 8.26. Comparison of the Cumulative Probabilities of Failure with Time for a Wall similat to Wall 6 in §4 with a Realistic Variation in Mechanical Properties and Loads, subjected to Real Fire. (Plots from Figure 8.24 are repeated to show comparisons.)

Table 8.4. Summary of Values Adopted for Random Variables in Applications of the Probability of Failure Model in §8.4.2, §8.4.3 and §8.4.4.

Variable	Mean	CoV of α' (random parameters)		
		§8.4.2 Wall 6 §4	§8.4.3 Standard Fire Real Loads Real Properties	§8.4.4 Real Fire Real Loads Real Properties
Fire Variables				
Temperature	§8.4.2 §8.4.3 §8.4.4	0.0	0.0	0.0
Emissivity	0.60 (§5.2.2)	0.0	0.0	0.0
Fuel ($kg.m^{-2}$)	10	NA	NA	as for live load
Enclosure = HxBxD (m^3)	3.0 x 5.0 x 4.0	NA	NA	0
Opening = H x B (m^2)	1.2 x 2.0	NA	NA	0
Thermal Properties of Wood				
Density, ρ	470 $kg.m^{-3}$	0.03	0.06	0.06
Specific heat	Janssens plot Fig 5.9	0.02	0.02	0.02
Conductivity[Note 1]	$[0.4 + 0.6\,\alpha_\rho]$xk(T)	0.02	0.02	0.02
Thermal Properties of Gypsum Board				
Density ($kg.m^{-3}$)	810, Fig 2.5	0.02	0.02	0.02
Specific heat	Figure 5.6	0.02	0.02	0.02
Conductivity	Fig 5.5 (Bold line) * $(0.1 + 0.9\,\alpha_\rho)$	0.02	0.02	0.02
Mechanical Properties of Timber (MPa)				
Compression strength	24 (Appendix C)	0.013	0.07	0.07
Tensile strength	24 (Appendix C)	0.013	0.07	0.07
Elastic modulus	7400 (Appendix C)	0.013	0.07	0.07
Structural Loads (kN/stud)				
Dead load	5.67	0	0.10	0.10
Live load	2.33	0	0.70	0.70
Total load	8.00	0	0.25 eq(8.44)	0.25

Notes.

1. k(T) is the conductivity obtained from Figure 5.8 (Janssens 1994), modified for moisture transfer as shown for plot C in Figure 7.4.
2. NA means not applicable.

The plot of the cumulative probability of failure with time for the wall exposed to real fire, can be used to evaluate whether the time of collapse is a threat to life safety. Horasan et al (1994) conducted a trial evacuation of a medium rise building with more than 1000 unsuspecting people who had not been given any prior practice evacuation drills. The people were a good representative sample of the general population of all ages and degrees of ambulence (from the word, amble, to walk with or without the aids such as crutches). Despite the presence of some people who need assistance with walking, and despite theformation of a crowd at the exit door at the street, which slowed evacuation, the total time for all people to evacuate was 11 minutes. Above it was observed that the CoV in Figure 8.26, for the time of failure for walls which collapse in real fire is 0.12; that is a standard deviation of approximately 7 minutes. The probability of collapse during evacuation is the cumulative probability of failure at 7 standard deviations below the mean. This number of standard deviations is a very large extrapolation of the probability indicated by the 100 simulations carried out with the probability of failure model. The number of standard deviations could be between 4-10. The essential point here is that the number of standard deviations is large and the probability of collapse during evacuation is extremely small (less than 10^{-5}). These probabilities indicate that there is scope for reducing the fire resistance time required for walls down to 30 minutes. Alternatively, walls could be designed to contain a fire to extinguishment and thus give the property protection required by the owner. These deductions, however, implicitly assume that there are no inadvertent service penetrations through the wall, resulting in a loss of fire resistance.

8.5 Conclusions

A probability of failure model has been developed, validated and applied.

Consensus is growing (§8.2.7) that the Monte Carlo method is most appropriate for analyses of the probability of failure of structures in fire, most likely due to the ever improving speed and computational abilities of personal computers. Models have not been sufficiently well developed and phenomena not well enough understood to make simplified models for faster methods of reliability analysis such as FOSM and transformation.

Applications (§8.4) have estimated coefficients of variation, CoV's for thermal and mechanical properties of materials in timber framed walls in fire. For a given density, the CoV's of the thermal properties of timber appear to be small (0.02) compared with the CoV's for mechanical properties (0.15-0.40, Table 8.2). The reason for the consistency of thermal properties of timber is the consistency of its constituents (Table 6.1). Although the variations in growth characteristics of timber greatly affect its mechanical properties, the characteristics do not affect its constituents.

Lognormal distributions seem most appropriate for all random variables other than fire variables which should be modelled by the extreme value distribution, the Weibull distribution.

Walls made from timber which is randomly selected from graded supplies (F8-AS1720.1 Leicester et al 1988) leads to a significant variation in the time of failure compared with failure times in experiments where the variation of timber with respect to elastic modulus is minimised. §8.4.3 showed that the CoV for the time of failure was similar to the CoV for the elastic modulus of the timber - approximately 0.12.

Walls in real fire have some maximum probability of failure, less than 1.00, independent of time (Figure 8.26). For the application demonstrated in §8.4.4, the variance of failure times, for those walls which failed, was similar to the variance of failure times for the walls in standard fire. This is but one example. Further investigation is required to establish the variability of failure times of walls in real fire compared with failure times in standard fires.

In §8.4.4, it was appears likely that the probability of walls collapsing in fires, is not a threat to life provided the occupants can escape by means of egress which conform to current building regulations. Walls should be designed to contain fire until it extinguishes, as the building owner requires.

Future research should be undertaken to increase the speed of the probability of failure model with the use of an importance sampling function (§8.2.5.5 and §8.3.1).

Surveys and research into the reduction of the times of failure due to service penetrations in walls and other construction details should be undertaken.

9. Conclusions and Recommendations for Further Research

9.1 Conclusions

9.1.1 General

In accordance with the aims in §1.5, the research for this thesis has developed time and probability of failure models to reduce the need for testing and to enable the design of light-timber framed walls in accordance with new performance-based building fire safety regulations which are gradually being introduced in countries around the world. The time of failure model comprises separate models for fire severity, heat transfer and structural response. The probability of failure model incorporates the time of failure model into a Monte Carlo analysis. The research and development of the time and probability of failure models achieved the following:

1. The development of a new heat transfer model (ADIDRAS) for structures containing cavities with re-entrant corners and smoke.
2. Eight full scale wall furnace experiments to validate ADIDRAS and the time of failure model.
3. A review of existing structural response models from which Young's (1999) model was found to be most appropriate for incorporation into the time and probability of failure models.
4. The development of a time of failure model that incorporated ADIDRAS and Young's structural response model and can incorporate most fire severity models.
5. The development of a model which can be used to estimate the probability of failure with time, for a light-timber framed wall exposed to real fires. For this model, a Monte Carlo analysis program was written.

It has been demonstrated with the time and probability of failure models, that timber can be used in loadbearing wall structures to achieve required times to failure at some nominated minimum risk.

The time and probability of failure models were developed for a wide range of light-timber framed walls exposed to standard and real fires. The scope includes those walls shown in Figure 9.1. The scope of validation against experimental results included ordinary hollow cavity walls (§5.1-5.4) and insulated double stud walls (§5.5), both of which were exposed to standard fires (AS1530.4). Although the time of failure model was written to predict the modes of failure of insulation, integrity and structural collapse, the walls in experiments for validation of the model, only failed by structural collapse, in particular, buckling. Despite experimental validation which is still required for real fires and the modes of failure

mentioned above, comparisons of predictions with the time of failure model, to results from the experiments have shown that the model can replace many wall furnace tests.

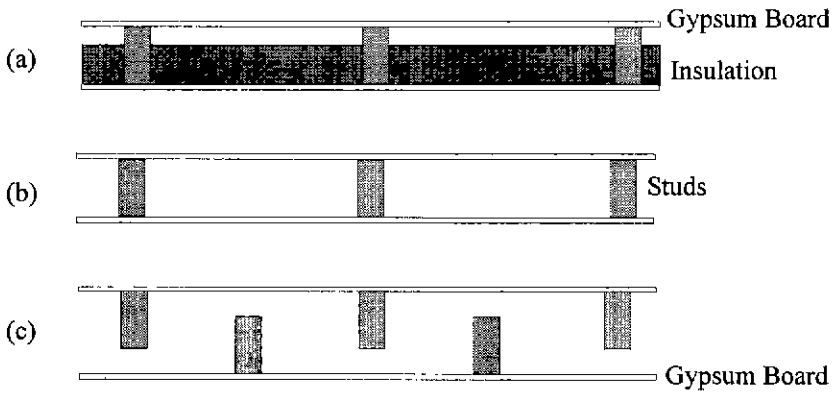

Figure 9.1 (Figure 1.3 repeated). Range of Light-Timber Framed Wall Sections for Heat Transfer Modelling: (a) Ordinary Insulated Stud Wall. (b) Uninsulated Ordinary Stud Wall. (c) Uninsulated Staggered Stud Wall.

Much of the efficacy of the time and probability of failure models in achieving the aims of the research described in this thesis, is due to a number of novel features in ADIDRAS and Young's (1999) structural response model. The novel features of ADIDRAS include:

1. Radiation analysis for cavities with re-entrant corners and smoke.
2. Simple modelling for the transfer of heat by the movement of moisture.
3. Modelling for the sloughing of individual sheets of gypsum board.
4. Implicit finite difference procedures which, for the analysis of thermal diffusion alone, are fast, stable and independent of time step.

Novel features of Young's model include rapid computation speed and a high level of refinement which is comparable with the refinement that can be achieved with three dimensional finite element analyses. The numerical analyses in his model consistently remain stable until collapse is predicted. His model involves such details as partial composite action of gypsum board with the studs, variable support conditions, non-linear mechanical properties which are different in compression and tension.

It is believed that the research for this thesis has clarified appropriate values for temperature-dependent material properties at elevated temperatures, from the wide ranges of values which have been previously published. Clarification was achieved with the use of the novel modelling features mentioned above and the results from a range of well controlled independent experiments. The material properties which were obtained from these experiments and were input into the time of failure model, led to good predictions compared with results for temperatures in walls and times to failure obtained from full scale wall furnace

experiments. An example of the well controlled conditions is the pinned supports adopted in some wall experiments. The rotational stiffness of these supports was clearly known to be zero compared with supports for walls, in standard tests (AS1530.4), which have some unknown rotational stiffness which varies between zero and large values (full fixity) during thermal degradation from fire exposure.

The time of failure model has been used to obtain useful knowledge for the design of light-timber framed walls for fire resistance. Variables for which relationships with the time of failure have been derived include structural load, wall height, thickness of gypsum board, various thermal properties and many characteristics relating to studs (elastic modulus, strength of studs, cross-sectional dimensions, initial crookedness).

Effects of moisture transfer have been revealed with experiments and the time of failure model (comprising ADIDRAS and Young's (1999) structural response model). Although it has been known that heat and moisture can be used to bend wood in the construction of furniture and wooden ships centuries ago, the research for this thesis has more clearly demonstrated the effects of moisture and heat on the time of failure of light-timber framed walls in fire. The simple modification of thermal conductivities (modification C in Figure 7.3) shows that the movement of moisture transfers heat approximately 10 times faster than thermal diffusion. The adoption of Young's (1999) properties for the elastic modulus of timber in compression (Figure 6.9) has shown that the creep or plastification caused by moisture approaching the vaporisation point, has the effect of reducing the elastic modulus relative to the ambient value from 0.90 to 0.20 . The effects of moisture transfer are not significant in timber at temperatures greater than 150°C. Soon after all moisture has vaporised, the timber stiffens. However, the creep deflections remain. There is a limited window of time which appears to be approximately 10 minutes when moisture transfer rather than charring, is the critical cause of potential failure. In this thesis, failure caused by the effects of moisture transfer has been called, "steaming failure". The research has indicated that the effects of moisture movement on heat transfer and mechanical properties are only of concern for walls that are either more slender than walls commonly built (that is, similar to Wall 6 in §4 but more than 4.00 metres tall) or more heavily loaded than is permitted in timber engineering codes such as AS1720.1. Consequently, it is unsafe to extrapolate failure times for such walls, on the basis of results from standard fire tests, unless allowance is made for the heat transferred by the movement of moisture and the reduction in the elastic modulus of timber in compression in regions where vaporisation is occurring.

The probability of failure model undertakes time-dependent probability analyses that are quite different in nature compared with previous time-dependent probability analyses. Previous analyses have been concerned with stationary ergodic stochastic processes; that is, random with time without having any trend which changes their statistical properties such as the mean and coefficient of variation such as wave

action, wind and fatigue. The process of light-timber framed walls degrading and possibly collapsing in fire does not involve behaviour that is stationary (repetitive) with time. The resistance of walls in fires substantially decreases with time and is a complex function of many variables. The probability of failure model has sufficient robustness to remain numerically stable for extreme values of random variables that can be generated in many simulations of walls exposed to fire. The model is sufficiently fast. One hundred simulations of walls exposed to fires of one hour duration, can be carried out in approximately 6 hours on a pentium 200MHz personal computer.

More detailed conclusions are given for the models for heat transfer, ADIDRAS, structural response, time and probability of failure in the following sections, §9.1.2 - §9.1.5

9.1.2 Conclusions on the Heat Transfer Model, ADIDRAS

In addition to the general conclusions in §9.1.1 which involve the heat transfer model, ADIDRAS, conclusions on the relative importance of the following thermal phenomena have been found:

1. Heat transfer is predominantly two dimensional in the horizontal plane. Heat transfer in the vertical direction is not dominant. Thus there is no significant vertical conductive heat flow (Figures 4.18, 4.24 and 4.25).
2. Thermal diffusion is the controlling mode of heat transfer in gypsum board and wood where temperatures are greater than 150°C. (§5.3 and §5.4)
3. As mentioned in §9.1.1, moisture transfer substantially increases heat transfer by approximately a factor of 10, in regions where temperatures are less than 100°C.
4. In the wall experiments reported in this thesis in §4, it was apparent that heat of pyrolysis in wood, was not significant and had no discernable effect on temperatures (§5.6.2).
5. The presence of smoke in cavities does not appear to significantly affect temperature distributions in walls (Figures 5.16, 5.17 and 5.20).
6. There is strong evidence (§5.4.3) that shrinkage gaps open up at the interface between studs and gypsum board, particularly on the fire side when the temperature at the interface exceeds 400°C as shown in Figure 9.2. Radiation in these gaps transfers much heat away from the fire side of studs towards the cavities. Gap widths as small as 1 mm, provide a significant path for radiant heat. The formation of these gaps appears to be the reason that temperatures which are predicted for wood on the fire side of studs, are overestimated by as much as 150°C by models which ignore heat transfer associated with the gaps.

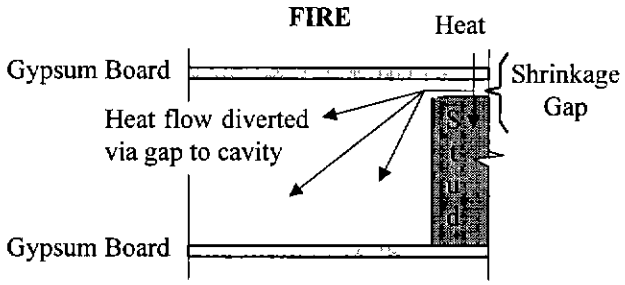

Figure 9.2. Part Horizontal Section through Ordinary Hollow Cavity Wall showing Diversion of Heat via Gap to Cavity. (Figure 1.3 repeated.)

Validation of the model with simple independent experiments to establish thermal properties, and with comparisons of model predictions with full scale wall furnace experiments have supported the use of the following thermal properties:

1. Relative density, specific heat and conductivity for wood by Janssens (1994) (§2.4.3 and §5.2.4).
2. Relative density of gypsum board by Mehaffey et al (1994) (Figure 2.5).
3. Conductivity of gypsum board below 400°C by Mehaffey et al (1994) (§5.2.3.2) modified for variations in density in accordance with equation (5.1). Above 400°C, the effective conductivity (for which the aim is to predict the same rate of heat transfer as the actual conduction together with the radiation through shrinkage cracks in the gypsum board) should be obtained by independent testing since the distribution of cracking varies substantially amongst boards produced by different manufacturers.
4. Specific heat of gypsum board by Sultan (1996) (Figures 2.6 and 5.6).

The numerical methods adopted for the model were designed to ensure sufficient speed and robustness for wide ranges of values for variables generated in failure probability modelling. These methods included:

1. The alternating direction implicit (ADI) method for thermal diffusion which has the numerical stability of implicit methods but unlike other implicit methods, has similar solution speed to explicit methods. (§2.5.2 and §3.2)
2. Discrete radiation analysis for smoke, gaps and re-entrant corners. Although this method is time consuming, the model only applies it once in the numerical simulation of a wall exposed to a fire. (§2.5.3 and §3.9.5)
3. The transformation of nodes for modelling the sloughing of gypsum board (§3.8)

4. The scaling of conductivities in regions where temperatures are less than the vaporisation temperature.(Figure 7.3).
5. Maintaining a constant grid of nodes with time, allowing for shrinkage gaps between studs and gypsum boards. This methodology improves predictions of temperatures at the fire side of studs by as much as 150°C when the temperatures in this vicinity rise above 400°C. (§5.4.3).

9.1.3 Conclusions on Young's (1999) Structural Response Model

Further to the conclusions in §9.1.1, details of Young's (1999) model which contributed to the efficacy of the time of failure model are subsequently summarised.

The iterative procedure he employed greatly simplifies the analysis of a complex combination of structural phenomena in the structural response of light-timber framed walls in fire. The procedure separates time dependent processes from deflection movements and analyses the processes on simple discrete elements. The modelling equations for the structural response of the individual discrete elements were simple and hence can be easily understood and facilitate any future enhancements by other researchers.

Young's (1999) method of discrete elements enabled the simple application of the equations for:

1. Stress as a function of strain.
2. Elasticity as a function of temperature.
3. Strength as a function of temperature and the removal of any elements which fail by rupture or crushing.
4. Relaxation modelling for creep (although this application is yet to be validated)
5. Thermal expansion and contraction
6. The reduction of elasticity due to moisture effects.

The modelling of the combined structural action of all elements within a wall section, with composite section analysis, has had several advantages. Any degree of partial composite action between gypsum board and the studs has been able to be modelled. Composite section analysis has enabled gypsum boards and studs to be modelled with single line members which can be analysed with frame analysis.

The frame analysis written in the model has the advantages of numerical robustness and computation speed compared with finite element analyses. Furthermore, the frame analysis has facilitated the implementation of second order analysis and the modelling of supports with variable rotational

stiffnesses. Thence, the model predicts structural collapse not only due to inadequate strength of materials, but also due to overall buckling.

The accuracy of Young's (1999) model has been well evaluated against classical solutions, finite element analyses and a number of independent experiments under well controlled conditions. The numerical accuracy of Young's model is within one percent of classical solutions and converged solutions of three dimensional finite element analyses. Young showed that this accuracy is not limited by any shear lag effects in gypsum board. From 30 full scale wall experiments at ambient conditions, measurements clearly established the load capacity, elastic modulus for studs, fastener stiffness and rotational stiffnesses of supports. Small scale experiments established mechanical properties for timber studs at elevated temperatures and gypsum board at ambient conditions. From these independently measured properties, Young compared his model predictions with results from furnace experiments on full scale walls made from materials which were very similar to the materials in the ambient and small scale experiments. His model predictions were within 5% of experimental results for walls within the slenderness and load limits mentioned above.

The assemblage of elements in Young's model have a similar grid pattern to a typical three dimensional finite element model. An advantage of Young's model over finite element models is the ease with which structural actions can be incorporated into his model. For example, most finite element programs have difficulty in modelling elements in which stress changes from compression to tension, especially when the properties also change which is the case for wood at elevated temperatures. Stress changes from compression to tension can be solved by Young's model with ease. Another example is the modelling for fastener stiffness in partial composite action between gypsum board and studs which was easily incorporated into Young's model. Attempts to model partial composite action in finite element models invariably led to numerical instabilities because of extreme variations in element dimensions and mechanical properties in the region of fasteners.

9.1.4 Conclusions on the Time of Failure Model

Further to the general conclusions in §9.1.1, more detailed conclusions are given for the time of failure model below.

The aims (§1.5 and §7.1) for the time of failure model have been satisfied. In §7.3 and §7.4 it was shown that model predictions of the time of failure compared well (within 5%) with experimental results for walls built according to common practice (TPC 1994) and exposed to standard fires, AS1530.4. Common practice means top and bottom plates secured against rotation, gypsum board nailed to studs (at spacings

less than 300 mm), heights less than 4.00 metres and loads within limits permitted by structural engineering codes such as AS1720.1. On the basis of this good comparison, the model could replace many standard wall furnace tests. The model has been written for standard and real fires, but is yet to be validated against a real fire test. The model is sufficiently fast and robust for incorporation into a probability of failure model. Relationships between a number of variables and the time of failure have been developed with the model. These relationships should be useful for the design of ordinary cavity walls for standard fire (AS1530.4).

Relationships for time of failure and design information which have been found that will be valuable to fire engineers are as follows:

1. The dominant mode of structural collapse is buckling, and hence, the modulus of elasticity for timber in compression is the dominant mechanical property controlling the time of failure.
2. Since the time of failure model repeats a frame analysis at frequent and regular time steps, an aim was to determine whether repetitions of the frame analysis was actually required at each time step; that is, whether the second order structural model could be simplified with a first order analysis. It was demonstrated in §7 that without second order analysis, the time of failure may be overestimated by 10 minutes, and thus, a second order frame analysis is indeed required at each time step.
3. As mentioned in §9.1.1, modelling of walls taller than 4.00 metres or more heavily loaded than permitted by timber engineering codes such as AS1720.1 must allow for the heat transferred by the movement of moisture and the reduction in the elastic modulus of timber in compression in regions of moisture vaporisation.
4. The dominant modes of heat transfer controlling the time of failure are those affecting heat transfer through solid material - thermal conduction, heat transferred in the movement of moisture, and at temperatures greater than 400°C, radiation through pores. Radiation and convection through cavities and at external surfaces do not dominate over heat transfer through the solid materials in walls (Table 7.2).
5. For the walls reported in this thesis, similar percentage changes in the depth and breadth of studs have approximately the same effect on the time of failure.
6. Time of failure is inversely related to initial crookedness at ambient conditions, although in increase in crookedness of the order of 10mm is unlikely to reduce the time of failure by more than 5%.
7. The time of failure is sensitive to the temperature at which glass fibres in gypsum board melt. When the minimum temperature in substantial portions of board reach this melting point, the portions tend to fall away, that is, "slough". The time of failure could be

increased, if fibres with higher melting temperatures were used in the manufacture of gypsum board.

8. For the walls researched for this thesis and for the thickness of gypsum board exceeding 25mm on the fire side, the shrinkage gaps mentioned in §9.1.2 significantly increase the time of failure compared with failure times when gaps are ignored. The increase in failure times was approximately 10 minutes.
9. For the wall studied, the component additive method (White 1988) was reasonably accurate and safe.

From the wide range of thermal and structural variables in both ADIDRAS and Young's (1999) structural response model, the sensitivity of the time of failure is greatest for the following variables in descending order (Table 7.2):

1. Fire temperature
2. Vertical Load
3. Elastic modulus of timber in compression
4. Density of timber
5. Specific heat of timber
6. Stud depth and breadth
7. The density, specific heat and thickness of gypsum board.

9.1.5 Conclusions on the Probability of Failure Model

Detailed conclusions on the probability of failure model, not mentioned in §9.1.1, are given below.

Log-normal probability distributions are appropriate for most variables for several reasons. From Turkstra's rule (Melchers 1987), it is unreasonable to consider probabilities associated with the simultaneous occurrence of more than one extreme event or one extreme random variable. In the analysis of the probability of collapse of walls in fire, fire temperature is the dominant variable affecting the time of failure, and thus should be considered as the extreme variable. Typical values should be chosen for all other variables; that is, the variables in the heat transfer and structural response models. Although it is appropriate to use extreme value probability distributions for loads for probability analyses for ambient conditions, it is more appropriate to adopt probability distributions for typical loads for fire conditions. Log-normal distributions are appropriate because they give typical non-negative values.

The model has been demonstrated using the Kawagoe-Lie (Lie 1992) real fire model (§8.4.4)

The probability of failure model was applied in three demonstrations which revealed that:

1. Coefficients of variation, CoV's of thermal properties can be controlled within values as small as, 0.02 (§8.4.2). The main reason for these small CoV's appears to be the small variability of the proportions of constituents in timber and gypsum boards (Table 6.1). Since the variability of the proportions of constituents is small for all timber, it is thus seems likely that the variability of thermal properties for timber generally is small. This small variability needs to be confirmed in future research. If the variability of thermal properties for timber is confirmed, it would contrast with the large variability (Table 8.2) of the mechanical properties of timber which is due to the growth characteristics of timber, such as knots, gum pockets, pith and the like. It is not expected that these characteristics affect the variability of thermal properties of timber.
2. The CoV for the time of failure for walls made from timber graded to AS1720.1, subjected to arbitrary-point-in-time live loads and standard fire (AS1530.4) was found to be 0.12 (§8.4.3).
3. For a particular real fire - namely, the Kawagoe-Lie model (Lie 1992) using the live loads in item (2) - the CoV for the time of failure was, coincidentally, similar to that for the case of standard fire (§8.4.4). However, failure was not inevitable. The time-independent probability of failure was approximately 0.6.

9.2 Recommendations for Further Research

9.2.1 General Recommendations for Further Research

As would be expected, there remain many areas for detailed research in experimentation and modelling of heat transfer, structural response and the time and probability of failure of light-timber framed walls in fire. Many of these areas have been identified throughout this thesis. These areas have been collated and are subsequently summarised below in §9.2.2 for areas in heat transfer requiring detailed research, in §9.2.3 for areas in structural response and in §9.2.4 for areas of concern in the modelling of time and probability of failure.

The detailed areas referred to above are mainly scientific issues. However, in order for the benefits of the research to be realised, future research should be pursued in implementation. Possible developments for implementation include simplified models and equations, recommendations of material properties, design charts and the establishment of simple performance targets through risk assessment. An important consideration in implementation is the minimisation of ambiguity; that is, for a particular design problem, different fire safety engineers should independently interpret similar assumptions, material properties,

appropriate means of design and similar performance targets, despite commercial and client pressures. Issues in implementation are discussed in further detail in §9.2.5 and recommendations for further research in this area are given.

9.2.2 Further Research on Heat Transfer Modelling

Further research is required to determine the following thermal properties:

1. Since the cracking patterns of gypsum boards from different manufacturers differs, the conductivities of gypsum board from each manufacturer should be determined from simple tests at temperatures greater than 400°C (§5.7.1); that is, conductivity which includes the radiant heat transfer through cracks. These experiments should simulate similar conditions experienced by gypsum board in walls exposed to fire, in particular the restraint of fasteners and timber framing against shrinkage of gypsum board.
2. Further testing is required to confidently establish the surface emissivity of gypsum boards with temperature as high as 1200°C (§5.3.2).
3. The conductivity of char needs to be obtained from simple tests because, as mentioned in §2.4.3.3, there have been few if any tests to determine the conductivity of char.

The following enhancements of the heat transfer model should be carried out:

1. The validation experiments reported in §4 (Figure 4.23) did not reach temperatures on the ambient side, that correspond to insulation failure (AS1530.4). Further research is required in the prediction of the time of this mode of failure because of the low temperature gradients near the ambient side and thus the high sensitivity of the time of this mode of failure to the specified insulation failure temperatures.
2. Further work needs to be undertaken to stabilize the numerical radiation computations for cavities at temperatures above 600°C. Some method of linearisation needs to be developed.
3. The research for this thesis has demonstrated (§9.1.4) that the movement of moisture substantially reduces the time of failure of slender walls (walls similar to Wall 6 in §4 but with heights greater than 4.0 metres), and the time of failure of walls with load ratios exceeding those permitted by timber structural engineering codes (AS1720.1). For these types of walls, it is necessary to theoretically model the heat transferred by the movement of moisture and vapour, as well as the creep or plastification of timber in regions affected by moisture vaporisation.
4. The capability of modelling heat transfer through insulation in cavities is required to be included. Modelling heat transfer through the insulation with thermal diffusion may be satisfactory. However, Young (1999b) observed that unlike walls with hollow cavities, there

was no sign of moisture transferring out of walls with insulation. Investigation of possible effects of moisture transfer in insulation is required.

5. There is some need to enable ADIDRAS to model surface movements associated with the shrinkage of timber, char and gypsum board at elevated temperatures. This modelling would enable the simple approach to moisture modelling in §5.4.4 to be used in conjunction with the modelling of heat transfer through gaps §5.4.3.

It was shown that smoke density (§5.3.3) and transmissivity (§5.3.4) had little effect on the temperature distributions in walls. Accordingly, a simplified model using Mehaffey's et al (1994) method of modelling heat transfer in a cavity with a single node should be further investigated.

The following tests are required to be undertaken:

1. It was concluded in §5.4.2 that gaps are expected to open at interfaces between studs and gypsum board on the fire side, when the temperatures at the interfaces exceed 400°C. It was also concluded that these gaps are the reason for temperatures measured in timber close to the interfaces being as much as 150°C less than predictions of models which ignore such gaps. These gaps should be confirmed with wire probes or devices to directly detect the time and temperatures when they occur, and the widths of the gaps should be measured.
2. As reported in this thesis the heat transfer model has been validated for standard fire (AS1530.4). In the future, the model should be validated against real fires.
3. In §5.3.2 it was shown that there are inadequacies in current procedures in measuring surface temperatures. Problems with radiation shielding and the accurate placement of thermocouples at surfaces needs to be researched.

Heat transfer modelling of other applications researched by others, should be developed with ADIDRAS. Examples include:

1. Panels tested by König (1991,97) involving cavities insulated with rock wool, and exposed to parametric fires. König noted that char penetrated between studs and insulation. This penetration can be explained with the use of shrinkage gaps (Figure 5.50).
2. The influx of heat through joints between sheets of gypsum board which was suspected by Takeda (1998).

9.2.3 Further Research in Modelling Structural Response.

The following further research required in the development of models for predicting the structural response of light-timber framed walls was identified in chapter 6.

1. To model the structural response of slender and heavily loaded walls (that is, walls similar to Wall 6 in §4 but with heights greater than 4.0 metres and load ratios exceeding those permitted by timber structural engineering codes such as AS1720.1), a model for creep or plastification of timber in compression in regions affected by moisture vaporisation, should be developed.
2. More detailed testing of compression properties of timber needs to be carried out for structural scale timber at elevated temperatures in a similar manner as was done by Lau (1996) for tension. Here, structural scale means timber samples with knots and other growth characteristics, and with dimensions similar to studs in walls. This testing is necessary to confirm whether the relationships for compression properties at elevated temperatures measured by Young (1999) for clear wood are applicable for structural scale timber. Furthermore, it is necessary to measure elastic moduli as well as strength; Lau only measured strength.
3. The potential problems and modelling for accelarated charring around nails (Collier 1993, and Fuller et al 1992) must be researched. Such charring can treble the charring rate in the vicinity of nails, reducing wood fibre stiffness and strength, and thus effectively create large notches.
4. Although creep in dry timber at temperatures above 200°C (Schaffer 1982) is not expected to significantly affect the time of failure of timber framed walls in fire, since studs of minimum temperatures exceeding 200°C should be close to failure, it does not seem that any modelling has been undertaken to justify this expectation. Such modelling should be undertaken in the future.

9.2.4 Further Research on Modelling Time and Probability of Failure

It was shown in Chapter 7 that fire temperature is the dominant variable affecting the time of failure. It is generally recognised that much research is required into the prediction of fire temperatures (IEAust 1989). Appropriate fire loads and the proportion of fire loads that actually combusts need to be determined. Post-flashover fire models (NRCC fire model - Beck et al 1995, Magnusson et al 1970) assume that the whole enclosure is consumed in fire at the sudden stage of flashover. Thomas and Bennetts (1999) have conducted experiments which have shown that sudden flashover does not occur in large enclosures such as open plan offices, nor does it occur in oblong enclosures such as corridors. In

these types of enclosures only part of the enclosure is consumed in fire. Thomas and Bennetts (1999) have referred to these types of fires as, "fully involved". The consequence of fully involved fires is that many building structures are only ever partly exposed to the intense heat of fire at any one time (IEAust 1989). Local exposure to heat allows the redundancies in cooler parts of structures to resist collapse. Once models for fully involved fires are developed, the use of such redundancies to increase the fire resistance should be explored in timber structures. More generally, research which leads to improvements in post-flashover fire severity modelling will produce the greatest benefit in designing fire resistant light-timber framed structures.

In Chapter 8, the random properties of some variables were judged. Surveys and experimental programs are required to improve the knowledge of these properties to obtain better estimates of the probability of failure. It was mentioned in §9.1.5 that the small variabilities expected for the thermal properties of timber need to be confirmed. Likewise, the variability of the elastic modulus of timber in compression at elevated temperatures needs to be measured.

Further work is required to make the input and output of models simple and expressed in terms which practicing engineers are familiar with; for example input of common gypsum board types and thicknesses instead of thermal properties.

Future research should be undertaken to increase the speed of the probability of failure model with the use of an importance sampling function (§8.2.5.5 and §8.3.1).

Surveys and research into the reduction of the times of failure due to service penetrations in walls and other construction details should be undertaken.

Further research is required in applying the probability of failure model, described in this thesis, within an overall risk assessment of building fire safety systems (which include protection from sprinklers, alarms, fire brigade and means of egress - Beck et al 1989). This research is underway in the Fire Code Reform Project 1993 and should determine appropriate fire resistance periods for particular fire scenarios in particular types of buildings.

Generally, ongoing research is required in developing the time and probability of failure models for use in fire engineering practice. Various issues, in this regard are raised in the next section, §9.2.5.

9.2.5 Implementation of Research in Fire Engineering Practice.

In the introduction, §1.1, to this thesis, it was explained that the research undertaken was driven by the need to develop models for new performance based building fire codes. The research in this thesis has made significant contributions to the understanding and modelling of a range of thermal and structural phenomena. The research has also synthesised these contributions to produce time and probability of failure models for light-timber framed walls exposed to standard and real building fires. Much work remains to implement the knowledge gained in the research for this thesis as well as that gained by other researchers such as Gammon (1987), Mehaffey et al (1994), Takeda (1998) and Thomas(1997).

With the possible exception of Mehaffey and Takeda's model (1994 and 1997), the input of wall sections and the thermal properties of materials in heat transfer models is not of a form which practicing fire engineers can readily use. It would be preferable for this input to be expressed in terms of particular components, for example gypsum board type and thickness, and stud dimensions and wood type. There will always be some difference of opinion on values for thermal properties. Thus these properties will vary depending the users of the models. The inevitable differences in selected property values undermines the basic requirements of codes of practice (Standards Australia 1995) that code methods must ensure safety and provide some basis for fair commercial competition which requires that different engineers will, independently, start from similar assumptions for loads, material properties and performance targets. For example, the Timber Engineering Code, AS1720.1 stipulates a basic flexural strength for F8 grade timber as 8.6 MPa despite actual flexural strengths typically varing between 10-50 MPa (Leicester et al 1988). Without a code of practice, a fair design value such as 8.6 MPa, would be ambiguous. Commercial competition would increase the values adopted for design and inevitably undermine confidence in safety and models used.

There are several approaches for implementing models to ensure fair, consistent and economical design of light-timber framed walls for fire:

1. Practices in well established codes could be followed. Structural engineering codes (for example, AS1170.1, AS1720.1, AS3600, AS4100) specify simple theoretically based design procedures, material properties and loads. Similarly, fire engineering codes require simple models. Such models are currently under development (Liew and Buchanan 1999, Pohl and Clancy 1999). The codes should specify thermal properties, gravity loads and appropriate fire severities. Fire severities are analagous to loads in structural engineering codes. Structural engineering has been practiced over 100 years more than fire engineering. In structural engineering dominant structural phenomena are understood much better than phenomena in fire engineering. Further, in fire engineering there is a much smaller statistical base of information on properties and fire severities from which to define rational

fair design values without being too conservative. Eventually, fire engineering should follow similar practices in structural engineering and other engineering disciplines. Until the knowledge base greatly increases, complementary means of implementing models will be necessary.

2. The principles of equivalence (Beck et al 1989) could be followed. In a very general sense, equivalence ties models to traditional practices in some particular way. The traditional approach to fire resistance engineering has been to prove performance with a standard fire test. The principles of equivalence could be applied by calibrating theoretical models to predict similar results to those of documented standard fire tests. The models could then be used to predict the behaviour of other walls with various restrictions on thicknesses of gypsum board and other items. The use of equivalence in this manner enables models to make predictions which are extrapolations of test results. Such an extrapolation method was developed by Collier (1991, 1993). However, with the exception of the models of Collier, and Mehaffey and Takeda (1994, 1997), the input data for theoretical models is too complex for most practicing fire engineers. The theoretical models are analagous to structural engineering finite element models. They are rigorous but require input data in a fundamental form which practicing engineers could not implement easily for common day-to-day projects. Future work is required to develop simple models with input data that is familiar to practicing engineers; such as the input of components as mentioned above. In such applications, models should assume default values for thermal properties and fire severities. Although this simplified approach does overcome the problems raised in approach (1) above, the author is concerned that models could be misused by people not appropriately trained in fire engineering.
3. Charts and simple empirical models could be developed from the generation of failure times from the models for various combinations of dimensions, materials, loads, and fire severities. There is a limited number of practical combinations of these variables. Charts and simple empirical models would be simple and fast to implement. Very importantly, they would be unambiguous. Future research should be undertaken to develop such charts and models. Appropriate real fire severities should be derived.

References

ABAQUS (1997), "ABAQUS/Standard Manual," Hibbitt, Karlsson and Sorenson Inc, 1080 Main Street, Pawtucket, RI, USA.

ASCE, ACSM and ASPRS (1994), "Glossary of the Mapping Sciences," prepared and published by the American Society of Civil Engineers, the American Congress of Surveying and Mapping, and the American Society for Photogrammetry and Remote Sensing.

ASTM E 119 (1995), "Standard Test Methods for Fire Tests of Building Construction and Materials", American Society of Testing and Materials, Philadelphia, Pennsylvania USA.

AS1170.1 (1989), "Minimum Design Loads on Structures, Part 1 - Dead and Live Loads and Load Combinations", Standards Association of Australia.

AS1530.4 (1990), "Methods for Fire Tests on Building Materials, Components and Structures and Structures, Part 4: Fire Resistance Tests of Elements of Building Construction", Standards Australia.

AS1720.1 (1988), "SAA Timber Structures Codes, Part 1- Design Methods", Standards Association of Australia.

AS1720.4 (1990), "Timber Structures, Part 4: Fire-Resistance of Structural Timber Members", Standards Australia.

AS1748 (1997), "Timber - Stress-graded - Product requirements for mechanically stress-graded timber", Standards Australia.

AS3600 (1988), "Concrete Structures", Standards Australia.

AS4100 (1990), "Steel Structures Code", Standards Australia.

Alloysius D (1996), "Significance of Plasterboard in Raising Load Resistance of Walls," Bachelor of Civil Engineering course subject, ECD4400 Fourth Year Civil Engineering Project, Victoria University of Technology, Melbourne Australia.

Amy L (1961), "The Physico-Chemical Bases of the Combustion of Cellulose and Ligneous Materials," Cah. Centre Tech. Bois 45:31. (in French)

Atreya A (1984), "Pyrolysis, Ignition and Fire Spread on Horizontal Surfaces of Wood," Division of Applied Sciences, Harvard University, Cambridge Massachussetts, USA.

Baber HL and Fowkes AHR (1984), "Fire Resistance of Loadbrearing Timber Walls," Proceedings of Pacific Timber Engineering Conference, Building Research Association of New Zealand, Judgeford, New Zealand.

Babrauskas V (1981) "A Closed-Form Approximation for Post-Flashover Compartment Fire Temperatures", Fire Safety Journal, Vol 4 pp63-73.

Babrauskas V and Williamson RB (1980a). "The Historical Basis of Fire Resistance Testing - Part 1." Fire Technology, Vol 14, pp184-194.

Babrauskas V and Williamson RB (1980b). "The Historical Basis of Fire Resistance Testing - Part 1." Fire Technology, Vol 14, pp304-316.

Babrauskas V and Williamson RB (1979a), "Post-Flashover Compartment Fires: Application of a Theoretical Model", Fire and Materials, vol 3, No 1.

Babrauskas V (1979b), "COMPF2, A Program for Calculating Post-Flashover Fire Temperatures", US Department of Commerce /National Bureau of Standards, NBS Technical Note 991.

Back EL, Htun MT, Jackson M and Johnson F (1967), "Ultrasonic Measurements of the Thermal Softening of Paper Products and the Influence of Thermal Auto-Cross-Linking Reactions," Tappi, vol 50, part 11, pp 542-547.

Bayley FJ (1955), "An Analysis of Turbulent Free Convection Heat Transfer," Proceedings of the Institution of Mechanical Engineers, Vol 169, p 361.

BCA (1996), "Building Code of Australia," The Australian Building Codes Board.

Beall FC (1968), "Thermal Degradation of Wood and Wood Components," PhD Dissertation, Dept Wood Products Engineering, State University College of Forestry, Syracuse, New York, USA.

Beck VR, Yaping H, Stewart S, Luo M, Szmalko E and White B (1995), "Experimental Validation of the NRCC Fire Growth Model", Research Report 95/01, Centre for Environmental Safety and Risk Engineering, Victoria University of Technology, Australia, 102pp.

Beck VR, Eaton C, Johnson P, Merewether T, Ramsay C, Richardson J, Freeman R, Lacey R, MacLennan H, Reddaway L and Thomas I (1989), "Fire Safety and Engineering: Project Report", The Warren Centre for Advanced Engineering, University of Sydney, December 1989.

Beck VR (1986), "Cost Effective Fire Safety and Protection Design Requirements for Buildings (Class V Occupancy)," Footscray Institute of Technology, Australia.

Beck VR (1985), "The Prediction of Probability of Failure of Structural Steel Elements Under Fire Conditions," Civil Engineering Transactions, The Institution of Engineers Australia, pp 111-118.

Bejan A (1984), "Convection Heat Transfer," John Wiley and Sons.

Bender DA, Woeste FE, Schaffer EL and Marx CM (1985), "Reliability Formulation for the Strength and Fire Endurance of Glued-Laminated Beams," Research Paper FPL 460, Madison Wisconsin, US Dept Agriculture, Forest Service, Forest Products Laboratory, 43 pp.

Benjamin JR and Cornell CA (1970), "Probability, Statistics, and Decision for Civil Engineers," McGraw-Hill. Library of Congress 79-97116, ISBN 07-004549-6, 684 pp.

Bizri H (1973), "Structural Capacity of Reinforced Concrete Columns Subjected to Fire Induced Thermal Gradients", University of California, Berkeley, Structural Engineering Laboratory Report No. UC SESM 73-1.

BHP Research - Melbourne Laboratories. Engineering and Scientific Research. Mulgrave, Melbourne, Australia.

Boral (1997), "Boral Plasterboard Installation Reference manual, Book 2, October 1997", Boral Australia.

Boral (1994), "Fire Rated and Sound-Rated Systems," Boral Australian Gypsum Limited.

British Gypsum Fireline, The White Book, 1996, UK.

British Gypsum Glasroc, The Glasroc Fire Book, January 1995, UK.

Bohren CF and Huffman DR (1983), "Absorption and Scattering of Light by Small Particles," John Wiley and Sons, New York.

Broding WC, Diederich FW and Parker PS (1964), "Structural Optimization and Design Based on a Reliability Criterion," Journal of Spacecraft, Vol. 1, No. 1, pp 56-61.

Brozetti J, Law M, Pettersson O and Witteveen J (1983), "Safety Concepts and Design for Fire Resistance for Steel Structures," IABSE Surveys S-22/83, Zurich, February 1983.

Browne FL and Tang WK (1962), "Thermogravimetric and Differential Thermal Analysis of Wood and Wood Treated with Inorganic Salts During Pyrolysis," Fire Research Abstract Review, vol 4, part 1, pp 76-91.

Browne FL (1958), "Theories of the Combustion of Wood and its Control," Forest Products Laboratory Report 2136, US Dept Agriculture, Forest Services, Forest Products Laboratory, Madison, Wisconsin, USA.

Buchanan AH (1994 Editor), "Fire Engineering Design Guide," Centre for Advanced Engineering, University of Canterbury, New Zealand, p40.

Buchanan AH (1986), "Combined Bending and Axial Load in Lumber", Journal of Structural Engineering, ASCE, Vol 112 No 12, pp2592-2609.

Bucher CG and Bourgund U (1990), "A Fast and Efficient Response Surface Approach for Structural Reliability Problems," Structural Safety, Elselvier, vol 7, pp 57-66.

Bukowski RW and Babrauskas V (1994), "Developing Rational, Performance-based Fire Safety Requirements in Model Building Codes," Fire and Materials, vol 18, pp173-191.

CAN/ULC-S101-M89 (1989), "Standard Methods of Fire Endurance Tests of Buidling Construction and Materials", Underwriters Laboratories of Canada, Scarborough, Ontario.

Carnahan B, Luther HA and Wilkes JO (1969), "Applied Numerical Methods," John Wiley, New York 604 pp.

Carne D (1995), "Melt Temperatures of Glassfibre Used in Fyrchek," CSR Gyprock Bradford Report Number 001292DC.

Carslaw HS and Jaeger JC (1959), "Conduction of Heat in Solids", 2nd edition, p76, Oxford University Press, Oxford, UK.

Churchill SW and Chu HHS (1975), "Correlating Equations for Laminar and Turbulent Free Convection from a Vertical Plate," International Journal of Heat and Mass Transfer, Vol 18, p1323.

CIB W14, "A Conceptual Approach Towards a Probability Based Design Guide on Structural Fire Safety," CIB W14 Workshop, "Structural Fire Safety."

Clancy P (1996), "Sensitivity Study of Variables Affecting Time-of-Failure of Wood Framed Walls in Fire", Proceedings of the International Wood Engineering Conference, New Orleans, Lousiana USA, October 28-31, Vol 2. pp 263-268.

Clancy P (1996a), "CESARE Fire Barrier, A Model for Time Dependent Probability of Failure of Barriers in Real Fire", Internal Report for CESARE, Centre for Environmental Safety and Risk Engineering, Victoria University of Technology, Australia, 250 pp.

Clancy P and Young SA (1996), "Full Scale Wall Furnace Tests", Report, Department of Civil and Building Engineering, Victoria University of Technology, Australia, 268 pp.

Clancy P and Young SA (1996a), "A Model for Predicting the Probability of Failure of Wood Framed Walls and Floors in Real Fire", Proceedings of the Third International Conference, Wood and Fire Safety, May 6-9, 1996, The High Tatras, Hotel Patria, Slovak Republic, pp33-42.

Clancy P, Beck VR and Leicester RH (1995), "Time Dependent Probability of Failure of Wood Frames in Real Fire", Proceedings, Fire and Materials, Fourth International Conference and Exhibition, November 15-16 1995, Marriot Hotel, Crystal City, Virginia, USA, pp85-94.

Clancy P and Young SA (1995), "Models for Light Timber Framed Assemblies in Real Fires", Proceedings of the Fifth East Asia-Pacific Conference on Structural Engineering and Construction, Gold Coast, Queensland, Australia, 25-27 July 1995, pp2271-2276.

Clancy P, Young SA, Beck VR and Leicester RH (1994), "Modelling of Timber Framed Assemblies in

Real Fires", Proceedings of the Pacific Timber Engineering Conference, Gold Coast, Australia, July 1994, Vol. 2 pp 282-293.

Coelho PJ and Carvalho MG (1997), "A Conservative Formulation of the Discrete Transfer Method," Journal of Heat Transfer, Transaction of the ASME, Vol 119, February, pp 118-128.

Collier P (1991), "Technical Recommendation N° 9. Design of Light Timber Framed Walls and Floors for Fire Resistance", Building Research Association of New Zealand, August, 17pp.

Collier P (1993), "A Method to Predict the Fire Resisting Performance of Loadbearing Light Timber Framed Walls", Building Research Association of New Zealand.

Collier P (1994), Personal communication.

Collins GE (1992), "Fire-Resistance Test on a Loadbearing Timber Stud Partition," Report FSV 0223, Commonwealth Scientific Industrial Research Organisation, CSIRO, Division of Building, Construction and Engineering, North Ryde, Australia.

Collins MJ (1989), "Allowable Heights for Gibraltar Board Lined Internal Wall Panels," Wood Technology Division Contract Report No. WTC 891, Forest Research Institute, Rotarua, New Zealand.

Cramer SM and White RH (1996), "Fire Endurance Modelling of Wood Structural Systems", Proceedings of the International Wood Engineering Conference, New Orleans, Lousiana USA, October 28-31, Vol 2. pp 249-256.

Croft DR and Lilley DG (1977), "Heat Transfer Calculations Using Finite Elements," Applied Science Publishers Ltd, London.

CSIRO Laboratories - Commonwealth Scientific and Industrial Research Organisation, Division of Building, Construction and Engineering, Highett, Melbourne, Australia.

CSIRO (1992), "Fire-Resistance Test on a Loadbearing, Timber Stud Partition", Report FSV 0187, CSIRO (Commonwealth Scientific Industrial Organisation), Division of Building, Construction and Engineering, North Ryde, Australia.

CSR Gyprock (1997), "CSR Plasterboard Installation Manual," August 1997, Australia.

Davis K (1998), CSR Insulation, Sydney Australia, personal communication.

Davis WH and Thompson WS (1964), "Influence of Thermal Treatments of Short Duration on the Toughness and Chemical Composition of Wood," Forest Products Journal, vol 14 part 8, pp 350-356.

de Kraker A, Tichleret JW and Vrouwenvelder ACWM (1982), "Safety, Reliability and Service Life of Structures," Heron, vol 27, No. 1, 87pp.

De Salvo GJ and Gorman RW (1989), "ANSYS Engineering Analysis System User's Manual," Revision 4.4, Swanson Analysis Systems Inc, Houston, Pennsylvania, USA.

Dee Snell F and Ettre LS (1971) - Editors of, "Encyclopedia of Industrial Chemistry Analysis," Interscience Publishers, John Wiley and Sons, vol 14, p88, Ref543.003 Eng, Victoria University of Technology Library.

Desch HE and Dinwoodie JM (1990), "Timber, Structure, Properties, Conversion and Use," 7th edition

di Li J (1998), Personal communication. Dr Jun di Li has written many journal papers on combustion.

DIN 18230 (1982), "Baulicher Brandschutz im Industrie-bau," Vornorm, Teil 1 und 2, Berlin.

Dinwoodie JM (1989), "Wood: Nature's Cellular Polymeric Fibre-Composite," The Institute of Metals.

Ditlevsen O and Arnbjerg-Nielsen T(1994), "Model-Correction-Factor Method in Structural Reliability," ASCE Journal of Engineering Mechanics, Vol 120, No 1, pp 1-10.

Ditlevsen O (1982), "Model Uncertainty in Structural Reliability," Structural Safety, Vol 1, pp 73-86.

Doyle DV and Markwardt LJ (1967), "Tension Parallel-to-Grain Properties of Southern Pine Dimension Lumber," Research Paper FPL 84, Forest Products Laboratory 64, USDA Forest Service, Madison, USA.

Doyle DV and Markwardt LJ (1966), "Properties of Southern Pine in Relation to Strength of Dimension Lumber," Research Paper FPL 64, Forest Products Laboratory, USDA Forest Service, Madison, USA.

Drysdale D (1985), "An Introduction to Fire Dynamics," John Wiley and Sons 424pp.

ECCS, European Convention for Constructional Steel Work (1981), "European Recommendations for the Fire safety of Steel Structures, Level 1: Calculation of the Fire Resistance of Loadbearing Elements and Structural Assemblies Exposed to Standard Fire," Technical Committee 3 - Fire Safety of Steel Structures, Delft, Netherlands.

Elms DG (1992), "Consistent Crudeness in System Construction", In BHV Topping (ed), Optimisation and Artificial Intelligence in Civil Engineering, Kluwer Academic Publishers, Vol 1, pp 61-70.

Eurocode 5-1.2 (1995), "Structural Fire Design," Final Draft, prEN 1995-1-2, prepared by CEN TC 250/SC 5/Project Team 10.

Eurocode (1993), "Eurocode Actions on Structures. Part 10. Actions on Structures Exposed to Fire", 1993 Draft.

Eurocode (1990), "Eurocode on the Actions on Structures," Chapter 20.

El-Zafrany A (1993), "Techniques of the Boundary Element Method," Ellis Horwood 321 pp.

Fernando AE (1999), "The Modelling of Fire Spread and the Growth of Fire in Buildings Using Computational Fluid Dynamics," PhD Thesis, Centre for Environmental Safety and Risk Engineering, Victoria University of Technology, Melbourne, Australia.

Fire Code Reform Project (1993), "Business Plan for the Fire Code Reform Program," Ove-Arup & Partners, Melbourne Australia.

Fredlund B (1988), "A Model for Heat and Mass Transfer in Timber Structures During Fire, A Theoretical, Numerical and Experimental Study", Lund University, Sweden, Institute of Science and Technology, Department of Fire Engineering, Report LUTVDG/(TVBB-1003), (a - p 178).

Fuller JJ, Leichti RJ and White RH (1992), "Temperature Distribution in a Nailed gypsum-stud Joint Exposed to Fire," Fire and Materials, Vol 16, pp 95-99.

Gammon BW (1987), "PhD Thesis, Reliability Analysis of Wood-Frame Wall Assemblies Exposed to Fire," University of California, Berkeley.

Gardner WD and Syme DR (1991), "Charring of Glued-Laminated Beams of Eight Australian-Grown Timber Species and the Effect of 13mm Gypsum Plasterboard Protection on their Charring," Technical Report No. 5, New South Wales Timber Advisory Council Ltd, Sydney Australia.

Geidl V and Saunders S (1987), "Calculation of Reliability for Time-Varying Loads and Resistances," Structural Safety, vol 4, pp285-292.

Gerhards CC (1982), "Effect of Moisture Content and Temperature on the Mechanical Properties of Wood: An Analaysis of Immediate Effects," Wood and Fibre, pp 4-36.

Golding KJ (1986), "Loadbearing Timber Framed Walls," The New Zealand Journal of Timber Construction, Vol 3, No 1, pp 11-13.

Goncalves T, Jong F, Clancy P and Poynter W (1996), "Mechanical Properties of Fire Rated Gypsum Board," Department of Civil and Building Engineering, Victoria University of Technology.

Goring DAI (1963), "Thermal Softening of Lignin, Hemicellulose and Cellulose," Pulp and Paper Magazine of Canada, vol 64, pp T517-T527.

Gray WA and Müller R (1974), "Engineering Calculations in Radiative Heat Transfer," Pergamon Press.

Griffiths E and Kay EWC (1923), "The Measurement of Thermal Conductivity," Proceedings of the Royal Society (London), Series A, 104:71-98, London.

Gypsum Association, Application and Finishing of Gypsum Board, GA-216-93, 1993, USA.

G+D Computing (1993), "Strand 6, Finite Element Analysis System, Reference Manual and User Guide," G+D Computing Pty Ltd, Suit 1 Level 7, 541 Kent Street, Sydney Australia.

Hadvig S (1981), "Charring of Wood in Building Fires, Practice, Theory, Instrumentation, Measurements, " Technical University of Denmark, Laboratory of Heating and Air-Conditioning, Denmark.

Harkin JM (1969), Private Communication to EL Schaffer, US Dept Agriculture, Forest Products Laboratory, Madison Wisconsin USA.

Harmathy TZ and Mehaffey JR (1982), "Normalized Heat Load: A Key Parameter in Fire Safety Design", Fire and Materials, Vol 6, No 1.

Harmathy TZ (1981), "The Fire Resistance Test and its Relation to Real-World Fires", Fire and Materials, Vol 5, No 3.

Harmathy TZ (1972), "A New Look at Compartment Fires", Parts 1 and 2, Fire Technology, vol 8 pp196-219, 326-351.

Hadjisophocleous G (1996), "Extract from Report on Furnace Tests on Walls for Department of National Defense, Canada", National Fire Laboratory, NRCC, National Research Council Canada 16pp.

Hasofer AM (1996), a leading exponent in reliability, personal communication.

Hasofer AM and Beck VR (1995), "A Stochastic Model for Compartment Fires," Centre for Environmental Safety and Risk Engineering, Victoria University of Technology, Melbourne, Australia.

He Y (1997), research engineer working for Beck VR, personal communication.

Heselden AJM and Thomas PH (1972), "Fully Developed Fires in Single Compartments", CIB Report No. 20, Joint Fire Research Organisation Research Note 923, Borehamwood, UK.

Hibbit, Karlson and Sorenson Inc. (1994), "ABAQUS User Manuals. Version 5.4", Pawtucket, Rhode Island, USA.

Holm C and Loikkanen P (1981), "Joint Investigation of Vertical Furnaces in Nordic Countries," Technical Research Centre of Finland, Research Notes 56/1981 ESPOO.

Hottel HC (1954), "Radiant Heat Transmission," in Mc Adams W (editor), "Heat Transmission," 3rd edition, chapter 4, McGraw-Hill Book Company, New York.

Horasan M, Johnson P and Beck VR (1994), "Use of Egress Modelling in Performance-Based Fire Engineering Design - Fire Safety Study at National Gallery of Victoria," Fourth International Symposium on Fire Safety Science Proceedings, ISFPA Maryland USA, pp 669-680.

Iding R, Bresler B and Nizamuddin Z (1977), "Fires-T3, A Computer Program for the Fire Response of Structures - Thermal", Report No. UCB FRG 77-15, Fire Research Group, Structural Engineering and Structural Mechanics, Department of Civil Engineering, University of California, Berkeley, USA.

IEAust (1989), "Fire Engineering for Building Structures and Fire Safety," Working Party on Fire Engineering, The National Committee on Structural Engineering, The Institution of Engineers, Australia.

Ince NZ and Launder BE (1989), "On the Computation of Bouyancy-Driven Turbulent Flows in Rectangular Enclosures," International Journal of Heat and Fluid Flow, Vol 10, No. 2, pp 110-117.

Incropera FP and De Witt DP (1990), "Fundamentals of Heat and Mass Transfer," John Wiley and Sons, (a - p A28; b - p A22).

Ingberg SH (1927), NFPA (National Fire Protection Association, USA) Quarterly, Vol 20, pp243-252.

ISO 834, "Fire-Resistance Tests- Elements of Building Construction", International Standards Organisation.

ISO/CD 13389, "Assessment and Verification of Mathematical Fire Models."

Janssens ML (1994), "Physical Properties for Wood Pyrolysis Models", Proceedings, Pacific Timber Engineering Conference, Gold Coast Australia, pp 607-618.

Janssens ML (1993), "Development of a Simple Model for the Charring of Fire-Exposed Wood Members", Presentation at Victoria University of Technology, Melbourne, Australia, September 1993.

Janssens ML (1991), "Fundamental Thermophysical Characteristics of Wood and their Role in Enclosure Fire Growth ," A dissertation submitted to the University of Gent, Belgium, p 4.32-4.33.

Jones WW and Forney GP (1990), "A Programmer's Reference Manual for CFAST, the Unified Model of Fire Growth and Smoke Transport," TN1283, National Institute of Standards and Technology, US.

Jong F (1999), " Fire Resistance of Slender Light Timber Framed Walls," PhD in progress.

Jönsson R and Pettersson O (1985), "Timber Structures and Fire - A Review of the Existing State of Knowledge and Research Requirements," Swedish Council for Building Research.

Kawagoe K and Sekine T (1963), "Estimation of Fire Temperature-Time Curve in Rooms," Research Paper No. 29. Building Research Institute, Tokyo, Japan.

Kelly KK, Southard JC and Anderson CT (1941), "Thermodynamic Properties of Gypsum and its Dehydration Products," Technical Paper 625, US Bureau of Mines, Department of the Interior, Washington.

Kline DE, Woeste FE and Bendtsen BA (1986), "Stochastic Model for Modulus of Elasticity of Lumber," Wood and Fiber Science, Vol. 18, Part 2, pp228-238.

Knauf Plasterboards, Publication B1 - Diamod Dry Wall Systems, January 1997, UK.

Knudson RM and Schniewind AP (1975), "Performance of Structural Wood Members Exposed to Fire," Forest Products Journal Vol 25 No. 2.

Kollmann and Côté (1984), "Principles of Wood Science and Technology," Springer Verlag, Berlin, pp 256-257.

Kollmann F and Fengel D (1965) "Changes in the Chemical Composition of Wood by Thermal Treatment," Holz Roh-Werkst, vol 23, part 12, pp 461-468. (in German)

Kollmann F (1952), "The Dependence of Some Mechanical Properties of Woods on Time, Notching and Temperature. III The Influence of Temperature on some Mechanical Properties of Wood," Holz Roh-Werkst, vol 10, part 7, pp 269-278.

Kollmann F (1940), "The Mechanical Properties of Wood of Different Moisture Content within -200° to +200°C Temperature Range," VDI-Forschungsh, vol 403, part 11, pp 1-18.

Kollman K (1934), "Uber Die Warmetechnischen Eigenshaften der Holzer," Gesundheits-Ing. Vol 57, part 18, pp 224-227.

König J and Norén J (1991), "Two Papers on Fire-Exposed Load Bearing Wood Frame Members - Presented at the 1991 Timber Engineering Conference, London and at Meeting 24 of CIB W18A - Timber Structures, Oxford", Trätek (The Swedish Institute for Wood Technology Research) Report I 9112080.

König J, Norén J, Olesen FB and Hansen FT (1997), "Timber Frame Assemblies Exposed to Standard and Parametric Fires, Part 1: Fire Tests," Trätek, Swedish Institute of Wood Technology, Report I 9702015.

Kreyszig E (1972), "Advanced Engineering Mathematics," Third Edition, John Wiley and Sons Inc.

Lahey (1995), "Lahey Fortran 90, Language Reference," Lahey Computer Systems, Inc, 865 Tahoe Boulevard, PO Box 6091, Incline Village, Nevada 89450, USA.

Lau PWC (1996), "Behaviour and Reliability of Wood Tension Members Exposed to Elevated Temperatures," PhD Thesis, Faculty of Graduate Studies, Department of Wood Science, The University of British Columbia, Canada.

Lau PWC and Foschi RO (1994), "Reliability Analysis of Light Framing During Fire Exposure - Concept and Approach", Proceedings, Pacific Timber Engineering Conference, Gold Coast Australia, Vol 1 pp 255-266.

Law JR (1997), "Time Varying Probability of Failure of Steel Floor Beams Subjected to Real Fire," Master of Engineering Thesis, Victoria University of Technology, Melbourne, Australia.

Law M (1983) "A Basis for the Design of Fire Protection of Building Structures", The Structural Engineer, Vol 61A, No 1, January, pp25-33.

Law M (1977), "A Relationship Between Fire Grading and Building Design and Contents", Fire Research Note Number 877, Fire Research Station (UK).

Lehoczky J (1990), "Statistical Methods," Handbooks in Operations Research and Management Science, Stochastic Models, Heyman DP and Sobel MJ (editors), Vol. 2, p 287.

Lide DR (1996), "CRC Handbook of Chemistry and Physics", CRC Press Incorporated, p10-261.

Lie TT (1992), "Structural Fire Protection," American Society of Civil Engineers, Structural Division, Manuals and Reports on Engineering Practice No. 78.

Leicester RH (1992), Personal communication. Chief Research Scientist, Division of Building, Construction and Engineering, CSIRO, Commonwealth Scientific Industrial Research Organisation, Highett Victoria, Australia. Author of AS1720.4.

Leicester RH, Grant DJ, Rumball BL and Young FG (1988), "Structural Engineering Properties of Machine Stress-Graded, Australian Grown Radiata Pine", DCE Technical Report TR88/1, CSIRO, Commonwealth Scientific Industrial Research Organisation, Australia.

Leicester RH (1985), "Computation of a Safety Index," Civil Engineering Transaction, The Institution of Engineers Australia, pp 55-61.

Levin ED and Belikova ZP (1968), "Thermographic Characteristics of the Thermal Degradation Process of Wood Components," Lesnoi Zh. vol 11, part 3, pp 112-115. (in Russian)

Luo M and He Y (1997), "Fire Growth and Smoke Spread Model for Fire Safety System Design: Experimental Verification", Centre for Environmental Safety and Risk Engineering, Victoria University of Technology, PO Box 14428, MCMC Melbourne Vic 8001, Australia.

MacGregor RK and Emery AP (1969), "Free Convection through Vertical Plane Layers: Moderate and High Prandtl Number Fluids," Journal of Heat Transfer, Vol 91, p 391.

MacLean JD (1941), "Thermal Conductivity of Wood, "Heating, Piping and Air Conditioning, Vol 13, No. 6, pp 380-391.

Magnusson SE and Pettersson O (1981), "Rational Design Methodology for Fire Exposed Load Bearing Structures," Fire Safety Journal, Vol. 3, No. 4.

Magnusson SE and Pettersson O (1977), "Functional Approaches - An Outline," CIB Symposium on Fire Safety in Buildings: Needs and Criteria, Amsterdam, CIB Publication 48.

Magnusson SE, Pettersson O and Thor J (1976), "Fire Engineering Design of Steel Structures," Manual, Swedish Institute of Steel Construction.

Magnusson SE and Thelandersson S (1970), "Temperature-Time Curves of the Complete Process of Fire Development, Acta Polytechnica Scandinavica, Civil Engineering and Building Construction Series, Number 65.

Maku T (1954), "Studies on the Heat Conduction in Wood," Kyoto University, Bulletin of the Wood Research Institute, No. 13, pp1-80.

Mann NR, Schafer RE and Singpurwalla ND (1974), "Methods for Statistical Analysis of Reliability and Lifer Data," John Wiley, New York.

Maruyama S and Aihara (1997), "Radiation Transfer of Arbitrary Three-Dimensional Absorbing, Emitting and Scattering Media and Specular and Diffuse Surfaces," Journal of Heat Transfer, Transaction of the ASME, Vol 119, February, pp 129-136.

McAdams WH (1954), "Heat Transmission," 3rd edition, McGraw-Hill, New York, chapter 7.

Mehaffey JR (1999), Facsimile explaining anomalous results from WALL2D (Takeda and Mehaffey, 1998).

Mehaffey JR (1997), "A Fire Safety Engineering Analysis of the Fire Resistance of Wood-Frame Buildings," Meeting of the North American Wood Products Fire Research Consortium Fire Modeling Group, Forintek Canada, 2665 East Mall Drive, University of British Columbia, Vancouver, Canada.

Mehaffey JR, Cuerrier P and Carisse G (1994), "A Model for Predicting Heat Transfer through Gypsum-Board/Wood-Stud Walls Exposed to Fire," Fire and Materials, Vol 18 pp 297-305.

Mehaffey JR (1991), "Development of Fire Endurance Models for Wood Stud Walls, Progress Report," Forintek Canada Corporation.

Melchers RE (1987), "Structural Reliability, Analysis and Prediction," Ellis Horwood Limited 400pp.

Melchers RE (1985), "Reliability Calculation for Structures," Civil Engineering Transaction, The Institution of Engineers Australia, pp 124-129.

Mikkola E (1991), "Charring of Wood Based Materials," Elselvier Applied science, Fire Safety Science - Proceedings of the Third International Symposium, pp 547-556.

Mitler HE and Rocket JA (1987), "User's Guide to FIRST, A Comprehensive Single Room Fire Model, NBSIR 853595", National Institute of Standards and Technology, Gaithersburg, Maryland, USA.

Morlier P (1994), "Creep in Timber Structures," Report 8 of Rilem Technical Committee 112-TSC, 149pp.

NAFI (1993), "Tests on Timber Framed Walls and Floors for Multi-Storey Housing," National Association of Forest Industries, Australia.

NAWPFRC (1997), communications at the North American Wood Products Fire Research Consortium, Wood and Fire Research Group, meeting at Vancouver.

NAWPFRC (1993), communications at the North American Wood Products Fire Research Consortium, Wood and Fire Research Group, meeting at Macon, Georgia USA.

NBFSS Project (1991), "Microeconomic Reform: Fire Regulation. An explanatory document describing developments leading to more effective Regulations for Fire Safety", National Building Fire Safety Systems Project of the Building Regulation Review Task Force, May 1991. (F REF 344.940 537)

Noren JB (1988), "Failure of Structural Timber Exposed to Fire", Proceedings on the 1988 Conference on Timber Engineering, Madison Wisconsin USA, Forest Products Research Society, Vol 2 pp 441-447.

Nusselt W (1908), V.D.I. BD. 52.

Ödeen K (1970), "Standard Fire Endurance Tests - Discussion, Criticism, and Alternatives," Fire Test Performance, ASTM STP 464, American Society for Testing and materials, pp 30-56.

Olesen FB and König J (1992), "Tests on Glued Laminated Beams in Bending Exposed to Natural Fires," Meeting 25, Ahus Sweden, International Council for Building Research Studies and Documentation, Working Commission W18 - Timber Structures.

Ouchi T (1988), "Thermal Conductivity of Wood at High Temperatures," Proceedings of the International Conference on Timber Engineering, Published by the Forest Products Research Society, vol 2, pp441-447.

Panshin AJ and de Zeeuw C (1980), "Textbook of Wood Technology: Structure, Idenification, Uses, and Properties of the Commercial Woods of the United States and Canada," 3rd edition, McGraw-Hill Book Company.

Parker WJ (1988), "Prediction of Heat Release Rate of Wood," Dissertation for Doctor Science, The George Washington University, USA, 160pp, (a - p80).

Parker WJ (1985), "Development of a Model for the Heat Release of Wood - A Status Report," National Bureau of Standards, Centre for Fire Research, NBSIR 85-3163, Gaithersburg, Maryland 2899, USA.

Patankar SV (1980), "Numerical Heat Transfer and Fluid Flow," Hemisphere Publishing Corporation, McGraw-Hill Book Company.

Peralta PN and Skaar C (1993), "Experiments on Steady-State Nonisothermal Moisture Movement in Wood," Wood and Fiber Science, vol 25 part 2 pp 124-135.

Pettersson O and Jönsson R (1983), "Fire Design of Wooden Structures," International Seminar, "Three Decades of Structural Fire Safety," Borehamwood, Herts, UK 22-23 February, 1983, pp229-246.

Pettersson O (1981), "Reliability Based Design of Fire Exposed Concrete Structures," Contemporary European Concrete Research, Stockholm, June 9-11, 1981.

Pettersson O and Ödeen K (1978), "Brandteknisk Dimensionering - Principer, Underlag, Exempel," ("Fire Engineering Design - Principals, Data, Examples"), Liber förlag, Stockholm.

Pham L (1985), "Load Combinations and Probabilistic Load Models for Limit State Load Codes," Civil Engineering Transactions, The Institution of Engineers, Australia.

Pohl A and Clancy P (1999), "EZ Barrier - An Easy-to-Use Spreadsheet Model to Estimate Time of Failure of Timber Framed Walls in Real Fire," School of the Built Environment, Victoria University of Technology, Melbourne Australia, Report No ERCC 265.

Pohl A and Young SA (1999), "Pilot Furnace Tests on Wall Panels," Warrington Fire Research Australia Pty Ltd, Melbourne, Australia.

Polensek A (1976), "Finite Element Analysis of Wood-Stud Walls," Journal of the Structural Division, Proceedings of the American Society of Civil Engineers, Vol 102, No. ST7, July, pp 1317-1335.

Prakash M, Turan OF and Thorpe GR (1999), "Program NATCON for the Numerical Solution in a Rectangular Cavity," Research Report, School of the Built Environment, Victoria University of Technology, 62pp.

Preusser R (1968), "Plastic and Elastic Behaviour of Wood Affected by Heat in Open Systems", Holztechnologie, Vol 9 No 4, pp 229-231.

Quintiere JG, Steckler KD and Corley D (1984), "An Assessment of Fire Induced Flows in Compartments," Fire Science and Technology, vol 4 p 1.

Quintiere JG, Birky M, MacDonald F and Smith G (1982), "An Analysis of Smoldering Fires in Closed Compartments and Their Hazard Due to Carbon Monoxide", Fire and Materials, Vol 6, p99.

Raithby GG and Chui EH (1990), "A Finite Volume Method for Predicting Radiant Heat Transfer in Enclosures with Participating Media," Journal of Heat Transfer, Volume 112, pp 415-423.

Rajashekhar MR and Ellingwood BR (1993), "A New Look at the Response Surface Approach for Reliability Analysis," Structural Safety, Elselvier, vol 12, pp 205-220.

Raznjevic K (1976), "Handbook of Thermodynamic Tables and Charts," Hemisphere Publishing Company, p54.

Rohsenow WM, Hartnett JP and Ganic EN (1985), "Handbook of Heat Transfer Fundamentals," second edition, p3-113.

Rowley FB (1933), "The Heat Conductivity of Wood at Climatic Temperature Differences ," Piping, Heating and Air Conditioning, Vol 5, pp 313-323.

Sano E (1961), "Effects of Temperature on the Mechanical Properties of Wood. I. Compression Parallel-to-Grain. II. Tension Parallel-to-Grain. III. Torsion test.," Journal of the Japanese Wood Research Society, vol 7, part 4, pp147-150; vol 7, part 5, pp189-191; vol 7, part 5, pp 191-193.

Schaffer EL (1984), "Structural Fire Design: Wood," United States Dept Agriculture, Forest Service, Forest Products Laboratory, Research Paper FPL 450, 17pp.

Schaffer EL (1982), "Influence of Heat on the Longitudinal Creep of Dry Douglas-Fir," Chapter 3 from Structural Use of Wood in Adverse Environments, edited by Meyer RW and Kellog RM, Society of Wood Science and Technology, Van Nostrand Reinhold Company.

Schaffer EL (1977), "State of Structural Timber Fire Endurance," Wood and Fiber, vol 9, part 2, pp 145-170.

Schaffer EL (1973), "Effect of Pyrolytic Temperatures on the Longitudinal Strength of Dry Douglas-Fir," ASTM Journal for Testing and Evaluation, vol 1, part 4, pp319-329.

Schleich JB (1993) (Chairman), "Fire Engineering Design of Steel Structures: State of the Art," International Iron and Steel Institute.

Sentler L (1983), "Service Life Predictions of Concrete Structures," Department of Structural Engineering, Lund Institute of Technology, Lund Sweden, Report TVBK-3018, 89pp.

Shooman ML (1968), "Probabilistic Reliability: An Engineering Approach," McGraw-Hill, New York.

Siegel R and Howell JR (1981), "Thermal Radiation Heat Transfer," second edition, Hemisphere Publishing Company, McGraw-Hill Book Company (a-pp 832-837).

Spalding DB (1992), "A Guide to the PHEONICS Input Language," Version 1.6, Document CHAM/TR100, revision 11, CHAM Bakery House, 40 High Street, Wimbledon Village, London SW19 5AU, UK

Stamm A (1956), "Thermal Degradation of Wood and Cellulose," Industrial Engineering and Chemistry, vol 48, part 3, pp 413-417.

Standards Australia (1995), "Australian Standards, Essential Cogs in the Nations Technical Infrastructure."

Steckler KD, Quintiere JG and Rinkinen WJ (1982), "Flow Induced by a Fire in a Compartment," NBSIR-82-2520, National Bureau of Standards, Gaithersburg, Maryland, US.

Sterner E and Wickstrom U (1990), "TASEF (Version 3.0) - Temperature Analysis of Structures Exposed to Fire", Fire Technology SP Report 1990:05, Swedish National Testing Institute.

Stray G and Bates J (1997), Industrial chemists at Boral Plasterboard Australia - Personal communications.

Sulzberger PH (1953), "The Effect of Temperature on the Strength of Wood, Plywood and Glue Joints, "Aeronautical Research Consultative Committee Report ACA-46, Melbourne, Australia.

Sultan MA (1996), "A Model for Predicting Heat Transfer Through Non-Insulated Steel Stud Gypsum Board Wall Assemblies Exposed to Fire," Fire Technology, Third Quarter, pp 239-259.

Takeda H (1998), "Model to Predict Fire Resistance of Wood-Stud Walls – The Effects of Insulation in the Cavity and Shrinkage of Gypsum Board," Proceedings of the World Conference on Timber Engineering, August 17-20, Montreux-Lausanne, Switzerland.

Takeda H and Mehaffey JR(1998), "WALL2D: a Model for Predicting Heat Transfer through Wood-stud Walls Exposed to Fire", Fire and Materials 22, 133-140 (1998).

Takeda H and Mehaffey JR (1996), "Model for Predicting Fire Resistance Performance of Wood-Stud Walls with or without Insulation", Proceedings of the International Wood Engineering Conference, New Orleans, Lousiana USA, October 28-31, Vol 2. pp 257-262.

Takeda H and Yung D (1992), "Simplified Fire Growth Models for Risk-Cost Assessment in Apartment Buildings", Vol 4, pp53-66.

Takeda H (1983), "Mixing Effect and Combustion Efficiency in Compartment Fires," Fire Safety Journal, Vol 5, p 199.

Tang WK (1967), "Effect of Inorganic Salts on Pyrolysis of Wood, Alpha-Cellulose and Lignin Determined By Thermogravimetric Analysis," US Forest Research Paper, FPL 71, Forest Products Laboratory, US Dept Agriculture Forest Service, Madison, Wisconsin, USA.

TCD3.0 (1990), "User's Manual for TCD 3.0, with Tempcalc," Fire Safety Design, Lund Sweden.

Tewarson A and Pion RF (1976), "Flammability of Plastics - I. Burning Intensity," Combustion and Flame, Vol 26, p 85.

Thomas GC (1997), "Fire Resistance of Light Timber Framed Walls and Floors," Fire Engineering Research Report 97/7, School of Engineering, University of Canterbury, Christchurch, New Zealand, p80.

Thomas GC, Buchanan AH, Carr AJ, Fleischmann CM and Moss PJ (1996), "Modelling Structural Fire Performance of Light Wood Frame Construction", Proceedings of the International Wood Engineering Conference, New Orleans, Lousiana USA, October 28-31, Vol 2. pp 241-248.

Thomas GC, Buchanan AH, Carr AJ, Fleischmann CM and Moss PJ (1995), "Light Timber-Framed Walls Exposed to Compartment Fires", Journal of Fire Protection Engineering, Vol 7 No. 1 pp25-35.

Thomas GC and Buchanan AH (1995), "Mechanical Properties of Timber at High Temperatures," Proceedings of the Fourth International Fire and Materials Conference, Marriot Hotel, Crystal City Virginia, USA.

Thomas IR and Bennetts ID (1999), "Fires in Enclosures with Single Ventilation Openings - Comparison of Long and Wide Enclosures," Proceedings of the Sixth International Symposium on Fire Safety Science, Ecole Nationale de Mécanique et d'Aérotechnique University of Poitiers, France, 5-9 July, 1999.

Thomas IR, Bennetts ID, Daywansa P, Proe DJ and Lewis RR (1992), "Fire Tests of the 140 William Street Office Building", BHP Research-Melbourne Laboratories, Report No. BHPR/ENG/R/92/043/SG2C, February, Australia.

Thomas IR, Bennetts ID, Proe DJ, Lewins RR and Almand KH (1990), "Fire in Mixed Occupancy Buildings", BHP Steel, Structural Steel Development Group, Melbourne, Australia.

Thomas PH (1986) (Coordinator), "Design Guide Structural Fire Safety, Workshop CIB W14 (Fire Commission of the Conseil International du Batiment," Fire Safety Journal, Vol 10 No 2, pp 77-137.

Trahair NS and Bradford MA (1994), "The Behaviour and Design of Steel Structures," second edition, Chapman and Hall, p261.

TPC (1994), "Victorian Timber Framing Manual", Victorian Timber Promotion Council, Australia.

Walton WD, Baer SR and Jones WW (1985), "User's Guide for FAST, NBSIR 85-3284", National Institute of Standards and Technology, Gaithersburg, Maryland, December 1985.

Wangaard FF (1940), "Transverse Heat Conductivity of Wood," Piping, Heating and Air Conditioning, Vol 12, pp 459-464.

Warner CY and Arpaci (1968), "An Experimental Investigation of Turbulent Natural Convection in Air at Low Pressure for a Vertically Heated Flat Plate," International Journal of Heat and Mass Transfer, Vol 11, p 397.

Warrington (1998), "WFRA Pilot Test R9701 - Thermal Properties, Boral Firestop 4x13mm Sheets," Warrington Fire Research Australia Pty Ltd, Melbourne, Australia.

Weimert D (1998), PhD student at Victoria University of Technology, researching the activation of sprinklers and alarms by smoke, personal communication.

White RH (1988), "Charring Rates of Different Wood Species", PhD Dissertation, University of Wisconsin, Madison, Wisconsin USA.

White RH (1988a), "Analytical methods for Determining Fire Resistance of Timber members," Section 3, Chapter 8, The SFPE Handbook of Fire Protection Engineering, National Fire Protection Association, Quincy, MA, USA

White RH and Schaffer EL (1981), "Transient Moisture Gradient in Fire-Exposed Wood Slab," Wood and Fiber, vol 13 part 1 pp 17-38.

White RH and Schaffer EL (1978), "Application of CMA Program to Wood Charring," Fire Technology, Vol 14, pp 279-290.

Wickstrom U (1977), "TASEF, A Numerical Procedure for Calculating Temperature in Hollow Structures Exposed to Fire", Report No. UCB FRG 77-9, Fire Research Group, Structural Engineering and Structural Mechanics, Department of Civil Engineering, University of California, Berkeley, USA.

Westroc Heavy, Communication from Hadjisophocleuos 1996.

Woeste FE and Schaffer EL (1981), "Reliability Analysis of Fire-Exposed Light-Frame Wood Floor Assemblies," United States Department of Agriculture, Forest Service, Forest Products Laboratory, Research Paper FPL 386, 15pp.

Wood Handbook (1987), "Wood Handbook: Wood as an Engineering Material," US Department of Agriculture, Forest Products Laboratory, Madison, Wisconsin, USA.

Wright CC (1995), "Structural Performance of Wood-Stud/Gypsum-Board Walls," Forintek Canada Corp.

Young SA (2000), "Structural Modelling of Plasterboard Clad, Light-timber Framed Walls in Fire", PhD thesis expected to be submitted March 31, 2000, Centre for Environmental Safety and Risk Engineering, Victoria University of Technology, Australia.

Young SA (1998), personal communication of test measurements.

Young SA and Clancy P (1998), "Degradation of the Mechanical Properties in Compression of Radiata Pine in Fire," 5th World Conference on Timber Engineering, August 17-20, Montreux, Switzerland, Natterer J and Sandoz JL (Editors) vol 1, pp 246-253.

Young SA (1996), "Elevated Temperature Mechanical Properties of Radiata Pine in Compression", Internal Report for CESARE, Centre for Environmental Safety and Risk Engineering, Victoria University of Technology, Australia, 200 pp.

Young SA, Clancy P and Beck VR (1996a), "Structural Modelling of Timber Walls in Fire", Proceedings of the First Australasian Congress on Applied Mechanics, 21-23 February 1996, Melbourne Australia, pp707-712.

Young SA and Clancy P (1996b), "Compression-Load Deformation of Timber Walls in Fire", Proceedings of the Third International Conference, Wood and Fire Safety, May 6-9, 1996, The High Tatras, Hotel Patria, Slovak Republic, pp127-136.

Young SA and Clancy P (1996c), "Full Scale Ambient Tests on Timber Framed Walls", Internal Report for CESARE, Centre for Environmental Safety and Risk Engineering, Victoria University of Technology, Australia, 164 pp.

Young SA, Clancy P, Beck VR and Leicester RH (1994), "Model for the Performance of Timber Framed Assemblies in Real Fires", Proceedings of the Australasian Structural Engineering Conference, Sydney Australia, September 1994, Institution of Engineers, Australia, Vol 2 pp 705-712.

Yung D (1995), Chief Fire Scientist National Research Council Canada, personal communication.

Yung D and Beck VR (1989), "A Risk-Cost Assessment Model for Evaluating Fire Risks and Protection Costs in Apartment Buildings," Proceedings of the International Symposium on Fire Engineering for Building Structures and Safety, Melbourne Australia, November 14-15, p15.

APPENDIX A Publications Arising from Research Undertaken Towards this Thesis

Clancy P (1996), "Sensitivity Study of Variables Affecting Time-of-Failure of Wood Framed Walls in Fire", Proceedings of the International Wood Engineering Conference, New Orleans, Lousiana USA, October 28-31, Vol 2. pp 263-268.

Clancy P (1996a), "CESARE Fire Barrier, A Model for Time Dependent Probability of Failure of Barriers in Real Fire", Internal Report for CESARE, Centre for Environmental Safety and Risk Engineering, Victoria University of Technology, Australia, 250 pp.

Clancy P and Young SA (1996), "Full Scale Furnace Tests on Timber Framed Walls", Report, Department of Civil and Building Engineering, Victoria University of Technology, Australia, 268 pp.

Clancy P (1996a), "A Model for Predicting the Probability of Failure of Wood Framed Walls and Floors in Real Fire", Proceedings of the Third International Conference, Wood and Fire Safety, May 6-9, 1996, The High Tatras, Hotel Patria, Slovak Republic, pp33-42.

Clancy P, Beck VR and Leicester RH (1995), "Time Dependent Probability of Failure of Wood Frames in Real Fire", Proceedings, Fire and Materials, Fourth International Conference and Exhibition, November 15-16 1995, Marriot Hotel, Crystal City, Virginia, USA, pp85-94.

Clancy P and Young SA (1995), "Models for Light Timber Framed Assemblies in Real Fires", Proceedings of the Fifth East Asia-Pacific Conference on Structural Engineering and Construction, Gold Coast, Queensland, Australia, 25-27 July 1995, pp2271-2276.

Clancy P, Young SA, Beck VR and Leicester RH (1994), "Modelling of Timber Framed Assemblies in Real Fires", Proceedings of the Pacific Timber Engineering Conference, Gold Coast, Australia, July 1994, Vol. 2 pp 282-293.

Young SA and Clancy P (1998), "Degradation of the Mechanical Properties in Compression of Radiata Pine in Fire," 5th World Conference on Timber Engineering, August 17-20, Montreux, Switzerland, Natterer J and Sandoz JL (Editors) vol 1, pp 246-253.

Young SA, Clancy P, Beck VR and Leicester RH (1994), "Model for the Performance of Timber Framed Assemblies in Real Fires", Proceedings of the Australasian Structural Engineering Conference, Sydney Australia, September 1994, Institution of Engineers, Australia, Vol 2 pp 705-712.

Young SA, Clancy P and Beck VR (1996a), "Structural Modelling of Timber Walls in Fire", Proceedings of the First Australasian Congress on Applied Mechanics, 21-23 February 1996, Melbourne Australia, pp707-712.

Young SA and Clancy P (1996b), "Compression-Load Deformation of Timber Walls in Fire", Proceedings of the Third International Conference, Wood and Fire Safety, May 6-9, 1996, The High Tatras, Hotel Patria, Slovak Republic, pp127-136.

Young SA and Clancy P (1996c), "Full Scale Ambient Tests on Timber Framed Walls", Internal Report for CESARE, Centre for Environmental Safety and Risk Engineering, Victoria University of Technology, Australia, 164 pp.

APPENDIX B Typical Load for Wall Stud

The table below is a copy of spreadsheet computations that show that a typical load on a stud in a lower storey in a two storey residential building is approximately 8 kN. It is thus appropriate that this load be applied to each stud in loadbearing wall furnace experiments.

Item	Sectional Dimensions		Density	Spacing	Load/m²	Spacing	Span/Height	**Load /Stud**
	mm	mm	kg.m⁻³	mm	kPa	mm	m	kN
Roof								
Tiles					1.00			
Timber - roof	45	150	500	450	0.08			
Timber - ceiling	45	150	500	450	0.08			
ceiling gypsum	16	1000	810	450	0.29			
					1.44	0.45	4.50	2.91
Walls								
Upper storey								
gypsum	32	1000	810	450	0.58			
timber	45	90	500	450	0.05			
					0.62	0.45	3.00	0.84
Lower storey					0.62	0.45	1.50#	0.42
Live Load					2.00	0.45	4.50	4.05
TOTAL								**8.22**

Notes:

1. Loads from AS1170.1. Typical dimensions from TPC1994.
2. # Self weight of wall approximated by assuming half at top and half at bottom of wall.

APPENDIX C. Time of Failure Model Input Data

Input to Young's (1998) Structural Response Model

Young's model is independent of units. The units used in applying his model are indicated below.

Wall Geometry

Height of wall (m)

3.0d0

Initial crookedness at mid-height (m)

10.0d-003

Thickness of gypsum board on fire side (m)

Effective width of gypsum board on fire side (m)

16.0d-003 **380d-003**

Depth of stud (m)

Width of stud (m)

90d-003 **45d-003**

Thickness of gypsum board on ambient side (m)

Effective width of gypsum board on ambient side (m)

16.0d-003 **380d-003**

Initial crookedness is the amplitude of the initial bow in the wall before any forces are applied. The bow is assumed to be a half sinusoidal wave which is a maximum at mid-height and zero at the top and bottom.

Effective width of gypsum board is the spacing between stud centres less any deductions for shear lag.

Discretisation Details

Number of nodes up the height of the wall. (The number of line members equals the number of nodes less 1.) Refer to Figure A.1.2 /pxx.

11

Gypsum board on fire side:

Number of elements through the thickness

Number of elements across the effective width

5 **15**

Stud:

Number of elements through the stud in the direction perpendicular to the plane of the wall

Number of elements through the stud in the direction parallel to the plane of the wall

18 **9**

Gypsum board on ambient side:

Number of elements through the thickness

Number of elements across the effective width

5 **15**

Elements for a particular component (gypsum board or stud) are equal in shape and size.

Restraint Details

Number of nodes with fully fixed restraints against one or more degrees of freedom

2

Node

Vertical restraint (0=free, 1=full fixity)

Horizontal restraint (0=free, 1=full fixity)

Rotational restraint (0=free, 1=full fixity)

1	**0**	**1**	**0**
11	**1**	**1**	**0**

Ambient rotational spring stiffnesses superimposed at ends of wall (N.m)

At first node

1.00d10

At last node

1.00d10

Load Details

Number of nodes with load

1

Node at which load is applied

Vertical load applied (N)

Horizontal load applied (N)

Moment applied (N.m)

1 8000 0 0

Distance vertical load is applied from face of wall on fire side (m)

51.d-003

Uniformly distributed load by any pressure from fire ($N.m^{-1}$)

0d0

If moment reaction at bottom support is equal and opposite to moment applied by eccentric load at top, enter "1", otherwise "0".

1

Mechanical Properties of Materials for a particular Temperatures

Strengths of materials at ambient conditions:

Compression strength (Pa)

Tensile strength (Pa)

Gypsum board:

1.0d006 1.0d006

Timber stud:

24.0d006 24.0d006

Elastic moduli of materials at ambient conditions:

Compression elastic modulus (Pa)

Tensile elastic modulus (Pa)

Gypsum board:

0.48d009 0.48d009

Timber stud:

7.4d009 7.4d009

Maximum strain before failure at ambient conditions:

Compression strain (Pa)

Tensile strain (Pa)

Gypsum board:

0.005 0.003

Timber stud:

0.00439 0.00325

Slip stiffnesses for partial composite action of stud and gypsum boards at ambient conditions (N.m-2):

Gypsum board on fire side

Gypsum board on ambient side

1.0d10 1.0d10

Thermal expansion(-), shrinkage (+) coefficients at ambient conditions ($°C^{-1}$):

Gypsum board:

1d-5

Timber stud:

0d-6

Usually the temperature at which mechanical properties above is 20°C. However, for thermal shrinkage of gypsum board, Young (1998) found alternative temperatures more convenient. The temperatures for which the above mechanical properties apply are those associated with a relative mechanical property of 1.00 below.

Joint information - elements with joints:

Number of horizontal joints in gypsum boards (assumed the same each side and in the same vertical position)

2

Nodes at where joints are located

2

7

Maximum tensile strain at failure of joint

0.003

Relative Mechanical Properties of Materials at Elevated Temperatures

Thermal expansion or shrinkage relative to value for particular temperature above:

Gypsum board:

Temperature (°C)

	Relative value
20.0	**0.00**
80.0	**-0.1**
150.0	**0.0**
200.0	**1.3**
250.0	**2.00**
300.0	**2.50**
400.0	**3.70**
500.0	**5.05**
510.0	**5.12**
600.0	**5.48**
700.0	**5.90**
800.0	**7.50**
900.0	**9.05**
980.0	**1.00**
990.0	**1.00**

Timber stud:

Temperature (°C)

	Relative value
20.0	**1.00**
40.0	**1.00**
60.0	**1.00**
100.0	**1.00**
120.0	**1.00**
160.0	**1.00**
180.0	**1.00**
200.0	**1.00**
220.0	**1.00**
240.0	**1.00**
260.0	**1.00**
280.0	**1.00**
300.0	**1.00**
400.0	**1.00**
500.0	**1.00**

Gypsum board elastic modulus in compression relative to value for particular temperature above:

Temperature (°C)

	Relative value
20.0	**1.00**
50.0	**1.00**
100.0	**1.00**
150.0	**0.00**
200.0	**0.00**
250.0	**0.00**
300.0	**0.00**
350.0	**0.00**
400.0	**0.00**
500.0	**0.00**
600.0	**0.00**
700.0	**0.00**
800.0	**0.00**
900.0	**0.00**
1000.0	**0.00**

Gypsum board elastic modulus in tension relative to value for particular temperature above:

Temperature (°C)

	Relative value
20.0	**1.00**
50.0	**1.00**
100.0	**1.00**
150.0	**0.00**
200.0	**0.00**
250.0	**0.00**
300.0	**0.00**
350.0	**0.00**
400.0	**0.00**
500.0	**0.00**
600.0	**0.00**
700.0	**0.00**
800.0	**0.00**
900.0	**0.00**
1000.0	**0.00**

Gypsum board strength in compression relative to value for particular temperature above:

Temperature (°C)

	Relative value
20.0	**1.00**
50.0	**1.00**
100.0	**1.00**
150.0	**0.30**
200.0	**0.13**
250.0	**0.13**
300.0	**0.13**
350.0	**0.13**
400.0	**0.13**
500.0	**0.13**
600.0	**0.13**
700.0	**0.00**
800.0	**0.00**
900.0	**0.00**
1000.0	**0.00**

Gypsum board strength tension relative to value for particular temperature above:

Temperature (°C)

	Relative value
20.0	**1.00**
50.0	**1.00**
100.0	**1.00**
150.0	**0.30**
200.0	**0.13**
250.0	**0.13**
300.0	**0.13**
350.0	**0.13**
400.0	**0.13**
500.0	**0.13**
600.0	**0.13**
700.0	**0.00**
800.0	**0.00**
900.0	**0.00**
1000.0	**0.00**

Gypsum board maximum strain in compression relative to value for particular temperature above:

Temperature (°C)

	Relative value
20.0	**1.00**
40.0	**1.00**
60.0	**1.00**
100.0	**1.00**
120.0	**1.00**
160.0	**1.00**
180.0	**1.00**
200.0	**1.00**
220.0	**1.00**
240.0	**1.00**
260.0	**1.00**
280.0	**1.00**
300.0	**1.00**
400.0	**1.00**
500.0	**0.00**

Gypsum board maximum strain in tension relative to value for particular temperature above:

Temperature (°C)

	Relative value
20.0	**1.00**
40.0	**1.00**
60.0	**1.00**
100.0	**1.00**
120.0	**1.00**
160.0	**1.00**
180.0	**1.00**
200.0	**1.00**
220.0	**1.00**
240.0	**1.00**
260.0	**1.00**
280.0	**1.00**
300.0	**1.00**
400.0	**1.00**

500.0	**0.00**

Timber elastic modulus in compression relative to value for particular temperature above:

Temperature (°C)	*Relative value*
20.0	**1.00**
70.0	**0.63**
110.0	**0.20**
200.0	**0.20**
288.0	**0.00**
300.0	**0.00**
305.0	**0.00**
310.0	**0.00**
320.0	**0.00**
340.0	**0.00**
400.0	**0.00**
420.0	**0.00**
440.0	**0.00**
460.0	**0.00**
480.0	**0.00**

Timber elastic modulus in tension relative to value for particular temperature above:

Temperature (°C)	*Relative value*
20.0	**1.00**
280.0	**0.20**
288.0	**0.00**
290.0	**0.00**
288.0	**0.00**
300.0	**0.00**
305.0	**0.00**
310.0	**0.00**
320.0	**0.00**
340.0	**0.00**
400.0	**0.00**
420.0	**0.00**
440.0	**0.00**

460.0	**0.00**
480.0	**0.00**

Timber strength in compression relative to value for particular temperature above:

Temperature (°C)

Relative value

20.0	**1.00**
40.0	**0.82**
50.0	**0.75**
70.0	**0.65**
100.0	**0.43**
120.0	**1.15**
140.0	**1.05**
160.0	**0.92**
180.0	**0.86**
200.0	**0.80**
220.0	**0.70**
240.0	**0.50**
260.0	**0.30**
280.0	**0.10**
300.0	**0.00**

Timber strength in tension relative to value for particular temperature above:

Temperature (°C)

Relative value

20.0	**1.00**
280.0	**0.20**
288.0	**0.00**
289.0	**0.00**
290.0	**0.00**
291.0	**0.00**
292.0	**0.00**
293.0	**0.00**
294.0	**0.00**
295.0	**0.00**
296.0	**0.00**
297.0	**0.00**

298.0	**0.00**
299.0	**0.00**
300.0	**0.00**

Timber strain in compression relative to value for particular temperature above:

Temperature (°C)

Relative value

20.0	**1.00**
40.0	**1.00**
60.0	**1.00**
100.0	**1.00**
120.0	**1.00**
160.0	**1.00**
180.0	**1.00**
200.0	**1.00**
220.0	**1.00**
240.0	**1.00**
260.0	**1.00**
280.0	**1.00**
300.0	**1.00**
400.0	**1.00**
500.0	**0.00**

Timber strain in tension relative to value for particular temperature above:

Temperature (°C)

Relative value

20.0	**1.00**
40.0	**1.00**
60.0	**1.00**
100.0	**1.00**
120.0	**1.00**
160.0	**1.00**
180.0	**1.00**
200.0	**1.00**
220.0	**1.00**
240.0	**1.00**
260.0	**1.00**

280.0	**1.00**
300.0	**1.00**
400.0	**1.00**
500.0	**0.00**

Stiffness of slip between gypsum board and studs, in partial composite action relative to value for particular temperature above:

Temperature (°C)

Relative value

20.0	**1.00**
40.0	**1.00**
60.0	**1.00**
100.0	**1.00**
110.0	**0.0015**
120.0	**0.0004**
130.0	**0.00013**
140.0	**0.00**
150.0	**0.00**
240.0	**0.00**
260.0	**0.00**
280.0	**0.00**
300.0	**0.00**
400.0	**0.00**
500.0	**0.00**

Rotational stiffness superimposed on end supports of wall relative to value for particular temperature above:

Temperature (°C)

Relative value

20.0	**1.00**
25.0	**1.00**
50.0	**1.00**
75.0	**1.00**
100.0	**1.00**
125.0	**1.00**
150.0	**1.00**
175.0	**1.00**

200.0	**1.00**
225.0	**1.00**
250.0	**1.00**
275.0	**1.00**
280.0	**1.00**
300.0	**1.00**
400.0	**1.00**

Analysis Options

Maximum number of second order iterations per time steps

Enter "0", only.

Enter "0" for non-linear mechanical properties of timber (Buchanan 1986), "1" for elasto-plastic behaviour in compression and elastic behaviour in tension.

Enter "0" if failure of wood fibres is controlled by stress, "1" if failure is controlled by maximum strain.

Convergence tolerance, that is the maximum difference between the applied vertical load and the load resistance computed from second order analysis, all divided by the applied vertical load.

20	**0**	**1**	**1**	**5d-002**

Time period of exposure (min.)

Size of discretised time steps (min.)

120.0d00	**1.00d00**